RECENT ADVANCES in ELECTRICAL and COMPUTER ENGINEERING

Proceedings of the 2014 International Conference on Circuits, Systems, Signal Processing, Communications and Computers (CSSCC '14)

Venice, Italy
March 15-17, 2014

RECENT ADVANCES in ELECTRICAL and COMPUTER ENGINEERING

Proceedings of the 2014 International Conference on Circuits, Systems, Signal Processing, Communications and Computers (CSSCC '14)

Venice, Italy
March 15-17, 2014

All papers of the present volume were peer reviewed by no less than two independent reviewers. Acceptance was granted when both reviewers' recommendations were positive.

ISBN: 978-1-61804-228-6

RECENT ADVANCES in ELECTRICAL and COMPUTER ENGINEERING

Proceedings of the 2014 International Conference on Circuits, Systems, Signal Processing, Communications and Computers (CSSCC '14)

Venice, Italy
March 15-17, 2014

Organizing Committee

General Chairs (EDITORS)

- Prof. Kleanthis Psarris,
  The City University of New York,
  USA
- Prof. Valeri Mladenov,
  Technical University of Sofia,
  Bulgaria
- Prof. Pierre Borne, IEEE France Section Chair,
  IEEE Fellow, IEEE/SMC Past President,
  Ecole Centrale de Lille, France
- Prof. George Vachtsevanos,
  Georgia Institute of Technology,
  Atlanta, Georgia, USA

Senior Program Chair

- Professor Philippe Dondon
  ENSEIRB
  Rue A Schweitzer 33400 Talence
  France

Program Chairs

- Prof. Filippo Neri
  Dipartimento di Informatica e Sistemistica
  University of Naples "Federico II"
  Naples, Italy
- Prof. Constantin Udriste,
  University Politehnica of Bucharest,
  Bucharest, Romania
- Prof. Sandra Sendra
  Instituto de Inv. para la Gestión Integrada de Zonas Costeras (IGIC)
  Universidad Politécnica de Valencia
  Spain

Tutorials Chair

- Professor Pradip Majumdar
  Department of Mechanical Engineering
  Northern Illinois University
  Dekalb, Illinois, USA

Special Session Chair

- Prof. Pavel Varacha
  Tomas Bata University in Zlin
  Faculty of Applied Informatics
  Department of Informatics and Artificial Intelligence
  Zlin, Czech Republic

Workshops Chair

- Prof. Ryszard S. Choras
  Institute of Telecommunications
  University of Technology & Life Sciences
  Bydgoszcz, Poland

Local Organizing Chair

- Assistant Prof. Klimis Ntalianis,
  Tech. Educ. Inst. of Athens (TEI),
  Athens, Greece

Publication Chair

- Prof. Gen Qi Xu
  Department of Mathematics
  Tianjin University
  Tianjin, China

Publicity Committee

- Prof. Reinhard Neck
  Department of Economics
  Klagenfurt University
  Klagenfurt, Austria
- Prof. Myriam Lazard
  Institut Superieur d' Ingenierie de la Conception
  Saint Die, France

International Liaisons

- Prof. Ka-Lok Ng
  Department of Bioinformatics
  Asia University
  Taichung, Taiwan
- Prof. Olga Martin
  Applied Sciences Faculty
  Politehnica University of Bucharest
  Romania
- Prof. Vincenzo Niola
  Departement of Mechanical Engineering for Energetics
  University of Naples "Federico II"
  Naples, Italy
- Prof. Eduardo Mario Dias
  Electrical Energy and Automation
  Engineering Department
  Escola Politecnica da Universidade de Sao Paulo
  Brazil

Steering Committee

- Professor Aida Bulucea, University of Craiova, Romania
- Professor Zoran Bojkovic, Univ. of Belgrade, Serbia
- Prof. Metin Demiralp, Istanbul Technical University, Turkey
- Professor Imre Rudas, Obuda University, Budapest, Hungary

Program Committee

Prof. Lotfi Zadeh (IEEE Fellow,University of Berkeley, USA)
Prof. Leon Chua (IEEE Fellow,University of Berkeley, USA)
Prof. Michio Sugeno (RIKEN Brain Science Institute (RIKEN BSI), Japan)
Prof. Dimitri Bertsekas (IEEE Fellow, MIT, USA)
Prof. Demetri Terzopoulos (IEEE Fellow, ACM Fellow, UCLA, USA)
Prof. Georgios B. Giannakis (IEEE Fellow, University of Minnesota, USA)
Prof. George Vachtsevanos (Georgia Institute of Technology, USA)
Prof. Abraham Bers (IEEE Fellow, MIT, USA)
Prof. David Staelin (IEEE Fellow, MIT, USA)
Prof. Brian Barsky (IEEE Fellow, University of Berkeley, USA)
Prof. Aggelos Katsaggelos (IEEE Fellow, Northwestern University, USA)
Prof. Josef Sifakis (Turing Award 2007, CNRS/Verimag, France)
Prof. Hisashi Kobayashi (Princeton University, USA)
Prof. Kinshuk (Fellow IEEE, Massey Univ. New Zeland),
Prof. Leonid Kazovsky (Stanford University, USA)
Prof. Narsingh Deo (IEEE Fellow, ACM Fellow, University of Central Florida, USA)
Prof. Kamisetty Rao (Fellow IEEE, Univ. of Texas at Arlington,USA)
Prof. Anastassios Venetsanopoulos (Fellow IEEE, University of Toronto, Canada)
Prof. Steven Collicott (Purdue University, West Lafayette, IN, USA)
Prof. Nikolaos Paragios (Ecole Centrale Paris, France)
Prof. Nikolaos G. Bourbakis (IEEE Fellow, Wright State University, USA)
Prof. Stamatios Kartalopoulos (IEEE Fellow, University of Oklahoma, USA)
Prof. Irwin Sandberg (IEEE Fellow, University of Texas at Austin, USA),
Prof. Michael Sebek (IEEE Fellow, Czech Technical University in Prague, Czech Republic)
Prof. Hashem Akbari (University of California, Berkeley, USA)
Prof. Yuriy S. Shmaliy, (IEEE Fellow, The University of Guanajuato, Mexico)
Prof. Lei Xu (IEEE Fellow, Chinese University of Hong Kong, Hong Kong)
Prof. Paul E. Dimotakis (California Institute of Technology Pasadena, USA)
Prof. M. Pelikan (UMSL, USA)
Prof. Patrick Wang (MIT, USA)
Prof. Wasfy B Mikhael (IEEE Fellow, University of Central Florida Orlando,USA)
Prof. Sunil Das (IEEE Fellow, University of Ottawa, Canada)
Prof. Panos Pardalos (University of Florida, USA)
Prof. Nikolaos D. Katopodes (University of Michigan, USA)
Prof. Bimal K. Bose (Life Fellow of IEEE, University of Tennessee, Knoxville, USA)
Prof. Janusz Kacprzyk (IEEE Fellow, Polish Academy of Sciences, Poland)
Prof. Sidney Burrus (IEEE Fellow, Rice University, USA)
Prof. Biswa N. Datta (IEEE Fellow, Northern Illinois University, USA)
Prof. Mihai Putinar (University of California at Santa Barbara, USA)
Prof. Wlodzislaw Duch (Nicolaus Copernicus University, Poland)
Prof. Tadeusz Kaczorek (IEEE Fellow, Warsaw University of Tehcnology, Poland)
Prof. Michael N. Katehakis (Rutgers, The State University of New Jersey, USA)
Prof. Pan Agathoklis (Univ. of Victoria, Canada)
Prof. P. Demokritou (Harvard University, USA)
Prof. P. Razelos (Columbia University, USA)
Dr. Subhas C. Misra (Harvard University, USA)
Prof. Martin van den Toorn (Delft University of Technology, The Netherlands)
Prof. Malcolm J. Crocker (Distinguished University Prof., Auburn University,USA)
Prof. S. Dafermos (Brown University, USA)
Prof. Urszula Ledzewicz, Southern Illinois University , USA.
Prof. Dimitri Kazakos, Dean, (Texas Southern University, USA)
Prof. Ronald Yager (Iona College, USA)
Prof. Athanassios Manikas (Imperial College, London, UK)

Prof. Keith L. Clark (Imperial College, London, UK)
Prof. Argyris Varonides (Univ. of Scranton, USA)
Prof. S. Furfari (Direction Generale Energie et Transports, Brussels, EU)
Prof. Constantin Udriste, University Politehnica of Bucharest , ROMANIA
Dr. Michelle Luke (Univ. Berkeley, USA)
Prof. Patrice Brault (Univ. Paris-sud, France)
Dr. Christos E. Vasios (MIT, USA)
Prof. Jim Cunningham (Imperial College London, UK)
Prof. Philippe Ben-Abdallah (Ecole Polytechnique de l'Universite de Nantes, France)
Prof. Photios Anninos (Medical School of Thrace, Greece)
Prof. Ichiro Hagiwara, (Tokyo Institute of Technology, Japan)
Prof. Metin Demiralp (Istanbul Technical University / Turkish Academy of Sciences, Istanbul, Turkey)
Prof. Andris Buikis (Latvian Academy of Science. Latvia)
Prof. Akshai Aggarwal (University of Windsor, Canada)
Prof. George Vachtsevanos (Georgia Institute of Technology, USA)
Prof. Ulrich Albrecht (Auburn University, USA)
Prof. Imre J. Rudas (Obuda University, Hungary)
Prof. Alexey L Sadovski (IEEE Fellow, Texas A&M University, USA)
Prof. Amedeo Andreotti (University of Naples, Italy)
Prof. Ryszard S. Choras (University of Technology and Life Sciences Bydgoszcz, Poland)
Prof. Remi Leandre (Universite de Bourgogne, Dijon, France)
Prof. Moustapha Diaby (University of Connecticut, USA)
Prof. Brian McCartin (New York University, USA)
Prof. Elias C. Aifantis (Aristotle Univ. of Thessaloniki, Greece)
Prof. Anastasios Lyrintzis (Purdue University, USA)
Prof. Charles Long (Prof. Emeritus University of Wisconsin, USA)
Prof. Marvin Goldstein (NASA Glenn Research Center, USA)
Prof. Costin Cepisca (University POLITEHNICA of Bucharest, Romania)
Prof. Kleanthis Psarris (University of Texas at San Antonio, USA)
Prof. Ron Goldman (Rice University, USA)
Prof. Ioannis A. Kakadiaris (University of Houston, USA)
Prof. Richard Tapia (Rice University, USA)
Prof. F.-K. Benra (University of Duisburg-Essen, Germany)
Prof. Milivoje M. Kostic (Northern Illinois University, USA)
Prof. Helmut Jaberg (University of Technology Graz, Austria)
Prof. Ardeshir Anjomani (The University of Texas at Arlington, USA)
Prof. Heinz Ulbrich (Technical University Munich, Germany)
Prof. Reinhard Leithner (Technical University Braunschweig, Germany)
Prof. Elbrous M. Jafarov (Istanbul Technical University, Turkey)
Prof. M. Ehsani (Texas A&M University, USA)
Prof. Sesh Commuri (University of Oklahoma, USA)
Prof. Nicolas Galanis (Universite de Sherbrooke, Canada)
Prof. S. H. Sohrab (Northwestern University, USA)
Prof. Rui J. P. de Figueiredo (University of California, USA)
Prof. Valeri Mladenov (Technical University of Sofia, Bulgaria)
Prof. Hiroshi Sakaki (Meisei University, Tokyo, Japan)
Prof. Zoran S. Bojkovic (Technical University of Belgrade, Serbia)
Prof. K. D. Klaes, (Head of the EPS Support Science Team in the MET Division at EUMETSAT, France)
Prof. Emira Maljevic (Technical University of Belgrade, Serbia)
Prof. Kazuhiko Tsuda (University of Tsukuba, Tokyo, Japan)
Prof. Milan Stork (University of West Bohemia , Czech Republic)
Prof. C. G. Helmis (University of Athens, Greece)
Prof. Lajos Barna (Budapest University of Technology and Economics, Hungary)
Prof. Nobuoki Mano (Meisei University, Tokyo, Japan)

Prof. Nobuo Nakajima (The University of Electro-Communications, Tokyo, Japan)
Prof. Victor-Emil Neagoe (Polytechnic University of Bucharest, Romania)
Prof. E. Protonotarios (National Technical University of Athens, Greece)
Prof. P. Vanderstraeten (Brussels Institute for Environmental Management, Belgium)
Prof. Annaliese Bischoff (University of Massachusetts, Amherst, USA)
Prof. Virgil Tiponut (Politehnica University of Timisoara, Romania)
Prof. Andrei Kolyshkin (Riga Technical University, Latvia)
Prof. Fumiaki Imado (Shinshu University, Japan)
Prof. Sotirios G. Ziavras (New Jersey Institute of Technology, USA)
Prof. Constantin Volosencu (Politehnica University of Timisoara, Romania)
Prof. Marc A. Rosen (University of Ontario Institute of Technology, Canada)
Prof. Alexander Zemliak (Puebla Autonomous University, Mexico)
Prof. Thomas M. Gatton (National University, San Diego, USA)
Prof. Leonardo Pagnotta (University of Calabria, Italy)
Prof. Yan Wu (Georgia Southern University, USA)
Prof. Daniel N. Riahi (University of Texas-Pan American, USA)
Prof. Alexander Grebennikov (Autonomous University of Puebla, Mexico)
Prof. Bennie F. L. Ward (Baylor University, TX, USA)
Prof. Guennadi A. Kouzaev (Norwegian University of Science and Technology, Norway)
Prof. Eugene Kindler (University of Ostrava, Czech Republic)
Prof. Geoff Skinner (The University of Newcastle, Australia)
Prof. Hamido Fujita (Iwate Prefectural University(IPU), Japan)
Prof. Francesco Muzi (University of L'Aquila, Italy)
Prof. Les M. Sztandera (Philadelphia University, USA)
Prof. Claudio Rossi (University of Siena, Italy)
Prof. Christopher J. Koroneos (Aristotle University of Thessaloniki, Greece)
Prof. Sergey B. Leonov (Joint Institute for High Temperature Russian Academy of Science, Russia)
Prof. Arpad A. Fay (University of Miskolc, Hungary)
Prof. Lili He (San Jose State University, USA)
Prof. M. Nasseh Tabrizi (East Carolina University, USA)
Prof. Alaa Eldin Fahmy (University Of Calgary, Canada)
Prof. Ion Carstea (University of Craiova, Romania)
Prof. Paul Dan Cristea (University "Politehnica" of Bucharest, Romania)
Prof. Gh. Pascovici (University of Koeln, Germany)
Prof. Pier Paolo Delsanto (Politecnico of Torino, Italy)
Prof. Radu Munteanu (Rector of the Technical University of Cluj-Napoca, Romania)
Prof. Ioan Dumitrache (Politehnica University of Bucharest, Romania)
Prof. Corneliu Lazar (Technical University Gh.Asachi Iasi, Romania)
Prof. Nicola Pitrone (Universita degli Studi Catania, Italia)
Prof. Miquel Salgot (University of Barcelona, Spain)
Prof. Amaury A. Caballero (Florida International University, USA)
Prof. Maria I. Garcia-Planas (Universitat Politecnica de Catalunya, Spain)
Prof. Petar Popivanov (Bulgarian Academy of Sciences, Bulgaria)
Prof. Alexander Gegov (University of Portsmouth, UK)
Prof. Lin Feng (Nanyang Technological University, Singapore)
Prof. Colin Fyfe (University of the West of Scotland, UK)
Prof. Zhaohui Luo (Univ of London, UK)
Prof. Mikhail Itskov (RWTH Aachen University, Germany)
Prof. George G. Tsypkin (Russian Academy of Sciences, Russia)
Prof. Wolfgang Wenzel (Institute for Nanotechnology, Germany)
Prof. Weilian Su (Naval Postgraduate School, USA)
Prof. Phillip G. Bradford (The University of Alabama, USA)
Prof. Ray Hefferlin (Southern Adventist University, TN, USA)
Prof. Gabriella Bognar (University of Miskolc, Hungary)

Prof. Hamid Abachi (Monash University, Australia)
Prof. Karlheinz Spindler (Fachhochschule Wiesbaden, Germany)
Prof. Josef Boercsoek (Universitat Kassel, Germany)
Prof. Eyad H. Abed (University of Maryland, Maryland, USA)
Prof. F. Castanie (TeSA, Toulouse, France)
Prof. Robert K. L. Gay (Nanyang Technological University, Singapore)
Prof. Andrzej Ordys (Kingston University, UK)
Prof. Harris Catrakis (Univ of California Irvine, USA)
Prof. T Bott (The University of Birmingham, UK)
Prof. Petr Filip (Institute of Hydrodynamics, Prague, Czech Republic)
Prof. T.-W. Lee (Arizona State University, AZ, USA)
Prof. Le Yi Wang (Wayne State University, Detroit, USA)
Prof. George Stavrakakis (Technical University of Crete, Greece)
Prof. John K. Galiotos (Houston Community College, USA)
Prof. M. Petrakis (National Observatory of Athens, Greece)
Prof. Philippe Dondon (ENSEIRB, Talence, France)
Prof. Dalibor Biolek (Brno University of Technology, Czech Republic)
Prof. Oleksander Markovskyy (National Technical University of Ukraine, Ukraine)
Prof. Suresh P. Sethi (University of Texas at Dallas, USA)
Prof. Hartmut Hillmer(University of Kassel, Germany)
Prof. Bram Van Putten (Wageningen University, The Netherlands)
Prof. Alexander Iomin (Technion - Israel Institute of Technology, Israel)
Prof. Roberto San Jose (Technical University of Madrid, Spain)
Prof. Minvydas Ragulskis (Kaunas University of Technology, Lithuania)
Prof. Arun Kulkarni (The University of Texas at Tyler, USA)
Prof. Joydeep Mitra (New Mexico State University, USA)
Prof. Vincenzo Niola (University of Naples Federico II, Italy)
Prof. Ion Chryssoverghi (National Technical University of Athens, Greece)
Prof. Dr. Aydin Akan (Istanbul University, Turkey)
Prof. Sarka Necasova (Academy of Sciences, Prague, Czech Republic)
Prof. C. D. Memos (National Technical University of Athens, Greece)
Prof. S. Y. Chen, (Zhejiang University of Technology, China and University of Hamburg, Germany)
Prof. Duc Nguyen (Old Dominion University, Norfolk, USA)
Prof. Tuan Pham (James Cook University, Townsville, Australia)
Prof. Jiri Klima (Technical Faculty of CZU in Prague, Czech Republic)
Prof. Rossella Cancelliere (University of Torino, Italy)
Prof. L.Kohout (Florida State University, Tallahassee, Florida, USA)
Prof. D' Attelis (Univ. Buenos Ayres, Argentina)
Prof. Dr-Eng. Christian Bouquegneau (Faculty Polytechnique de Mons, Belgium)
Prof. Wladyslaw Mielczarski (Technical University of Lodz, Poland)
Prof. Ibrahim Hassan (Concordia University, Montreal, Quebec, Canada)
Prof. Stavros J.Baloyannis (Medical School, Aristotle University of Thessaloniki, Greece)
Prof. James F. Frenzel (University of Idaho, USA)
Prof. Mirko Novak (Czech Technical University in Prague,Czech Republic)
Prof. Zdenek Votruba (Czech Technical University in Prague,Czech Republic)
Prof. Vilem Srovnal,(Technical University of Ostrava, Czech Republic)
Prof. J. M. Giron-Sierra (Universidad Complutense de Madrid, Spain)
Prof. Zeljko Panian (University of Zagreb, Croatia)
Prof. Walter Dosch (University of Luebeck, Germany)
Prof. Rudolf Freund (Vienna University of Technology, Austria)
Prof. Erich Schmidt (Vienna University of Technology, Austria)
Prof. Alessandro Genco (University of Palermo, Italy)
Prof. Martin Lopez Morales (Technical University of Monterey, Mexico)
Prof. Ralph W. Oberste-Vorth (Marshall University, USA)

Prof. Vladimir Damgov (Bulgarian Academy of Sciences, Bulgaria)
Prof. Menelaos Karanasos (Brunel University, UK)
Prof. P.Borne (Ecole Central de Lille, France)

Additional Reviewers

Angel F. Tenorio	Universidad Pablo de Olavide, Spain
Ole Christian Boe	Norwegian Military Academy, Norway
Abelha Antonio	Universidade do Minho, Portugal
Xiang Bai	Huazhong University of Science and Technology, China
Genqi Xu	Tianjin University, China
Moran Wang	Tsinghua University, China
Minhui Yan	Shanghai Maritime University, China
Jon Burley	Michigan State University, MI, USA
Shinji Osada	Gifu University School of Medicine, Japan
Bazil Taha Ahmed	Universidad Autonoma de Madrid, Spain
Konstantin Volkov	Kingston University London, UK
Tetsuya Shimamura	Saitama University, Japan
George Barreto	Pontificia Universidad Javeriana, Colombia
Tetsuya Yoshida	Hokkaido University, Japan
Deolinda Rasteiro	Coimbra Institute of Engineering, Portugal
Matthias Buyle	Artesis Hogeschool Antwerpen, Belgium
Dmitrijs Serdjuks	Riga Technical University, Latvia
Kei Eguchi	Fukuoka Institute of Technology, Japan
Imre Rudas	Obuda University, Budapest, Hungary
Francesco Rotondo	Polytechnic of Bari University, Italy
Valeri Mladenov	Technical University of Sofia, Bulgaria
Andrey Dmitriev	Russian Academy of Sciences, Russia
James Vance	The University of Virginia's College at Wise, VA, USA
Masaji Tanaka	Okayama University of Science, Japan
Sorinel Oprisan	College of Charleston, CA, USA
Hessam Ghasemnejad	Kingston University London, UK
Santoso Wibowo	CQ University, Australia
M. Javed Khan	Tuskegee University, AL, USA
Manoj K. Jha	Morgan State University in Baltimore, USA
Miguel Carriegos	Universidad de Leon, Spain
Philippe Dondon	Institut polytechnique de Bordeaux, France
Kazuhiko Natori	Toho University, Japan
Jose Flores	The University of South Dakota, SD, USA
Takuya Yamano	Kanagawa University, Japan
Frederic Kuznik	National Institute of Applied Sciences, Lyon, France
Lesley Farmer	California State University Long Beach, CA, USA
João Bastos	Instituto Superior de Engenharia do Porto, Portugal
Zhong-Jie Han	Tianjin University, China
Francesco Zirilli	Sapienza Universita di Roma, Italy
Yamagishi Hiromitsu	Ehime University, Japan
Eleazar Jimenez Serrano	Kyushu University, Japan
Alejandro Fuentes-Penna	Universidad Autónoma del Estado de Hidalgo, Mexico
José Carlos Metrôlho	Instituto Politecnico de Castelo Branco, Portugal
Stavros Ponis	National Technical University of Athens, Greece

Table of Contents

ISBN: 978-1-61804-228-6

ISBN: 978-1-61804-228-6

ISBN: 978-1-61804-228-6

ISBN: 978-1-61804-228-6

Keynote Lecture 1

On the Distinguished Role of the Mittag-Leffler and Wright Functions in Fractional Calculus

Professor Francesco Mainardi
Department of Physics, University of Bologna, and INFN
Via Irnerio 46, I-40126 Bologna, Italy
E-mail: francesco.mainardi@bo.infn.it.it

Abstract: Fractional calculus, in allowing integrals and derivatives of any positive real order (the term "fractional" is kept only for historical reasons), can be considered a branch of mathematical analysis which deals with integro-di erential equations where the integrals are of convolution type and exhibit (weakly singular) kernels of power-law type. As a matter of fact fractional calculus can be considered a laboratory for special functions and integral transforms. Indeed many problems dealt with fractional calculus can be solved by using Laplace and Fourier transforms and lead to analytical solutions expressed in terms of transcendental functions of Mittag-Leffler and Wright type. In this plenary lecture we discuss some interesting problems in order to single out the role of these functions. The problems include anomalous relaxation and diffusion and also intermediate phenomena.

Brief Biography of the Speaker: For a full biography, list of references on author's papers and books see:
Home Page: http://www.fracalmo.org/mainardi/index.htm
and http://scholar.google.com/citations?user=UYxWyEEAAAAJ&hl=en&oi=ao

ISBN: 978-1-61804-228-6

Keynote Lecture 2

Latest Advances in Neuroinformatics and Fuzzy Systems

Yingxu Wang, PhD, Prof., PEng, FWIF, FICIC, SMIEEE, SMACM
President, International Institute of Cognitive Informatics and Cognitive Computing (ICIC)
Director, Laboratory for Cognitive Informatics and Cognitive Computing
Dept. of Electrical and Computer Engineering
Schulich School of Engineering
University of Calgary
2500 University Drive NW,
Calgary, Alberta, Canada T2N 1N4
E-mail: yingxu@ucalgary.ca

Abstract: Investigations into the neurophysiological foundations of neural networks in neuroinformatics [Wang, 2013] have led to a set of rigorous mathematical models of neurons and neural networks in the brain using contemporary denotational mathematics [Wang, 2008, 2012]. A theory of neuroinformatics is recently developed for explaining the roles of neurons in internal information representation, transmission, and manipulation [Wang & Fariello, 2012]. The formal neural models reveal the differences of structures and functions of the association, sensory and motor neurons. The pulse frequency modulation (PFM) theory of neural networks [Wang & Fariello, 2012] is established for rigorously analyzing the neurosignal systems in complex neural networks. It is noteworthy that the Hopfield model of artificial neural networks [Hopfield, 1982] is merely a prototype closer to the sensory neurons, though the majority of human neurons are association neurons that function significantly different as the sensory neurons. It is found that neural networks can be formally modeled and manipulated by the neural circuit theory [Wang, 2013]. Based on it, the basic structures of neural networks such as the serial, convergence, divergence, parallel, feedback circuits can be rigorously analyzed. Complex neural clusters for memory and internal knowledge representation can be deduced by compositions of the basic structures.

Fuzzy inferences and fuzzy semantics for human and machine reasoning in fuzzy systems [Zadeh, 1965, 2008], cognitive computers [Wang, 2009, 2012], and cognitive robots [Wang, 2010] are a frontier of cognitive informatics and computational intelligence. Fuzzy inference is rigorously modeled in inference algebra [Wang, 2011], which recognizes that humans and fuzzy cognitive systems are not reasoning on the basis of probability of causations rather than formal algebraic rules. Therefore, a set of fundamental fuzzy operators, such as those of fuzzy causality as well as fuzzy deductive, inductive, abductive, and analogy rules, is formally elicited. Fuzzy semantics is quantitatively modeled in semantic algebra [Wang, 2013], which formalizes the qualitative semantics of natural languages in the categories of nouns, verbs, and modifiers (adjectives and adverbs). Fuzzy semantics formalizes nouns by concept algebra [Wang, 2010],

verbs by behavioral process algebra [Wang, 2002, 2007], and modifiers by fuzzy semantic algebra [Wang, 2013]. A wide range of applications of fuzzy inference, fuzzy semantics, neuroinformatics, and denotational mathematics have been implemented in cognitive computing, computational intelligence, fuzzy systems, cognitive robotics, neural networks, neurocomputing, cognitive learning systems, and artificial intelligence.

Brief Biography of the Speaker: Yingxu Wang is professor of cognitive informatics and denotational mathematics, President of International Institute of Cognitive Informatics and Cognitive Computing (ICIC, http://www.ucalgary.ca/icic/) at the University of Calgary. He is a Fellow of ICIC, a Fellow of WIF (UK), a P.Eng of Canada, and a Senior Member of IEEE and ACM. He received a PhD in software engineering from the Nottingham Trent University, UK, and a BSc in Electrical Engineering from Shanghai Tiedao University. He was a visiting professor on sabbatical leaves at Oxford University (1995), Stanford University (2008), University of California, Berkeley (2008), and MIT (2012), respectively. He is the founder and steering committee chair of the annual IEEE International Conference on Cognitive Informatics and Cognitive Computing (ICCI*CC) since 2002. He is founding Editor-in-Chief of International Journal of Cognitive Informatics and Natural Intelligence (IJCINI), founding Editor-in-Chief of International Journal of Software Science and Computational Intelligence (IJSSCI), Associate Editor of IEEE Trans. on SMC (Systems), and Editor-in-Chief of Journal of Advanced Mathematics and Applications (JAMA). Dr. Wang is the initiator of a few cutting-edge research fields or subject areas such as denotational mathematics, cognitive informatics, abstract intelligence (□I), cognitive computing, software science, and basic studies in cognitive linguistics. He has published over 160 peer reviewed journal papers, 230+ peer reviewed conference papers, and 25 books in denotational mathematics, cognitive informatics, cognitive computing, software science, and computational intelligence. He is the recipient of dozens international awards on academic leadership, outstanding contributions, best papers, and teaching in the last three decades.

http://www.ucalgary.ca/icic/

http://scholar.google.ca/citations?user=gRVQjskAAAAJ&hl=en

Editor-in-Chief, International Journal of Cognitive Informatics and Natural Intelligence
Editor-in-Chief, International Journal of Software Science and Computational Intelligence
Associate Editor, IEEE Transactions on System, Man, and Cybernetics - Systems
Editor-in-Chief, Journal of Advanced Mathematics and Applications
Chair, The Steering Committee of IEEE ICCI*CC Conference Series

Keynote Lecture 3

Recent Advances and Future Trends on Atomic Engineering of III-V Semiconductor for Quantum Devices from Deep UV (200nm) up to THZ (300 microns)

Professor Manijeh Razeghi
Center for Quantum Devices
Department of Electrical Engineering and Computer Science
Northwestern University
Evanston, Illinois 60208
USA
E-mail: razeghi@eecs.northwestern.edu

Abstract: Nature offers us different kinds of atoms, but it takes human intelligence to put them together in an elegant way in order to realize functional structures not found in nature. The so-called III-V semiconductors are made of atoms from columns III (B, Al, Ga, In. Tl) and columns V(N, As, P, Sb,Bi) of the periodic table, and constitute a particularly rich variety of compounds with many useful optical and electronic properties. Guided by highly accurate simulations of the electronic structure, modern semiconductor optoelectronic devices are literally made atom by atom using advanced growth technology such as Molecular Beam Epitaxy (MBE) and Metal Organic Chemical Vapor Deposition (MOCVD). Recent breakthroughs have brought quantum engineering to an unprecedented level, creating light detectors and emitters over an extremely wide spectral range from 0.2 mm to 300 mm. Nitrogen serves as the best column V element for the short wavelength side of the electromagnetic spectrum, where we have demonstrated III-nitride light emitting diodes and photo detectors in the deep ultraviolet to visible wavelengths. In the infrared, III-V compounds using phosphorus ,arsenic and antimony from column V ,and indium, gallium, aluminum, ,and thallium from column III elements can create interband and intrsuband lasers and detectors based on quantum-dot (QD) or type-II superlattice (T2SL). These are fast becoming the choice of technology in crucial applications such as environmental monitoring and space exploration. Last but not the least, on the far-infrared end of the electromagnetic spectrum, also known as the terahertz (THz) region, III-V semiconductors offer a unique solution of generating THz waves in a compact device at room temperature. Continued effort is being devoted to all of the above mentioned areas with the intention to develop smart technologies that meet the current challenges in environment, health, security, and energy. This talk will highlight my contributions to the world of III-V semiconductor Nano scale optoelectronics. Devices from deep UV-to THz.

Brief Biography of the Speaker: Manijeh Razeghi received the Doctorat d'État es Sciences Physiques from the Université de Paris, France, in 1980.
After heading the Exploratory Materials Lab at Thomson-CSF (France), she joined Northwestern University, Evanston, IL, as a Walter P. Murphy Professor and Director of the Center for

ISBN: 978-1-61804-228-6

Quantum Devices in Fall 1991, where she created the undergraduate and graduate program in solid-state engineering. She is one of the leading scientists in the field of semiconductor science and technology, pioneering in the development and implementation of major modern epitaxial techniques such as MOCVD, VPE, gas MBE, and MOMBE for the growth of entire compositional ranges of III-V compound semiconductors. She is on the editorial board of many journals such as Journal of Nanotechnology, and Journal of Nanoscience and Nanotechnology, an Associate Editor of Opto-Electronics Review. She is on the International Advisory Board for the Polish Committee of Science, and is an Adjunct Professor at the College of Optical Sciences of the University of Arizona, Tucson, AZ. She has authored or co-authored more than 1000 papers, more than 30 book chapters, and fifteen books, including the textbooks Technology of Quantum Devices (Springer Science+Business Media, Inc., New York, NY U.S.A. 2010) and Fundamentals of Solid State Engineering, 3rd Edition (Springer Science+Business Media, Inc., New York, NY U.S.A. 2009). Two of her books, MOCVD Challenge Vol. 1 (IOP Publishing Ltd., Bristol, U.K., 1989) and MOCVD Challenge Vol. 2 (IOP Publishing Ltd., Bristol, U.K., 1995), discuss some of her pioneering work in InP-GaInAsP and GaAs-GaInAsP based systems. The MOCVD Challenge, 2nd Edition (Taylor & Francis/CRC Press, 2010) represents the combined updated version of Volumes 1 and 2. She holds 50 U.S. patents and has given more than 1000 invited and plenary talks. Her current research interest is in nanoscale optoelectronic quantum devices.

Dr. Razeghi is a Fellow of MRS, IOP, IEEE, APS, SPIE, OSA, Fellow and Life Member of Society of Women Engineers (SWE), Fellow of the International Engineering Consortium (IEC), and a member of the Electrochemical Society, ACS, AAAS, and the French Academy of Sciences and Technology. She received the IBM Europe Science and Technology Prize in 1987, the Achievement Award from the SWE in 1995, the R.F. Bunshah Award in 2004, and many best paper awards.

ISBN: 978-1-61804-228-6

ISBN: 978-1-61804-228-6

Bayesian Inference for Phase Unwrapping using Multiple Interferograms Based on Statistical Mechanics of Three-state Ising Model

Yohei Saika and Tatsuya Uezu

***Abstract*—**We construct a method of phase unwrapping using multiple interferograms on the basis of Bayesian inference which corresponds to the statistical mechanics of the three-state Ising model. Then, in order to clarify performance from statistical mechanical viewpoint, we describe phase diagram using Monte Carlo simulation for a typical wave-front in synthetic aperture interferometry. We clarify that phase unwrapping carried out perfectly by the present method without using prior information under a constraint of surface-consistency condition, if observed interferograms are not corrupted by any noises. Then, we clarify that the present method phase unwrapping with high degree of accuracy using prior information under the constraint of the surface-consistency condition.

***Keywords*—**Maximizer of the posterior marginal estimate, multiple interferograms, phase unwrapping, statistical mechanics.

I. Introduction

WAVE-FRONTS often carry information through noisy channels. Therefore, many researchers [1]–[6] have constructed methods of utilizing information on wave-fronts in various fields. Engineers have constructed optical systems to observe wave-fronts using the synthetic aperture radar (SAR) interferometry [1]. Then, researchers have constructed a technique called as phase unwrapping to reconstruct original wave-fronts from a set of principal values of phase differences derived from an interferogram observed by interferometer. Various techniques have been proposed for this problem, such as the least squares estimation [1], [2], the MAP estimation via conjugate gradient method [7], simulated annealing [8], [9] and maximum entropy [9]. Now, in order to improve the accuracy of\ phase unwrapping, researchers tried various approaches, such as the edgelist phase unwrapping algorithm [10].

On the other hand, theoretical researchers have investigated information science [11]-[20], such as image restoration and error-correcting codes based on an analogy between statistical mechanics and Bayesian inference via the maximizer of the posterior marginal (MPM) estimate and the maximum A posteriori (MAP) estimation. In this field, researchers have applied statistical mechanics to information science, such as information communication. Then, a research field called as statistical mechanics of information has developed as an established research field. Present author has utilized statistical mechanics to various problems, such as image restoration [14], inverse process of digital halftoning [15]-[17] and noise reduction in JPEG-compressed images [18]. Saika and Nishimori [19] have applied statistical mechanics to phase retrieval under a restricted condition. Recently, Saika and Uezu [20] have studied wave-front reconstruction with the use both of the MPM estimate for phase unwrapping and maximum entropy for noise reduction. Here, they investigated the availability of the MPM estimate for phase unwrapping from the viewpoint of statistical mechanics.

In this study, on the basis of Bayesian inference using the MPM estimate utilizing the statistical mechanics of the three-state Ising model, we first construct a method of phase unwrapping using multiple interferograms in remote sensing using the SAR interferometry. We try this approach with a hope that the accuracy of the present method with respect to phase unwrapping may be improved by utilizing information on multiple interferograms. In this method, we carry out phase unwrapping by searching the MAP solution based on the framework of the Bayesian inference using the MPM estimate. When we here estimate the posterior probability, we assume following model prior and likelihood. We use the model prior which decreases the number of non-zero states of the three-state Ising spin at each sampling point so as to suppress the occurrence of residues in the patterns of interferograms. Then, we use the likelihood with following two terms: One is the term which suppresses differences between neighboring wave-front slopes so as to enhance smooth structures in wave-fronts. The other is the term which satisfies the surface-consistency condition at each plaquette. Next, in order to clarify the performance of the MPM estimate for phase unwrapping, we describe a phase diagram in the hyper-parameter space by using the Monte Carlo simulation for the wave-front in remote sensing via SAR interferometry. Here, we examine stability of a “PU phase” in the hyper-parameter space, where the term “PU phase” is referred to be a domain where the MPM estimate succeeds in phase unwrapping perfectly/accurately. We clarify from the phase diagram that the constraint of surface-consistency condition is essential to succeed in phase unwrapping with high accuracy in the MPM estimate using the multiple interferograms. Also, we find that the prior information

Yohei Saika is with the Gunma National of Technology, Toriba 580, Maebashi 371-8530, Japan (phone: +81-27-254-9256; fax:+81-27-254-9009; saika@ice.gunma-ct.ac.jp).

Tatsuya Uezu is with Nara Women’s University, Nara, 630-8506, Japan (e-mail: uezu@nara-wu.ac.jp).

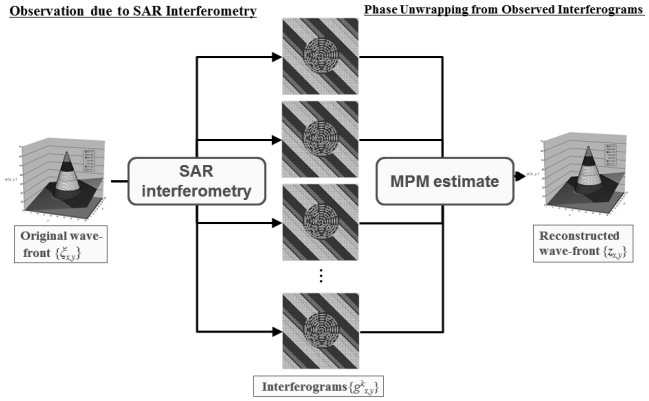

Fig. 1 General formulation for phase unwrapping using multiple interferograms based on the Bayesian inference via the MPM estimate.

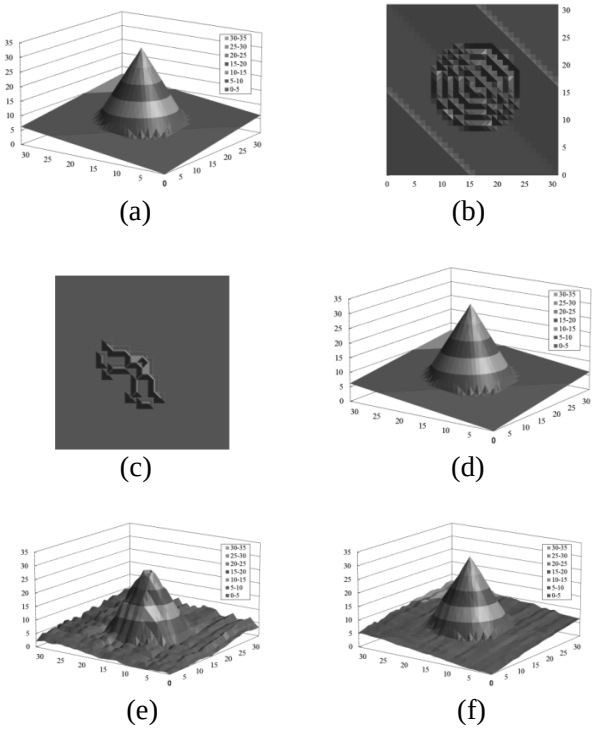

Fig. 2 (a) An original wave-front, (b) an interferogram of the original wave-front in Fig. 2(a), (c) a residues of the interferogram in Fig. 2(b), (d) a wave-front reconstructed using the MPM estimate without using the prior information, if the interferogram was not corrupted by any noises, (e) a wave-front reconstructed by the MPM estimate using the single interferogram corrupted by the Gaussian noises, (f) a wave-front reconstructed by the MPM estimate using 8 interferograms corrupted by the Gaussian noises.

is useful for extending the PU phase along the T_m axis under the constraint of the surface-consistency condition. Next, we evaluate how the performance of the MPM estimate depends on the number of the interferograms. We find that the MPM estimate becomes more accurately with the increase in the number of the interferograms. Next, we find that the MPM estimate using fluctuations around the MAP solution carries out phase unwrapping more smoothly than the deterministic version of the MPM estimate.

The content of this paper is organized as follows. First, we show the general formulation of phase unwrapping based on Bayesian inference using the MPM estimate via the multiple interferograms. Next, we investigate both static and dynamic properties of the MPM estimate for phase unwrapping using the Monte Carlo simulation for typical wave-fronts in SAR interferometry. Last part is devoted to a summary and discussion.

II. Statistical Mechanics

In this chapter, we briefly show the framework of statistical mechanics. A principal goal of statistical mechanics is clarifying thermodynamic property of many-body systems starting with interactions between microscopic elements. In general prescription of statistical mechanics, thermal average of macroscopic physical quantity is estimated as an ensemble average:

$$\Pr(\{S\}) = \frac{1}{Z}\exp\left[-\beta H(\{S\})\right] \tag{1}$$

for a given Hamiltonian $H(\{S\})$, where $\{S\}$ is a set of the Ising spin system which is a typical example of the microscopic elements in physical systems. Then, we take the unit of temperature such that Boltzmann's constant k_B is unity and then $\beta=1/T$. Then, normalization factor:

$$Z = \sum_{\{S_1\}}\sum_{\{S_2\}}\cdots\sum_{\{S_N\}}\exp\left[-\beta H(\{S\})\right]. \tag{2}$$

is called as "partition function" in statistical mechanics. The probability distribution in eq. (1) is termed the "Boltzmann factor". Using the Boltzmann distribution, we estimate thermal average of macroscopic quantity $A(\{S\})$ as

$$\langle A\rangle = \frac{1}{Z}\sum_{\{S_1\}}\sum_{\{S_2\}}\cdots\sum_{\{S_N\}}\exp\left[-\beta H(\{S\})\right]A(\{S\}). \tag{3}$$

Though it is difficult to calculate this macroscopic quantity directly, however it is estimated via approximation theories, such as the mean-field theory, and numerical simulations, such as the Monte Carlo simulations.

III. General Formulation

As shown in Fig. 1, we here show a general formulation of the problem of phase unwrapping on the basis of Bayesian inference using the MPM estimate.

Let us first consider an original wave-front $\{\xi_{x,y}\}$ ($0<\xi_{X,Y}<\infty$, x, y=1,...,L) in this study. If we treat a realistic case, we can use the wave-front in Fig. 2(a). If we investigate the statistical performance, we need to consider a set of wave-fronts $\{\xi_{x,y}\}$ which are generated by the assumed true prior expressed as the probability distribution $\Pr(\{\xi_{x,y}\})$. Then, each original

ISBN: 978-1-61804-228-6

wave-front $\{\xi_{x,y}\}$ is rewritten into $\{\eta_{x,y}\}$ ($0<\eta^k_{x,y}<\infty$, x, y=1,...,L, k=1,…,N_s) by some noises, such as atmospheric disturbance, with the conditional probability $\Pr(\{\eta^k_{x,y}\}|\{\xi_{x,y}\})$. Here, we use Gaussian noise expressed as

$$\Pr(\{\eta^k_{x,y}\}|\{\xi_{x,y}\}) = \left(\frac{1}{\sqrt{2\pi}\sigma_1}\right)^{\frac{L^2}{2}} \exp\left[-\frac{1}{2\sigma_1^2}\sum_{(x,y)}\sum_{k=1}^{Ns}(\eta^k_{x,y}-\xi_{x,y})^2\right]. \quad (4)$$

Here σ_1^2 denotes variance of the Gaussian noise. Then, as seen in Fig. 2(b), we observe the interferogram $\{\zeta^k_{x,y}\}$ as:

$$\zeta^k_{x,y} = \mathrm{mod}(\eta^k_{x,y}+\pi, 2\pi)-\pi. \quad (5)$$

Then, we obtain two sets of phase differences:

$$\tau^{k,x}_{x,y} = \mathrm{mod}(\zeta^k_{x+1,y}-\zeta^k_{x,y}+\pi, 2\pi)-\pi+n^k_{x,y}(0,\sigma_2^2), \quad (6)$$

$$\tau^{k,y}_{x,y} = \mathrm{mod}(\zeta^k_{x,y+1}-\zeta^k_{x,y}+\pi, 2\pi)-\pi+n^k_{x,y}(0,\sigma_2^2), \quad (7)$$

both of which are derived from the interferograms $\{\zeta^k_{x,y}\}$ restricted to the principal interval $[-\pi, +\pi]$. Here, σ_2^2 is the variance of the Gaussian noise. As shown in eqs. (6) and (7), these phase differences are often corrupted by some noises through the procedure of optical measurements using the interferometer. Here, we assume that the phase differences are rewritten by the Gaussian noise $n_{x,y}(0, \sigma_2^2)$ at each sampling point. Here, we discuss accuracy of the optical measurements due to the interferometer from the theoretical point of view. As shown in Fig. 3(a), if aliasing does not occur at each sampling point, the Nyquist theorem holds as

$$|\eta^k_{x+1,y}-\eta^k_{x,y}|<\pi, \quad (8)$$

at every sampling point. Then, as shown in Fig. 3(b), if aliasing occurs, the Nyquist theorem does not hold as

$$|\eta^k_{x+1,y}-\eta^k_{x,y}|>\pi, \quad (9)$$

at several sampling points. In this case, as shown in Fig. 2(c), there appears residue corresponding to a plaquette where the surface-consistency condition:

$$\tau^{k,x}_{x,y}+\tau^{k,y}_{x+1,y}-\tau^{k,x}_{x,y+1}-\tau^{k,y}_{x,y}=0, \quad (10)$$

does not hold, even if each phase difference in eq. (10) is not corrupted by any noises.

Next, we carry out phase unwrapping by utilizing the set of principal values for the phase differences, $\{\tau^x_{x,y}\}$ and $\{\tau^y_{x,y}\}$ based on the Bayesian inference using the MPM estimate which corresponds to statistical mechanics of the three-state Q-Ising models $\{n^x_{x,y}\}$ ($n^x_{x,y}$ =-1, 0, +1, x=1,…,L-1, y=1,…,L) and $\{n^y_{x,y}\}$ ($n^y_{x,y}$ =-1,0, +1, x=1,…,L, y=1,…,L-1). Here, we reconstruct the original wave-front so as to maximize the marginal posterior probability as

$$\hat{n}^x_{x,y} = \arg\max_{n^x_{x,y}} \sum_{\{n^x\}\neq n^x_{x,y}} \sum_{\{n^y\}} \Pr(\{n^x\},\{n^y\}|\{\tau^x\},\{\tau^y\}) \quad (11)$$

and

$$\hat{n}^y_{x,y} = \arg\max_{n^y_{x,y}} \sum_{\{n^y\}\neq n^y_{x,y}} \sum_{\{n^x\}} \Pr(\{n^x\},\{n^y\}|\{\tau^x\},\{\tau^y\}). \quad (12)$$

Here, the posterior is estimated via the Bayes formula:

$$\Pr(\{n^x\},\{n^y\}|\{\tau^x\},\{\tau^y\}) \propto \frac{\Pr(\{n^x\},\{n^y\})\Pr(\{\tau^x\},\{\tau^y\}|\{n^x\},\{n^y\})}{\sum_{\{\tau^x\}}\sum_{\{\tau^y\}}\Pr(\{n^x\},\{n^y\})\Pr(\{\tau^x\},\{\tau^y\}|\{n^x\},\{n^y\})} \quad (13)$$

using the likelihood and the model of the true prior. In this study, We assume the model of the true prior by suppressing the number of non-zero states of the three-state Ising spins, $\{n^x_{i,j}\}$ and $\{n^y_{i,j}\}$, as

$$\Pr(\{n^x\},\{n^y\}) \propto \exp\left[-\frac{h}{T_m}\sum_{(x,y)}\left\{|n^x_{x,y}|+|n^y_{x,y}|\right\}\right]. \quad (14)$$

We then assume the likelihood that would enhance the smooth structures, as seen from natural wave-fronts, by suppressing the differences in wave-fronts as

$$\Pr(\{\tau^x\},\{\tau^y\}|\{n^x\},\{n^y\}) \propto \exp\left[-\frac{1}{T_m}\left\{\frac{J}{(2\pi)^2}H_{\mathrm{int}}(\{n^{\nu}{}_{i,j}\})+\frac{\Gamma}{(2\pi)^2}H_{\mathrm{sc}}(\{n\})\right\}\right], \quad (15)$$

$$\begin{aligned} H_{\mathrm{int}}(\{n^x\},\{n^y\}) = &\sum_{(i,j)}\sum_{k=1}^{N_m}\left(\tau^{k,x}_{i,j}-\tau^{k,x}_{i+1,j}+2\pi(n^x_{i,j}-n^x_{i+1,j})\right)^2 \\ &+\sum_{(i,j)}\sum_{k=1}^{N_m}\left(\tau^{k,y}_{i,j}-\tau^{k,y}_{i,j+1}+2\pi(n^y_{i,j}-n^y_{i,j+1})\right)^2 \\ &+\alpha\sum_{(i,j)}\sum_{k=1}^{N_m}\left(\tau^{k,x}_{i,j}-\tau^{k,x}_{i,j+1}+2\pi(n^x_{i,j}-n^x_{i,j+1})\right)^2 \\ &+\alpha\sum_{(i,j)}\sum_{k=1}^{N_m}\left(\tau^{k,y}_{i,j}-\tau^{k,y}_{i+1,j}+2\pi(n^y_{i,j}-n^y_{i+1,j})\right)^2 \end{aligned} \quad (16)$$

under the constraint of the surface-consistency condition:

$$H_{\mathrm{int}}(\{n^x\},\{n^y\}) = \sum_{(i,j)}\sum_{k=1}^{N_m}\left(\tau^{k,x}_{i,j}+\tau^{k,y}_{i+1,j}-\tau^{k,x}_{i+1,j}-\tau^{k,y}_{i,j}+2\pi(n^x_{i,j}+n^y_{i+1,j}-n^x_{i+1,j}-n^y_{i,j})\right)^2. \quad (17)$$

As seen from eqs. (14)-(16), the likelihood which we use here is composed of two terms. One is the term which enhances smooth structures, as seen in natural wave-fronts, in the pattern of original wave-fronts. The other is the term which shows the surface-consistency conditions at each plaquette.

A reconstructed wave-front is constructed in this study as an expectation value for a wave-front slope as

$$\hat{n}^{\nu}_{x,y} = \Theta(\bar{n}^{\nu}_{x,y}) \quad (18)$$

where

$$\hat{n}^{\nu}_{x,y} = \sum_{\{n^x\}}\sum_{\{n^y\}}\Pr(\{n^x\},\{n^y\}|\{\tau^x\},\{\tau^y\})\cdot n^{\nu}{}_{x,y}, \quad (19)$$

$$\Theta(x) = \sum_{k=-1,0,+1}\theta\left(x-k+\frac{1}{2}\right)-\theta\left(x-k-\frac{1}{2}\right). \quad (20)$$

Here, ν=x, y. The wave-fronts are then reconstructed by making use of solutions $\{n^x\}$ and $\{n^y\}$ as

$$z_{x,y} = z_{0,0}+\sum_{l=0}^{x-1}(\tau_{l,0}+2\pi\hat{n}_{l,0})+\sum_{m=0}^{y-1}(\tau_{x,n}+2\pi\hat{n}_{x,m}). \quad (21)$$

Here, we assume $z_{0,0}$=0 and $\xi_{0,0}$=0 for convenience.

Next, in order to improve the accuracy of the present method for wave-front reconstruction, we introduce a method of removing noises on the reconstructed wave-front based on statistical mechanics of the spin system which is composed of a set of continuous spins $\{\theta_{x,y}\}$($0<\theta_{x,y}<2\pi$, x,y=1,…,L) on the square lattice. In this method, we carry out the maximum likelihood algorithm as

$$\hat{\theta}^x_{x,y} = \sum_{\{\theta^x\}}\sum_{\theta^y\}}\Pr(\{\tau^x\},\{\tau^y\}|\{\theta^x\},\{\theta^y\};\{\hat{n}^x\},\{\hat{n}^y\})\cdot\theta^x_{x,y} \quad (22)$$

$$\hat{\theta}^y_{x,y} = \sum_{\{\theta^x\}}\sum_{\theta^y\}}\Pr(\{\tau^x\},\{\tau^y\}|\{\theta^x\},\{\theta^y\};\{\hat{n}^x\},\{\hat{n}^y\})\cdot\theta^y_{x,y} \quad (23)$$

Then, the likelihood which we use here is assumed to enhance smooth structures as

$$\Pr(\{\tau^x\},\{\tau^y\}|\{\theta^x\},\{\theta^y\};\{\hat{n}^x\},\{\hat{n}^y\}) \propto \exp\left[-\frac{1}{T_m}\left\{\frac{J}{(2\pi)^2}H_{\mathrm{int}}(\{\theta\},\{\theta\})+\frac{\Gamma}{(2\pi)^2}H_{\mathrm{sc}}(\{\theta\},\{\theta\})\right\}\right] \quad (24)$$

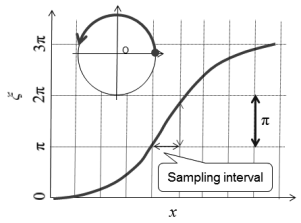

(a)

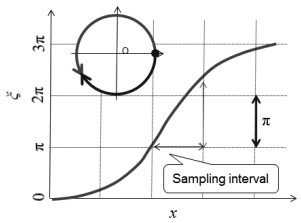

(b)

Fig. 3 Nyquist sampling theorem. (a) In this case, aliasing does not occur at every sampling point, (b) In this case, aliasing occurs at some sampling points.

$$\begin{aligned} H_{\text{int}}(\{\theta^x\},\{\theta^y\}) &= \sum_{(i,j)}\left(\theta^x_{i,j}-\theta^x_{i+1,j}+2\pi(\hat{n}^x_{i,j}-\hat{n}^x_{i+1,j})\right)^2 \\ &+\sum_{(i,j)}\left(\theta^y_{i,j}-\theta^y_{i,j+1}+2\pi(\hat{n}^y_{i,j}-\hat{n}^y_{i,j+1})\right)^2 \\ &+\alpha\sum_{(i,j)}\left(\theta^x_{i,j}-\theta^x_{i,j+1}+2\pi(\hat{n}^x_{i,j}-\hat{n}^x_{i,j+1})\right)^2 \\ &+\alpha\sum_{(i,j)}\left(\theta^y_{i,j}-\theta^y_{i+1,j}+2\pi(\hat{n}^y_{i,j}-\hat{n}^y_{i+1,j})\right)^2 \end{aligned} \tag{25}$$

under the constraint of the surface-consistency condition:

$$\begin{aligned} H_{\text{sc}}(\{\theta^x\},\{\theta^y\}) &= \sum_{(x,y)}(\theta^x_{x,y}+\theta^y_{x+1,y}-\theta^x_{x+1,y}+\theta^y_{x,y} \\ &+2\pi(\hat{n}^x_{x,y}+\hat{n}^y_{x+1,y}-\hat{n}^x_{x+1,y}+\hat{n}^y_{x,y}))^2 \end{aligned} \tag{26}$$

In the following part of this chapter, we study the present method for phase unwrapping with the use both of the three-state Q-Ising and the continuous spin models from the statistical mechanical point of view. As shown in above, the present method first carries out phase unwrapping based on statistical mechanics of the three-state Q-Ising model and then carries out noise reduction via the continuous spin model. We construct a probability distribution regarded as an equilibrium state of the Q-Ising models whose Hamiltonian is given by

$$\begin{aligned} H(\{n^x\},\{n^y\}) &= h\sum_{(x,y)}(|n^x_{x,y}|+|n^y_{x,y}|) \\ &+\frac{J}{(2\pi)^2}H_{\text{int}}(\{n^x\},\{n^y\})+\frac{\Gamma}{(2\pi)^2}H_{\text{sc}}(\{n^x\},\{n^y\}) \end{aligned} \tag{27}$$

at finite temperature T_m. Next, we carry out phase unwrapping by searching the ground state of the Hamiltonian in eq. (27) utilizing thermal fluctuations around the ground state from an initial state set randomly. We explain how thermal fluctuations are effective for phase unwrapping in the present method for typical wave-fronts in the SAR interferometry in the following.

In order to clarify the performance of the present method, we numerically evaluate the mean square error:

$$\sigma=\frac{1}{L^2}\sum_{x=1}^{L}\sum_{y=1}^{L}(z_{x,y}-\xi_{x,y})^2, \tag{28}$$

where $\{z_{x,y}\}$ is the reconstructed wave-front for a realistic image. On the other hand, we estimate statistical performance for the set of the original wave-front $\{\xi_{x,y}\}$ which are generated by the true prior expressed as probability distribution $\Pr(\{\xi_{x,y}\})$ as

$$\sigma=\sum_{\{\xi\}}\Pr(\{\xi\})\frac{1}{L^2}\sum_{x=1}^{L}\sum_{y=1}^{L}(z_{x,y}-\xi_{x,y})^2. \tag{29}$$

These variables become zero, if all kinds of wave-fronts are completely reconstructed.

IV. Performance

We investigated the performance of the present method for phase unwrapping using the Monte Carlo simulation for the single artificial wave-front which was typical in remote sensing using the SAR interferometry. Here, we clarified static property of the present method for phase unwrapping from the phase diagram in the hyper-parameter space.

In order to estimate the performance of the MPM estimate, we used the artificial wave-front $\{\xi_{x,y}\}$ in Fig. 2(a). Then, the original wave-front was corrupted by additive white Gaussian noise $\{n_{x,y}(0,{\sigma_1}^2)\}$ with ${\sigma_1}^2=0$, and the interferogram $\{\zeta^k_{x,y}\}$ in Fig. 2(b) was observed by the interferometer. Here, the residue pattern of the interferogram was shown in Fig. 2(c). Then, we derived from the interferogram in Fig. 2(c) the sets of principal phase differences $\{\tau^{k,x}_{x,y}\}$ and $\{\tau^{k,y}_{x,y}\}$ corrupted by the Gaussian noise with ${\sigma_2}^2$ = 0, 0.3. We carried out phase unwrapping from the phase differences $\{\tau^{k,x}_{x,y}\}$ and $\{\tau^{k,y}_{x,y}\}$ by using the Monte Carlo simulation with 20000 Monte Carlo steps (MCSs). Next, we estimated statistical performance based on the mean square error between the original and reconstructed wave-fronts.

On the basis of the phase diagram in the hyper-parameter space, we investigated statistical performance of the MPM estimate via the multiple interferograms for phase unwrapping. For this purpose, as shown in Fig. 4, we evaluated the parameter dependence of the mean square error, if the interferograms were not corrupted by any noises. Figure 4 showed that the present method perfectly reconstructed the original wave-front in Fig. 2(a), if we introduced the constraint of the surface-consistency condition into the cost function. Using these estimates, we described the phase diagram in the hyper-parameter space. As shown in Fig. 5(a), we found that the present method succeeded in phase unwrapping up to T_m~0.4 (1.2, 2.0), if we set $\Gamma/(2\pi)^2=0$ (0.1, 0.2) at J=1, α=0, and h=0. Also, we found that the PU phase was extended up to T_m=3.1, if we introduced the constraint of the surface-consistency condition into the model system at J=1, α=0, and h=0. These results indicated that the surface-consistency condition was useful for extending the range of the PU phase along the T_m axis. Then, we examined how the prior information was useful for phase unwrapping due to the present method. For this purpose, we evaluated how mean square error depends on the hyper-parameter h to describe the phase diagram in hyper-parameter space. As seen in Fig. 5(b), we clarified that the prior information is useful for extending the PU phase up to T_m=4.9 under the constraint of surface-consistency condition.

ISBN: 978-1-61804-228-6

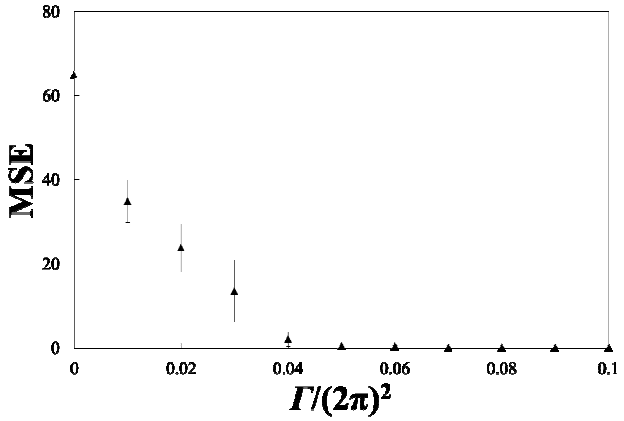

Fig. 4 Mean square error as a function of the parameter Γ obtained by the Bayesian inference using the MPM estimate, if we set to σ=0, J=1, α=0 and h=0.

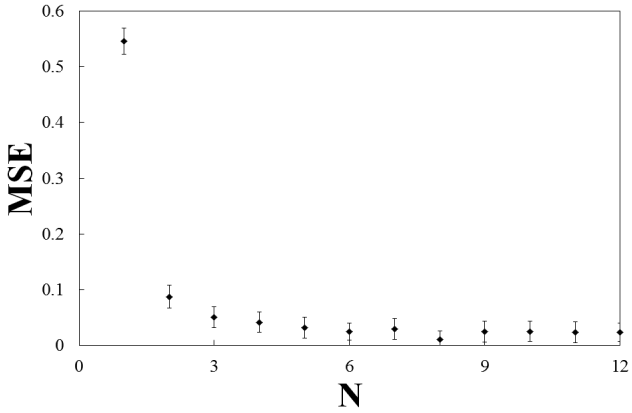

Fig. 6 Mean square error as a function of the number of the interferograms observed by the remote sensing using the SAR interferometry due to the Monte Carlo simulation for the original wave-front in Fig. 2(a).

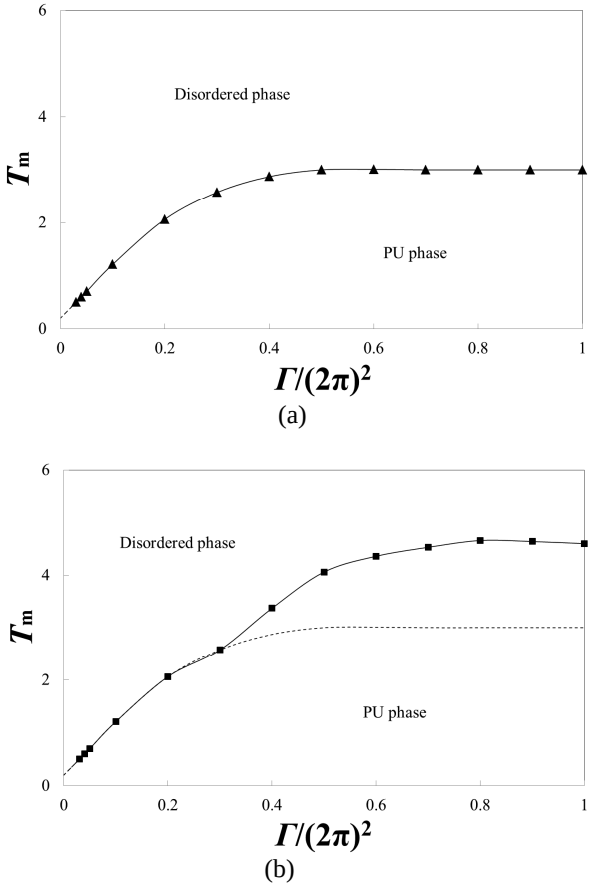

Fig. 5 (a) Phase diagram which shows the stability of the PU phase due to the MPM estimate via 8 interferograms without using prior information in the T_m-Γ space, where ▲ shows the upper phase boundary of the PU phase, if we set to σ_1=0, σ_2=0, J=1, α=0 and h=0. (b) Phase diagram which shows the stability of the PU phase due to the MPM estimate via 8 interferograms with prior information in the T_m-Γ space, where ■ denotes the upper phase boundary of the PU phase, if σ_1=0, σ_2=0, J=1, α=0 and h=1.

information was not useful for extending the PU phase, if h<0.6.

Then, we investigated the performance of the present method with respect to the observed interferograms corrupted by the Gaussian noises with σ_2= 0.3. As shown in Fig. 5, we found that the performance was improved by introducing the prior information under the constraint of the surface-consistency condition at each plaquette.

Next, we estimated the performance of the present method for phase unwrapping with respect to the number of the interferograms corrupted by the Gaussian noises with σ_2= 0.3. Using the Monte Carlo simulation for wave-front in Fig. 2(a), we found in Fig. 6 that the present method became more accurately with the increase in the number of the interferograms observed by the SAR interferometry.

In addition, we investigated the dynamical property of the present method with respect to the single wave-front in Fig. 2(a). We found that the phase unwrapping was carried out more smoothly, as the set of hyper-parameters were assumed so that the point in the hyper-parameter space was located more closely to the upper phase boundary in the PU phase described in Figs. 5 (a) and (b).

V. Summary and Discussion

In previous chapters, we have constructed the method of phase unwrapping using the multiple interferograms based on the Bayesian inference using the MPM estimate corresponding to the statistical mechanics of the three-state Q-Ising model on the square lattice. Then, from the statistical mechanical point of view, we have examined the performance of the present method both from the static and dynamic properties of the present method by utilizing the Monte Carlo simulations for the artificial wave-front typical in remote sensing using the SAR interferometry. For this purpose, we have described the phase diagram in the hyper-parameter space. We have first treated the case if the observed interferograms were not corrupted by any noises. The phase diagram showed that the constraint of the surface-consistency condition was very important for stabilizing

the PU phase in the MPM estimate, and also that the prior information was available of extending the PU phase under the constraint of the surface-consistency condition. Next, we have evaluated the performance for phase unwrapping, if observed interferograms were corrupted by the Gaussian noises. Here, we found that the mean square error took its optimal value, if we appropriately tuned the hyper-parameters respective of the choice of the original wave-front under the constraint of the surface-consistency condition. In addition, we have clarified the dynamic properties of the present method for phase unwrapping using the Monte Carlo simulation for the single wave-front. We found that the present method carried our phase unwrapping more smoothly, if the hyper-parameters were set so that the location of the hyper- parameters were set more closely to the upper phase boundary of the PU phase. This result have indicated that fluctuations around the MAP solution were useful to realize smooth phase unwrapping.

As a future problem, we apply the present method for realistic case, such as the digital elevation model of the Japanese volcanos. Also, we construct the method for this problem via the approximation theory established in statistical mechanics.

REFERENCES

[1] D. L. Fried, "Least-square fitting of a wave-front distortion estimate to an array of phase differences measurements," J. Opt. Soc. Am, vol. 67, pp. 370-375, 1977.

[2] R. H. Hudgin, "Wave-front reconstruction for compensated imaging," J. Opt. Soc. Am, vol. 67, pp. 375-378, 1977.

[3] R. J. Noll, "Phase estimation from slope-type wave-front sensors," J. Opt. Soc. Am, vol. 68, 139-140, 1978.

[4] R. M. Goldstein and H. A. Zebker, "Interferometric radar mapping of ocean currents," Nature, vol. 328, pp. 707-709, 1987.

[5] D. C. Ghiglia and. L. A. Romero, "Robust two-dimensional weighted and unweighted phase unwrapping that uses fast transforms and iterative method," J. Opt. Soc. Am. A, vol. 11, pp. 107-117, 1994.

[6] D. C. Ghiglia and M. D. Pritt, "Two-Dimensional Phase Unwrapping Theory Algorithms and Software," New York: Wiley, 1998.

[7] J. L. Marroquin and M. Rivera, "Quadratic regularization functionals for phase unwrapping", J. Opt. Soc. Am. A, vol. 12, pp. 2393-2400, 1995.

[8] L. Guerriero, G. Nico, G. Pasquariello and Stramaglia, "A new regularization scheme for phase unwrapping," Appl. Opt. vol. 37, no. 14, pp. 3053-3058, 1998.

[9] G. Nico, G. Palubinskas and M. Datcu, "Bayesian Approaches to Phase Unwrapping: Theoretical Study", IEEE Trans. Signal Processing, vol. 48(4), pp.2545-2556, 2000.

[10] A. P. Shanker and H. Zebker, "Edgelist phase unwrapping algorithm for time series InSAR analysis," J. Opt. Soc. Am. A, vol. 27(3), pp. 605-612, 2010.

[11] H. Nishimori, "Theory of spin glasses and information; An introduction," Oxford, London, 2001.

[12] K. Tanaka, "Statistical mechanical approach to image processing," Journal of Physics A: Mathematical and General, vol. 35(37), R31-R150, 2002.

[13] K. Tanaka, J. Inoue and D. M. Titterington, "Probabilistic image processing by means of the Bethe approximation for the Q-Ising model," Journal of Physics A: Mathematical and General, vol. 36(43), pp. 11023-11035, 2003.

[14] Y. Saika and H. Nishimori, "Statistical mechnics of image restoration using the plane rotator model," Journal of the Physical Society of Japan, vol. 71(4), pp. 1052-1058, 2002.

[15] Y. Saika, J. Inoue, H. Tanaka and M. Okada, "Bayes-optimal solution to inverse halftoning based on statistical mechanics of the Q-Ising Model", Central European Journal of Physics, vol. 7(3), pp. 444-456, 2009.

[16] Y. Saika, "Statistical mechanics of inverse halftoning", Numerical Simulations and Engineering Process (Book's Chapter), pp. 525-540, 2011.

[17] Y. Saika and T. Aoki, "Thermodynamics-inspired inverse halftoning via multiple halftone images", CAAI-Transactions on Intelligent Systems, vol. 7(1), pp. 86-94, 2012.

[18] Y. Saika and Y. Haraguchi, "Maximizer of the Posterior Marginal Estimate for Noise Reduction of JPEG-compressed Image", International Journal of Computer and Information Technology, vol. 6(1), pp. 13-17, 2012.

[19] Y. Saika and H. Nishimori, "Statistical mechanical approach to phase retrieval Yusing the Q-Ising model", Progress Theoretical Physics Supplement, vol. 157, pp. 292-295, 2005.

[20] Y. Saika and T. Uezu, "Statistical Mechanical Approach to Phase Unwrapping in Remote Sensing Using the Synthetic Aperture Radar Interferometry", Interdisciplinary Information Sciences, vol. 19(1), pp. 73-78, 2013.

ISBN: 978-1-61804-228-6

Fourier optics for investigating the impact of roughness to scatterometry

H. Gross, S. Heidenreich, and M. Bär

***Abstract*—Efficient algorithms are proposed for stochastical investigations of the impact of structure roughness on light diffraction pattern of photo masks. This is important for the scatterometry, i.e. the accurate, indirect determination of geometry parameters from scattered light intensities in wafer metrology. The sensitivity to roughness increases the smaller the wavelengths of the incident light are. For EUV scatterometry at 13.5 nm, many higher diffraction orders can be measured and they are sensitive to structure details. We calculate the light diffraction patterns of apertures with many rough slits in the far field. Applying Fraunhofer approximation, a 2D-Fourier transform of the light distribution of the aperture plane yields the sought diffraction pattern. The rough edges of the aperture are created by means of power spectrum density (PSD) functions used with a random complex exponential phase term. The comparison of the calculated light intensities to those of the undisturbed, 'non-rough' aperture, whose edges are straight lines, reveal a systematic decrease in terms of the diffraction order and the standard deviation of the roughness amplitude. Ensembles of rough apertures with different values for the imposed standard deviation of the roughness amplitude, the linear correlation length, and the roughness exponent were examined. Former results, obtained by rigorous calculations with computational expensive finite element methods (FEM) have been confirmed. The sensitivity of the method is demonstrated for bi-periodic arrays of hole-space structures too.**

***Index Terms*—critical dimensions (CDs), scatterometry, line edge roughness (LER), Fourier optics.**

I. Introduction

Non-imaging metrology methods like scatterometry (cf. Fig. 1) are in contrast to optical microscopy non diffraction limited and grant access to the geometrical parameters of periodic structures like structure width (critical dimension CD), period (pitch), sidewall angle or height of trapezoidal bridges (lines) [1], [2]. Scatterometry is an indirect optical method. From scattered relative light intensities, i.e. the measured efficiencies, the geometrical parameters of irradiated surface profiles and their uncertainties are reconstructed. The evaluation of structure dimensions on photo masks and wafers in lithography [3], [4] is an important application. In the semiconductor industry both the feature sizes and the required limit of measurement uncertainty decrease continuously and shorter wavelengths like extreme ultraviolet (EUV) at 13.5 nm will be applied. Besides conventional metrology techniques like atomic force, electron and optical microscopy, scatterometry is an established tool for the characterization of such structures (cf. e.g. [5], [6]). However, scatterometry requires a-priori knowledge for an appropriate modeling of the light diffraction pattern and reconstruction of geometrical profiles. Typically, the surface structure is sought in a certain class of gratings described by a finite number of parameters, and these parameters are confined to certain range.

The conversion of measurement data into desired geometrical parameters depends crucially on a high precision rigorous modeling by Maxwell's equations [7], [8], [9] which reduce to the two-dimensional Helmholtz equation if geometry and material properties are invariant in one direction. For the numerical solution, a lot of methods have been developed (cf. e.g. [10], [11], [12], [13], [14], [15], [16]). The finite element method (FEM) is used too and the infinite domain of computation is truncated to a finite one by coupling with boundary elements (cf. e.g. [17], [18], [19] and compare the alternative approach in e.g. [20]). To compute highly oscillatory fields, generalized finite element methods are available (cf. e.g. [21], [22], [23], [24]) and accurate numerical solutions for wavelengths λ in the EUV range are possible.

Apart from the forward computations by solving the Helmholtz equation, the solution of the inverse problem, i.e., the reconstruction of the grating profiles and interfaces from measured diffraction data, is the true task in scatterometry. Like many inverse problems, the inverse problem of scatterometry is ill-posed [25] and prior knowledge is required. A common approach for its regularization is to set up an equivalent low dimensional optimization problem with a weighted least squares function of the residuals [26], [27]. The prior knowledge in this case includes information not only about the geometrical profile of the investigated probe, but also knowledge of the variances of the measured data, i.e., the statistical error model of the measurements has to be known.

A comparison of the reconstructed profiles using EUV-scatterometry and the results obtained using atomic force and electron microscopy [28] has revealed that scatterometry can underestimate the sidewall angle, an important feature of the EUV-mask, by several degrees. Imperfect modeling is supposed to be one of the main reasons for this result [26], [29], [30]. In particular, to get more reliable simulations and reconstructions, effects like line edge roughness (LER) and further model based impacts have to be taken into account (cf. [31], [32], [33], [34] for the details).

Torcal-Mila et al. [35], and also Kato and Scholze [30] have suggested approximative analytical expressions for the impact of line edge roughness on the scattered efficiencies. They have applied Fraunhofer's diffraction method on gratings with randomly disturbed periodicity, i.e., the Fourier transform of the reflectivity function of perturbed binary gratings were investigated. They found damping of the mean efficiencies with increasing diffraction orders, which was confirmed by rigorous FEM simulations for a real EUV mask [31]. In these FEM investigations, large computational domains containing

ISBN: 978-1-61804-228-6

many line-space structures with stochastically chosen widths were used. Hence, these results were still obtained for a simplified model of rough line edges, i.e., without modeling the line edges as a stochastic process with a prescribed autocorrelation function analogously to what is often done in the metrology of rough geometries. There are several publications [36], [37], [38], where the modeling of line edge roughness as a stochastic process starts with an exponentially decaying autocorrelation function for the position $p(r)$ of an edge point at distance r: $p(r) = \sigma^2 e^{-(r/\xi)^{2\alpha}}$ where σ is the standard deviation of the roughness amplitude, ξ is the linear correlation length, and α is a roughness exponent. Randomized line edge profiles can be generated by calculating or approximating the associated power spectrum density function $\mathrm{PSD}(r^{-1})$ belonging to the autocorrelation function $p(r)$ and subsequently applying an inverse Fourier transform with a random phase uniformly distributed in the range of $[0, 2\pi]$. For instance, Bergner et al. [36] use a similar approach to generate rough line edge profiles of 2D-binary gratings to calculate its impact on the angular dependence of the specular, 0th order reflectance at wavelengths around 633 nm. Torcal-Milla et al. [35] have investigated gratings with rough edges in the visible optical range by applying the Rayleigh-Sommerfeld approach for near field simulations and the Fraunhofer approximation for the far field pattern. They found light intensities with exponential attenuation factors depending on σ and the diffraction order. Schuster et al. [39] have studied the impact of LER for silicon gratings on the basis of sinusoidal perturbations for the line positions with amplitudes in the range of 2–8 nm and for wavelengths of 400 and 250 nm, respectively.

The objective of the present paper is to demonstrate that the LER-induced attenuation of the mean efficiencies for higher diffraction orders is supported by a stochastic model of line edge roughness combined with a fast approximative calculation of the relative light intensities in the far field. The LER simulation uses a 2D binary aperture plane with many slits whose boundary lines are rough. The roughness is controlled by an autocorrelation function depending on a standard deviation σ, a correlation length ξ and a roughness exponent α. To avoid time consuming rigorous numerical calculations, the light intensity is approximately computed by a fast 2D-Fourier transform of the light distribution of the binary aperture plane applying the Fraunhofer approximation.

II. Exponential Damping of Efficiencies

The mathematical models for the scatterometric measurement process consist of a nonlinear operator that maps the geometry parameters onto the aforementioned efficiencies. The unknown parameters are mapped into the measured efficiencies. The vector of parameters $\mathbf{p} := (p_j)_{j=1}^N$ fixes the grating geometry and the solution of the boundary value problem for every set of parameter values gives a vector of efficiencies values $f_1(\mathbf{p}), \ldots, f_M(\mathbf{p})$, defining point-wise the nonlinear operator

$$\mathbf{p} \mapsto \Big(f_j(\mathbf{p})\Big)_{j=1}^{M}. \tag{1}$$

Note that these calculated efficiencies are compared to the measured ones and optimization of $\mathbf{p}$ is used to minimize

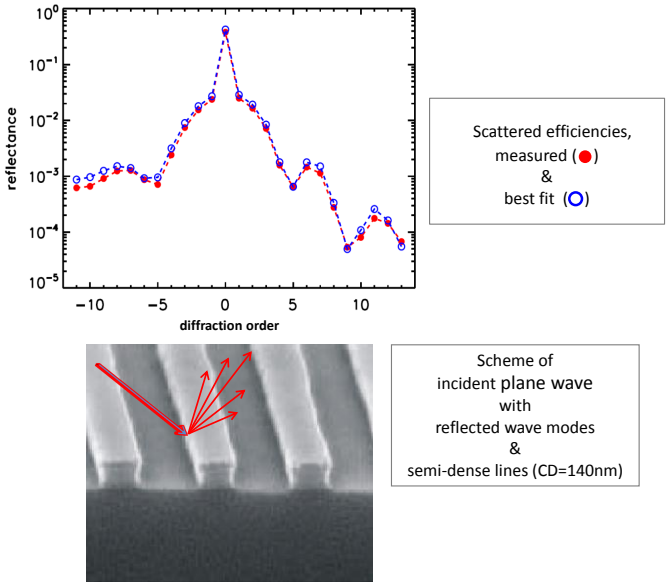

Fig. 1. Measurement prinicple of scatterometry.

the residuals. Additionally, there is a noise on the measured efficiencies, which is assumed to be Gaussian distributed. Unfortunately, in realistic geometries the ideally periodic line-space structures are slightly perturbed.

In the aforementioned previous studies, it was shown that there is a significant systematic damping for the measured efficiencies especially of higher diffraction orders due to perturbations of the periodicity of the lines. More precisely, scattered efficiencies measured from rough line structures are damped according to

$$\widetilde{f}_j\left(\sigma_\mathrm{r}, \mathbf{p}\right) = \exp(-\sigma_\mathrm{r}^2 k_j^2) \cdot f_j\left(\mathbf{p}\right), \tag{2}$$

where $k_j = 2\pi n_j/d$, n_j is the order of the diffractive mode and d the period of grating. The symbol σ_r denotes the variance of the line edge position. In rigorous finite element simulations the expression for the analytical damping factor was confirmed [31]. Note, that the results obtained with rigorous FEM calculations of $f_j(\mathbf{p})$ were obtained by means of a simplified model of line roughness, i.e., large periods for the cross section of the EUV mask containing many line-space pairs with stochastically chosen widths, but still with straight edges, were used (cf. [31]). In the following the hypothesis (2) will be tested by a more realistic model of line edge roughness based on a stochastic process considering the impact of correlation length ξ, roughness exponent α and the standard deviation σ of the roughness amplitude.

III. Apertures with Non-Straight Edges

In order to examine the impact of LER on the measured efficiencies (cf. Eq. (2)) in dependence on different roughness patterns, we open with the creation of randomly perturbed 2D binary line-space structures. Their edge positions are controlled by an exponentially decaying autocorrelation function allowing a significantly more realistic modeling of line edge roughness.

ISBN: 978-1-61804-228-6

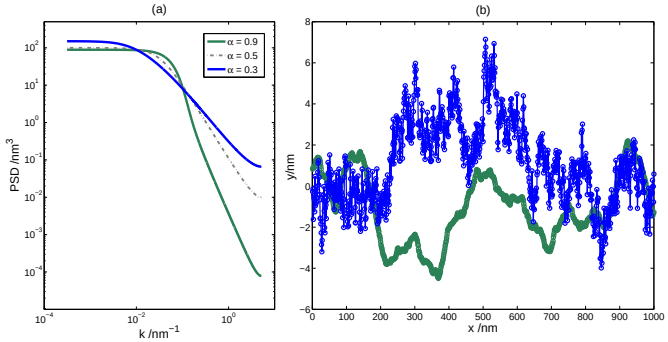

Fig. 2. Power spectral density (PSD) and generated rough lines a) PSD for σ = 1 nm, correlation length ξ = 50 nm and three different roughness exponents α = 0.3, 0.5, 0.9; (b) samples of rough lines calculated by the corresponding PSD with α=0.3 and 0.9.

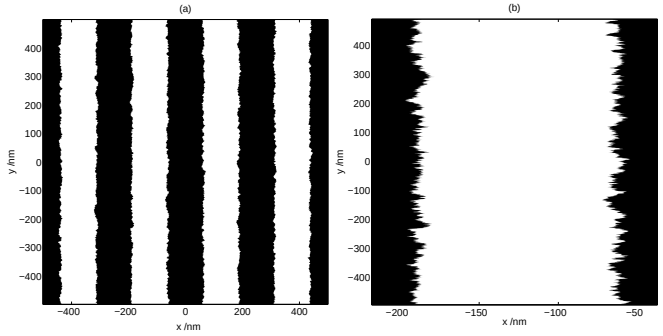

Fig. 3. (a) Example of a rough aperture used for 2D Fourier transform approach; size 1μm in both directions with a resolution of 0.1 nm ($\Longleftrightarrow$ 10000 x 10000 points); four slits per aperture, i.e., 125 nm width of the slits and a period of 250 nm; all edges are non-correlated; used PSD with σ=3 nm, α=0.5, and ξ=10 nm. (b) Zoomed (in x-direction) area of the same aperture.

We represent 2D-binary line-space gratings by square arrays of strip shaped slits, i.e., square apertures composed of many slits. In order to create rough boundary lines for the slits, we use an autocorrelation function to describe the variations along the edges. Considering lines $\{(x(y), y) : y \in \mathbb{R}\}$ with random variables $x(y)$, we assume a constant mean value $\langle x(y)\rangle = x_0$ and that the correlation depends on the distance $r = |y_1 - y_2|$ only, i.e. $x(y_1, y_2) = x(r)$. Furthermore, we assume the exponentially decaying autocorrelation function

$$x(r) = \sigma^2 e^{-(r/\xi)^{2\alpha}}, \tag{3}$$

where σ is the standard deviation of the edge positions, ξ is the linear correlation length along the line, and α is called roughness exponent. Recent publications, e.g. Mack and Bergner et al. [36], [37], [38], are starting with such an exponentially decaying function for modeling a stochastic process which ends up in randomized line edges or surfaces. The investigations here are addressing the 1D case of randomly rough lines. Randomized line edge profiles x are generated by calculating the associated power spectrum density function $\mathrm{PSD}(r^{-1})$ that belongs to the autocorrelation function $x(r)$ in a first step. Then we apply to the calculated PSD a random complex exponential phase term, being uniformly distributed in the range of $[0, 2\pi]$. Subsequently, the inverse Fourier

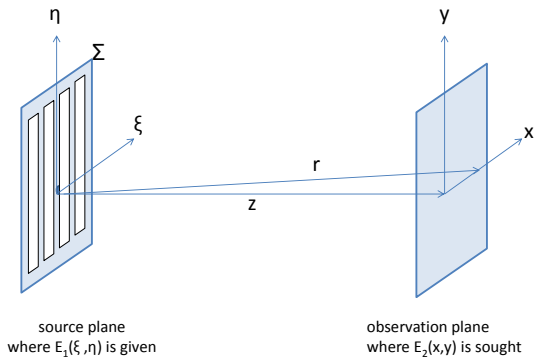

Fig. 4. Scheme of aperture plane and parallel observation in a distance z.

transform of that disturbed PSD provides a rough line edge profile x. Fig. 2 demonstrates the impact of different roughness exponents α on the PSD and the generated rough lines for a correlation length ξ of 50 nm. The edges of the aperture slits are created by repeating this process independently from each other. Fig. 3 gives an example of a whole aperture created with σ=3 nm, ξ=10 nm and α=0.5.

To get a sufficient resolution, the pixel size (stepsize of discretization for the Fourier transform) is 0.1 nm in both directions of the 2D apertures broadening upon a total range of 1μm $\times$ 1μm. The investigated rough apertures are typically composed of four periodically arranged slits, i.e., the corresponding grating period is 250 nm and the mean width of the rough slits is 125 nm (cf. Fig. 3). There is no restriction to choose other line-to-space ratios. We choose several slits per apertures to improve the spatial averaging of the irradiance pattern associated with the randomized aperture.

IV. Fraunhofer Approximation

Fourier optics is well known for being a cornerstone for the analysis of imaging, diffraction, coherence and propagation through random media [40], [41]. The mathematical description of the propagation of an optical field from one location, for example a diffractive aperture, to another is one of its most essential tasks. In general the propagation behavior of electro-magnetic waves in matter is based on Maxwell's equations, where the electric field E and the magnetic field H are coupled. However, assuming a linear and isotropic dielectric medium, where additionally the material properties are invariant in one direction, both fields are decoupled and scalar diffraction equations can be applied.

Under these ideal conditions a monochromatic plane wave with wavenumber k and orthogonal incidence on a diffractive aperture is considered. Its propagating radiation in a parallel observation plane far away from the aperture can be elegantly expressed as the Fourier transform of the field distribution in the source plane applying the Fraunhofer approximation. According to Huygens' principle each point of the wave

ISBN: 978-1-61804-228-6

front in the source plane can be considered as the source of superimposing spherical waves generating secondary wave fronts. That is, the field distribution $E_2(x, y)$ in an observation plane parallel to the source plane (cf. Fig. 4) can be calculated by means of the field distribution $E_1(\xi, \eta)$ of the source plane:

$$E_2(x, y) = \frac{z}{j\lambda} \iint_{\Sigma} E_1(\xi, \eta) \frac{e^{jkr}}{r^2} \mathrm{d}\xi d\eta, \tag{4}$$

here given in Rayleigh-Sommerfeld's diffraction notation with

$$r = \sqrt{z^2 + (x - \xi)^2 + (y - \eta)^2}. \tag{5}$$

Σ is the domain of the source plane. It can be shown very easily (cf. [42], [43]) that for propagation distances that are very long compared to the size of the aperture, i.e., for distances z with

$$z \gg \max_{(\xi,\eta)\in\Sigma} \frac{k(\xi^2 + \eta^2)}{2}, \tag{6}$$

$E_2(x, y)$ from equation (4) can be written as

$$E_2(x, y) = \frac{e^{jkz}}{j\lambda z} e^{\frac{jk(x^2+y^2)}{2z}} \iint_{\Sigma} E_1(\xi, \eta) e^{\frac{-j2\pi}{\lambda z}(x\xi+y\eta)} \mathrm{d}\xi \mathrm{d}\eta. \tag{7}$$

Equation (7) represents the Fraunhofer diffraction expression.

It consists of multiplying the source field E_1 by the characteristic function of the slit domain Σ, of applying the Fourier transform together with the frequency variable substitution

$$f_\xi \to \frac{x}{\lambda z}, f_\eta \to \frac{y}{\lambda z}. \tag{8}$$

and of multiplying by a complex exponential function. Note that the multiplicative complex exponentials in front of the double integral disappear, provided only the irradiance is of interest.

We apply this Fraunhofer expression with a wavelength λ of 13.5 nm and a distance z of 1 m to calculate the irradiance pattern of the rough apertures and the corresponding unperturbed non-rough aperture in this paper. Fig. 5 shows an example for an aperture composed of four periodically arranged slits with a width of 200 nm and a period of 250 nm, i.e., the bridge-to-slit ratio is 1:4. The irradiance pattern along the x-direction at the central position $y = 0$ is shown for the unperturbed aperture. Note that depending on the bridge-slit ratio equivalent to the line-space ratio of 2D binary grating, the irradiance becomes zero for special diffraction orders. These diffraction orders are not considered for the evaluations and only those with values significantly greater than zero are selected. In the example of Fig. 5 this is the case for the orders $n_j = \pm 5$.

V. Irradiance Pattern Relative to Those of 'Non-Rough' Structures

The key for analyzing the impact of roughness is to compare the mean light intensities calculated for ensembles of rough apertures to that of the unperturbed non-rough aperture, i.e., the corresponding aperture whose slits are composed of straight lines. Any systematic impact on the mean efficiencies should then be identified obviously. In previous investigations

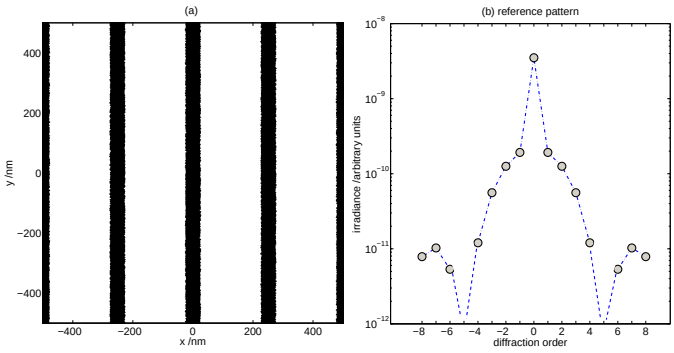

Fig. 5. (a) Rough aperture (σ=1 nm; α=1; ξ=2 nm) with a slit width of 200 nm at a period of 250 nm and (b) reference irradiance pattern of the corresponding unperturbed aperture (with straight edges).

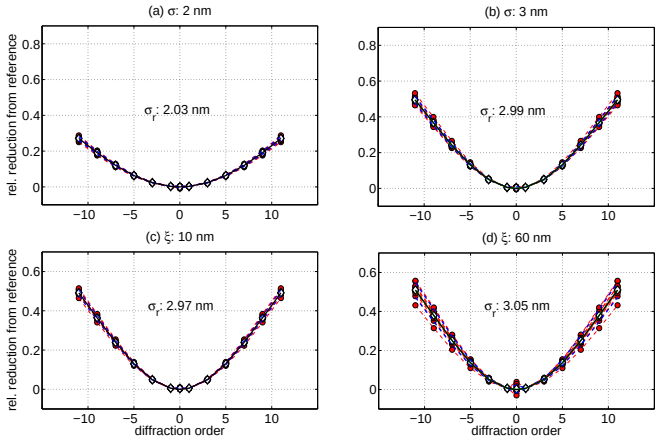

Fig. 6. Normalized deviations from the efficiencies of the unperturbed aperture, depicted as circles; diamond symbols represent the mean deviations of all samples and solid line the exponential approximation according Eq. (9); (a)-(b) for two different standard deviations σ and α=1, ξ=10 nm; (c)-(d) for tow different linear correlation lengths ξ and σ=3 nm, α=0.5.

that made use of computationally expensive FEM simulations [31], this strategy has already been applied successfully.

The relative deviations of light intensities in dependence on the diffraction orders for several ensembles of rough apertures are depicted in Fig. 6. The two examples in the upper part of Fig. 6 differ from each other by an increasing standard deviation σ of the autocorrelation function (cf. Eq. (3)) from 2 nm to 5 nm used to generate the rough edges of the apertures. The roughness exponent α was fixed to 1.0 and the correlation length ξ was set to 10 nm. Each ensemble has eleven samples of rough apertures whose relative deviations are depicted as circle symbols. Their mean values are marked by diamond symbols. The bridge to slit ratio was 1:1, i.e., both parameters have a nominal value of 125 nm. Only the orders with intensities significantly greater than zero are considered.

A systematic nonlinear decrease of the mean efficiencies for higher diffraction orders along with slightly increasing variances is observed. This is established for different degrees of roughness expressed by the different σ values for two ensembles. Only a few ten samples for each ensemble are necessary to reveal a stable bias of the mean efficiencies.

ISBN: 978-1-61804-228-6

Quite similar outcomes are obtained for the two ensembles generated with different correlation lengths $\xi = [10, 60]$ nm as shown in the lower part of Fig. 6. Here α was changed to 0.5 and σ was fixed to 3 nm. One can recognize that the correlation length ξ effects the variances around the mean values of the light intensities. They rise slightly in particular for higher diffraction orders. Nevertheless, the essential impact on the biased mean values is stemming from the imposed σ values and appears to follow an exponential function depending on the diffraction order and σ, just like the above-mentioned findings of the 2D FEM simulations.

Consequently, we conclude that the revealed attenuation of the mean light intensities with higher diffraction orders can be modeled by

$$\frac{f_{n_j,\mathrm{ref}} - \overline{f_{n_j,\mathrm{pert}}}}{f_{n_j,\mathrm{ref}}} \approx 1 - e^{-(\frac{2\pi n_j}{d})^2 \sigma_\mathrm{r}^2}$$

$$\Longleftrightarrow \overline{f_{n_j,\mathrm{pert}}} \approx e^{-(\frac{2\pi n_j}{d})^2 \sigma_\mathrm{r}^2} f_{n_j,\mathrm{ref}}. \qquad (9)$$

Here $f_{n_j,\mathrm{ref}}$ denotes the light intensities of the unperturbed aperture at diffraction order n_j and $\overline{f_{n_j,\mathrm{pert}}}$ the corresponding mean values of the generated ensemble of rough apertures, d is the period of the bridge-slit structure and σ_r depicts that value for the standard deviation which represents the best-fit results for the mean normalized deviations applying equation (9). In fact, the solid lines in Figs. 6 are depicting these best-fit results for σ_r obtained by minimizing the Euclidean norm $\|\overline{f_{n_j,\mathrm{pert}}} - \exp(-(\frac{2\pi n_j}{d})^2 \sigma_\mathrm{r}^2) f_{n_j,\mathrm{ref}}\|$. Note that, according to our hypothesis (9), the evaluated σ_r values are good estimations of the imposed standard deviations characterizing the generated ensembles of rough apertures.

We have examined many different samples of rough apertures representing variant roughness patterns characterized by different values of σ, ξ, and α (cf. [44] for more details). Only a slight increase within a range of maximal 5% were found for the determined σ_r compared to the imposed standard deviation σ of the associated rough ensemble. That means, that our hypothesis (2) is valid for different kinds of roughness pattern.

Furthermore we have applied the described method to bi-periodic arrays of binary hole-space structures as shown in Fig. 7. To demonstrate the sensitivity of the method, we have imposed different values of σ to generate the hole edges in x- and y-direction.

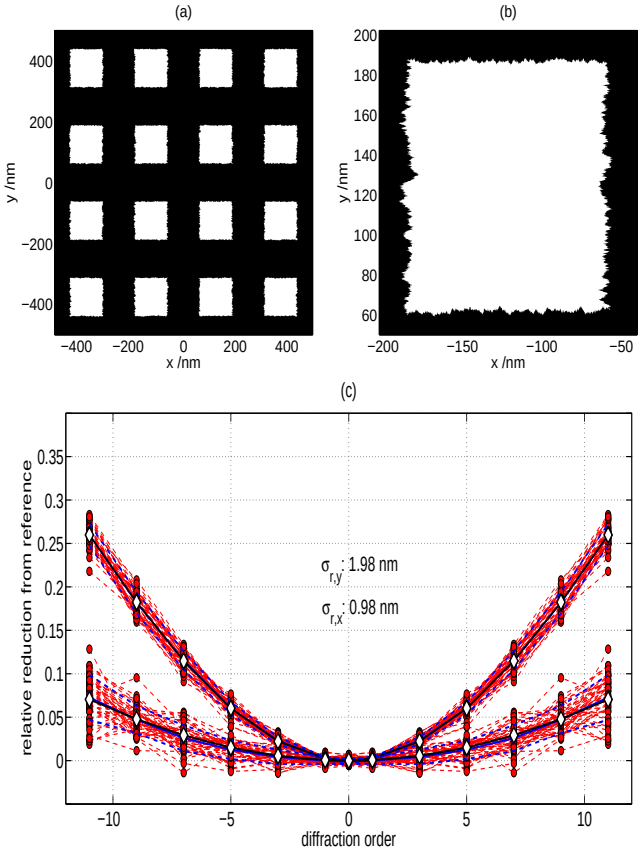

Fig. 7. (a-b) Array of holes and zoomed hole from a square area with a length of $1\mu m$ and different σ values along x- and y-direction. (c) Normalized deviations from the efficiencies of the unperturbed aperture in x- and in y-direction, depicted as circles; diamond symbols represent the mean deviations of all 50 samples and solid line the exponential approximation according Eq. (9); different imposed standard deviations along x- and y-direction σ_x=1 nm and σ_y=2 nm; ξ=3 nm and α=0.5 for both directions.

VI. Summary

We have proposed a 2D-Fourier transform method as a simple and efficient algorithm to complement previous investigations on the systematic impact of line edge roughness on light diffraction patterns of periodic line-space structures. In particular, this has been done in the EUV regime, where the light diffraction pattern is characterized by many significant wave modes with higher diffraction orders. The irradiance of illuminated rough apertures far away from the source plane is numerically calculated very efficiently as the 2D-Fourier transform of the light distribution in the aperture plane and then compared to those of the unperturbed, 'non-rough' aperture. Rough random boundaries are generated for the aperture slits by PSD functions ensuring realistic line edge profiles comparable to those of 3D AFM measurements along the sidewalls of the absorber lines (cf. [44]). For apertures of a typical size of 1 μm in both directions and a pixel size of 0.1 nm, there is already a strong spatial averaging in each single sample of a rough aperture. Consequently, a few samples (e.g. ten) are sufficient to determine a stable estimate for the bias of the mean values at different diffraction orders. Compared to the diffraction pattern of the unperturbed aperture, the mean efficiencies of the rough apertures show a systematic exponential decrease for higher diffraction orders. The standard deviation of the edge fluctuations σ_r and the diffraction order n_j govern the revealed exponential damping factor. In fact, this dependence has been investigated for ensembles of rough apertures with different roughness pattern, i.e., with different values for the imposed standard deviation σ, the linear correlation length ξ, and the roughness exponent α. Compared to the σ used for the generation of our simulated geometry, only a slight increase within a range of 5% has been found for the σ_r determined a posteriori by our damping

ISBN: 978-1-61804-228-6

formula. Thus former results on the damping, obtained by rigorous FEM computations, have been confirmed on the base of a much more realistic model of line edge roughness. The binary distributions in the aperture are not restricted to line-space structures. For example, arrays of rough hole-space structures can be treated by the proposed method too, and the sensitivity of the method was demonstrated by an example with different σ values for the x- and y-borders of the holes.

ACKNOWLEDGMENT

Results are part of the projects IND17 Scatterometry and NEW04 Uncertainty within the European Metrology Research Programme (EMRP).

REFERENCES

[1] B.K. Minhas, S.A. Coulombe, S. Sohail, H. Naqvi, and J.R. McNeil. Ellipsometric scatterometry for metrology of sub-0.1μm-linewidth structures. *Appl.Optics*, 37:5112–5115, 1998.

[2] H.T. Huang and F.L. Terry Jr. Spectroscopic ellipsometry and reflectometry from gratings (scatterometry) for critical dimension measurement and in situ, real-time process monitoring. *Thin Solid Films*, 455:828–836, 2004.

[3] C.J. Raymond, M.R. Murnane, S. Sohail, H. Naqvi, and J.R. McNeil. Metrology of subwavelength photoresist gratings using optical scatterometry. *J. Vac. Sci. Technol., B*, 13(4):1484–1495, 1995.

[4] C.J. Raymond, M.R. Murnane, S.L. Prins, S. Sohail, H. Naqvi, J.R. McNeil, and J.W. Hosch. Multiparameter grating metrology using optical scatterometry. *J. Vac. Sci. Technol., B*, 15(2):361–368, 1997.

[5] M. Wurm, B. Bodermann, and W. Mirandé. Evaluation of scatterometry tools for critical dimension metrology. *DGaO Proceedings*, 106, 2005.

[6] H. Gross, R. Model, M. Bär, M. Wurm, B. Bodermann, and A. Rathsfeld. Mathematical modelling of indirect measurements in scatterometry. *Measurement*, 39(9):782–794, 2006.

[7] R. Petit and L.C. Botten. *Electromagnetic theory of gratings*. Springer-Verlag, Berlin Heidelberg, 1980.

[8] D.C. Bao, G. and Dobson. Modeling and optimal design of diffractive optical structures. *Surveys on Mathematics for Industry*, 8:37–62, 1998.

[9] A. Chen, X. and Friedmann. Maxwell's equation in a periodic structure. *Trans. Amer. Math. Soc.*, 323:811–818, 1991.

[10] T.K. Moharam, M.G. and Gaylord. Rigorous coupled wave analysis. *J.Opt.Soc.Amer.*, 71:811–812, 1981.

[11] A. Tavrov, M. Totzeck, N. Kerwien, and H.J. Tiziani. Rigorous coupled-wave analysis calculus of submicrometer interference pattern and resolving. *Opt.Eng.*, 41:1886–1892, 2002.

[12] M.G. Moharam, E.B. Grann, D.A. Pommet, and T.K. Gaylord. Stable implementation of the rigorous coupled-wave analysis for surface-relief gratings: enhanced transmittance matrix approach. *JOSA A*, 12:1077–1086, 1995.

[13] G.M. Lalanne, P. and Morris. Highly improved convergence of the coupled-wave method for TM-polarization. *JOSA A*, 13:779–784, 1996.

[14] L. Li. New formulation of the Fourier modal method for crossed surface-relief gratings. *JOSA A*, 14:2758–2767, 1997.

[15] J. Chandezon, G. Raoult, and D. Maystre. A new theoretical method for diffraction gratings and its numerical application. *J. Opt.*, 11:235, 1980.

[16] B.H. Kleemann. *Elektromagnetische Analyse von Oberflächengittern von IR bis XUV mittels einer parametrisierten Randintegralmethode: Theorie, Vergleich und Anwendungen*. PhD thesis, TU Ilmenau, 2002.

[17] H.P. Urbach. Convergence of the Galerkin method for two-dimensional electromagnetic problems. *SIAM J. Numer. Anal.*, pages 697–710, 1991.

[18] G. Bao. Finite element approximation of time harmonic waves in periodic structures. *SIAM J.Numer.Anal.*, 32:1155–1169, 1995.

[19] J. Elschner, R. Hinder, and G. Schmidt. Finite element solution of conical diffraction problems. *Adv. Comput. Math.*, 16(2):139–156, 2002.

[20] A. Schaedle, L. Zschiedrich, S. Burger, R. Klose, and F. Schmidt. Domain decomposition method for Maxwell's equations: Scattering of periodic structures, ZIB-Report 06-04, Konrad Zuse Institut, Berlin, 2006.

[21] F. Ihlenburg. *Finite element analysis of acoustic scattering*. Springer-Verlag, Berlin Heidelberg, 1998.

[22] JM Melenk and I. Babuška. The partition of unity finite element method: basic theory and applications. *Comput. Meth. Appl. Mech. Eng.*, 139(1-4):289–314, 1996.

[23] O. Cessenat and B. Despres. Application of an ultra weak variational formulation of elliptic PDEs to the two-dimensional Helmholtz problem. *SIAM J. Numer. Anal.*, 35(1):255–299, 1998.

[24] J. Elschner, R. Hinder, A. Rathsfeld, and G. Schmidt. http://www.wias-berlin.de/software/DIPOG.

[25] A. Tarantola. *Inverse problem theory*. Elsevier Amsterdam etc., 1987.

[26] H. Gross, A. Rathsfeld, F. Scholze, and M. Bär. Profile reconstruction in extreme ultraviolet (EUV) scatterometry: modeling and uncertainty estimates. *Meas. Sci. Technol.*, 20:105102, 2009.

[27] R.M. Al-Assaad and D.M. Byrne. Error analysis in inverse scatterometry. I. Modeling. *J. Opt. Soc. Am. A:*, 24(2):326–338, 2007.

[28] M.Wurm. *Über die dimensionelle Charakterisierung von Gitterstrukturen auf Fotomasken mit einem neuartigen DUV-Scatterometer*. PhD thesis, Friedrich-Schiller-Universität Jena, 2008.

[29] H. Patrick, T. Germer, R. Silver, and B. Bunday. Developing an uncertainty analysis for optical scatterometry. *Proc. SPIE*, 7272:72720T, 2009.

[30] A. Kato and F. Scholze. Effect of line roughness on the diffraction intensities in angular resolved scatterometry. *Appl. Opt.*, 49(31):6102–6110, 2010.

[31] H. Gross, M-A. Henn, S. Heidenreich, A. Rathsfeld, and M. Bär. Modeling of line roughness and its impact on the diffraction intensities and the reconstructed critical dimensions in scatterometry. *Appl. Optics*, 51:7384–7394, 2012.

[32] M.-A. Henn, H. Gross, F. Scholze, M. Wurm, C. Elster, and M. Bär. A maximum likelihood approach to the inverse problem of scatterometry. *Optics Express*, 20, No. 12:12771–12786, 2012.

[33] M-A. Henn, S. Heidenreich, H. Gross, A. Rathsfeld, F. Scholze, and M. Bär. Improved grating reconstruction by determination of line roughness in extreme ultraviolet scatterometry. *Optics Letters*, 37 (24):5229–, 2012.

[34] M-A. Henn, H. Gross, S. Heidenreich, F. Scholze, C. Elster, and M. Bär. Improved reconstruction of Critical Dimensions in Extreme Ultraviolet Scatterometry by Modeling Systematic Errors. *Measurement Science and Technology*, 2014, at press.

[35] F.J. Torcal-Milla, L.M. Sanchez-Brea, and E. Bernabeu. Diffraction of gratings with rough edges. *Optics Express*, 16:19757–19769, 2008.

[36] B.C. Bergner, T.A. Germer, and T.J. Suleski. Effective medium approximations for modeling optical reflectance from gratings with rough edges. *J. Opt. Soc. Am. A*, 27:1083–1090, 2010.

[37] C.A. Mack. Analytic form for the power spectral density in one, two, and three dimensions. *J. Micro/Nanolith. MEMS MOEMS*, 10(4):040501–, 2011.

[38] C.A. Mack. Generating random rough edges, surfaces, and volumes. *Appl. Optics*, 52:1472–1480, 2013.

[39] T. Schuster, S. Rafler, V.F. Paz, F. Frenner, and W. Osten. Fieldstitching with Kirchhoff-boundaries as a model based description for line edge roughness (LER) in scatterometry. *Microelectronic Engineering*, 86:1029–1032, 2009.

[40] J.W. Goodman. *Introduction to Fourier Optics*. Roberts & Company, Greenwood Village, 2005.

[41] O.K. Ersoy. *Diffraction, Fourier Optics, and Imaging*. Wiley-Interscience, New York, 2006.

[42] D. Voelz. *Computational Fourier Optics*, volume TT89. SPIE PRESS, 2011.

[43] D.C. Champeney. *Fourier transforms and their physical applications*. Academic Press, London and New York, 1973.

[44] H. Gross, S. Heidenreich, M.-A. Henn, G. Dai, F. Scholze, and M. Bär. Modelling line edge roughness in periodic line-space structures by Fourier optics to improve scatterometry. *J. Europ. Opt. Soc. Rap. Public.*, 9:14003, 2014.

Symbolic Computer-Aided Design for Wireless Power Transmission

Takuya Hirata, Univ. Miyazaki, Kazuya Yamaguchi, Univ. Miyazaki, Yuta Yamamoto, Univ. Miyazaki and Ichijo Hodaka, Univ. Miyazaki

Abstract—This paper develops a computer-aided analysis method for wireless power transfer systems. Conventional rersearch for wireless power transfer systems has been dominated mainly by experimental analysis and numerical analysis. This situation does not deny that circuit theoretical observation of wireless power transfer circuits is also useful. However, such an observation largely depends on the skill of engineer who tries to observe the circuits, and it needs a large amount of efforts or time. This leads to a restriction on the size of circuits to be observed. This paper realizes a computer algorithm for wireless power transfer systems, which enables to replace the engineer's observation by symbolic modelling of circuits with help of computer power.

Keywords—symbolic circuit analysis, modelling, power transfer

I. Introduction

THERE are numerous number of products powered by electric power in the world, such as mobile phones, cars, computers and televisions — the heart of those products is electric circuits which are proposed, tested, and fabricated by circuit engineers. Nowadays, the design process is dominated by circuit numerical simulators such as SPICE, a de facto standard tool in academia as well as industry. Using SPICE, engineers and designers can analyze the circuits which may contain nonlinear elements such as diodes and transistors, and any complex circuits supposing real electric parts in the time and frequency domains. Circuit engineers design their circuits with deep consideration of how the circuit parameters will affect the outputs of the circuits. Since the consideration sums up the results from each value of parameters, they need to repeat many sets of numerical simulation on SPICE. On the other hand, it is obvious that if their circuit is simple enough to write equations they will be able to understand the whole behavior of the circuit. In this situation, they have symbolic equations which govern the behavior of the circuits in terms of voltages and currents. However, it is also true that such a symbolic analysis is not popular in practical use. One reason for it is that computer aided tools available now with symbolic expressions are less sophisticated than SPICE. A symbolic solution to practical circuits are very difficult to find due to an explosion of computation steps as the number of elements increase. Even if the symbolic solution is found, it tends to be too complicated to be interpret by engineers. Some of these problems have been handled by recent studies[1]-[4], but other problems have been still open, and engineers continue to use SPICE. The heart of a wireless power transfer system with magnetic resonance is to transmit much electric power with high efficiency to the loads in the secondary from a voltage source in the primary. The system is realized by the circuits which is composed of resistors, inductors, and capacitors, thus, linear circuits. The efficiency and quantity of the transfer power are different from among different circuits. Additionally, the way to design the circuits which can transmit the power maximally is not established. Thus we have to design many circuits and compare the circuits from the point of view of efficiency and the quantity of the power.

In this paper, we propose the method to automatically make circuit models which express the wireless transmission behavior from a primary circuit to a secondary circuit. The model is expressed in so-called state equation fully embedded with symbols of the value of electrical elements as well as voltages and currents in the circuit. Some of conventional software[1]-[4] does not handle wireless situation. The software which can compute wireless circuit equations are based on transfer functions. Since our algorithm outputs a state equation instead of transfer functions, one has a benefit: we can utilize other sophisticated computation tools seamlessly with our algorithm, and apply theoretical idea arranged and developed on a state equation in other academic field.

II. Proposed Method

In general circuit equations which represent the behavior of provided circuits are composed of KVL (Kirchhoff's Voltage Law), KCL (Kirchhoff's Current Law) and Laws which are voltage and current law of the elements. We consider here that a circuit is composed of resistors, inductors, capacitors and a voltage source. Then circuit equations are written by linear differential equations and linear algebraic equations. The circuit equations contain variables (function of time) – each of voltages and currents –representing circuit states. In these equations, there are *redundant* quantities, voltage and current of resistors, current of capacitors and voltage sources, voltage of inductors and nodes.

We call circuit equations which contain the redundant quantities redundant circuit equations. Additionally, we call circuit equations which are expressed as a linear combination of only independent quantities *non-redundant* circuit equations. In this paper, we propose a method which is suitable for a computer algorithm and is to transform redundant circuit equations into non-redundant circuit equations systematically.

Linear differential equations in redundant circuit equations are written as

$$z = F\dot{x} \tag{1}$$

where z, x are a vector which arranges vertically voltage of inductors and current of capacitors respectively. A matrix F

ISBN: 978-1-61804-228-6

is determined by x consistency.

Algebraic equations in redundant circuit equations can be written as (2) after eliminating voltage and current of resistors, current of a voltage source, voltage of nodes.

$$K_1 z + K_2 x + K_3 u = 0 \tag{2}$$

Where z is a vector which arranges voltage of inductors and transformers and current of capacitor vertically, and u are voltage of a voltage source. Matrices K_1, K_2, K_3 are determined consistency by z, x, u respectively.

We define a matrix Q as the following equation.

$$Q = \begin{bmatrix} K_1 & K_2 & K_3 \end{bmatrix} \tag{3}$$

If $\operatorname{rank} Q = r$, then we can transform (2) into the following equation.

$$z = -(K_1^T K_1)^{-1} K_1^T (K_2 x + K_3 u) \tag{4}$$

Even if $\operatorname{rank} Q \neq r$, we can transform Q into $\operatorname{rank} Q = r$ after that we eliminate linear dependence rows of Q.

By using (1), if $\det F \neq 0$, we can rewrite (4) as the following equation.

$$\dot{x} = -F^{-1}(K_1^T K_1)^{-1} K_1^T (K_2) x - F^{-1}(K_1^T K_1)^{-1} K_1^T (K_2) u \tag{5}$$

If

$$A = -F^{-1}(K_1^T K_1)^{-1} K_1^T (K_2) \tag{6}$$

$$B = -F^{-1}(K_1^T K_1)^{-1} K_1^T (K_3), \tag{7}$$

then (5) can be rewritten as

$$\dot{x} = Ax + Bu \tag{8}$$

and we can obtain non-redundant circuit equations. The matrices A, B contains symbolic computing of the inverse matrix. Generally, the more a matrix size increases and more the computing is hard to finish performing in practical time. Thus, we found a way of being illustrated Fig. 1 in a process of eliminating voltage and current of resistors, current of a voltage source, voltage of nodes in redundant circuit equations. Hereby, we can perform the computing in little computational effort.

A. Implementation

Our proposed method is shown in Fig. 1 by a flowchart. Where v_{Node}, I, v_R, i_R represent voltage of nodes, current a voltage source, and voltage and current of resistors respectively.

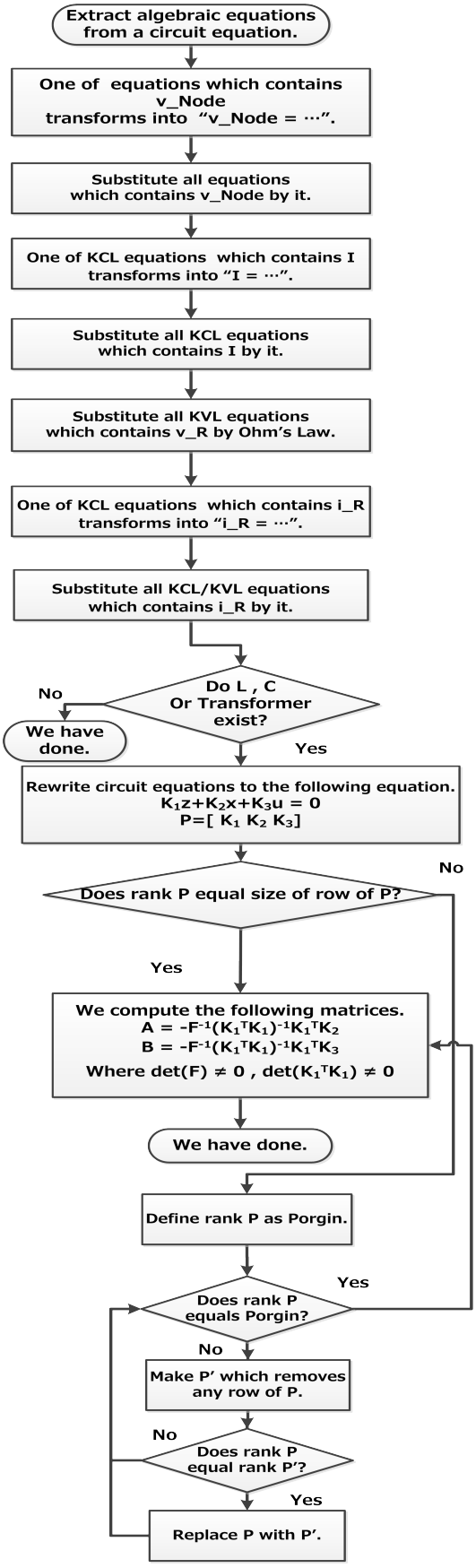

Fig. 1. A flowchart of our method

III. A Model of Transformer for Wireless Transfer

As a model for received and transmitted coils of a wireless power transfer, we consider that there are $n-1$ loads in the secondary windings in the model on Fig. 2.

By Neumann's law, we can write the mutual inductor M in the following equation[6]-[8].

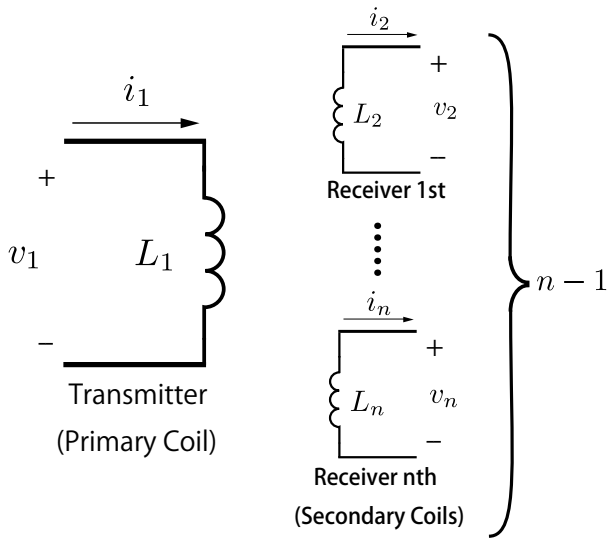

Fig. 2. A transformer model for a wireless power transfer system

$$M_{ij} = \frac{\mu_0}{4\pi}\oint_{C_i}\oint_{C_j}\frac{dl_i \cdot dl_j}{r_{ij}} \quad (9)$$

Where $1 \le i \le n$, $1 \le j \le n$, as $i = j$, M_{ij} represents L_i. C_i, C_j represent the path around Coil i, Coil j respectively. dl_i, dl_j show vectors of Coil i and Coil j respectively. r_{ij} represents the distance between Coil i and Coil j. A mutual inductance M is determined by the distance between coils and a shape of a coil(the number of turns) and so on.

We can consider that a model of a transmission coil and a receiver coil is in the case of a variable mutual inductance M by a distance between coils and a relative position of a coil in a general electric circuit. Hence we adopt the relation expression between voltage and current in an ideal transformer in the case of the variable mutual inductance M as the model for a wireless power transfer.

$$v = \begin{bmatrix} L_1 & \pm M_{12} & \pm M_{13} & \dots & \pm M_{1n} \\ \pm M_{21} & L_2 & \pm M_{23} & \dots & \pm M_{2n} \\ \vdots & \vdots & \vdots & \vdots & \vdots \\ \pm M_{n1} & \pm M_{n2} & \dots & \pm M_{nn-1} & L_n \end{bmatrix} \dot{i} \quad (10)$$

where v, i are $v = \begin{bmatrix} v_1 & v_2 & \dots & v_n \end{bmatrix}^T$, $i = \begin{bmatrix} i_1 & i_2 & \dots & v_n \end{bmatrix}^T$, respectively.

IV. An example of calculating efficiency

We consider a wireless power transfer system which consists of a circuit that is composed of resistors, inductors(including coils), capacitors and a voltage source. Thus, we can make a model by proposed method and by use it, we can analyze an effect of power transfer by variation of circuit parameters. This modeling is performed by Wasabi that we implement our proposed method as a computer program.

$$\dot{x} = Ax + Bu \quad (11)$$

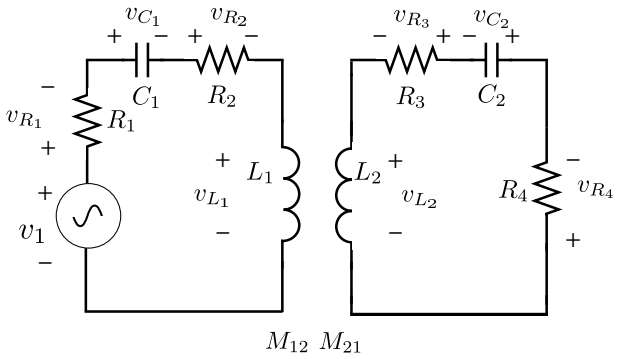

Fig. 3. Wireless power transfer circuit

TABLE I
Notation

Symbol	Representation	Note
v_1	Voltage of a voltage source	
R_1, R_2, R_3, R_4	Resistor	
L_1, L_2	Coil(Inductor)	The winding direction of L_1 is the same as the direction of L_2.
C_1, C_2	Capacitor	
v_*	Voltage of *	* represents any element in the circuit.
i_*	Current of *	* represents any element in the circuit. The Direction of current of * is opposite to its voltage respectively.

$$A = \begin{bmatrix} 0 & 0 & \frac{1}{C_1} & 0 \\ 0 & 0 & 0 & \frac{1}{C_2} \\ \frac{-L_2}{\Delta} & \frac{M_{12}}{\Delta} & \frac{(-R_1-R_2)L_2}{\Delta} & \frac{(R_4+R_3)M_{12}}{\Delta} \\ \frac{M_{21}}{\Delta} & \frac{-L_1}{\Delta} & \frac{(R_1+R_2)M_{21}}{\Delta} & \frac{(-R_4-R_3)L_1}{\Delta} \end{bmatrix} \quad (12)$$

$$B = \begin{bmatrix} 0 \\ 0 \\ \frac{L_2}{\Delta} \\ \frac{-M_{21}}{\Delta} \end{bmatrix} \quad (13)$$

$$x = \begin{bmatrix} v_{C_1} & v_{C_2} & i_{L_1} & i_{L_2} \end{bmatrix}^T \quad (14)$$

$$u = v_1 \quad (15)$$

where $\Delta = L_2L_1 - M_{12}M_{21}$. The other symbols are represented in Table I.

In this system, by using symbols that are an average power $\bar{P_4}$ of a load resistor R_4 and an average power $\bar{P_1}$ of a voltage source, including an internal resistance, we can write an efficiency η as the following equation.

$$\eta = \left|\frac{\bar{P_4}}{\bar{P_1}}\right| \quad (16)$$

If we choose v_1 which is the voltage of a voltage source for $v_1(t) = \sin(\omega t)$, then we can write the efficiency η as

$$\eta = \frac{C_2^2 M_{12}^2 R_4 \omega^4}{\alpha} \quad (17)$$

where

$$\alpha = |C_2^2 M_{12} M_{21}(R_3 + R_4)\omega^4 + R_2(1 - 2C_2L_2\omega^2 + C_2^2\omega^2(R_3^2 + 2R_3R_4 + R_4^2 + L_2^2\omega^2))|$$

ISBN: 978-1-61804-228-6

and ω, t are angular frequency, time respectively. Note the obtained equation is complexity, but we can analyze the efficiency by leaving symbolic parameters that we are only interested in. Since the model as expressed in symbolic equations, it is possible. Next we introduce concretely this point through some examples.

A. A case of only variations of M_{12} and M_{21}

By (9), mutual inductances M_{12}, M_{21} vary with a distance between the primary coil L_1 and the secondary coil L_2. Thus, if we would like to analyze that how the distance effects the efficiency, then we regard (16) as a function about the mutual inductances. For example, Let $M_{12} = M_{21} = M$ and let M be a variable. We consider the case of varying with $0.01L_1 \leq M \leq 0.1L_1$ by changing the distance.

TABLE II
PARAMETER VALUE

Element	Value
R_1, R_4	50Ω
R_2	0.03Ω
R_3	0.012Ω
L_1	5μH
L_2	5μH
C_1	286pF
C_2	1.43nF
ω	13Mrad/s

Then by (17), the efficiency $\eta(M)$ is expressed as

$$\eta(M) = \frac{2.92022 \times 10^{12} M^2}{0.0272338 + 2.92092 \times 10^{12} M^2}. \quad (18)$$

A change of the efficiency $\eta(M)$ is shown in Fig. 4.

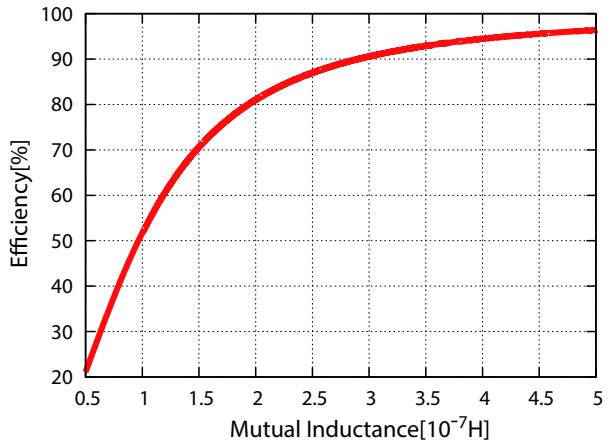

Fig. 4. Efficiency $\eta(M)$ $[0.01L_1 \leq M \leq 0.1L_1]$

B. A case of only a variation of angular frequency ω

If we are interested in angular frequency ω that maximizes the efficiency $\eta(M)$, we can analyze the ω. Now let ω is a variable and $M_{12} = M_{21} = 0.05L_1$, the other parameters are on Table II. Then the efficiency $\eta(M)$ is expressed as

$$\eta(\omega) = \frac{6.39031 \times 10^{-30} \omega^4}{0.03 - 2.75559 \times 10^{-16} \omega^2 + 7.92552 \times 10^{-30} \omega^4}. \quad (19)$$

We plot the efficiency $\eta(M)$, $|\bar{P}_4|$, $|\bar{P}_1|$ in $10^5 \leq \omega \leq 10^8$ on Fig. 5.

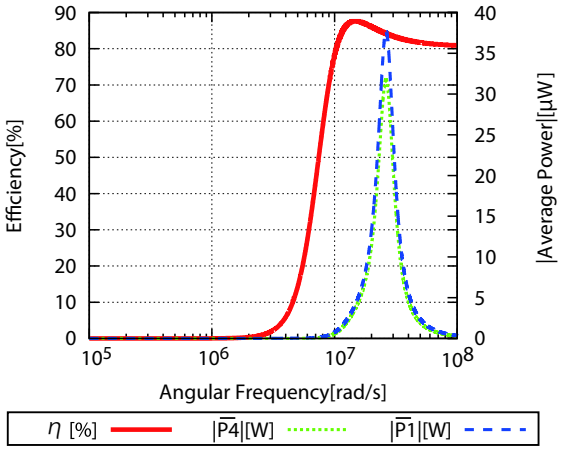

Fig. 5. Efficiency and average power $[10^5 \leq \omega \leq 10^8]$

This result shows that the peak of the efficiency, $\omega_1 = 14.8$Mrad/s is different from the peak of the average power, $\omega_2 = 26.3$Mrad/s. Furthermore, the efficiency at ω_1 lower than it at ω_2, but the average power greater at ω_2 than it at ω_1. Thus, even if the efficiency is lower, to choose the frequency of the voltage source for ω_2 is able to supply the power to the load resistor in the secondary coil, we can judge.

C. The variation of the power transfer due to varying the load

In a state space equation, a general solution is well known as (20).

$$x(t) = e^{At}x(0) + \int_0^t e^{A(t-\tau)}Bu(\tau)d\tau \quad (20)$$

where e^{At} is a state transition matrix. The first term of (20) represents a response of an initial state and the second term of it represents behavior which is from a transitional response until a steady-state response. In general, the more eigen values of the matrix A is near the imaginary axis, the longer the time of the initial state response takes, and it takes longer to get the steady state. Most studies[5][6][8] view the consumption power of the load if it is fixed, but it is time varying generally, and we choose the frequency of a voltage source which maximize the quantity of transfer power. Thus the system is largely affected by the initial state response. We consider this situation next.

TABLE III
PARAMETER VALUE

Element	Value
L_1, L_2	50mH
R_1	50Ω
R_2	0.03Ω
R_3	0.012Ω
M_{12}, M_{21}	0.05 L_1
C_1	2.86μF
C_2	14.3μF
ω	2.5krad/s

ISBN: 978-1-61804-228-6

The parameters of the circuit are represented on Table III. In this circuit, we consider the situation which varies from $R_4 = 50[\Omega]$ to $R_4 = 49[\Omega]$ at $t = 0.3$[s]. This situation until 0.4s is shown on Fig. 6. Where the initial state $x(0) = 0$.

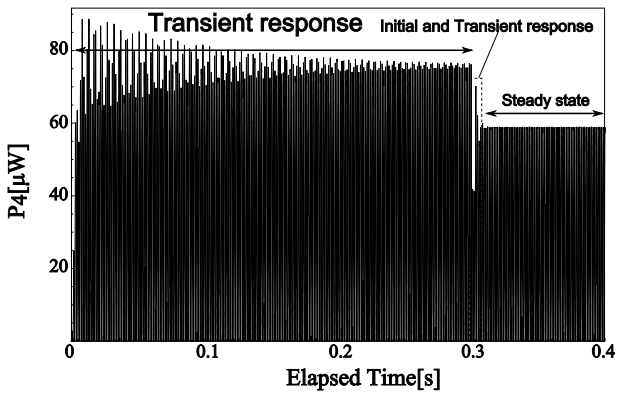

Fig. 6. Response of P_4

It takes 3s to get the steady state from 0s. At 3s, the load resistor R_4 varies to 49Ω, and it takes 0.01s to get the steady state again. After all, in 0.4s, it takes 0.31s and the average power only expresses in the power if a steady state has remained since 0s, thus, there is an extra estimation about the load power.

V. Conclusion

In wireless power transfer, we must search a suitable frequency of a voltage source for high efficiency and high power supplying capability. We have proposed a method of circuit modeling automatically for computing the suitable frequency and the efficiency. We define a model a transfer model between the coils for wireless power transfer and we have been able to analyze more circuit through simplifying the process which makes models for searching high efficiency circuits.

We have shown that we can analyze the behavior of circuits with leaving the symbolic parameters that we interested in since models are expressed in symbolic equations. We have confirmed the achievement of these objects by our proposed method.

In this paper, we have been able to reduce the computing time of analysis of circuits, and analyze circuits if the circuit topology is large and the circuit is composed of many elements, and as a consequence, we have been able to search suitable circuits for wireless power transfer systems more widely.

References

[1] Hassoun, M. M. and Lin, P. M., *A hierarchical network approach to symbolic analysis of large-scale networks*, Circuits and Systems I: Fundamental Theory and Applications, IEEE Transactions on(Volume: 42,Issue: 4).

[2] Starzyk, J. A.andKonczykowska, A., *Flowgraph analysis of large electronic networks*, Circuits and Systems, IEEE Transactions on (Volume: 33, Issue: 3).

[3] Xiang-Dong Tan and C. J. Richard Shi, *Hierarchical Symbolic Analysis of Analog Integrated Circuits via Determinant Decision Diagrams*, Computer-Aided Design of Integrated Circuits and Systems, IEEE Transactions on （Volume: 19, Issue: 4 April 2000).

[4] C. J. Richard Shi and Xiang-Dong Tan, *Canonical Symbolic Analysis of Large Analog Circuits with Determinant Decision Diagrams*, Computer-Aided Design of Integrated Circuits and Systems, IEEE Transactions on （Volume: 19, Issue: 1 January 2000).

[5] Alexey Bodrov and Seung-Ki Sul, *Analysis of Wireless Power Transfer by Coupled Mode Theory (CMT) and Practical Considerations to Increase Power Transfer Efficiency*, Wireless Power Transfer - Principles and Engineering Explorations.

[6] Huy Hoang and Franklin Bien, *Maximizing Efficiency of Electromagnetic Resonance Wireless Power Transmission Systems with Adaptive Circuits*, Wireless Power Transfer - Principles and Engineering Explorations.

[7] Takehiro Imura and Yoichi Hori, *Maximizing Air Gap and Efficiency of Magnetic Resonant Coupling for Wireless Power Transfer Using Equivalent Circuit and Neumann Formula*, Industrial Electronics, IEEE Transactions on(Volume: 58, Issue: 10).

[8] Hiroshi Hirayama, *Equivalent Circuit and Calculation of Its Parameters of Magnetic-Coupled-Resonant Wireless Power Transfer*, Wireless Power Transfer - Principles and Engineering Explorations.

[9] Andr Kurs, Aristeidis Karalis, Robert Moffatt, J. D. Joannopoulos, Peter Fisher and Marin Soljačić, *Wireless Power Transfer via Strongly Coupled Magnetic Resonances*, 6 July 2007 Vol. 317 Science.

The TLS to study deformations using ICP algorithm

V. Barrile, G. M. Meduri and G. Bilotta

Abstract— This contribute describes a methodology for the monitoring and control of mountainous areas with TLS, crossing data acquired in two different epochs. The next phase of data processing was performed using ICP algorithm (Iterative Closest Point) for recording each time scans. To generate DEMs for the analysis of ΔDEM differences between the two epochs, the Ransac algorithm (Random Sample Consensus) has been used.

***Keywords*—** TLS, ICP algorithm, DEM, Ransac algorithm.

I. Introduction

THE research activity carried out within the Laboratory of Geomatics of the Faculty of Engineering of the University "Mediterranea" of Reggio Calabria. The aim of study is to assess the possible deformations of a portion of land located within the University (Fig. 1) and simultaneously test, experiment and verify the TLS (and more specifically of Riegl LMS-Z420i instrument shown in Figs 2 and 3) finalized to environmental monitoring.

Fig. 1 study area

II. Design and Execution of the Survey

For data collection was enough to use two instrumental positions (Fig. 4), using spherical targets, not really needed for the type of performed processing, but useful for verification and / or any other processes. Since surveys were carried out in two different epochs, it was necessary to create a targets handling and fix the exact positions and settings of the acquisition tools.

III. Scan Registration

After acquiring data set in the test site, the first operation carried out in the laboratory was the recording of different scans.

Fig. 2 view during the scan

V. Barrile is with the DICEAM Department, Faculty of Engineering Mediterranean University of Reggio Calabria, Reggio Calabria 89100 IT (phone: +39-0965-875-301; e-mail: vincenzo.barrile@unirc.it).

G. M. Meduri is with the DICEAM Department, Faculty of Engineering Mediterranean University of Reggio Calabria, Reggio Calabria 89100 IT (phone: +39-0965-875-301; e-mail: giumed@libero.it).

G. Bilotta was with the Department of Planning, IUAV University of Venice, Venice 30135 IT. She now collaborates with the DICEAM Department, Faculty of Engineering Mediterranean University of Reggio Calabria, Reggio Calabria 89100 IT (e-mail: giuliana.bilotta@gmail.com).

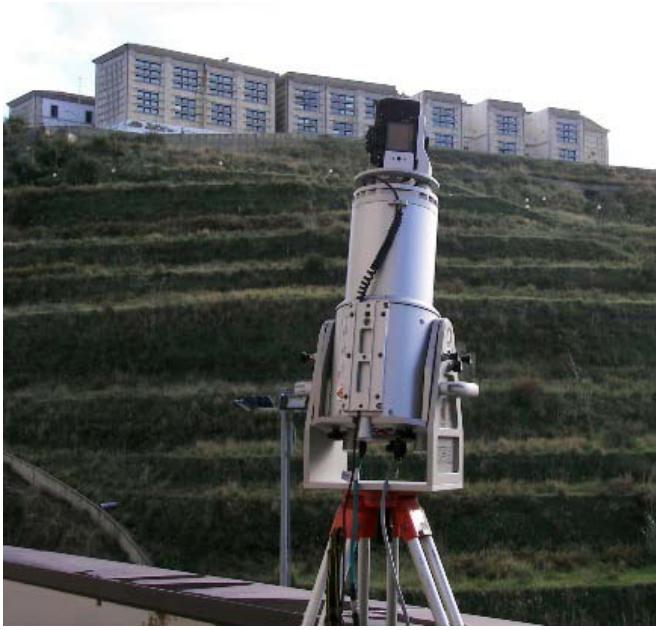

Fig. 3 another view during the scan

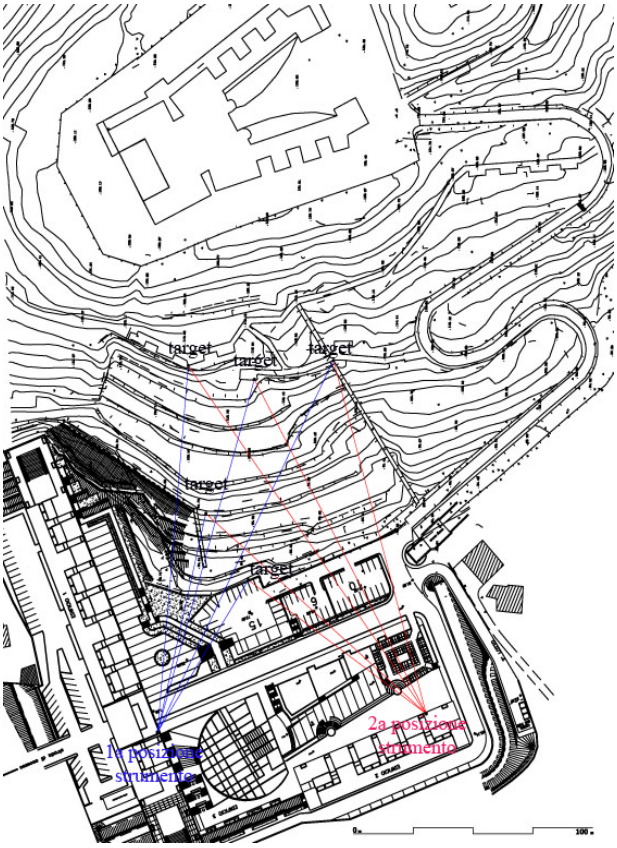

Fig. 4 survey area and shooting design

It made possible to generate a unique point cloud representing the investigated object (Fig. 5 a, b).

To record the clouds and generate the whole cloud, each time was used the ICP algorithm (Interactive closest Point) implemented in the Matlab environment.

The ICP algorithm iteratively applied a rigid roto-translation in one of the two clouds, considered to be mobile, so that overlap in the best possible way to another cloud, considered fixed.

Given a point cloud V^j and a point cloud V^i to align with each other, for each y_i point of V^j, exists at least one x_i point on the cloud V^i, said corresponding point, which is the closest to y_i compared to all other points in X.

The algorithm is an efficient method to tackle rigid registration between two point sets. Its goal is to find a rigid transformation, with which Y is registered to be in the best

(a)

(b)

Fig. 5 point cloud after registration at t_1 and t_2 ages

ISBN: 978-1-61804-228-6

alignment with X, that is, let T of Equation:

$$\min_{T,\, j\in\{1,2,\ldots,N_x\}} \left(\sum_{i=1}^{N_y} \left\| T(y_i) - x_j \right\|_2^2 \right) \tag{1}$$

be rotation and translation transformations, hence the rigid registration between two point sets is

$$\min_{\vec{R},\vec{t},\, j\in\{1,2,\ldots,N_x\}} \left(\sum_{i=1}^{N_y} \left\| \left(\vec{R} y_i + \vec{t} \right) - \vec{x}_j \right\|_2^2 \right) \tag{2}$$

s.t. $R^T R = I_x$; $\det(R)=1$

In an iteration, ICP assumes that the closest points correspond, computes the absolute orientation and applies the resulting rigid transformation to V^j. In practice, at step 1 for each point of mobile cloud (V^j set), are sought, within the fixed point cloud, the points (closest point) contained in a sphere of a certain radius (multiple of a parameter introduced by user) belonging to V^i set. The closest of these will be held and considered the corresponding point.

$$C_k(i) = \arg\min_{j\in\{1,2,\ldots,N_x\}} \left(\left\| \left(R_{k-1} \vec{y}_i + \vec{t}_{k-1} \right) - \vec{x}_j \right\|_2^2 \right) \tag{3}$$

With these matches found, in step 2, the algorithm computes the incremental transformation (rotation matrix $R_{i,j}$ and translation vector T and solving the absolute orientation) by applying it to the elements of V^j; If the mean square error is less than a certain threshold, the iteration terminates otherwise return to step 1;

$$(R_k, \vec{t}_k) = \arg\min_{R^T R = I_m,\, \det(R)=1,\, \vec{t}} \left(\left\| \left(R \vec{y}_i + \vec{t} \right) - \vec{x}_{c_k(i)} \right\|_2^2 \right) \tag{4}$$

The principle on which is based this algorithm is that the alignment between the two point clouds corresponds to the minimization of the quadratic error of the minimum distances between the two objects. In fact, Besl and McKay demonstrated that the algorithm converges to a local minimum of the error (Fig. 6).

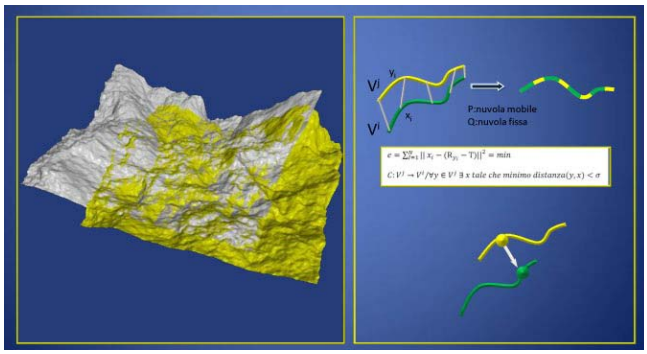

Fig. 6 interactive closest point

$$e = \sum_{i=1}^{N} \| x_i - (R_{y_i} - T) \|^2 = min \tag{5}$$

$$C: V^j \rightarrow \frac{V^i}{\forall y} \in V^j \; \exists \; x \; such \; that \; min \; distance \; (y,x) < \sigma \tag{6}$$

IV. Subsequent Processing

Completed the registration steps, cleaning and filtering, repeated for two epochs that characterize the methodology tested, and in order to delimit the areas of interest and eliminate the present vegetation, we proceed to the generation of DEM, segmenting the entire point cloud in small regions 2.5 D (Figs. 7 and 8).

For this purpose was used the Ransac (Random Sample Consensus) algorithm with a voxel approach that generates a pyramidal structure from which are extracted flat elements. (Figs. 9 and 10). These plans were subsequently aggregates, using a hierarchical clustering, to build a single plane of greater dimensions.

Thus transforming the point cloud of all ages in DEM in the form of a square grid of δDEM resolution, proceed with the analysis of the ΔDEM differences between the two epochs t_1 and t_2 .

However, from previous experience with the segmentation of LIDAR data, and because of the amount of data from scans with TLS, it would be impossible enter all points on the algorithm.

For these reasons, it has been developed a system of multi resolution. We create a pyramid (Fig. 8), each level is processed and the results are transferred to the next.

From the cloud are filled levels of the pyramid. At each level, from bottom to top, the surface of the soil is simplified by reducing the number of points ("smoothing"). This is done with a "voxel", enclosing the point cloud in a box (Fig. 9, Table I).

The generation of the pyramid starts from the lowest level, where the cells have smaller size. The points corresponding to each cell are replaced by their center of gravity. From one level to the next, 8 cells of lower level are grouped in a new cell of the upper layer. The point associated with the cell becomes the center of gravity of the 8 mothers cells. This leads to a reduction factor of 4 for each level. Then the problem becomes more computationally easy.

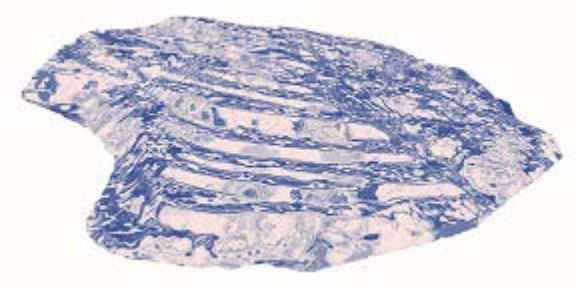

Fig. 7 DEM created after segmentation of new cloud at t_1 age

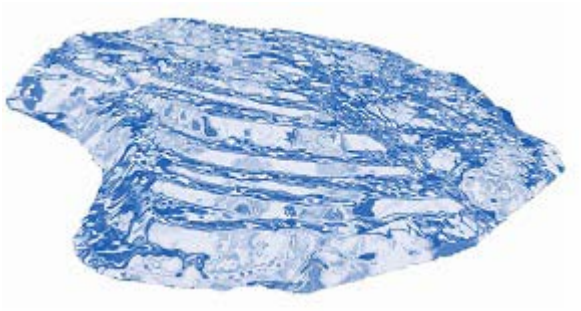

Fig. 8 DEM created after segmentation of new cloud at t_2 age

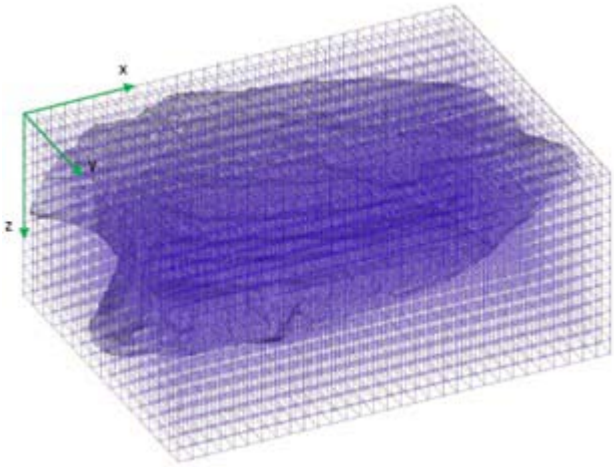

Fig. 9 voxel generation

Fig. 10 pyramid of DEM generation

Table I plans extracted in each level of the pyramid

LVL No.	Points No.	Avg. dist (cm)	STD (cm)	Planes No.
0	2,700,000	0.0	0.0	1117
1	1,345,000	2.3	4.8	805
2	430,632	4.3	5.0	496
3	257,389	7.9	15.0	376

From the data of the segmentation, and the relative plans, two zones (Fig. 11) are chosen for the control of the deformations: a well in reinforced concrete and a zone with exposed rock.

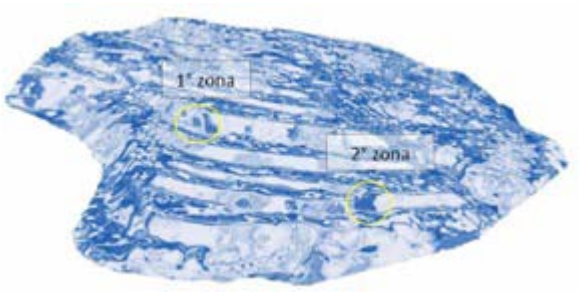

Fig. 11 DEM and chosen plans to the deformation control

The algorithm of deformation analysis uses some parameters regulating research (Table II). First, the size of the average window (W_{def}) defines the range within which to calculate the deformation on ΔDEM. The individual average windows are spaced by an interval Δw.

$\delta w(r,s)$ is the deformation and $\sigma_{\delta w}$ its s.q.m the value of which will be much lower, the greater will be the ability to detect even small deformations.

For discriminating whether the average $\delta w(r,s)$ of the displacements within each window represents or does not represent a significant value, there will be a statistical test.

In particular, since the parameter $\delta w(r,s)$ is the average of a sample of data that, for now, are considered independent from each other, we test the hypothesis H_0:δw=0. If the null hypothesis will be tested, the displacement δw will not be considered significant. Otherwise, the alternative hypothesis matches the significance of the deformation within the window. The statistical analysis used for the test is the following:

$$\xi = \frac{\delta_w}{\sigma_{\delta w}} \approx N(0,1) \tag{7}$$

Set a given level of risk α and its corresponding critical value $\xi_{\alpha/2}$, H_0 is rejected if

$$. |\xi| > \xi_{\alpha/2}$$

It is therefore possible to set a minimum threshold for accepting the significance of a deformation as:

$$\delta_{wdef} = \sigma_{\delta w} \cdot \xi_{\alpha/2} \tag{8}$$

ISBN: 978-1-61804-228-6

Table II thresholds of the process input

	Zone 1 (cockpit in reinforced concrete)		Zone 2 (exposed rock)	
parameters	cm	DU	cm	DU
w_{def}	35	7	35	7
Δ_W	5	1	5	1
η(%)	95	95	90	90
$\sigma_{\delta w}$	±0.05	±0.01	±0.05	±0.01
δ_{wdef}	±0.5	±0.1	±0.5	±0.1

In Fig. 12 we can assess, with a false-color scale, the displacements in the two areas (cockpit and rock).

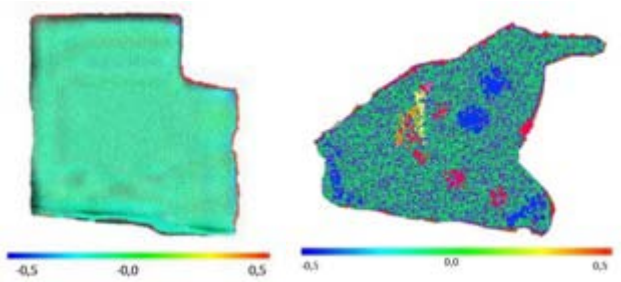

(a) (b)

Fig. 12 well (a) and exposed (b) rock deformations

V. Conclusions

The used methodology and particularly the use of the ICP algorithm, which does not need in the phase of record of the scansions of the use of targets, has supplied of the appreciable results allowing to obtain results comparable with the classic methods. The latters instead need of homologues targets for the generation of the whole point cloud. ICP algorithm might be fundamental where, because of the possible deformations, the monumentation of the targets might not guarantee the certainty of the obtained datum, distorting the results and checks to be achieved.

References

[1] C. S. T. Werner, A. Wiesmann and U. Wegmueller, U. (2008) Gamma's Portable Radar Interferometer", *in Proceedings of the 13th FIG International Symposium on Deformation Measurements and Analysis*, 2008.

[2] T. J. M. Kennie and G. Petrie (Eds.) Blackie, "Engineering surveying technology", 1990.

[3] R. Van Gosliga, R. Lindenbergh and N. Pfeifer, "Deformation analysis of a bored tunnel by means of terrestrial laser scanning", in IAPRSSIS vol. 36, no. 5, pp. 167-172, 2006, on CD-ROM.

[4] R. W. Schnabel and R. Klein, "Ransac Based Out-of-Core Point-Cloud Shape Detection for City-Modeling", in *Proceedings of "Terrestrisches Laserscanning* (TLS 2007), Beiträge zum 74. DVW Seminar, Fulda, Germany, 2007.

[5] G. Bitelli, G., M. Dubbini. and A. Zanutta, "Terrestrial laser scanning and digital photogrammetry techniques to monitor landslides bodies". IAPRSSIS vol. 35, pp. 246-251, 2004.

[6] G. Teza, A. Galgaro., N. Zaltron. and R. Genevois, "Terrestrial laser scanner to detect landslide displacement field: a new approach", 2007.

[7] D. Schneider, "Terrestrial laser scanning for area based deformation analysis of towers and water dams" in *Proc. of 3rd IAG Symp. on Deformation Measurements and Analysis / 12th FIG Symp. on*, 2006.

[8] R. Lindenbergh, R. and N. Pfeifer, "A statistical deformation analysis of two epochs of terrestrial laser data of a lock", in *Proc. of 7th Conf. on Optical 3-D Measurement Techniques*, Austria, 3–5 October 2005, vol. 2, pp. 61-70.

[9] A. Abellán, M. Jaboyedoff, T. Oppikofer and J. Vilaplana, "Detection of millimetric deformation using a terrestrial laser scanner: experiment and application to a rockfall event", 2009.

[10] V. Barrile, G. M. Meduri, G. Bilotta, "Laser scanner surveying techniques aiming to the study and the spreading of recent architectural structures", in *Recent advances in signals and systems, Proceedings of the 9th WSEAS International Conference on Signal, speech and image processing* 2009, pp. 92-95. Available: http://www.wseas.us/e-library/conferences/2009/budapest/MIV-SSIP/MIV-SSIP15.pdf

[11] V. Barrile, G. M. Meduri, G. Bilotta, "Laser scanner technology for complex surveying structures", *WSEAS transactions on signal processing*, vol. 7 no. 3, July 2011, pp. 65-74. Available: http://www.wseas.us/e-library/transactions/signal/2011/53-180.pdf

[12] V. Barrile, G. Bilotta, G. M. Meduri, "Least Squares 3D Algorithm for the Study of Deformations with Terrestrial Laser Scanner", in *Recent Advances in Electronics, Signal Processing and Communication Systems, Proceedings EUROPMENT 2013 International Conference on Electronics, Signal Processing and Communication Systems*, ESPCO 2013, Venice, Italy, September 28-30, pp. 162-165. Available: http://www.europment.org/library/2013/venice/bypaper/ESPCO/ESPCO-24.pdf

Efficient Wireless Power Transfer – Resonance Does Not Imply High Efficiency

Kazuya Yamaguchi, *University of Miyazaki* Ichijo Hodaka, *University of Miyazaki*

Abstract—This paper naively inquires when power transmission is optimized by tuning possible parameters of a wireless power transfer system. It is well known that tuning the frequency of the AC supply input implies maximizing the magnitude of transmitted power into a receiver side. This type of tuned wireless power transfer system, however, may cause a low efficiency of power transfer. The paper illustrates that such an undesired situation exists, and suggests that tuning parameters in the both views of large magnitude of transmitted power and high efficient transmission will be desirable for better wireless power transfer systems.

Keywords—wireless power transfer, highly efficient power transmission, resonance

I. Introduction

MOST of devices that are driven by electric power are usually fed via electric wires connected to AC power supply. On the other hand, some of electric devices are required or designed to be fed without electric wires — in the way of called WPT (wireless power transfer). Since the amount of power provided by WPT is usually restricted compared with wired power transfer, WPT has not been used for many applications.

In 2007, a successful experiment that could wirelessly transfer practical amount of power away from sixty centimeters was reported[1]. The heart of the experiment was to generate resonant phenomena of electromagnetic coupling between transmitting and receiving coils. After the pioneering study[1], many researchers have tried to develop theory and experiments for WPT. In [2] a structure of circuit was devised in order to raise the factor Q of circuits, since better WPT needs higher values of the factor Q. In [3] devised antennas are proposed to be used for a directed energy radiation in order to implement efficient WPT. In [4] the effect of radiation energy to human body was discussed.

It is generally understood that resonant phenomena will be caused if one tunes the frequency of AC power supply to the natural frequency of a circuit. The natural frequency is determined by the values of circuit elements; especially, the mutual inductances which relate transmitting and receiving sides of the circuit play an important role. These values are determined by the radii, winding numbers, and relative position of two coils[5]. It is important to know the relation between the relative position of coils and mutual inductances because the position of the coils could be changed in various reasons.

For extending the usage of WPT, the most important specification for WPT is power and efficiency of transmission. In many literatures, causing resonant phenomena should lead to high power and efficient WPT. However, little is known about how resonance brings the best performance of WPT based on a concrete and mathematical aspects.

In this paper, we propose a series of procedures to analyze relations between the resonant frequency, obtained average power at the receiving side, and the ratio of the average power at the receiving side to the average power at the transmitting side that is called an efficiency of WPT. Our procedures are based on the differential equations in the form which commonly used in control theory. This gives us a benefit that we can manipulate different transfer functions and write the relations under investigation in a clear and unified manner. Consequently, we will assert that resonance does not imply the optimization of efficiency of WPT in general, by observing derived equations.

To illustrate this situation that should be carefully treated, we pick one of most common circuits for WPT, and put practical values into the circuit elements, and then we demonstrate the situation numerically. In fact, although we have the case when resonance is equivalent to maximization of efficiency of WPT, we have another case when resonance leads to loss of efficiency of WPT. Thus we propose to use the way of modelling by mathematical equations and to describe the targets into equations for WPT systems.

II. Analysis of Wireless Power Transfer Circuit

A. Self inductance and mutual inductance

We consider the situation that current i flows in a coil with a radius r_1 and a winding number n_1, called coil 1. This generates magnetic flux in the whole space by the Biot-Savart law. Here we consider a magnetic flux density B which is away from the current i by z and which is along the central axis of the coil 1[6]. That is,

$$B = \frac{\mu i}{4\pi} \frac{2n_1 \pi r_1^2}{(z^2 + r_1^2)^{3/2}}. \tag{1}$$

Where μ is the permeability.

Now we consider another coil 2 with a radius r_2 and a winding number n_2. From equation (1), self inductances L_1 of the coil 1 and L_2 of the coil 2, and mutual inductances M_1 and M_2 between the coils 1 and 2 can be written as below.

$$\begin{aligned} L_1 &= \frac{\mu \pi n_1^2 r_1}{2},\ L_2 = \frac{\mu \pi n_2^2 r_2}{2} \\ M_1 &= \frac{\mu \pi n_1 n_2 r_1^2 r_2^2}{2(z^2 + r_1^2)^{3/2}},\ M_2 = \frac{\mu \pi n_1 n_2 r_1^2 r_2^2}{2(z^2 + r_2^2)^{3/2}}. \end{aligned} \tag{2}$$

ISBN: 978-1-61804-228-6

From the above equations, note that these mutual inductances are inversely proportional to cube of the distance z between two coils[7].

B. Wireless power transfer circuit and its mathematical model

We study a typical circuit for WPT depicted below[8]. Despite of the placement of two coils in the figure, we assume they have a common central axis as explained in the previous section.

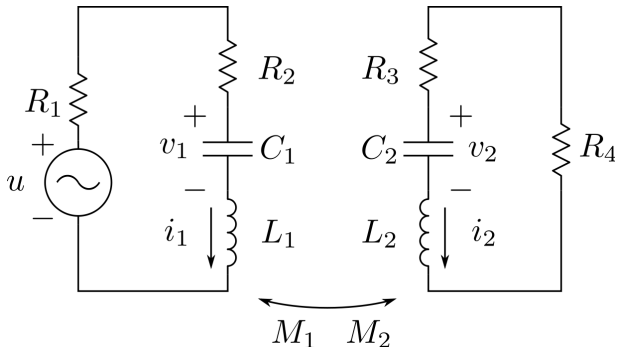

Figure 1 A Wirelss Power Transfer Circuit

The resistor R_1 is supposed to represent an internal impedance of the power supply, and R_4 the load. R_2, R_3, C_1, C_2 are parasitic factors of transmitting and receiving coils. This circuit is mathematically modelled as the following state equation. This type of expression is widely used in control theory. In particular one can write the model of WPT circuits in a compact form, and obtain a clear perspective to analysis of stability and responses with a sinusoidal input.

$$\dot{x} = Ax + Bu$$

$$x = \begin{bmatrix} v_1 \\ v_2 \\ i_1 \\ i_2 \end{bmatrix}$$

$$A = \frac{1}{\Delta} \begin{bmatrix} 0 & 0 & \frac{\Delta}{C_1} & 0 \\ 0 & 0 & 0 & \frac{\Delta}{C_2} \\ -L_2 & M_2 & -(R_1+R_2)L_2 & (R_3+R_4)M_2 \\ M_1 & -L_1 & (R_1+R_2)M_1 & -(R_3+R_4)L_1 \end{bmatrix}$$

$$B = \frac{1}{\Delta} \begin{bmatrix} 0 \\ 0 \\ L_2 \\ -M_1 \end{bmatrix}$$

$$\Delta = L_1L_2 - M_1M_2. \tag{3}$$

C. Formulation of average power and efficiency

The purpose of this paper is to investigate the relation between the frequency of AC supply voltage, the average power delivered to the receiving side, and the efficiency of average power transmission. The efficiency is defined as the ratio of the average power obtained at the receiving side against the average power supplied at AC power supply. Thus we formulate equations of the average powers at transmitting and receiving sides, and of the efficiency in the following.

Since the matrix A in the equation (3) is stable, i.e., all eigenvalues of the matrix A have negative real parts, the solution to the equation (3) will be stationary after time have passed adequately. The stationary solution with a sinusoidal input $u = \sin\omega t$, will have the same frequency of the input.

In general, the average powers P_1 and P_4 which are at the AC supply and the load in the receiving side respectively, and then the efficiency η depends on the frequency of AC supply. These stationary values can be all expressed in terms of transfer functions.

$$\begin{aligned} P_1 &= \frac{1}{2}\left|\mathrm{Re}[G_1(j\omega)] - R_1|G_1(j\omega)|^2\right| \\ P_4 &= \frac{1}{2}R_4\left|G_2(j\omega)\right|^2 \\ \eta &= \frac{P_4}{P_1}. \end{aligned} \tag{4}$$

Here $G_1(s)$ and $G_2(s)$ are the transfer functions from the input u to i_1 and i_2, respectively. With the equation (3), these transfer functions are written in $G_1(s) = H_1(sI - A)^{-1}B, G_2(s) = H_2(sI - A)^{-1}B$, where $H_1 = [0, 0, 1, 0]$ and $H_2 = [0, 0, 0, 1]$.

D. Resonance and average power

In view of the equation (4), we see that if one puts an AC input voltage with the frequency which gives the maximal gain of the transfer function $G_2(s)$ (the gain is called H_∞-norm), one will have the maximal average power at the receiving side. To illustrate the situation, we set values of circuit elements as below. These values are given by consulting a practical situation of WPT[2].

TABLE I
PARAMETERS

elements	values	elements	values
R_1	50Ω	L_2	10μH
R_2	0.1Ω	M_1	0.5μH
R_3	0.1Ω	M_2	0.5μH
R_4	50Ω	C_1	1nF
L_1	10μH	C_2	1nF

The bode diagram of $G(s)$ is shown as below.

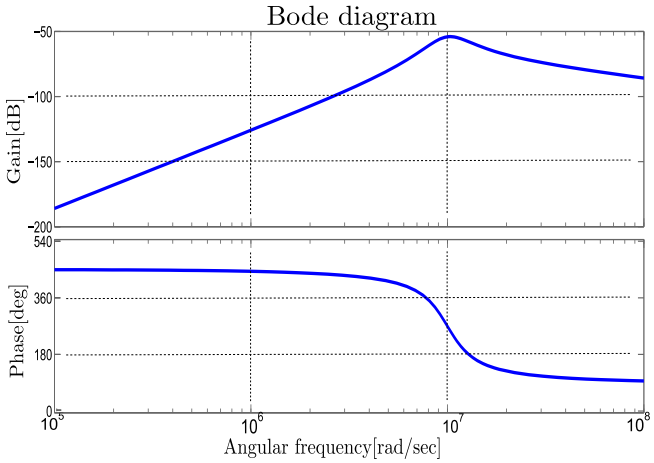

Figure 2 Bode Diagram

In this case the resonance will occur at the unique frequency $\omega = 1.00 \times 10^7 \mathrm{rad/sec}$ and we have the maximal average power at the receiving side if we use a sinusoidal wave with the resonant frequency.

E. Resonance and efficiency

Based on the equation (4), we can observe that the relation between the input frequency and the efficiency of WPT is not straightforward. Many other papers state that using an AC input voltage with a resonant frequency is optimal or better in the design of WPT. In the previous section, we have clarified that using the input with resonance maximizes the average power at the receiving side. However, the efficiency of power transmission can be maximized either when one use resonance or when one use nonresonance. This difficult situation is illustrated by numerical examples in the following.

First, power P_4 and efficiency η with the condition of TABLE I are shown as below.

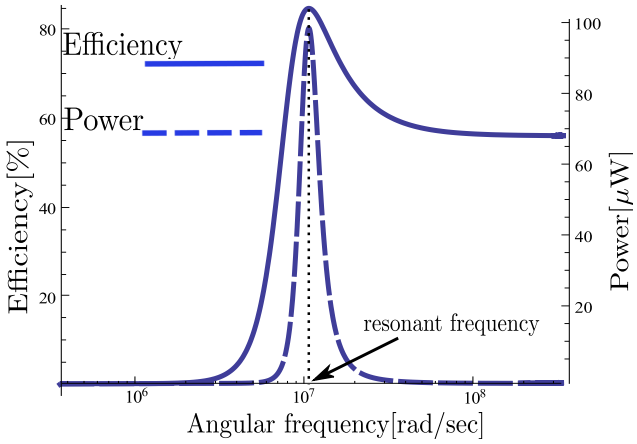

Figure 3 Power and Efficiency for TABLE I

Then, η is maximized when

$$\omega = 1.07 \times 10^7 \mathrm{rad/sec} \tag{5}$$

as previously known in [9].

Another example is shown as below. The values of elements are set as TABLE II. The only difference between TABLE I and TABLE II is the value of C_1.

TABLE II
PARAMETERS

elements	values	elements	values
R_1	50Ω	L_2	10μH
R_2	0.1Ω	M_1	0.5μH
R_3	0.1Ω	M_2	0.5μH
R_4	50Ω	C_1	0.1nF
L_1	10μH	C_2	1nF

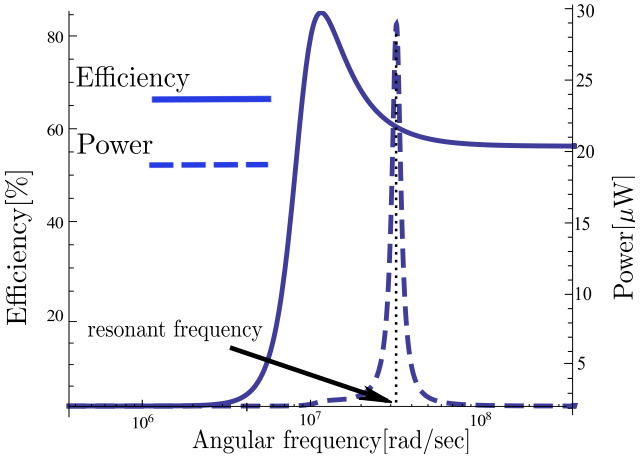

Figure 4 Power and Efficiency for TABLE II

By comparing Figure 3 and Figure 4, we see that the frequencies which respectively maximize power and efficiency are different.

III. Conclusion

In this paper, we have pointed out that using a resonant frequency of AC voltage input does not lead to maximize the efficiency of average power transmission, although resonance is equivalent to maximization of output average power, in general WPT systems. In fact, we have illustrated a situation that non-resonance maximizes the efficiency of power transmission by numerical examples. This suggests that we should take both of output power and efficiency into account and then decide a balanced working frequency, in the case that resonance is not equivalent to the maximal efficiency. For example, the maximum power is desirable if an AC power supply can serve enough power, but the maximum efficiency is best if the supply can serve less power.

Even one of the simplest WPT circuits treated in this paper may have disagreement between resonance and efficiency. Therefore, one will face on further difficulty to design better WPT when one tries more complex circuit with more elements in order to meet an increasing design specification.

ISBN: 978-1-61804-228-6

REFERENCES

[1] Andr Kurs, Aristeidis Karalis, Robert Moffatt, J. D. Joannopoulos, Peter Fisher, Marin Soljacic´ , ”Wireless Power Transfer via Strongly Coupled Magnetic Resonances”, Science 317, PP.83-86, 2007.

[2] Huy Hoang, Franklin Bien, ”Maximizing Efficiency of Electromagnetic Resonance Wireless Power Transmission Systems with Adaptive Circuits”, Wireless Power Transfer - Principles and Engineering Explorations, PP.207-226, 2012.

[3] Ick-Jae Yoon, Hao Ling, ”Realizing Efficient Wireless Power Transfer in the Near-Field Region Using Electrically Small Antennas”, Wireless Power Transfer - Principles and Engineering Explorations, pp.151-172, 2012.

[4] Ji-Yeon Mun, Min-Gyeong Seo, Woo-Geun Kang, Hae-Young Jun, Yong-Ho Park, Jeong-Ki Pack, ”Study on the Human Effect of a Wireless Power Transfer Device at Low Frequency”, PIERS Proceedings, pp.322-324, 2012.

[5] Hiroshi Hirayama, ”Equivalent Circuit and Calculation of Its Parameters of Magnetic-Coupled-Resonant Wireless Power Transfer”, Wireless Power Transfer - Principles and Engineering Explorations, pp.117-132, 2012.

[6] Youngjin Park, Jinwook Kim, Kwan-Ho Kim, ”Magnetically Coupled Resonance Wireless Power Transfer (MR-WPT) with Multiple Self-Resonators”, Wireless Power Transfer - Principles and Engineering Explorations, pp.51-64, 2012.

[7] Henri Bondar, Shailendra Oree, Zafrullah Jagoo, Keiichi Ichikawa, ”Estimate of the maximum range achievable by non-radiating wireless power transfer or near-eld communication systems”, Journal of Electrostatics, Volume71, Issue4, pp.648-655, 2013.

[8] Marco Dionigi, Alessandra Costanzo, Mauro Mongiardo, ”Network Methods for Analysis and Design of Resonant Wireless Power Transfer Systems”, Wireless Power Transfer - Principles and Engineering Explorations, pp.65-94, 2012.

[9] Takashi Komaru, Masayoshi Koizumi, Kimiya Komurasaki, Takayuki Shibata, Kazuhiko Kano, ”Compact and Tunable Transmitter and Receiver for Magnetic Resonance Power Transmission to Mobile Objects”, Wireless Power Transfer - Principles and Engineering Explorations, pp.133-150, 2012.

ISBN: 978-1-61804-228-6

A fully-differential Regulated Telescopic Operational Transconductance Amplifier

J. Mallek, H. Mnif, H. Daoud, and M. Loulou

***Abstract*—**A fully-differential Regulated Telescopic Operational Transconductance Amplifier (OTA) is proposed. In fact, the conventional OTA is a version of simple telescopic circuit with the gate voltage of the cascode transistor is controlled by a feedback amplifier. To obtain more DC gain, the feedback is applied around the cascode transistor. The proposed OTA is designed in AMS 0.35µm technology and simulated with Advanced Design System. Simulation results show that Regulated Telescopic OTA has 15% improvement in the DC gain compared to that of conventional Telescopic OTA. Moreover, the slew rate and Common Mode Rejection Ratio (CMRR) are also enhanced and the settling time of Regulated Telescopic OTA is reduced by 11% compared to that of conventional Telescopic OTA.

***Keywords*—**DC gain, fully- differential, Operational transconductance amplifier, Regulated telescopic OTA.

I. Introduction

DESIGNING high-performance base band analog circuits is still a hard task toward reduced supply voltages and increased frequency. Current tendency focus on some radio-software receivers which suppose an RF signal conversion just after the antenna. Thus, a very higher sampling frequency and resolution analog-to-digital converter design is required. The OTA is a basic element in this type of circuit [1].

It is very difficult to design an amplifier with both high gain and high bandwidth. High gain amplifiers use cascode structures or multi-stage designs with long channel length transistors biased at low current levels. High bandwidth amplifiers use single-stage designs with short channel length transistors biased at high current levels [2].

Our target was to design a wideband regulated telescopic OTA circuit in sight of continuous-time sigma-delta ADC design, using for Mobile WiMAX applications.

This paper is organized as follows. Telescopic OTA circuit design is described in section II. Section III presents the Regulated Telescopic OTA. Section IV gives simulation results. Finally some concluding remarks are provided.

J. Mallek is with the Laboratory of Electronics and Information Technologies, University of Sfax, Tunisia, E-Mail: jihenemallek@yahoo.fr.

H. Daoud is with the Electronic and Communication Institute, University of Sfax, Tunisia, E-Mail: daoud.houda@tunet.tn.

H. Mnif is with the Electronic and Communication Institute, University of Sfax, Tunisia, E-Mail: hassene.mnif@ieee.org.

M. Loulou is with the Laboratory of Electronics and Information Technologies, University of Sfax, Tunisia, E-Mail: mourad.loulou@ieee.org.

II. Conventional fully-differential wideband telescopic OTA

A. Design and performance

There are three kinds of OTAs: two stage OTAs, folded-cascode OTAs, and telescopic OTAs. The telescopic amplifier consumes the least power compared with the other two amplifiers, so it is widely used in low power consumption applications. A conventional single-stage telescopic amplifier is shown in Fig. 1 [3].

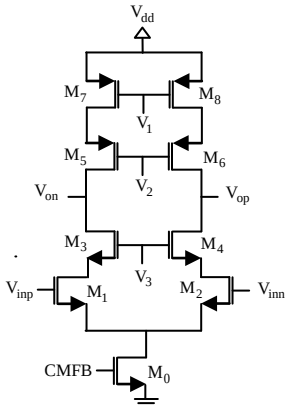

Fig. 1 Single-stage telescopic OTA

The OTA is designed to be fully-differential for a number of reasons. This doubles the effective output swing and the amount of current available for slewing. Because the signal power quadruples while the noise power only doubles, the dynamic range is also doubled. Moreover, fully-differential circuits have been shown to effectively attenuate even-order harmonic distortion, substrate noise, supply noise, and common mode disturbances [4].

The single-stage telescopic OTA employs differential input pairs (M_1 and M_2), cascode devices (M_3 and M_4) and current source loads (M_5, M_6, M_7 and M_8). An input device (M_1 and M_2) generates drain current proportional to input voltages (V_{inp} and V_{inn}). The cascode devices simply routes the current to current loads. Furthermore, cascode devices will increase the output resistance. Therefore, the OTA gain increases. OTA is loaded with PMOS cascode current sources (M_5, M_6, M_7 and M_8) to increase output impedance [5].

ISBN: 978-1-61804-228-6

B. Theoretical study

Open loop gain is one of the most important parameter for OTA design. In the OTA circuit, output current is given by the following equation:

$$i_{out} = i_{d1} - i_{d2} \tag{1}$$

where:

$$i_{d1} = g_{m1} V_{inp},\ i_{d2} = g_{m1} V_{inn} \tag{2}$$

with g_{mi} is the transconductance of transistor T_i for i = (1, 3, 5, 7). Assuming: $g_{m1}=g_{m2}$, and substituting (2) into (1), we obtain:

$$i_{out} = g_{m1}(V_{inp} - V_{inn}) \tag{3}$$

The output resistance is given by (4).

$$R_{out} \approx (g_{m3} ro_3 ro_1) // (g_{m5} ro_5 ro_7) \tag{4}$$

Where ro_i is the drain-source resistance of transistor T_i for i = (1, 3, 5, 7). Combining (3) and (4), the output voltage is then given by:

$$\begin{aligned} V_{out} &= i_{out} R_{out} \\ &= g_{m1}(V_{inp} - V_{inn})\left[(g_{m3} ro_3 ro_1) // (g_{m5} ro_5 ro_7)\right] \end{aligned} \tag{5}$$

and the open loop gain is:

$$A_v = g_{m1}\left(g_{m5} ro_5 ro_7\right) // \left(g_{m3} ro_3 ro_1\right) \tag{6}$$

High frequency model of single-stage telescopic OTA is investigated clearly in [5]. High frequency model of cascode stage can be seen in Fig. 2.

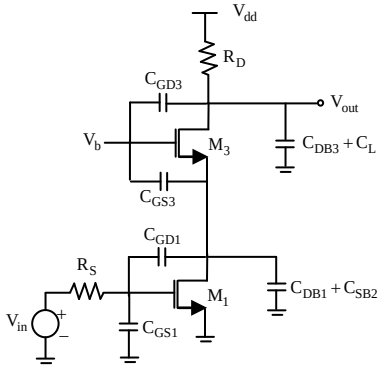

Fig. 2 High frequency model of cascode stage

Output node creates a pole which is dominant pole/bandwidth of the OTA, is given by (7).

$$W_{p,out} = \frac{1}{R_{out}\left(C_{DB3} + C_{GD3} + C_L + C_S\right)} \tag{7}$$

GBW is the product of open loop gain and bandwidth. Combining Equation (6) and Equation (7), the GBW is then given by:

$$GBW = \frac{g_{m1}}{2\pi\left(C_{DB3} + C_L + C_{GD3}\right)} \tag{8}$$

where C_L is the capacitance at the output node. The slew rate is given by:

$$SR = \frac{I_{out\text{-max}}}{C_L} \tag{9}$$

The CMRR of a differential amplifier measures the tendency of the device to reject input signals common to both input leads. A high CMRR is important in applications where the signal of interest is represented by a small voltage fluctuation superimposed on a (possibly large) voltage offset, or when relevant information is contained in the voltage difference between two signals [6]. The CMRR is given by the following equation:

$$CMRR = \frac{A_v}{A_c} \tag{10}$$

With A_v is given by (6) and A_c is given by the following equation:

$$A_c = \frac{ro_7}{2ro_0} \tag{11}$$

According to [7], we use the following formula:

$$\frac{1}{A_v} \le \frac{1}{2} q \Leftrightarrow A_v \ge 59.576\text{dB} \tag{12}$$

Where q is the quantum of the sigma-delta ADC and it is expressed by (13).

$$q = \frac{V_{Full\_scale}}{2^N} \tag{13}$$

with the V_{Full_scale} of the ADC is equal to 13dBm and N is equal to 11bits. In this case, we assume the overall gain A_v more than 60 dB and to ensure good stability op-amp phase margin should be also more than 60 degrees [8]. In [9], It is mentioned that:

$$GBW \geq 3F_S \Leftrightarrow GBW \geq 750MHz \quad (14)$$

III. Regulated Telescopic OTA

A. Design and performance

Regulated Telescopic OTA is a version of simple telescopic circuit with the gate voltage of the cascode transistor being controlled by a feedback amplifier. To obtain more gain, feedback is applied around the cascode transistor. This feedback is actually parallel-series feedback, causing the output impedance to rise by amount of feedback gain. The gain goes up by the same amount. However, that gain boosting adds another gain enhancement at low frequencies. It will not alter the GBW [5]. A schematic of the Regulated Telescopic OTA is shown in Fig. 3.

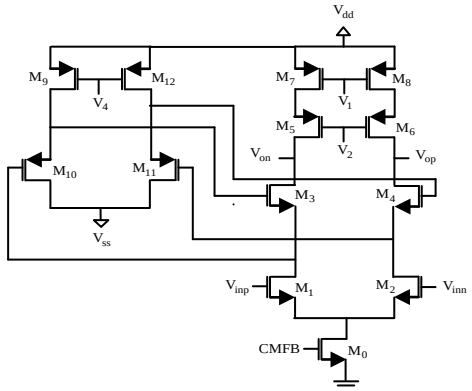

Fig. 3 Schematic of the Regulated Telescopic OTA

B. Theoretical study

The new output resistance equation is given by the following equation:

$$R_{out} = ((gm_3 + gm_{10})ro_3\left(ro_{10} // ro_9\right)ro_1) // \left(gm_5 ro_5 ro_7\right) \quad (15)$$

As a result, open loop gain for Regulated telescopic OTA circuit is given (16).

$$A_v = G_m R_{out} = g_{m1}((gm_3 + gm_{10})ro_3\left(ro_{10} // ro_9\right)ro_1) // \left(gm_5 ro_5 ro_7\right) \quad (16)$$

The GBW is same for conventional Telescopic OTA and Regulated Telescopic OTA due to no change in transconductance G_m. The slew rate and the CMRR are given respectively by (9) and (10).

IV. Simulation Results

Now that design trade-offs have been discussed in detail, the device sizes and load capacitor value are summarized in Table I.

TABLE I
Regulated Telescopic OTA parameters values

Devices	Value	
M_1, M_2	W= 800µm	L= 0.85µm
M_3, M_4	W= 800µm	L= 0.85µm
M_5, M_6	W= 1100µm	L= 0.55µm
M_5, M_6	W= 1100µm	L= 0.55µm
M_0	W= 590µm	L= 0.55µm
M_9, M_{12}	W= 900µm	L= 0.85µm
M_{10}, M_{11}	W= 200µm	L= 0.85µm
Supply voltage	V_{dd}= 3.3V	
Load capacitance	C= 1pF	

By using Advanced Design System, we proceed to simulate the Conventional Telescopic OTA and Regulated Telescopic OTA. We determine various characteristics of different represented architectures of telescopic OTA such as DC gain, phase margin, slew rate, settling time and Common Mode Rejection Ratio (CMRR).

A. Design and performance

The open-loop AC analysis of different architectures of represented Telescopic OTA is shown in Fig.4. Regulated Telescopic OTA has the most important DC gain, which is equal to 60.93 dB. In fact, simulation results show that Regulated Telescopic OTA has 15% improvement in the DC gain compared to that of conventional Telescopic OTA. In addition, the different presented architectures of Telescopic OTA have the same large GBW, which is equal to 790 MHz and the phase plot gives the same phase margin of 60 degrees to ensure a good stability.

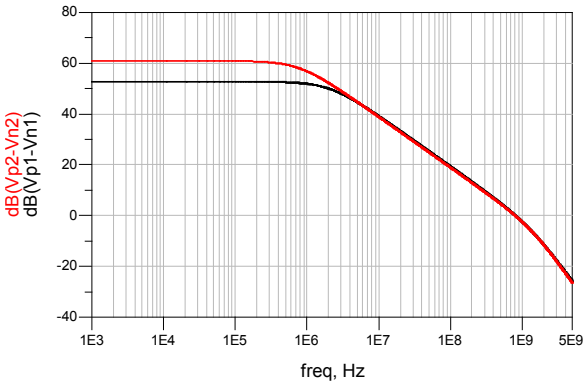

(a)

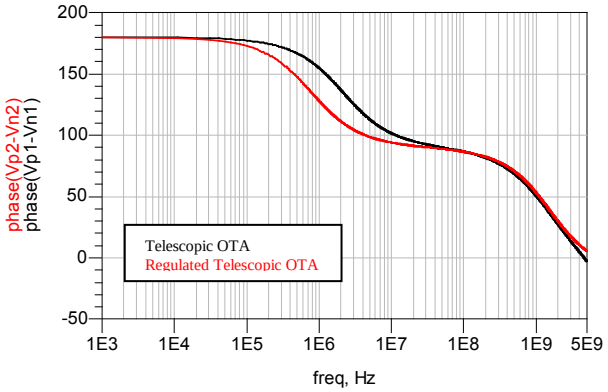

(b)

Fig. 4 Simulated transfer function of (a) Amplifier Magnitude and (b) Phase of the Conventional and Regulated Telescopic OTA

B. *Unity feedback analysis*

As shown in Fig. 6, a step is applied from 0 V to 3.3 V at the input with unity feedback configuration. As was measured, the Regulated Telescopic OTA has the most important slew rate, which is equal to 351 V/µs. In addition, the settling time of Regulated Telescopic OTA is equal to 14.24 ns. So, it is reduced by 11% compared to that of conventional Telescopic OTA.

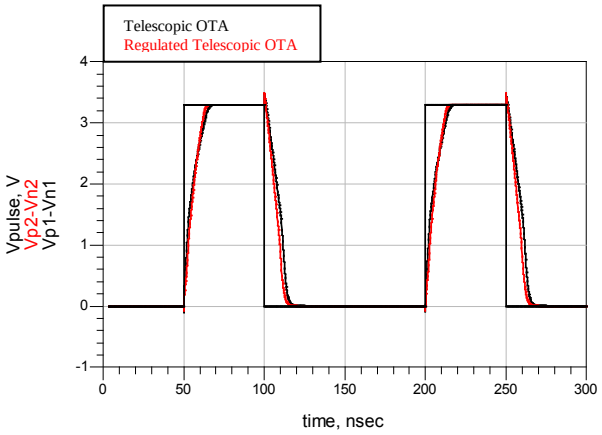

Fig. 6 Step transient response of the Conventional and Regulated Telescopic OTA

C. *Common Mode Rejection Ratio*

In order to simulate common mode rejection, first we find the common mode gain. When the simulator seeps the frequency, there will be a 1V AC source on both the positive and negative inputs and hence the AC signal at the output will be the common mode gain. The previously calculated gain can be divided by this gain to give the CMRR. As shown in Fig. 7, the common mode rejection ratio was found to be 47.60 dB in the case of Conventional Telescopic OTA and 49.242 dB in the case of Regulated Telescopic OTA.

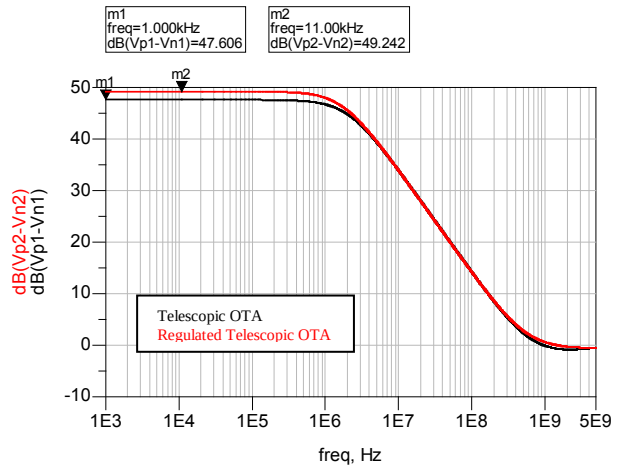

Fig. 7 CMRR of the Conventional and Regulated Telescopic OTA

V. Conclusions

The design approach for fully-differential wideband Regulated telescopic OTA is presented. Behavioral simulation indicated that Regulated Telescopic OTA has 15% improvement in the DC gain compared to that of Conventional Telescopic OTA. In addition, the different represented architectures of Telescopic OTA have the same wide GBW, which is equal to 790 MHz and the same phase margin of 60 degree to ensure a good stability. Moreover, the slew rate and Common Mode Rejection Ratio are also enhanced and the settling time of Regulated Telescopic OTA is reduced by 11% compared to that of Conventional Telescopic OTA.

References

[1] H. D. Dammak, S. Bensalem, S. Zouari, M. Loulou, "Design of Folded Cascode OTA in Different Regions of Operation through gm/ID Methodology," *International Journal of Electrical and Computer Engineering*, 2008, pp. 977 – 982.

[2] B. K. Thandri, J.S. Martinez, "An overview of feed-forward design techniques for high gain wideband operational transconductance amplifiers," *Microelectronics Journal 37 (2006)*, pp. 1018 – 1029.

[3] L. Tianwang, Y. Bo, J. Jinguang, "A novel fully differential telescopic operational transconductance amplifier," *Journal of Semiconductors, Vol. 30, N. 8*, August 2009.

[4] H. D. Dammak, "Etude des Potentialités des Nouvelles Technologies CMOS pour la Conception des OTAs. Applications à la Conception des CANs pour les Nouvelles Générations des Systèmes Radio-Mobiles," *Thesis*, National Engineering School of Sfax, 2012.

[5] A. Karakuzulu, "Design of a Low Current Leakage Integrator for Non-Coherent Ultra-WideBand Receiver," *Master*, Royal Institute of Technology, Stockholm, Sweden, 2012.

[6] J. P. M. Brito, S. Bampi, "A DC offset and CMRR analysis in a CMOS 0.35 mm operational transconductance amplifier using Pelgrom's area/accuracy tradeoff," *Microelectronics Journal*, 2008.

[7] F. Chaahoub, "Etude des méthodes de conception et des outils de CAO pour la synthèse des circuits intégrés analogique," *Thesis*, Polytechnic National institute of Gronoble, 1999.

[8] T. C. Caldwell, "Delta-Sigma Modulators with low oversampling ratios," *Thesis*, University of Toronto, 2010.

[9] F. Silveira, D. Flandre, P.G.A. Jespers, A gm/ID based methodology for the design of CMOS analog circuits and its application to the synthesis of a silicon-on-insulator micropower OTA, *IEEE Journal of solid-state circuits, vol. 31, N. 9*, September 1996.

ISBN: 978-1-61804-228-6

A Novel Delay and Overshoot Estimation model for VLSI Global Interconnects

M. Kavicharan, N.S. Murthy, and N. Bheema Rao

***Abstract*—** In this paper, we propose a novel, simple and accurate delay and overshoot estimation model for VLSI Global Interconnects, based on new matrix Pade-type approximant (MPTA). This model reduces the computational complexity by considering rational function denominator as scalar polynomial and avoiding matrix inversion. The proposed model provides a simpler rational function approximation for estimating delay and overshoot in lossy VLSI interconnects. With the reduced order lossy interconnect transfer function, finite ramp responses are obtained and line delay and signal overshoot are estimated. The estimated delay and overshoot values are compared with the Pade model and HSPICE W-element model. The 50% delay results are in good agreement with those of HSPICE within 0.5% error while the overshoot error is within 1% for a 1 mm long interconnects. For global lines of length more than 1 mm in SOC (system on chip) applications, the proposed model is found to be nearly two times more accurate than existing model. Furthermore the proposed model is computationally more efficient than HSPICE and Pade model.

***Keywords*—** Delay, matrix rational model, ramp input, RLC interconnects, transient analysis, transfer function, new MPTA approximant.

I. Introduction

ACCURATE estimation of delay and overshoot is crucial for the design of high speed systems at VLSI technology. As the physical dimensions in VLSI technologies scale down, interconnect delay dominates the gate delay in determining circuit performance [1]. Hence, for the design of complex circuits, simple, fast and more accurate analytic models are useful for IC designers to predict the interconnect effects.

Originally VLSI interconnects were modeled as RC lines and single pole Elmore-based models [2], [3] because of long channel device delay dominance over negligible interconnect delay. However the Elmore model fails at high frequencies since it does not consider the inductance effects [4]. It is necessary to use a second-order model, which includes the effect of inductance. Kahng et al. considered equivalent Elmore delay model based on the Resistance Inductance and Capacitance (RLC) of the interconnects [4] and [5]. Ismail et al. [6] proposed two pole model to capture far end time domain solution for single line interconnect.

A simplified voltage transfer function obtained using Taylor series approximation for transient analysis [7], [8] has less accuracy in delay calculation. Nakhla et al. [9] use modified nodal analysis (MNA) for obtaining far end and near end responses of interconnects. Roy [10] extended [9] for obtaining more accurate far end responses of coupled RLC interconnects using delay algebraic equations.

A matrix rational-approximation model for SPICE analysis of high-speed interconnects is presented by Dounavis et al. [11], [12]. However, the approximations made to derive these models contributed to more inaccuracy. This has been improved using Pade approximation model [13] to estimate the delay of interconnects. All the above models still suffer from accuracy and computational efficiency and need better models to efficiently estimate delay and overshoot of interconnects.

In this paper, we present an improved analytic delay model by extending the concepts developed by Dounavis et al. [11]-[13] for on-chip RLC interconnects. The estimated delay and overshoot values of the proposed model are compared with Pade model [13] and HSPICE. The proposed model is based on new matrix Pade type approximant (MPTA) [14] and [15], which is simple in structure and easier to implement. For the same order (2/2), the proposed model offers better accuracy than Pade model for global interconnects of length 1-5 mm. The proposed model is used to solve the Telegrapher's equations for the first time.

The new MPTA model [15] has matrix Pade-type approximation, whose denominator is a scalar polynomial in terms of a matrix-valued linear functional on the polynomial space. The Pade model with rational matrix approximation has numerator and denominator matrices which need inverse matrix operations leading to severe computational complexity. The proposed model reduces the computational complexity by considering rational function denominator as scalar polynomial and avoiding matrix inversion.

This work was sponsored by the MHRD, Govt. of India as a Research Project on Modeling and Noise Reduction in VLSI Interconnect Structures in the DSM Regime.

M. Kavicharan is pursuing his Ph.D in the Dept. of ECE at the National Institute of Technology, Warangal, India. (phone: 91-9010614822; e-mail: kavicharan@nitw.ac.in).

N. S. Murthy is a senior Professor at the National Institute of Technology, Warangal, India. (e-mail: nsm@nitw.ac.in).

N. Bheema Rao is is a Assoc. Professor in the Dept. of ECE at the National Institute of Technology, Warangal, India. (e-mail: nbr.rao@gmail.com).

The remainder of the paper is organized as follows. Section II briefly describes the mathematical analysis to determine the linear transfer function of RLC interconnects and to find the transient analysis. Section III presents the proposed new MPTA model for single RLC line, while section IV deals with the comparison of the proposed model with Pade and standard HSPICE models. Conclusions appear at the section V.

II. Analysis of RLC Interconnect

The analysis of on-chip RLC interconnects begins with Telegrapher's equations in frequency domain. All the closed-form RLC interconnects models assume quasi-TEM (transverse electromagnetic) mode of signal propagation. The Telegrapher's equations are a pair of linear partial differential equations, which illustrate the voltage and current on a transmission line with distance and time as transmission line variables.

The solution of interconnects are described by telegrapher's equations as

$$\frac{\partial}{\partial x}V(z,s) = -(R + sL)I(z,s) \quad (1)$$

$$\frac{\partial}{\partial x}I(z,s) = -sCV(z,s) \quad (2)$$

where 's' is a Laplace-transform variable, z is a variable which represents position; $V(z,s)$ and $I(z,s)$ stand for the voltage and current vectors of the transmission line, respectively, in the frequency domain; and R, L and C are the per unit length (p.u.l.) resistance, inductance, and capacitance matrices, respectively.

The solution of (1) and (2) can be written as an exponential matrix function as

$$\begin{bmatrix} V(d,s) \\ -I(d,s) \end{bmatrix} = e^{\phi d}\begin{bmatrix} V(0,s) \\ I(0,s) \end{bmatrix} \quad (3a)$$

where

$$\phi = \begin{bmatrix} 0 & -Z \\ -Y & 0 \end{bmatrix}$$

In (2) 'd' is the length of the transmission line, with Z=R+sL and Y=sC. The exponential matrix of (3a) can be written in terms of cosh and sinh functions as

$$e^{\phi d} = \begin{bmatrix} \cosh\left(d\sqrt{ZY}\right) & -Y_0^{-1}\sinh\left(d\sqrt{YZ}\right) \\ -Y_0\sinh\left(d\sqrt{YZ}\right) & \cosh\left(d\sqrt{YZ}\right) \end{bmatrix} \quad (3b)$$

where

$$Y_0 = Y(\sqrt{YZ})^{-1}$$

Equation (3a) does not have a direct representation in the time domain, so it is difficult to analytically predict the delay and overshoot of transmission lines. Hence, there exists demand for approximate models. The basic idea of the matrix rational-approximation model is to use predetermined coefficients to analytically obtain rational functions for (3a). To obtain a passive model, the exponential function is approximated and the resultant model is used for obtaining time response.

A single RLC line is shown in Fig. 1. The line is driven by a 1-V finite ramp with rise times of 0.1 ns and 0.05 ns. This represents a point-to-point interconnection driven by a transistor (modeled as a resistance R_s) and connected to the next gate (modeled as a capacitance C_l).

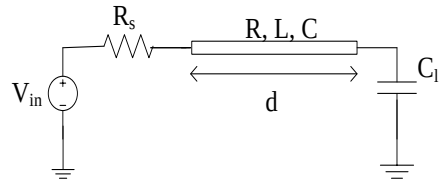

Fig.1. Circuit model of the single-line distributed RLC interconnect.

$$V_f = \frac{V_{in}}{(1+sR_sC_l)\cosh(\Gamma d) + (R_sY_0 + sC_lY_0^{-1})\sinh(\Gamma d)} \quad (4)$$

where

$$\Gamma = \sqrt{YZ},$$

In (4), R_s is the source resistance at the near end, C_l is the load capacitance at the far end, and V_{in} is the input voltage. It is extremely difficult to find the time domain response of this complex transfer function, hence an approximate transfer function has been derived using new MPTA model. The time response of this function is used for estimation of delay and overshoot in single RLC interconnect.

III. Proposed New MPTA Model

This model is based on new MPTA approximation [14], [15]. For the power series expansion of a function f(x), where 'x' is a complex variable

$$f(x)=C_0+C_1x+C_2x^2+\ldots+C_nx^n+\ldots,\ C_i=(C_i^{(uv)}) \in C^{sxt};\ x \in C \quad (5)$$

The exponential matrix (4) can be written as above series and the closed form rational function approximation for an exponential matrix in (4) is written as

$$R_{mn}(x) = P_{mn}(x)/\tilde{v}(x) \quad (6)$$

is called as new MPTA approximant and is denoted by (m/n) f(x)

where

$$P_{mn}(x) = \tilde{v}(x)\sum_{i=0}^{m-n} c_i x^i + x^{m-n+1}\tilde{W}_l(x), \quad (7)$$

$$\tilde{v}(x) = x^n v(x^{-1}), \quad (8)$$

Let 'v' be a scalar polynomial of degree n

$$v(x) = b_0 + b_1x + \ldots\ldots + b_nx^n \quad (9)$$

These coefficients b_0 to b_n can be calculated using [15].

Further more

$$\tilde{W}_l(x) = x^{n-1} W_l(x^{-1}), l = m - n + 1 \quad (10)$$

$$\tilde{W}_l(x) = \sum_{l=0}^{n-1} \left(\sum_{i=0}^{l} b_{n-l+i} c_{i+m-n+1} \right) x^l \quad (11)$$

For the 2/2 approximation order, the rational approximation is

$$R_{22}(x) = P_{22}(x) / \tilde{v}(x) \quad (12)$$

where

$$P_{22}(x) = \tilde{v}(x) c_0 + z \tilde{W}_l(x)$$

and

$$v(x) = b_0 + b_1 x + b_2 x^2$$

$$(x) = b_0 + b_1 x + b_2 x$$

Thus, R_{22} represents a table of rational functions, each element of which is an approximant of original series (5) and obtained from the series of below steps.

Calculation procedure for estimating delay and overshoot using new MPTA approximants are as follows.

(i) Telegrapher's equations are solved and the solution is written as exponential matrix and the derived transfer function (4) is approximated using the new MPTA model.
(ii) The coefficients W_1 of the resultant exponential function are calculated using (11).
(iii) $P_{mn}(x)$ can be calculated for any order of m/n from the relation (7). However, for validation with Pade model (2/2), the proposed model (12) is calculated with m=n=2
(iv) Total sums of the numerator $P_{22}(x)$ and the denominator are calculated and the approximated transfer function is obtained.
(v) Ramp response of the transfer function is obtained to estimate delay and overshoot of interconnect.

IV. Simulation Results

A single RLC line is presented in this section to demonstrate the validity and efficacy of the proposed model. The results obtained using MATLAB R2010a operating on HP 64-bit Intel i5 processor with clock speed of 2.53 GHz, are compared with HSPICE W-element model.

The typical interconnect parameters [13] considered for simulation of single RLC interconnect are given in Table-I. The Pade approximation [13], and proposed new MPTA model are implemented in MATLAB for the same set of input parameters.

Table I: The values of Interconnects parameters [13]

V_{dd}	1 V
Length	0.1 mm to 0.5 cm
Resistance	88.29 Ω/cm
Capacitance	1.8p F/cm
Inductance	15.38 nH/cm
Input ramp rise/fall time	0.1 ns
Source resistance	20 Ω to 100 Ω
Load capacitance	0.05 fF to 0.1 fF

The far-end response to a finite ramp input of single interconnect is plotted in Fig. 2. The plots compare the responses of proposed and Pade model [13]. It is evident from Fig. 2 that, the proposed new MPTA model and Pade model [13] match very closely for the same order of 2/2. However, computational complexity of the proposed model is less than that of the Pade model, because for the same accuracy the former needs less number of poles than the latter.

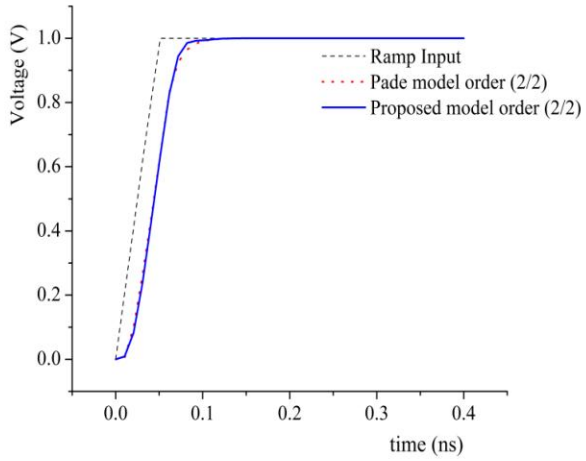

Fig.2. Transient response of single interconnect line, with length = 0.5 mm, R_s=50 Ω, C_l=50 fF and rise time=0.05 ns.

Fig. 3 shows the results of finite ramp response for the rise time of 0.1 ns, line with length of 0.5 mm, source resistance of 100 Ω and load capacitance of 100 fF. The obtained overshoot of proposed model matches with existing Pade model [13] for the same approximation order of 2/2.

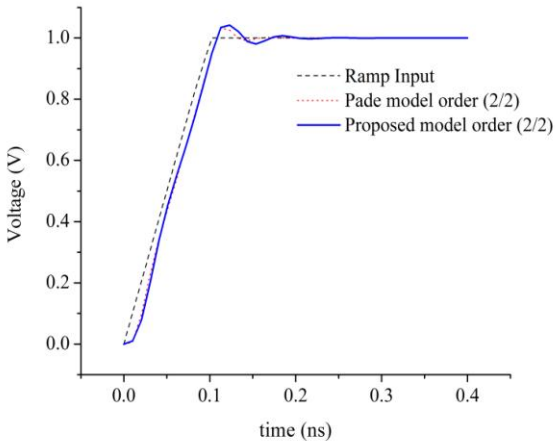

Fig.3. Ramp response of single line when length =0.5 mm, R_s=50 Ω and C_l=50 fF and rise time=0.1 ns.

Tables II and III give the comparisons of 50% delay and overshoot values obtained using HSPICE W element model, Pade model [13] and proposed model for various lengths,

source Resistances, load Capacitances and rise times. These tables include the average and maximum error percentages values of Pade model and proposed model with respect to HSPICE. From Table II, the Pade model of order 2/2 has average and maximum error of 0.73% and 3.9%, whereas proposed model has 0.41% and 1.53% respectively.

For global interconnects (1-5 mm) the proposed model works much better than Pade model for delay and overshoot estimation. Both Pade and proposed models perform similarly for smaller length (<1 mm) interconnects, but for longer lengths of 5mm, proposed model has less error percentage.

From Table III, it is observed that the Pade model [13] has maximum overshoot error of 1.05%, while the proposed model has an error of 0.96%. In the case of overshoot estimation the proposed model is best for all cases. Overall, the average error percentages of delay and overshoot estimations are within 1% for the proposed model.

Table II: Comparisons of 50% delay of HSPICE W Element, Pade model and proposed model for various lengths, source Resistances, load Capacitances and input Ramp rise times.

L (mm)	R_S (Ω)	C_l (fF)	t_r (ns)	HSPICE	Pade model [13] order 2/2	Proposed Model order (2/2)
				50% delay (ps)	*50% delay (ps)*	*50% delay (ps)*
0.1	50	50	0.1	53.45	53.5	53.5
	100	100	0.05	36.45	36.5	36.5
0.5	50	50	0.1	57.33	57.5	57.6
	100	100	0.05	43.79	43.9	43.95
1	50	50	0.1	61.92	61.95	61.94
	100	100	0.05	52.94	53.1	53.05
5	50	50	0.1	135.6	136.7	136.5
	100	100	0.05	125.11	120.2	123.2
Average error % w.r.t. HSPICE					0.73	0.41
Maximum error % w.r.t. HSPICE					3.9	1.53

Table III: Comparisons of Overshoot of HSPICE W Element, Pade model and proposed model for various lengths, source Resistances, load Capacitances and input Ramp rise times.

L (mm)	R_S (Ω)	C_l (fF)	t_r (ns)	HSPICE	Pade model [13] order (2/2)	Proposed Model order (2/2)
				Overshoot (V)	*Overshoot (V)*	*Overshoot (V)*
0.1	50	50	0.1	1.004	1.005	1.005
	100	100	0.05	1	1	1
0.5	50	50	0.1	1.035	1.045	1.045
	100	100	0.05	1	1	1
1	50	50	0.1	1.071	1.081	1.075
	100	100	0.05	1	1	1
5	50	50	0.1	1.143	1.155	1.147
	100	100	0.05	1	1	1
Average error % w.r.t. HSPICE					0.378	0.209
Maximum error % w.r.t. HSPICE					1.05	0.96

The computational complexity of the proposed model is less as compared to Pade model, because inverse matrix operation is not needed, which reduced the number of poles required from 5 to 3 at the same approximation order (2/2). As a result the CPU computation time is less as compared to Pade model.

Table IV: CPU time comparison of various models with HSPICE models

Pade model [13] (ms)	Proposed model (ms)	HSPICE W element model (ms)
40	28	15

The CPU computation time to calculate the transfer functions of various models into poles and residues is provided in Table IV. The CPU time of proposed model is a onetime expense to find poles and residues for any input switching pattern, whereas HSPICE analysis is based on numerical integration that has to be performed for each input switching pattern, thus proving that the proposed model is computationally more efficient.

V. CONCLUSION

This paper presents a novel MPTA based closed form model for delay and overshoot estimation of high speed VLSI interconnects in DSM regime. A single line interconnect has been used for validating the proposed model by comparing with the Pade model and HSPICE. The delay and overshoot estimations average error percentages are within 1% for the proposed model. In SOC (system on chip) applications, for global lines of lengths 1-5 mm the proposed model is found to be more accurate than existing model. The proposed model is computationally more efficient than HSPICE and Pade model.

ISBN: 978-1-61804-228-6

REFERENCES

[1] Semiconductor Industry Association, The International Technology Roadmap for Semiconductors, 1999.

[2] W. C. Elmore, "The transient response of damped linear networks with particular regard to wideband amplifiers," *J. Appl. Phys*., vol. 19, no.1, pp. 55–63, Jan. 1948.

[3] T.Sakurai, "Closed-form expressions for interconnection delay, coupling, and crosstalk in VLSI's," *IEEE Trans. Electron Devices*, vol. 40, no. 1, pp. 118–124, Jan. 1993.

[4] Kahng A B, Muddu S, "An analytical delay model for RLC interconnects", *IEEE Trans. Computer-Aided Design of Integrated Circuits and Systems*, pp. 1507−1514, 1997.

[5] Kahng A B, Muddu S, "Two-pole analysis of interconnection trees", in *1995 Proc. of IEEE MCMC Conf.(MCMC-95)*, Santa Cruz, California, USA, pp. 105−110, 1995.

[6] Xiaopeng Ji, Long Ge, Zhiquan Wang, "Analysis of on-chip distributed interconnects based on Pade expansion," *Journal of Control Theory and Applications*, 7 (1) pp. 92–96, 2009.

[7] Ren Yinglei, Mao Junfa and Li Xiaochun, "Analytical delay models for RLC interconnects under ramp input", *Frontiers of Electrical and Electronic Engineering in China*, vol. 2, pp. 88-91, March 2006.

[8] Y. I. Ismail, E. G. Friedman, and J. L. Neves, "Equivalent Elmore delay for RLC trees," *IEEE Trans. Comput.-Aided Design Integr. Circuits Syst*.,vol. 19, no. 1, pp. 83–97, Jan. 2000.

[9] N.Nakhla, A.Dounavis, R.Achar, M.Nakhla,"DEPACT:Delayextraction based Passive Compact Transmission-Line Macromodeling algorithm," *IEEE Transactions on Advanced Packaging*, vol. 28, issue 1, pp. 13-23, Feb 2005.

[10] S.Roy, A. Dounavis, "Efficient Delay and Crosstalk Modeling of RLC Interconnects using Delay Algebraic Equations," *IEEE Transactions on Very Large Scale Integration Systems*, vol. 2, issue 2, pp. 342-345, Feb. 2011.

[11] A. Dounavis, R. Achar, and L. Xin, "Passive closed-form transmission-line model for general-purpose circuit simulators," *IEEE Trans. Microw. Theory Tech*., vol. 47, no. 12, pp. 2450–2459, Dec. 1999.

[12] A. Dounavis, R. Achar, and M. Nakhla, "A general class of passive macromodels for lossy multiconductor transmission lines," *IEEE Trans. Microwave Theory Tech*., vol. 49, no. 10, pp. 1686–1696, Oct. 2001.

[13] S. Roy and A. Dounavis, "Closed-Form Delay and Crosstalk Models for RLC On-Chip Interconnects using a Matrix Rational Approximation," *IEEE Transactions on Computer-Aided Design of Integrated Circuits and Systems*, vol. 28, issue 10, pp. 1481 - 1492, Oct.2009.

[14] C. Brezinski. Pade-Type Approximation and General Orthogonal Polynomials. Birkhäuser, Basel, 1980.

[15] C. Q. Gu. Matrix Pade-type approximant and directional matrix Pade approximant in the inner product space. *J Comput. Appl. Math*. 2004, 164-165: 365-385.

Using Non-Sinusoidal Inputs for Efficient Wireless Power Transmission

Yuta Yamamoto, Ichijo Hodaka, Kazuya Yamaguchi and Takuya Hirata

***Abstract*—One of most important specification for wireless power transmission is power efficiency from a primary power supply to a secondary power consumption. It is common in many literature to use a sinusoidal voltage at the primary supply with a resonant frequency for the purpose of maximizing power consumption at the secondary load. However, in general, it might be possible that one has better power efficiency when using non-sinusoidal waves as the power supply voltage. This paper proposes to use non-sinusoidal voltage inputs for an efficient wireless power transmission. Proposed idea is to add a feedback to a sinusoidal wave. Illustrative examples how efficiently our input with a feedback will adjust the purely sinusoidal input are shown.**

***Keywords*—wireless power transmission, non-sinusoidal voltage, feedback.**

I. Introduction

WIRELESS power transmission has attracted many researchers for demand of a new type of power transmission. In 2007, wireless power transmission was proven to have a practical value of power transmission with a longer distance than it was used before [3]. After the pioneering work, the main interest of performance of wireless power transmission has been the magnitude of average power transmitted from a primary side to a secondary side. Maximizing the transmitted power is achieved by adjusting the frequency of voltage supply at the primary side to the resonant frequency of the whole circuit, as pointed out and utilized in many literature. Another important performance of wireless power transmission system is how efficiently one can transmit power from the primary side to the secondary side. It is revealed in [1][2] that using the resonant frequency does not lead to optimization of efficiency. Thus a problem to be solved is how to keep the total transmitted power with raising the efficiency of power transmission, if the resonance is not equivalent to the maximal efficiency. This situation, of course, depends on the circuit to be used for wireless power transmission. This paper proposes that we use the idea of feedback with the resonant sinusoidal supply voltage. The feedback mechanism has in nature ability of adjustment against change or variation of circuit parameters. Therefore, using feedback has a possibility to attain better efficiency without losing transmitted power. Numerical examples will show the possibility is indeed the case.

Y. Yamamoto is with the Department of Agriculture and Engineering, University of Miyazaki, 1-1, Gakuen-kibanadai-nishi Miyazaki, 889-2192 JAPAN e-mail: (nc12006@student.miyazaki-u.ac.jp).

I. Hodaka is with the Department of Environmental Robotics, University of Miyazaki, 1-1, Gakuen-kibanadai-nishi Miyazaki, 889-2192 JAPAN e-mail: (hij@ieee.org).

K. Yamaguchi is with the Department of Agriculture and Engineering, University of Miyazaki, 1-1, Gakuen-kibanadai-nishi Miyazaki, 889-2192 JAPAN e-mail: (nc13001@student.miyazaki-u.ac.jp).

T. Hirata is with the Department of Electrical and Electronic Engineering , University of Miyazaki, 1-1, Gakuen-kibanadai-nishi Miyazaki, 889-2192 JAPAN e-mail: (tc12030@student.miyazaki-u.ac.jp).

II. Problem statement

In this paper, we study how to attain better efficiency of wireless power transmission circuits. Typical configuration of wireless power transmission circuits is depicted in Fig. 1.

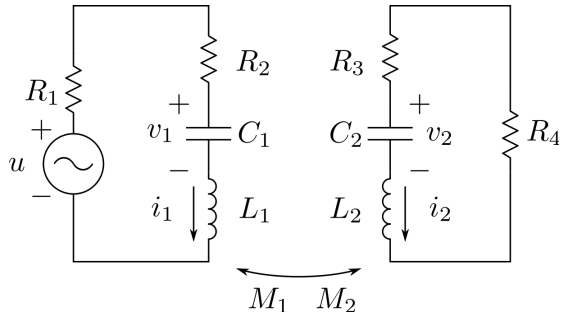

Fig. 1. Wireless power transmission circuit

Any wireless power transmission has a pair of inductors (L_1 and L_2 in Fig. 1) which enables power transmission with wireless connection. In practical situation, inductors are not ideal, i.e., they have unexpected characteristics besides the pure relation that the voltage across the inductor is proportional to the time-derivative of the current through the inductor. These unexpected characteristics are actually expected when we use them for the purpose of wireless power transmission − they include capacitive characteristics even if the capacitance (C_1 and C_2 in Fig. 1) would be very small. Thus we recognize that a pair of coils could bring a phenomenon of resonance when using a sinusoidal input [4][5][6](u in Fig. 1). This leads to maximization of average power into the receiving side, as the other literature stated. Maximization of power at the receiving side is one of desired specification on wireless power transmission, and it is accomplished by tuning the frequency of voltage supply input around the resonant frequency. This principle is valid even if we want to take resistive characteristics (represented by R_2 and R_3 in Fig. 1) of coils or output resistance (R_1 in Fig. 1) in the supply voltage into account. Another important specification on wireless power transmission is efficiency of the circuits. In general, efficiency of wireless power transmission system is defined as a ratio of the average power consumed at a load (R_4 in Fig. 1) in

ISBN: 978-1-61804-228-6

a receiving side to the average power generated at a supply voltage in a transmitting side. If we decide to neglect any resistive element except for a load, we will have one hundred percent efficiency simply because we have no element with energy consumption. However, in order to aim a detailed analysis, if we decide to consider resistive elements in the coils, we will inevitably waste a small amount of power, that is, we have to suppose an efficiency less than one hundred percent in practice. The problem of our study is to investigate how to accomplish:

(1) Maximizing the average power at the load in the receiving side and
(2) Increasing the average power efficiency from the transmitting side to the receiving side.

Notice that there are cases that we cannot accomplish the both above simultaneously when we use a sinusoidal input with a pure frequency [1]. Thus we stands on the point of view that we should not necessarily use sinusoidal inputs in this paper.

III. Proposed Idea

Our problem is to obtain a method to maximize the average power at the load with improving efficiency of wireless power transmission. Our idea is that we can use non-sinusoidal inputs of supply voltage. To be precise, we use a *feedback* plus a sinusoidal signal for a possible supply input. To explain our idea in a mathematical setting, we describe the set of equations governing the dynamics of the wireless power transmission circuit in Fig. 1. Especially we prefer to describe them as a so-called *state-space equation* in the following.

$$\dot{x} = Ax + Bu \tag{1}$$

$$A = \begin{bmatrix} 0 & 0 & \frac{1}{C_1} & 0 \\ 0 & 0 & 0 & \frac{1}{C_2} \\ \frac{-L_2}{\Delta} & \frac{M_2}{\Delta} & \frac{(-R_1-R_2)L_2}{\Delta} & \frac{(R_4+R_3)M_2}{\Delta} \\ \frac{M_1}{\Delta} & \frac{-L_1}{\Delta} & \frac{(R_1+R_2)M_1}{\Delta} & \frac{(-R_4-R_3)L_1}{\Delta} \end{bmatrix} \tag{2}$$

$$B = \frac{1}{\Delta}\begin{bmatrix} 0 \\ 0 \\ L_2 \\ -M_1 \end{bmatrix} \tag{3}$$

$$\Delta = L_1L_2 - M_1M_2 \tag{4}$$

$$x = \begin{bmatrix} v_1 & v_2 & i_1 & i_2 \end{bmatrix}^T \tag{5}$$

A common strategy is to use a sinusoidal input u with the resonant frequency. On the other hand, our idea is to use an input in the form

$$u = u_0 + Kx, u_0 = sin\omega t \tag{6}$$

where omega is set to a frequency and K is a state feedback gain. The problem here is how to choose the feedback gain K. To solve it, we notice that the matrix A is decomposed into $A = A_0 - BK$, where

$$A_0 = \begin{bmatrix} 0 & 0 & \frac{1}{C_1} & 0 \\ 0 & 0 & 0 & \frac{1}{C_2} \\ \frac{-L_2}{\Delta} & \frac{M_2}{\Delta} & \frac{-R_1L_2}{\Delta} & \frac{(R_4+R_3)M_2}{\Delta} \\ \frac{M_1}{\Delta} & \frac{-L_1}{\Delta} & \frac{R_1M_1}{\Delta} & \frac{(-R_4-R_3)L_1}{\Delta} \end{bmatrix} \tag{7}$$

$$K = \begin{bmatrix} 0 & 0 & R_2 & 0 \end{bmatrix} \tag{8}$$

If we apply the input (6) with K above, the state-space equation is also rewritten as

$$\dot{x} = A_0x + Bu_0, \tag{9}$$

whose ' A-matrix ' A_0 is equivalent to A with $R_2 = 0$. That is, we can cancel out R_2 which is one of factors causing undesired energy consumption. Now our problem is reduced into a usual situation. That is, we concentrate on maximization of average power at the load. Therefore, we just choose omega as the resonant frequency of the system (9). Our proposed idea is described by the block-diagram in Fig. 2.

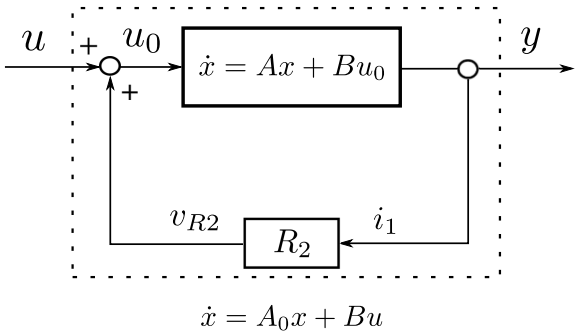

Fig. 2. feedback system

To realize the input, we have to measure the current i_1 by using an appropriate sensor, and feed it back into the supply voltage. This will be done by using a microcontroller or operational amplifiers.

IV. Numerical Examples

To illustrate the effect of the proposed idea in the previous section, we use numerical values of elements in the circuit as I below.

Table. I
CIRCUIT PARAMETERS

	value
R_1, R_4	10 [Ω]
R_2, R_3	0.01 [Ω]
C_1, C_2	1 [nF]
L_1, L_2	10 [μH]
M_1, M_2	0.1 [μH]

We select angular frequency ω based on resonance angular frequency ω_r which is known from the gain diagram of this system in Fig. 3. In this case, we adopt $\omega = 9.95 \times 10^6$[rad/s].

ISBN: 978-1-61804-228-6

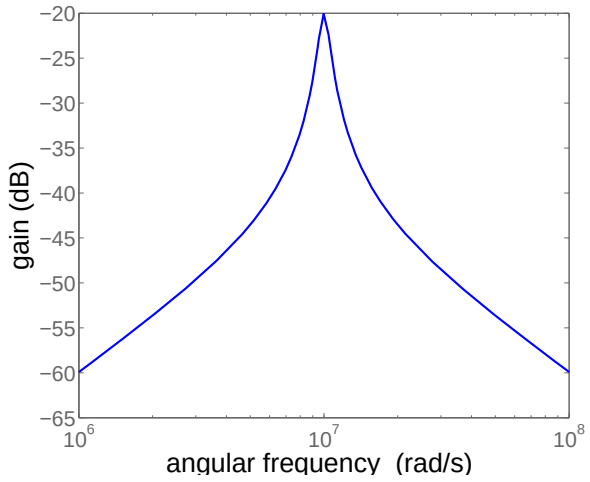

Fig. 3. gain diagram

V. COMPARING THE POWER SUPPLY EFFICIENCY

We compare the power transmission efficiency of each voltage power source u_0 and u. The average power $\bar{P}_1$ at power source and $\bar{P}_4$ at R_4 are expressed in

$$\bar{P}_1 = \beta_3 - R_1(\alpha_3^2 + \beta_3^2) \quad (10)$$

$$\bar{P}_4 = R_4(\alpha_4^2 + \beta_4^2) \quad (11)$$

where

$$\begin{bmatrix} \alpha_1 & \alpha_2 & \alpha_3 & \alpha_4 \end{bmatrix}^T = -\omega(\omega^2 I + A^2)^{-1}B \quad (12)$$

$$\begin{bmatrix} \beta_1 & \beta_2 & \beta_3 & \beta_4 \end{bmatrix}^T = -A(\omega^2 I + A^2)^{-1}B. \quad (13)$$

Then, the power transmission efficiency η is

$$\eta = \frac{\left|\bar{P}_4\right|}{\left|\bar{P}_1\right|}. \quad (14)$$

We show $\left|\bar{P}_1\right|$, $\left|\bar{P}_4\right|$, η of each voltage power source u_0 and u in II.

Table. II
CIRCUIT PARAMETER

	R_2=0.01[Ω]	R_2=0[Ω]
$\left\|\bar{P}_1\right\|$[w]	1.05×10^{-3}	9.51×10^{-4}
$\left\|\bar{P}_4\right\|$[w]	9.49×10^{-4}	9.51×10^{-4}
η[%]	90.6	99.9

According to II, we obtained better η when we use u for voltage power source.

VI. CONCLUSION

In this paper, we proposed a method to improve the power transmssion efficiency of the wireless power transmission system. We shown numerical examples of canceling the parasitic resistance by adding v_{R_2} to voltage power source. We compared power transmission efficiency of sinusoidal input u_0 and our proposed input u. Finally, we demonstrated our proposed input is better than sinusoidal input as an input for wireless power transmission.

REFERENCES

[1] K. Yamaguchi and T. Hirata, *"Efficient Wireless Power Transfer-Resonance Does Not Imply High Efficiency,"* private communication

[2] T. Hirata and K. Yamaguchi, *"Symbolic Computer-Aided Design for Wireless Power Transmission,"* private communication

[3] A. Kurs, and A. Karalis, *"Wireless Power Transfer via Strongly Coupled Magnetic Resonances,"* Science 317, pp. 83-86, August 2007

[4] C. Huang and T. Nimje, *"Goodbye Wires: Approach to Wireless Power Transmission,"* ISSN 2250-2459, Volume 2, Issue 4, April 2012

[5] R. L. Vitale and D. Civilian, *"DESIGN AND PROTOTYPE DEVELOPMENT OF A WIRELESS POWER TRANSMISSION SYSTEM FOR A MICRO AIR VEHICLE,"* Submitted in partial fulfillment of the requirements for the degree of MASTER OF SCIENCE IN ELECTRICAL ENGINEERING, June 1999

[6] M. Yang and Q. Ma, *"Wireless power transmission system for charging the inspection robot on power transmission lines,"* Proceedings of the 2nd International Conference on Computer Science and Electronics Engineering (ICCSEE 2013)

An Efficient Distributed Tree Structure Modelling for VLSI circuits

M.Kavicharan, N.S.Murthy, and N. Bheema Rao

***Abstract*—**In this paper a closed-form matrix rational model for the computation of finite ramp responses of distributed Resistance Inductance Capacitance (RLC) tree in VLSI circuits is presented. This model allows the numerical estimation of delay in distributed RLC tree. The proposed method is based on the U-transform, which provides rational function approximation for obtaining passive interconnect model. With the reduced order lossy interconnect transfer function, finite ramp responses are obtained and tree structure delay at various nodes are estimated. The estimated delay is compared with the Pade method and HSPICE W-element model. The average 50% delay results are in good agreement with those of HSPICE within 4% error. For global lines of each branch lengths 0.5 mm and above the proposed method is found to be more accurate than existing Pade model.

***Keywords*—**Delay, matrix rational model, ramp input, RLC interconnects, transient analysis, transfer function, tree structure, U-approximation.

I. Introduction

IN general interconnects in digital VLSI circuits are in the form of tree structure and driven by CMOS gates. As the physical dimensions in VLSI technologies scale down and operating speed continues to increase, interconnect delay dominates the gate delay in determining circuit performance [1]. The nets in a VLSI circuit are often structured as tree interconnects rather than as single interconnect. Hence, for the design of complex circuits in DSM regime it is necessary to have computationally economical and accurate tree interconnect delay models.

Traditionally VLSI interconnects were modelled as RC lines and single pole Elmore-based models [2], [3] because of long channel device delay dominance over negligible interconnect delay. However for high speed DSM VLSI interconnects, inductance effects are becoming progressively important and can no longer be ignored. Under these circumstances, the Elmore model fails since it does not consider the inductance effects [4]. It is necessary to use a second-order model, which includes the effect of inductance. Kahng et al. considered equivalent Elmore delay model based on the Resistance Inductance and Capacitance (RLC) of the interconnects [4] and [5]. Ismail et al. [6] proposed two pole model to capture far end time domain response for single line interconnect. Many delay models have been proposed to calculate delay of single line interconnects [7]-[9]; however, these models did not consider the analysis of tree structures.

Interconnects of ICs (integrated circuits) are generally in the form of tree rather than a single line. Thus, the time-domain response and delay estimation for interconnect trees are of primary importance. Various techniques have been proposed for delay estimation of interconnect trees, which can be classified as simulation techniques and analytical formulas. Simulation techniques such as SPICE are most accurate, but inefficient. Initially, the Elmore delay model was developed for lumped resistor-capacitor (RC) trees in [10] and later it was extended to distributed RC trees in [11] and lumped resistor-inductor-capacitor (RLC) trees in [12] and [13]. These models provide analytical delay formulas by simplifying the sub-tree interconnect with capacitance model, which results in limited accuracy. To include transmission line effect, a numerical method based on ABCD matrix and moment matching technique was developed for distributed RLC trees in [14]. All the above models still suffer from various inaccuracies and need improvement for accurate delay estimations.

The performance of a synchronous circuit is heavily dependent on the design of a clock distribution network. RLC interconnect trees are common structures in clock networks. An accurate model of an RLC interconnect tree, therefore, is critical in modern digital circuit design. In this paper, an analytic delay model is presented by extending the concepts developed in [16] for on-chip RLC interconnect trees. The proposed model is based on U-transform [18] and [19], which is simple in structure and easier to implement. For a given number of terms used in the transform, the U-approximant requires less algebraic manipulations than the Pade scheme and thus computationally less expensive. The U-transform is used to solve the Telegrapher's equations of tree interconnect model for the first time. The proposed algorithm is tested for both single interconnect and tree structure networks.

This work was sponsored by the MHRD, Govt. of India as a Research Project on Modeling and Noise Reduction in VLSI Interconnect Structures in the DSM Regime.

M. Kavicharan is pursuing his Ph.D in the Dept. of ECE at the National Institute of Technology, Warangal, India. (phone: 91-9010614822; e-mail: kavicharan@nitw.ac.in).

N. S. Murthy is a senior Professor at the National Institute of Technology, Warangal, India. (e-mail: nsm@nitw.ac.in).

N. Bheema Rao is is a Assoc. Professor in the Dept. of ECE at the National Institute of Technology, Warangal, India. (e-mail: nbr.rao@gmail.com).

Significant improvement in 50% delay estimation is achieved when compared to existing pade model [17].

The remainder of the paper is organized as follows. Section II briefly outlines the mathematical background to determine the transfer function of RLC interconnect to find the transient analysis. Section III presents the proposed U-model for single RLC line, whereas distributed tree modeling is presented in section IV. For validation of the proposed model simulation results are compared with standard HSPICE and reported in sections V. Conclusions and future scope appear at the end.

II. Analysis of RLC Interconnect

The solution of interconnects are described by telegrapher's equations as

$$\frac{\partial}{\partial x}V(z,s) = -(R+sL)I(z,s) \quad (1)$$

$$\frac{\partial}{\partial x}I(z,s) = -sCV(z,s) \quad (2)$$

where 's' is the Laplace-transform variable, z is a variable which represents position; $V(z,s)$ and $I(z,s)$ stand for the voltage and current vectors of the transmission line, respectively, in the frequency domain; and R, L and C are the per unit length (p.u.l.) resistance, inductance, and capacitance matrices, respectively.

The solution of (1) and (2) can be written as an exponential matrix function as

$$\begin{bmatrix} V(d,s) \\ -I(d,s) \end{bmatrix} = e^{\phi d}\begin{bmatrix} V(0,s) \\ I(0,s) \end{bmatrix} \quad (3)$$

Where

$$\phi = \begin{bmatrix} 0 & -Z \\ -Y & 0 \end{bmatrix}$$

In (3) 'd' is the length of the transmission line, with Z=R+sL and Y=sC. The exponential matrix of (3) can be written in terms of cosh and sinh functions as

$$e^{\phi d} = \begin{bmatrix} \cosh\left(d\sqrt{ZY}\right) & -Y_0^{-1}\sinh\left(d\sqrt{YZ}\right) \\ -Y_0\sinh\left(d\sqrt{YZ}\right) & \cosh\left(d\sqrt{YZ}\right) \end{bmatrix} \quad (4)$$

where

$$Y_0 = Y(\sqrt{YZ})^{-1}$$

Equation (3) does not have a direct representation in the time domain, so it is difficult to analytically predict the delay of transmission lines.

III. Proposed U Model

This model is based on a generalized U-transform [18], [19]. For the power series expansion of a function f(x)

$$f(x) = \sum_{n=0}^{\infty} a_n x^n \quad (5)$$

where ' x ' is a complex variable

$$s_n = \sum_{k=0}^{n-1} a_k x^k \quad (6)$$

where the sequence $\{S_n\}$ is a partial sum of original series f(x).

The closed form rational function approximation for an exponential matrix is

$$u_{kn}(\{S_n\}) = \frac{\sum_{j=0}^{n+k-1} x^i \sum_{j=0}^{k} w_{knj} a_{j-i}}{\sum_{j=0}^{k} w_{knj} x^i} \quad (7)$$

where

Where

$$w_{knj} = (-1)^j \frac{k!}{j!(k-j)!}\frac{(n+k-j)^{k-2}}{a_{n+k-j-1}} \quad (8)$$

Thus u_{kn} represents a table of rational functions, each element of which is obtained from n + k terms of the original sequence $\{S_n, n = 1, 2,...\}$ and is an approximant of the function f(x) specified above.

The basic idea of the matrix rational-approximation model is to use predetermined coefficients to analytically obtain rational functions for (3). To obtain a passive model, the exponential function $e^{\Phi d}$ is approximated using (7) and the resultant model is used for obtaining time response.

A single RLC line is shown in Fig. 1.The line is driven by 1-V finite ramp with rise time of 0.1 ns. This represents a point-to-point interconnection driven by a transistor (modelled as a resistance R_s) and connected to the next gate (modelled as a capacitance C_l).

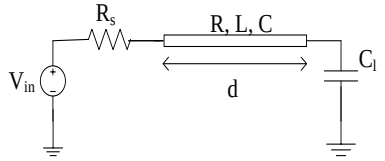

Fig.1. Circuit model of the single-line distributed RLC interconnect.

The frequency-domain solution at the far end is expressed as

$$V_f = \frac{V_{in}}{(1+sR_sC_l)\cosh(\Gamma d) + \left(R_sY_0 + sC_lY_0^{-1}\right)\sinh(\Gamma d)} \quad (9)$$

Where

$\Gamma = \sqrt{YZ}$,

In (9), R_s is the source resistance at the near end, C_l is the load capacitance at the far end, and V_{in} is the input voltage. The exact transfer function of distributed RLC transmission line has cosh and sinh terms, which are multiplied with Y_o and its inverse. It is extremely difficult to find the time domain response of this complex transfer function, hence several approximations are proposed in literature to find the time domain response. An approximate transfer function has been derived using U-transform. This transfer function is inverse Laplace transformed to get time domain response for estimation of delay in single RLC interconnect.

IV. Modelling of Distributed Trees

Interconnect trees are widely used in clock distribution networks. In this section, the proposed U transform model is extended to tree structures. Arbitrarily accurate results can be obtained by increasing the order of model. The computational complexity is linear with the size of the tree and the order of model.

Based on the analysis of single interconnect, the transfer functions for distributed trees can be derived from the above iterative method. The exact transfer functions are hyperbolic, exact, but very complicated. To simplify the transfer functions for distributed trees, the U approximation technique is used.

Fig. 2 shows an example of a distributed RLC tree which is often used to analyze clock distribution networks. Here the driver is modelled as a resistance R_s and connected to the Node N_o. The leaf nodes (N_4 to N_6) are called leaves and connected with load buffers which can be used to drive the RLC trees in the next level. The load buffers are modelled by capacitors C_0 to C_3. All of the branches in the tree are represented by distributed RLC lines. The load capacitances of all leaf nodes are assumed to be same (80 fF). The lengths of interconnect line T_0 to T_6 are 1mm to 3mm as shown in Fig. 2.

The transfer function from N_0 to N_1 is similar to that of single interconnect modeling as presented in last section. The total transfer function from N_0 to N_k is the product of all of the transfer functions along the path.

The transfer function of a single branch can be obtained by (9), in which replace source resistance R_s by 0 and sC_l by Z_L.

The resultant transfer function can be written as

$$V_{f1} = \frac{V_{in}}{\cosh(\Gamma d) + \left(Y_0^{-1} / Z_L\right)\sinh(\Gamma d)} \tag{10}$$

The transfer function between voltage source and certain node N_i can be written as

$$V_{f,i}(s) = \frac{Z_{L,0}}{R_S + Z_{L,0}} \prod_i \left\{ \frac{V_{in}(s)}{\cosh(\Gamma_i d_i) + \left(Y_{0,i}^{-1} / Z_{L,i}\right)\sinh(\Gamma_i d_i)} \right\} \tag{11}$$

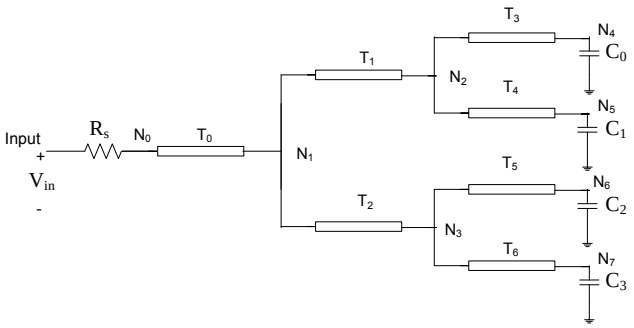

Fig. 2 General interconnect tree.

V. Simulation results

A distributed RLC tree is presented in this section to demonstrate the validity and efficacy of the proposed method. The results obtained using MATLAB R2010a operating on HP 64-bit Intel i5 processor with clock speed of 2.53 GHz, are compared with HSPICE using the W-element method. The Pade approximation and proposed U-approximation are implemented in MATLAB for the same set of input parameters.

The far-end responses to a finite ramp input of tree structure single branch are plotted in Fig. 3 and Fig. 4. The plots compare the responses of proposed, Pade and HSPICE W-element models. Figs. 5 to 6 plot the response at N_2 branch of given tree structure for various interconnect parameters, whereas Figs. 7 to 8 plot the response at N_4. The branches of the tree are assumed to have different interconnect parameters. The branches in the tree can have different parasitic interconnect parameters. The interconnect parameters of T_0, T_3, T_4, T_5 and T_6 structure are R=1480 Ω/cm, L=3.2 nH/cm and C=1.78 pF/cm whereas, T_1 and T_2 have R=88.29 Ω/cm, L=15.38 nH/cm and C=1.8 pF/cm [17]. The time domain responses obtained by various models at nodes N1, N2, N3, N4 and N6 is presented in Figs. 3-8.

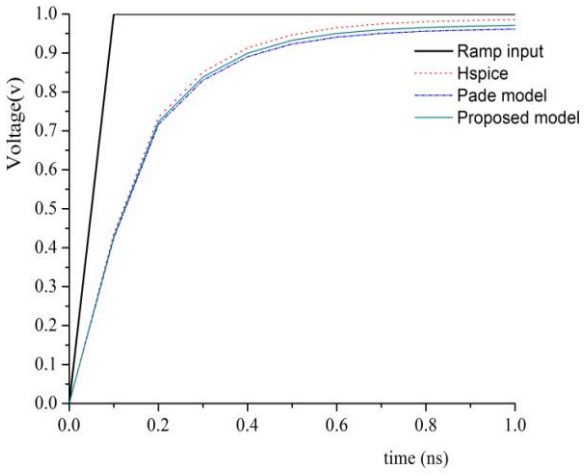

Fig 3. Time domain response at the node N1 of the given Tree structure with branch length = 0.1cm, R_s=50Ω and C_l=80fF.

ISBN: 978-1-61804-228-6

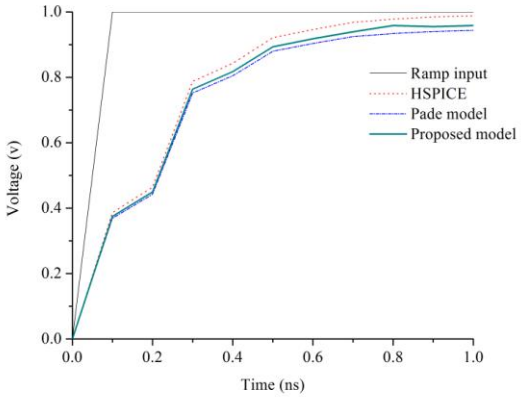

Fig 4. Time domain response at the node N1 of the given Tree structure with branch length = 0.1cm, R_s=100Ω and C_l=100fF.

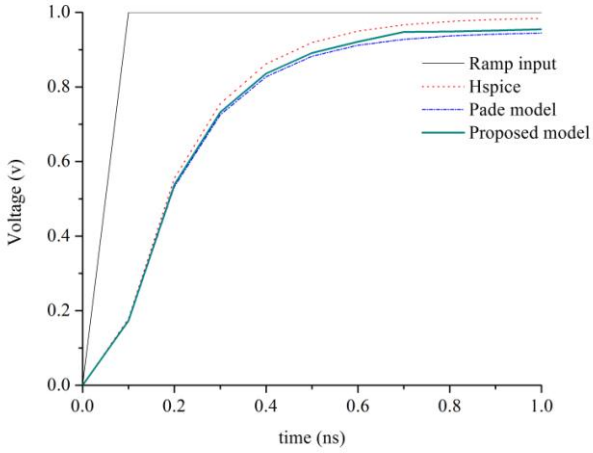

Fig 5. Time domain response at the node N2 of the given Tree structure with branch lengths 0.1cm and 0.2cm, R_s=50Ω and C_l=80fF.

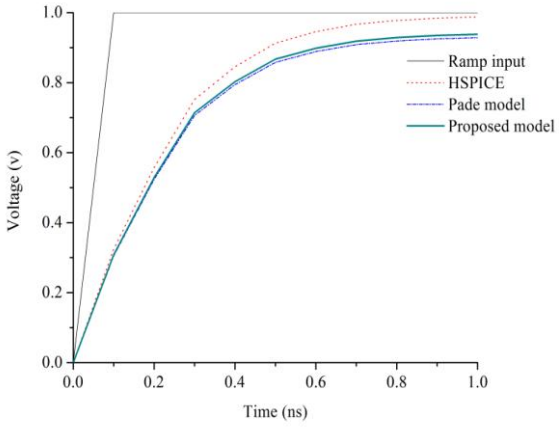

Fig 6. Time domain response at the node N3 of the given Tree structure with branch lengths 0.1cm and 0.2cm, R_s=100Ω and C_l=100fF.

Table II. Comparisons of 50% delay of HSPICE W Element, Pade model and proposed model for various lengths, source Resistances and load Capacitances at nodes N4 and N6.

L (mm)	R_S (Ω)	C_l (fF)	Node	HSPICE	Pade model order 2/2	Proposed model order (2/2)
				50% delay (ps)	*50% delay (ps)*	*50% delay (ps)*
0.1	50	100	N4	32.61	31.76	31.58
	100	50	N6	21.93	22.69	22.65
0.5	50	50	N4	66.98	64.36	65.3
	100	100	N6	64.68	61.05	63.15
1	100	50	N4	184.36	198.18	196.28
	50	100	N6	96.74	90.16	92.09
Average error % w.r.t. HSPICE					4.95	3.78
Maximum error % w.r.t. HSPICE					7.5	6.47

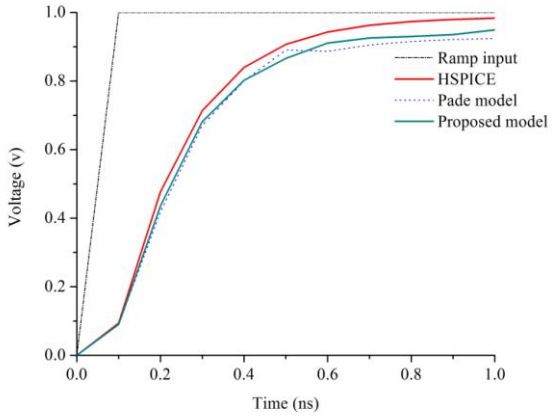

Fig 7. Time domain response at the node N_4 of the given Tree structure with branch lengths 0.1cm, 0.2cm and 0.3cm, R_s=50Ω and C_l=80fF.

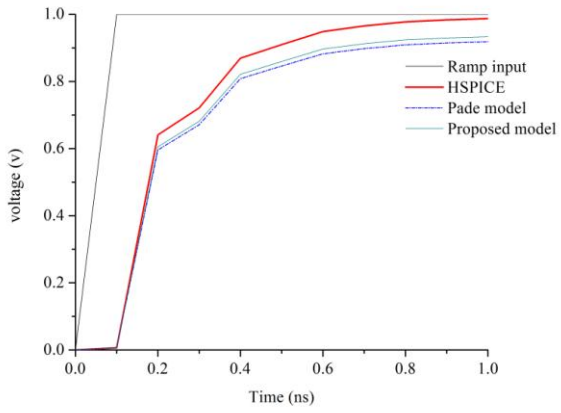

Fig 8. Time domain response at the node N6 of the given Tree structure with branch lengths 0.1cm, 0.2cm and 0.3cm, R_s=100Ω and C_l=100fF.

ISBN: 978-1-61804-228-6

A finite ramp signal with rise time of 0.1ns is applied at the input of the tree. Tables II compares the 50% delay values obtained using Pade model of order 2/2, proposed model of order (2/2) and HSPICE for various lengths, source Resistances and load Capacitances. These values are calculated at nodes N_4 and N_6. This table also includes the percentage error values with respect to HSPICE. The Pade model of order 2/2 has average error of 4.95%, whereas proposed model has 3.78%.

VI. Conclusion

This paper presents a U-transform based closed form model for delay estimation of VLSI interconnect tree structure in DSM regime. A distributed RLC tree has been used for validating the proposed model by comparing with the Pade model and the HSPICE. In SOC (system on chip) applications, for global lines of each branch lengths 0.5 mm and above the proposed method is found to be more accurate than existing Pade model. This model can be used for the analysis of hierarchical clock-distribution network in SOC applications.

References

[1] Semiconductor Industry Association, The International Technology Roadmap for Semiconductors, 1999.

[2] W. C. Elmore, "The transient response of damped linear networks with particular regard to wideband amplifiers," *J. Appl. Phys*., vol. 19, no.1, pp. 55–63, Jan. 1948.

[3] T.Sakurai, "Closed-form expressions for interconnection delay, coupling, and crosstalk in VLSI's," *IEEE Trans. Electron Devices*, vol. 40, no. 1, pp. 118–124, Jan. 1993.

[4] Kahng A B, Muddu S, "An analytical delay model for RLC interconnects", *IEEE Trans. Computer-Aided Design of Integrated Circuits and Systems*, pp. 1507−1514, 1997.

[5] Kahng A B, Muddu S, "Two-pole analysis of interconnection trees", in *1995 Proc. of IEEE MCMC Conf.(MCMC-95)*, Santa Cruz, California, USA, pp. 105−110, 1995.

[6] Xiaopeng Ji, Long Ge, Zhiquan Wang, "Analysis of on-chip distributed interconnects based on Pade expansion," *Journal of Control Theory and Applications*, 7 (1) pp. 92–96, 2009.

[7] K. Banerjee and A. Mehrotra, "Analysis of On-Chip Inductance Effects for Distributed RLC Interconnects," *IEEE Trans. on CAD*, vol. 21, no. 8, pp.904–915, Aug. 2002.

[8] Y. I. Ismail and E. G. Friedman, "Effects of Inductance on the Propagation Delay and Repeater Insertion in VLSI Circuits," *IEEE Trans. on VLSI*, vol. 8, no. 2, pp. 195–206, Apr. 2000.

[9] K. T. Tang and E. G. Friedman, "Delay and Power Expressions Characterizing a CMOS Inverter Driving an RLC Load," in *Proceedings of the IEEE International Symposium on Circuits and Systems*, pp. III.283-III.286, May 2000.

[10] J. Rubinstein, P. Penfield, Jr., and M. A. Horowitz, "Signal delay in RC tree networks," *IEEE Transactions on Computer-Aided Design*, vol. 2, no. 3, pp. 202–211, July 1983.

[11] K. Yamakoshi and M. Ino, "Generalized Elmore delay expression for distributed RC tree networks," *Electronics Letter*, vol. 29, no. 7, pp. 617–618, Apr. 1993.

[12] Y. I. Ismail, E. G. Friedman, and J. L. Neves, "Equivalent Elmore delay for RLC trees," *IEEE Transactions on Computer-Aided Design*, vol. 19, no. 1, pp. 83–97, Jan. 2000.

[13] Y. I. Ismail and E. G. Friedman,"Fast and accurate simulation of tree structured interconnect," in *Proc. 43rd IEEE Circuits and Systems Mid-west Symp.*, vol. 3, Aug. 2000, pp. 1130–1134.

[14] X.-C. Li, J.-F. Mao, and H.-F. Huang, "Accurate Analysis of Interconnect Trees with Distributed RLCModel and Moment Matching", *IEEE Transactions on Microwave Theory and Techniques*, vol. 52, no. 9, pp. 2199 – 2206, Sept. 2004.

[15] Guoqing Chen, Friedman E.G "An RLC interconnect model based on fourier analysis," *IEEE Transactions on Computer-Aided Design of Integrated Circuits and Systems*, vol.24, no.2, pp.170,183, Feb. 2005.

[16] Kavicharan M, Murthy N.S, Rao N.B, "An efficient delay estimation model for high speed VLSI interconnects," in *International Conference on Advances in Computing, Communications and Informatics (ICACCI)*, 2013, pp.1358-1362, 22-25 Aug. 2013.

[17] S. Roy and A. Dounavis, "Closed-Form Delay and Crosstalk Models for RLC On-Chip Interconnects using a Matrix Rational Approximation," *IEEE Transactions on Computer-Aided Design of Integrated Circuits and Systems*, vol. 28, issue 10, pp. 1481 - 1492, Oct.2009.

[18] Roy D, Bhattacharya R, and Bhowmick S, "Rational approximants generated by the U-transform," *Comput. Phys. Commun*. vol. 78, pp. 29-54 (1993).

[19] Tarun Kumar Sheel, MS Thesis "Rational approximants generated by Pade approximation and U-transform (Thesis or Dissertation style)," Ph.D. dissertation, University of Dhaka, Bangladesh March 1997.

Software Maintenance from the Change Theory Perspective

Maeda Hanafi and Amal Abdel-Raouf
Computer Science Department
Southern Connecticut State University
New Haven, US

Abstract—-In current software engineering research, software maintenance is alwaysstudied in terms of certain factors, namely maintenance methodology used by developers and software features and properties. In this paper, we introduce a different perspective on software maintenance from the standpoint of change theory. We use three change theories to model the software maintenance process. Our findings suggest that considering software maintenance from a different perspective will further benefit the software maintenance process, help developers to better understand their role and increase the possibility of success.

Keywords—software engineering,software maintenance, software quality, change theory

I. INTRODUCTION

Software maintenance is one of phases of the software development cycle. Traditionally, software maintenance is defined as"the modification of a software product after delivery to correct faults, to improve performance or other attributes or to adapt the product to a modified environment" [1]. Software maintenance is very important, as it is a critical factor to determine the software cost. Statistics show that it represents almost 60% of the total cost of any software product[2]. Moreover, software maintainability, the ease with which a software system can be modified, is considered one of the attributes to assess software product quality.

It is very challenging to study software maintenance because it deals with many factors ranging from software features to human dynamics. Software features include correctness, modularity, coupling, code size, and complexity. On the other hand, human dynamics include team activity rate, communication structure, familiarity with the system, skill levels, and leadership. As a result, the variety of the factors affecting the maintenance process limits the generalization of the finding of individual studies.

Yet most of the research studies have paid little attention to how software engineers understand the system and the information needed to perform a maintenance task. Pizka et al[3] showed that maintainability is dependent on more than just the technical properties of the system; it depends on three different dimensions:

1) The people performing software maintenance (team members and a project manager)
2) The maintenance goals and tasks
3) The technical properties of the system under consideration

Most of the work to investigate software maintenance only considers the technical properties of the system, the third dimension, thus ignoring the first two dimensions and limiting the scope and accuracy of these approaches. One major problem is that the effect of the first two dimensions on software maintenance depends on a deeper understanding of the context of the system. Therefore there is a need for a context model to describe the software maintenance process.

In this paper, we propose the use of change theory to model the software maintenance process in order to incorporate contextual information and help maintainers to better understand the software maintenance task.

The remainder of this paper is organized as follows: the literature related to software maintenance is reviewed in Section II. Section III summarizes three change theories and assumptions about the nature of change. Section IV presents our model to represent software maintenance in terms of change theories principles. Then, Section V provides a generalization of the three models together with a brief comparison. Finally, section VI draws our conclusions and presents potential future work.

II. PREVIOUS WORKS IN SOFTWARE MAINTENANANCE

In the literature, the term "Software Maintenance" started back in 1960s and was widely accepted after the publication of Cannie's work [4] in 1972. The next significant work was Swanson's [5] that was published in 1976 and included taxonomy of the software maintenance that is still in use. It classifies software maintenance as follows: corrective, adaptive, perfective and preventive maintenance.

Other research has presented alternative taxonomies of software maintenance. Chapin et al. in [6] presented taxonomy of 12 categories based on the nature of changes of the software system's activities. Mens et al. in [7] proposed

ISBN: 978-1-61804-228-6

maintenance taxonomy based on characterizing the factors that influence the software changes.

The distinguished work by Lehman et al. [8], [9] in 1997-98 is still considered for software evolution/maintenance and included in all software engineering textbooks. Lehman et al. carried out several empirical studies of very large-scale industrial systems. From these studies they proposed Lehman's Laws concerning system change.

In recent years, with the emerging use of open source, software services, components, and frameworks some research has challenged Lehman's laws [10],[11] resulting in the need for new models to update them.

In 2011, Kumar [12] did a comprehensive review on the major studies regarding maintainability models for object-oriented software systems. Kumar compiled literature in this particular field along with the variables, methods, and datasets used. For instance, Oman and Hagemeister's [13] research was on constructing and testing software maintainability assessment models. The variables employed in this research are as follows: aveLOC (Average Line of Code), ES (Executable Statement), CM (Line of Comment), and NES (Number of executable Statement). Kumar has compiled other works, which also employed similar variables. Such variables clearly describe software's factors and features.

Moreover, Kumar identified that the methods used in Oman and Hagemeister's research are as follows: MAT (Maintainability Analysis Tool), Regression, Halsted metrics, Cyclomatic Complexity, Assessment Model, and Entropy. The other publications Kumar compiled mostly employ regression models as a method to evaluate software maintenance of object oriented system. Based on Kumar's comprehensive literature review,most of the literature considers software maintenance in terms of the software's factors and features. There is a need for a context model to describe the software maintenance process. In thiswork, we model software maintenance using change theories principles.

III. Change Theories

Change theories attempt to describe and organize the process in which human behavior changes. In this work, we have extrapolated the use of change theory to the field of software maintenance.

The most basic of change theories is Kurt Lewin's theory of change [14], used to describe human behaviors, and defined in three stages as follows:

1) Unfreezing: Stage in which change is needed
2) Moving: The change is initiated
3) Refreezing: Equilibrium is reached

Lewin's theory emphasizes the analysis of driving forces and restraining forces before a change is implemented. A change will occur when forces that promote change combined are greater than the forces that resist change combined. In the unfreezing stage, the aim is to unfreeze the current situation, also known as the equilibrium state. During the moving phase, the equilibrium state is in alteration in order to move to a different level of equilibrium. In this phase the driving forces establish a newer equilibrium state that is better than the current one. The last step is refreezing, in which the goal is to make the new equilibrium state continuous and to prevent reverting to the previous equilibrium state. Policies, procedures, and community actions can help uphold a new equilibrium[14].

A more extended and detailed change theory is defined by Ronald Lippit, Watson, and Westley [14]. Lippit's theory includes sevenstepsto implement a change, as follows:

1) Diagnosing the problem
2) Assess motivation and capacity for change
3) Assess change agent's motivation and resource (examples of change agents: cheerleader, facilitator, expert)
4) Select progressive change objective; Develop action plans and establish strategies
5) Choose appropriate role of the change agent
6) Maintain change through strong group dynamics
7) Terminate the helping relationship.

Lippit's theory of change consists first of scrutiny of the problem, and thereupon moving on to evaluating the ability to change and the change agent's ability to change. It is important that the change agents clearly understand their roles in order for them to carry out their duty in facilitating change. Lippit, Watson, and Westley pointed out that a change is more likely to be adopted if the neighboring system adapts to it. Once a change is widespread, the behavior would be observed as the norm. An example of applying Lippit's theory of change is given from the research of Gary Mitchell [15] that analyzes planned change in nursing management. However, much of Lippit's theory focuses on the change agents rather than on the change itself.

The third theory of change is Prochaska and DiClemente's cyclical model of change [14], which defines a more general process of change. It was originally developed for the purposes of explaining the patterns of staged behavior change.The defined stages are as follows:

1) Pre-contemplation
2) Contemplation
3) Preparation
4) Action
5) Maintenance

In the pre-contemplation stage, the problem is denied by the individual, and there is absolutely no will to change. The awareness of the problem will occur in the contemplation stage, where change is being thought about. In the preparation stage, the individual is prepared to change their behavior, and consequently the action stage occurs. The action stage is where the individual actually changes their behavior.Finally, the

ISBN: 978-1-61804-228-6

maintenance stage attempts to sustain the change. This process is a spiral since individuals can exit any stage and return to the previous stages. However, it is also possible for the individual to return to the contemplation stage at any time in order to prepare for future action. This model pushes the idea that an individual will not always circle the spiral forever.

The three theories presented so far relate to social and management fields. However, there has been similar research on change in software-related fields. For instance, Lassila [16] proposed the adoption and utilization of new software through the punctuated equilibrium model. The punctuated equilibrium model utilizes incremental adaptations with organizational changes in long periods of stable infrastructures. During these adaptations the equilibrium is disrupted but returns back to stability.

In the following section, we present how these change theories can be applied to model software maintenance.

IV. Software Maintenance Model based on Change Theories

Our research surrounds the question, "How is software maintenance can be modeled in terms of change theories instead of its features and factors?" We gathered and scrutinize the techniques of other researchers in the field of change theory and compared it to the software maintenance process. In the following subsection, we introduce software maintenance based on the three change theories described in section III.

A. Software Maintenance Model Using Kurt Lewin's Theory

In Lewin's theory, there are only three stages, which place much focus on the idea of equilibrium and moving from one state of equilibrium to another. In terms of software maintenance, such equilibrium can be translated to any running software that is servicing the user and running on a stable system. The system's stability can be quantifiedwith the stability condition from queuing theories, which state that the servicing rate must be greater than the customer's incoming rate [17].In Table I, we show the stages of software maintenance process based onLewin's theory.

TABLE I. Software Maintenance Model using Lewin's Theory of Change

Stage	*Lewin*	*Description*	*Maintenance Stage*
1	Unfreezing	Stage in which change is needed.	Prepare and plan for software maintenance/change. Perform force-field analysis.
2	Moving	The change is initiated.	Maintenance occurs.
3	Refreezing	Equilibrium is reached.	Software must pass all tests, be stable, and serve users.

In the unfreezing stage, much of the aim is to plan and prepare for the change. Maintainers at this stage prepare for a maintenance project.Lewinsuggested force-field analysis, where positive and negative factors are compared. Mitchell's research in change management for the nursing field [15] also employs force-field analysis to address resistance and induce stress. The same can be applied to software maintenance. According toDehaghani et al [18], the factors to be considered are the tools used in maintenance, current practice of proper software development techniques, team stability and skillset, contractual responsibilities, software age and architecture. Once force-field analysis is performed and a plan is finalized, the preparation for change is complete. The benefit of force-field analysis is that it ensures that a change in the software maintenance successfully occurs, while overcoming obstacles.

In the moving stage, the maintenance project begins and the system is analyzed and undergoes change. The change made to the system may be as simple as correcting code or more extensive change to correct design errors or accommodate new system requirements.

Finally, the refreezing stage aims to re-stabilize the system. In this stage, all tests must be passed and the system must be able to serve its users while incorporating the new changes.

B. Software Maintenance Model Using Lippit's Theory

Lippit's theory consists of more stages, but targets the change agent's ability. In software maintenance, the change agent is the maintainer,sincechange mostly occurs within the software and only a maintainer is able to do it. Lippit's theory emphasizes the maintainer's skillset and knowledge in order to accomplish the change.

The first three steps of Lippit's theory revolve around analyzing the current status. Diagnosing the problem requires the maintainer's being able to give a brief description of the problem, and perhaps a speculation of its source. Then, the assessment of motivation and capacity of changeevaluates the priority, ability, and profit of the proposed maintenance project. If the need for the proposed change is high, then the priority should be high as well. However, assessment of the change agent mainly deals with the team's ability to continue on with the proposed project. For instance, if the proposed maintenance project is dependent on another project, then the team wouldn't be able to continue the first project without the other being completed.

Once assessment is completed, an action plan must be developed. If there are dependent projects, then those projects must be completed.This stage stresses the importance of an action plan. This action plan can be greatly guided with a maintenance methodology. A maintenance methodology, whether standard or individually defined, can be any process that is defined within a set of tasks and timeline that is feasible and agreed upon by the stakeholders [19]. The maintainers must reassess if the methodology used is consistent with their aims. Factors to consider when choosing a maintenance methodology include project factors (frequency of change or immediate change), developer factors (skill set, enjoyment for collaboration, or desire to be "in fashion"), and organizational factors (organization structure and cultural issues).

Afterwards, the roles of the team members must be determined. Then, the change is put in action. Lippit's theory emphasizes the group dynamics. This is especially important for teams that have scattered members, where each member must be constantly communicating with the rest of the team.

During this stage, a maintainer constantly faces unfamiliar code. In this case, the maintainer would search and pick a relevant node to begin comprehending the structure and program flow. The maintainer would decide if the current node is relevant to the change. This process of searching for relevant nodes would continue until there is enough information to implement a solution and create changes in code. Searching and comprehending is easier on the maintainer when the environment provides ease for judging a node's relevancy. Another factor that provides further straightforwardness is the environment's reliability to provide relevant information for a given node [20]. If these two factors are not considered, this stage will take longer time.

When a solution is implemented and the tests are passed, then the maintenance project ends. If needed, tests can be recreated to cover new cases, and the system can be retested. However, if a need for change i.e. bug, fault, new feature, or adaption change, appears due to the new change, then the team must aim to continue to maintain the change. Once those needs are addressed, the project may be terminated. The system must be running and stable as well. The tabular form of software maintenance tasks based on Lippit's theory is shown in TableII.

TABLE II. SOFTWAE MAINTENANCE MODEL USING LIPPIT'S THEORY OF CHANGE

Stage	*Lippit*	*Software Maintenance Tasks*
1.	Diagnosing the problem	Give a brief description of the problem. Recommended to speculate on its source.
2.	Assess motivation and capacity for change	Evaluate ability, priority, and profit.
3.	Assess change agent's motivation and resource	Evaluate team's ability.
4.	Select progressive change objective; Develop action plans and establish strategies	Reassessmaintenance methodology and develop action plans.
5.	Choose appropriate role of the change agent i.e. cheerleader, facilitator, expert	Pick appropriate maintainers, and set roles for each one.
6.	Maintain change through strong group dynamics	Make necessary changes while upholding team communication.
7.	Terminate the helping relationship.	End the project. Return the system to running and stable.

C. Software Maintenance Model Using Prochaska and DiClemente's Theory

In Prochaska and DiClemente's theory, there is a pre-contemplation stage that doesn't exist in the other theories we have described. This stage considers the situation where a need for change is required but is not yet noticed by the maintenance team. The users may perceive it, but it requires the maintenance team to notice it before a maintenance project is initiated, moving to the contemplation stage. The software is similar to a patient at this stage; others perceive his or her abnormal behavior, but the patient has no intention of changing.

But even in this stage, it is advised that the possibilities of future requirements are analyzed. The aim of this is to ensure that all architectural changes are explored and thoroughly defined [21]. In fact, the pre-contemplation stage defines a stage for the team to have special attention to the architecture's changeability. A coherent architecture allows flexibility to meet the constant altering of user's requirements. In order to have extensive architecture coherence, the team must gain enough knowledge about it so that the software can evolve. If the architectural knowledge is lost, then the software goes through coherent architectural loss known as code decay [21]. In other words, the team may make changes that do not take advantage of the software's architecture, thus losing its coherency.

Moreover, Prochaska and DiClemente's spiral model allows for flexibility that is not offered by Lippit's and Lewin's. At any stage, the team can suspend a maintenance project and exit a stage. Anytime the team decides to return to the maintenance project, the project's stage winds back to the contemplation stage. This is a convenience for the team especially when an emergency maintenance happens or a need for change appears due to the current change.

The contemplation stage occurs when the team considers the change, but is not yet ready to analyze and implement it. At this point, the team is conscious of the need for change and a maintenance project must be formulated. The priority, profit, and ability of the proposed changeare decided before it is moved to the preparation stage.

The preparation stage is when the team decides that it is ready to undertake the change. This is when a definite action plan is set and the re-analysis of current methodology is done and revised as needed. Consequently, the team re-analyzes the code and changes as needed, which is the action stage. In Prochaska and DiClemente's patient model, the patient is supported with counseling, social support, and assistance.In software maintenance, the tools and environment assist the maintainers in searching for relevant nodes to form a solution [22]. The pressure from users provides motivation, and the maintenance team members provide further assistance in the process.

TABLE III. SOFTWAE MAINTENANCE MODEL USING PROCHASKA AND DICLEMENTE'S THEORY OF CHANGE

Stage	*Prochaska and DiClemente's*	*Maintenance Stage and Tasks*
1.	Pre-contemplation	The need for change is not yet perceived by maintainers. Speculate about future changes especially architectural changes.
2.	Contemplation	The problem is detected by the team, and priority, ability, and profit are decided.
3.	Preparation	Reassess maintenance methodology and develop action plans.
4.	Action	Analyze, search, and change code.
5.	Maintenance	Rerun tests to ensure the new change is passed, and the users are updated about it. Evaluation of the changes is recommended.

ISBN: 978-1-61804-228-6

Once the changes are done and the tests are revised and passed, the changes are integrated into the running system. A change in software can be maintained if all the tests are successful, the users are updated about it, and the system is stable. If the system is not stable, then another maintenance project is initiated and repeats throughout all the defined steps. Moreover, it is recommended that a change be evaluated by surveying the users. A tabular form of software maintenance tasks based on Prochaska and DiClemente's theory is shown in Table III.

V. Generalization and comparison

Lewin's theory is the most basic with only three stages, with a focus on analyzing negative and positive factors through force-field analysis.Lippit's theory is more detailed, helping to define more specific tasks in the software maintenance process.Lippit's theory also emphasizes the importance of assessing the specific team's abilities, since a stress is placed on the change agent.Furthermore, the team's dynamics, including communication, areemphasized. On the other hand, Prochaska and DiClemente's theory is a more evolved theory, allowing flexibility for the maintenance team to spiral around the stages. Moreover, their theory has a pre-contemplation stage, which propels the team to constantly think of the future changing requirements and needs.

The three theories and the maintenance tasks can be combined to explain a more generalized situation, as shown in Table IV.In Table IV, we provide a comparison of the three change theories stages together with the corresponding software maintenance tasks in each stage.

A. Assessing the current situation

Prochaska and DiClemente's pre-contemplation stage does not correspond to any stages from the other theories. However,the next stage of contemplation corresponds toLewin'sunfreezing stage and encompasses Lippit's first three stages. These stages all share the characteristics of reviewing and reassessing the current situation. The highlighted task is force-field analysis of driving forces and negating forces. Lippit's theory splits the tasks into 1) the analysis of the problem itself, where a maintenance request is sent in andamaintenance project is initiated, 2) analyzing ability to change, and 3) analyzing the change agent's ability, i.e. team's ability.

B. Developing an action plan

Lewin's moving stage corresponds to Prochaska and DiClemente's preparation and action stages. Lewin's moving stage also corresponds to the next three stages of Lippit's theory. These stagesarespecific to developing an action plan and acting upon it. Lippit's theory divides Prochaska and DiClemente's preparation stage into two stages: 1) developing action plans and 2) choosing team member roles.

Finally, change takes place in Lippit's last stage in this category, which corresponds to Prochaska and DiClemente's action stage.

C. Maintenance

The final stagein all theories depicts a maintenance stage. Lewin's refreezing stage aims to incorporate the new changes into the operational system successfully. Lippit's theory explains that the team terminates the maintenance project and return the system to the running state. Prochaska and DiClemente'slast stage elucidates the importance of maintaining the change, with passing all tests, addressing all other needed changes, and ensuring the stability of the system.

TABLE IV. General Maintenance Tasks in Terms of Change Theories

Lewin	***Prochaska and DiClemente's***	***Lippit***	***Maintenance Stage and Tasks***
	Pre-contemplation		The need for change is not yet perceived by maintainers. Speculate about future changes especially architectural changes.
Unfreezing	Contemplation	Diagnosing the problem	The problem is detected by the team, and priority, ability, and profit are decided. Give a brief description of the problem. Recommended to speculate on its source.
		Assess motivation and capacity for change	Perform force-field analysis. Evaluate ability, priority, and profit.
		Assess change agent's motivation and resource	Perform force-field analysis. Evaluate team's ability.
Moving	Preparation	Select progressive change objective; Develop action plans and establish strategies	Reassess maintenance methodology and develop action plans.
		Choose appropriate role of the change agent i.e. cheerleader, facilitator, expert	Pick appropriate maintainers, and set roles for each one.
	Action	Maintain change through strong group dynamics	Maintenance occurs. Analyze, search, and change code. Make necessary changes while upholding team communication.
Refreezing	Maintenance	Terminate the helping relationship.	End the project. Ensure passing of tests. Return the system to running and stable. The users must be updated about it. Evaluation of the changes is recommended.

ISBN: 978-1-61804-228-6

VI. Conclusions

While other researchers have sought to study software maintenance in terms of feature and factors, our research proposes the use of change theories to model software maintenance. We utilize three change theories:Lewin's, Prochaska and DiClemente's, and Lippit's theories to introduce three different software maintenance models.These models consider both software features and human dynamics to bring about a successful change.

Lewin's model is the most basic with only three stages, with a focus on analyzing negative and positive factors through force-field analysis. Lippit's model is more detailed, emphasizing the maintainer's skillset and knowledge in order to accomplish the change. Lastly, Prochaska and DiClemente's model is a more evolved model, allowing flexibility for the maintenance team to spiral around the stages.

Our future work includes extending the models to reflect the different types of software maintenance i.e.corrective, adaptive, perfective and preventive maintenance.

References

[1] K. Denis, J. Koskinen, and M. Sakkinen,"Fault-Proneness Of Open Source Software: Exploring Its Relations To Internal Software Quality And Maintenance Process," *Open Software Engineering Journal* , vol. 7, pp. 1-23, 2013.

[2] P. Bhatt, K. Williams, G. Shroff, and K. Misra, "Influencing Factors on Outsources Software Maintenance," *ACM SIGSOFT Software Engineering Notes*, 31, 3, pp. 44-49, May 2006.

[3] M. Pizka, and F. Deissenboeck, "How to effectively define and measure maintainability," *Software Measurement European Forum*, Rome, Italy, 2007.

[4] R. Canning, "That maintenance iceberg," *EDP Analyzer*, 10(10), 1972.

[5] E. B. Swanson, "The dimensions of maintenance," *Proceedings of the 2nd Intl. Conference on Software Engineering*, San Francisco, CA, October 1976.

[6] N. Chapin, J. Hale, K. Khan, J. Ramil, and W. Tan, "Types of software evolution and software maintenance," *Journal of Software Maintenance and Evolution*: *Research and Practice*, 13(1), January/February 2001.

[7] T. Mens, J. Buckley, M. Zenger, A. Rashid, and G. Kniesel, "Towards a taxonomy of software change," *Journal of Software Maintenance and Evolution: Research and Practice*,17(5), September 2005.

[8] M. M. Lehman, D. E. Perry, and J. F. Ramil, "Implications of evolution metrics on software maintenance," *Proceedings Of the 1998 IEEE Intl. Conference on Software Maintenance*, Bethesda, Maryland, November 1998.

[9] M. M. Lehman, J. F. Ramil, P. D. Wernick, D. E. Perry, and W. M. Turski, "Metrics and laws of software evolution," The nineties view. In *Proceedings of the Fourth Intl. Software Metrics Symposium*, Albuquerque, NM, November 1997.

[10] M. W. Godfrey and Q. Tu., "Evolution in open source software: A case study. In *Proceedings of 2000 IEEE Intl. Conference on Software Maintenance*, October 2000.

[11] G. Robles, J. M. Gonzalez-Barahona, M. Michlmayr, J. J. Amor, and D. M. German, "Macro-level software evolution: A case study of a large software compilation," *Empirical Software Engineering*,vol. 14, pp. 262–285, 2009.

[12] D. Kumar, Sanjay, A. Sharma, and A. Rana,"Analysis Of Maintainability Models For Object Oriented System," *International Journal On Computer Science & Engineering* 3.12 , pp. 3837-3844, 2011.

[13] F. Zhuo, B. Lowther, P. Oman and J. Hagemeister, "Constructing and testing software maintainability assesement models," *IEEE Computer Society*pp.61-70, 1993.

[14] A. Kritsonis, "Comparison of Change Theories,"*International Journal of Scholarly Academic Intellectual Diversity*vol. 8.1 pp. 1-7, 2004-2005.

[15] G. Mitchell, "Selecting The Best Theory To Implement Planned Change," *Nursing Management* - UK 20.1, pp. 32-37, 2013.

[16] Lassila, Kathy S., and James C. Brancheau,"Adoption And Utilization Of Commercial Software Packages: Exploring Utilization Equilibria, Transitions, Triggers, And Tracks," *Journal Of Management Information Systems*, vol. 16.2 , pp. 63-90, 1999.

[17] J.Virtamo, "Queueing Theory / Priority Queues." Web. 10 Feb., 2014.<http://www.netlab.tkk.fi/opetus/s383143/kalvot/E_priority.pdf>.

[18] Dehaghani, S. M. Hejazi, and N. Hajrahimi,"Which Factors Affect Software Projects Maintenance Cost More?," *Acta Informatica Medica* , vol. 21.1, pp. 63-66, 2013.

[19] D. Edberg, P. Ivanova, and W. Kuechler, "Methodology Mashups: An Exploration of Processes Used to Maintain Software," *Journal of Management Information Systems*, vol. 28.4, pp. 271-303, 2012.

[20] Ko. J. Andrew, B. Myers, M. Coblenz, and H. Aung, "An Exploratory Study of How Developers Seek, Relate, and Collect Relevant Information during Software Maintenance Tasks," *IEEE Computer Society*, vol. 32.12 , pp. 971-987, 2006.

[21] K. Bennet, and V. Rajlich, "Software Maintenance and Evolution: A Roadmap." *ACM*, pp.73-87, 2000.

[22] Ian Sommerville, *Software Engineering*, 9th Edition, Addison-Wesley Publishers Ltd, New York, 2011.

Proposal of A Flexible and Efficient System Development Approach

Michiko Oba and Taku Yamaguchi

***Abstract*—**The business environment has accelerated sharply year by year. However, the information system does not catch up the rapid change. A certain gap arises between the business strategy and IT. Approaching this problem, this paper aims to resolve a combination of two concepts of SOA and BPM,. In the proposal approach, we apply the agile development process to which the change in the requirement is brilliantly accepted. The grasped requirement is listed and the order of priority is applied at the time of beginning of development. Next, it develops from the function with high priority one by one. When the change and the addition of the requirement occur, priority is reviewed. As mentioned above, our approach accepts the change and the addition of the requirement, and develops them according to priority. As a result, system implementation to be worthy for the customer in the delivery date becomes possible. In this paper, we propose the design-approach that combines BPM, SOA, and agile development for the system development to which the specification is not fixed. Additionally, we prove the effectiveness of our proposal by the application experience.

***Keywords*—**Agile Development Process, BPM, Component, Feature List, Information System Development, SOA

I. Introduction

RECENTLY, the business environment has changed rapidly. There is a problem that the information system cannot follow rapidly to the change in this business environment. Consequently, a certain gap seems to arise in the business strategy and IT. In an enterprise, unchangeableness of the information system initially designed to match to the accelerating business environment becomes nonnegligible problem of management. There is an approach for attempting the solution by combining two concepts for this problem BPM(Business Process Management)[1] and SOA(Service Oriented Architecture)[2].

BPM is an approach from the business side. On the other hand, SOA is the one from the system side. The gap between the business strategy and IT can be patched by two approaches. The change in the business environment can be absorbed by the flexibility of the business process in BPM. Moreover, it is possible to develop systems efficiently by the combination development of service in SOA. Therefore, we come to be able to construct the information system that can follow the change of business promptly.

Up to now, we have practiced the development approach based on the method above. However, our development approach has the problem that the implementation cost becomes large when the specification has not been fixed. The reason is that the rework often occurs in the development of the information system because of the change in a frequent specification.

Therefore, the purpose of this paper is to suppress the implementation cost for the system development to which the specification is not fixed, and to propose a design approach that secures customer satisfaction. In the proposal approach, we apply the agile development process to which the change in the requirement is brilliantly accepted. The grasped requirement is listed and the order of priority is applied at the time of beginning of development. Next, it develops from the function with high priority one by one. When the change and the addition of the requirement occur, priority is reviewed. As mentioned above, our approach accepts the change and the addition of the requirement, and develops them according to priority. Resultantly, system implementation to be worthy for the customer in the delivery date becomes possible.

In this paper, we propose the design approach that combines BPM, SOA, and agile development for the system development to which the specification is not fixed. Additionally, we show the effectiveness of our proposal by the application experience.

II. Development Approach That can Flexibly Step with Change

2.1 System Development Approach by BPM and SOA

There was a gap between the business and IT in the system development of the past. Therefore, there was a problem of taking time to absorb the change to the information system when the business environment changed[3]. A past information system was a structure of the tight coupling overall. The change part of the information system becomes wide-ranging when the business environment changes, and it costs time to change them.

These problems can be solved by the development approach that combines BPM and SOA. In BPM, a real business is abstractly expressed by the business process. Therefore, the change in a real business is absorbed by changing the business process definition. The change in the program doesn't occur in this case. Changes can

Michiko Oba Author is with the Media Architecture Department, Future University Hakodate, 116-2 Kameda-Nakano Hakodate Hokkaido, Japan (e-mail: michiko@fun.ac.jp).

Taku Yamaguchi Author with the Graduate School of Systems Information Science, Future University Hakodate, 116-2 Kameda-Nakano Hakodate Hokkaido, Japan (e-mail: g3111008@fun.ac.jp).

ISBN: 978-1-61804-228-6

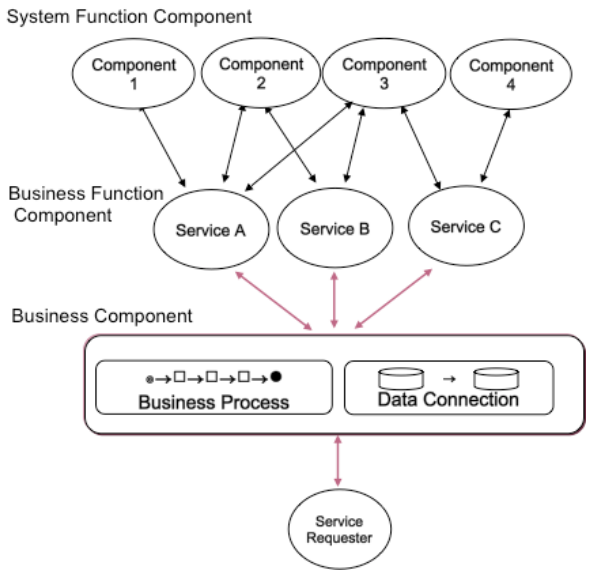

Fig. 1. Relation with Business Processes, Services, and Components.

Business Analysis (CIM)		Difinition of non-functional requirements
	1 Arrangement of the target business development	
	2 Activity diagram	Creating a term dictionary and maintenance
Requirements Analysis (PIM)		
	3 Definition of scope to be systematized	Software architecture design
	4 Use case diagram	
	5 Usecase scenario	User interface and form design
	6 External specification diagram of components	
System Analysis (PIM)		Database design
	7 Analysis level class diagram	
	8 Logical data model	
	9 State diagram	
	10 Compornent diagram	
Logical Design (PSM)		
	11 Logical class diagram	
	12 Logical class diagram	
	13 Logical sequence diagram	
	14 Request mapping	
	15 Database mapping	
Implimentation and Test		
	16 Implementation class diagram	
	17 Sequence diagram for implementation	
	18 Implementation	
	19 Test Specifications	
	20 unit test	
	21 integration test	

( ): MDA process
CIM : Computation Independent Model
PIM: Platform Independent Model
PSM: Platform Specific Model

Fig. 2. Development Process.

be seen only in the definition. On the other hand, SOA is an architecture that constructs the system with the combination of service. The change on the implementation side can be absorbed by the change in service.

The change on the implementation side can be absorbed by the change in service. Flexible correspondence to the information system becomes possible by these.

In other words, in a real business, when there is a change the business process model has been changed: service is hit to a new business process in the rediscount. It ends only when the business process model changes which is possible to allocate it with an existing service group. The change in the component that achieves an insufficient part and the change part and the development of the addition are only executed when service is insufficient or the change occurs.

2.2 COMPORNENT BASED MODELING

The design of the business process and the design of the composing service component are important to achieve the approach of the foregoing section.

Fig. 1. shows the relation between these business processes and service and components.

Here, the granularity of the component is defined by the following three hierarchies.

(1) Business component

It is one settled disposal of business affairs such as order and estimate, etc. It is composed of the compound of the business function component.

(2) Business function component

It is a unit of the element of the business processing of the order receipt and estimate answer, etc.

(3) System function component

They are part groups of the system functions of registration, update, reference and attestation, etc. of information. And the business function component is made by using these.

Up to now, we have practiced the development approach by BPM and SOA[4][5]. This practice is object-oriented type application development that uses both MDA[6][7] and UML[8]. We derive the business process from the stage of the job analysis, and make the analytic model on the assumption of deriving the component. Fig. 2. shows this development process.

In general, making the component is attempted in the making process of logical class chart in object-oriented development. The component with high recycling level cannot be derived when the process is in the upstream. There is no process where the component is derived. The component is derived at the stage of the use case chart and the use case scenario in this development process. They are refined in the following processes, and, in addition, the internal analysis model is made. The development style of an iterative type is general in object-oriented development. The iteration is executed in each phase of MDA in this development process. The iteration is executed in each phase of MDA. If the iteration in each phase is approved by the customer, it is a proceed in the following phase.

2.3 PROBLEM OF THE COMPORNENT BASED MODELING

In the system development by the component base modeling, the specification is fixed in the business analysis process. The implementation phase is developed by the water fall type. The problems are as follows:

(1) If the requirements specification is not fixed, it takes a lot of time in the business analysis. As a result, process delay can easily occur. There are a lot of cases where the request is not fixed in a new

ISBN: 978-1-61804-228-6

business model.

(2) The return to the former process occurs when the specification changes in the implementation process. The cost of correction and test increases by becoming the post-processing. It leads to the delay of delivery.

(3) The man-hour making the document becomes large through the job analysis, the requirements analysis and the systems analysis process.

Moreover, it takes time to acquire the knowledge of UML.

III. Agile development Approach based on BPM and SOA

THE target of the proposal approach is developing a system that the specification is not fixed. Our purpose is to decrease the implementation cost, to defend the delivery date, and to secure customer satisfaction. To achieve this purpose, the agile development process where the change in the requirement can be brilliantly accepted is applied. Moreover, the modeling for the business process and the service development is used based on the component base modeling. To take much time to documentation in this modeling, however, the idea of agile modeling[9] is introduced. As a result, using the documentation of the modeling tool can be simplified.

Agile development consists of a series of short period that is called "Iteration" with a technique for repeating development and release. It becomes possible to improve covering, realizability, and the correspondence of the requirement by developing while confirming the movement of the system. Agile development has a lot of techniques such as XP or scrummage, etc. [10].

"Feature drive type development (FDD)" is used in our proposal approach[11]. FDD is a method to define the function by using unit of feature in order to implement the function, according to the priority of the request of the customer. Changing management by priority is flexibly enforceable in FDD by the feature list.

3.1 CHANGE MANAGEMENT AND ITERATION

In new system development, it is difficult to decide the detail in the scope of development in the requirement definition phase. Scope is a meaning of range of requirement that a system should achieve. There are a lot of change management methods[12]. In this proposal, scope is decided based on the priority of the feature list or the use case. An example of the feature list is explained below.

The feature list is a table where the requirement was arranged according to the priority level. The process of the change management by the feature list is as follows:

(1) The requirement is understood when developing starting is dug up. According to each requirement, they are ranked into the following three stages. Priorities are set in each rank. They are sequentially filled on the feature list from A to C.

A: absolutely necessary

B: may be necessary

C: may not be necessary

Moreover, the estimate of the scale of each requirement is filled in there. The scope of development is decided based on a delivery date and past development production results.

(2) When a new requirement occurs, the rank is applied to it. After an existing requirement in the same rank is compared with the priority level, it is added to the feature list.

(3) After the requirement for the correspondence in the feature list is changed, the rank and the priority level are reviewed when the requirement changes. In this case, the feature list is updated if necessary.

When the project begins, the length of the iteration is decided. On the way, it is important not to change the length. It is general to delimit to iterations of one-four weeks in agile development and to repeat the development.

3.2 PROPOSAL OF AGILE DEVEROPMENT PROCESS

The agile development process based on the change management and on the iteration described in the foregoing section is shown below.

(1) After the feature is listed, the requirement for the amount that can be developed by the iteration of the times when the iteration begins is sequentially selected from the place. The amount of development at first time is estimated based on a past development production.

(2) In each iteration, the requirements analysis and the design based on the content of the next section are executed.

(3)After the iteration ends, the development production is calculated. The amount of development in the following iteration is judged based on this result, and the requirement is selected and developed from the feature list.

(4) If it is necessary to narrow scope, it removes from scope in order with low priority.

(5) Development ends in any of the following cases.

- When the delivery date comes
- When all iterations end
- When all of the feature list are developed

Without corresponding the above-mentioned process, returns to (1).

The function with high priority can be implemented in the limited time according to the above-mentioned process.

3.3 APPLIED MODELING

In agile development process of the proposal, the practice of the following agile modeling is executed

(1) Think modeling as a mean of understanding and the discussion, not of the information transmission between work.

(2) Various modeling techniques are used widely, and shallowly.

In (1), modeling assumes execution by multiple people. Modeling is executed by an easy method here. It is as an example by using making the model of the card type in XP, writing the model of UML on a white board, and the tag paper.

In (2), various modeling techniques including UML are used widely and shallowly. The modeling technique recommended by agile modeling reaches the technique of 32 kinds. In the proposal method, the modeling technique is freely selected from component base modeling and agile modeling. For instance, the design of the business process are drawn as the activity diagram on the whiteboard. Therefore, information is shared.

IV. Application of the Proposed Method

WE applied the proposed method to the development of the prototype system of the inventory management of the IT operations system. An existing IT operation system is that manages the asset of hardware and the software license. This system takes an inventory regularly by online and the person. This system for development is an additional function of this system, and the

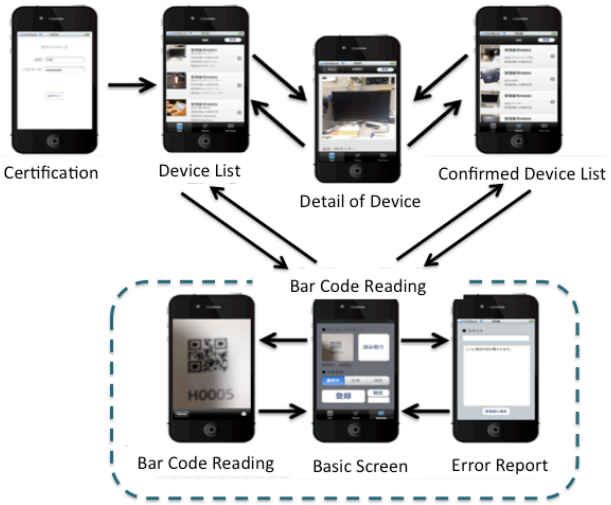

Fig. 3 Screen Transition of This System.

Table 1. Development Process.

	Client	Server
Hardware	iPhone 4S	Dell Power Edge
OS	iOS5	Cent OS
Development Environment	X Code 4.2	Apache/MySQL/PHP
Language	Objective-C	PHP/HTML5/Java Script

Table 2. Result of Development

Iteration	Preliminary Work or Development Function	Change	Development time(Week)
	Creation of an Environment for Development and Technology Investigation		2
1	Bar Code Reading	Modifed	1
2	Devices List	Modifed	1
3	Certification	Modifed	
3	Confirmed Devices List	Added	1
5	Report	Added	
6	Selection of Device Condition	Added	1
	Total	6	6

Table 3. Number of Business Processes, Components, and reusability.

Business Process	4
Compornents	11
Common Compornents	4
reusability	36%

prototype system of the application to manage the inventory of hardware with a smart phone.

In this development, the firstly fixed requirement was the following.

(1)The application uses a feature function of a smart phone.

(2)The application makes the inventory faster and easier.

The condition of this development was following.

It was a commissioned business from the client, and the delivery date was six weeks.

The system development for which the client and the developer used a smart phone was an initial experience.

Fig. 3 shows the screen transition of this system.

Table 1 shows details of the implementation environment.

Table 2 shows the development result.

In this development, the entire development period was six weeks, six times iterations

The addition of the function and the correction occurred six times.

Using modeling tool is as follows. Here, the simplification was aimed at besides with whiteboard and card, etc. though use case scenario was made as a document. Other documentation used the whiteboard and the card and the simplification was attempted.

- Feature list
- Mind map
- Use case chart
- Use case scenario
- Class chart
- Component chart

Table 3 shows number of business processes, total components, common components and the recycling rate of a common component.

The action of the change, the delivery date, and the efficiency improvement of development are as follows:

(1) Action of change

The addition and the correction occurred six times on the way. It was possible to deal flexibly by the addition of six components and the change in the business process.

(2) Efficiency improvement of delivery date and development

The system development ended before due date. The client was satisfied with the prototype system. We think that recycling the absorption of the change in the simplification of the document, the business process and the component contributed to the efficiency improvement of development.

Therefore, we were able to develop the system that the client satisfied before due date by the proposal approach in spite of the requirement for the uncertainty. A further verification is necessary for large-scale system development. However, it is conclusive that this proposal method was able to show effectiveness in the development of the small system and the prototype system.

V. Conclusion

In this paper, concerning about the system development to which the specification is not fixed, we suppressed the implementation cost by the approach that combines BPM, SOA and agile development, and to propose the design approach that secures customer satisfaction, offering the effectiveness of our proposal by the application experience.

This proposal approach was applied to the development of the prototype system in which effectiveness was shown.

The application experience must be increased in order to the improvement and the effectiveness of the problem will be pursued in the future.

References

[1] Mathias Weske: "Business Process Management: Concepts, Languages, Architectures", Springer Publishing Company (2010)

[2] Thomas Erl,: "Service-Oriented Architecture: Concepts, Technology and Design," PRENTICE HALL (2008)

[3] S. Latronico, F. Battista: " How a business process vision may boost innovative ideas", Transformation and Innovation (2007)

[4] Shinichi Kirikoshi, Mai Asai, Hiroshi Hamaguchi: " Report of component base modeling for SOA", Information Processing Society

of Japan Research Report, IS-57, pp.35-42 (2007) (in Japanese)
[5] Hiroshi Hamaguchi, Keiji Fujii, Takuya Haraguchi, Shinichi Kirikoshi: "Structure of documents for component base modeling", Information Processing Society of Japan Research Report, DD-53, pp.25-31 (2006) (in Japanese)
[6] MDA http://www.omg.org/mda/
[7] David S.Frankel, " Model Driven Architecture: Applying MDA to Enterprise Computing (OMG)", Wiley (2003)
[8] UML http://www.omg.org/spec/UML/
[9] Robert C. Martin: "Agile Software Development, Principles, Patterns, and Practices", Pearson Education; International ed. (2011)
[10] Scott W. Ambler: "Agile Modeling: Effective Practices for eXtreme Programming and the Unified Process", John Wiley & Sons. (2002)
[11] Palmer, S.R., & Felsing, J.M.: A Practical Guide to Feature-Driven Development. Prentice Hall, (2002)
[12] Scott W. Ambler, Mark Lines: "Disciplined Agile Delivery: A Practitioner's Guide to Agile Software Delivery in the Enterprise", IBM Press (2012)

A genetic programming approach to telecommunications fraud detection and classification

Constantinos S. Hilas, Spyridon A. Kazarlis, Ioannis T. Rekanos, and Paris A. Mastorocostas

***Abstract*—** Telecommunications fraud has drawn the researchers' attention due to the huge economic burden on companies and to the interesting aspect of users' behavior modeling. In the present paper, an application of genetic programming to fraud detection is presented. Genetic programming is used for case classification in order to distinguish between normal and fraudulent activities in a telecommunications network. Implications to appropriate user behavior modeling are, also, discussed. Real world cases of defrauded user accounts are modeled by means of selected usage features and comparisons with other approaches are made.

***Keywords*—** Fraud detection, genetic programming, user profiles, feature selection, telecommunications

I. Introduction

FRAUD detection is important to the telecommunications industry because companies and suppliers of telecommunications services lose a significant proportion of their revenue as a result. The Communications Fraud Control Association (CFCA) recently announced the results of a global survey carried out in 2013. Experts estimate 2013 fraud losses at $46.3 billion (USD), up 15 % from 2011. As a percent of global telecom revenues, fraud losses are approximately 2.09%, a 0.21% increase from 2011. The main reason for the relative increase in fraud is due to more fraudulent activity targeting the wireless industry [1].

Several categories of telecommunications fraud have been reported in the literature. The most prominent are the technical fraud, the contractual fraud, the procedural fraud, and the hacking fraud [2]. The first three usually burden the economics of the service provider, while hacking fraud also harms the subscriber. Hacking fraud is usually met in the form of the superimposed fraud, where the fraudster (cracker) uses a service concurrently with the subscriber and burdens his account. The present paper focuses on superimposed fraud identification.

Exchange of information in fraud detection is limited by the fact that it makes no sense to describe the methods in detail, as it gives fraudsters the information they require to evade detection. Moreover, companies and organizations that have been defrauded refrain from revealing the situation due to reputation concerns. Additionally, fraud detection problems involve huge data sets which are constantly evolving. Data sets can be as large as tenths of thousands of calls per weekday for a large organization with 3 or 4 thousand employees, to hundreds of millions of calls for national carriers. One should also consider the size of the related metadata.

Another difficulty with fraud detection is the fact that, nowadays, the term telecommunications is wider than ever. It includes both wired and wireless systems, mobile and cellular systems, legacy systems (PSTN, ISDN), terrestrial and satellite networks, and a plethora of Internet based communication applications. The diversity of network types and applications, along with the deregulation of the market and the relocation of services to the cloud makes fraud detection a complex task.

One way to detect fraud is by analyzing the activity of a user and comparing recent transactions with his historical behavior. In order to achieve this task one needs to build a user model or profile. This is a representation of the so called historical, normal or typical behavior of the user. Analysis is then achieved by means of statistical and probabilistic methods, neural networks and rule based systems that search for diversions from the normal. There are generally two approaches: the "absolute analysis" that searches for limits between legal and fraudulent behavior, and the "differential approach" that tries to detect extreme changes in the user's behavior.

Apart from the fraud detection task, the modeling and characterization of users' behavior in telecommunications can be used to improve network security and services, provide personalized applications, and optimize the operation of electronic equipment and/or communication protocols.

Research in telecommunications fraud detection is mainly motivated by fraudulent activities in mobile technologies [2], [3]. Recent research also focuses on VoIP technologies [4].

This work has been co-financed by the European Union (European Social Fund – ESF) and Greek national funds through the Operational Program "Education and Lifelong Learning" of the National Strategic Reference Framework (NSRF) - Research Funding Program: ARCHIMEDES III. Investing in knowledge society through the European Social Fund.

C. S. Hilas, S. A. Kazarlis, and P. A. Mastorocostas (corresponding author) are with the Department of Informatics Engineering, Technological Educational Institute of Central Macedonia, Terma Magnisias, 62124, Serres, Greece (phone: 0030-23210-49380; fax: 0030-23210-49118; e-mail: chilas@teicm.gr; kazarlis@teicm.gr; mast@teicm.gr).

I. T. Rekanos is with the School of Electrical and Computer Engineering. Aristotle University of Thessaloniki, Thessaloniki, 54124, Greece (e-mail: rekanos@auth.gr).

ISBN: 978-1-61804-228-6

Fraud detection methods can be based on statistical or machine learning techniques and may be supervised or unsupervised [5]-[7]. Fawcett and Phua [8] have assembled the bibliography on the use of data mining and machine learning methods for automatic fraud detection up to 2005. A user behavior characterization model that gives good results towards superimposed fraud detection has been proposed in [9].

In the present paper, Genetic Programming is applied to test the ability of the method to correctly classify cases of normal and fraudulent behavior. This is a first step in an attempt to examine the performance of several evolutionary algorithms in the problem of telecommunications fraud detection.

Genetic Programming has already been applied on problems of credit card fraud detection. Carlos *et al*. propose the use of Genetic Programming (GP) to model and detect fraud (charge back) in electronic transactions, more especially in credit card operations [10]. Techniques of finding optimal solutions for the problem of fraud in a credit card payment system and implicitly generate the results using a genetic algorithm are examined in [11]. The aim is to develop a method of generating test data and to detect fraudulent transactions with the algorithm proposed.

The paper proceeds as follows. In the next chapter a brief introduction to genetic programming is made. In chapter 3, the data, the user modeling and the feature selection process are presented. Experimental results are given in chapter 4. In the last chapter conclusions are drawn.

II. Genetic Programming

Genetic Programming (GP) is one of a number of evolutionary algorithms that are inspired by natural evolution. The founding idea behind its birth was that computer software development could be seen as an optimization problem that could be tackled by an evolutionary algorithm. However, GP has moved beyond the evolution of software, and has been successfully applied to a variety of complex problems where possible solutions are represented by complex structures, like analog and digital circuit optimization, symbolic regression, network routing, engineering design, and so on. Moreover, GP's ability to discover novel and innovative solutions has reasonably led to its designation as an "invention machine" [12].

Many researchers have applied GP to various systems by employing linear strings, non-linear trees or graphs. Some blend GP with linear regression or context free grammars (CFGs) while others use GP to model ontogeny and organism [13], [14]. Although GP can be easily applied to classification problems, [15], mostly due to its tree like structure, there are proposals to use genetic programming for data clustering [16].

The most significant difference of GP to other evolutionary methods, like genetic algorithms, lies in the representation of the solutions. GP employs a tree structure, whereas genetic algorithms represent the solutions as strings of symbols [13], [14]. The trees consist of two types of elements: nodes and leaves. Nodes are functional elements which connect other elements using the functions assigned to the nodes. On the other hand, leaves are endpoints consisting of values or inputs, and have no further connections below.

An example of such a tree is depicted in Fig. 1. The tree contains 3 nodes and 4 leaves and the expression reads as $\{(x_1/x_2)+(x_2-0.2)\}$. Here, the leaves normally take the values of any real number or input variables. Fitness function is the quantitative measure of how well a program has learned to predict the output(s) in terms of the input(s) [14]. It gives a feedback to the learning algorithm regarding which individuals should have a higher probability of being allowed to survive and reproduce. The fitness function should be designed in such a way to fully reflect the physical objective of the problem.

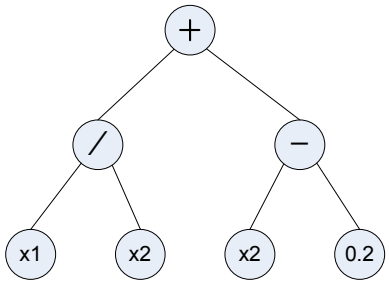

Fig. 1 An example of a tree structure representation of a program

After evaluating the quality of individuals, the algorithm decides which individuals are maintained and how new individuals are created (Fig. 2). This task can be carried out by the parent selection and the reproduction operators. Parent selection is usually performed by means of a probabilistic method, which selects parents with a probability proportional to their fitness. Reproduction is the method that creates new individuals within the population. Many reproduction operators may exist, with the most prominent being the crossover and the mutation functions. Reproduction aims to the exploration of promising regions in the search space [13], [14]. In other words, selection and reproduction are responsible for the population evolution, and affect the progress of the population fitness towards optimality and also the speed of convergence. As such, a decision on the type of reproduction to be applied is one of the most important tasks.

Due to the uniqueness in the representation (i.e., tree) of GP, crossover is different from that of usual evolutionary algorithms [13], [14]. The simplest way to perform crossover on the tree-type structure is to use branch cutting and splicing. The method of exchanging proper subtrees (of parents) is very effective in increasing the exploratory power of GP.

Unlike crossover, mutation is performed on only a single individual with a small probability [13], [14]. It plays an important role in maintaining search diversity of GP. Many mutation operators may be implemented in a GP paradigm, like simple node content mutation, or leaf content mutation operators, but one has also to consider architecture-altering mutation operators that alter the geometry of the tree-encoded genotypes. For example, when an individual has been selected

ISBN: 978-1-61804-228-6

for mutation, a point (i.e., node) in the tree is randomly chosen, and then the existing sub-tree at that point is replaced with a newly generated sub-tree. The mutated individual is then placed back into the population.

III. User Modeling and Feature Selection

In telecommunications systems, user transactions and hence user behavior is contained in the Call Detail Record (CDR) of any Private Branch Exchange (PBX). The CDR contains data such as: the caller ID, the chargeable duration of the call, the called party ID, the date and the time of the call, etc, [17]. These features may be used to construct appropriate user profiles.

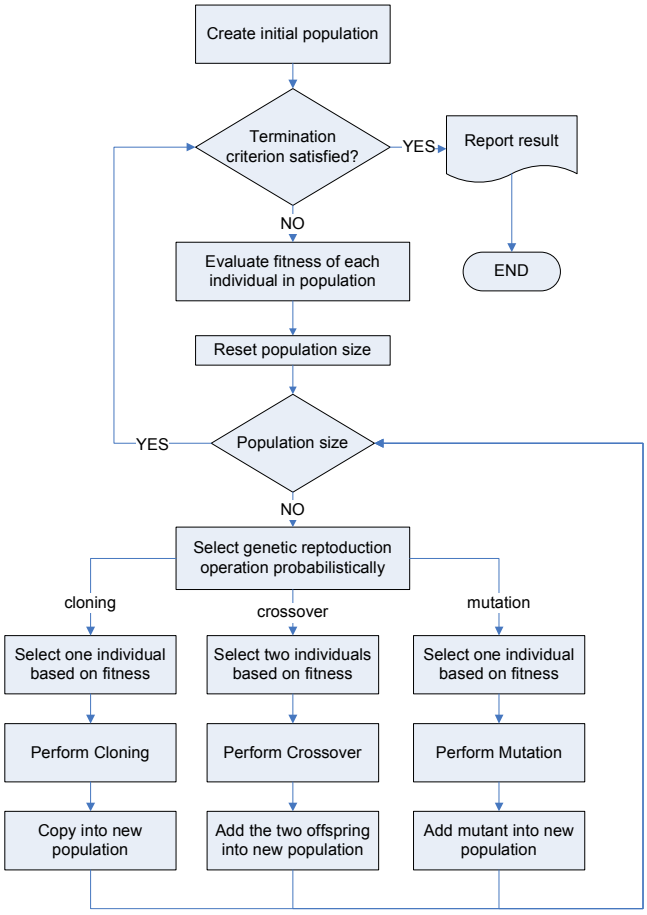

Fig. 2 The basic genetic programming algorithm

Our experiments are based on real world data extracted from a database that holds the CDR records from an organization's PBX, and span in a period of eight years. Several defrauded user accounts, which contain both examples of legitimate and fraudulent activity, have been identified and marked by a field expert. Each phone call has been marked as either normal or defrauded. If at least one fraudulent call was present then the whole day was marked as fraud, else it was marked as normal.

The daily data used for the construction of the profiles are the number of calls per day (Calls), the duration of these calls (Dur), the corresponding charging units (Units), the maximum duration of one call (MaxDur), and the maximum units for one call in this day (MaxUnits). These features are combined in one profile, (Fig. 3), to test the daily characteristics of fraud.

Prior research on the topic has concluded that accumulated characteristics of a user give better discrimination results [6], [9]. The most promising user profile is shown in Fig.4. It consists of seven fields which are the mean and the standard deviation of the number of calls per week (calls), the mean and the standard deviation of the duration (dur) of calls per week, the maximum number of calls, the maximum duration of one call and the maximum cost of one call. All maxima are computed within a week period. This profile representation has also been used in this study.

The original data set consists of 22,000 phone calls. The calls correspond to 5,541 days (2,702 days of legitimate behavior and 2,839 of fraudulent one). The weekly aggregation of these calls for each user is represented by means of the user profile in Fig.4. This yielded 2,014 vectors (weeks) with 7 variables each. Normal usage constitutes the 51.1% of the whole data set (class 1), while fraudulent usage is the remaining 48.9% (class 2). It is pointed out that the rate of weeks and days is not 1:7, because the weekly aggregation was performed per user, so days with zero activity were omitted. It is also noted that data in the fraud detection field are usually unbalanced in the sense that the examples of at least one learning class are rare [15]. However, in our case the number of data in the classes is comparable since the user accounts that were selected were defrauded for a long time and have both examples of the legitimate users' behavior as well as examples of the superimposed fraudulent behavior.

Calls	Dur	Units	MaxDur	MaxUnits

Fig. 3 The basic vector for the daily user behavior representation

mean(calls)	std(calls)	mean(dur)	std(dur)	max(calls)	max(dur)	max(cost)

Fig. 4. The basic vector for the weekly user behavior representation

A. Feature Selection

When constructing behavior profiles, one needs to use the most relevant features, i.e. the features that are more capable of discriminating the problem classes. The process of profile construction is by itself a feature selection process, performed by a field expert who uses his specific knowledge in order to select the most appropriate features. However, automated methods also exist and are used to assist the feature selection process and reduce the problem's dimensionality. By doing so, one may have a more easily interpretable representation of the problem. There are two main approaches in feature selection, namely the filter methods and the wrapper methods [18]. Most methods search the attribute space in order to select the

ISBN: 978-1-61804-228-6

attributes that are strongly correlated with the problem classes and less correlated with each other. Feature selection works either with forward selection or with backward elimination [19].

In the present paper four different feature selection methods were applied. These are the Exhaustive Search, the Genetic Search, the Greedy Forward Selection, and the Ranker method [20]. The last one was applied with the Information Gain as relevance measure.

Table I: Feature selection for the weekly representation of the users

Attribute		***Feature Selection Method***			
		Exhaustive Search	Genetic Search	Greedy Forward Selection	Ranker (Information Gain)
		Number of folds (%)			Average rank (rank)
1	MeanCalls	10(100%)	10(100%)	10(100%)	1,6 ± 0,49 (1)
2	StdCalls	8(80%)	8(80%)	8(80%)	3,8 ± 0,4 (4)
3	MeanDur	10(100%)	10(100%)	10(100%)	5 ± 0 (5)
4	StdDur	10(100%)	10(100%)	10(100%)	1,9 ± 1,22 (2)
5	MaxCalls	2(20%)	2(20%)	2(20%)	2,7 ± 0,46 (3)
6	MaxDur	0(0%)	0(0%)	0(0%)	7 ± 0 (7)
7	MaxUnits	0(0%)	0(0%)	0(0%)	6 ± 0 (6)

Table II: Feature selection for the daily representation of the users

Attribute		***Feature Selection Method***			
		Exhaustive Search	Genetic Search	Greedy Forward Selection	Ranker (Information Gain)
		Number of folds (%)			Average rank (rank)
1	Calls	10(100%)	10(100%)	10(100%)	1 ± 0 (1)
2	Dur	10(100%)	10(100%)	10(100%)	2,6 ± 0,49 (3)
3	Units	10(100%)	10(100%)	10(100%)	2,4 ± 0,49 (2)
4	MaxDur	0(0%)	0(0%)	0(0%)	5 ± 0 (5)
5	MaxUnits	0(0%)	0(0%)	0(0%)	4 ± 0 (4)

Stratified ten-fold cross validation was used for the selection of samples. All methods gave similar results which are presented in Table I. Attributes 1 – 4 are characterized as highly relevant by most of the methods, attribute 6 and 7 are characterized as irrelevant, while the characterization of attribute 5 depends on the method. The procedure was also applied to the daily representation of user behavior. The corresponding feature selection is shown in Table II.

B. Evaluation statistics

Since we intend to use GP as a classifier, we need some statistics to evaluate its performance. This cannot be evaluated by a single numeric measure. The number of correct and false classifications are used instead, and they are expressed with measures like the true positive (TP) or the false positive (FP) rate. Two parameters that are commonly used are the recall and the precision. Recall is actually the same as TP. Precision is the number of objects correctly classified over the total number of objects that were classified in the same class, *precision*=TP/(TP+FP). The *F-measure* statistic is equally often used:

$$F-measure=\frac{2\times recall\times precision}{recall+precision}=\frac{2\mathrm{TP}}{2\mathrm{TP}+\mathrm{FP}+\mathrm{FN}} \quad (1)$$

IV. Experimental procedure and results

In order to test the weekly profiles of the users several configurations of a Genetic Programming classifier were examined. Typical configuration parameters of the GP classifiers that were used in our experiments are given in Table III and in Table IV. The weekly data consist of 2014 vectors. These were divided into two sets, i.e. the training set which holds 70% of the data and the validation set which consists of the remaining 30%. All data were normalized to have mean 0.0 and standard deviation 1.0.

The initial population for each GP run was set to 100 instances. The termination criterion used was the maximum number of allowed generations which was set to 1,000. The confidence on one class recognition was used as the solution's fitness evaluation. We believe that this is the most appropriate fitness indicator to our problem.

ISBN: 978-1-61804-228-6

For each of the two user profiles eight experiments were conducted. Each profile was tested both with and without feature selection. Due to space limitations only the statistics for the weekly representation of users is given here. For the other profile, the daily one, results are in general about 20% worse.

Table III. Basic parameters of the GP classifier

Genetic Programming Parameters	
Population Size	100
Max depth of program trees	8
Max no of leaf nodes	21
Proportion of inputs in terminals (leaves)	0,5
Possible Node Functions	+, -, /, *, If, >, <, &, |, Max, Min
Selection Method	Selection with probability proportional to the solution's relative fitness (fitness/ sumfitness)
Elitism	The best parent (1) is copied to offspring population
Termination Criterion	
Max generations	1,000

Table IV. Operator usage

Crossover Operator	
Crossover Type	"Crosses" two programs together, switching a random sub-tree from each of the programs
Probability	0.8 (0.2 Cloning)
No of parents recombined	2
No of offspring produced	2
Mutation Operator 1	
Mutation Type	Mutates a whole randomly selected sub-tree from a program
Probability	0.05
No of parents involved	1
No of Offspring produced	1
Mutation Operator 2	
Mutation Type	Random Genotype (creates a completely random program)
Probability	0.05
No of parents involved	1
No of Offspring produced	1
Mutation Operator 3	
Mutation Type	Mutates a randomly selected node
Probability	0.05
No of parents involved	1
No of Offspring produced	1
Mutation Operator 4	
Mutation Type	Produces a clone of the selected program for the next generation.
Probability	0.05
No of parents involved	1
No of Offspring produced	1

The possible node functions that were used are the comparison operators (less than) and (more than), the logical functions IF, And, and Or, and the arithmetic functions of addition, subtraction, multiplication and division. The arithmetic functions were not used in half the experiments, as to our understanding of the problem it would be difficult to explain a relationship of the type (MeanDur/MaxDur). However, they were used in the other half of the experiments just to test the performance of the GP classifier. Last, we asked the classifier to build either large or small trees. Large trees, with more than 8 levels of depth, are expected to fit better to the data and give better performance statistics, however, it would be difficult to interpret, compared to their smaller counterparts.

Table V presents the performance of each configuration given all other parameters are kept constant. The classifier is asked to keep the elite 5 programs for each class and the mean outcome from each program is reported in Table V. One may observe that when all features are used, or when larger trees are build or when more functions are used, fitness is better. Nonetheless, since differences are small one may prefer a classifier with less functions and smaller size that would be easier to interpret.

Table V. Performance of the GP classifier for different configurations

Case no.	*Feature selection, tree depth, {functions}*	*Mean Fitness*	*Mean tree size*
1	No, 8, {+, -, /, *, If, >, <, &, |}	0.7918	33.28
2	No. 8, { If, >, <, &, |}	0.7737	17.80
3	No, 4, {+, -, /, *, If, >, <, &, |}	0.8302	14.00
4	No, 4, { If, >, <, &, |}	0.7498	9.25
5	Yes, 8, {+, -, /, *, If, >, <, &, |}	0.7714	43.25
6	Yes, 8, { If, >, <, &, |}	0.7209	22.75
7	Yes, 4, {+, -, /, *, If, >, <, &, |}	0.7628	11.75
8	Yes, 4, { If, >, <, &, |}	0.7328	9.25

In this work the genetic programming algorithm was used to produce multiple one-class classifiers, by keeping some of the elite programs after each run. One way to enhance the classification ability of the approach is to combine the elite programs' descriptive ability. In other words, one may create a multiclass classifier from multiple one-class classifiers (multiple GP runs). In order to achieve this, one may apply some kind of boosting technique. Boosting is a machine learning approach based on the idea of creating a highly accurate prediction rule by combining many relatively weak and inaccurate rules. In our case AdaBoost was used [21]. The AdaBoost algorithm was the first practical boosting algorithm, and remains one of the most widely used and studied, with applications in numerous fields [21], [22].

Table VI presents five accuracy statistics for the aforementioned cases, i.e. the cases of Table V that correspond

ISBN: 978-1-61804-228-6

to the weekly profiles of users. These are the TP rate, the FP rate, the Recall, the Precision, and the F-measure. The confusion matrices for the four best cases are also presented, (Table VII). The percentage of objects that are correctly classified is more than 75% for all the cases. If the results are compared in pairs one may observe that the classifier's performance deteriorates slightly for GPs with fewer functions. However, the use of fewer and more relevant to the problem functions allow us to better interpret the results.

Table VI. Statistics for the classifiers that correspond to the weekly representation of users (cases of Table V) without feature selection, after the application of AdaBoost

Statistics for Case1 (target tree depth: 8, all functions)					
TP Rate	FP Rate	Precision	Recall	F-Measure	class
0.942	0.109	0.901	0.942	0.921	1
0.891	0.058	0.936	0.891	0.913	2
Statistics for Case2, (target tree depth: 8)					
TP Rate	FP Rate	Precision	Recall	F-Measure	class
0.929	0.228	0.81	0.929	0.866	1
0.772	0.071	0.912	0.772	0.837	2
Statistics for Case3, (target tree depth: 4, all functions)					
TP Rate	FP Rate	Precision	Recall	F-Measure	class
0.962	0.126	0.889	0.962	0.924	1
0.874	0.038	0.957	0.874	0.913	2
Statistics for Case4, (target tree depth: 4)					
TP Rate	FP Rate	Precision	Recall	F-Measure	class
0.858	0.205	0.814	0.858	0.836	1
0.795	0.142	0.843	0.795	0.818	2
Statistics for Case5 (target tree depth: 8, all functions)					
TP Rate	FP Rate	Precision	Recall	F-Measure	class
0.933	0.175	0.848	0.933	0.889	1
0.825	0.067	0.922	0.825	0.871	2
Statistics for Case6, (target tree depth: 8)					
TP Rate	FP Rate	Precision	Recall	F-Measure	class
0.953	0.258	0.794	0.953	0.867	1
0.742	0.047	0.938	0.742	0.829	2
Statistics for Case7, (target tree depth: 4, all functions)					
TP Rate	FP Rate	Precision	Recall	F-Measure	class
0.923	0.175	0.847	0.923	0.883	1
0.825	0.077	0.911	0.825	0.866	2
Statistics for Case8, (target tree depth: 4)					
TP Rate	FP Rate	Precision	Recall	F-Measure	class
0.936	0.259	0.791	0.936	0.857	1
0.741	0.064	0.917	0.741	0.82	2

V. Conclusion

In the present paper, an application of genetic programming to fraud detection has been presented. GP algorithm has been used as a classifier in order to distinguish between normal and fraudulent activity in a telecommunications network. The data used came from real defrauded user accounts. Feature selection methods have been applied before tree building.

The outcome of this work coincides with the findings of [23], where decision trees had been applied on the same problem and data. The performance statistics derived here are comparable and sometimes better than those in [23], especially after boosting.

Regarding the problem of fraud detection and the more appropriate representation of a user's activity, it has also been concluded that the aggregated weekly profile gives better classification results.

Table VII. Confusion matrices for the four best cases of Table VI

Confusion matrix for Case1			*Confusion matrix for Case3*		
1	2	Classified as ←	1	2	Classified as ←
970	60	1	991	39	1
107	877	2	124	860	2
Confusion matrix for Case6			*Confusion matrix for Case8*		
1	2	Classified as ←	1	2	Classified as ←
982	48	1	964	66	1
254	730	2	255	729	2

Implications to the fraudsters' behavior have also been found. Since the statistics for Class 1 (normal usage) were always better than those for Class 2 (fraudulent activity), it has been concluded that typical usage tends to be more consistent. On the other hand, fraudsters may differentiate their activity heavily between each other, thus resulting in worst classification outcomes.

One problem with genetic programming is that the solution evolves for some number of generations and the fittest solution is kept and reported to the analyst. This solution is a combination of functions and features whose interpretation may not always be profound to the analyst. Additionally, the fittest solution may alter, due to the evolutionary nature of the algorithm, after a second run. On the other hand, decision trees may be left to evolve to their full size and then be pruned in order to become more easily comprehendible. A solution retrieved by a decision tree algorithm, e.g. C4.5, should always be the same, given the same initial conditions.

Nonetheless, the application of genetic programming to the problem of telecommunications fraud detection looks promising and as a next step to our research we plan to apply Evolutionary Learning Classifier Systems on it.

Acknowledgment

The authors would like to thank the staff of the Telecommunications Center of the Aristotle University of Thessaloniki for their contribution of anonymised data.

References

[1] Communications Fraud Control Association. "2013 Global Fraud Loss Survey," Press Release, Roseland, NJ (CFCA) October 10, 2013, available online: http://www.cfca.org/press.php.

[2] P. Gosset and M. Hyland, "Classification, detection and prosecution of fraud in mobile networks," *Proceedings of ACTS Mobile Summit*, Sorrento, Italy, June 1999.

[3] Y. Moreau, B. Preneel, P. Burge, J. Shawe-Taylor, C. Stoermann, and C. Cooke, "Novel Techniques for Fraud Detection in Mobile Telecommunication Networks," *ACTS Mobile Summit*. Granada Spain 1997.
[4] T. Kapourniotis, T. Dagiuklas, G. Polyzos, P. Alefragkis, "Scam and fraud detection in VoIP Networks: Analysis and countermeasures using user profiling," *50th FITCE Congress (FITCE)*, Palermo Italy, 2011.
[5] R. J. Bolton and D. J Hand, "Statistical fraud detection: a review," *Statistical Science*, vol. 17, no. 3, 2002. pp. 235–255.
[6] C. S. Hilas and P. As. Mastorocostas, "An Application of Supervised and Unsupervised Learning Approaches to Telecommunications Fraud Detection," *Knowledge-Based Systems*, 21, pp 721 – 726, 2008.
[7] D. Olszewski, "A probabilistic approach to fraud detection in telecommunications," *Knowledge-Based System,*. 26, 246-258, 2012.
[8] T. Fawcett, and C. Phua, Fraud Detection Bibliography, Accessed From: http://liinwww.ira.uka.de/bibliography/Ai/fraud.detection.html. 2005.
[9] C. Hilas, and J. Sahalos, "Testing the fraud detection ability of different user profiles by means of FF-NN classifiers," In S. Kollias et al. (Eds.): *ICANN 2006, Part II, NCS 4132*, Springer-Verlag Berlin Heidelberg, 2006, 872 – 883.
[10] C. Assis, A. Pereira, M. Pereira, and E. Carrano, "Using Genetic Programming to Detect Fraud in Electronic Transactions," *19th Brazilian Symposium on Multimedia and the Web - WebMedia'13*, November 5–8, 2013, Salvador, Brazil.
[11] K. RamaKalyani, D.UmaDevi, "Fraud Detection of Credit Card Payment System by Genetic Algorithm," *International Journal of Scientific & Engineering Research*, Volume 3, Issue 7, July-2012.
[12] J. R. Koza, F. H. Bennett III, D. Andre and M. A. Keane, *Genetic Programming III: Darwinian Invention and Problem Solving*, 1st ed., Morgan Kaufman, 1999.
[13] J. R. Koza, *Genetic Programming: On the programming of Computers by Means of Natural Selection*. The MIT Press, 1992.
[14] W. B. Langdon. *Genetic Programming and Data Structures: Genetic Programming + Data Structures = Automatic Programming!*. Kluwer, Boston, 1998.
[15] U. Bhowan, M. Johnston, and M. Zhang, "Evolving Ensembles in Multi-objective Genetic Programming for Classification with Unbalanced Data," *Genetic and Evolutionary Computation Conference - GECCO'11*, July 12–16, 2011, Dublin, Ireland.
[16] Ch. W. Ahn, S. Oh, and M. Oh, "A Genetic Programming Approach to Data Clustering," *International Conference on Multimedia, Computer Graphics and Broadcasting - MulGraB 2011, Part II, CCIS 263*, T.-h. Kim et al. (Eds.), pp. 123–132, 2011.
[17] S. F. Hinde, "Call Record Analysis," *Making Life Easier - Network Design and Management Tools* (Digest No: 1996/217), IEE Colloquium on, 1996, pp 8/1 – 8/4.
[18] G. H. John, R. Kohavi, and P. Pfleger, "Irrelevant features and the subset selection problem," *Proc. 11th Int. Conf. on Machine Learning*, New Brunswick, NJ. 1994, pp 121 – 129.
[19] K. Kira and L. Rendell, "A practical approach to feature selection," *Proc. 9th Int. Workshop on Machine Learning*, Aberdeen Scotland, 1992, pp. 249 – 258.
[20] I. H. Witten and E. Frank, *Data mining: practical machine learning tools and techniques with Java implementations*. London: Academic Press, 2000.
[21] Y. Freund and R. E. Schapire, "Experiments with a new boosting algorithm," *Proc International Conference on Machine Learning*, 1996, pp 148-156, Morgan Kaufmann, San Francisco.
[22] Y. Levasseur, "Artificial intelligence techniques for biological object classification in 2D images," M.Sc. Thesis, École de technologie supérieure, Université du Québec, 2008.
[23] C. S. Hilas, and J. N. Sahalos. "An application of decision trees for rule extraction towards telecommunications fraud detection". *KES 2007/ WIRN 2007, Lecture Notes in Artificial Intelligence*, vol. 4693, Part II, Eds. B. Apolloni et al. Berlin-Heidelberg: Springer – Verlag, pp. 1112–1121, 2007.

Investigating the Reliability of Nano-Scaled BDD-Based Gates

Azam Beg and Ajmal Beg

***Abstract*—**Binary decision diagrams have been useful for synthesis and verification of digital circuits. This paper, for the first time, looks into the reliability of a fewrudimentary gates that were implemented usingbinary decision diagram representations.The gates were designed using 22nm metallic oxide semiconductortechnology node and subject to threshold-voltage variations. The results of the Monte Carlo Spice simulations show that these gates are significantly more reliable than their conventional counterparts.

***Keywords*—**Reliability, static noise margin (SNM),digital circuits, nano-circuits, binary decision diagrams (BDDs), threshold voltage (V_{TH}) variation, Monte Carlo simulations

I. Introduction

A. Nano-scaled circuits and their reliability

Nanotechnology is science, engineering, and technology conducted at the scale between 1 to 100 nm[1]. Nanotechnology is an important technology of the 21st century, and is used for producing different products including integrated circuits (ICs). New nanodevices and nanomaterials are expected to continue contributing to the improvement of the quality of life.

In 2007, Intel started the mass production of 45 nm ICs. In 2010, Intel and Micron introduced 25nm NAND devices. In 2012, Intel introduced Atomprocessor based on 22nm process, and most recently, i.e., in 2013, Intel announced using 14nm technology[2].

Scaling the semiconductor technology deep into the nano-scale allows novel applications such as wireless sensor networks, wearable computers, implantable devices, etc. The emergence of real-life applications depends to a great extent on the ability to fabricate small, ultra low power/energy, yet reliable circuits. However, as the transistor/devicesizes are aggressively shrunk, the manufacturing of ICs becomes more complex and unavoidably introduces more defects. The nano-scaleddevices requiresmall amount of energy for switching, but are highlysusceptible to transient failures[3], [4]. Parameter variation is yet another challenge for reliable operation of circuits and systems[5], [6]. This means that besides the traditional design vectors (power, delay, and area), the reliability also needs to be considered as a design criterion [7].

As transistors are scaled to nano-dimensions, it becomes harder to limit the variation of the threshold voltages (V_{TH}) of the myriads of transistors on a large IC. Formetallic oxide semiconductor (MOS) transistors, the variations of V_{TH} occur primarily due to the randomness of the count andthe positions of the dopant atoms. In[8], it has been shown that V_{TH} can be estimatedwithnormal distribution, with a standard deviation of:

$$\sigma_{V_{TH}} \approx 3.19\times10^{-8}\cdot\frac{t_{ox}\times N_A^{0.4}}{\sqrt{L_{eff}\times W_{eff}}} \quad (1)$$

wheret_{ox} is the oxide thickness, N_A is the channel doping, W_{eff} is the effective channel width, and L_{eff} is the effective channel length. Understandably, the V_{TH}fluctuation can be alleviated by increasing either L_{eff} or W_{eff}, or both[9].

B. Binary Decision Diagrams

The high complexity of today's ICs requires efficient handling of Boolean functions. An important task of a design (CAD) tool is to handle and manipulate the Boolean functions as efficiently as possible. In the past two decades, the binary decision diagrams (BDDs) have gained popularity for efficient synthesis and verification of digital systems.The BDDs were introduced by Lee [11] and popularized by Akers [12] and Boute [13]. The BDDs are based on the principle of Shannon expansion [10].

Any Boolean function $F(x_1, x_2, \ldots x_n)$ can be represented with aBDD[14].In general, a BDD is a *levelized* acyclic graph of nodes. The nodes on a given level represent one input of the function. There is an additional level (at the bottom) with nodes 0 and 1. All nodes (except the 0- and 1-nodes) have two outgoing edges connecting to the lower level nodes. An upper level node can have multiple incoming inputs from the lower levels. A set of inputs results in a path leading 0- or 1-node to the top-level node(s), i.e., the output(s). A fully-specified input-set takes exactly one complete path in the BDD. A sample BDD representing the Boolean function(*sum-of-products*/SOP)$f(x,y,z) = \sum m(0,2,5,7)$ is shown in Fig. 1(a).

The typical BDD-based design procedure consists of the following steps:

1. A truth table of the logic function is determined.
2. Output with 1's in the truth table are mapped to a BDD.
3. The BDD is *reduced*(while retaining its logical properties).
4. Each node in the BDD is implemented using a multiplexer circuit.

Azam Beg is with the College of Information Technology, United Arab Emirates University, Al-Ain, United Arab Emirates (phone: +971-3-713-5565; fax: +971-3-767-2018;e-mail: abeg @ uaeu.ac.ae).

Ajmal Beg is with Cortex Business Solutions, Calgary, Canada jmal_beg@yahoo.com).

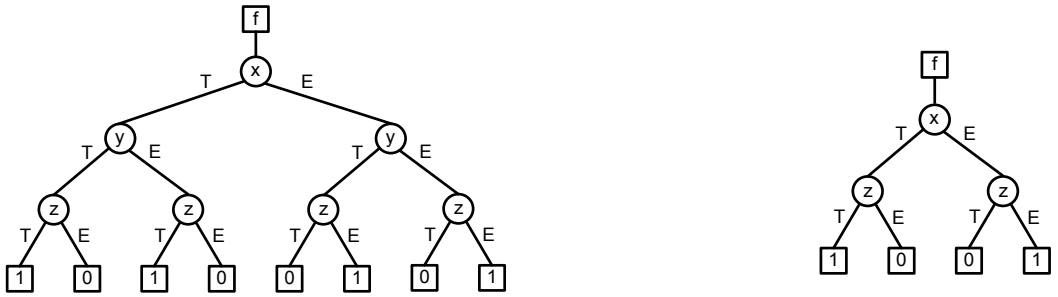

(a) (b)

Fig. 1. Example of BDD in (a) its original form, and (b) in the reduced form (T=true; E=else/false)

Generally speaking, the BDDscan be manipulated and simplified using two techniques:

1. *Redundant nodes* are deleted. A redundant node is a node whose two *child*nodes are identical.
2. *Equivalent nodes* are shared. Equivalent nodes are two or more nodes which have the same variable and the same pair of child nodes.

The unsimplifiedBDD for the aforementioned SOP is drawn in Fig. 1(a); after simplification the BDD reduces to the form shown inFig. 1(b).

A. About this paper

Ours is the first known effort to evaluate the reliability of BDD-based circuits when they are implemented using nano-scaled (22nm) technology node. This paper presents the findings of an initial study of the reliability of the basic gates when implemented with multiplexers. We use *static noise margin* (SNM) as a metric for reliability [15].

II. Related Work

The BDDs have been extensively used for designing optimum logic circuits[16][17]. Simple Boolean functions like adder and comparator has been implemented using BDDs[18]–[20]. More complex computing circuits such as cipher and crypto have also been designed [21].

The evaluation time of a BDD is related to its *path length* and this relationship was investigated and modeled in [22][23].

Low power BDD-based designs have been investigated in [24]–[27]. In addition to power, [26] also considers delaysof the circuits. Power and area-efficient design of an asynchronous adder was looked at in [28].

The BDD representations have been used to model the reliability of different systems [29]–[31]but the reliability of BDD-based circuits themselves has not been reported in any research literature.

Our research in the past few years has focused on the reliability studies of existing and new gate design schemes [32]–[37]. This paper presents the results of our investigation of the reliability ofa few basic BDD-based gates.

III. Experimental Results And Analysis

For estimating V_{TH} and its variations, we have used the MOS model from BSIM4 v4.7 level 54 [38]. For modelling the conventional and BDD-based gates, we have used 22 nm PTM HP v2.1 (high-*k*/metal gate and stress effect)transistor models[39] [40]. We have simulated the gates using NGSpice[41].

The BDDs for the three fundamental gates, INV, NAND2, and NOR2 are shown in Figs. 2 (a)–(c), and the corresponding multiplexer-based implementations are shown in Figs. 2 (d)–(f). The multiplexers are built using the well-known *compound-AOI*22 configuration ofFig. 3. The transistor dimensions in all the experiments are fixed at:$L_{nMOS} = L_{pMOS} = L_{min}$ = 22 nm,W_{pMOS} = 88 nm, and W_{nMOS} = 44 nm. The supply voltage (V_{DD}) is set at 0.8V (the nominal voltage specified in 22nm PTM HP models [39] [40]).

We used the SNM as a measure of reliable operation of the gates. In order to measure the SNM, we used the test setup of Fig. 4(a) for the INV, and the setup of Fig. 4(b) for both NAND2 and NOR2. Understandably, for the INV, a single ramp input is sufficient, while the other gates need different combinations of constant and ramp inputs that result in transitioning of the outputs. For NAND2, the inputsare: 10→11, 01→11, and 00→11; and for NOR2, the inputs are: 00 →01, 00→10,and 00→11.

In order to find the SNMs, we use *shell* and Matlab scripts.The shell script parses through the file simulation log files to create *clean* data files that are easily readable by the Matlab script; the latteractually calculates the SNMs. The script automatically determines: the highest allowed input voltage for logic *low* (V_{IL}); the lowest allowed input voltage for logic *high*(V_{IH}); highest output voltage for logic *low* (V_{OL}); and lowest output voltage for logic *high* (V_{OH}). These four voltage levels arethen used to calculate the SNM as follows:

$$SNM_{low} = V_{IL} - V_{OL} \quad (2)$$

$$SNM_{high} = V_{OH} - V_{IH} \quad (3)$$

$$SNM = \min (SNM_{low}, SNM_{high}). \quad (4)$$

An INV has a single value of SNM (refer to the plot of Fig.

ISBN: 978-1-61804-228-6

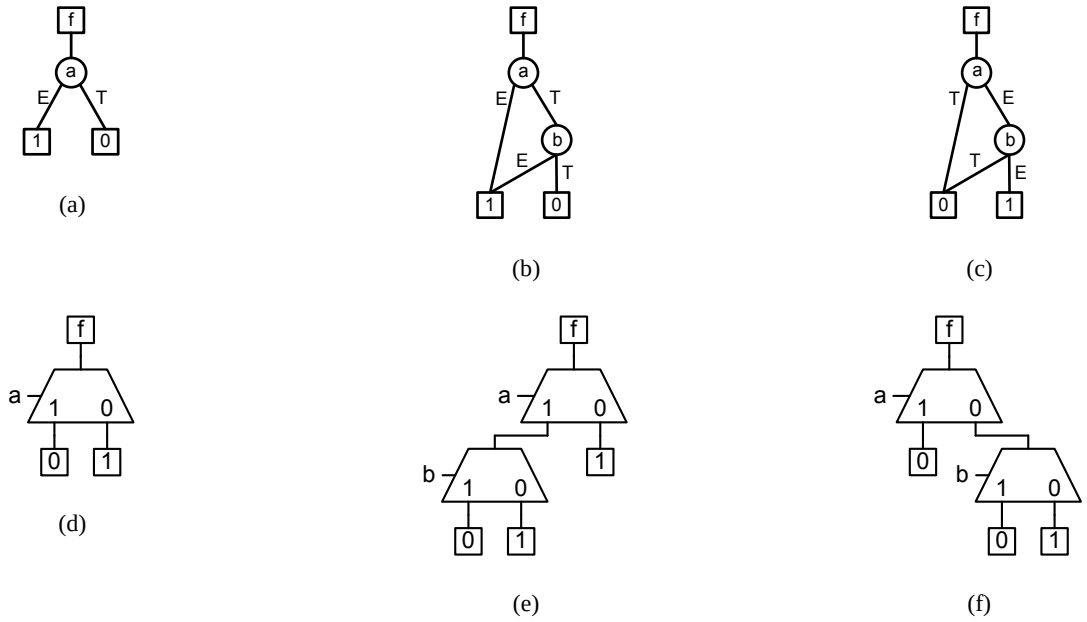

Fig. 2. BDDs for (a) INV, (b) NAND2, and (c) NOR2; multiplexer-based implementation of (d) INV, (e) NAND2, and (f) NOR2

5(a)). In comparison, NAND2 and NOR2 have three different sets of input-output curves (as inFig. 5(b)), resulting in three different SNMs – we consider the worst of the three values as a gate's SNM.

For the purpose of this work, we selected 20% (a common threshold) as the minimum acceptable SNM. This means that if the simulation of gate results in SNM < 20% of V_{DD}, it is considered a *failure*.

We conducted 1000 Monte Carlo simulations for each of three gates (INV, NAND2, and NOR2) in two different configurations (in other words, a total of 6000 simulations): (1) the normal/conventional CMOS design[42], and (2) BDD-based design (Figs. 2(d)–(f)). The V_{TH}'s of the transistors were varied according to equation (1).

A numerical comparison of the SNM variations for the three gates in the normal- and the BDD-implementations is shown in Tables 1 and 2. The histograms of SNMs of the gates are shown in Figs. 6–8.

From Table 1, we observe that BDD-based gates have consistently lower failures than the normal ones. The normal INV has 6% failures as compared to none for the BDD version. NAND2's failures rates are 25% and 2.7% for the normal and the BDD-types, respectively. Normal NOR2 fails 17.5% of the time, while the BDD-version fails in just 0.2% of the simulations. These statistics show that a BDD-based gate is appreciablymore reliable than a normal one. Additionally, the INV due to its simpler construction has lower failure rates than the two-input gates. Both types of NOR2s have higher reliability than NAND2s. Besides the structural differences between the NAND2 and NOR2, the reliability of NAND2 and NOR2 also depends on the input vectors [43].

Table 2 summarizes the effect of V_{TH} variationson the SNMs of the three gates. INVs of both types, normal and BDD, have the highest SNMs. NOR2s have higher average-SNMs(5-7%) than NAND2s. The BDD-based INV has 71% higher average-SNM than the normal one, whereas NAND2 and NOR2 have 85% and 83% higher SNMs, respectively. The standard deviations for SNMs of normal and BDD-gates are quite comparable. BDD-NAND2 shows higher *spread* than the normal one, while NOR2 is just the opposite.

The findings from our experimentsshow thatthe BDD-based gates can be more robust and reliable alternatives to the

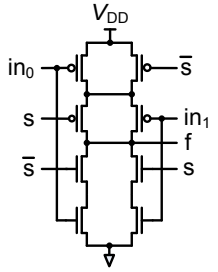

Fig. 3. Schematic of a 2-1 multiplexer

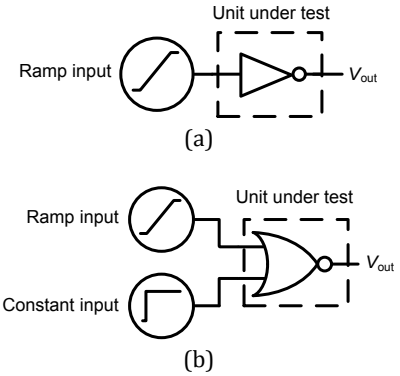

Fig. 4. Test setups for measuring the SNMs of (a) an INV, and (b) NOR2 gate

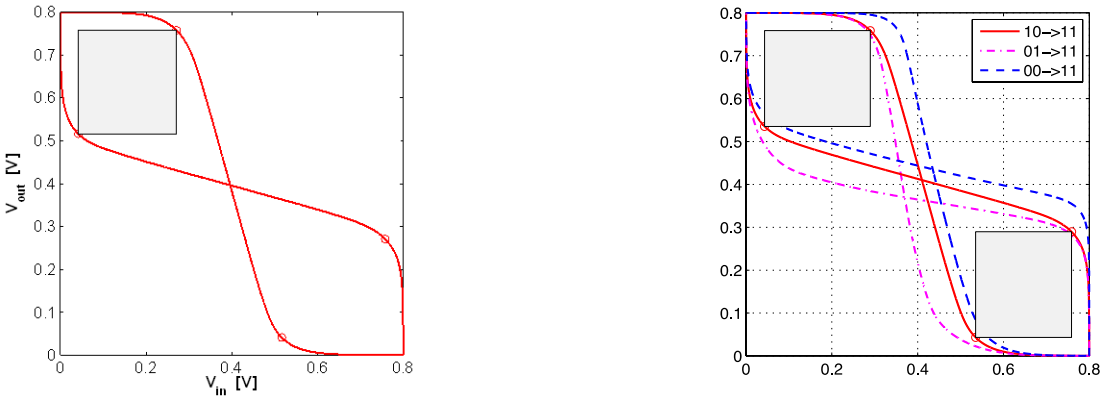

(a) (b)

Fig. 5. Voltage transfer curves for (a) an INV, and (b) a NAND2, for measuring the SNM

conventional gates.However, it is obvious that the BDD-manifestations of the basic gates occupy more area than the conventional ones. One should compare the power and the delay of the BDD and the normal gates –a focus of our current work.

IV. Conclusions

We have explored the reliabilities (measured in terms of noise margin) of BDD-based gates and compared them to the conventional CMOS gates. The BDD-gates have significantly higher SNMs than the conventional gates.

The higher noise margins come at the higher cost in terms of area and possibly the delay and power – a subject of our continued investigation. Use of different multiplexer circuits for the realization of the BDD-nodes is also being looked into.

The three BDD-based basic gates have been *handcrafted*. To facilitate reliability studies of other gates/cells and larger circuits, we would need an automated mechanism for creating both the BDD-descriptions and the corresponding multiplexer-based implementations – this would be yet another extension to our work.

Table 1. Number of failures (defined as SNM < 0.2 x V_{DD}) for normal and BDD-based gates.
(Number of simulations for each gate = 1000)

Gate type	Normal	BDD
INV	60	0
NAND2	250	27
NOR2	173	2

Table 2. SNM (volts) for normal and BDD-based gates

Gate type	Normal		BDD	
	Mean	Std. dev.	Mean	Std.dev
INV	0.2027	0.0251	0.346	0.0242
NAND2	0.1745	0.0332	0.322	0.0924
NOR2	0.1859	0.0419	0.3393	0.028

References

[1] "What is nanotechnology?" [Online]. Available: http://www.nano.gov/nanotech-101/what/definition.[Accessed: 31-Jan-2014].

[2] "Global-Intel-Manufacturing_FactSheet.pdf." [Online]. Available: http://download.intel.com/newsroom/kits/22nm/pdfs/Global-Intel-Manufacturing_FactSheet.pdf. [Accessed: 31-Jan-2014].

[3] C. Constantinescu, "Trends and challenges in VLSI circuit reliability," *IEEE Micro*, vol. 23, no. 4, pp. 14–19, 2001.

[4] P. Shivakumar, M. Kistler, S. W. Keckler, D. Burger, and L. Alvisi, "Modeling the effect of technology trends on the soft error rate of combinational logic," in *International Conference on Dependable Systems and Networks*, 2002, pp. 389–398.

[5] SIA, "International Technology Roadmap for Semiconductors (ITRS)," Semiconductor Industry Association, SEMATECH, Austin, TX, USA, 2009.

[6] Y. Cao and L. T. Clark, "Mapping Statistical Process Variations Toward Circuit Performance Variability: An Analytical Modeling Approach," *IEEE Trans. Comput. Des. Integr. Circuits Syst.*, vol. 26, no. 10, pp. 1866–1873, Oct. 2007.

[7] A. Beg and W. Ibrahim, "Relating reliability to circuit topology," in *IEEE North Eastern Workshop on Circ. & Syst. (NEWCAS'09)*, 2009, pp. 1–4.

[8] A. Asenov, A. R. Brown, J. H. Davies, S. Kaya, and G. Slavcheva, "Simulation of intrinsic parameter fluctuations in decananometer and nanometer-scale MOSFETs," *IEEE Trans. Electron Devices*, vol. 50, no. 9, pp. 1837–1852, 2003.

[9] A. Beg, V. Beiu, and W. Ibrahim, "Unconventional transistor sizing for reducing power alleviates threshold voltage variations," in *Int. Semiconductor Conf. (CAS)*, 2012, pp. 429–432.

[10] C. E. Shannon, "A symbolic analysis of relay and switching circuits," *Trans. Am. Inst. Electr. Eng.*, vol. 57, no. 12, pp. 713–723, Dec. 1938.

[11] C.Y. Lee, "Representation of Switching Circuits by Binary-Decision Programs," *Bell Syst. Tech. J.*, vol. 38, pp. 985–999, 1959.

[12] Sheldon B. Akers, "Binary Decision Diagrams," *IEEE Trans. Comput.*, vol. 27, no. 6, pp. 509–516, 1978.

[13] R. T. Boute, "The binary decision machine as programmable controller," *Euromicro Newsl.*, vol. 2, no. 1, pp. 16–22, Jan. 1976.

[14] R. E. Bryant, "Graph-Based Algorithms for Boolean Function Manipulation," *IEEE Trans. Comput.*, vol. C–35, no. 8, pp. 677–691, Aug. 1986.

[15] A. Beg, "Enhancing Static Noise Margin While Reducing Power Consumption."

[16] M. Ciesielski, "BDS: a BDD-based logic optimization system," *IEEE Trans. Comput. Des. Integr. Circuits Syst.*, vol. 21, no. 7, pp. 866–876, Jul. 2002.

ISBN: 978-1-61804-228-6

[17] R. I. Bahar, E. A. Frohm, C. M. Gaona, G. D. Hachtel, E. Macii, A. Pardo, and F. Somenzi, "Algebraic decision diagrams and their applications," in *Proceedings of 1993 International Conference on Computer Aided Design (ICCAD)*, pp. 188–191.

[18] P. R. Panda, B. V. N. Silpa, A. Shrivastava, and K. Gummidipudi, "Power-efficient System Design," 2010.

[19] and M. B. Singh, Preeti, Chetan Gupta, "Power optimization in a 4-bit magnitude comparator circuit using BDD and pre-computation based strategy," *Int. J. Appl. Eng. Res.*, vol. 7, no. 11, pp. 1482–1485, 2012.

[20] M. Bansal and A. Agarwal, "Ordering and reduction of BDDs for multi-input adders using evolutionary algorithm," in *2013 International Conference on Advanced Electronic Systems (ICAES)*, 2013, pp. 127–130.

[21] S. Morioka and A. Satoh, "A 10-Gbps full-AES crypto design with a twisted BDD S-Box architecture," *IEEE Trans. Very Large Scale Integr. Syst.*, vol. 12, no. 7, pp. 686–691, Jul. 2004.

[22] A. Beg and P. W. C. Prasad, "Prediction of area and length complexity measures for binary decision diagrams," *Expert Syst. With Appl.*, vol. 37, no. 4, pp. 2864–2873, 2010.

[23] P. W. C. Prasad, A. Assi, and A. Beg, "Binary decision diagrams and neural networks," *J. Supercomput.*, vol. 39, no. 3, pp. 301–320, 2007.

[24] P. Lindgren, M. Kerttu, M. Thornton, and R. Drechsler, "Low power optimization technique for BDD mapped circuits," in *Asia and South Pacific Design Automation Conference 2001 (ASP-DAC 2001)*, 2001, pp. 615–621.

[25] S. N. Pradhan, G. Paul, A. Pal, and B. B. Bhattacharya, "Power Aware BDD-based Logic Synthesis Using Adiabatic Multiplexers," in *2006 International Conference on Electrical and Computer Engineering*, 2006, pp. 149–152.

[26] G. P. R. Reddy, J. Ghosh, A. P. C. R. Mandal, and B. B. Bhattacharya, "Power-delay efficient technology mapping of BDD-based circuits using DCVSPG cells," in *2008 3rd International Design and Test Workshop*, 2008, pp. 123–128.

[27] Q. Dinh, D. Chen, and M. D. F. Wong, "BDD-based circuit restructuring for reducing dynamic power," in *2010 IEEE International Conference on Computer Design*, 2010, pp. 548–554.

[28] G. Paul, R. Reddy, C. R. Mandal, and B. B. Bhattacharya, "A BDD-Based Design of an Area-Power Efficient Asynchronous Adder," in *2010 IEEE Computer Society Annual Symposium on VLSI*, 2010, pp. 29–34.

[29] K. S. Trivedi, "A BDD-based algorithm for reliability analysis of phased-mission systems," *IEEE Trans. Reliab.*, vol. 48, no. 1, pp. 50–60, Mar. 1999.

[30] T. Tsuchiya, "A BDD-Based Approach to Reliability Optimal Module Allocation in Networks," in *2012 IEEE 18th Pacific Rim International Symposium on Dependable Computing*, 2012, pp. 121–126.

[31] R. Hu, J. Mi, T. Hu, M. Fu, and P. Yang, "Reliability research for PV system using BDD-based fault tree analysis," in *2013 International Conference on Quality, Reliability, Risk, Maintenance, and Safety Engineering (QR2MSE)*, 2013, pp. 359–363.

[32] A. Beg and W. Ibrahim, "On teaching circuit reliability," in *2008 38th Annual Frontiers in Education Conference*, 2008, pp. T3H–12–T3H–17.

[33] A. Beg, "Reviewing high-level estimation of reliability of nanometric digital circuits," in *9th Int. IEEE Conf. Nanotech. (NANO 2009)*, 2009.

[34] A. Beg and W. Ibrahim, "Relating reliability to circuit topology," in *Circuits and Systems and TAISA Conference, 2009. NEWCAS-TAISA '09. Joint IEEE North-East Workshop on*, 2009.

[35] W. Ibrahim, V. Beiu, and A. Beg, "GREDA: A Fast and More Accurate Gate Reliability EDA Tool," *IEEE Trans. Comput. Des. Integr. Circuits Syst.*, vol. 31, no. 4, pp. 509–521, 2012.

[36] W. Ibrahim, V. Beiu, and A. Beg, "On optimum reliability sizing for complementary metal oxide semiconductor gates," *IEEE Trans. Reliab.*, vol. 61, no. 3, pp. 675–686, 2012.

[37] W. Ibrahim, A. Beg, and H. Amer, "A Bayesian based EDA tool for accurate VLSI reliability evaluations," in *International Conference on Innovations in Information Technology, 2008 (IIT 2008)*, 2008.

[38] B. J. Sheu, D. L. Scharfetter, P.-K. Ko, and M.-C. Jeng, "BSIM: Berkeley short-channel IGFET model for MOS transistors," *IEEE J. Solid-State Circuits*, vol. 22, no. 4, pp. 558–566, Aug. 1987.

[39] W. Zhao and Y.Cao, "New generation of predictive technology modeling for sub-45nm early design exploration," in *7th Int. Symp. Quality Electron. Des.*, 2006, pp. 585–590.

[40] W. Zhao and Y. Cao, "New generation of predictive technology modeling for sub-45nm early design exploration," *IEEE Trans. Electr. Dev.*, vol. 53, pp. 2816–2823, 2006.

[41] "NGSpice – Mixed mode – Mixed level circuit simulator." [Online]. Available: http://ngspice.sourceforge.net/.

[42] J. M. Rabaey, A. P. Chandrakasan, and B. Nikolić, *Digital integrated circuits: A design perspective*, 2nd ed. Prentice Hall, NJ, USA, 2003.

[43] V. Beiu and W. Ibrahim, "Devices and Input Vectors are Shaping von Neumann Multiplexing," *IEEE Trans. Nanotech.*, vol. 10, no. 3, pp. 606–616, 2011.

Azam Beg (M'07) received an MS degree in computer/electrical engineering in 1994, and a PhD degree in computer engineering in 2005, from Mississippi Sate University, MS, USA. From 1991 to 1997, he worked as a test/product engineer and a team lead at Motion Control Engineering, Rancho Cordova, CA, USA. In 1997, he joined Intel Corporation, Folsom, CA, USA, as a Flash Memory Test Engineer. In 1999, he moved to company's Microprocessor Division. There he first worked as a Pre-Silicon Architecture Validation Engineer and then as a Microprocessor Design Engineer. In 2005, he joined the College of Information Technology, United Arab Emirates University, Al Ain, UAE. He is currently an Associate Professor in Computer System Design department of the Faculty. He is the author and co-author of 76journal and conference papers, and book chapters. His current research interests include design and modeling of low-energy and reliable digital circuits, and the application of artificial intelligence to different fields. He holds a UK patent on low-energy instruction caches.

Ajmal Beg received Bachelor of Electronics Degree from Kyoto University, Japan and Master of Electrical Engineering degree from University of Calgary, Canada. He has worked at IBM and SAP for 16 years in different roles such as Hardware Engineer, Software Engineer, Consultant Project Lead and Senior Researcher. Currently he is associated with Cortex Business Solutions and works on reliability/quality assurance of system integration.

ISBN: 978-1-61804-228-6

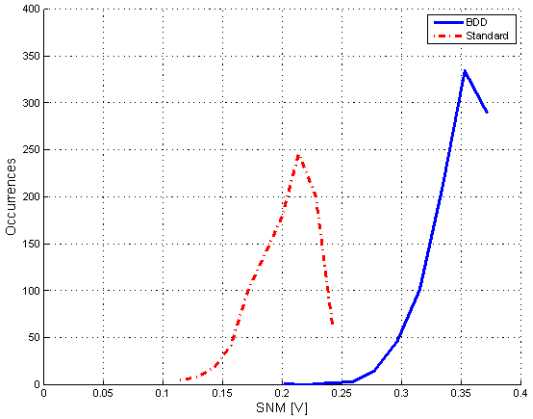

Fig. 6. Histograms of SNM for normal and BDD-based INV's

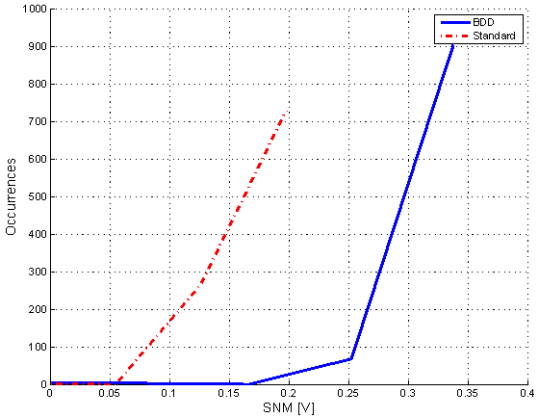

Fig. 7. Histograms of SNM for normal and BDD-based NAND2's

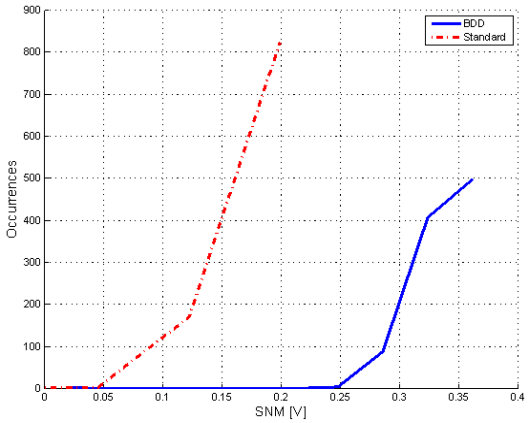

Fig. 8. Histograms of SNM for normal and BDD-based NOR2's

ISBN: 978-1-61804-228-6

An Analysis of Social Media Usage in Teaching and Learning: The Case of SEEU

Lejla A. Bexheti, Burim E. Ismaili and Betim H. Cico

***Abstract*—** Social media are becoming the most important tools for interaction among people, where everybody can share, exchange, comment, discuss and create information and knowledge in a collaborative way. The aim of this study is to analyze the use of social media in teaching and learning based on literature study and experiences in different faculties at South East European University. The study examines the impact of the social media applications on personal and teaching use. Based on a representative sample of teaching staff from all the faculties at SEE University, the study investigates their level of awareness and their experiences in the use of social media, as well as the opportunities and value they see for addition of social media applications as part of the teaching process.

The starting point of the study is to examine impacts of personal use of social media on teaching. In this examination phase we evaluate teachers' level of awareness of the various social media applications. Is the teaching staff as well-informed about the existence of the various social media applications as the general population is or their students are? Like the general population, the teachers might use social media for different purposes. This study attempts to differentiate between two different kinds of use: for personal use only, with no connection to teaching responsibilities and for use in teaching and learning. Further aspects on what value, if any, they distinguish in social media applications and how they use them in the teaching process are also explored.

***Keywords*—**social media, teaching, learning, higher education

I. Introduction

ALTHOUGH the mission of higher education has remained the same for centuries, the environment in which that mission exists is changing dramatically. Consequently, teachers should come up with innovative strategies that anticipate and embrace this change. The main driver of this change is the digital revolution which has shifted many aspects of teaching and learning.

There is a growing recognition that the skills needed to succeed in the knowledge society today and into the future are different in kind from those that were required earlier. Therefore, it is essential for teachers to familiarize themselves with the contemporary social tools or they will simply not be prepared to serve the learning needs of their students.

Teachers exploring this moving landscape will also be able to discover the real potential of social media to transform drastically the pedagogical basis of their teaching experience, giving them tools that they can use in order to create truly adapted and flexible learning experiences for students [1].

II. Literature review

Many current studies suggest that the high take up of social media applications as an addition to formal educational settings offers new opportunities for innovating and modernizing education institutions and for preparing learners for the 21st century [1],[11], [12].

While social media's start was for personal use, it has evolved to be used in virtually all domains. From a preliminary check, it appears that almost every college and university in the world has adopted some form of social media, using it for general outreach, to attract potential students, maintain alumni relations, and increase institutional reputation and pride [2].

A primary reason to adopt social media in the classroom is because it is familiar to almost everybody and also because it doesn't cost and requires minimal training. One of the largest surveys of social media in higher education to date shows that universities can lever social media into the classroom and ensure its used more than it is now [3][4].

Some academic experts believe that social media can be used as an effective teaching tool in higher education because of its ease of use, ready availability, and individual affordability and network effects.

Facebook has been used in university courses to facilitate teacher/student discussion, and wikis and blogs have been used to collaborate on projects and receive rapid feedback [5].

Some courses have also used YouTube as a platform for students to create and share videos for their course [6]. In other courses, students have used Twitter to discuss course topics during class, with Tweets being displayed on a large screen to encourage cross group communication [7].

Not only can social media facilitate peer communication and collaboration, it can facilitate communication between students and teachers. Studies have shown that students are more likely to communicate with their professors if they are Facebook friends with them [8].

In general, the research conducted in the field identifies four main dimensions in which social media can lead to innovations in teaching and learning [11]:

1) Content. Social media allow students to access a enormous variety of learning materials in most of the cases free of charge. It supports teaching and learning in a lifelong learning scale; it contributes to fairness and inclusion and increases standards on Higher Education

institutions to improve the quality and availability of their course content.

2) Creation. Social media gives the possibility to the students to create digital content on their own and publish it online, increasing a vast resource of user-created content from which learners and teachers can jointly benefit, also encouraging more active and proactive approaches to learning.
3) Connecting. Social media is a network that connects students with one another, and to their teachers, allowing them to share their knowledge and at the same time have access to specific and targeted knowledge in a given field of interest.
4) Collaboration. Social media makes possible collaboration between learners and teachers on a given task or project or a joint objective, pooling resources and gathering the expertise of a group of people working towards a common objective.

III. Study of Social Media Usage

Social media are becoming more and more widespread in higher education. The trend can be observed in many higher education institutions around the world [9][10]. There are many ways of appropriating online social media for teaching and learning. Higher education institutions including SEEU are putting their efforts into developing such environments. The aim of this study is to observe the personal (private) as well as the use of social media web sites for teaching by the teaching staff at SEEU.

In this study, teachers' use of social media as a tool for enhancing the teaching and learning process was explored. Like the wider public, teachers may use social media web sites for numerous reasons. This research will distinguish and observe the influence of the social media web sites for personal and for teaching use.

Additional information on the value that teachers identify in social media web sites and how they employ them in their teaching classes will be also explored.

A more detailed explanation of the survey sample and design is provided below.

A. General Information about the sample

The analysis is conducted by using data gathered from a survey carried out at SEEU on the years 2011 and 2013. The survey has been delivered by Google form via domain email to all academic staff at SEEU. Considering the sample size, the data consist of 82 observations for 2011 and 36 observations for 2013.

The survey covers several well-known social media like Facebook, Youtube, Twitter, LinkedIn, SlideShare. Blogs, wikis, video and podcasts were included as well.

This research involves academic and administrative staff engaged in the teaching process from all faculties at South East European University (SEEU). The survey sample represents 59% of all full time academic and administrative staff involved in teaching at SEEU what provided a sufficient number of responses for this study.

Additionally, in order to indentify the trends and drawbacks in the use of social media sites at SEEU, for several topics the study compares data from the survey carried out on 2011 with the latest results from 2013 among the staff.

B. Survey Design

The survey included a mixture of open and closed questions. The closed questions were check boxes where respondents could select one response from a range of possible answers. Open questions allowed respondents to fill in a text box with as much information as necessary. The survey questions were arranged into 3 sections as listed below.

Section 1 - General. On this part were gathered some general data about the profile of the respondents such as: teaching experience, department and age.

Section 2 - Social Media Usage. This section is the central part of the survey and included more detailed questions regarding the specific social media tools and their importance in improving teaching and learning process.

Section 3 - Interviews. This part had open questions regarding the use of social media in teaching and learning. The responders gave their personal opinions, experiences and views about social medial use in teaching and learning process.

IV. Survey Results on the Usage of Social Media in Teaching and Learning at SEEU

In this part are presented and discussed the results gained from the survey on the teacher's use of social media for teaching and learning at SEEU. These results include data from the survey carried out in 2011 and 2013.

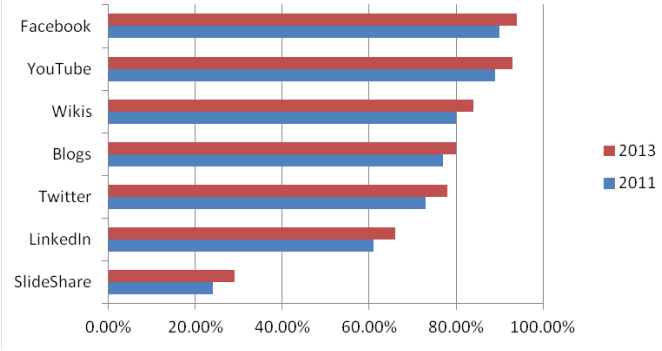

Fig.1 Teacher awareness of social media sites

A. Teachers' awareness with popular social media sites

Initially was observed the level of teachers' awareness for several most popular social media sites (Fig.1).

As it can be expected given the high level of awareness of social media among the general population, 90% of the

ISBN: 978-1-61804-228-6

teachers report they are aware of social sites such as Facebook and YouTube. Around 80% report they know about blogs and wikis. The awareness level fails for other less common sites, with 70% saying that they know of Twitter, 60% LinkedIn and a lower percentage around 30% report they are aware of presentation-sharing site SlideShare. Also in general there is a slight enhancement of approximately 5% higher awareness for the social media sites from 2011 to 2013.

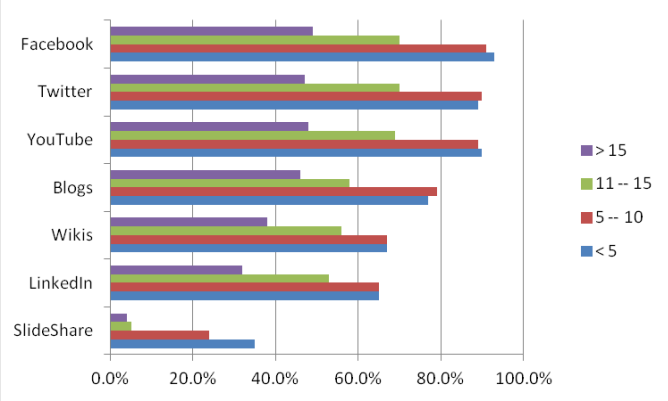

Fig.2 Teachers' use of social media in teaching by experience in teaching

Based on the fact that social media is a more or less contemporary issue, the survey also investigates whether contemporariness influences in differences in social media awareness by teachers age or by years of experience in teaching. When examined by experience in teaching, teachers' responses indicated that there is no significant difference in the awareness of social media. Regardless their experience in teaching the awareness levels among teachers was nearly universal. But there was a major difference on the level of usage of the social media in teaching process based on the years of experience. The study showed that the more experienced teachers were more reluctant towards application of the social media in their teaching (Fig.2). And on the other side the younger staff with less experience in teaching adopt a variety of social media in their classes.

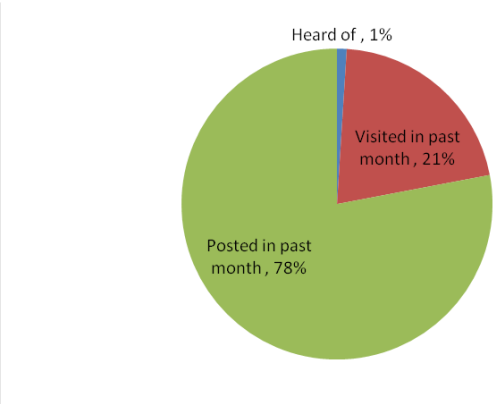

Fig. 3 Teacher personal use of social media

B. Teachers' personal use of social media sites

In this part of the survey was explored the teachers' personal use of social media sites. Actually it's not the same if you have just heard of some social media sites and if you make use of these sites.

To discover these elements, SEEU teaching staff was asked about their use of social media for personal purposes. With the exception of those "Heard of" with 1%, teachers' personal use of social media sites is quite high. As shown in Fig.3, 21% of all teachers just visited a social media site within the past month for personal use, and 78% visited and posted some content during that period. At the same time, teachers' use is not confined to a single site. The majority of teachers have visited more than one social media site, with nearly 28% visiting three or more sites.

Social media use among teachers does not consist only of passive reading and/or viewing. Teachers who posted some content during the past month are doing so on more than one site. However, even though the level of teachers' awareness does not vary with age or with experience in teaching, the usage level does.

Following on, as we can see from Fig.4, teachers have different patterns of personal use for different social media oriented sites. Based on the data from the survey carried out on the 2013, 70% of all teachers' visited Facebook during the past month. This is closely followed by visits to YouTube (62%). The visiting frequency is much lower for other social media sites, having 37% of the teachers visited Wikis, 30% LinkedIn and 22% Twitter, while the visiting rates for SlideShare is 11%.

The posting frequencies are much lower than the visiting ones. Almost half of the teachers who visited Facebook also posted (70% visited and 34% posted). Posting rates for other sites are much lower (Fig.4).

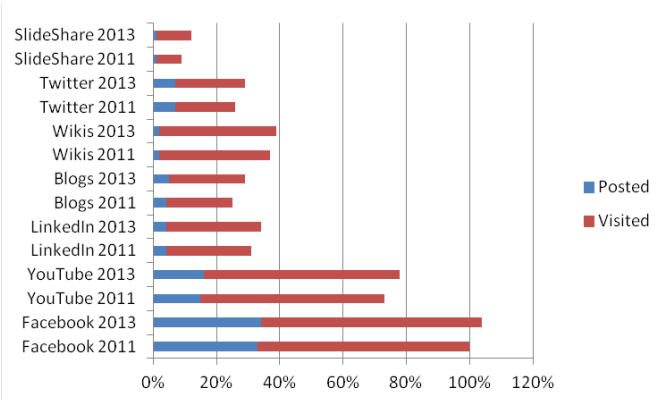

Fig. 4 Teachers personal social media use by site

C. Teachers' use of social media sites for teaching purposes

The majority of surveyed SEEU teachers are well aware of social media, and most are using them for personal purposes. But, in order to identify if they also think that social media can be a part of their course syllabuses, teachers were asked to identify their use of social media in their classes, posting for

student use out of class, and use as part of student homework or in class assignments. It is obvious, based on the results, that teachers include considerably social media in their teaching classes. Online video from either YouTube or other online video sites are seen as having the greatest value for use in classes. This corresponds with the usage pattern of those sites, where online video is the most-used form of social media in courses.

As shown in Fig.5, almost half of the overall usage of social media in teaching is on online videos and the other half is distributed among the other social sites (Facebook, Blogs, Twitter and Wikis). These results show good and active use for classroom and out of class activities and comparing with the results from the 2011 show a positive trend.

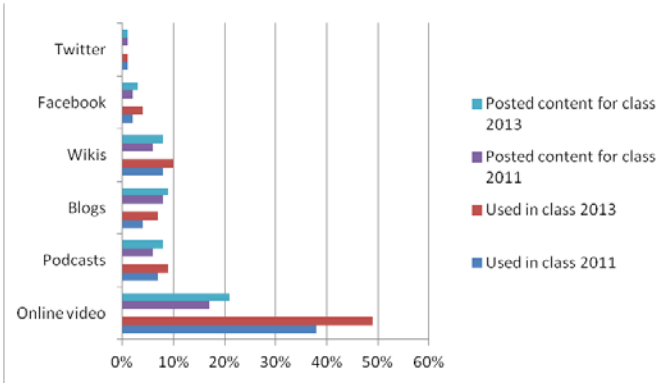

Fig.5 Teachers use of social media for teaching

The result is also strong for the level of integration of social media into course assignments (Fig.6). 23% of teachers have assigned students to read or view social media as part of course assignments and 18% have assigned students to comment on or post to social media sites.

In total, 52% of teachers report using social media for some aspect of a course they are teaching.

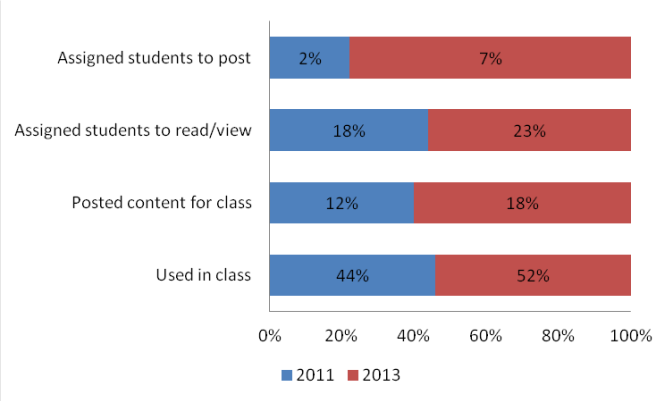

Fig. 6 Teachers use of social media for student assignments during the lesson

D. Estimations and barriers

Regardless the positive approach for social media inclusion in teaching and learning, the process itself is very time consuming and faces a lot of barriers. Participants of the survey indicated that their number one concern of using social media in the classroom is the truthfulness of student submissions, followed closely by concerns about privacy. The data from the 2013 are to some extend more positive than data from 2011, but yet more than 60% of teachers have concerns regarding the privacy; more than 70% do not trust the student submissions, around 40% are not satisfied with the support from the institution and the integration with the LMS (Fig. 7).

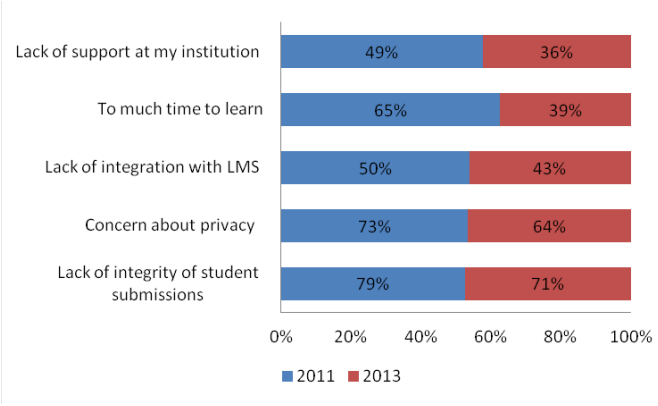

Fig. 7 Teacher views of barriers to use of social media in teaching

Even though teachers had a lot of comments on the barriers for the adoption of the social media into their teaching, still they find significant value in many social media sites for improvement of teaching and learning (Fig.8). When asked about the potential of social media for positive change in education, more than 70 % of the teachers answer agree or strongly agree. Teachers opinion on the overall value of social media for teaching via the statement “Video, podcasts, blogs, and wikis are valuable tools for teaching” is answered with 52% ‘Agree’ and 18 % ‘Strongly agree’, with 22% neutral and just 4% of them disagreeing with the statement. There is slightly less agreement but still a majority of teachers (68%) agreeing that social media can be valuable for collaborative learning.

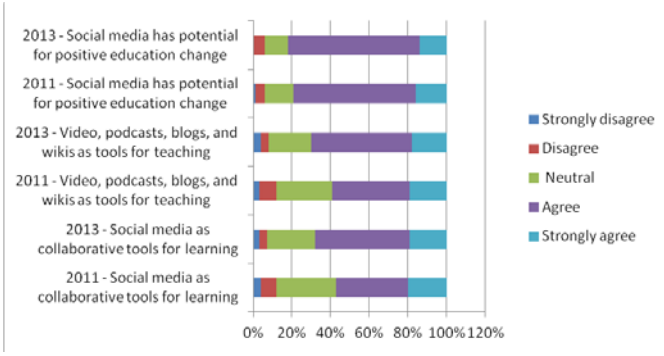

Fig.8 Teachers opinions on the value of social media for teaching

ISBN: 978-1-61804-228-6

V. Conclusion

The study showed that social media are already affecting the ways in which teachers find, create, share and learn knowledge, through the media opportunities and in collaboration with each other.

Teachers find social media as a very useful tool for enhancing teaching and learning. It is important to think about the characteristics of social media that were mentioned above and think about how this relates to classrooms. Almost all teachers (participants in the survey) are aware of the major social media sites; more than 75% visited a social media site within the past month and nearly 25% posted content.

However there is a large diversity among the patterns of use from one social media site to another. For personal use, Facebook is both the most visited site. YouTube and online videos are almost half of the overall usage of social media for online videos in teaching.

The study also pointed out the teachers' difficulties and concerns in the use of social media. Most teachers are concerned with the time it requires. The main concerns in teachers' use of social media in teaching and learning are: privacy and integrity. More than 70% report the lack of integrity of student submissions, and over 60% report privacy concerns as an important barrier.

Regardless of those concerns, however, teachers believe that social media sites offer value in teaching. The majority report they believe that video, podcasts, and wikis are valuable tools for teaching and also that social media sites can be valuable tools for collaborative learning.

References

[1] Redecker, C. (2009). *Review of Learning 2.0 Practices: Study on the Impact of Web 2.0 Innovations on Education and Training in Europe*, JRC Scientific and Technical Report, EUR 23664 EN: http://ipts.jrc.ec.europa.eu/publications/pub.cfm?id=2059.

[2] Center for Marketing Research. (2013, September 15). *Social Media Research*. [Online]. Available: http://www.umassd.edu/cmr/socialmediaresearch/

[3] E. Qualman. (2009). *Socialnomics: How Social Media Transforms the Way We Live and Do Business*. Adapted by permission of John Wiley & Sons, Inc. ISBN: 978-0-470-47723-6. [Online]. Available: http://www.ebscohost.com/uploads/corpLearn/pdf/bbs_socialnomics.pdf

[4] B. Alexander, A. Levine. "Web 2.0 Storytelling: Emergence of a New Genre." EDUCAUSE Review, vol. 43, no. 6. November/December 2008.

[5] G. Grosseck, (2009, January 4). *To use or not to use web 2.0 in higher education?* Procedia: Social and Behavioral Sciences. ScienceDirect. [Online]. Available: http://webpages.csus.edu/~sac43949/pdfs/to%20use%20or%20not%20to%20use.pdf

[6] L. Johnson, A.Levine, S. Stone, R. S. Smith. (2009). *2010 Horizon Report: Deutsche Ausgabe*. The New Media Consortium & EDUCAUSE Learning Iniciative, Austin, Texas. ISBN: 978-0-9825334-5-1. [Online]. Available: http://www.nmc.org/pdf/2010-Horizon-Report.pdf

[7] S. Hamid, J. Waycott, S. Chang, S.Kurnia. Appropriating Online Social Networking (OSN) activities for higher education: Two Malaysian cases. *Ascilite Conference*. pp.526 – 538. 2011

[8] H.F.C. Davis, R. Deil-Amen, C. Rios-Aguilar, M. S. G. Canche. *Social Media in Higher Education: A literature review and research directions.* (2012). The Center for the Study of Higher Education at The University of Arizona. [Online]. Available: http://www.academia.edu/1220569/Social_Media_in_Higher_Education_A_Literature_Review_and_Research_Directions

[9] A.Mrva-Montoya. (Summer 2012). Social Media: New Editing Tools or Weapons of Mass Distraction? *Journal of Electronic Publishing*. Volume 15, Issue 1, Available: http://quod.lib.umich.edu/j/jep/3336451.0015.103/--social-media-new-editing-tools-or-weapons-of-mass?rgn=main;view=fulltext

[10] Jacques Bughin and Michael Chui, The rise of the networked enterprise: Web 2.0 finds its payday. McKinsey Quarterly. (December 2010). [Online].

[11] Available: http://www.mckinseyquarterly.com/The_rise_of_the_networked_enterprise_Web_20_finds_its_payday_2716.

[12] C.Redecker, K. Ala-Mutka and Y. Learning 2.0 - The Impact of Social Media on Learning in Europe. Institute for Prospective technological Studies [Online]. Available: http://www.ict-21.ch/com-ict/IMG/pdf/learning-2.0-EU-17pages-JRC56958.pdf

[13] Pearson Social Media Survey. 2010. [Online]. Available: http://www.slideshare.net/PearsonLearningSolutions/pearson-socialmediasurvey2010.

Image Security with Different Techniques of Cryptography and Coding: A Survey

Mona F. M. Mursi[1], Hossam Eldin H. Ahmed[2], Fathi E. Abd El-samie[3], Ayman H. Abd El-aziem[4]

[1]Professor, Dept. Of Electrical Engineering Shubra Faculty of Engineering Benha University, Egypt.

[2]Dept. Of Electronics Comm. Eng. P. Dean of the Faculty of Electronic Eng. Menouf-32952, Menufiya University, Egypt.

[3]Assoc. Prof. Dept. of Electronics& Comm. Eng. Faculty of Electronic Eng - Menufiya University. Egypt.

[4]Student, Dept. Of Electrical Engineering, Shubra Faculty of Engineering, Benha University, Egypt.

[1]monmursi@yahoo.com,[2]hhossamkh@yahoo.com,[3]fathi_sayed@yahoo.com,[4]eng_aymnhassnin@yahoo.com

Abstract:

Due to the growth of multimedia applications, the protection of this multimedia data becomes a very important issue of communication and storage; especially when it is transferred over an insecure channel, where apart from preventing illegal data access, images are used in many fields such as medical science and military. The protection of images can be done with image encryption. The majority of encrypted image transmission schemes does not adequately take into account the effect of bit errors occurring during transmission and this issue is considered a problem that should be handled by an efficient coding scheme. Hence, error correction code should be applied after encryption to protect encrypted images against channel errors. In this paper, we present a survey of image encryption techniques and channel coding techniques.

Keywords: Image Encryption, Channel coding, chaotic theory.

1. Introduction

Image encryption techniques try to convert the original image to another image that is hard to understand. There are two main types of cryptography: Secret key cryptography and public key cryptography. In secret key cryptography both the sender and the receiver know the same secret code, but public key cryptography, uses a pair of keys for encryption and decryption.

Encryption algorithms can be classified with respect to the mode of operation of the algorithms: block or stream cipher. A block cipher is a type of symmetric key encryption algorithm that transforms a fixed length of plaintext data into a block of ciphertext data of the same length, stream ciphers typically operate on smaller units of plain text, usually bits. A block cipher may also be divided into two groups: chaos and non-chaos based methods. Moreover, it can be further divided into full encryption and partial encryption according to the percentage of the data encrypted. Finally it can be classified into compression and non-compression methods [1].

Traditional encryption algorithms such as AES, RSA and IDEA are used in text or binary data. It is difficult to use them for image encryption because of the high correlation among pixels, high redundancy, bulk capacity of data, so that these algorithms are not suitable for real-time application [2].

Chaos theory has properties of deterministic nonlinear systems that exhibit sensitivity to initial conditions and have random like behaviors. Many researchers have noticed that there exists the close relationship between chaos and cryptography [4].

Chaotic maps and cryptographic algorithms have some similar properties as sensitivity to tiny changes in initial conditions and parameters, both have random-like behavior. There are two differences in characteristics between cryptography and chaos; in cryptography, the encryption operations are defined on finite sets of integers while chaos is defined on real numbers; cryptographic algorithms shuffle and diffuse data by rounds of encryption, while chaotic via iterations [4]. There are two general principles that guide the design of block ciphers; diffusion and confusion, which are closely related to the mixing and ergodicity properties of chaotic maps.

Hence we can use a chaotic map in image encryption because it satisfies the requirements of a good cryptosystem [5-7].

In this paper we present a survey of the security of images using chaotic map and the channel coding techniques. The rest of the paper is organized as follows: In section2 we describe some image encryption schemes. Section 3 presents channel coding technique, Section 4 present relations between coding and encryption. Finally, the conclusions of the paper are presented in section 5.

2. Some Image Encryption Schemes

We introduce a brief description of the various techniques used for image encryption.

ISBN: 978-1-61804-228-6

A new encryption algorithm based on using the chaotic logistic map produced pseudo random sequence on image and makes double time encryption with improved DES. The combination of Chaos and improved DES makes the final algorithm more secure, faster and more suitable for digital image encryption [8].

A new image encryption scheme based on a chaotic system is presented in [8]. It is based on power and the tangent function instead of linear function. It uses a chaotic sequence generated by chaotic map to encrypt image data with different keys for different images. Plain-image can be encrypted by the use of the XOR operation with the integer r sequence.

A block based transformation algorithm is used in [9], where the image is divided into a number of blocks. These blocks are transformed before going through an encryption process. It uses blowfish algorithm for encryption. At the receiver side these blocks are retransformed into their original position and decryption process is performed. It has the advantage of no loss of information in reconstruction of image for the encryption and decryption process.

An algorithm using two chaotic systems is in [10]. One chaotic system generates a chaotic sequence, which was changed into a binary stream using a threshold function. The other chaotic system was used to construct a permutation matrix. Firstly, using the binary stream as a key stream, random the pixel values of the images were modified. Then, the modified image was encrypted again by a permutation matrix.

In [13], two kinds of schemes based on higher dimensional chaotic maps are presented. By using a discretized chaotic map, pixels in an image are permuted in shuffling after several rounds of operations between every two adjacent rounds of permutations, a diffusion process is performed, which can significantly change the distribution of the image histogram which makes statistical attack infeasible.
Image encryption scheme utilizes the SCAN language to encrypt and compress an image simultaneously in [14].Fridrich [15] demonstrated the construction of a symmetric block encryption technique based on two-dimensional standard Baker map. There are three basic steps in the method of Fridrich

- Choose a chaotic map and generalize it by introducing some parameter.
- Discretize the chaotic map to a finite square lattice of points that represent pixels.
- Extend the discredited map to three dimensions and further composes it with a simple diffusion mechanism.

A chaotic Kolmogorov-flow-based image encryption technique was designed [16], in which whole image is taken as a single block and which is permuted through a key-controlled chaotic system. In addition, a shift registers pseudo random generator is also adopted to introduce the confusion in the data.

An encryption method called BRIE based on the chaotic logistic map is presented in [17]. The basic principle of BRIE is bit recirculation of pixels, which is controlled by a chaotic pseudo random binary sequence. The secret key of BRIE consists of two integers and an initial condition of the logistic map.

An encryption method called CKBA (Chaotic Key Based Algorithm) [18], in which a binary sequence as a key is generated using a chaotic system. The image pixels are rearranged according to the generated binary sequence and then XORed and XNORed with the selected key.

An image encryption algorithm using logistic map in [3], uses a chaotic map with suitable initial condition for varying the pixel values randomly with respect to its initial values of the original image. Next the chaotic sequences of the logistic map are used for pixel shuffling. The algorithm uses a secret key of 32 characters (256-bits).

A chaos-based image encryption scheme was introduced in [20]. An image is first converted to a binary data stream by masking these data with a random keystream generated by the chaos-based PRKG, the corresponding encrypted image is formed.

In most of the previous algorithms a security analysis is made; such as key space analysis, statistical analysis and differential analysis. A comparison between original image and encrypted image in terms of correlation between the initial and transformed images, number of pixels change rate and unified average changing intensity are also performed.

3. Channel Coding Theory

The goal of any communication system is to transmit information from an information source to a destination via a communication channel. There are many factors that cause the output of a communication channel to be different from its input. Among these factors are attenuation, nonlinearities, bandwidth limitations, multipath propagation and noise [13].

The main objective when transmitting information over any communication channel is reliability,

ISBN: 978-1-61804-228-6

which is measured by the probability of correct reception at the receiver.

3.1 CHANNEL CAPACITY

Entropy H (X) defines a fundamental limit on the rate at which a discrete source can be encoded without errors in its reconstruction. A fundamental result of information theory is that reliable transmission is possible even over noisy channels as long as the transmission rate is less than the channel capacity [21]**.** The capacity of a discrete memoryless channel is given by

$$C = \max p(x)\, I(X; Y) \quad (1)$$

Where I (X; Y) is the mutual information between the channel input X and the output Y, If the transmission rate R is less than C, then for any $\delta > 0$ there exists a code with block length n large enough whose error probability is less than δ. If R >C, the error probability of any code with any block length is bounded away from 0. The communication channel is characterized by a number called capacity that determines how much information can be transmitted over it [23].

3.2 Bounds On Communication

The capacity of an additive white Gaussian noise channel is given by

$$c = W * \log X \left(1 + \frac{p}{X * W}\right) \quad (2)$$

The basic factors that determine the channel capacity are the channel bandwidth W, the noise power spectrum No and the signal power P. There exists a trade-off between P and W in the sense that one can compensate for the other. Increasing the input signal power obviously increases the channel capacity, because when one has more power to spend, one can choose a larger number of input levels that are far apart and, therefore, more information bits/transmission are possible.

3.3 Channel Coding Techniques

Channel coding techniques are divided into two main types; block codes and convolution codes. In a block code, the information sequence is broken into blocks of length k and each block is mapped into channel inputs of length n. This mapping is independent from the previous blocks. In convolutional codes, there exists a shift register. The information bits enter the shift register bits at a time and then output bits which are linear combinations of various shift register bits are transmitted over the channel. The main difference between block codes and convolutional codes is the existence of memory in convolutional codes.

3.3.1 Linear Block Codes

A block code is completely defined by(n, k),$M = 2^k$ binary sequences of length n called code words. A code C consists of M code words Ci for $1 \le i \le 2^k$.
C = {c1, c2, . . . ,cM}
where each Ci is a sequence of length n with components equal to 0 or 1 and it denoted by.

$$C = X \times G \quad (3)$$

Where g is the generator and the parity check matrix, the generator matrix of a code completely describes the code. If we denote the generator matrix of the dual code by H, which is an $(n - k) \times n$ matrix, then any code word of the original code is orthogonal to all rows of H.

$$C.H^t = 0 \quad (4)$$

Soft decision decoding is used for decoding information as follow after receiving the output of the channel and passing it through the matched filters, we choose one of the message signals that is closest to the received signal in the Euclidean distance sense. These are bounds on the error probability of a coded communication system when optimal demodulation is employed. By optimal demodulation, we mean passing the received signal r (t) through a bank of matched filters to obtain the received vector **r**, and then finding the closest point in the constellation to **r** in the Euclidean distance sense.

Hard decision decoding is simpler and more frequently used decoding scheme to make hard binary decisions on the components of the received vector **r**, and then to find the code word that is closest to it in the Hamming distance sense. There are three basic steps involved in hard-decision decoding. First, we perform demodulation by passing the received r (t) through the matched filters and sampling the output to obtain the **r** vector. Second, we compare the components of **r** with the thresholds and quantize each component to one of the two levels to obtain the **y** vector. Finally, we perform decoding by finding the code word that is closest to **y** in the Hamming distance sense.

3.3.2 Cyclic Codes

Cyclic codes are a subset of linear block codes with the extra condition; it is easily implementable encoders and decoders. A cyclic code is a linear block code that if **C** is a code word, a cyclic shift of it is also a code word. It is easier to represent each codeword as a polynomial, called the code word polynomial. The code word polynomial corresponding to

C=(c1, c2, . . . ,cn−1, cn) is simply defined to be

$c_i p_{n-i} = c_1 p_{n-1} + c_2 p_{n-2} + \cdots + c_{n-1} p + c_n$

And the code word polynomial corresponding to **x** is given by

$$C(p) = X(p) \times g(p). \quad (7)$$

Any code word polynomial is the product of the generator polynomial and the information sequence polynomial, this fact is very important in designing cyclic encoders.

Cyclic codes have more built in structure and this extra structure makes the implementation of their encoders easier. The main advantage of cyclic codes is the existence of an easily implementable decoder for them.

3.3.3 Convolution Codes

denoted
by lines connecting these boxes. On each line both the inputs causing that transition and the corresponding output are specified. The number of lines emerging from each state is, therefore, equal to the number of possible inputs to the encoder at that state

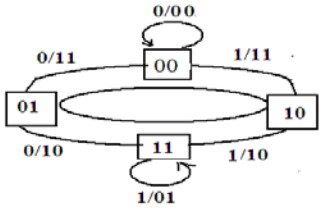

Fig1 State transition diagram for convolution code

The second and more popular method to describe convolutional codes is to specify their trellis diagram as shown in figure 2 . The trellis diagram is a way to show the transition between various states as the time evolves. The trellis diagram is obtained by specifying all states on a vertical axis and repeating this vertical axis along the time axis. Then, each transition from a state to another state is denoted by a line connecting the two states on two adjacent vertical axes. In a sense, the trellis diagram is nothing but a repetition of the state transition diagram along the time axes.

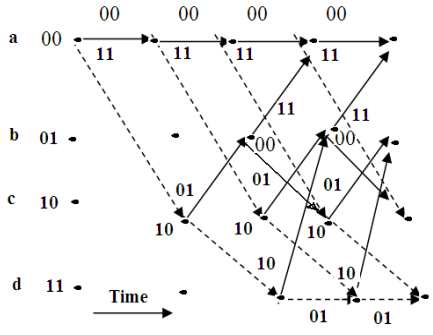

Fig 2. Trellis diagram for convolution code

3.3.4 Complex codes

The performance of block and convolutional codes depends on the distance properties of the code and, in particular, the minimum distance in block codes

Convolutional codes are different from the block codes by the existence of memory in the encoding scheme. In convolutional codes, each block of k bits is again mapped into a block of n bits to be transmitted over the channel, but these n bits are not only determined by the present k-information bits but also by the previous information bits.

Because a convolutional encoder has finite memory, it can easily be represented by a state-transition diagram as shown in figure 1.

In the state-transition diagram, each state of the convolutional encoder is represented by a box and transitions between states are

and the free distance in convolutional codes. In order to design block codes with a given rate and with high minimum distance, we have to increase n, but increasing n and increasing the constraint length will, increases the complexity of the decoding. We discuss two widely used methods for combining simple codes to generate more complex codes. These techniques generate product codes, and turbo codes.

Product Codes

The structure of product codes is very similar to a crossword puzzle as shown in figure 3.

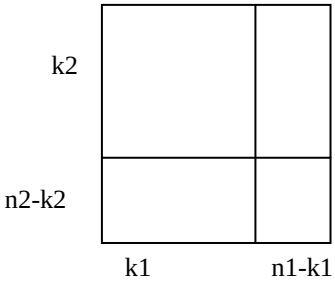

Fig 3.Product codes

Product codes are generated by using two linear block codes arranged in a matrix form. Two linear block codes, one with parameters n1, k1, d1 and another with parameters n2, k2, d 2, are used in a matrix of the resulting code is an (n1n2, k1k2) linear block code. It can be shown that the minimum distance of the resulting code is the product of the minimum distances of the component codes.

d = d1*d 2, and is capable of correcting d1* d2−1

This process can be repeated in an iterative fashion, improving the quality of the guess in each step. This process is known as iterative decoding and is very similar to the way a crossword puzzle is solved. To employ this decoding procedure, we need to decode schemes for the row and column codes that are capable of providing guesses about each individual bit. In other words, decoding schemes with soft outputs (usually, the likelihood values) are desirable.

ISBN: 978-1-61804-228-6

Turbo Codes

Turbo codes use an interleaver between two parallel or serial encoders as shown in figure 4. The existence of the interleaver results in very large code word lengths with excellent performance, particularly at low SNRs. Using these codes, it is possible to get as close as 0.7 dB to the Shannon limit at low SNRs. The turbo encoder consists of two constituent codes separated by an interleaver of length N.

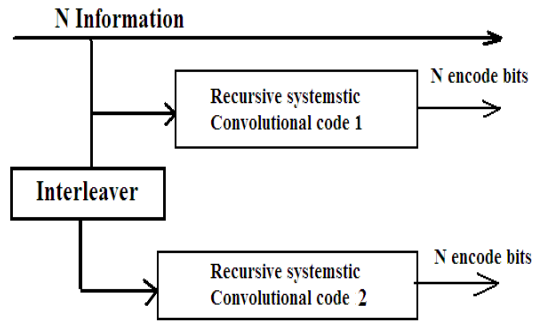

Fig 4. Block diagram of Turbo encoder

Because the encoders are systematic, each encoder generates the N-information bits applied to its input followed by N parity check bits. After the encoding, the N information bits and the 2N parity check bits of the two encoders, a total of 3N bits, are transmitted over the channel. Therefore, the overall rate is R = N/3N =1/3.

The interleaver in turbo codes is usually very long, in the order of thousands of bits. Pseudorandom interleavers perform well, although some improvement in the performance of the code can be obtained by clever choice of the interleaver. This improvement is more noticeable at short interleaver lengths. Due to the existence of the interleaver, it is, in most cases, impossible to return both codes to the all-zero state.

Since turbo codes have two constituents-code components, an iterative algorithm is appropriate for their decoding. Any decoding method that yields the likelihood of the bits as its output can be used in the iterative decoding scheme as shown in figure 4. One such decoding scheme is the maximum a posteriori (MAP) decoding method.

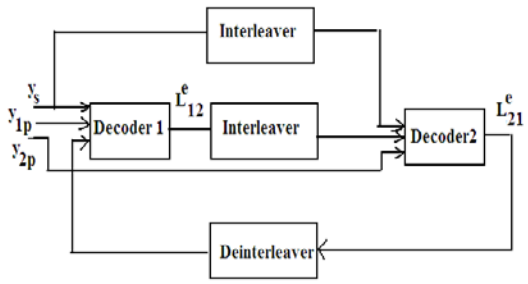

Fig 5. Block diagram of Turbo decoder

3.4 Bit error rate performance

The measure of that performance is usually bit-error rate (BER), which quantifies the reliability of the entire radio system from “bits in” to “bits out”, including the electronics, antennas and signal path in between. On the surface, BER is defined as: BER = Errors/Total Number of Bits with a strong signal and an unperturbed signal path, this number is too small as to be insignificant. It becomes significant when we wish to maintain a sufficient signal-to-noise ratio in the presence of imperfect transmission through electronic circuitry.

The two performance parameters used are Message Error Rate MER and Bit Error Rate BER, MER define as = (No. of messages received in Error after error correction) / (Total no. of messages transmitted), Expressed as a percentage for a given signal to interference ratio.

While the basic concept of BER measurement is simple send a data stream through the system and compare the output to the input. However, we don’t want to wait forever to make a BER measurement! So a pseudorandom data sequence is used for this test, some smart mathematicians have worked out sufficient approximations of random behavior so we can quickly make accurate BER measurements.

4.1 Relation between Source coding and encryption

There is a relation between source and channel coding and encryption we introduce the combine of error correction code with encryption and the combine of compression and encryption as follow in sub sections.

4.1 Combine Encryption and Error Correction Code

While cryptographic algorithms, in order to provide information security, in the process of decryption need an errorless input, error-correcting algorithms are meant to handle a certain amount of errors in the input data, but they are not designed to provide any security of the data they process. However, there are many situations where both information security and error-correction are needed or required.

In this case a combination of cryptographic algorithms and error correction code introduces, called “A Combined Encryption and Turbo Coding which basically means encryption, decryption, encoding and decoding, is realized by AES-TURBO”. AES was chosen for the encryption and decryption process, and turbo codes for encoding and decoding [12]. According to the general perspective of the system turbo encoder block is embedded in an AES encrypted block in the first round after subbytes block. The remaining steps of

ISBN: 978-1-61804-228-6

the AES encryption are followed normally. In the decryption phase turbo decoder block is embedded in an AES decryption block in the last round before Subbytes block.
Turbo codes mimic the good performance of random codes using an iterative decoding algorithm based on simple decoders individually matched to the simple constituent codes. The turbo decoder iterates between the outputs of the two constituent decoders until reaching satisfactory convergence. The final output is a hard-quantized version of the likelihood estimates of either of the decoders.

4.2 Combine Source and Channel Coding

Nowadays source compression and channel coding techniques are necessary for transmitting images efficiently [20], source coding is needed to remove as much redundancy as possible and to combat the errors introduced by noisy channels, channel coding is often employed to add controlled redundancy. Therefore, using characteristics of channels and compressed bit stream may be interested in practical systems. When transmitting progressively coded images, such as those encoded by set partitioning in hierarchical trees SPHIT or JPEG2000 that can provide efficient compression, over wireless channels. Due to its embedded property, the source bit stream is susceptible to transmit noise and sensitive to bit errors. Typically, a single error could render a whole bit stream useless. Thus it is important to combine source and channel coding to protect such bit stream over noisy channels. Given a particular source encoder, the key point lies in how to partition the limited total bit budget between source and channel coders such that the image distortion is minimized. We introduce a robust image transmission strategy over wireless channels by adding a coding controller between source code and channel coding, According to the characteristics of the channel and compressed bit stream, the coding controller dynamically allocates the coding rate for source code and channel coder.
Error protection with different coding rates. On the receiving side, the decoding controller extracts the important priority of the demodulated data.

4.3 Joint authentication and channel coding

We present a joint authentication, integrity verification and channel coding scheme, applied to secure image transmission through wireless networks and make it suitable for real-time image applications [6]. In noisy environments, channel coding has to be performed after encryption. Forward Error Correction (FEC) has to be specified in order to guarantee that the original messages can be properly deciphered and authenticated. A tight cooperation between channel coding and security mechanisms should be exploited to reduce the security overhead, to decrease the requested computational complexity, and to achieve the secrecy capacity limit. The guarantees a strong resilience to the errors introduced by noisy channels, while providing the means to discriminate between data modifications performed by malicious attackers, and data distortions due to noise. Moreover, data encryption, performed before channel coding to prevent illegal data access, is also exploited to improve the performances of the scheme. The encoder employed to safely transmit an authenticated image over a noisy channel in the presence of a malicious opponent, and the decoder employed to receive the image and determine if it is original.

4.4 Combine Image-Encryption and Compression

A new and efficient method to develop secure image-encryption techniques may be realized by combining two techniques: encryption and compression. In this technique, a wavelet transform was used to decompose the image and decorrelate its pixels into approximation and detail components. The most important component is encrypted using a chaos-based encryption algorithm. The remaining components are compressed using a wavelet transform. This algorithm was verified to provide a high security level. This algorithm produces a good diffusion and confusion properties [19].

6. CONCLUSION

In this paper we presented a survey of some recent image encryption techniques and channel coding. We see that image encryption techniques using chaotic map give high security and a high rate of security and is suitable for real time applications. Each technique has advantages and the advantage depends on the design of these algorithms.
We find that it is not sufficient to secure the multimedia image by applying image encryption, especially when transmitting it over noisy channels.
It is necessary to apply channel coding after encryption. Forward Error Correction (FEC) has to protect the encrypted image from noise induced error, and make BER small as possible and close to the Shannon limit[11]. We introduced some different types of channel coding.
Also source coding as JPEG, JPEG2000 and SPHIT should be applied to the image to remove as much redundancy as possible before it is encrypted. There is a close relationship between channel coding and source coding; and security mechanisms should be exploited to increase the security of multimedia, and to decrease the requested computational complexity. These relations should be taken into consideration in the design to render high performance of security.

ISBN: 978-1-61804-228-6

References:

[1] Komal D Patel, Sonal Belani "Image Encryption Using Different Techniques: A Review" International Journal of Emerging Technology and Advanced Engineering www.ijetae.com (ISSN 2250-2459, Volume 1, Issue 1, November 2011).

[2] Varsha S. Nemade, R. B.Wagh "Review of different image encryption techniques" National Conference on Emerging Trends in Computer Technology (NCETCT-2012).

[3] Mrinal K. Manual, GourabD. Banik, DebasishChattopadhyay and DebashisNandi"An Image Encryption Process based on Chaotic Logistic Map " IETE Technical Review Vol 29 ISSUE 5 - SEP- OCT 2012.

[4] Yaobin Mao and Guanrong Chen" Chaos-Based Image Encryption"

[5] Shubo Liu, Jing Sun, ZhengquanXu"An Improved Image Encryption Algorithm Based on Chaotic System" 1100 Journal Of Computer, VOL. 4, NO. 11, November 2009.

[6] 6 Alessandro Ne., Daniele BL., Patrizio CA., and Emanuele Ma." Joint Authentication and forward Error Correction of Still Images "18th European Signal Processing Conference (EUSIPCO-201 Aalborg, Denmark, August 23-27, 2010.

[7] J. Fridrich. "Secure image ciphering based on chaos," Technical Report RL-TR-97-155, the Information Directorate (former Rome Laboratory) of the Air Force Research Laboratory, New York, USA, March 1997.

[8] Rajinder Kaur, Er. Kanwalprit Singh"Image Encryption Techniques: A Selected Review" IOSR Journal of Computer Engineering (IOSR-JCE) e-ISSN: 2278-0661, p- ISSN: 2278-8727Volume 9, Issue 6 (Mar. - Apr. 2013), PP 80-83 www.iosrjournals.org

[9] A. Gautam, M. Panwar, Dr.P.R Gupta "A New Image Encryption Approach Using Block Based Transformation Algorithm" 2011 (IJAEST) Vol No. 8, Issue No. 1, 090 - 096 .

[10] Rinki Pakshwar, Vijay Kumar Trivedi, Vineet Richhariy "A Survey On Different Image Encryption and Decryption Techniques."

[11] C.E. Shannon, A Mathematical Theory of Communication, Bell Sys. Tech. J., 27:379 {423, 623 {656, 194.

[12] Hakan Cam, Volkan O. Osman N. UCAN " A cobmnine Encryption and Error Correction Scheme: AES-TURBO" Journal of Electrical&Electronics Engineering, VOL 9 ,2009, (891-896) 05.01.2009.

[13] Fridrich J (1998) Symmetric ciphers based on two-dimensional chaotic maps. Int J Bifurcation and Chaos 8 (6): 1259 – 1284.

[14] N. Bourbakis, C. Alexopoulos, Picture data encryption using SCANpattern, Pattern Recogn. 25 (1992) 567–581.

[15] Fridrich Jiri, "Symmetric ciphers based on two dimensional chaotic maps" Int. J. Bifurcat Chaos 8 (6) (1998) 1259–1284.

[16] J. Scharinger, "Fast encryption of image data using chaotic Kolmogrov flow", J. Electronic Eng 7 (2) (1998) 318–325.

[17] J.C. Yen, J.I. Guo, A new image encryption algorithm and its VLSI architecture, in: Proceedings of the IEEE workshop signal processing systems, 1999, pp. 430–437.

[18] J.C. Yen, J.I. Guo, A new chaotic key based design for image encryption and decryption, Proceedings of the IEEE International Symposium Circuits and Systems, vol. 4, 2000, pp. 49–52.

[19] Somaya Al-Maadeed, 1 Afnan Al-Ali, 2 and Turki Abdalla" A New Chaos-Based Image-Encryption and Compression Algorithm "Journal of Electrical and Computer Engineering Volume 2012, Article ID 179693, 11 pages

[20] Daniel J. Costello, Jr. and G. David Forney, Jr" "Channel Coding: The Road to Channel Capacity" IEEE | Vol. 95, No. 6, June 2007.

[21] Jorge C. Moreira and Patrick G. Farrell. "Essential of Error Control Coding," John Wiley & Sons Ltd, The Atrium, Southern Gate, Chichester,West Sussex PO19 8SQ, England. 2006.

Computer-Vision Based Visual Inspection and Crack Detection of Railroad Tracks

Mohammad Farukh Hashmi[1], Avinash G. Keskar[2]

[1-2]Department of Electronics Engineering
[1-2]Visvesvaraya National Institute of Technology, Nagpur, India
farooq78699@gmail.com, agkeskar@ece.vnit.ac.in

***Abstract*-**Surface analysis is a very important measurement for track maintenance for Railroad Tracks, because deviations in surface geometry indicate where potential defects may exist. A rail surface defects inspection method based on computer vision system is proposed in the paper. Various algorithms related denoising, filtering, thresholding; segmentation and feature extraction are applied for processing the images of Railroad surface defect and cracks. It has mostly been implemented on computers. For better speed and complexity, the algorithms need to be implemented on embedded platforms. These methods were designed for different software setups, namely MATLAB and C++ using the Intel OpenCV library. Then accurate region of Interest in respective to defect is extracted and recognized by adaptive thresholding and feature matching methods. Percentage of wear of rail head and length of cracks in surface are calculated next as an evaluation of flaw on inspected rail head section. Experimental results of the proposed algorithms are presented in the results sections along with bench marking with software algorithms.

***Keywords*-** OpenCV, Track Inspection, Dynamic Threshold, Computer Vision, Optimal Thresholding.

I. INTRODUCTION

The incidence of railway accidents in our country is greater as compared to other countries of the world. Accidents occur due to the errors and negligence of the employees. Many high speed and heavy railways have been built and applied in recent years. The reliability of railway tracks needs to be paid more attention than before. In the past, majority of rail problems were attributed primarily to the propagation of internal defects in the rail web and head due to fatigue and excessive wear. As some advanced manufacturing technology were introduced, such as higher carbon steels and cleaner steel-making processes, the probability of inner defects reduced a lot.

Rail failures caused by surface defects in the rail head have become much more common within the rail industry these days. Surface defects can be distinguished into following types:

a) The cracks in the rail surface and the rolling contact fatigue damage which have occurred due to high stresses and resistance. In most cases, cracks grow out of some internal defects and can be defined as severe damage directly.
b) The main two kinds of rolling contact fatigue damage, including spalling of rail head and rail corrugation, are also of great significance to the track inspection [15, 16].

Experiments have shown that the rolling contact fatigue damage could exert a negative effect on ultrasonic rail track inspection and moreover, corrugation of rail is able to expand downward and turn into some more threatening flaws, such as nucleus flaw [2]. A machine vision system is being developed to automate, or enhance the visual inspection of track and track components [4]. Machine vision algorithms are being designed to recognize track components, identify their proper location and condition, and detect and quantify the extent of the defects found. Automated vision systems are typically used to measure the rail profile and calculate the percentage of wear of the rail head [1, 3].

The primary focus of this research is inspection of Indian railroad mainline and siding tracks, as these generally experience the highest traffic densities. Although the primary focus of this research is the inspection of high-density track, algorithms are also being tested on lower track classes to ensure robustness to component variability and condition. The algorithms currently under development will also be adaptable to many types of track and track components [9]. These interim solutions include video capture using vehicle-mounted cameras, image enhancement using image processing software, and assist the system automatically using various vision based algorithms [8, 17].

In this paper, the continuous images of rail track surface acquired by CCD camera in a high frame rate is taken and the image is processed using various software's to extract the defects, and other purposes like parameters computation, and information extraction using a personal computer. If the defects found are negligible, tracks need not be replaced whereas in the case of considerable amount of crack or wear in the railway track, immediate action needs to be taken. Using the information of the defects found, tracks can be replaced in time and many railway accidents can be avoided.

II. SYSTEM OVERVIEW

Railway applications of computer-vision technology that were previously developed have three main components is shown in Figure 1. The first component of this system is the image acquisition system, in which digital cameras are used to capture the video or images in the visible or infrared spectrum [4, 14]. The next element is the

image analysis system, where the images or videos are processed using computer-vision or image processing based algorithms that identify specific parts of interest and assess the condition of the detected parts [5, 7]. The final element is the data analysis system or embedded processing hardware, which compares and verifies whether or not the condition of track features or mechanical components comply with parameters specified by the individual railroad tracks. Finally the data is transported to embedded Image processing system [8, 17].

The work of image processing algorithms which finished in embedded system consists of three main parts. First, some pre-processing should be used to acquire the original image. Then finally apply the designed algorithm for selecting the region of interest and extract all valuable defects from the processed images. At last, required features of defects are computed and classified for calculating evaluation of defects on the target rail track section [6]. Block Diagram of Block Diagram of Vision based Railroad Detection/Inspection System is shown in Fig. 1.

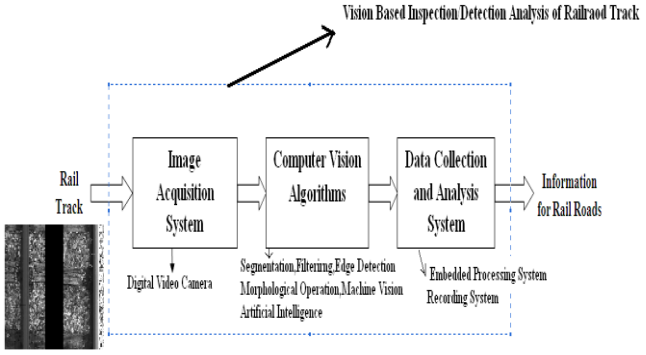

Figure 1. Block Diagram of Vision based Railroad Detection/Inspection System

III. METHOODS AND MATERIALS

A. *Thresholding*

Gary-level thesholding is the simplest segmentation process. Many objects or images regions are categorized by constant reflectivity or light absorption of their surfaces; a brightness constant or threshold can be determined to segment objects and background. Thresholding is computationally inexpensive and fast-it is the oldest segmentation method and it still widely used in simple applications; thresholding can easily be done in real time using specialized hardware [10, 11].

A complete segmentation of a Railroad image R is a finite set of regions R_1…., Rs,

$$\bigcap_{i=1}^{S} Ri \qquad Ri \cap Rj = 0, \quad i \neq j. \qquad (1)$$

Complete segmentation can result from thresholding in simple process. Thresholding is the transformation of an input image f to an output (segmented) binary image g as follows:

$$g(i,j) = 1 \quad \text{for} \quad f(i,j) \geq T$$
$$= 0 \quad \text{for} \quad f(i,j) < T \qquad (2)$$

Where is the threshold g(i,j)=1 for image elements of objects, and g(i,j)=0 for image elements of the background (for vice versa).

Algorithm-1: Basic Thresholding

Search all the pixels $f(i,j)$ of the image .An image element $g(i,j)$ of the segmented image is an object pixel if $f(i,j) \geq T$, and is a background pixel otherwise [11].

Segmentation using variable thresholds (also called adaptive thesholding), in which the threshold value varies over the image as a function of local image characteristics, can produce the solution in these cases.

A global threshold is determined from the whole Railroad image f:

$$T = T(f) \qquad (3)$$

On the other hand, local thresholds are position dependent

$$T = T(f, fc), \qquad (4)$$

Where f_c is that image part in which the threshold is determined.

B. *Optimal Thresholding*

Methods based on approximation of the histogram of an image using a weighted sum of two or more probality densities with normal distribution represent a different approach called optimal thresholding [11].

Algorithm -2: Iterative (optimal) threshold selection

1. Assuming no knowledge about the exact location, consider as a first approximation that the four corners of the image contain background pixels only and the remainder contains object pixels.
2. A step t,

$$\boldsymbol{\mu}^{t}_{B} = \frac{\sum_{(i,j)\in background} f(i,j)}{\#background\_pixels},$$

$$\boldsymbol{\mu}^{t}_{O} = \frac{\sum_{(i,j)\in objects} f(i,j)}{\#objects\_pixels},$$

3. Set $\mathbf{T}^{(i+1)} = \frac{\boldsymbol{\mu}^{t}_{B} + \boldsymbol{\mu}^{t}_{B}}{2}$

$\mathbf{T}^{(i+1)}$ now provides an upward background-object distinction

4. If $\mathbf{T}^{(i+1)} = \mathbf{T}^{(t)}$, halt; otherwise return to step 2.

This method performs well under a large variety of Railroad image contrast conditions.

A combination of optimal and adaptive thresholding (equation) was used for Railroad images segmentation from cracks of Tracks image data. The method determines optimal gray-level segmentation parameters in local sub-regions for which local histograms are constructed.

C. *Morphological Analysis*

ISBN: 978-1-61804-228-6

a) Dilation

Mathematical Morphology is one of the most productive areas in image processing. The content of mathematical morphology is based on set theory [10, 11].

The morphological transformation dilation $\oplus$ combines two sets using vector addition (or Minkowski set addition e.g. (a,b)+(c,d)=(a+c,b+d).The dilation $X \oplus B$ is the point set of all possible vector additions of pairs of elements, one from each of the sets X and B.

$$X \oplus B = \{ p \in \varepsilon^2 : p = x + b, x \in X and b \in B \} \quad (5)$$

Dilation with an isotropic 3x3 structuring elemnt might be described as a transformation which changes all bacground pixels neighbouring the object to object pixels.

Dilation is an increasing transformation:

If $X \subseteq Y$ then $X \oplus B \subseteq Y \oplus B$ (6)

b) Erosion

Erosion $\odot$ combines two sets using vector subtraction of set elements and is the dual operator of dilation. Neither erosion nor dilation is an invertible transformation

$$X \odot B = \{ p \in \varepsilon^2 : p = x + b, x \in X for\ every b \in B \} \quad (7)$$

The formula says that every point p from the image is tested; the result of the erosion is given by those points p for which all possible p+b are in X.

Erosion is used to simplify the structure of an object-object or their parts with width equal to one will disappear. It might thus decompose complicated objects into several simpler ones.

And like dilation ,is an increasing ransformation:

If $X \subseteq Y$ then $X \odot B \subseteq Y \odot B$ (8)

c) Openiong and Closing

Erosion and dilation are not inverse transformations, if an image is eroded and then dilated,the original image is not re-obtained. Instead ,the result is a simplified and less detailed version of the original image [10,11].

Erosion folowed by dilation creates an important morphological transformation called opening.The opening of an image X by the structuring elements B is denoted by $X \circ B$ and is defined as

$$X \circ B = (X \odot B) \oplus B \quad (9)$$

Dilation followed by erosion is called closing .The closing of an image X by the structuring elemt B is denoted by $X \bullet B$ and is defined as

$$X \bullet B = (X \oplus B) \odot B \quad (10)$$

IV. PROPOSED METHODOLOGY

Rail inspection is the practice of examining rail tracks for flaws that could lead to catastrophic failures. The proposed work is based on analysis of railway track surface to detect various problems to avoid any kind of possible accidents as these days most of the accidents in railways are happening due to railway track surface defects. This proposed work successfully helps in determining some kind of track defects which are:

A. Crack detection

Rail crack is a kind of severe damage which will lead to rail track fracture. Timely detection of crack in the rail track is crucial for the safety of railway transportation. Avoiding this problem may cause accidents as well as the might become larger. In this work, an image of the track is taken and is processed in MATLAB to detect the crack. The image is divided into horizontal strips (for profiling) and vertical columns, such that one point from each strip belongs to a column. An image profile is then taken along a strip of the image and is checked if there is any crack. However there are some cracks in the railway track profile that cannot be detected through software simulation due to surface irregularities and noise.

B. Object detection

The railway tracks must be smooth and should not have any obstacles on them. A stray rock or any object on the railway track can scratch, wear and damage the railway track as well as the railway wheels and can even cause major accidents. In this work, the unwanted objects on the railway track are detected using frame differencing method. Detection of object on the railway track in advance, can avoid accidents by removing the object from the track before the train arrives. It can also avoid suicide problems on railway tracks by detecting human on the track and alarming the railway station about the problem.

C. Detection of Rail head Spalling

The spalling of rail head, widespread over rail track in service, is able to increase noise and instability of fast moving trains. Failure to detect this problem in time causes increase of the track wear. If the amount of spalling is large, if may lead to accidents as well. In this work, an image of the track is taken and is processed using MATLAB as well as OpenCV [12]. The exact amount of track wear is obtained and the percentage area of wear is also calculated. In this paper, the continuous images of rail track surface acquired by CCD camera in a high frame rate is taken and the image is processed using various software's to extract the defects, and other purposes like parameters computation, and information extraction using a personal computer. The proposed work uses visual inspection to determine defects in the rail surface. Two different platforms (OpenCV and MATLAB) are tried for software simulation [13, 18].

V. EXPERIMENTAL RESULTS

A. Inspection of rail head spalling using OpenCV

The spalling of rail head i.e. upper surface of the rail track, widespread over rail track, is able to increase noise and instability of fast moving train. Information about percentage of wear of rail track is very useful which can be acquired from the area of spalling. The objective of image processing is to extract regions of wear, then get some valuable features belong to those regions and compute the

results. This has been implemented using MATLAB and embedded C language using OpenCV functions [12, 13]. The image processed and used in this paper is shown in the following Fig .2.

Figure 2. Railway track with spalling

Algorithm:

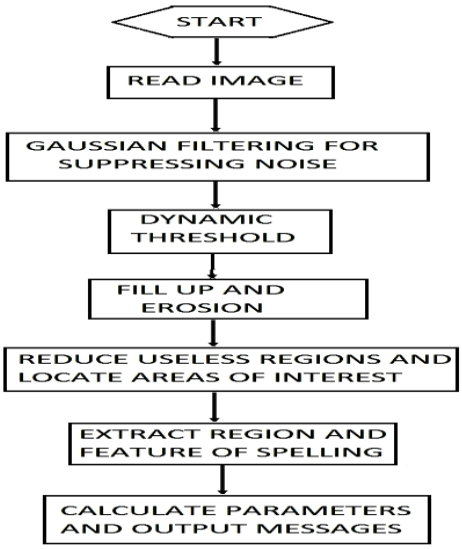

Figure 3. Proposed Flow chart of Track wears examination

Images of spalling and wear on the railway track are taken and it is processed using OpenCV library functions [18] with the method shown in the above flowchart given Fig. 3.The application of Gaussian filter suppresses noise in the image and obtains a foggy image meanwhile. The foggy image will be used as a local background in the operation of dynamic threshold next. Filter is designed in such a way and of suitable size so that it is ensured that all local structures are eliminated by the smoothing, and hence to better suppress noise in the segmentation. The image of railway track surface is always influenced by many factors such as in homogeneous illumination and motion speed difference. Typical threshold operation based on gray value histogram of the image cannot fulfill requests anymore. It can be seen that the defects and wear of interest can be characterized by being locally brighter or darker than their local background. Therefore, instead of specifying global thresholds or using multiple thresholds, the work changes to specify by how much a pixel must be brighter or darker than its local background. The dynamic threshold with local background estimated by the mean filter is superior to other methods. Information about defects shows clearly and the edges-effect is suppressed a lot too.

It is observed that there are many little holes in connected regions and some regions are linked by just a few pixels. Relative algorithms need to be employed to avoid having influence on the following operation. First find the holes inside and fill it up. Then select proper structuring element of erosion to separate two regions if their connection is very small. At the same time, single tiny regions including several pixels caused by noise are eliminated. The next step is to reduce useless region in the binary image and locate regions of interest. All the connected regions are extracted and some feature parameters are computed. After analyzed from the processed image, it is found that the width of region is able to be used to remove the two long borders. One other point needs to be mentioned is the computation of rail head surface area. Two regions of borders have been recognized, so the area between them is able to stand for the total area of rail surface and the value will be applied for the following calculation .After locating area of interest i.e. rail head spalling area, edge detection of these areas is done followed by area calculation of the wear included in these edges. Percentage wear area is also calculated [1]. Results obtained for rail head wear detection are shown in Fig. 4.

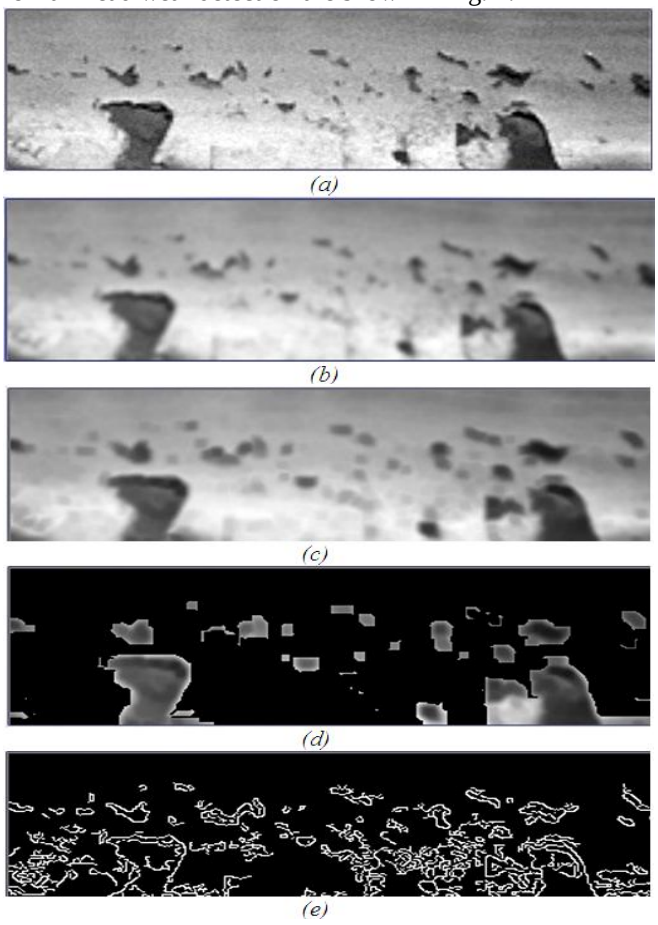

Figure 4.Results obtained for rail head wear detection: (a)source image, (b)filtered image, (c)eroded image, (d)image obtained after thresholding, (e)image showing edges of wear area, (f)final image showing track wear.

The percentage of wear calculated the given image comes out to be 9.229737. The time required to calculate the surface wear area is 0.535 seconds.

B. *Selection of suitable filter and Thresholding* :

The current module required the selection of a filter which would clear out the noise (granular) present on the rail track image and would smoothen the overall image without affecting any of the spalled zones. Both the Gaussian and Median filter with the same kernel sizes were tried, but the Gaussian filter yielded far more satisfactory results, which are illustrated in Fig.5 shown below. Comparison of different threshold methods is shown in Fig. 6 [11].

(a)

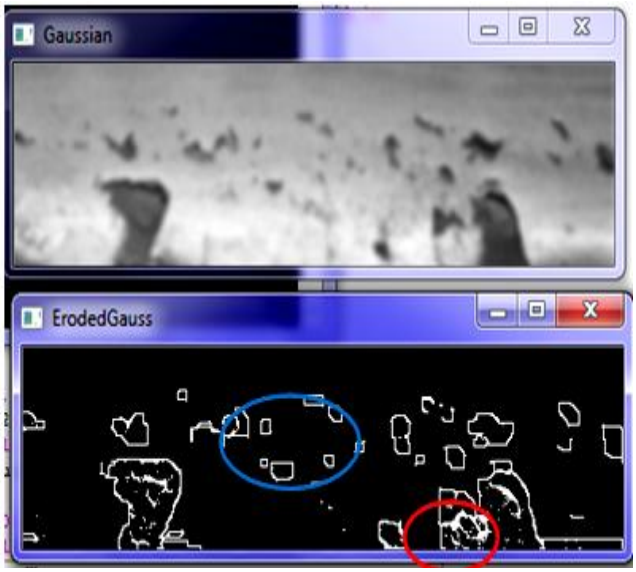

(b)

Figure 5.Results of erosion and adaptive thresholding after (a) median filtering with 3x3 kernel and (b) Gaussian filtering with 3x3 kernels. The highlighted areas show where spalled areas are removed by the median filter.

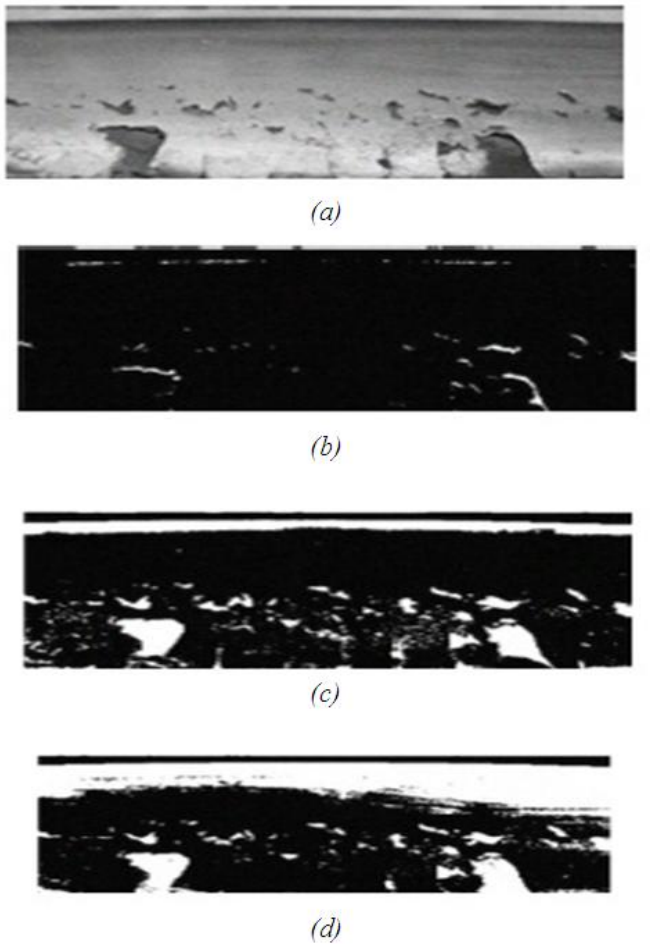

Figure 6. Comparison of different threshold methods: (a)source image, (b)image obtained by Auto thresholding, (c) image obtained by Dynamic thresholding, (d) image obtained by Manual thresholding.

The dynamic threshold with local background estimated by the mean filter is superior to other methods. Information about defects shows clearly and the edges-effect is suppressed a lot too.

C. *Inspection of rail head spalling using MATLAB*

The Image of a worn track surface is first read. This image is then converted into gray scale image. A global threshold is applied on the entire grayscale image and the image is converted into a binary image. The pixels in grayscale image with their pixel values greater than the threshold value are represented as black pixels in the binary image. Similarly, the pixels with their pixel values smaller than or equal to the threshold value are represented as white pixels in the binary image. The amount of wear area detected depends on the value of the global threshold applied. Hence, the value of the global threshold must be

selected appropriately. The wear is detected and is represented as black pixels in the binary image.

Algorithm:

The flow chart of calculation the area of the worn surface on the railway track is as follows as shown in Fig.7.

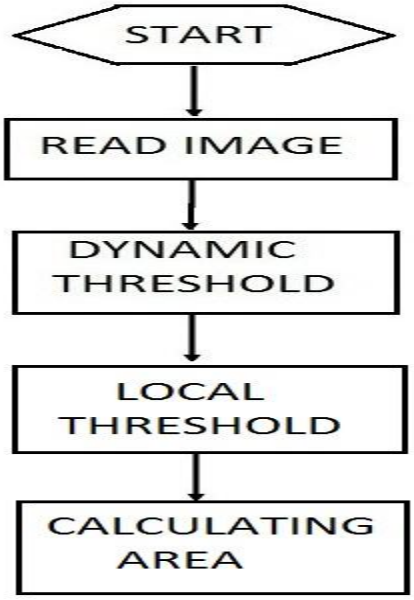

Figure 7.Proposed Flowchart of wear area calculation using MATLAB

- *Pixel Connectivity:*

A pixel is surrounded by 8 neighboring pixels. Connectivity defines which pixels are connected to other pixels. A set of pixels in a binary image that form a connected group is called an object or a connected component. Determining which pixels create a connected component depends on how pixel connectivity is defined.

Pixel connectivity in a 2D image can be of two types:

- 4 Connected

Pixels are connected if their edges touch. This means that a pair of adjoining pixels is part of the same object only if they are both on and are connected along the horizontal or vertical direction.

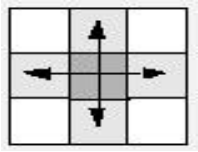

- 8 Connected

Pixels are connected if their edges or corners touch. This means that if two adjoining pixels are on, they are part of the same object, regardless of whether they are connected along the horizontal, vertical, or diagonal direction.

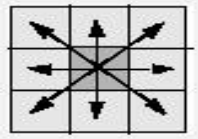

Thus, we have objects that contain number of connected pixels in them. The value of objects is the number of pixels connected. We apply local thresholding that removes from the binary image all connected components (objects) that have fewer than 100 pixels. Thus small patches (objects with less than 100 pixels in them) of white pixels in black background are removed in our example.

The white patches in the detected wear area are removed after applying local thresholding.

- *Image Complementation and wear area calculation:*

The image is complemented. By complementing a binary image, we simply convert the white pixel into black and black pixels into white. The worn railway track surface is now represented by the white pixels. To calculate the area of the railway track, we basically calculate the area of the white pixels in the binary image. The area of an individual pixel is determined by looking at its 2-by-2 neighborhood. There are six different patterns, each having different area values:

Patterns with zero white pixels have area = 0

Patterns with one white pixel have area = 1/4

Patterns with two adjacent white pixels have area = 1/2

Patterns with two diagonal white pixels have area = 3/4

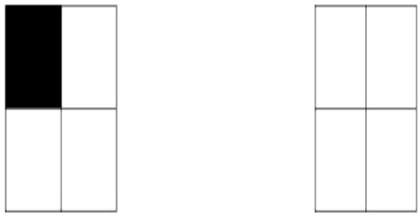

Patterns with three white pixels have area = 7/8

Patterns with all four white pixels have area = 1

Thus each pixel is part of four different 2-by-2 neighborhoods. This means, for example, that a single white pixel surrounded by all white pixels has a total area of 1 (1/4*4=1).Thus we calculate the area of each white pixel in

ISBN: 978-1-61804-228-6

the binary image and sum it up to get the total area of the wear on the railway track [1]. Results of wear area calculation using MATLAB are shown in Fig.8.

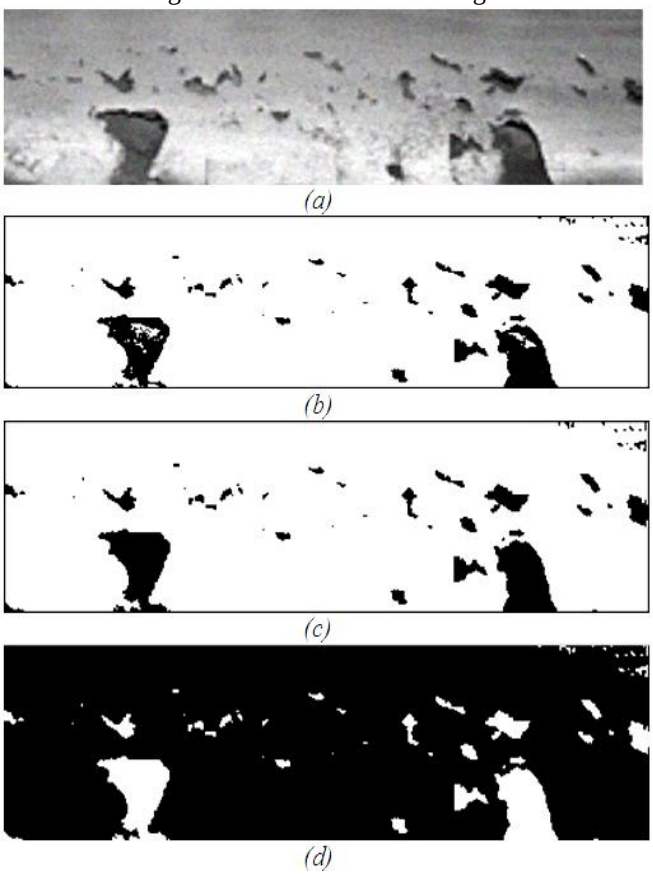

Figure 8.Results of wear area calculation using MATLAB (a) grayscale image of railway track wear, (b) Binary image obtained by global thresholding, (c) Binary image after applying local thresholding, (d) Complemented binary image of worn railway track

The percentage of wear calculated the given image comes out to be 8.346. The time required to calculate the surface wear area is 1.064653 seconds.

D. Detection of foreign objects on railway tracks

The railway tracks must be smooth and should not have any obstacles on them. A stray rock or any object on the railway track can scratch, wear and damage the railway track as well as the railway wheels. In this method, the unwanted objects on the railway tracks will be detected using frame differencing methods.

The method for detecting change between two frames is by using frame differencing and background subtraction. This method directly compares the similar pixels of two frames to decide whether they are the same. In the simplest form, a binary difference picture B(x, y) is difference between frames F1(x, y) and F2(x, y) obtained by: τ

$$B(x,y)=\begin{cases} 1, & F1(x,y)-F2(x,y)>\tau \\ 0, & \text{otherwise} \end{cases} \quad (11)$$

where F1(x,y) is the latest image with the object to be detected in it and F2(x,y) is the previous image without object in it. In a difference picture, pixels which have value 1 may be considered to be the result of object motion or illumination changes [10, 11].

Algorithm:

i. Take images of railway track after fixed time intervals.
ii. Compare the present image (the image has object to be detected in it) with previous image (image which does not have object in it) by using frame differencing method.
iii. The frame differenced image contains zero(R=0,G=0,B=0) and non zero value pixels in it.
iv. A pixel to be categorized as a non-zero pixel, it has to have its pixel value above a fixed threshold. In this method the threshold applied is of the value 20.
v. The non-zero value pixels (pixels with pixel value above the threshold) are the pixels of the object to be detected and zero value pixels (pixels with pixel value equal or below 20) are that of the background.
vi. These non-zero value pixels are then replaced by the corresponding pixels of the image with object in it and zero valued pixels are given zero pixel value.
vii. Thus the final image only consists of the object that was to be detected.

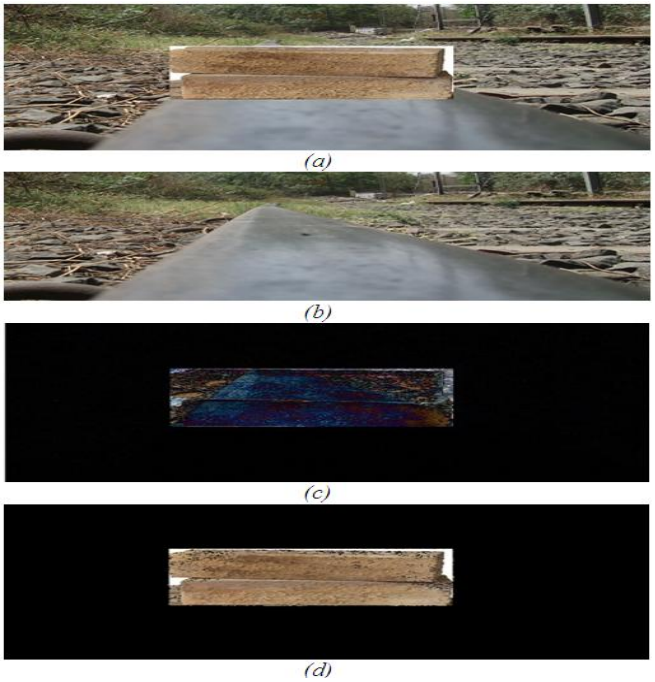

Figure 9.Results of object detection (a)Track image with the object to be detected, (b)Track image without object, (c)The frame differenced image, (d) Final image containing the detected object.

The non-zero value pixels in the frame differenced image are replaced by the corresponding pixels of the image with object in it and zero valued pixels are given zero pixel value.

The final image contains the object to be detected in it and results of object detection are shown in above Fig. 9.

E. *Crack Detection*

Extreme temperature differences, wearing, faulty manufacture or accidents can crack a railway track. A crack in the railway track must be detected at an early stage. The crack widens and expands each time the heavy railway passes over it. These cracks can later break the railway track and fatal accidents can occur. Basic Block Diagram of processing of crack detection system is shown in Fig.10.

Figure 10. Block Diagram for Proposed crack detection system

Algorithm:

- The image is read into the system memory for processing using the computer vision tools.
- The image is analyzed and the corresponding intensity histogram is obtained. The histogram contains the pixel intensity values in all three primary colour spaces (red, green and blue). A uniform surface should show homogeneity in the intensity levels throughout the image, which is indicated by the entire histogram lying in a specific band of values.
- The histogram obtained in the above step is analyzed for regions where the pixel intensity values (red, green and blue) show an immediate and large departure from the rest of the graph. These areas indicate that the surface at these points is not uniform as the rest of the image, and hence are an indication of deformities on the surface. Such areas are identified as cracks.

Results of crack detection with Test image containing crack, and Image test profile showing crack location are shown in Fig.11.

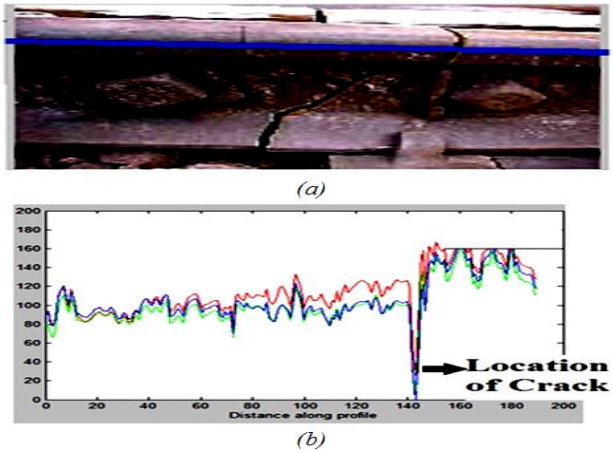

Figure11.Results of crack detection (a) Test image containing crack, (b) Image test profile showing crack location

VI. CONCLUSION

A sharp drop in the intensity values, which is consistent for a significant number of strips, indicates a crack on the surface. In this paper, we have developed computer vision methods for reliable identification and localization of structural defects in railroad tracks. Percentage of wear of rail head and length of cracks, as evaluation of defects of rail head section, Object detection, are calculated by various image processing methods and compare the simulation results using OpenCV and MATLAB. We have developed three software modules for analysis of different types of defects in railway tracks, namely, stray objects on the track, cracks on the track surface and wear of the rail head due to spalling. While the methodology developed and described in this paper involves a purely software-based approach, a conceptual hardware schematic is included which shows how the techniques can be successfully implemented by mounting the required hardware on a rail carriage and the measurements can be conducted without much disruption to the regular functioning of the railways.

ACKNOWLEDGMENT

The work is the outcome of project taken up by students Raj Inamdar, Sonam Sagar and Devjeet Dutta.

REFERENCES

[1] Ze Liu, Wei Wang, Xiaofei Zhang, Wei Jia, “Inspection of Rail Surface Defects Based on Image Processing”, 2nd International Asia Conference on Informatics in Control, Automation and Robotics, 2010,pp 472-475.

[2] Tomas Karis, “Track Irregularities for High-Speed Trains” , Master of Science Thesis,Stockholm, Sweden 2009.

[3] PavelBabenko, “Visual Inspection of Railroads Tracks”, Fall term, MS. University of Central Florida, 2009.

[4] Cesare Alippi, Ettore Casagrande, Matteo Fumagall', Fabio Scotti, Vincenzo Piur, Luigi Valsecchi, “Embedded System Methodology for Real-time Analysis of Railway Track Profile”, IEEE Instrumentation and Measurement Technology Conference Anchorage, AK, USA, 21-23 May 2002,pp 747-751.

[5] Wei Sun, Tian Luan, “Enclosure Method for Reconstruction of 2-D Cracks”, International Conference on Mechatronic Science, Electrical Engineering and Computer, Jilin, China, 2011.pp. 180-1483.

[6] Qingjie Tang, “Railway track geometry real-time inspecting system”, Instrumentation and Measurement Technology Conference,IMTC-92, 9th IEEE, 1992,pp. 656-660.

[7] E. Deutschl, C. Gasser, A.Niel, J. Werschonig, “Defect Detection on Rail Surfaces by a Vision based System”, IEEE Intelligent Vehicles Symposium, University of Parma, Italy, 2004,pp. 507-511.

[8] Luis Fernando Molina Camargo,Esther Resendiz,John Hart,J.Riley Edwards,Narendra Ahuja, Christopher P. L. Barkan, “Machine Vision Inspection of Railroad Track” , USDOT Region V Regional University Transportation Center Final Report, NEXTRANS Project No. 0281Y02, January 10,2011.

[9] Dr.Mubarak Shah, “Automated Visual Inspection/Detection of Rialroad track”, Final Report ,Computer Vision Lab,University of Central Florida, , Contarct No:BD550RPWO#8, July ,2010.

[10] Rafael C. Gonzalez, Richard E. Woods, Digital Image Processing (Second Edition), Publishing house of electronics industry, BEIJING, 2008.

[11] Milan Sonka, Vaclav Hlavac, Roger Boyle,Digital Imag eProcessing and Comuter Vison(First Edition), Cengage Learning India(2008).

[12] Bin He, Tianyu Ma, and Yunjian Wang, Visual C++ Digital Image processing(Second Edition), Posts and Telecommunications Press, 2003.

[13] Ruizhen Liu, Shiqi Yu, Course of OpenCV , Beijing University of Aeronautics and Astronautics Press, 2009.

[14] Stella E., Mazzeo P. L., Nitti M., Cicirelli G., Distante A., and D'Orazio T., "Visual recognition of missing fastening elements for railroadmaintenance," In Proceedings of the IEEE-ITSC International Conference on Intelligent Transportation system, Singapore, 2002, pp. 94-99.

[15] Cannon D. F. "An international cross reference of rail defects," UIC Rail Defect Management Report, June 2003.

[16] Federal Railroad Administration(FRA) "Office Of Railroad Safety Rail Defect" Reference Manual, first edition ,August 2011.

[17] Esther Resendiz, Luis Fernando Molina Camargo,John Hart,J.Riley Edwards,Narendra Ahuja, Christopher P. L. Barkan, "Development Of A Machine Vision System For Inspection Of Railway Track Components", 12th WCTR, July 11-15, 2010 – Lisbon, Portugal ,pp 1-21.

[18] Gary Bradski and Adrian Kaebler"Learning OpenCV: Computer Vision with the OpenCV Library", Sebastopol: O'ReillyMedia Inc.,2008.

Analysis the Effect of Pedagogical Agent using Leaners' Eye Movements

Noh, Kyung-Bo, Ki-Sang Song, and Sang Chun Nam

***Abstract*—**There exists controversies introducing pedagogical agents into digital contents, pros are fostering learner motivation and learning outcomes based on the pedagogical agents' social cues, and cons are distracting learners from the learning content. To identify the impact of applying a pedagogical agent, we have measured the differences of cognitive load and achievements by analyzing the learners' eye movements. Three groups consisting of 45 high school students have been tested to measure the effect of three types of contents; image and text based multimedia with a pedagogical agent, multimedia as figure and text with narration, and multimedia only. The learners' eye movements were recorded while they studied the provided contents, and self-reports of cognitive loads and learning achievements surveys were conducted to analyze learners' performance. From the analysis, we found that group of contents using pedagogical agents and narration, outperformed the other two groups, and showed that the positive impact of pedagogical agents' presence on learners' cognitive load and achievements.

***Keywords*—**Pedagogical agent, Multimedia learning, Eye-tracking, Cognitive load

I. Introduction

The importance of providing appropriate interactions between *i*) learner and content, *ii*) learner with other learners, and *iii*) learners with instructor [1] are crucial aspects of e-learning systems. The interaction between learner and content needs to consider the learner's isolation status from other learners or the instructor[2]. The computer tutor needs to provide human educators' teaching strategies such as observing students' progress and giving appropriate feedback.

For providing more vivid interactions, research was carried out to apply pedagogical agents into an e-learning environment. The pedagogical agent is a software program working as a helpful aid in computer based learning. Usually an animated character that has a persons' motions and emotions is sometimes inserted into typical e-learning contents, to help learners to interact with the contents.

This work was supported by the National Research Foundation of Korea Grant funded by the Korean Government (NRF- 2012-R1A1A-2008560). The authors also express thanks to KRISS for sharing utilities.

K.B. Noh was with the Korea National University of Education, ChungBuk, 363-791 Korea. (e-mail: boya1110@naver.com).

K.-S. Song is with the Korea National University of Education, ChungBuk, 363-791 Korea. (corresponding author to provide phone: +82-10-6402-8644; fax: +82-43-231-3790; e-mail: kssong@knue.ac.kr).

S. C. Nam is with the Korea National University of Education, ChungBuk, 363-791 Korea. (e-mail: happynsc@naver.com).

The main reason for applying a pedagogical agent is to reduce the learners feeling of isolation towards an instructor, and to provide the function of encouragement into content, so that learners may feel more one on one tutoring or personalized learning with a human instructor. Wouter and his colleagues [3] have reported that pedagogical agents may provide more social interactions between learners and content, and therefore improving the learners motivations and engagements in the learning process. However, there exist different opinions on the effect of pedagogical agents. For example, Heidig and Clare reported that [4] the agents may give positive effect to affective characteristic to learners, but not give positive effect to the scholastics achievements. Dogmagk [5] also reported similar results, and suggested that the social agency theory needs to be modified.

Because of pedagogical agents appearing in the same display with learning contents, the learner's attention may be split between both objects. Some researchers explained this to create less effective learning outcomes [3], and Ryu [6]. To overcome such distraction, presenting text information and figures needs to be converted into audio information according to Mayer's multimedia principle [7].

It is necessary to identify the effect of pedagogical agents for reducing cognitive overload in multimedia contents based on evidence based methods. In this paper, we have applied eye movement measurement technique to analyze the effect of pedagogical agents on learners visual attention. Also, we want to find the most effective ways of interaction between learner and contents with pedagogical agents.

II. Procedure for Experiment

A. Contents Design

Three types of contents have been designed with multimedia. The multimedia includes text and figures. Also pedagogical agents were designed using computerized characters.

The selected topic of content was the 'human organ of scent,' and this subject was selected considering the test subjects grade level. The test participants were in Grade 11 and therefore the experimental content's subject was selected from the science topics of Grade 10. The designed contents contain 2 frames, one for the structure of the scent organ smell, and the other was the sensory system delivering information to the brain.

The narration for explaining the contents on each page was designed using TTS from Oddocast. Also the animated agent

was created using CrazyTalk Animator Pro, to imitate a human's emotions and expressions. The designed frames are shown in Figure 1.

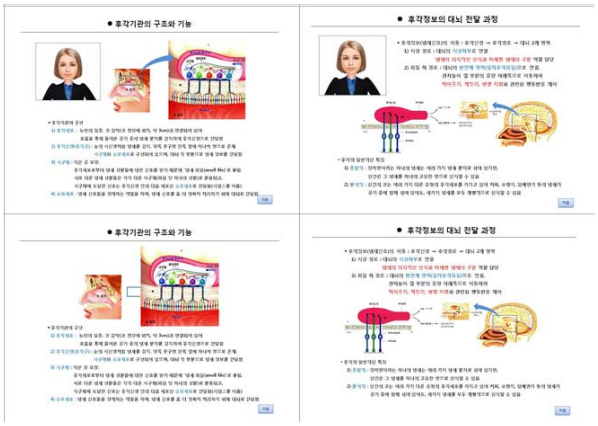

Fig 1. Designed contents

The test contents G1 has an pedagogical agent as shown in the upper two squares in Fig. 1. The G2 has a narration of a media file instead of a pedagogical agent in the bottom two squares in Fig. 1. The contents of G3 does not have either a pedagogical agent or narration media file as shown in Fig. 1.

B. *Participants*

The test subjects were randomly selected from Grade 10 high school students, 9 males and 36 female students. The 45 students were divided into 3 groups with 15 students in each group. To assure the same learning capabilities between groups we performed a pre-test, and the results are as following.

Table 1. The Pre-test of priori knowledge between groups

Item	G1	G2	G3
Mean	2.30	2.21	2.27
S.D.	0.72	0.80	0.94

Based on the test data, we have analyzed the scores using the whole area covariance analysis, and they show that all three groups have no differences in terms of learning capabilities.

C. *Experiment*

The playing time of the narration file embodied in the1st page is 1Min and 52 Seconds, 2nd page is 1Min and 49 Seconds. These are the minimum times to spend on each page, but if a user needs more time they can proceed to the next page according to their pace. While they use the contents, their eye movements have been captured and recorded with Facelab 4.6 eye tracker. The eye movements were captured 60 frames/sec, and the captured data was stored immediately for processing. The data was analyzed with EyeWorks Analyzer 3.7 Premiere Software.

The experiment consists of following steps;

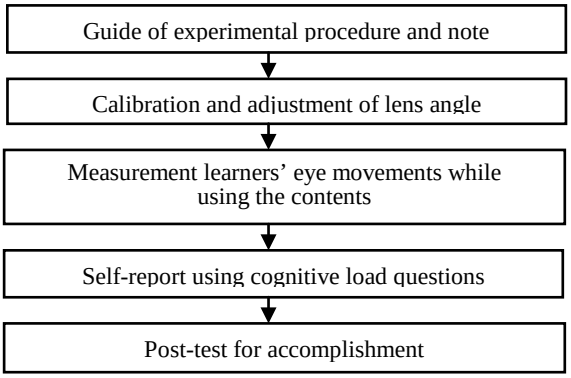

Fig 2. Experimental procedures

D. *Measurement Cognitive Overload*

Among the measurement techniques of cognitive load such as physiological measurement, double task, and questionnaire survey, we have applied the questionnaire test of self-reporting style for allocation during the test period. Although there exists controversies that self-reporting may depend on individual perception, it is also reported that this technique is useful for understanding cognitive process [8].

The questionnaire was originally designed by Ryu and Lim [8], and has been modified Lim[9]. It has Likert 7 scale levels, and has 5 sub factors such as physical effort, mental effort, task difficulty, self-evaluation, and usability. The cognitive load sub factors, and their reliability are given in Table 2.

Table 2. The sub factors of cognitive load

Factor	Meaning	Item reliability
Physical effort	Physical fatigue and consumption of physical strength	0.850
Mental effort	The perceived amount of mental activities	0.807
Task difficulty	The individually perceived task difficulty	0.832
Self-evaluation	The sense of accomplishment after studying	0.870
Usability	The effect of instructional design to learner's understanding	0.909

After the experiment, subjects were asked to take post-tests for their retention and level of understanding of the tasks. There was no time limitation to the paper and pencil test of accomplishments.

III. Data Analysis and Discussion

A. *The Results of Cognitive Load Questions*

To check the cognitive load differences of users according to different types of contents, we have tested cognitive load and

analyzed with MONOVA. The technical statistics of each contents are given in Table 3.

Table 3. The technical statistics of cognitive load of each content

Factor	G1	G2	G3	Total
	Mean(S.D.)	Mean(S.D.)	Mean(S.D.)	Mean(S.D.)
Physical effort	3.31(1.09)	2.98(1.08)	3.10(1.22)	3.13(1.12)
Mental effort	5.35(0.89)	5.03(0.80)	4.63(1.11)	5.00(0.97)
Task difficulty	4.45(0.97)	4.56(0.97)	5.41(1.12)	4.81(1.09)
Self-evaluation	4.85(1.11)	5.10(1.16)	4.28(1.00)	4.74(1.11)
Usability	4.98(1.11)	5.03(1.02)	4.00(1.03)	4.67(1.14)

Among the three types of contents, users expressed the least physical effort from the narration inserted content G2. The most mentally challenging activity content type was G1, where the pedagogical agent was inserted. The highest task difficulty was found in the G3, where the content used only text and images. The highest self-evaluation and usability factors are found in the G2 content with text, image and narration.

The post comparison analysis of task difficulty between G1, G2, and G3, only G1 and G3 shows statistically significant differences with the significance level of 0.05. Also, usability analysis shows that G1 and G3, and G2 and G3 show statistically significant differences. From these results, we can say that the narration applied in the pedagogical agent might affect the task difficulty and usability of the content.

B. *The Results of Accomplishment Test*

To check the accomplishment results using three types of contents, the subjects have taken a post-test, and their statistical results are given in Table 4.

Table 4. The technical statistics of accomplishment

Content	G1	G2	G3	Total
Mean	23.13	22.40	19.46	21.66
S.D.	3.52	3.33	2.82	3.54

We have applied ANOVA for checking the significant difference between the content types based on this data, and it shows that there exist significant differences among the three types of contents. The statistical analysis of accomplishments between G1 and G3, and G2 and G3 show significant difference level of 0.05. This indicates that the narration used in the pedagogical agent affect the accomplishment difference between contents.

C. *The Eye Movements Analysis*

1) *Eye Fixation Analysis to Specific Element in Content*

While users viewed the different types of contents, their eye fixation characteristics were tracked.

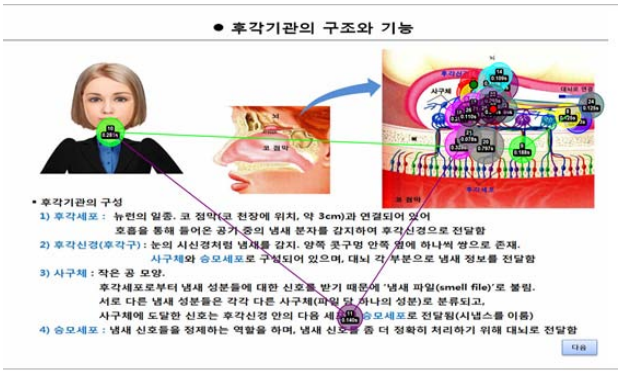

Fig. 3 The eye fixations to specific elements in the content

From the measurements, it was found that contents G1 and G2, where text message and visual exploration guide were provided, users spent more time on figures than G3 where no narration was used. This indicates that users pay more attention to explanative figures without splitting their attention to text elements. However, when users use G3 contents, they frequently switched their focus from text to image vice versa. This means they might spend more time on text reading instead of figures.

2) *Eye Fixation Analysis to Specific Element in Content*

To check the effect of narration to G1 and G2 contents, we have analyzed the gaze path according to the time slot while users viewed the contents.

Time slot (sec)	Content type: G1
(a) 0-17 Guide for using the content	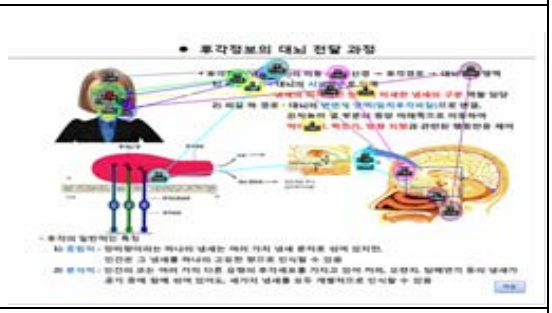
(b) 17-46 The olfactory delivery path	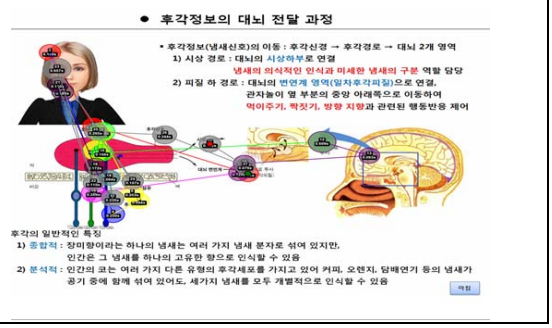

Time slot (sec)	Content type: G1
(c) 75-109 General character istics	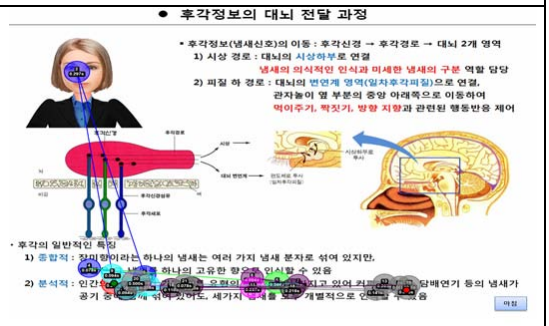
(d) After narration is ending	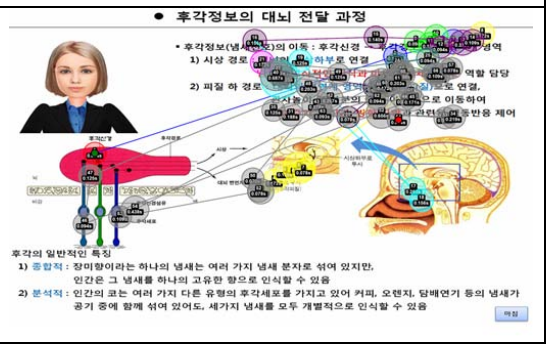

Fig 4. The gaze paths of users' with content G1

When users viewed the pedagogical agent embedded content G1, users gazes stay with the pedagogical agent before the narration started (Refer Fig. 4 (a)). Once narration was started, users' eyes move to a specific area of the content according to the explanation. When the narration was stopped after a sentence, users' eyes moved to the pedagogical agent again. This indicates users naturally gaze at the pedagogical agent as a means of social interaction in face to face human communication. Almost 10% of attention occupation was observed towards the pedagogical agent, but this does not impose additional cognitive load to a user according to the analyzed results of the cognitive load questionnaire and accomplishment test.

(b) 17-46 The olfactory delivery path	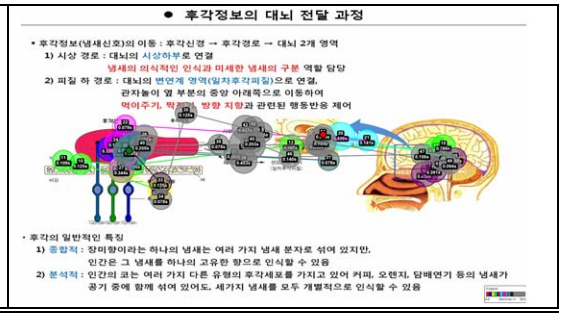
(c) 75-109 General character istics	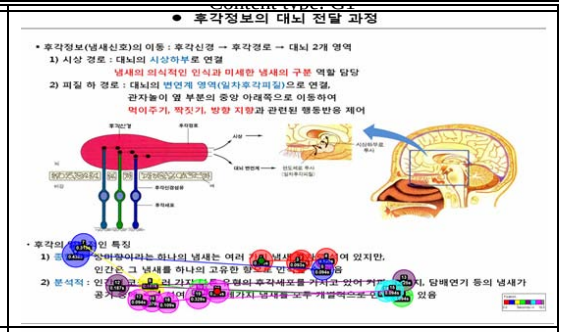
(d) After narration is ending	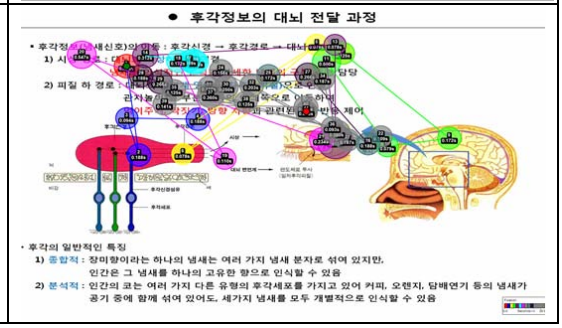

Fig 5. The gaze paths of users' with content G2

Compared with G1 and G2 contents, the eye movement patterns of G3 content has two characteristics; one is reading text and quickly passing by the figures and returning to the text again as shown in the top of Fig 6., and the other is reading text and referring to figures often that frequent gaze movements are caused.

Time slot (sec)	Content type: G2
(a) 0-17 Guide for using the content	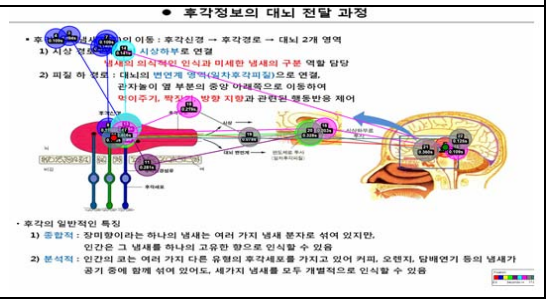

Pattern 1	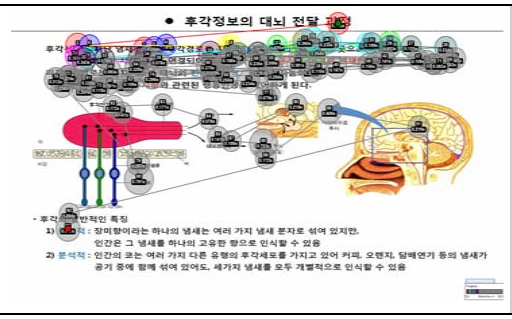

Pattern 2	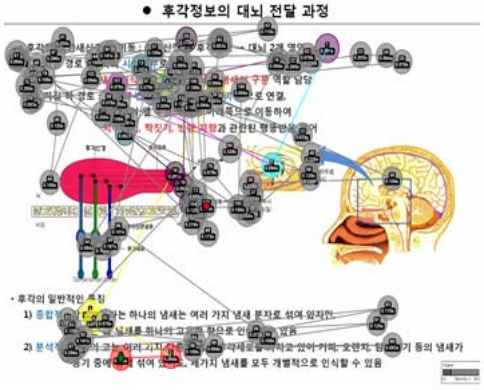

Fig. 6. The two eye movement patterns in G3 content

These patterns can be explained in that users use both text and image information to process information simultaneously in the cognition process as Mayer described [10].

Content	Heat map diagram
G1	
G2	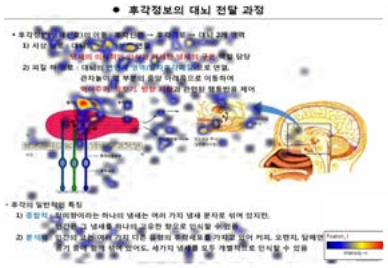
G3	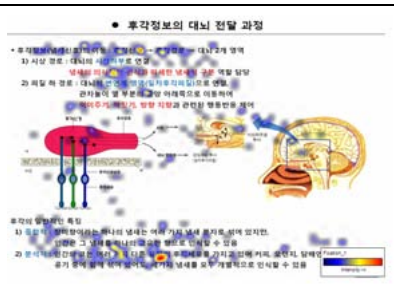

Fig. 7 Heat map diagram of g1, G2, and G3 content

Comparing the heat maps of three types of contents as in Fig. 7, G1 and G2 spent more time on figures, and listening explanations from the narration than G3. The narration helps users focus on figures, and the result is easy integration of audio and visual information compared with G3. This causes positive results in terms of cognitive load and accomplishment tests.

IV. Conclusion

Although the purpose of a pedagogical agent application in multimedia learning contents is fostering a learner's motivation and eventually enhancing learning outcomes, sometimes the pedagogical agent is blamed for distracting learners attention.

From this rationale, we have designed three types of learning contents, and tested them in various ways including eye tracking techniques to observe learners' attention points by measuring eye movements.

From the eye fixation time analysis, a heat map diagram and gaze path observations, the pedagogical agent helps the user to provide social interactions with content. Even though the existence of a human image of pedagogical agent's does cause significant differences in learning outcomes and cognitive load compared with content using narration, text and image, users spend time frequently looking at the human image. This implies that if the image may convey more human-like feedback, it may contribute positively towards learners' overcoming the sense of isolation associated with an e-learning environment.

Also, the outperformance of learning content with pedagogical agents and narration, the pedagogical agent itself does not distract a user's attention, but rather can have a positive effect on creating a better e-learning environment.

References

[1] M. G. Moore, *Three types of interaction*. In K. Harry, M. John & D. Keegan (Eds.), Distance education: New perspectives (pp. 12-24). London: Routlege, 1993.

[2] K.S. Song, J. H. Park, and S. M. Jeung, "Enhancing e-Learning Interactivity via Emotion Recognition through Facial Expressions," in the proceeding of ICL 2006, September 27 -29, 2006 Villach, Austria

[3] P. Wouter, F. Pass & J. J. G. van Merrienboer, "How to optimize learning from animated models: A Review of guidelines based on cognitive load," *Review of Educational Research*, 78(3), 645-675, 2008.

[4] S. Heidig, & G. Clarebout, "Do pedagogical agents make a difference to student motivation and learning?," *Educational Research Review*, 6, 27-54, 2011.

[5] S. Domagk, "Do pedagogical agents facilitate learner motivation and learning outcomes? The role of the appeal of agent's appearance and voice," *Journal of Media Psychology*, 22(2), 82-95, 2010.

[6] J. Ryu, and C. Son, "Attentional guidance of visual cueing and levels of realism of pedagogical agent on cognitive load factors and achievement," *Journal of Educational Technology*, 27(3), 507-533, 2011.

[7] R. E. Mayer, R. Moreno, "Nine ways to reduce cognitive load in multimedia learning," *Educational Psychologist*, 38, 43-52, 2003.

[8] J. Ryu, and J. Lim, "An Exploratory Validation for the Constructs of Cognitive Load," *Educational Information Media Research*, 15(2), 1-27, 2009.

[9] T. Lim, On the Effect of Reading Purpose and Display Mode to Performing Task and Cognitive Factors, M.S. Thesis, ChunNam National University, 2012.

[10] R. E. Mayer, Multimedia Learning, 2nd ed. Cambridge University Press, NY, 2010.

Hand-off performance Enhancement in Heterogeneous Mobile Networks using Radio Access Technology Selection Algorithm

Ibraheem M. Fayed

***Abstract*—**CRRM can bring significant benefits in the heterogeneous wireless network, such as load balancing, interference distribution, reduction of unnecessary handoffs and reduction of call dropping blocking probability. A major issue for CRRM is the RAT selection. An efficient CRRM RAT selection algorithms have been described and deployed depending on four different techniques; load balancing (LB), service based (SB), random selection (RS), and priority based (PB). Cooperative HWN operator is assumed with three different RATs used in GSM, DCS and UMTS networks. A comparative study has been presented based upon the presented CRRM deployment scenarios for fixed user model and mobile user model. In the mobile user model, the effect of velocity variation will be investigated. It is shown that UMTS is best utilized via the deployment of PB algorithms. This occurs as a result of huge number of the RRUs in the UMTS network. DCS is best utilized via the deployment of LB algorithm. This occurred as a result of normalized load calculations, in other words, the percentage of the available RRUs will not be biased to any RAT, but the system will try to use the lowest loaded RAT. On the other hand, GSM is best utilized with a deployment of SB algorithm. Finally, the handoff performance and the overall performance (represented by the percentage of un-served users) will be improved by introducing CRRM RATs algorithms. This will give minimal opportunities for un-served customers in the RATS under the predefined operational conditions.

***Keywords*—**Access Selection Algorithms, Heterogeneous Wireless Network, hand-off, GoS and CRRM.

I. Introduction

WIRELESS mobile communication networks have become essential for human life. On order that, great booming and huge investments are devoted to the development and best utilization of different radio access technologies (RAT's). So the operators are facing a lot of problems for the efficient utilization of the different RATs that they may have. A heterogeneous wireless network (HWN),integrates a number of overlapped RATs such as Global Service Mobile (GSM) and its enhanced version (EDGE).GSM/EDGE Radio Access Network (GERAN) are based on two different carriers (900&1800Mhz) namely GERAN900 and GERAN1800 [1]. A major challenge for such HWN is the collaborative Radio Resource Management (RRM) strategy. Currently RRM strategies are implemented independently in different kinds of RATs. Individually these RRM strategies work well in its own RAT for which it is designed for. However none of them is suitable for management of cooperative HWN. This arises from the fact that each RAT only considers the situation of one particular radio resources RRM is based upon what is called the Radio Resource Unit (RRUs). These physical transmission parameters depend on the multiple access technique being used [2]. The objective of a network operator is the deployment of a network able to support its customers with the required Grade of Service (GoS) under the factor of coverage area.

The handoff process is of major importance within any cellular telecommunications network. It is necessary to ensure that it can be performed reliably and without disruption to any calls. Failure for it to perform reliably can result in dropped calls, and this is one of the key factors that can lead to customer dissatisfaction, which in turn may lead to them changing to another cellular network provider. Accordingly handoff is one of the key performance indicators monitored so that a robust cellular handoff regime is maintained on the cellular network [3], [4].

RRM functions are in charge of allocating and managing the provisioned RRUs. In order to solve this problem in case of HWN deployment scenario, the common RRM (CRRM) strategy has been proposed to coordinate radio resource utilization across a number of different RATs in an optimized way. CRRM is deployed in order to jointly manage radio resource among different access technologies (RATs) in an optimized way [5]. The RAT selection algorithm, including initial RAT selection and the vertical handover (VHO), is one of the key research areas in CRRM. A suitable RAT selection algorithm can maximize system performance and GoS by allocating users to the most suitable RAT in the case of two or more RATs co-locating in the same coverage area.

II. Common Radio Resource Management Algorithms

The RAT selection algorithm, including initial RAT selection and Vertical Handover (VHO) is a key research issue in CRRM at the current stage. Four different algorithms are introduced in a mixed CRRM GREAN900, GREAN1800, and UTRAN scenarios. The proposed CRRM algorithms will be applied on the defined active users in the cell using the four different CCRM RAT selection

techniques. These techniques are: Load Balancing (LB), Service Based (SB), Priority Based (PB) and Random Selection (RS) algorithms. Since the initial x& y coordinates, RSS, status and distance of the active users have already been saved in an excel sheet, we can easily reread them in order to be used in the CRRM RAT selection [6].

a) Load Balancing Algorithm

If the number of voice active calls in the system is i calls, and the number of active data sessions is j sessions. Hence, the TDMA- based RATs loading factor L(i,j)(namely: GERAN900 and GERAN1800), is measured as follows [7] :

For GERAN900:

$$L(i,j) = \left(\frac{\min\{(i+j), Cg\text{-max}\}}{Cg\text{-max}}\right) \quad (1)$$

For GERAN1800:

$$L(i,j) = \left(\frac{\min\{(i+j), Cd\text{-max}\}}{Cd\text{-max}}\right) \quad (2)$$

Where, Cg-max and Cd-max are the maximum capacity of GERAN900 and GERAN1800 respectively. Note that this definition of load will not account for multiple users sharing a same time slot, nor users using multiple time slots.

On the other hand the load in a WCDMA-based system may be calculated by means of the UTRAN loading factor L(k,l), which is defined by:

$$L(k,l) = \left(\frac{k}{Cu\text{-max}}\right) + \left(\frac{l}{Cu\text{-max}}\right) \quad (3)$$

Where, Cu-maxis the maximum capacity of UTRAN network with k users using a voice service and l users using data service. Then different RAT loads are compared, and the CRRM will select the lowest loaded RAT.

Initially, loading factor for each RAT will be set to zero. The loading factor is a key factor for users' allocation in this algorithm. The RSS will be calculated and will be used and compared with the RATs sensitivities in the following cases.

i. Case 1:

UMTS is the most eligible RAT for allocation.

The received power of the user is greater than the UMTS power threshold and less than GSM and DCS power threshold taking into consideration that the capacity of UMTS is less than the maximum capacity. This user will be UMTS allocated and is given a frequency carrier in the 2100 band and then the loading factor will be recalculated. If the UMTS is fully capacitated then this user will be blocked.

ii. Case 2:

GSM and UMTS are both eligible RAT allocation.

In this case we must take into consideration the loading factor of each RAT to decide which RAT is the most eligible. If the loading factor of the UMTS is less than the loading factor of GSM and there is free allocation in the UMTS this user will be UMTS allocated, but if the loading factor of GSM is less than the loading factor of UMTS and there is free allocation in GSM then this user will be GSM allocated.

iii. Case 3:

All RATS are eligible

All RATS are eligible because the received signal strength is sufficient for all RATS. We will choose which RAT is the most eligible according to the loading factor and the capacity of each RAT.

iv. Case 4:

No RAT is eligible

No RAT is eligible because the received signal strength is not sufficient for any RAT so this user will be blocked. Finally after allocating all users in the most eligible RAT the frequency of each user is saved in an excel sheet so we can reread them later and choose which RAT selection algorithm is the best.

b) Priority Based

In the priority based scheme we are only looking at the RSS of the active user and the capacity of the desired RAT. The management of this technique is done according to the operator's desire for allocating the proposed active users to certain RAT. The proposed methodology, at first allocates the users to DCS1800. Then, GSM 900 is the next preferred RAT. Finally UMTS based RAT, is the last algorithm used. These arrangements are based on the path loss which is proportional to the operating frequency. This is done in order to achieve less number of un-served users. Then the RSS will be calculated and will be used and compared with the RATs sensitivities in the four cases mentioned before will be applied.

c) Service based

Under the service based RAT selection policy, the RAT is selected based on the service type. There are two service policy algorithms: voice based service is preferred to be served by DCS or GSM according to the power threshold conditions. So, voice users are always allocated to DCS/GSM first. On the other hand, the broad band data service users are preferred to be served by UMTS. We have already defined a variable status S before if it's equal to '1'then this user is voice user and if its equal to '0' then this user is data user. Then the RSS will be calculated and will be used and compared with the RATs sensitivities in the four cases mentioned before will be applied.

d) Random Selection

The RAT is selected based on the random function normally distributed between the three available RATs. Random variable N is generated randomly to decide which RAT will be allocated. Then the RSS will be calculated and will be used and compared with the RATs sensitivities in the

four cases mentioned before will be applied.

III. System Parameters and Assessment Criteria

The main objective is to propose an algorithm to help user to make the discovery of available heterogeneous networks around and makes the decision of which network will be connected, depending on specific Quality of Service (QoS) parameter. The proposed algorithm will be implemented using MATLAB and its performance will be evaluated by simulations.

A certain number of customers (N), which are to be efficiently distributed on the different radio access technologies in our proposed cell using the common radio resource management selection algorithm (CRRM) are assumed. This model assumes random distribution for fixed users around the cell with available RATs in (DCS, GSM and UMTS networks). CRRM RAT selection techniques (load balancing, random selection, service based and priority based) are applied. After applying CRRM the best algorithm will be determined to help the operator to utilize the bandwidth so that the operator can allocate the maximum number of users.

After the fixed users start motion, the CRRM is applied again taken into consideration the handoff process for the users in the cell boarder. Vertical and horizontal handover will be applied to enhance the system as decrease its call dropping rate. Different CRRM policies will be tested in conjunction with different selection algorithms. The system model is based on three co-located sites that belong to three different RATs. Customers are distributed normally over the service area. In addition, the deployment for practical propagation models for downtown deployment is taken into consideration. The presented system model parameters are summarized in the following table [8], [9]. The proposed model assumes that there are different radio access technologies (RATs), namely, GERAN900, GERAN1800, and UMTS, It is assumed that the three RATs coexist and the channel is modelled via practical propagation models, the path loss is evaluated practically based on the Okumura-Hata Model for GERAN900, whereas both of the GERAN1800 and UTRAN are modelled via COST231-Hata propagation model [10].

Table 1. *System Parameters*

BTS/NodeB antenna height (ht)	45m	GERAN900 Power Threshold (Prg_min)	-90dBm
MS antenna height (hr)	1.5m	GERAN1800 Power Threshold (Prd_min)	-85dBm
BTS/Node antenna Gain (Gt)	18dBi	UTRAN Power Threshold (Prd_min)	-112dBm
MS antenna Gain (Gr)	2dBi	GERAN900 Maximum Capacity (Cg_min)	63
GERAN900 central frequency (fg)	900MHz	GERAN1800 Maximum Capacity (Cd_min)	63
GERAN1800 central frequency (fd)	1800MHz	UTRAN Maximum Capacity (Cu_min)	480
UTRAN central frequency (fu)	2100MHz	BTS Transmitting Power Range (Pt)	~50
Feeder Loss (Lf) for all RATs	6dB		

The path loss equations are presented in the following set of equations:

$$LpGERAN900 = 69.55+26.16\log(fg)-13.82\log(hr)-a(hr)+(44.9-6.55(ht)\log(d) \quad (4)$$

$$LpGERAN1800 = 49.3+33.9\log(fd)-13.82\log(hr)-a(hr)+(44.9-6.55(ht)\log(d) \quad (5)$$

$$LpUTRAN = 49.3+33.9\log(fu)-13.82\log(hr)-a(hr)+(44.9-6.55(hr)\log(d) \quad (6)$$

$$a(hr)=(11.1\log(fc)-0.7)hr-(1.56\log(fc)-0.8); \quad fc \begin{cases} 900; \text{GERAN900} \\ 1800; \text{GERAN1800} \\ 2100; \text{UTRAN} \end{cases}$$

IV. The Proposed Model

In the proposed algorithm, N users are to be are served by one BTS in an already planned site which supports 3 RAT technologies (GSM, DCS, and UMTS) where, Identically Independent Distributed (IID) cells are being assumed. The number of active users is kept fixed for simulation purposes. Where, each active user can only use one class of service either data or voice. And the probability of a user to demand a voice service is considered to be 65%, while the probability of a user to demand a data service is 35%.

The coverage area for each RAT was calculated by substituting with the RAT's sensitivity in the Link budget equation to determine the value of the path loss at the cell's edge. Therefore, substituting with the value obtained for the path loss and with the central frequency of each RAT, a cell radius is obtained.

The values of the radiuses obtained are as follows:

- DCS Cell Radius= 2.294 km
- GSM Cell Radius= 7.633 km
- UMTS Cell Radius= 12.208 km

a) Users Generation

A thousand users are generated randomly around the BTS/NodeB. The position of each user is then determined by its x and y coordinates and its distance away from the BTS/NodeB and direction (θ) is calculated. 250 users out of the thousand are set to be idle users and are excluded, the remaining 750 are then given a random bit (0 or 1) to determine the service requested (0 denotes data service and 1 denotes a voice service). The probability of a user to require a data service is limited to 35% of the active users.

ISBN: 978-1-61804-228-6

b) Calculation of the Received Signal Strength for Active Users

According to the user's distance away from the BTS/NodeB its Received Signal Strength will be determined [11].

If the distance of the user is greater than the UMTS cell radius then this user is out of coverage area and therefore will not be able to acquire a service and is therefore given very low received signal strength to avoid confusion in further calculation throughout the simulation process. The RSS of such a user is set to -500dBm.

If the distance of the user is smaller than the DCS cell radius, the capacity of the DCS RAT is checked and compared with the DCS maximum capacity. If the DCS current capacity is lower than the DCS maximum capacity, then there is free allocation in DCS the user's path loss is calculated according to equation (5). While if the DCS current capacity is greater than the DCS maximum capacity, the GSM current capacity is compared with its maximum capacity. If the GSM current capacity is lower than the GSM maximum capacity, then there is free allocation in GSMthe user's path loss is calculated according to equation (4). While if the GSM current capacity is greater than the GSM maximum capacity, the user is given an allocation in the UMTS RAT and its path loss is calculated according to equation (6).

If the distance of the user is greater than the DCS cell radius, and smaller than the GSM cell radius, the GSM current capacity is compared with its maximum capacity. If the GSM current capacity is lower than the GSM maximum capacity, then there is free allocation in GSM the user's path loss is calculated according to equation (5). While if the GSM current capacity is greater than the GSM maximum capacity, the user is given an allocation in the UMTS RAT and its path loss is calculated according to equation (6).

While if the distance of the user is greater than the GSM cell radius and smaller than the UMTS cell radius, the user is given an allocation in the UMTS RAT and its path loss is calculated according to equation (6) directly.

As a result an array of the received signal strengths is obtained. To be used as an input for the proposed CRRM algorithms. Figure 1 shows users generation for active and idle users with in the cell.

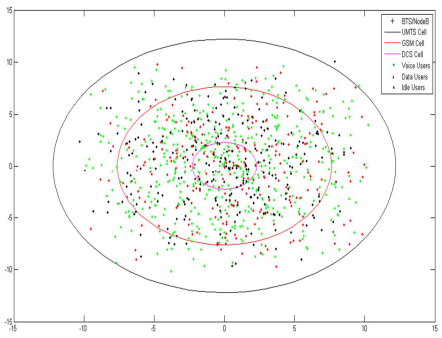

Figure 1. *Active and Idle Users With in the Cell*

c) Mobility Model

Up to this point all users where thought to be fixed and maintaining their distance away from the BTS/NodeB, but cell phone systems provide mobility, therefore it is impractical to just distribute the active users to different RATs based on their fixed positions only.

The assumption that users are to change location is necessary to be dealt with. Therefore, in the case where mobility is applied to fixed users, their initial distance and coordinates will change.

To simulate this change, in our proposed algorithm it is assumed that the active users of total number 750 will change their location randomly by assuming a random variable dx and dy which gives values of (1, 0, -1), this variable tends to give a certain direction to each user. Each 10 seconds the new locations of the users will be monitored and saved. GSM RAT will be taken as an example for results.

i. Users' Location and Distance Calculation after Mobility

First we will reread the initial x & y coordinates of each user and their distances with respect to the BTS. Two variables are defined (dx, dy) to move the fixed users in a different directions [11]. These variables are either (-1, 0, 1) which tends to represent the location of each user whether he/she moves forward towards the BTS, or away from the BTS or user stays still and maintains initial position. We will calculate the new value of x & y coordinates after each value of Ts (10 seconds) from a time span of 120 seconds at a certain value of the given velocities.

After calculating the new values of x &y coordinates, we can determine also the direction of the user from the BTS, since we are assuming a circular cell;

$$\tan(\theta) = y/x$$

After applying mobility we noticed that the new location of some users were located outside the coverage area of the UMTS cell radius. These users will make successful horizontal handoff in the neighboring cells and a new user will enter instead of this user since we are assuming identically independent distributed cells (IID). The new values of x & y coordinates will be saved after each sample to be used as initial values to the next sample.

To determine the changes to the initial distribution of the users the time span of 120 seconds was divided into 4 sessions each of an average duration of 30 seconds. At the start of each session the users will be distributed into the different RATs using the CRRM algorithms discussed earlier. While during each session the user's movement is monitored and if user needs to change his/her initially provided RAT due to crossing of the coverage of area of its operating RAT the user is to perform vertical handoff if possible or its call is to be dropped. The average number of vertical handoff and dropped calls is calculated every session to help in comparing between different CRRM algorithms at different velocities.

ISBN: 978-1-61804-228-6

ii. Load Balancing Handoff and Mobility

If a user previously allocated in DCS RAT, is crossing the DCS cell radius then the system will need to check and compare between the loading factors of the GSM and UMTS. The new RAT provided for this user will be the one with the lower loading factor. While if both RATs are fully capacitated the user's call or service will be terminated.

Similarly, if a user previously allocated in GSM RAT, is crossing the GSM cell radius then the system will need to check the loading factors of UMTS and if possible use vertical handoff to change from GSM to UMTS or else his call will be dropped.

iii. Service Based Handoff and Mobility

Here, the decision of handoff from DCS to either UMTS or GSM is based on the service type of the given user, if the service is a voice service the GSM is of a higher priority, and if the service is a data service then the UMTS is of a higher probability.

iv. Random Selection Handoff and Mobility

Similar to the Service based handoff algorithm the sequence of RATs that the users is to be handed to if possible is determined by the a random integer similar to the service type of the user.

v. *Priority Based Handoff and Mobility*

In priority based the operator sets the sequence or the priority of the RATs independent to the service type, loading factors or random integers.

V. Results and Analysis

First, CRRM RAT selection policies are deployed under the condition that the users are statics and before applying any movement.

Second, applying CRRM and observing handoff performance after applying the mobility proposed model, where users are no more static and moving with certain velocities. The system parameters are chosen as stated in the previous section. These parameters are in consistence with previously published work. In addition, it is the most commonly used in the current deployment scenarios in the practical rollouts. Each CRRM policy has been evaluated via both of the percentage of served and un-served customers.

a) 5.1 Fixed Users Model

GSM Performance after applying CRRM RAT selection, figure 2 shows GSM/GERAN900 Served users for different CRRM Algorithms with different transmitted powers. As shown in this figure, the sufficient power for having best utilizing (i.e. 95% usage), is about 50 dBm. It has to be recognized that these results are for the downtown deployment scenario. Eventually, the LB algorithm is the most efficient power algorithm whereas it suffers from the unfairness that will affect the performance of the shared RATs. On the other hand, SB will require large computational power to stabilize the fairness between the usages of different RATs. The simplest technique is the RS which has minimum computational power, but at the expense of the possibility of bad utilization.

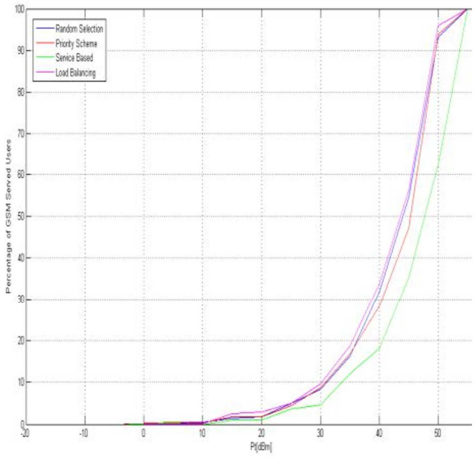

Figure 2. *GSM/GERAN900 Served users for different CRRM algorithms with different transmitted powers.*

DCS performance after applying CRRM RAT selection, figure 3 shows the percentage of served DCS/GERAN1800 customers against transmitted power.

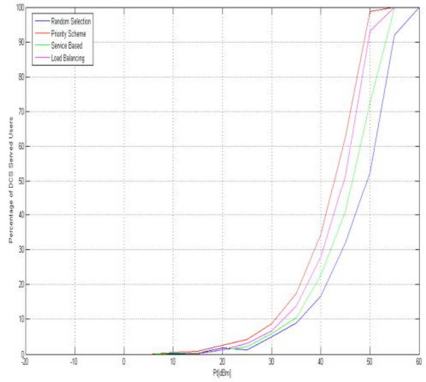

Fig. 3 DCS/GERAN1800 served users for different CRRM algorithms with different transmitted powers.

As shown in figure 4, DCS has the same performance like GSM after applying CRRM RAT selection. ie, the LB algorithm is the most efficient power algorithm whereas it suffers from the unfairness that will affect the performance of the shared RATs. On the other hand, SB will require large computational power to stabilize the fairness between the usages of different RATs. The simplest technique is the RS which has minimum computational power, but at the expense of the possibility of bad utilization.

UMTS performance after applying CRRM RAT selection, figure 4 shows the percentage of served UMTS customers against transmitted power.

ISBN: 978-1-61804-228-6

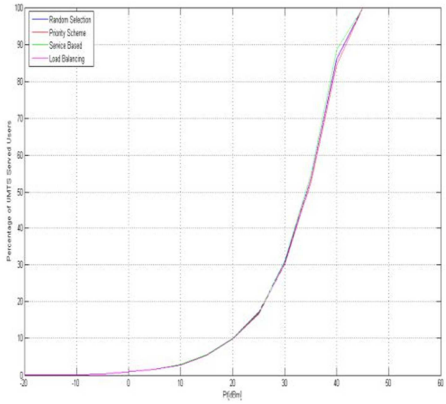

Fig. 4 UMTS served users for different CRRM algorithms with different transmitted powers.

Figure 4 shows that, the sufficient power for having best utilizing (i.e. 95% usage), is about 45 dBm. Eventually, the LB and PB algorithms are the most power efficient algorithms that may be deployed in order to decrease the number of un-served DCS users. On the other hand, the deployment of SB or RS algorithms will require much transmitted power. This is explained as a result of losses that may occur to the received signal strength due to the higher frequency band of DCS. This is not the case for UMTS, because UMTS has extra gain coming from WCDMA coding gain will give extra advantage for UMTS selection and degrade the performance of DCS in spite of the losses increase due to the operation in higher frequency bands. These phenomena maybe overcome via the deployment of SB algorithms in CRRM. The figure above shows that the UMTS is less dependent on the CRRM algorithm. This will be at the expense of the unfairness of the other RATs. This is explained as a result of UMTS has huge number of available RRU's when it is compared to the other competitive RATs. It's shown that, the sufficient power for having best utilizing (i.e. 95% usage), is about 35 dBm.

Call blocking probability after applying CRRM RAT selection, figure 5, shows the percentages of un-served (blocked) users after applying CRRM RAT for each algorithm.

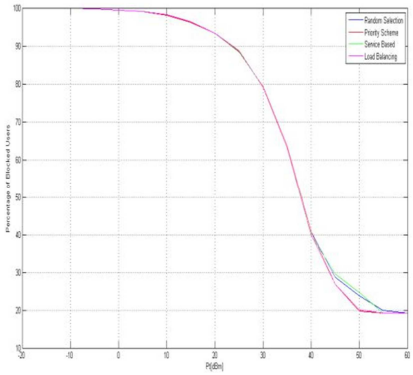

Fig. 5 percentages of un-served/blocked users

Figure 5 shows that the sufficient power for having best utilizing (i.e. about 5% blocking), is about 45 dBm. So, the HWN operators have to consider this result into the operational scenarios. So, it may be concluded that; operation with about 45 dBm transmitted power will minimize the number of un-served users due to RRU power and occupancy conditions.

b) 5.2 Mobile Users Model

The following results, give a determination for the customers capacity in each RAT versus the range of different transmitted powers at velocities mimicking the various area types (rural area, highly dense area, etc) that the customer can be moving with.

GSM Performance after Mobility, Figures 6, 7, 8, 9, and 10 shows the GSM Performance after customers move with velocities V1, V2, V3, V4, and V5 respectively.

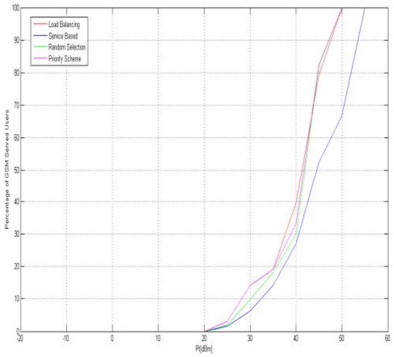

Fig. 6 GSM Performance after customers mobility with velocity V1

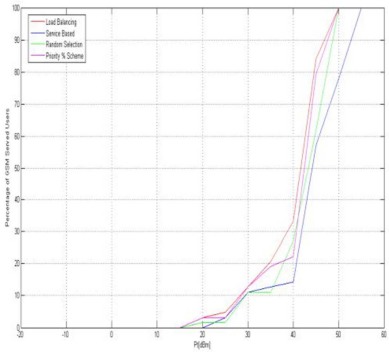

Fig. 7 GSM Performance after customers mobility with velocity V2

ISBN: 978-1-61804-228-6

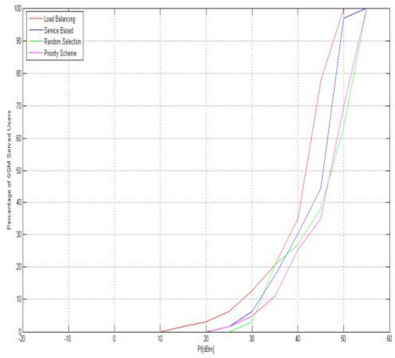

Fig. 8 GSM performance after customers mobility with velocity V3

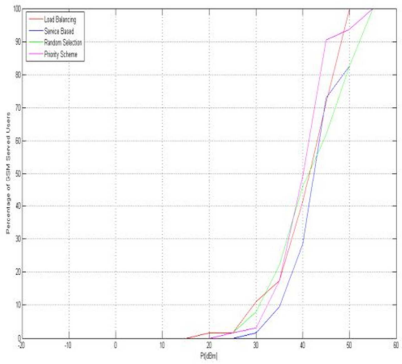

Fig. 9 GSM performance after customers mobility with velocity V4

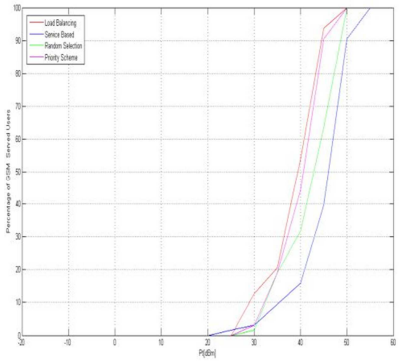

Fig. 10 GSM performance after customers mobility with velocity V5

From figures 7, 8, 9, 10, and 11, it is recognized that the LB algorithm is the most efficient power algorithm whereas it suffers from the unfairness that will affect the performance of the shared RATs. On the other hand, SB will require large computational power to stabilize the fairness between the usages of different RATs. The simplest technique is the RS which has minimum computational power, but at the expense of the possibility of bad utilization.

VI. Conclusion

It was shown that having different CRRM contributions will decrease the number of un- served customers. By comparing the obtained results from the different simulated scenarios throughout this paper it may be formed that different CRRM RAT selection algorithms are needed to be used in different cases of customer mobility. CRRM can bring significant benefits in the heterogeneous wireless network, such as load balancing, interference distribution, reduction of unnecessary handoffs and reduction of call dropping blocking probability. It is shown that UMTS is best utilized via the deployment of LB algorithm. This occurs as a result of huge number of the RUs in the UMTS network. This occurred as a result of normalized load calculations, In other words, the percentage of the available RRUs will not be biased to any RAT, but the system will try to use the lowest loaded RAT. DCS is best utilized via the deployment of PB algorithm. On the other hand, GSM is best utilized with a deployment of SB algorithm.

Finally, the overall performance (represented by the percentage of un-served users) may be improved if the transmitted power is around 40dBm. This will give minimal opportunities for un-served customers in the RATS under the predefined operational conditions.

The presented work in this paper may be extended by having different users priority schemes to serve users with different classes of service that may not have the same radio resources needed. CRRM placing will be crucial in order to achieve minimal number of un-served customers.

References

[1] G.Corazza, D. Giancristofaro, and F.Santucci, "Characterization of Handover Initialization in Cellular Mobile Radio Networks," in Proceedings of IEEE VTC'94, June 1994.

[2] G. P. Pollini, "Trends in Handover Design," IEEE Communication Magazine, March 1996

[3] Fang Zhu and Janise McNair, "Optimizations for Vertical Handoff Decision Algorithms," in Proceedings of the IEEE Wireless Communications and Networking Conference (WCNC),March 2004

[4] H. Bertoni, Radio Propagation for Modern Wireless Systems, Prentice Hall, 2000.

[5] Bijan Jabbari, Giovanni Colombo, Akihisa Nakajima and Jayant Kulkarni, "Network issues for wireless communications", IEEE Communications Magazine,Volume 33, Issue 1, page(s): 88-99, 1995.

[6] Andreas Festag, T.Assimakopoulos, L. Westerhoff and A. Wolisz, "Rerouting for handover in mobile networks with connection-oriented backbones: an experimental testbed", Proceedings of the IEEE Conference on High Performance Switching and Routing, page(s): 491-499, 2000.

[7] Ramachandran, Ramjee, Ramesh Nagarajan and Don Towsley, "On optimal call admission control in cellular networks", INFOCOM 96, Fifteenth Annual Joint Conference of the IEEE Computer Societies. Networking the Next Generation, Proceedings IEEE, Volume 1, page(s):43-50, 1996.

[8] Hesham M. ElBadawy, "Optimal RAT Selection Algorithm through Common Radio Resource Management in Heterogeneous Wireless Networks ",28th National Radio Science Conference (NRSC 2011), National Telecommunication Institute, Egypt, April, 2011.

[9] H. Eriksson, B. Gudmundson, J. Skold, J.K. Ugland and P. Willars, "Multiple access options for cellular based personal communications", 43rd IEEE Vehicular Technology Conference, page(s): 957-962, 1993.

[10] A. Medeisis, A.Kajackas, On the Use of the Universal Okumura-Hata Propagation Prediction Model in Rural Areas, IEEE Vehicular Technology Conference Proceeding, Vol. 3, May 2000.

[11] Hesham ElSawy, Ekram Hossain, and Martin Haenggi, "Stochastic Geometry for Modeling, Analysis, and Design of Multi-Tier and Cognitive Cellular Wireless Networks: A Survey," IEEE Communications Survey & Tutorials, Vol. 15, No. 3, third quarter 2013.

Identification of Direct and Indirect Discrimination in Data Mining

P. Priya and Dr. J. C. Miraclin Joyce Pamila

Department of Computer Science and Engineering, Govt. College of Technology, Coimbatore-13

Abstract--Discrimination is the prejudicial treatment which involves denying opportunities to members of one group in favor of other groups. It is unfair to discriminate people because of their gender, religion, nationality, age and so on, especially when those attributes are used for making decisions about them like giving them a job, loan, insurance, etc. If the training data are inherently biased for or against a particular community, discriminatory decisions may ensue. Discovering the potential biases and eliminating them from the training data without harming their decision-making utility is therefore highly desirable which forms the primary goal of anti-discrimination techniques in data mining. Discrimination can be either direct or indirect. Direct discrimination occurs when decisions are made based on sensitive attributes. Indirect discrimination occurs when decisions are made based on non-sensitive attributes which are strongly correlated with biased sensitive ones. This paper aims at identifying potential discrimination using an acceptable level of discrimination.

Key words--discrimination, direct and indirect discrimination

I Introduction

Discrimination is a very important issue when considering the legal and ethical aspects of data mining. It is more than obvious that most people do not want to be discriminated because of their gender, religion, nationality, age and so on, especially when those attributes are used for making decisions about them like giving them a job, loan, insurance, etc.

It involves denying to members of one group opportunities that are available to other groups. There is a list of **antidiscrimination** acts, which are laws designed to *prevent* discrimination on the basis of a number of attributes (**e.g., race, religion, gender, nationality, disability, marital status, and age**) in various settings (**e.g., employment and training, access to public services, credit and insurance, etc.**). At first sight, automating decisions may give a sense of fairness: classification rules do not guide themselves by personal preferences. However, at a closer look, one realizes that classification rules are actually learned by the system (**e.g., loan granting**) from the training data. If the training data are inherently biased for or against a particular community (**e.g., foreigners**), the learned model may show a discriminatory prejudiced behavior?. In other words, the system may infer that just being foreign is a legitimate reason for loan denial. Discovering such potential biases and eliminating them from the training data without harming their decision making utility is therefore highly desirable. One must prevent data mining from becoming itself a source of discrimination, due to data mining tasks generating discriminatory models from biased data sets as part of the automated decision making. In [12], it is demonstrated that data mining can be both a source of discrimination and a means for discovering discrimination. Discrimination can be either direct or indirect (also called systematic).

1.1 Direct discrimination

Direct discrimination consists of rules or procedures that explicitly mention minority or disadvantaged groups based on sensitive discriminatory attributes related to group membership. Discriminatory (sensitive) attributes like gender, race, religion, etc.,

1.2 Indirect discrimination

Indirect discrimination consists of rules or procedures that, while not explicitly mentioning discriminatory attributes, intentionally or unintentionally could generate discriminatory decisions. Redlining by financial institutions (refusing to grant mortgages or insurances in urban areas they consider as deteriorating) is an archetypal example of indirect discrimination, although certainly not the only one. With a slight abuse of language for the sake of compactness, in this paper indirect discrimination will also be referred to as redlining

ISBN: 978-1-61804-228-6

and rules causing **indirect discrimination will be called redlining rules** [12].

In direct discrimination could happen because of the availability of some background knowledge (rules), for example, that a certain zip code corresponds to a deteriorating area or an area with mostly black population. The background knowledge might be accessible from publicly available data (e.g., census data) or might be obtained from the original data set itself because of the existence of nondiscriminatory attributes that are highly correlated with the sensitive ones in the original data set. .

1.3 Basic definition

Some basic definitions related to data mining [17]. After that, we elaborate on measuring and discovering discrimination.

- **A data set** is a collection of data (records) and their attributes. Let DB be the original data set.
- *An* **item** is an attribute along with its value, e.g., Race = black.
- *An* **item set** is a collection of one or more items, e.g.,{ Foreign worker = Yes, City = NYC}.
- *A* **classification rule** is an expression X -> C, where C is a class item (a yes/no decision), and X is an item set containing no class item, e.g., {**Foreign worker = Yes, City = NYC-> Hire = no}**. X is called the premise of the rule.
- The support of an item set, supp(X), is the fraction of records that contain the item set X. We say that a rule X -> C is completely supported by a record if both X and C appear in the record.
- The confidence of a classification rule, conf(X)->C, measures how often the class item C appears in records that contain X. Hence, if supp(X) > 0 then
- **Conf(X)->C =** $\frac{supp(X,C)}{supp(X)}$

Support and confidence range over (0,1)

- **A frequent classification rule** is a classification rule with support and confidence greater than respective specified lower bounds. Support is a measure of statistical significance, whereas confidence is a measure of the strength of the rule. Let FR be the database of frequent classification rules extracted from DB.
- **Discriminatory attributes and item sets** *(protected by law):* Attributes are classified as discriminatory according to the applicable anti-discrimination acts (laws). For instance, U.S. federal laws prohibit discrimination on the basis of the following attributes: race, color, religion, nationality, sex, marital status, age and pregnancy (Pedreschi et al. 2008). Hence these attributes are regarded as discriminatory and the item sets corresponding to them are called discriminatory item sets. {Gender=Female, Race=Black} is just an example of a discriminatory item set. Let *DAs* be the set of predetermined discriminatory attributes in *DB* and *DIs* be the set of predetermined discriminatory item sets in *DB.*
- **Non-discriminatory attributes and item sets:** If A*s* is the set of all the attributes in *DB* and *Is* the set of all the item sets in *DB*, then *nDA*s (*i.e.* set of *nondiscriminatory attributes*) is *As - DAs* and *nDIs* (*i.e.* set of *non-discriminatory item sets*) is *Is - DIs*. An example of non-discriminatory item set could be {**Zip= 10451, City=NYC**}.

II RELATED WORK

Some proposals are oriented to the discovery and measure of discrimination. The discovery of discriminatory decisions was first proposed by Pedreschi et al. [12], [15]. The approach is based on mining classification rules (the inductive part) and reasoning on them (the deductive part) on the basis of quantitative measures of discrimination that formalize legal definitions of discrimination. For instance, the US Equal Pay Act [18] states that: “a selection rate for any race, sex, or ethnic group which is less than four-fifths of the rate for the group with the highest rate will generally be regarded as evidence of adverse impact.”

This approach has been extended to encompass statistical significance of the extracted patterns of discrimination in [13] and to reason about affirmative action and favoritism [14]. Moreover it has been implemented as an Oracle-based tool in [16]. Current discrimination discovery methods consider each rule individually for measuring discrimination without considering other rules or the relation between them. Three approaches are conceivable: **pre-processing, in processing and post-processing approaches**. We next describe these groups

2.1 Pre processing.

Transform the source data in such a way that the discriminatory biases contained in the original data are removed so that no unfair decision rule can be mined from the transformed data and apply any of the standard data mining algorithms. The preprocessing approaches of data transformation and hierarchy-based generalization can be adapted from the privacy

ISBN: 978-1-61804-228-6

preservation literature. Along this line, [7], [8] perform a controlled distortion of the training data from which a classifier is learned by making minimally intrusive modifications leading to an unbiased data set. The preprocessing approach is useful for applications in which a data set should be published and/or in which data mining needs to be performed also by external parties (and not just by the data holder).

2.2 In-processing

Change the data mining algorithms in such a way that the resulting models do not contain unfair decision rules. For example, an alternative approach to cleaning the discrimination from the original data set is proposed in [2] whereby the Non discriminatory constraint is embedded into a decision tree learner by changing its splitting criterion and pruning strategy through a novel leaf relabeling approach. However, it is obvious that in processing discrimination prevention methods rely on new special-purpose data mining algorithms; standard data mining algorithms cannot be used.

2.3 Post processing.

Modify the resulting data mining models, instead of cleaning the original data set or changing the data mining algorithms. For example, in [13], a confidence-altering approach is proposed for classification rules inferred by the CPAR algorithm. The post processing approach does not allow the data set to be published, only the modified data models can be published (knowledge publishing), hence data mining can be performed by the data holder only. One might think of a straightforward pre processing approach consisting of just removing the discriminatory attributes from the data set. Although this would solve the direct discrimination problem, it would cause much information loss and in general it would not solve indirect discrimination. As stated in [12] there may be other attributes (e.g., Zip) that are highly correlated with the sensitive ones (e.g., Race) and allow inferring discriminatory rules.

Preprocessing approach seems to be the most flexible one, it does not require changing the standard data mining algorithms, unlike the inprocessing approach, and it allows data publishing (rather than just knowledge publishing), unlike the post processing approach.

III SYSTEM MODEL

There are two types of rules:
1. PD Rule
2. PND Rule

3.1 Potentially discriminatory rule

A classification rule X -> C is potentially discriminatory (PD) when X = A, B with A is a discriminatory item set and B a nondiscriminatory item set

For example,(Foreign worker = Yes, City = NYC-> Hire = No). The word "potentially means that a PD rule could probably lead to discriminatory decisions. Therefore, some measures are needed to quantify the direct discrimination potential.

3.2 Direct discrimination measure

One of these measures is the extended lift (elift) Let A, B -> C be a classification rule such that Conf (B -> C) > 0. The extended lift of the rule is elift **(A, B -> C) =** $\frac{conf(A,B \rightarrow C)}{conf(B \rightarrow C)}$

The idea here is to evaluate the discrimination of a rule as the gain of confidence due to the presence of the discriminatory items (i.e., A) in the premise of the rule. Whether the rule is to be considered discriminatory can be assessed by thres holding elift as follows.

Let α € R be a fixed threshold and let A be a discriminatory item set. A PD classification rule

c = A, B ->C c is taken as α -discriminatory w.r.t. elift if elift(c) > α. Otherwise is taken as α-protective,. The purpose of direct discrimination discovery is to identify α -discriminatory rules. In fact, α –discriminatory rules indicate biased rules that are directly inferred from discriminatory items (e.g., Foreign worker = Yes).

We call these rules direct α -discriminatory rules. In addition to elift, two other measures slift and olift were proposed by Pedreschi et al. in [13].

ISBN: 978-1-61804-228-6

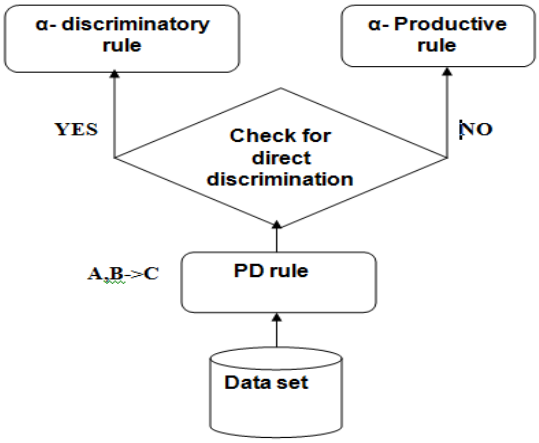

Fig:3.1 Direct discrimination measure

Fig 3.1 says that PD rule of the form A,B->C A is a discriminatory item set and check for direct discrimination such a measure is called Elift .if Elift>α α-discriminatory rule otherwise α-protective rule

3.3 Potentially non discriminatory rule

A classification rule X -> C is potentially nondiscriminatory (PND) when X = D, B is a nondiscriminatory item set. For example,
{Zip =10451, City = NYC -> Hire = No} or
{Experience = Low, City = NYC -> Hire = No}
PND rule could lead to discriminatory decisions in combination with some background knowledge.
e.g., if the premise of the PND rule contains the zip code as an attribute and one knows that zip code 10451 is mostly inhabited by foreign people. Hence, measures are needed to quantify the indirect discrimination potential as well

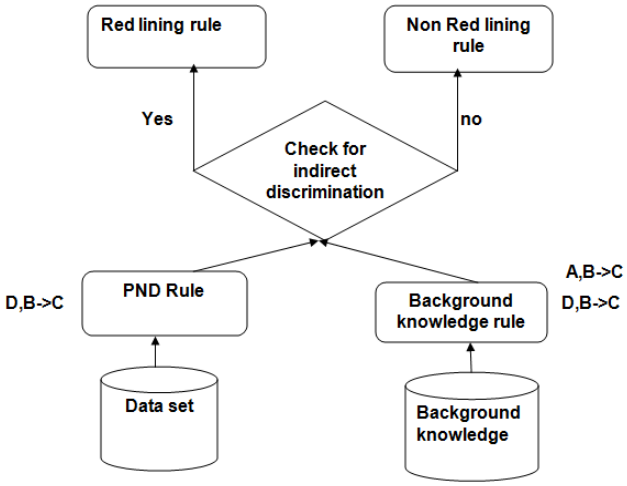

Fig:3.2 Indirect discrimination measure

Fig: 3.2 says that PND rule of the form D,B->C where D is not directly discriminated but highly correlated with discriminatory attribute A . and check for indirect discrimination such a measure is called elb. If elb>α is taken as readlining rule otherwise is taken as non lining rule.

3.5 Indirect discrimination measure

The purpose of indirect discrimination discovery is to identify redlining rules. In fact, redlining rules indicate biased rules that are indirectly inferred from nondiscriminatory items (e.g., Zip = 10451) because of their correlation with discriminatory ones. To determine the redlining rules, Pedreschi et al. in [12] stated the theorem below which gives a lower bound for α discrimination of PD classification rules, given information available in PND rules (γ , δ), and information available from background rules (β1, β2). They assume that background knowledge takes the form of classification rules relating a nondiscriminatory item set D to a discriminatory item set A within the context B.

Theorem Let r: D, B -> C be a PND classification rule, and let
γ= conf(r: D, B -> C) δ= conf (B -> C) > 0:
Let A be a discriminatory item set, and letβ1, β2 such that
Conf (rb1: A, B -> D) ≥β1
Conf (rb2: D, B -> A) ≥β2

$$\mathbf{F(x)} = \frac{\beta 1}{\beta 2}(\beta 2 + x - 1)$$

$$\mathbf{elb(x, y)} = \begin{cases} \frac{f(x)}{y} & \text{if } f(x) > 0 \\ 0 & \text{otherwise} \end{cases}$$

It holds that, for α ≥ 0, if elb (γ, δ) ≥ α, the PD classification rule r': A,B -> C is α-discriminatory. Based on the above theorem, the following formal definitions of redlining and non redlining rules are presented:

A PND classification rule r : D,B -> C is a redlining rule if it could yield an α-discriminatory rule r' : A,B -> C in combination with currently available background knowledge rules of the form rb1 : A,B -> D and rb2 : D,B -> A, where A is a discriminatory item set. For example,
{Zip= 10451, City = NYC}-> Hire = No}.

A PND classification rule r : D,B -> C is a non redlining or legitimate rule if it cannot yield any α-discriminatory rule r': A,B -> C in combination with currently available background knowledge rules of the form

rb1 : A,B -> D and rb2 : D,B -> A, where A is a discriminatory item set. For example,
{Experience = Low, City = NYC} -> Hire= No}.

IV EXPERIMENTAL RESULTS AND ANALYSIS

4.1 Data sets

Two data sets are considered: adult and German credit data set.

4.1.1 Adult data set: We used the Adult data set [10], also known as Census Income, in our experiments. This data set consists of 48,842 records, split into a "train" part with 32,561 records and a "test" part with 16,281 records. The data set has 14 attributes (without class attribute). We used the "train" part in our experiments. The prediction task associated with the Adult data set is to determine whether a person makes more than 50K$ a year based on census and demographic information about people. The data set contains both categorical and numerical attributes. For our experiments with the Adult data set, we set DIs= {Sex = Female, Age = Young}. Although the Age attribute in the Adult data set is numerical, we converted it to categorical by partitioning its domain into two fixed intervals: Age <= 30 is renamed as Young and Age > 30 is renamed as old.

4.1.2 German credit data set: we also used the German Credit data set [11]. This data set consists of 1,000 records and 20 attributes (without class attribute) of bank account holders. This is a well-known real-life data set, containing both numerical and categorical attributes. It has been frequently used in the antidiscrimination literature [12], [7]. The class attribute in the German Credit data set takes values representing good or bad classification of the bank account holders. For our experiments with this data set, we set DIs = {Foreign worker = Yes, Personal Status =Female and not Single, Age = Old}; (cut-off for Age = Old: 50 years old).

4.2 Experimental result for adult data set

```
Rule : martial_status='Never-married' and gender='Male' => salary='<=50K'

A : martial_status='Never-married'
B : gender='Male'
C : salary='<=50K'

Number of tuples which satisfy A , B and C : 5591
Number of tuples which satisfy A and B : 5916
Number of tuples which satisfy B and C : 15128
Number of tuples which satisfy B : 21790

Confidence of A , B -> C : 0.9450642325895876
Confidence of B -> C : 0.6942634235888022
Elift : 1.3612473313145896
Rule : relationship='Own-child' and race='White' => salary='<=50K'

A : relationship='Own-child'
B : race='White'
C : salary='<=50K'

Number of tuples which satisfy A , B and C : 4196
Number of tuples which satisfy A and B : 4255
Number of tuples which satisfy B and C : 20699
Number of tuples which satisfy B : 27816

Confidence of A , B -> C : 0.9861339600470035
Confidence of B -> C : 0.7441400632729365
Elift : 1.3251993928531547
Rule : age='old' and captial_loss='Zero' => salary='<=50K'

A : age='old'
B : captial_loss='Zero'
C : salary='<=50K'

Number of tuples which satisfy A , B and C : 9652
Number of tuples which satisfy A and B : 10275
Number of tuples which satisfy B and C : 23974
Number of tuples which satisfy B : 31041

Confidence of A , B -> C : 0.939367396593674
Confidence of B -> C : 0.7723333655487903
Elift : 1.216271934498383
```

Fig4.1 Direct discrimination measure for adult data set

The α- discriminatory rule identification has been done using the following series of steps:

1. For the given data set, association rules have been generated.

2. From the set of rules, PD rules have been extracted where each PD rule contains at least one discriminatory attribute.

3. For the given data set, elift measure for all the PD rules has been calculated**.**

if elift value is > α,

α discriminatory rule

else

α- protective rule

Table 4.1 gives the number of discriminatory rule for various value of threshold

Table 4.1 Result of Adult data set

Threshold	No of discriminatory rule
0.0	392
0.4	392
0.8	352
0.9	346
1.0	222
1.1	157
1.2	63
1.3	35
1.4	16
1.5	6
1.7	6
1.8	0

From the above table it is seen that as the threshold value is increased, number of discriminatory rule decreases. The maximum threshold value is 1.8 because it gives 0 discriminatory rule. The maximum number of discriminatory rule is 392 because it taken at threshold value 0. Taking an approximately intermediate value for both threshold and number of discriminatory rule the α value has been chosen to be 1and also analyzing set of discriminatory rule for both the previous threshold value 0.9 and next threshold value 1.1seems to be a suitable choice for α

4.3 Experimental result for German credit data set

```
Rule : purpose='A43' and foreign='A201' => class='One'

A : purpose='A43'
B : foreign='A201'
C : class='One'

Number of tuples which satisfy A , B and C : 213
Number of tuples which satisfy A and B : 275
Number of tuples which satisfy B and C : 667
Number of tuples which satisfy B : 963

Confidence of A , B -> C : 0.7745454545454545
Confidence of B -> C : 0.6926272066458983
Elift : 1.1182717732043068
Rule : property='A121' and age='young' => class='One'

A : property='A121'
B : age='young'
C : class='One'

Number of tuples which satisfy A , B and C : 191
Number of tuples which satisfy A and B : 247
Number of tuples which satisfy B and C : 609
Number of tuples which satisfy B : 875

Confidence of A , B -> C : 0.7732793522267206
Confidence of B -> C : 0.696
Elift : 1.1110335552049886
Rule : property='A121' and foreign='A201' => class='On

A : property='A121'
B : foreign='A201'
C : class='One'

Number of tuples which satisfy A , B and C : 203
Number of tuples which satisfy A and B : 263
Number of tuples which satisfy B and C : 667
Number of tuples which satisfy B : 963

Confidence of A , B -> C : 0.7718631178707225
Confidence of B -> C : 0.6926272066458983
Elift : 1.114399074227145
```

Fig4.2 direct discrimination measure for German credit data set

Table 4.2: Result of German credit data set

Threshold	No of discriminatory rule
0.0	68
0.4	68
0.8	68
0.9	66
1.0	37
1.1	10
1.2	3
1.3	0

From the above table it is seen that as the threshold value is increased, number of discriminatory rule decreases. The maximum threshold value is 1.3 because it gives 0 discriminatory rule. The maximum number of discriminatory rule is 68 because it taken at threshold value 0. Taking an approximately intermediate value for both threshold and number of discriminatory rule the α value has been chosen to be 1and also analyzing set of discriminatory rule for both the previous threshold value 0.9 and next threshold value 1.1 seems to be a suitable choice for α

4.4 Indirect discrimination measure for adult data set

```
Rule : native_country='United-States' and work_class='Private' => salary='<=50K

D : native_country='United-States'
B : work_class='Private'
C : salary='<=50K'
A : race='White'

 Number of tuples which satisfy D , B and C :15594
 Number of tuples which satisfy  D and B : 20135
 Number of tuples which satisfy  B and C : 17733
 Number of tuples which satisfy  B :22696
 Number of tuples which satisfy A , B and D :17728
 Number of tuples which satisfy  A and B : 19404
 Number of tuples which satisfy D , B and A : 17728
 Number of tuples which satisfy  D and B : 20135
Confidence of A , B -> D :0.9136260564831994
Confidence of D , B -> A :0.8804569158182269
Confidence of D , B -> C :0.7744723118947107
Confidence of  B -> C :0.7813271060979908
 Function value : 0.679602143887858
 Elb : 0.8698048980814767
```

Fig4.3 Indirect Discrimination measure for adult data set

Fig 4.3 shows that indirect discrimination measure for Adult data set

ISBN: 978-1-61804-228-6

4.5 Indirect discrimination measure for German credit data set

```
Rule : exp='A73' and no_of_credit='One' => class='One'

D : exp='A73'
B : no_of_credit='One'
C : class='One'
A : age='young'

Number of tuples which satisfy D , B and C : 154
Number of tuples which satisfy D and B : 226
Number of tuples which satisfy B and C : 433
Number of tuples which satisfy B : 633
Number of tuples which satisfy A , B and D : 209
Number of tuples which satisfy A and B : 558
Number of tuples which satisfy D , B and A : 209
Number of tuples which satisfy D , B: 226

Confidence of A , B -> D : 0.37455197132616486
Confidence of D , B -> A : 0.9247787610619469
Confidence of D , B -> C : 0.6814159292035398
Confidence of B -> C : 0.684044233807267
Function value : 0.24551971326164873
Elb : 0.3589237378628722
```

Fig 4.4 shows that indirect discrimination measure for German credit data set

V CONCLUSION

The purpose of this paper is to measure direct and indirect discrimination and identify categories and groups of individuals that have been directly discriminatory in the decision-making processes. The choice of the acceptable level of discrimination has been made. By analyzing the measures of each classification rule, direct discriminatory decision rules have been identified in order to convert them into legitimate (nondiscriminatory) classification rules. The experimental results reported demonstrate that the proposed techniques are quite successful.

REFERENCES

[1] S. Hajian and J. Domingo-Ferrer. A methodology for direct and indirect discrimination prevention in data mining. Manuscript, 2012.
R. Agrawal and R. Srikant, "Fast Algorithms for MiningAssociation Rules in Large Databases," Proc. 20th Int'l Conf. Very Large Data Bases, pp. 487-499, 1994.
[2] T. Calders and S. Verwer, "Three Naive Bayes Approaches for Discrimination-Free Classification," Data Mining and Knowledge Discovery, vol. 21, no. 2, pp. 277-292, 2010.
[3] European Commission, "EU Directive 2004/113/EC on Anti-Discrimination," http://eur-lex.europa.eu/LexUriServ/ LexUriServ.do?uri=OJ:L:2004:373:0037:0043:EN:PDF, 2004.
[4] European Commission, "EU Directive 2006/54/EC on Anti-Discrimination," http://eur-lex.europa.eu/LexUriServ/ LexUriServ.do?uri=OJ:L:2006:204:0023:0036:en:PDF, 2006.
[5] S. Hajian, J. Domingo-Ferrer, and A. Martı´nez-Balleste´, "Discrimination Prevention in Data Mining for Intrusion and Crime Detection," Proc. IEEE Symp. Computational Intelligence in Cyber Security (CICS '11), pp. 47-54, 2011.
[6] S. Hajian, J. Domingo-Ferrer, and A. Martı´nez-Balleste´, "Rule Protection for Indirect Discrimination Prevention in Data Mining," Proc. Eighth Int'l Conf. Modeling Decisions for Artificial Intelligence (MDAI '11), pp. 211-222, 2011.
[7] F. Kamiran and T. Calders, "Classification without Discrimination," Proc. IEEE Second Int'l Conf. Computer, Control and Comm. (IC4 '09), 2009.
[8] F. Kamiran and T. Calders, "Classification with no Discrimination by Preferential Sampling," Proc. 19th Machine Learning Conf. Belgium and The Netherlands, 2010.
[9] F. Kamiran, T. Calders, and M. Pechenizkiy, "Discrimination Aware Decision Tree Learning," Proc. IEEE Int'l Conf. Data Mining (ICDM '10), pp. 869-874, 2010.
[10] R. Kohavi and B. Becker, "UCI Repository of Machine Learning Databases," http://archive.ics.uci.edu/ml/datasets/Adult, 1996.
[11] D.J. Newman, S. Hettich, C.L. Blake, and C.J. Merz, "UCI Repository of Machine Learning Databases," http://archive. ics.uci.edu/ml, 1998.
[12] D. Pedreschi, S. Ruggieri, and F. Turini, "Discrimination-Aware Data Mining," Proc. 14th ACM Int'l Conf. Knowledge Discovery and Data Mining (KDD '08), pp. 560-568, 2008.
[13] D. Pedreschi, S. Ruggieri, and F. Turini, "Measuring Discrimination in Socially-Sensitive Decision Records," Proc. Ninth SIAM Data Mining Conf. (SDM '09), pp. 581-592, 2009.
[14] D. Pedreschi, S. Ruggieri, and F. Turini, "Integrating Induction and Deduction for Finding Evidence of Discrimination," Proc. 12th ACM Int'l Conf. Artificial Intelligence and Law (ICAIL '09), pp. 157- 166, 2009.
[15] S. Ruggieri, D. Pedreschi, and F. Turini, "Data Mining for Discrimination Discovery," ACM Trans. Knowledge Discovery from Data, vol. 4, no. 2, article 9, 2010.
[16] S. Ruggieri, D. Pedreschi, and F. Turini, "DCUBE: Discrimination Discovery in Databases," Proc. ACM Int'l Conf. Management of Data (SIGMOD '10), pp. 1127-1130, 2010.
[17] P.N. Tan, M. Steinbach, and V. Kumar, Introduction to Data Mining. Addison-Wesley, 2006.
[18] United States Congress, US Equal Pay Act, http://archive. eeoc.gov/epa/anniversary/epa-40.html, 1963.
[19] V. Verykios and A. Gkoulalas-Divanis, "A Survey of Association Rule Hiding Methods for Privacy," Privacy-Preserving Data Mining: Models and Algorithms, C.C. Aggarwal and P.S. Yu, eds., Springer, 2008. Sara Hajian

Priya.P received BE degree in Computer Science and Engineering from Jayaraj Anna packiam CSI College of engineering, Nazareth. She is currently doing ME in the Department of Computer Science and Engineering of Government College of Technology, Coimbatore.

Miraclin Joyce Pamila J.C. is an Assistant Professor (Senior Grade) in the Department of Computer Science and Engineering, Government College of Technology, Coimbatore, Tamilnadu, India. She received her Master and Doctoral degree in Computer Science and Engineering from Anna University, Chennai, India. Her fields of interest include Mobile Computing, Data Management Systems, Network Security and Recovery system design for mobile networks. She is a life member of ISTE. She teaches and guides courses at both B.E. and M.E. levels in Computer Science and Information Technology. She has published 30 technical papers in national and international conferences and journals.

Suitable Propagation Loss Models for Mobile Communications in Jordan

M. S. H. Al Salameh and M. M. Al-Zu'bi
Department of Electrical Engineering
Jordan University of Science and Technology
Irbid 22110, Jordan
salameh@just.edu.jo

Abstract— Extensive outdoor measurements for mobile phone base stations in Irbid city, Jordan, were performed by the authors. In order to determine the model that can accurately predict the propagation in this environment, different well-known propagation models are compared with these measurements. Among these models, the comparison reveals that the COST-231 Hata model is the most suitable model for Irbid city, Jordan. To further improve the prediction accuracy, this paper proposes a propagation model based on optimizing the COST-231 Hata model by the particle swarm optimization (PSO) method. The proposed model is validated by comparison with measurements conducted in other locations in Irbid. It is shown that the root mean square error (RMSE) between the predicted and the measured data for the proposed model, is improved by up to 5 dB compared with Hata model and by up to 29 dB compared with Egli model, in all the areas under study. Furthermore, this model is expected to be suitable for other areas in Jordan similar to Irbid.

Keywords— Mobile communications, Measurements, Propagation, Hata, Wireless, PSO.

I. INTRODUCTION

Mobile phone communications are the most widely used systems across the world. For efficient communication network planning, accurate radio frequency (RF) propagation models are needed. In fact, many propagation models are available. However, every model is mainly suitable for the area conditions under which the measurements were performed. Thus, it is important to determine the most suitable model for a specific environment.

Various propagation models were optimized to match specific areas in different parts of the world. For instance, Hata model was customized by the least squares (LS) method for suburban areas within Cyberjaya and Putrajaya areas in Malaysia [1]. The Bertoni-Walfisch model was tuned using the mean square error (MSE) method for global system for mobile communications (GSM) at 900 MHz in Istanbul, Turkey [2]. Hata model was also tuned using the MSE method for Brno, Czech Republic [3]. In [4], Lee model was calibrated by the least square regression method for Jiza town in Jordan based on data supplied by the mobile operators. Okumura model was optimized by the use of the regression fitting method for code division multiple access (CDMA) network in Kuala Lumpur, Malaysia [5]. The COST-231 Hata model was optimized for 3G radio network in Banciao city, Taiwan [6]. In [7], COST-231 Walfisch-Ikegami (WI) path loss model was tuned by the particle swarm optimization (PSO) method for 3G network in the south-western Amman, Jordan.

In this paper, different well-known propagation models are compared with extensive measurements performed by the authors for mobile communications in Irbid, Jordan. Among these models, the comparison reveals that the COST-231 Hata model is the most suitable model for Irbid city, Jordan. To further improve the prediction accuracy, this paper proposes a propagation model based on optimizing the COST-231 Hata model by the particle swarm optimization (PSO) method. The proposed model is validated by comparison with measurements conducted in other locations in Irbid. It is shown that the prediction accuracy of the proposed model is enhanced by up to 5 dB compared with Hata model and by up to 29 dB compared with Egli model, in all the areas under study. This model should be suitable for other areas in Jordan similar to Irbid. As a matter of fact, the COST-231 Hata model was also optimized by the least squares (LS) method, but due to the limit placed on the paper number of pages, only the PSO optimization results will be shown here.

II. PROPAGATION LOSS MODELS AND THE DRIVE TEST

The propagation loss models considered here are COST-231 Hata [3, 6], COST-231 WI [8, 9], and Egli models [10]. Details of these models can be found in [3], [6], [8],[9], [10].

The path loss in dB is calculated from the measured received power using the following equation [8]:

$$PL = P_t + G_t + G_r - P_r - L_t - L_r \qquad (1)$$

Where, P_t is the transmitted power, P_r is the received power, G_t is the transmitter antenna gain, G_r is the receiver antenna gain, L_t is the transmitter feeder losses (e.g., cables and connector losses), and L_r is the receiver feeder losses (e.g., cables and car body losses). In this paper, the values of these

ISBN: 978-1-61804-228-6

parameters are: P_t= 42 dBm, G_t= 18 dB, G_r= 2.15 dB, L_t= 2 dB, and L_r=8 dB. The value of L_r is due to the car body penetration loss and it equals to 8 dB on average based on the experiments and this value is similar to the car body loss reported in [11], [12]. The values of L_t, P_t, and G_t were obtained from the mobile communications operators in Jordan.

The definitions of the parameters used in this paper are: f_c: the operating frequency in MHz, d: the distance between the transmitter and the receiver in km, h_m: the receiver antenna height in m, h_b: the transmitter antenna height in m.

The measurements have been carried out, for over a year, by using RF measuring tools while driving a car on many routes in Irbid city around cellular phone base stations for Umniah mobile operator in Jordan at 1800 MHz. The measuring tools consist of TEMS (Test Mobile System) RF measuring software [13], GPS receiver, Laptop, and mobile phone. The mobile phone is equipped with RF measuring firmware [14] in order to extract the received RF signal strengths and deliver these readings to the laptop. The collected data mainly include the received signal strength levels of the serving base stations for each ARFCN (Absolute Radio Frequency Channel Number) scanned channel, cell-ID, and mobile station (MS) location coordinates.

III. OPTIMIZATION PROCESS

The optimization process is intended to enhance the accuracy of the path loss model in order to suit the environmental area under consideration. To that end, the COST-231 Hata model consists of three parts: initial offset, initial system design parameter and slope of model curve, which are expressed as:

$$P_{offset} = 54.27$$

$$P_{system} = 33.9 \log_{10}(f_c) - 13.82 \log_{10}(h_b) - 3.2[\log_{10}(11.755 h_m)]^2$$

$$P_{slope} = 44.9 - 6.55 \log(h_b) \quad (2)$$

Thus, COST-231 Hata model can be written as follows:

$$PL = [P_{offset} + P_{system}] + [P_{slope}] \log_{10}(d) \quad (3)$$

The role of the optimization process is to modify the expressions between the square brackets in equation (3) so that a better match will be created between the resulting optimized equation and the measured data. This can alternatively be done through introducing two coefficients, say $\acute{x}$ and $\acute{y}$, associated with the square brackets. According to that, equation (3) becomes:

$$PL = \acute{x}\,[P_{offset} + P_{system}] + \acute{y}\, P_{slope} \log_{10}(d) \quad (4)$$

The PSO method will be used to find the optimum values of $\acute{x}$ and $\acute{y}$.

Particle Swarm Optimization (PSO)

The PSO algorithm is a recently developed, in 1995, global optimization technique for the solution of non-linear problems [15]. The idea is related to the social intelligent behavior of organisms such as swarms of bees, flocks of birds, schools of fish, herds of animals, colonies of ants, molds, and bacterial growth. Each particle in the search space of PSO consists of position vector (**x**), velocity vector (**v**) and personal best vector (i.e., best previous position) and its fitness value. The PSO algorithm is applied in two phases: initialization and iteration [16]. In the initialization phase, the initial velocity and position vectors of each particle are randomly assigned in n-dimensional search space. Each particle moves toward the best solution by modifying its velocity and position in accordance with its best previous experience. The best solution of each particle is called personal or local best (X_{pbest}). The best solution among all particles in the search space is called global best (X_{gbest}). In the iterations phase, each coordinate component of n-dimensional search space for a specific particle, updates its velocity and position according to the following equations [17]:

$$v^{n+1}{}_{id} = C\,[\,\omega\, v^{n}{}_{id} + c_1\, r^{n}{}_{1d}\,(X^{n}_{pbest\,id} - X^{n}{}_{id}) + c_2\, r^{n}{}_{2d}\,(X^{n}_{gbest\,d} - X^{n}{}_{id})\,] \quad (5)$$

$$X^{n+1}{}_{id} = X^{n}{}_{id} + v^{n+1}{}_{id}\,\Delta t \quad (6)$$

Where,

- $v^{n+1}{}_{id}$, $v^{n}{}_{id}$: Velocity of d^{th} coordinate in velocity vector of i^{th} particle at the $n+1^{th}$ and n^{th} iterations, respectively.
- $X^{n+1}{}_{id}$, $X^{n}{}_{id}$: Position of d^{th} coordinate in position vector of i^{th} particle at the $n+1^{th}$ and n^{th} iterations, respectively.
- $X^{n}{}_{pbest\,id}$: Personal best position of d^{th} coordinate in the personal best vector of i^{th} particle at n^{th} iteration.
- $X^{n}{}_{gbest\,d}$: Global best position of d^{th} coordinate in the global best vector at n^{th} iteration.
- Δt: Time step; as usual it is chosen here to be 1 s.
- $i = 1,..,N_p$, where N_p is the swarm size
- $d = 1,\ldots,N_d$, where N_d is the search space dimension

The inertia weight ω and the convergence factor C in (5) above are given by [17], [18]:

$$\omega = \omega_{max} - \frac{(\omega_{max} - \omega_{min})}{N_j}\, j \quad (7)$$

$$C = \frac{2}{\left|2 - \alpha - \sqrt{\alpha^2 - 4\alpha}\right|} \qquad (8)$$

Where N_j is the maximum number of iterations, and j is the current iteration number. In this paper, $\omega_{min}= 0$, $\omega_{max}= 1$; where the experiments have shown that when the value of ω_{max} falls between 0.8 and 1.2, the PSO algorithm has the largest convergence speed.

The cognitive parameter c_1 and social parameter c_2 are positive acceleration constants used to increase the new velocity towards personal best (X_{pbest}) and global best (X_{gbest}). The parameter $\alpha= c_1+c_2$, and c_1, c_2 are chosen to be: $c_1=2$, $c_2=2$, accordingly $\alpha=4$, $C=1$. The experiments showed that the acceleration coefficients should be selected as $c_1=c_2=2$ in order to obtain the best performance. The parameters, r^n_{1d} and r^n_{2d}, are random numbers of the d^{th} coordinate at the n^{th} iteration that are uniformly distributed between 0 and 1.

In each iteration, the fitness function is evaluated for all the particles. For each particle, if the current fitness value is better than the local best value, then the local best position is replaced by the current position value. Moreover, all local best values are examined in order to determine the global best position.

IV. RESULTS

The location map of the ten cellular phone base stations (BS1 to BS10) under study in Irbid city is shown in Fig. 1.

Fig. 1: Locations of the ten cellular phone base stations (BS1 to BS10) under study in Irbid City.

The COST-231 Hata model is optimized using PSO. In this work, the swarm size value is selected to be 10; this choice is based on several trials in order to get the best results. For all the cases examined in this paper, the optimal solution is reached, on average, after 40 iterations. The optimization process is implemented through the use of the measurements accomplished in six sites (BS1 to BS6) in Irbid city, see Fig. 1. The measurements in the remaining four base stations (BS7 to BS10) are used to validate the optimized model. Figures 2 and 3 show a comparison between the existing path loss models, the measured path loss data, and the proposed optimized model for BS1 and BS2 sites at different frequencies and different sectors. The results of base stations BS3-BS6 are not shown here due to the limit on the number of paper pages. The accuracy of the path loss models are calculated in terms of the root mean square error RMSE [10]:

$$RMSE = \sqrt{\frac{\sum_{i=1}^{N} [PL_{mi} - PL_i]^2}{N-1}} \qquad (9)$$

Where, PL_{mi} is the measured path loss at position i in dB, PL_i is the calculated path loss at position i in dB, and N is the number of measured path loss samples. Due to the huge number of measured samples for each base station and in order to remove the effects of fast fading, the measured data were averaged over every 1 m of the path between the base station and the receiver.

The optimization process of the COST-231 Hata model gives the optimized values of $\acute{x}$ and $\acute{y}$ in (4) as listed in Table 1 for each base station.

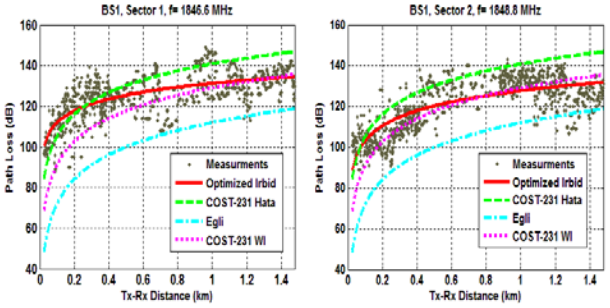

Fig. 2: Path loss vs. distance in kilometres for BS1 site.

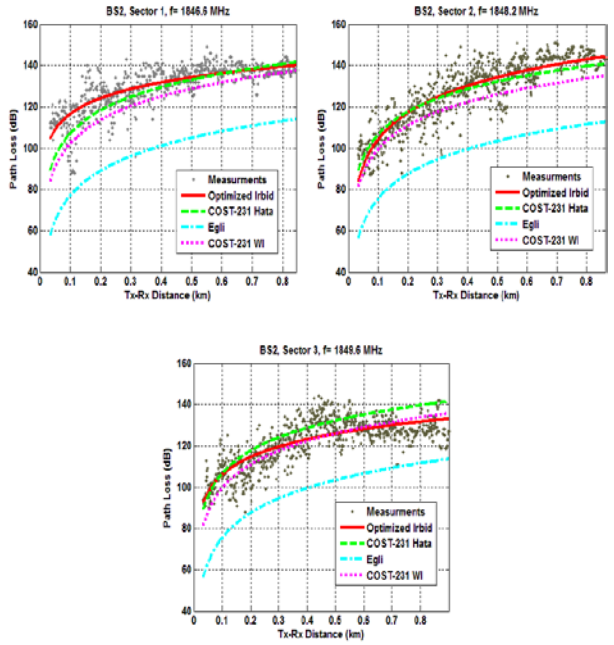

Fig. 3: Path loss vs. distance in kilometres for BS2 site.

ISBN: 978-1-61804-228-6

Table 1: The RMSE values and optimized coefficients for base stations: BS1 to BS6.

	RMSE (dB)				Optimized coefficients	
Base Station	Proposed optimized Model	Hata	Egli	WI	ẋ	ẏ
BS1	8.09	12.6	25.02	11.65	0.92	0.62
BS2	6.92	8.32	29.81	9.73	0.95	0.68
BS3	8.16	10.8	29.81	10.91	0.91	0.50
BS4	7.69	9.32	35.88	16.28	0.95	0.62
BS5	8.74	10.9	30.46	14.87	0.93	0.69
BS6	8.31	9.91	30.69	11.73	0.92	0.70

From Table 1, we can see that the proposed optimized model has the best RMSE values in all the base station sites compared with the other examined models. Substituting the average values of ẋ and ẏ from Table 1 into equation (4), the proposed optimized model can be written as follows:

$$PL = \dot{x}\,[P_{offset} + P_{system}] + \dot{y}\,[P_{slope}]\log_{10}(d)$$
$$= 50.57 + 31.59\log_{10}(f_c) - 12.88\log_{10}(h_b) - 2.98\,[\log_{10}(11.755h_m)]^2 + [29 - 4.23\log(h_b)]\log(d) \quad (10)$$

The measured data in the remaining four locations in Irbid city, i.e., BS7-BS10, are utilized to verify the validity and accuracy of the proposed optimized model. Fig. 4 compares the optimized model with the COST-231 Hata model for base station BS8. Table 2 shows the root mean square error (RMSE), between the predicted and the measured data, of the proposed optimized model as well as the other models.

Table 2: The RMSE values for the base station sites (BS7 to BS10), which were used to validate the proposed model.

	RMSE (dB)			
Base station	Optimized model	Hata	Egli	WI
BS7	8.38	11.82	37.43	11.81
BS8	7.26	10.19	29.27	11.19
BS9	7.89	13.04	29.24	13.69
BS10	9.58	13.09	24.68	11.27

Table 2 confirms that the proposed optimized model has the best RMSE values in all the base station sites compared with the other models. In particular, the prediction accuracy of the proposed model is improved by up to 5.15 dB as compared with Hata model, and by up to 29.05 dB as compared with Egli model. Moreover, it is expected that this new model will be suitable for other similar areas in Jordan.

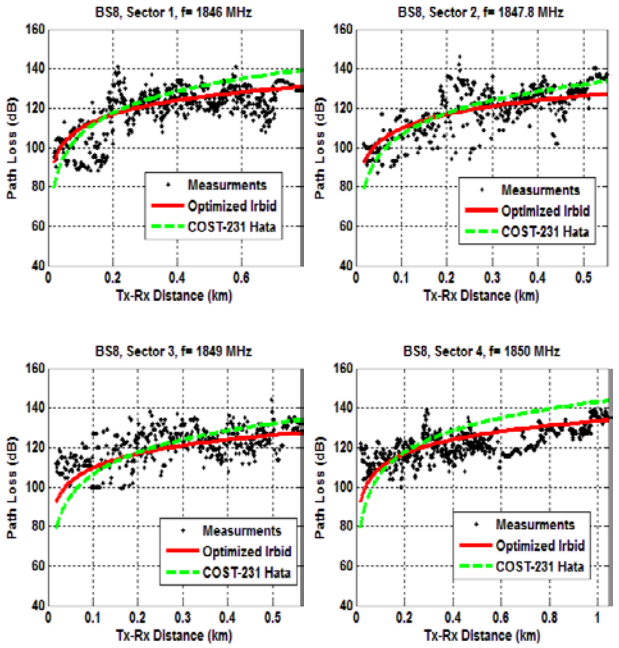

Fig. 4: Path loss vs. distance in kilometres for BS8 site.

V. CONCLUSIONS

This study proposes an optimized path loss model for Irbid city in Jordan. The optimization is based on the particle swarm optimization (PSO) technique in addition to outdoor measurements for mobile phone base stations performed by the authors for over a year. The measured path loss data for other base stations are used to confirm the validity and accuracy of the optimized model, where the path loss predictions of the proposed model show enhanced accuracy of up to 5 dB as compared with Hata model and up to 29 dB as compared with Egli model.

Finally, the optimized model is expected to suit other similar areas in Jordan. The proposed model can help the mobile operator companies in Jordan to make accurate predictions for many system design parameters.

REFERENCES

[1] R. Mardeni, K.F. Kwan, "Optimization of Hata propagation prediction model in suburban area in Malaysia," Progress In Electromagnetic Research, vol. 13, pp. 91-106, 2010.

[2] B.Y. Hanci, I.H. Cavdar, "Mobile radio propagation measurements and tuning the path loss model in urban areas at GSM-900 band in Istanbul–turkey," IEEE 60th Vehicular Technology Conference, Los Angeles, USA, Sept. 2004, vol. 1, pp. 139-143.

[3] L. Klozar, J. Prokopec , "Propagation path loss models for mobile communication," In Proceedings of 21st International Conference Radioelektronika, Brno, *Czech Republic*, April 2011, vol. 48, pp. 1-4.

ISBN: 978-1-61804-228-6

[4] L.A. Nissirat, M. Ismail, M. Nisirat, M. Singh, "Lee's path loss model calibration and prediction for Jiza town, south of Amman city, Jordan at 900 MHz," IEEE International RF and Microwave Conference (RFM), Seremban, Negeri Sembilan, Dec. 2011, pp. 412-415.

[5] R. Mardeni, Lee Yih Pey., "Path loss model development for urban outdoor coverage of code division multiple access (CDMA) system in Malaysia," International Conference on Microwave and Millimeter Wave Technology (ICMMT), Chengdu, China, May 2010, pp. 441-444.

[6] Y.H. Chen, K.L. Hsieh, "A dual least-square approach of tuning optimal propagation model for existing 3G radio network," IEEE 63rd Vehicular Technology Conference (VTC), Melbourne, Australia, May 2006, vol. 6, pp. 2942-2946.

[7] A. Tahat, M. Taha, "Statistical tuning of Walfisch-Ikegami propagation model using particle swarm optimization," IEEE 19th Symposium on Communications and Vehicular Technology in the Benelux (SCVT), Eindhoven, Netherlands, Nov. 2012, pp. 1-6.

[8] Simon R. Saunders, Alejandro Aragón-Zavala., Antennas and propagation for wireless communication system, 2nd ed. Wiley, 2007.

[9] M.V.S.N. Prasad, S. Gupta, M.M. Gupta, "Comparison of 1.8 GHz cellular outdoor measurements with AWAS electromagnetic code and conventional models over urban and suburban regions of northern India," IEEE Antennas and Propagation Magazine, vol. 53, pp. 76-85, 2011.

[10] J. Chebil, A.K. Lwas, M.R. Islam, A. Zyoud, "Comparison of empirical propagation path loss models for mobile communications in the suburban area of Kuala Lumpur," 4th International Conference On Mechatronics (ICOM), Kuala Lumpur, *Malaysia*, May 2011, pp.1-5.

[11] H. Holma, A. Toskala, "WCDMA for UMTS: HSPA evolution and LTE," 5th ed. John Wiley & Sons, 2010.

[12] H. Holma, A. Toskala, "LTE for UMTS: OFDMA and SC-FDMA based radio access," UK: John Wiley & Sons, 2009.

[13] TEMS Investigation [Online]. Available: http://www.ascom.com/nt/en/index-nt/tems-products-3/tems-investigation-5.htm#overview

[14] TEMS Pocket [Online]. Available: http://www.ascom.com/nt/en/index-nt/tems-products-3/tems-pocket-5.htm#overview

[15] J. Kennedy, R. Eberhart, "Particle swarm optimization," IEEE International Conference on Neural Networks, Perth, WA, Nov./Dec. 1995, vol. 4, pp. 1942-1948.

[16] M. Zambrano-Bigiarini, M. Clerc, R. Rojas, "Standard particle swarm optimization 2011 at CEC-2013: A baseline for future PSO improvements," IEEE Congress on Evolutionary Computation (CEC), Cancun, June 2013, pp. 2337-2344 .

[17] Qinghai Bai., "Analysis of particle swarm optimization algorithm," Computer and Information Science, vol. 3, pp. 180-184, 2010.

[18] Singiresu S. Rao, S. S. Rao, Engineering optimization: theory and practice. 4th ed. Wiley, 2009.

PSCM: Proxy Server Cache Mechanism for Video on Demand System

Saleh Ali Alomari[1], Putra Sumari[2]
[1,2] School of Computer Science, Universiti Sains Malaysia
Pulau Penang 11800, Malaysia
[1]Faculty of Science and Information Technology, Jadara Universeity
Irbid 21110, Jordan
omari08@jadara.edu.jo and sumari@cs.usm.my

Abstract—Video on Demand (VOD) system is being one of the emerging systems that allow the user to view a video at anytime and anywhere. One of the important elements in this system is the broadcasting technique that is used to disseminate the video to the users. In this paper, a caching scheme was proposed to reduce the service waiting time in Video on Demand (VOD) system. The proposed caching schemes called Proxy Server Cache Mechanism (PSCM) scheme to overcome the service delay. This delay is accursed when a client misses the broadcasting phase of the 1st segment from broadcasting channels. Therefore, this paper proposed a caching scheme that denote as the (PSCM) to overcome the start-up service delay. In PSCM scheme, the 1st segment of the video is stored on a stationary proxy server. The late clients can request the 1st segment directly from the proxy server rather than waiting for the next broadcast of the 1st segment. The PSCM scheme guarantees obtaining the 1st segment by the mobile clients once they arrive. This scheme presents balance technique to maintain the requests over the local proxy server in order to ensure a fair distribution of these requests. The performance of the caching scheme is evaluated by implementing the VOD system. The results show that the proposed scheme has reduced the service delay substantially compared to the best existing schemes.

Keywords—VOD, PSCM, SB, LF's, LPS, All-Cache

I. INTRODUCTION

VIDEO on Demand (VOD) system is one of the most important applications for the future internet. It is became an interactive multimedia service that helps clients to playback any of the large collection of videos at anytime through public communication networks more freely after waiting for a short period of time, where they can be capable of making use of interactive services and download many videos at the same time [1]. Typically, these video files are stored in a set of central video servers, and distributed through high-speed communication networks to geographically dispersed clients. Wireless and mobile computing devices gave more flexibility and convenience to clients in order to enjoy viewing videos, and obtain flexible services from the distance video server while they are moving freely within the coverage of their wireless network. The choice of the suitable system architecture will be based on the location of the server, communication systems, available storage and other factors.

This project is part of a larger research work in the MCRG and this work was supported by Universiti RU's grant (1001 / PKOMP/ 817066) from the Universiti Sains Malaysia (USM).

The VOD system provides ubiquitous services to users (especially mobile users) in almost daily routines. For instance, VOD system allows university students to watch an educational video of their interests online anywhere and anytime. It also allows them to watch earlier recorded videos from lectures they were not able to attend. The VOD system allows people at the airport to instantly watch videos using their own PDAs while they are waiting for their flights' schedules. There are many other VOD applications, such as IPTV [2], Facebook [3], Youtub [4], Educclip [5], E-learning (digital video library) [6], On-line shopping, medical information services and etc.

The basic elements of the VOD system are servers, networks and user display equipment. The server is responsible for storing large number of videos and broadcasting them to users. Users may make requests of the videos and watch them by using users to display equipments, such as smart phone, iPad, PDA's and etc.

The characteristics of the VOD system, which include the long-lived session, high bandwidth requirements and QoS-sensitive service has made the design of the VOD system become a challenge. This is because of the nature of the video data. The video data are the real time data that has to satisfy certain QoS. Besides, the issues are how rapid a video can be watched, once requested. It is here referred to as the delay, which is the average period of time a client waits until being serviced. In other words, it determines an end-to-end time that is considered to be the difference between the times of requests for a packet travels from the source to the time of receiving at the user's destination. There are many elements influence the delay issue. The choice of the system architecture is one of the elements that influence the overall performance, especially, the location of the servers, the protocol of communication systems, and the availability of storage and other factors can contribute to the delay.

The subsequent sections are organized as follows. Section II presented the related background, while in Section III shown the cache proxy server mechanism (CPSM), the broadcasting technique for PSCM scheme presented in Section VI. In Section V described the caching mechanism of the PSCM scheme. The scenario of the playback video in the PSCM scheme for Video in Demand (VOD) system is presented in Section IV. The experimental results and discussions are

presented in Section IIV. Finally, the conclusion is presented in Section IIIV.

II. RELATED BACKGROUND

The designs of VOD systems are categorized into three main approaches; such as, Client/Server, Peer-to-Peer (P2P) and Periodic Broadcast [7] , [8] , [9], each of these approaches has such limitations. In the Client/Server approach [10] does not simply fit well for MANETs due to the limitation encountered in the wireless bandwidth. This limitation of wireless bandwidth creates problems when the number of request increases. In addition, the Peer-to-Peer (P2P) approach is not suggested to transmit the long video through more than one wireless hop, as this is inefficient for both; bandwidth and energy that are being used. Periodic Broadcast approaches are considered to be the better approaches in terms of bandwidth, since any number of mobile clients could be efficiently served. Particularly, the client can tune to one or more server channels and view the video. In this case, the number of the request will not effect on the server bandwidth. All broadcasting protocols, such as, [11-18], divided the video into a number of segments, then broadcasted these segments repeatedly over the number of channels.

The broadcasting method at the server is another element in contributing to the delay, as well as, the number of concurrent users of which the VOD system can support. Broadcasting is related to the scenario of handling clients who are watching different portions of the same video at any given moment. In particular, the server has to have an efficient broadcasting mechanism so that it can broadcast the video to many users as possible in a simultaneous fashion with the stringent delay requirements.

Broadcasting technique is a method of distributed video from a server to many simultaneous users. Broadcasting schemes can work with different network infrastructures [19], including cable TV, direct broadcast satellite and local area network. The idea behind the broadcasting schemes is to provide effective ways in reducing the waiting time for clients. This time refers to the interval time between requests for a video and receives the video from the beginning.

There are several researchers have been proposed to the VOD system to provide optimal services to the mobile ad hoc devices. MobiVoD [10], [20] is the latest VOD system, which provided the video services to homogeneous devices (i.e. laptop) through homogeneous network (i.e. WiFi 802.11b). MobiVoD allows the mobile clients to watch their movies at anytime and anywhere. As well as the system is composed of three main component the video server, Local forwarder (LF) and the mobile clients. The entire video files are stored on the main server. The LF's are a number of scattered stationary devices, which used as a relay for the video to the mobile clients by broadcasting video segments to its service coverage area. The server cannot transmit the video using wireless technique to wide coverage area; therefore, LF's are used to expand the transmission coverage area. Staggered Broadcast (SB) protocol has been used to broadcasting video segments repeatedly to mobile clients over number of wireless channels. SB is considered as the best choice for broadcasting the video to the mobile devices, since the limitation of the mobile devices [10]. The main advantages of using the SB protocol in VOD system is that, at first, a zero cache space is required in the mobile client devices. In addition, the required bandwidth by the clients' device does not exceed the playback rate, while in other protocols; the bandwidth is at least twice more than the playback rate. Furthermore, the clients just need to connect one channel, while in other broadcasting techniques the client should connect to at least two channels. The disadvantage is a high service delay that is accursed when the client misses up the broadcasting of the 1st segment of the video. The client should wait for a long time until broadcasting the 1st segment again on one of the channels.

Many researchers have been proposed a caching technique to solve delay problem. In [10] proposed several types of caching, such as, All Caching, Random Caching and DSC. The author proposed PCSB1 work attempted to solve the problem of the late clients, which missed the 1st segment of the current broadcasting channel. In order to solve this problem, and make the client obtain the video segment (1st segment) without waiting for the next broadcast channel of the 1st segment, the proposed scheme helps the clients to obtain it directly from the Pool of RAM (PoR) of the existing MF, where it used a procedure to store the 1st segment of the entire videos in the PoR of the MF, when the videos are broadcasted. In other words, the PCSB scheme can minimize the delay by guaranteeing that the late client can obtain the 1st segment as soon as it arrives. The author in [21] enhanced the cache by providing the on-going video streaming in the Relay Station (RS) in order to minimize the waiting time. Proxy prefix caching for Multimedia Streams has been proposed by [22] to reduce the user perceived latency and network resource requirements in the Internet, where a proxy is used to store the initial frames of audio or video locally. Upon the request, the proxy immediately transmits the data to the client. All Cache and Random Caching schemes have been proposed [10]. In the All-Cache scheme, all the clients in the Local forwarder coverage have to save the 1st segment in the Random Caching. The random number of clients has to save the 1st segment. The late clients in both schemes can cache the missed 1st segment from their neighbor who already saves the 1st segment in their buffer. DSC scheme has been proposed [10]. In this scheme, the new client X can get the 1st segment from client Y in the same transmission area, meanwhile, Y should not forward the segment to any other clients. But if Y is not in the transmission area of X, then Y will find client Z that share the same transmission area with itself and client X, then Y will forward the 1st segment to X through Z. There are many proposed caching techniques such present in [23], [24], [25].

III. CACHE PROXY SERVER MECHANISM (CPSM)

The caching scheme proposed in this paper is called the Cache Proxy Server Mechanism (CPSM). This caching scheme minimizes the start-up delay in VOD systems. In CPSM, the 1st segments of all broadcasting movies are stored in the local Proxy Server. If a client arrives after the local forwarder broadcasts the 1st segment, the clients cannot get it, where the

client must wait till the next broadcasting channel to broadcast the 1st segment. To overcome this problem, we suggest to install stationary proxy called the Local Proxy Server to make ensure that the late mobile client can get the 1st segment as soon as arrive with less start-up delay compared to with others. In this paper, the main content of the VOD system is classified into four components, main server, local forwarders (LF), local proxy server (LPS) and number of mobile clients. The main server is a server that is used to store a lot of video files. LF is a stationary device used to replay the videos to its wireless coverage area. LPS is a stationary server used to store the 1st segment of each broadcasting video in order to reduce the delay. Clients are mobile devices which can receive and watch videos. The interconnection between the main server and LF either will be via a wired LAN or via an infrastructure- based wireless network. The devices (LF, LPS, and Clients) are equipped with a wireless network interface card (wNIC) in order to communicate with each other through IEEE 802.11b technique. The video file is divided into a number of equal-size segments. These segments are broadcast to LF's by the main sewer. The LF will disseminate the video into its coverage area by broadcasting these segments through a number of channels. Clients join one of these logical channels and view the video as shown in Figure 1, the figure shows the logical broadcasting channels of the LF, and how the clients join these channels.

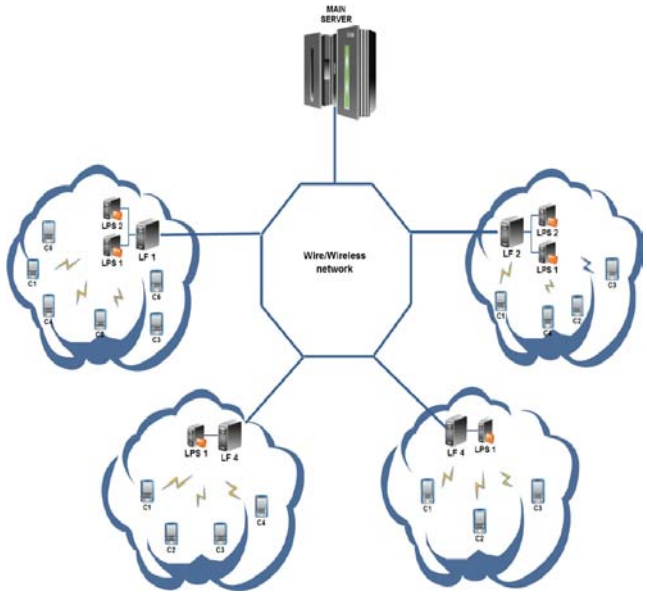

Fig.1. System Architecture of PSCM Scheme for VOD System

IV. BROADCASTING TECHNIQUE FOR PSCM SCHEME

In the main server sends the videos to the LF. The LF utilizes SB protocol as a broadcasting technique to broadcast the video to the clients where the video is classified into a number of equal-sized segments. These segments are periodically broadcasted over number of logical channels one by one according to the scheduled time of the SB protocol. In SB protocol, the number of segments is equal to the number of logical broadcasting channels. The number of the logical broadcasting channels is determined according to the bandwidth of the transmission media. This bandwidth is logically divided into k logical broadcasting channels. Each video is broadcasted over K logical channels in order to increase the chance of the clients to get the video at the proper time.

The bandwidth required by the system is considered constant and system can meet any number of requests. This justifies the use of the broadcasting technique in the system. In the PSCM scheme, the whole video is divided into K equal size segments (Seg1, Seg2, Seg3, …, SegK). The duration of each segment is Di = V/K. The numbers of every logical broadcasting Channeli must be between (Channeli = $1 \leq i \leq K$). It is decided that the provider bandwidth is Pb*K for the 2nd video and so on. This bandwidth is partitioned into physical channels (Channeli) repeatedly by broadcasting the video starting from (Seg1) and until the end of the video (SegK) with a transmission rate (Tr) that is equal to the playback rate (Pb) as shown in Figure 2. The Client_x can join Channel1 and wait for the beginning of 1st segment (Seg1) to download and playback it. After that, Client_x switches to the next segment (Seg2) for playback. This process is repeated for the subsequent segments until the last segment (SegK) is downloaded from Channel1. Equation 1 and 2 follows the definition.

$$Di = \frac{V}{K} \qquad (1)$$

$$V = \sum_{i=1}^{k} Di \qquad (2)$$

Where, Di is the duration of each segment, V is the length of the video and K is the number of the channels. The equation that is used to determine the number of logical channels (k) is as follows:

$$Tr \times K \times Nvi \leq b \qquad where\ i = \{1,2,\ldots,n\} \qquad (3)$$

Where Tr is the bandwidth transmission media, Nvi is the number of videos and K is the number of logical channels.

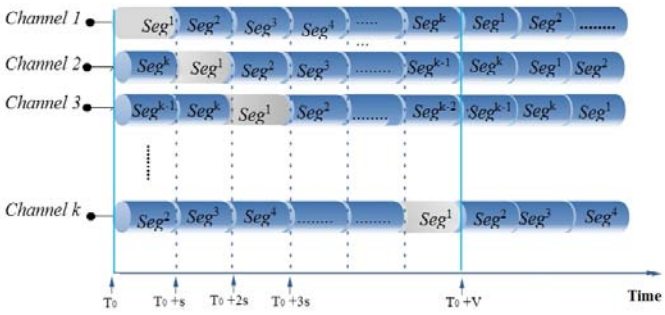

Fig. 2. Broadcasting Mechanism of PSCM scheme

Figure 2 illustrates the details of SB mechanism of broadcasting the video over the logical channels, where Channel 1 starts broadcasting the video segments sequentially. After a period of time (equals to the time of the segment), Channel 2 also starts broadcasting the segments the same way as in Channel 1. The same mechanism is achieved for the rest of channels.

In SB technique, the video can be watched directly when the client arrives at the time T0 of the video broadcasting on LF channel where (T0) is the time when the broadcasting of the 1st segment starts. The client has to wait for a period of time (until the next broadcasting of the 1st segment starts on another channel) if this client arrive at (T0+s) of the 1st segment broadcasting time.

V. CACHING MECHANISM OF THE PSCM SCHEME

The caching technique proposed in this thesis aims at reducing the delay that is caused by the broadcasting technique used. The delay occurs when the client misses the broadcast of the 1st segment of the video. To view the video, the client has to wait for the next broadcasting of the 1st segment on the same or a different channel. To reduce this delay, a new caching scheme called PSCM is proposed. Figure 3 illustrates a representation of one VOD system service area. In this representation, two clients (PDA 2 and PDA5) cache the 1st segment from LPS after it is missed form LF. When these clients miss the 1st segment that is broadcasted by LF1, the clients are cached the 1st segment form the LPS1. The rest of the segments should be retrieved from the LF after tuning into one of the LF logical broadcasting channels.

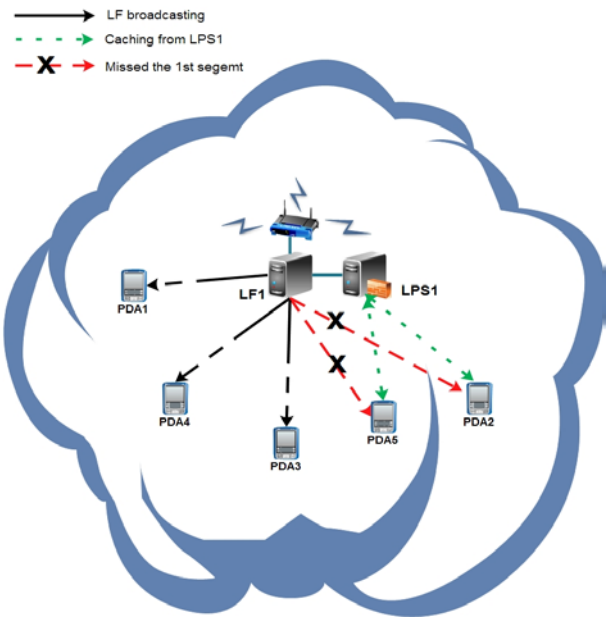

Fig. 3. A representation of one VOD System Service Area.

The PCSM scheme proposes using LPS. LPS is used for providing the 1st segment to late clients that miss broadcasting the 1st segment as soon as they arrive. The immediate provide of the 1st segment saves the clients time. This can be performed by avoiding the delay when waiting for the next broadcast of the 1st segment. In the PSCM scheme, each LF is responsible for passing a copy of the 1st segment of the videos to the neighbor LPS within its area. Figure 4 shows how the LF passes the 1st segment of the broadcasted videos to the neighboring LPS.

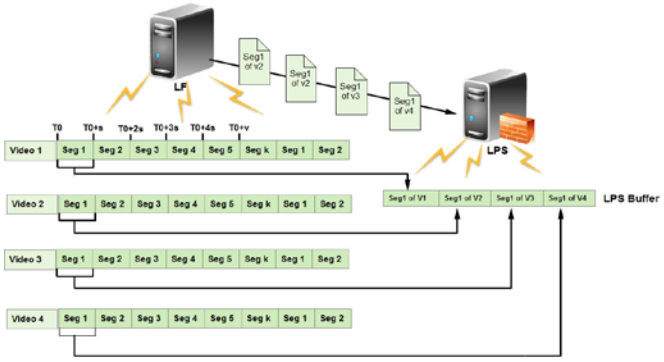

Fig. 4. The Process of Sharing the Videos 1st Segment of LF with LPS

VI. THE SCENARIOS OF PLAYBACK VIDEO IN PSCM SCHEME FOR VOD SYSTEM

In CPSM, the client can request to watch movie after one inters in the LF's areas. LF will check the arrival time of new client to know if the new client missed the 1st segment of the video or not. t0 is the start time of the broadcasting video, so if the client arrive at time Arrival Time = (T0, T0+s, T0+2s, T0+3s,T0+4s or T0+V), he/she can join that channel and watch the video, otherwise, if the client arrives at Arrival-Time of the broadcasting time= (T0+ δ, T0+s+δ, T0+2s+δ, T0+3s+δ, T0+4s+δ 0r T0+V+δ), where (0<δ<s). This impels the client has missed the 1st segment. In this case, the LF will look up in the table to find which LPS is suitable for streaming the 1st segment of the video to the late client; then the LF sends information about the LPS. The client sends a request to the LPS and asks the 1st segment; at the same time the client joins the LF channel to get the rest of the segments. In the PSCM scheme, each LF maintains the information about the LPSs that are located in their area. Figure 5 illustrates the scenario and the LF table that are used for the load balancing of the client requests. The information in the table is used to balance the assigned requests among the LPSs in order to maintain the resources of the LPSs. Besides, by using this information in the table the CPSM can ensure a fair distribution of the requests among the LPSs, where none of the LPS has more loads than others. When late clients' request

ISBN: 978-1-61804-228-6

a video, the LF check it table in order to know which LPS has less number of requests then retrieve the information about the suitable LPS and sends it to that client. The late client will cache the 1st segments from the LPS's who have less number of clients, in case that the LPSs have equal number of requests, LPS who has less ID address will handle the request of the late client. After that the LF will send the LPS which has less ID number as shown in Figure 5. The LPS will guarantee the new client to get the 1st segment as soon as he/she arrives with a less waiting time on mobile clients and with a reasonable delay.

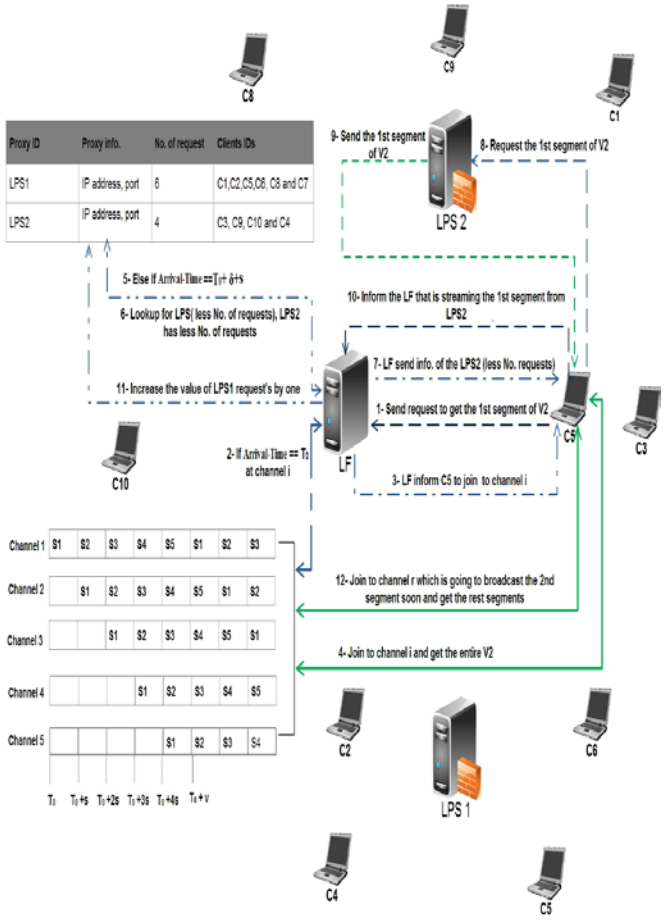

Fig.5. Shows a scenario when the late client (C5) missed the 1st segment

VII. EXPERIMENTAL RESULT AND DISCUSSION

This section represents the results that are produced by implementing the PSCM scheme for the VOD system. In addition, the following subsections discuss the service delay of requesting the video under multiple effective cases. The service delay is the time average of which a client has to spend starting from requesting the video till receiving its service. In particular, it is used to measure the way the VOD system performs as a truly on demand video service.

A. *The Effects of The Number of Arrival Requests With Delay*

The results of the delay effective of VOD system when it is measured depending on the number of the client's requests at a period of time as illustrated in Figure 6(a) and Figure 6(b). The results show the average delay of two caching scheme which are All-Cache and PSCM scheme. In All-Cache, needs at least one other client located in the area to cache the 1st segment and minimize the delay. In PSCM scheme, the late client cache the delay is effective even if there is one client in the area. It contributed to make the probability of the getting the video service is same for all clients. That means the client can get the 1st segment regardless if there is previous clients in the area.

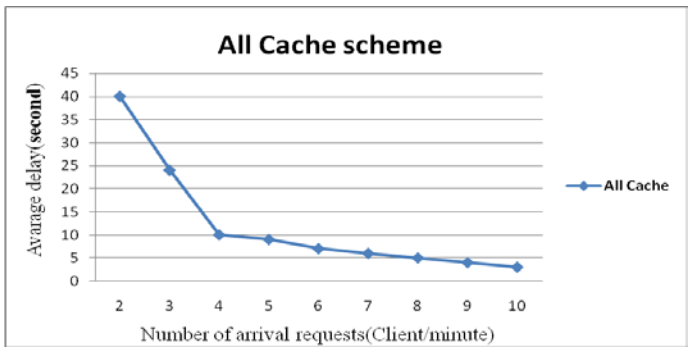

Fig.6. (a) Average service delay of All-Cache scheme depending on the number of arrival requests

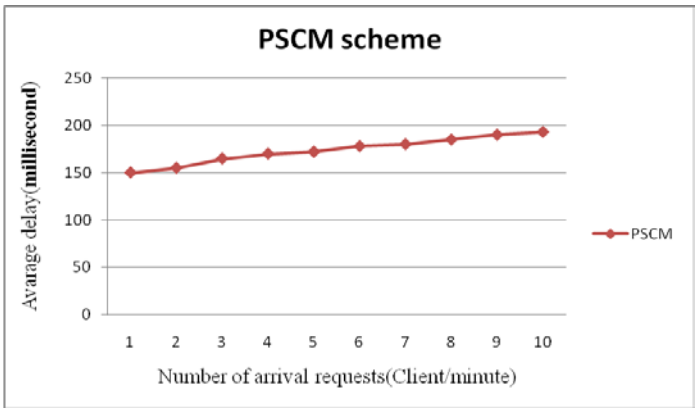

Fig.6. (b) Average service delay of PSCM Scheme depending on the number of arrival requests

B. *The Effective of The Average Delay Depending n The Length Of The Video*

The impact of the average delay depending on different video lengths where the VOD system is capable to handle different lengths of a video. According to Formula (2), the length of each segment can be maximized or minimized based on the total video length and the number of broadcasting

ISBN: 978-1-61804-228-6

logical. Figures 7 (a) and Figures 7 (b) illustrate the effects of video length on the service delay in the All- Cache scheme and the PSCM scheme, respectively.

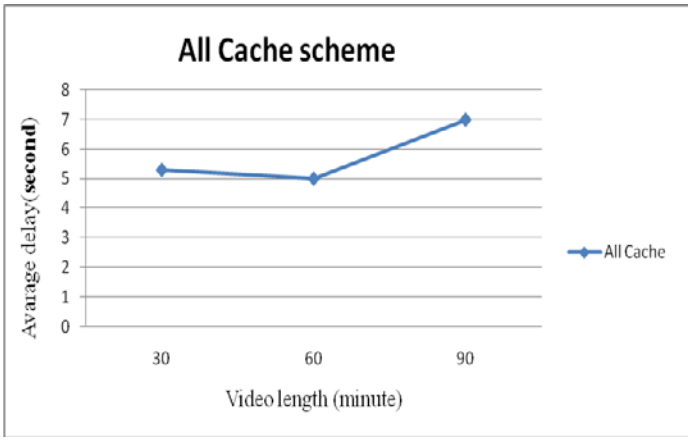

Fig.7. (a) Average delay of All-Cache scheme depending on different video lengths

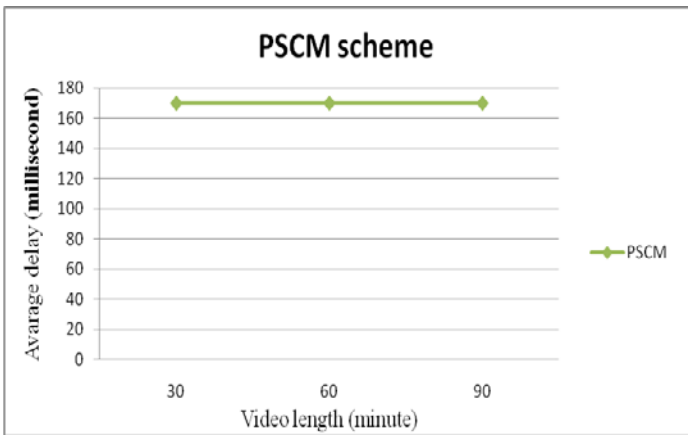

Fig. 7. (b): Average delay of the PSCM scheme depending on different video lengths

In Particular, the average of the delay is 5 seconds when the video length is 60 minutes in the All-Cache scheme, while in the PSCM scheme, the average service delay is 170 milliseconds. Besides that, the average service delay is 7 seconds when the length of the video is 90 minutes. In contrast, the average delay of the PSCM scheme maintained the same (170 milliseconds) when the length of the video is 90 minutes.

C. The Results of the Fail Probability Depending on the Number of Arrival Requests

The results of the fail probability that obtains the 1st segment video of the two caching schemes which are; the All-Cache scheme and the PSCM scheme depending on the arrival request number. As shown in Figure 8, the All-Cache scheme, a failure is detected once the new client fails to find a free neighbor client who has already cached the 1st segment. In addition, a failure is also detected once the new clients fail to get the 1st segment video from the current cache. This failure of getting the video is due to the fact that the client who is caching the 1st segment is moved or is terminated from the system.

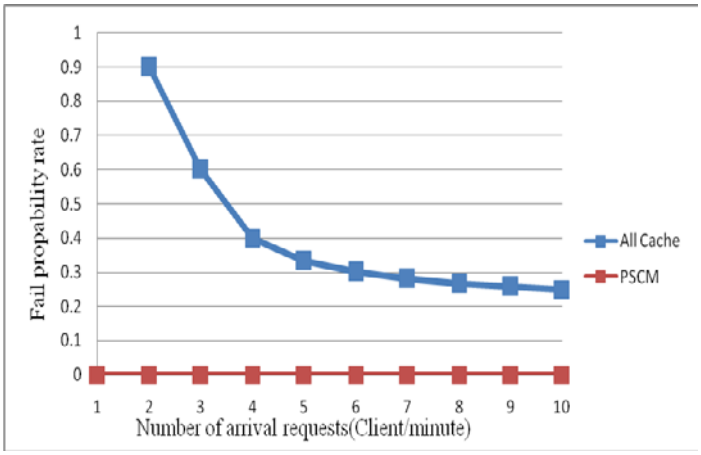

Fig.8. The results of the failure probability to get the 1st segment of the video.

VIII. CONCLUSIONS

This paper proposed a new caching scheme, which is called the Proxy Server Caching Mechanism (PSCM) for VOD system. This caching scheme proposed to solve the delay problem in mobile clients caused by using a broadcasting technique in that mobile VOD system over Ad Hoc network. In PSCM, the 1st segment of all videos is stored in a stationary server (LPS). This caching will minimize the delay by guaranteeing the late client to get the 1st segment as soon as it arrives. In order to maintain the recourses of the LPSs in the system, a load balancing method has proposed.

ACKNOWLEDGMENT

This project is part of a larger research work in the MCRG and this work was supported by Universiti RU's grant (1001 / PKOMP/ 817066) from the Universiti Sains Malaysia (USM).

REFERENCES

[1] Saleh Ali Alomari and putra Sumari.,(2012), Effective Broadcasting and Caching Technique for Video on Demand over Wireless Mobile Network. KSII Transactions on Internet and Information Systems (TIIS), VOL. 6, NO. 3, pp. 919- 940.
[2] Shiroor, R.G. (2007), IPTV and VoD services in the context of IMS. International Conference on IP Multimedia Subsystem Architecture and Applications, Vol. 2, No. 1, pp.1-5.
[3] Facebook (2012). http://www. facebook.com/ (Accessed on 2 Jan)
[4] YouTube .(2012). http://www.youtube.com/t/press_statistics (Accessed on 2 Feb 2012).
[5] Educlip (2012). http://www.educclip.com/ (Accessed on 4 Nov)
[6] Williams, B. and Camp, T. (2002). Comparison of Broadcasting Techniques for Mobile Ad Hoc Networks. In ACM Symposium on

Mobile Adhoc Networking and Computing (MOBIHOC 2002). New York, NY, USA, pp. 194 – 205.
[7] Duc AT, Thinh N.(2008). Broadcasting Techniques for Video-on-Demand in Wireless Networks. Book Chapter 1, department of Computer Science, University of Dayton, Dayton, OH 45469. Oregon State University, Corvallis, OR 97331.
[8] Gruber S, Rexford J, Basso A. (2000). Protocol considerations for a pre-caching proxy for multimedia streams, in Proc. of the 9th International WWW Conference, pp. 657-668.
[9] Park YW, Baek KH, Chung KD.(2000). Reducing network traffic using two-layered cache servers for continuous media on the internet, in Proc. Of the IEEE Int'l Conf. on Computer Software and Applications, pp. 389-394.
[10] Duc AT, Minh L, Kien AH. (2004). MobiVoD: A Video-on Demand System Design for Mobile Ad hoc Networks. Proceedings of the 2004 IEEE International Conference on MobileData Management (MDM'04). Berkeley, CA, pp. 212 223.
[11] Li-Shen J, Li-Ming T. (1998). Fast data broadcasting and recive scheme for polpular video service. IEEE transactions on broadcasting, Vol. 44, No. 1, 1998.
[12] Paris JF, Carter SW, Long DDE. (1999). A hybrid broadcasting protocol for video on demand. In Proc. 1999 Multimedia Computing and Networking Conference (MMCN'99), San Jose, CA, pp 317-326.
[13] kien AH, Simon S. (1997) skyscraper broadcasting, A new broadcasting scheme for metroplitan Video on Demand systems. In Proceedings of ACM SIGCOMM 1997, Cannes, France.
[14] Hee J, Seong-min J, Sung-kwon P, Seung-hwan S, Dong-hwa Y. (2008). Interleaving harmonic staggered broadcasting scheme for video-on-demand services. Tenth IEEE International Symposium on Multimedia, 2008
[15] Kwon JB, Heom HY.(2002).Providing vcr functionality in staggered video broadcasting. IEEE Transactions on Consumer Electronics, Vol.48, No.1, pp.41–48.
[16] Gui YQ, Jung E, Choi Y, Choi HK. (2007). an efficient periodic broadcast scheme for mobile video –on demand system" In Proc. Of international Confernce on Information Technology (ITNG'07), pp. 888-889.
[17] L. Juhn and L. Tseng. Harmonic broadcasting for videoon- demand service. IEEE Transactions on Broadcasting. Vol 43, No.3, pp.268–271.
[18] Saleh Ali Alomari, Putra Sumari, Sadik Ali Taweel. (2011). An Efficient Popularity Cushion Staggered Broadcasting for Homogeneous and Heterogeneous Mobile Video-on-Demand System. International Conference on Wireless and Optical Communications (ICWOC 2011), Vol.4, pp.272-277.
[19] Liao, W. and Li, V. O. K. (1997). The split and merge protocol for interactive video on demand. IEEE Multimedia , Vol. 4, No. 4, pp.51–62.
[20] Saleh Ali Alomari, Putra Sumari. (2010). A Video on Demand System Architecture for Heterogeneous Mobile Ad Hoc Networks for Different Devices. International Conference on Computer Engineering and Technology, Vol.7, pp.700 – 707.
[21] Xie F, Hua K. (2009). A caching-based video-on-demand service in wireless relay networks. IEEE International Conference on Wireless Communications and Signal Processing, , pp. 1–5.
[22] Subhabrata S, Jennifer YR, Don T. (1999). Proxy Prefix Caching for Multimedia Streams. CMPSCI Technical Report 98-27 University of Massachusetts.
[23] Saleh Ali Alomari, Putra Sumari. (2010). A Video on Demand System Architecture for Heterogeneous Mobile Ad Hoc Networks for Different Devices. International Conference on Computer Engineering and Technology, Vol.7, pp.700 – 707.
[24] Saleh Ali Alomari, Putra Sumari. (2010). A new Peer to Peer Caching Techniques for Transmitting the Video over Wireless Ad Hoc Network. (IJCSIS) International Journal of Computer Science and Information Security, Vol. 8, No. 3,pp. 239-245.
[25] Vaithegy D, Saleh Alomari, Putra S. (2011). Video on Demand Caching System using NIPBCS over Mobile Ad Hoc Network. JDCTA: International Journal of Digital Content Technology and its Applications, Vol.5, No.6, pp. 142 -154.

Saleh Ali K. Alomari obtained his MSc and PhD in Computer Science from Universiti Sains Malaysia (USM), Pulau Penang, Malaysia in 2008 and 2013 respectively. He is a lecturer at the faculty of Science and Information Technology, Jadara University, Irbid , Jordan. He is Assistance Professor at Jadara University, Irbid , Jordan 2013**.** He is the candidate of the Multimedia Computing Research Group, School of Computer Science, USM. He is research assistant with Prof. Dr. Putra, Sumari. He is managing director of ICT Technology and Research and Development Division (R&D) in D&D Professional Consulting Company. He has published over 35 papers in international journals and refereed conferences at the same research area. He is a member and reviewer of several international journals and conferences (IEICE, ACM, KSII, JDCTA, IEEE, IACSIT, etc). His research interest are in area of multimedia networking, video communications system design, multimedia communication specifically on Video on Demand system, P2P Media Streaming, MANETs, caching techniques and for advanced mobile broadcasting networks as well.

Putra Sumari is currently working as Assistant Professor of School of Computer Science, Universiti Sains Malaysia, Penang in 2009. Assoc. Prof Dr. Putra received his MSc and PhD in 1997 and 2000 from Liverpool University, England. Currently, he is a lecturer at the School of Computer Science, Universiti Sains Malaysia, Penang. He is the head of the Multimedia Computing Research Group, School of Computer Science, USM. He is Member of ACM and IEEE, Program Committee and reviewer of several International Conference on Information and Communication Technology (ICT), Committee of Malaysian ISO Standard Working Group on Software Engineering Practice, Chairman of Industrial Training Program School of Computer Science USM, and Advisor of Master in Multimedia Education Program, UPSI, and Perak.

General study of self excited induction generator used in isolated renewable energy conversion source

Mohamed. Barara, Ahmed. Abbou, Mohamed. Akherraz , Abderrahim.Bennassar and Mohamed larbi. ELhafyani

***Abstract*—**In this paper we have present a general study of self excited induction generator used in isolated renewable energy conversion source ,the behavior of generated voltage under variable load ,rotor speed and excitation capacitance is presented ,also we have proposed a robust controller suitable in order to control the terminal DC voltage under different speed and AC load conditions for supplied an isolated DC load, the experimental characteristic curve of the generator and simulation result of proposed control scheme are presented.

Keywords—*Renewable energy, Self-excited induction Generator, DC link control.*

I. Introduction

The energy demand around the world increases the great opposition facing the nuclear energy in some countries have spur researchers attentions for renewable energy. The self excited induction generator is a very popular machine used in isolated areas to generate electrical energy because of its low price, mechanical simplicity, robust structure.
When capacitors are connected across the stator terminals of an induction machine, and driven at a given speed, the voltage will be induced from a remnant magnetic flux in the core.

The induced emf and current in the stator windings will continue to rise until steady state is attained. This behavior is influenced by the Magnetic saturation of the machine. At this operating point the voltage and current will continue to oscillate at a given peak value and frequency[6] , However, its major disadvantage is the inability to control the terminal voltage under variable load and speed conditions

The objective of this work is divided into two parts: in the first part we present the experimental curve of variation speed and capacitance with the SIEG connected to load and no load in order to show the behavior of our machine, The relationship between magnetizing inductance (Lm)and phase voltage for induction machine was obtained experimentally, and in the second part we are more interested in the control of the DC bus voltage in order to provide an essentially constant terminal DC voltage in spite of the presence of disturbances such as step change in rotor speed and application of sudden AC load for supplied an isolated DC load ,the simulation results are given to demonstrate the effectiveness of the proposed method.

II. System Configuration without control scheme

The proposed system starts excitation process from capacitors bank which are connected across the stator terminals of an induction machine driven by unregulated prime mover (DC motor in laboratory test) and supplying AC load

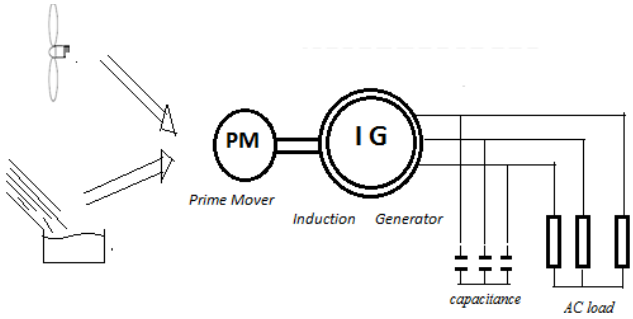

Fig.1: self excited induction generator system

When the induction machine when used for motoring application, it is important to determine the magnetizing inductance at rated voltage. In the SEIG, the variation of

Mohamed . Barara , Ahmed abbou ,Mohammed Akherraz and abderrahim bennassar are with the Electrical Department Laboratory of Power Electronic and Control Mohamed V University , Mohammadia School of Engineering Agdal Rabat Morocco :Mohamed-barara@hotmail.fr.

Mohamed,larbi Elhafyani is with Université Mohamed I, EST,LGEM. 473, 60000 Oujda, Morocco: m_elhafyani@yahoo.fr

magnetizing inductance Lm is the main factor in the dynamics of voltage build up and stabilization[3].

The relationship between magnetizing inductance (Lm) and phase voltage for induction machine was obtained experimentally as show in Fig 3:

the magnetizing inductance is calculated by driving the induction machine at synchronous speed and taking measurements when the applied voltage was varied from zero to 100% of the rated voltage.

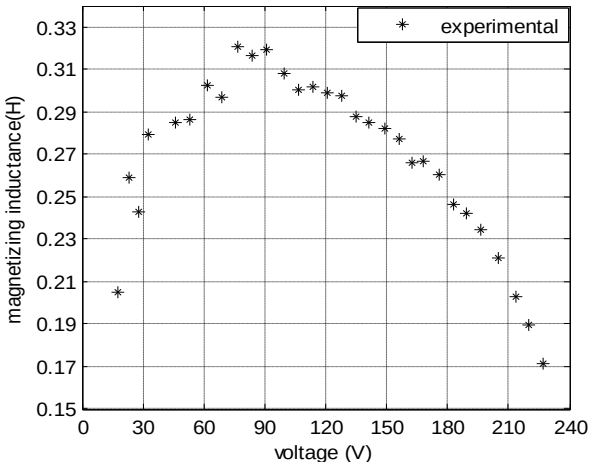

Fig.2: Variation of magnetizing inductance with phase voltage

The variation of magnetizing inductance, increases until it reaches a peak value and decreases until it attains saturated value as shown n Fig.2

A. Self Excited induction Generator

The state-space form of the induction generator in the q-d synchronously rotating reference frame is given by[3]:

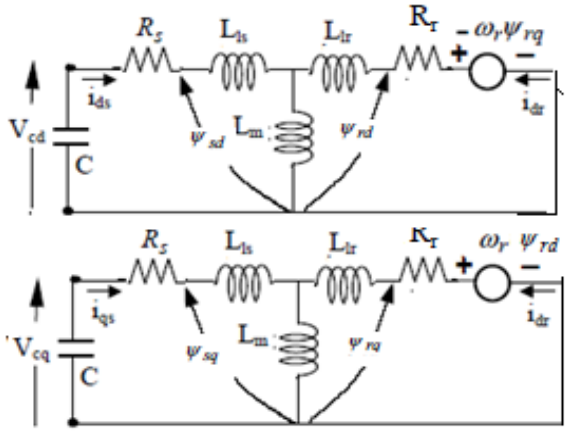

Fig.3: d-q model of SEIG at no load

$$\mathrm{PI} = AI + B$$

Where:

$$I = \begin{bmatrix} i_{qs} \\ i_{sd} \\ i_{qr} \\ i_{dr} \end{bmatrix}$$

$$\mathrm{B} = \begin{bmatrix} L_m K_q - L_r V_{cq} \\ L_m K_d - L_r V_{cd} \\ L_m V_{cq} - L_s K_q \\ L_m V_{cd} - L_s K_d \end{bmatrix}$$

$$A = \frac{1}{L}\begin{bmatrix} -L_r R_s & -L_m^2 w_r & L_m R_r & -L_m w_r\ L_r \\ L_m^2 w_r & -L_s R_s & L_m w_r\ L_r & L_m R_r \\ L_m R_s & L_s w_r\ L_m & -L_s R_r & -L_s w_r\ L_r \\ -L_s w_r\ L_r & L_m R_s & -L_s w_r\ L_r & -L_s R_r \end{bmatrix} \quad (1)$$

Where $\mathrm{L} = L_r\ L_s - L_m^2$

Modeling of The excitation system model:

$$V_{cq} = 1/c \int (i_{qs} \_ i_{rlq} \_ i_{rq})\ dt \quad (2)$$

$$V_{cd} = 1/c \int (i_{ds} \_ i_{rld} \_ i_{rd})\ dt \quad (3)$$

Where $i_r d$, $i_r q$ are input currents of three-phase diode bridge rectifier and i_{rlq} , i_{rld} are the AC load current

The instantaneous amplitude of the magnetizing current of the SEIG, which is computed as:

$$im = sqrt\ ((i_{qs} + i_{qr})^2 + (i_{ds} + i_{dr})^2) \quad (4)$$

B. Experimental results of variation speed and capacitance while the SIEG is connected to load and no load

In the laboratory test rig, a three phase squirrel cage induction machine was coupled to a DC motor operating as the prime mover.

The experimental setup includes the variation of rotor speed with capacitance bank respectively with no load and load, in this investigation for have a fixed generated voltage of 400V and 250 V as show in Fig.4 and Fig.5 respectively.

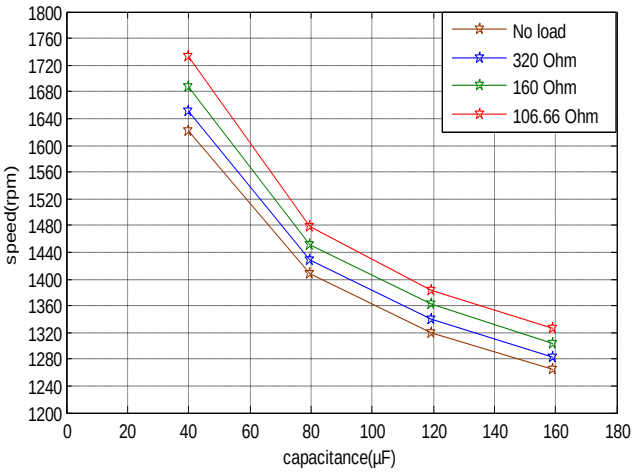

Fig.4: Variation of capacitance with different speed and loads for constant terminal voltage of 400V

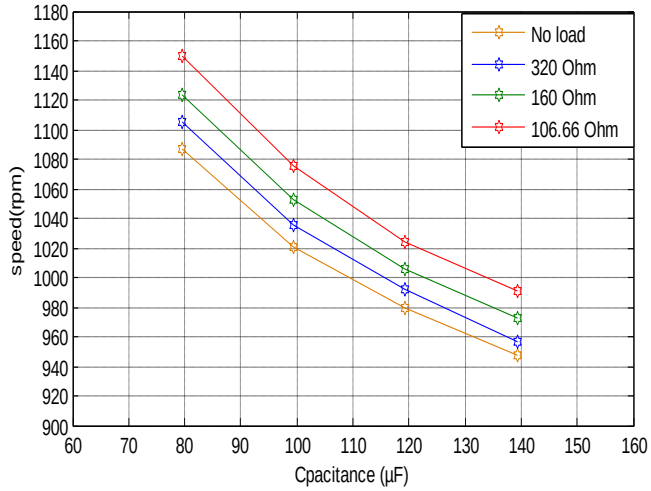

Fig.5 :Variation of capacitance with different speed and loads for constant terminal voltage of 250V

From these figure is well observed that the variation of output voltage is affected by the application of Load, variation of speed and excitation capacitance.

When the generator runs at the speed of 1087 rpm, the necessary value of capacitance will be at 80 μF for no load connected ,in order to have a fixed terminal voltage of 250V. In the same condition with load connected of 320 ohm the rotor speed will be increased at 1105 rpm for maintain the same value of the terminal voltage ,Similar analysis will be followed to track different value of speed ,capacitance with load and no load as summarized in Fig.5,Fig.4.

III. Proposed Control Scheme of SIEG

For proper operation of the use for this machine in standalone renewable energy Source, cases (Wind-, micro hydro) we must provide a control system capable of controlling the output voltage for a good functioning .

Recently the application of semiconductor devices, controlled converter circuits, and control algorithms has resulted in suitable and good regulating schemes for SIEG.In literature many researchers have proposed numerous control for regulating the terminal voltage[2 4 5 7 10 15 17]. Since this paper present a simple and uncomplicated control scheme.

The motivation of this work is to study the feasibility of this system by providing a detailed transient and steady-state analysis in order to keeps the DC bus voltage at a constant value even the rotor speed change and application of sudden AC load. Detailed Matlab/Simulink-based simulation studies are carried out to demonstrate the effectiveness of the scheme.

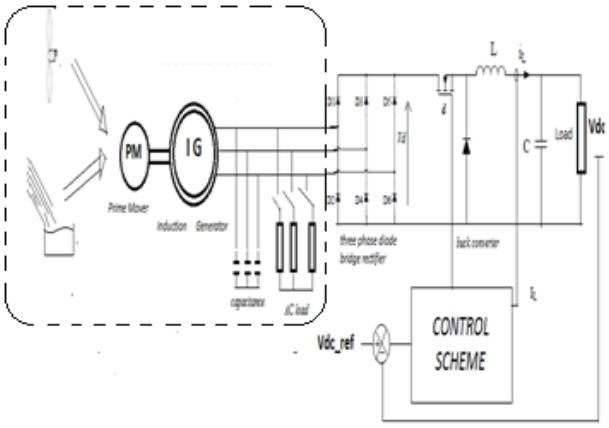

Fig.6: Proposed control of self excited induction generator

The variable output voltage from the generator is first rectified using diode bridge rectifier and then controlled by dc-dc buck converter as shown in Fig 6.

A. *Three Phase Diode Rectifier*

Three phase diode bridge rectifier is used to convert variable magnitude, variable frequency voltage at the induction generator terminal into DC voltage the circuit consists of 6 diodes, a top group of 3 diodes and a bottom group of 3 diodes

ISBN: 978-1-61804-228-6

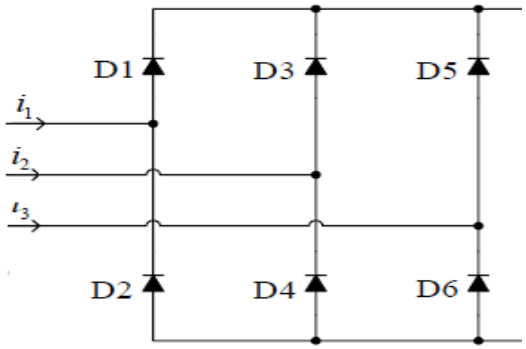

Fig. 7.Three-phase diode bridge rectifier

B. Buck Converter

The DC-DC converter inputs are generally unregulated DC voltage input and the required outputs should be a constant or fixed voltage. Application of a voltage regulator is that it should maintains a constant or fixed output voltage under variation of input voltage.

.

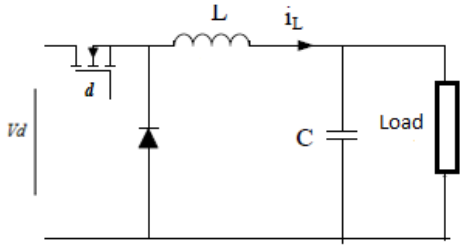

Fig. 8.Buck converter circuit

The mathematical model of the buck type dc-dc converter with the control input **d** are given by following equation :

$$\frac{di_L}{dt} = \frac{Vd}{L}(d) - \frac{Vc}{L} \qquad (6)$$

$$\frac{dVc}{dt} = \frac{iL}{C} - \frac{Vc}{R*C} \qquad (7)$$

Where R= resistive load

C. Control scheme

Current-mode control is a dual loop control method, including current and voltage control loops[8]. In this method, the error signal between output voltage Vdc and reference voltage Vdc_ref is used to generate reference current iref. Then, this reference current is compared with sensed inductor current iL to control the duty cycle As show in Figure 9

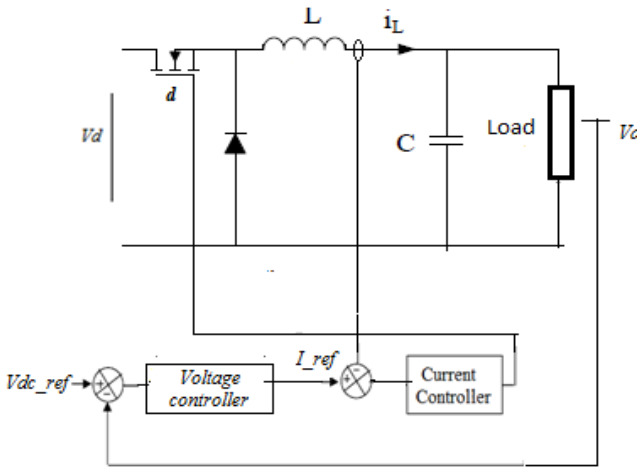

Fig. 9.Block diagram of control scheme

IV. Simulation Results and Discussion

MATLAB/Simulink® modelling is used to observe the proposed control. The residual magnetism in the machine is taken into account in simulation process without which it is not possible for the generator to self excite.

The induction generator is rated at 3 kw and the system parameters approximation are given in Table I.

The SIEG is tested during 7 s, when the system is subjected to step change in the rotor speed and sudden application AC load. The proposed system starts excitation process from AC capacitors bank of 100µF and variation rotor speed between 1500rpm, 1096rpm to 1296rpm, respectively at 0s,3s,4s, as shown in Fig.3

in his section, for investigate the response of the system with sudden application of AC load the generator is initially excited at no-load and suddenly a AC load of Rac=80 Ω applied at t = 6sec

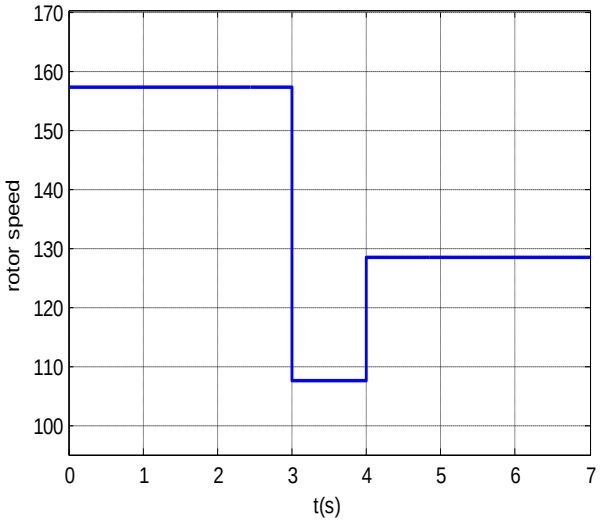

Fig.10: Rotor speed (rad/s)

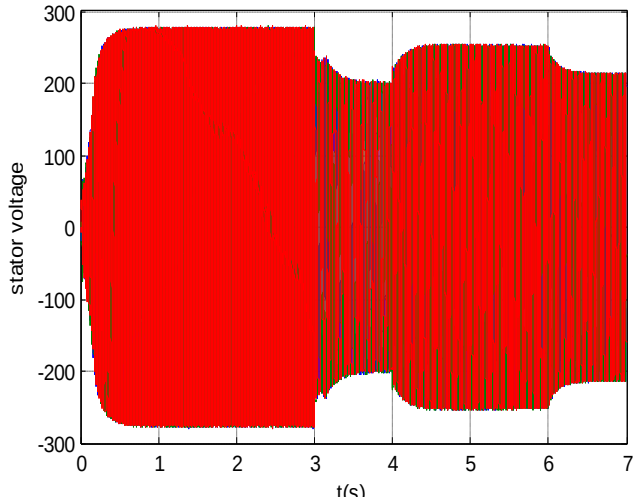

Fig.11: generate voltage of the SIEG

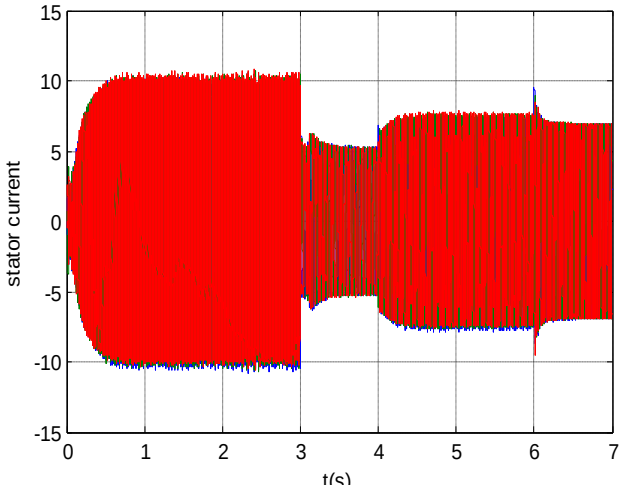

Fig.12:generate current of the SIEG

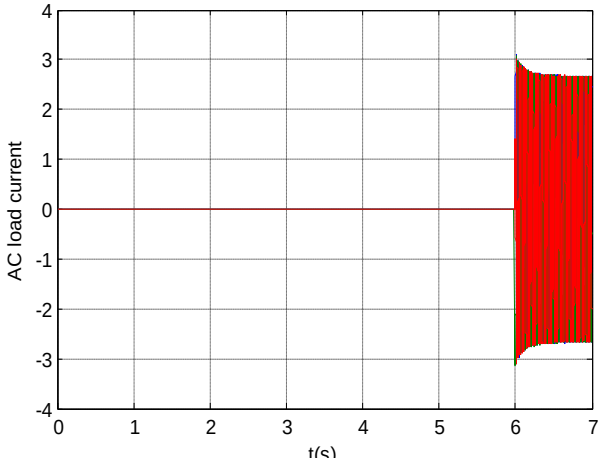

Fig .13: AC load current

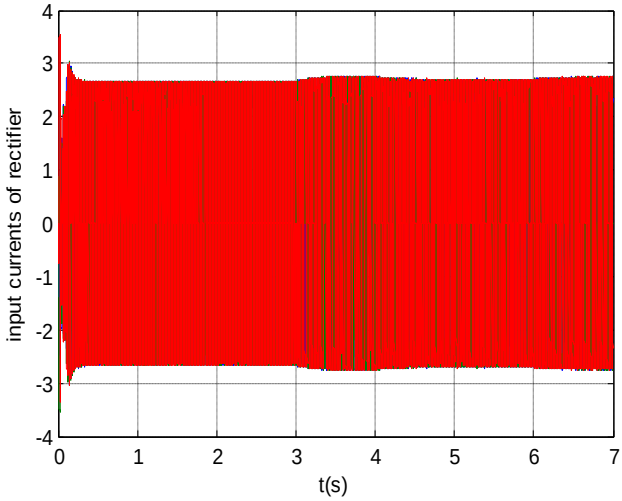

Fig.14: input current of three phases rectifiers

Any variation in rotor speed of the SEIG is directly indicated by the variation in the terminal voltage and current of the generator as shown in Fig.11, Fig.12

After connecting the AC load at t = 6s, we see the generated current increases during this time and then decreases to its initial value then the terminal voltage dropped ,the load current is created as shown in Fig.12, Fig.11 Fig.813 respectively.

.

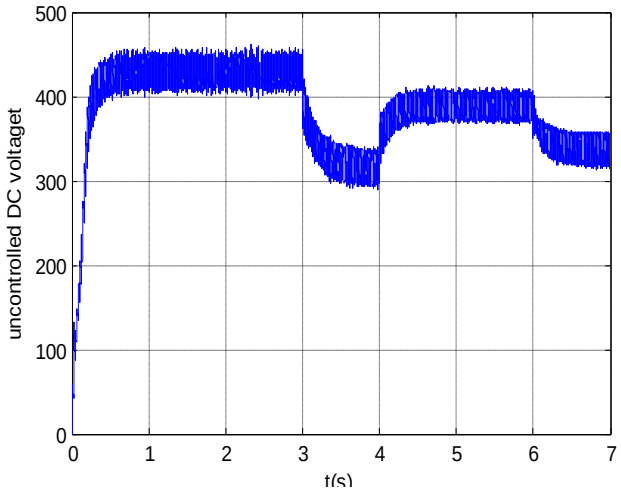

Fig.15: Uncontrolled DC link voltage

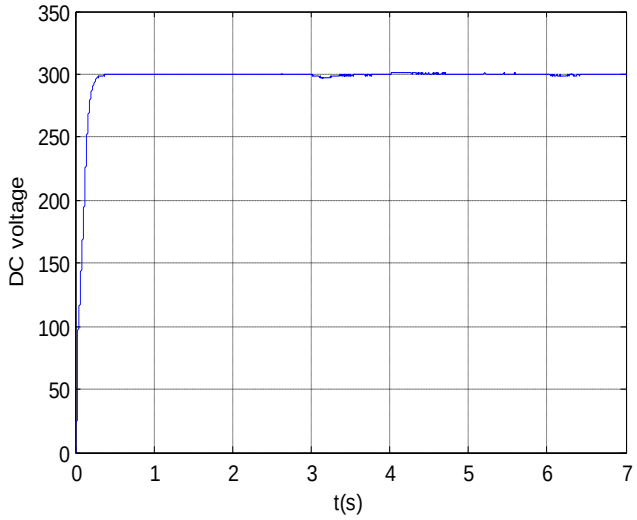

Fig.16: controlled DC link voltage

The value of the DC bus voltage is maintained at constant value of 300 V even if the rotor speed changes at 3s , 4s and application of AC load at 6s . The controller provides a rapid and accurate response for the reference as shown in Fig.16 it has been demonstrated that the system is able to feed an isolated DC loads with a robust regulated voltage.

V. Conclusion

This paper presents a general studies of SIEG include dynamic behavior ,the variation of magnetizing inductance are considered, also we propose a simple and uncomplicated control scheme in order to provide a regulated DC voltage The controller has been tested for different transient conditions such as, sudden application for both three-phase loads , and variable rotor speed. The simulated results show a good performance and efficiency of the global SEIG conversion system.

Appendix

Table I: Generator and buck converter Parameters

designation	value
R_s	2.2Ω
R_r	2.68Ω
l_s, lr	12 mH
C	600F
L	50mH
Rdc	120 Ω

Acknowledgment

This work has been developed within the framework of the Activities of the Project: "analysis, application and advanced control of self excited induction generator used in isolated renewable energy source» and has been carried out for the Electrical Department Laboratory of Power Electronic and Control Mohamed V University , Mohammadia School of Engineering Agdal Rabat Morocco The authors wish to place on record its deep sense of gratitude to Mr driss Deppagh and Mr Mohamed moutchou, of, for their valuable assistance in this work .

References

[1] M.L. Elhafyani, S. Zouggar, Y. Zidani and M. Benkaddour, „Permanent and Dynamic Behaviours of Selfexcited Induction Generator in Balanced Mode", M. J. Condensed Mater, Vol. 7, pp. 49 - 53, 2006.

[2] Ahmed, T.; Nishida, K.; Nakaoka, M.; Tanaka ''Advanced Control of a Boost ACDC PWM Rectifier for Variable-Speed Induction Generator''K.Applied Power Electronics Conference and Exposition, 2006. APEC '06. Twenty First Annual IEEE 956-962 March 19, 2006.

[3] Seyoum D., Grantham C. and Rahman F,"Analysis of an Isolated Self-Excited Induction Generator Driven by Variable Speed Prime Mover", Proc.AUPEC"01, 2001, pp. 49-54

[4] Karim H. Youssef, Manal A. Wahba, Hasan A. Yousef and Omar. A. Sebakhy ''A New Method for Voltage and Frequency Control of Stand-Alone Self-Excited Induction Generator Using PWM Converter with Variable DC link Voltage''2008 American Control Conference Westin Seattle Hotel, Seattle, Washington, USA June 11-13, 2008

[5] [3] M.L. Elhafyani , S. Zouggar , A. Aziz et M. Benkaddour"" Conception et modélisation d"un système éolien contrôlé par un régulateur de tension"" Revue des Energies Renouvelables CER"07 Oujda (2007) 41 – 45.

[6] Debta, Birendra Kumar and Mohanty, K.B., "Analysis on the effect of dynamic mutual inductance in voltage build up of a stand-alone brushless asynchronous generator", Procc. of National Power Electronics Conference, IIT Roorkee, June 2010.

[7] Mohamed barara Ahemd Abbou Mohammed Akherraz and abderrahim Bennasar,,"Modeling and Control Voltage of Wind Pumping Systems using a Self Excited Induction Generator,,,, International Journal on Electrical Engineering and Informatics - Volume 5, Number 2, June 2013

[8] Kai wan., Advancd current-mode control techniques for DC-DC Power electronic converter, PhD Thesis, MISSOURI UNIVERSITY OF SCIENCE & TECHNOLOGY ,2009

[9] Soltane BELAKEHAL ,Conception & Commande des Machines à Aimants Permanents Dédiées aux Energies Renouvelables,,PhD Thesis,UNIVERSITE DE CONSTANTINE

[10] T. Ouchbel *, S. Zouggar †, M. Seddik, M. Oukili et M. El Hafyani"" Régulation de la puissance d"une éolienne asynchroneà vitesse variable à l"aide d"un compensateur d"énergie réactive (SVC) Revue *des Energies Renouvelables Vol. 15 N°3 (2012) 439 – 450*

[11] Hanifi. Guldemir"" Study of Sliding Mode Control of Dc-Dc Buck Converter Energy and Power Engineering, 2011, 3, 401-406

[12] Sonam Singh, A.N Tiwari"" VOLTAGE AND FREQUENCY CONTROLLER FOR SELF EXCITED INDUCTION GENERATOR IN MICRO HYDRO POWER PLANT: REVIEW"" International Journal of Advanced Research in Electronics and Communication Engineering (IJARECE) Volume 2, Issue 2, February 2013

[13] B.BOSSOUFI, M.KARIM, S.IONITA, A.LAGRIOUI, "Low-Speed Sensorless Control of PMSM Motor drive Using a NONLINEAR Approach BACKSTEPPING Control: FPGA-Based Implementation" Journal of Theoretical and Applied Information Technology JATIT, pp154-166, Vol. 36 No.1, 29th February 2012.

[14] Tariq Riouch, Rachid El Bachtiri"" Robust Control of the Active and Reactive Power Exchanged With the Rotor of the DFIG and the Grid"" WSEAS TRANSACTIONS on ENVIRONMENT and DEVELOPMENT Issue 1, Volume 9, January 2013

[15] El -Sousy, F. F. M., Orabi, M., & Godah, H. (2006). Maximum Power Point TrackingControl Scheme for Grid Connected Variable Speed Wind Driven Self-Excited InductionGenerator. Journal of Power Electronics (JPE), 6(1), 52-66.

[16] Luc Moreau., modélisation, conception et commande de génératrices a reluctance variable basse vitesse, PhD Thesis, Université de Nantes France, 2005.

[17] L. Louze, A.L. Nemmour, A. Khezzar, M.E. Hacil and M. Boucherma"" Cascade sliding mode controller for self-excited induction generator "" Revue des Energies Renouvelables Vol. 12 N°4 (2009) 617 – 626.

[18] A.M. BOUZIDa, M. BENGHANEMb, B.HAMANEc,A.BELABBESd,M.BOUHAMIDAe,A.DRAO,," Current Control of the Isolated Self-Excited Inductio Generator using Shunt Active Filter"" Energy Procedia 18 (2012) 349 – 358.

Efficient Answering of XML Queries using Holistic Twig Pattern Matching

Divya Rajagopal and Dr. Miraclin Joyce Pamila J. C.

***Abstract*—**XML is used as a standard for expressing semi structured data, a form of data that does not conform to the formal structure of relational data models but nonetheless contains tags to separate semantic elements and enforce hierarchies of records and fields within the data. Semi structured data model allows information from several sources with related but different properties to be integrated, thereby enabling sharing of information. Improving the efficiency of answering the queries issued on such data is therefore a great challenge. Twig pattern matching is a critical operation for XML query answering and holistic approaches have shown superior performance over other methods. In this paper, we propose a novel holistic twig pattern matching algorithm which performs optimal matching for twigs with both AD (Ancestor Descendent) edges as well as PC (Parent Child) edges, while prior algorithms claim optimality for twigs with only AD edges.

***Keywords*—**ancestor-descendant, holistic, parent-child, XML

I. INTRODUCTION

An XML document consists of data enclosed within a set of user-defined tags. The tags should be properly nested, they should be paired, and there should be one and only one root tag and so on. XML offers simplicity, flexibility, standardization and interoperability. Hence XML is being widely used as a data representation format for representing nearly all kinds of data. However XML documents are often very large and have a deeply nested structure. And also the XML data can be very complex. Hence efficient pattern matching algorithms are needed to retrieve the data from the XML documents by answering the queries given on the documents.

A query on the XML document describes a tree-shaped or hierarchical search pattern, which is often referred to as a twig pattern [2]. XML queries are thus called tree queries or twigs and the relationships (AD or PC) between the components of the twig are represented as edges. Single backslash (/) is used to represent a parent-child edge or PC edge. When / is used at the beginning of a query, for example /book, it will define an absolute path to node "book" relative to the root. In this case, it will only find "book" nodes at the root of the XML tree. When / is used in the middle of a query, for e.g. /book/author, it will define a path to node "author" that is a direct descendant (i.e. a child) of node "book". Double backslash (//) is used to represent an ancestor-descendant edge or AD edge. When // is used at the beginning of a query, for example //book, it will define a path to node "book" anywhere within the XML document. In this case, it will find "book" nodes located at any depth within the XML tree. When // is used in the middle of a query, for e.g. /book//author, it will define a path to node "author" that is any descendant of node "book".

The core operation of XML query answering is twig pattern matching: finding in an XML document tree ‘D’, all matches of a given tree-type query ‘Q’ called twig. A match is identified by a mapping from nodes in ‘Q’ to nodes in ‘D’ such that query node predicates are satisfied by the corresponding document tree nodes and also the structural relationships (AD or PC) between query nodes are satisfied by the corresponding document tree nodes.

The answer to query ‘Q’ with ‘n’ nodes can be represented as an n-ary relation where each tuple (d1,…,dn) consists of the document tree nodes that identify a distinct match of ‘Q’ in ‘D’.

Holistic twig pattern matching approaches avoid large sets of irrelevant intermediate results by considering the structural inter-dependencies among the XML elements. Holistic approaches optimize pattern matching in two phases:

1. Labeling: assigning to each node x in the data tree t, an integer label label(x) that captures the structure of t.
2. Computing: exploiting the labels to match a twig pattern p against t without traversing t again.

In this paper, we propose a novel holistic twig pattern matching algorithm which performs optimal matching [2] for twigs with both AD (Ancestor-Descendent) edges as well as PC (Parent-Child) edges.

II. EXISTING SYSTEMS

TwigStack [2] is a holistic twig join algorithm that ensures that no large intermediate results are produced. When the query has only ancestor-descendant relationships between the elements, TwigStack is I/O and CPU optimal but it is suboptimal when the query has parent-child relationship among the elements. It is suboptimal as the overall computation cost for a twig pattern is proportional not just to the sizes of the input and the final output but also to the sizes of the intermediate results. GTwigMerge [3], a basic framework for holistic processing of AND/OR-twigs works correctly when AND/OR twig queries contain parent-child QNodes. However, the optimality in terms of worst-case I/O and CPU cost is no longer guaranteed. There are two reasons for the sub-optimality. First, if some output nodes are parent-child QNodes, a path solution may turn out not to join with any other path solutions. Thus, irrelevant I/O access is caused. Second, if some OR-predicates in an AND/OR-twig contain

parent-child QNodes, a path solution may contain an element node that eventually turns out not to satisfy all its OR-predicates. TwigStackList [4] is another holistic twig join algorithm which is I/O optimal for queries with only ancestor-descendant relationships below branching nodes. The optimality cannot be proved for the case where parent-child relationships appear only in edges below non-branching nodes. TwigStackList¬ [5] is a new algorithm to match NOT-twig queries holistically. In a NOT-twig, this algorithm can guarantee the I/O optimality only when all the positive edges below branching nodes are ancestor-descendant relationships.

III. TREE REPRESENTATION OF XML AND TWIG

As the XML and the twig are hierarchical, they are represented using a tree data structure. A sample XML tree representation is shown in Fig. 1. Each node in the tree corresponds to an XML element. The root node corresponds to the root element, the intermediate nodes to sub elements, the leaf node to values. Each edge corresponds to an element-sub element or element-value relationship.Each non-leaf node in the XML tree can have multiple, variable number of children. Hence instead of a linked list implementation of the tree, a more optimized tree representation (shown in Fig. 2) is used. In this representation, each non-leaf node has two pointers: a pointer to the first child and a pointer to the next sibling. The optimized XML tree representation of the tree used in Fig. 1 is demonstrated in Fig. 3. Because each node has at most only two children, the new tree is a binary representation of the previous tree.

The twig considered in this paper is a plain twig which contains only a single path from root to leaf. Sample query trees are shown in Fig. 4. Every node in the twig, called a QNode or query node, associates to an element type or tag name in a tree database. For programmatic purposes, a QNode records its location step axis or edge type as either "//" or "/" for edge test, and a tag name for node test. Therefore, the content of a QNode takes the general format of "/tag" or "//tag."

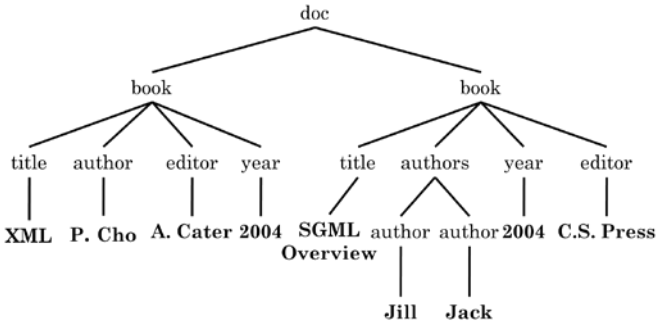

Fig. 1. Representation of XML tree

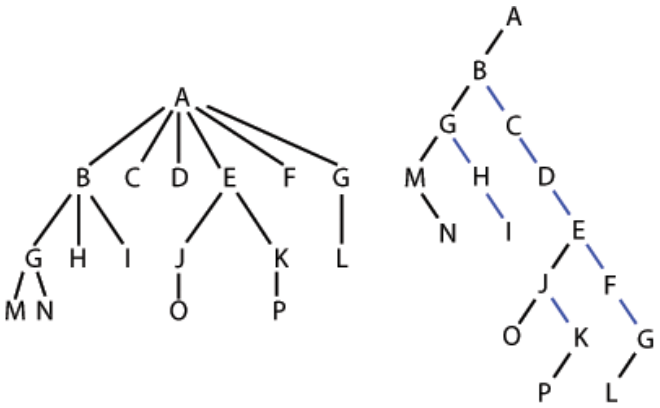

Fig. 2. Data structure for XML tree representation

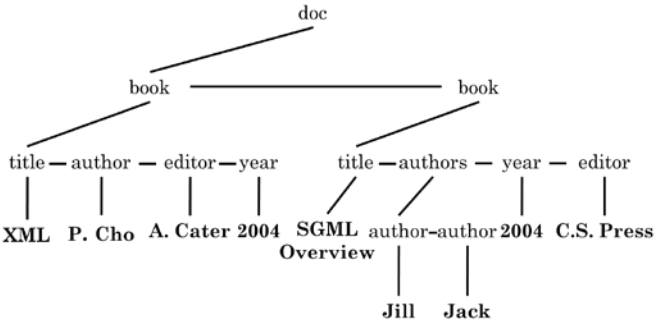

Fig. 3. Optimized representation of XML tree

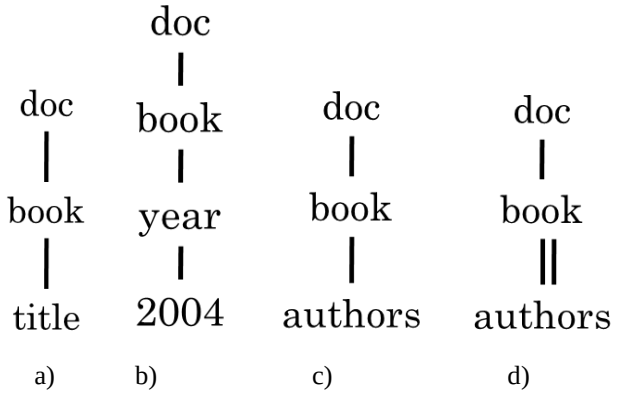

Fig. 4. Representation of XML query trees

IV. XML TREE LABELING

The aim of data tree labeling schemes is to determine the relationship (i.e., Parent-Child or Ancestor-Descendant) between two nodes of a tree from their labels alone. Each node in the XML tree is given a unique identity called label or region code. In this paper, the triplet region encoding scheme which is obtained through pre-order traversal of the document tree is used. Each label consists of three parts: start position, end position, level. The encoded version of the XML tree shown in Fig. 1 is shown in Fig. 5.

ISBN: 978-1-61804-228-6

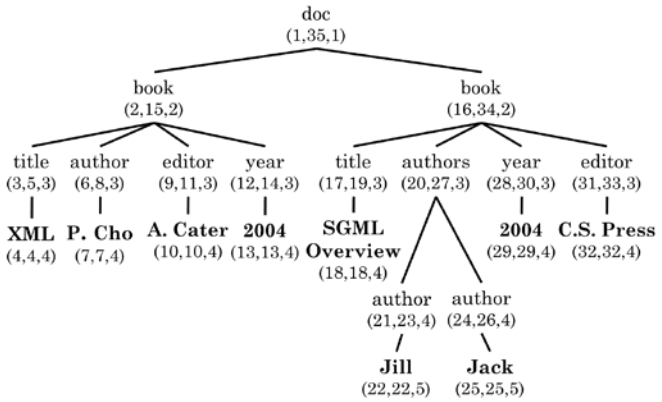

Fig. 5. Encoded XML tree representation

The relative positional information obtained is as follows: Let x and x' be two nodes labeled (S, E, L) and (S', E', L'), respectively. Then,

- x' is a descendant of x if and only if S' > S and E > E'. Thus the edge between x and x' represents an ancestor-descendant edge.
- x' is a child of x if and only if S' > S and E > E' and L'=L+1. Thus the edge between x and x' represents a parent-child edge.

V. TWIG PATTERN MATCHING MAIN ALGORITHMS

Fig. 6 presents the main algorithm "TwigMerge" of the second phase called the computing phase of the proposed twig pattern matching process. TwigMerge uses the labels to compute the answers to the twig. All the supporting functions are as described in [1].

```
ALGORITHM TwigMerge(root)
1: while not end(root) do
2:    q = GetQNode(root);
3:  if q == null then
4:     continue;
5:  if not isRoot(q) then
6:        cleanStack(S_QParent(q),C_q);
7:    cleanStack(S_q, C_q);
8: if isRoot(q) or (not empty(S_QParent(q))) then
9:       if not isLeaf(q) then
10:          push(S_q, C_q,isRoot(q)? -1 : top(S_QParent(q)));
11:      else
12:          outputPathSolutions(C_q);
13:   C_q ->advance();
14: end while
```

Fig. 6. TwigMerge holistic twig pattern matching algorithm

Some important features of TwigMerge are highlighted as follows:

1. TwigMerge receives (from GetQNode shown in Fig. 7) either a valid QNode q or an invalid QNode, denoted by null (the validness is checked at line 3). An invalid QNode is generated when a non-top level recursive call into this function fails to find a QNode associated with a fully qualified element. But since noncontributing elements have been skipped, the main algorithm quick jumps to its next iteration (at line 4) to start a new call to GetQNode for getting the next valid QNode.
2. No stacks are allocated for non-output QNodes nor for any leaves since the contributing elements which correspond to the leaf can be directly grabbed from the associated stream.
3. All critical processing logics are encapsulated in the key supporting function, GetQNode and other lower level supporting functions edgeTest and hasExtension. In addition to feeding the main algorithm with the next query node to be processed, GetQNode also checks the candidacy of the elements in the input streams and guarantees that for the next QNode returned to the main algorithm the current element in the associated stream is fully qualified. Therefore, TwigMerge achieves both I/O and CPU optimality not only with AD edges but also with PC edges.
4. "Stack cleaning" (lines 6 and 7) is needed in TwigMerge solely because each time after outputting path solutions, some elements on the stacks may become irrelevant for future path solutions and must be cleaned out. In most prior algorithms such as TwigStack, stack cleaning is required to get rid of those noncontributing elements that may have been tentatively added to the stacks but are actually noncontributing.
5. TwigMerge moves the element associated to q from stream to stack if it is not a leaf (at lines 8 to 10), otherwise (q is a leaf) outputs the path solutions currently on the stacks (lines 9 and 10).

Another critical supporting function, hasExtension (refer Fig. 8), implements our definition of a match for a twig. It helps in ensuring that only relevant contributing nodes are taken for processing. For leaf nodes, it performs edgeTest to confirm the relevancy with respect to edge-type (AD or PC) and for non-leaf nodes, it performs testing of further extensions.

```
FUNCTION GetQNode(q)
1: if isLeaf(q) then
2:    return q;

3: for each q_i ∈ Qchildren(q) do
4:    q_0 = GetQNode(q_i);
5:  if q_0 != q_i then
6:       return q_0;
7: end for
8: q_max = getMaxQChild(q);
9: while C_q ->end < C_qmax ->start do
10:  C_q ->advance();
11: end while

12: q_min = argmin_qi { C_qi ->start}, q_i ∈ Qchildren(q);
13: while C_q ->start < C_qmin ->start do
14:  if hasExtension(q) then
```

```
15:      return q;
16:   else
17:      Cq ->advance();
18: end while
19: if hasExtension(qmin) then
20:      return qmin;
21:   else
22:      Cqmin ->advance();
23. if end(q) then
24:   return null;
25: else
26:   return GetQNode(q);
```

Fig. 7. Pseudocode for GetQNode function

```
FUNCTION hasExtension(q)

1: for each qi ∈ children(q) do
2:    if isLeaf(qi) then
3:       return edgeTest(Cq, qi)
4:    else
5:       return (edgeTest(Cq, qi) and hasExtension(qi))
6: end for
```

Fig. 8. Pseudocode for hasExtension function

The function edgeTest is presented in Fig. 9. The while loop (at lines 8 and 9) brings an important optimization: fast skipping noncontributing elements in stream T_q until the cursor moves over the range of the parent element e. Holistic twig joins typically disallow backtracking of stream cursors to guarantee linear time complexity.

```
FUNCTION edgeTest(e,q)
1: while not end(Cq) do
2:    if e.start < Cq ->start and e.end > Cq ->end then
3:       if q.edgeType == '//' then
4:          return true
5:    else if e.level == Cq ->level-1 then
7:       return true
8: if Cq ->end < e.end then
9:       Cq ->advance()
10:   else
11:      break
12: end while
13: return false
```

Fig. 9. Pseudocode for edgeTest function

VI. COMPLEXITY OF TWIGMERGE

Given a twig query Q, the parameters used are:

- |Input| stands for the total size of all the input streams relevant to query Q
- |Output| stands for the total count of the data elements included in all output twig instances produced for query Q

The I/O cost of TwigMerge consists of three parts: the I/O cost for accessing all the relevant input stream elements and the I/O cost for dealing with the intermediate path solutions plus the I/O cost for outputting the final twig solutions. Since in TwigMerge, the stream cursors are always advanced and never backtracked, the first part of the I/O cost is the total size of all relevant input streams. For the second part, since TwigMerge is optimal with both AD and PC edges—i.e., it never produces useless intermediate path solutions, the I/O cost of this part is two times (for first output and then input) of the total final output size, i.e., 2 * |Output|. And the third part (for outputting the final results), of course, is |Output|. The total I/O cost for TwigMerge is the sum of the above three parts = |Input| + 3 * |Output|

The CPU cost analysis for TwigMerge is analogous. The CPU cost also consists of three parts. The first part is the time spent on computing the path solutions, the second part is the time spent on dealing with the obtained intermediate path solutions (output, input, and merging), and the third part is on outputting the final twig solutions. The main structure of TwigMerge is a loop that repeats no more than |Input| times, which is the total number of elements in all the input streams because noncontributing elements are skipped at line 10, 17, and 22 of GetQNode (refer Fig. 7) or by the optimization rendered by the primitive function edgeTest (refer Fig. 9). So the first part of the CPU cost is linear to the input size. The second part depends on how many intermediate path solutions are produced and how many of them are going to be merged to form the final output twig solutions. As TwigMerge does not produce any unused intermediate path solutions (it actually does not push any noncontributing elements onto any stack), the second part of the cost is linear to and solely decided by the output size |Output|. And the third part of course is also linear to the output size. Added together, for the overall CPU cost of TwigMerge, exactly the same result as that derived for the I/O cost is obtained (cost equations omitted). The above cost analysis results shows that TwigMerge has both optimal I/O cost and optimal CPU cost for twigs with both AD and PC edges.

VII. RESULTS

To avoid potential bias of using a single data set, two XML data sets are used for this study. The first is a docBook data set which contains the details of various books. The second data set is the TreeBank data set, downloaded from the University of Washington XML Repository website [6]. The XML document of the TreeBank data set is deep and has many recursions in structure. This data set takes 82 MB memory, consisting of 2.4 million data nodes. The average depth of TreeBank is 7.8 and the max depth is 36. Fig. 10 shows the parsing of docBook XML document, construction of the XML tree. The number of leaf nodes, non-leaf nodes, total number of nodes and maximum depth are also shown. The twig results for the queries on the docBook XML Document are shown in Fig. 11, Fig. 12. The twigs contain combinations of ancestor-descendant and parent-child edges. The corresponding execution time (in milliseconds) is also displayed. Fig. 13 shows the parsing of treebank XML document, construction of and labelling of the XML tree. The number of leaf nodes, non-leaf nodes, total number of nodes and maximum depth are also shown. The twig results for the query on the treebank XML Document is shown in Fig. 14. The twig contains an ancestor-

descendant edge. The corresponding execution time (in milliseconds) is found to be 10395.

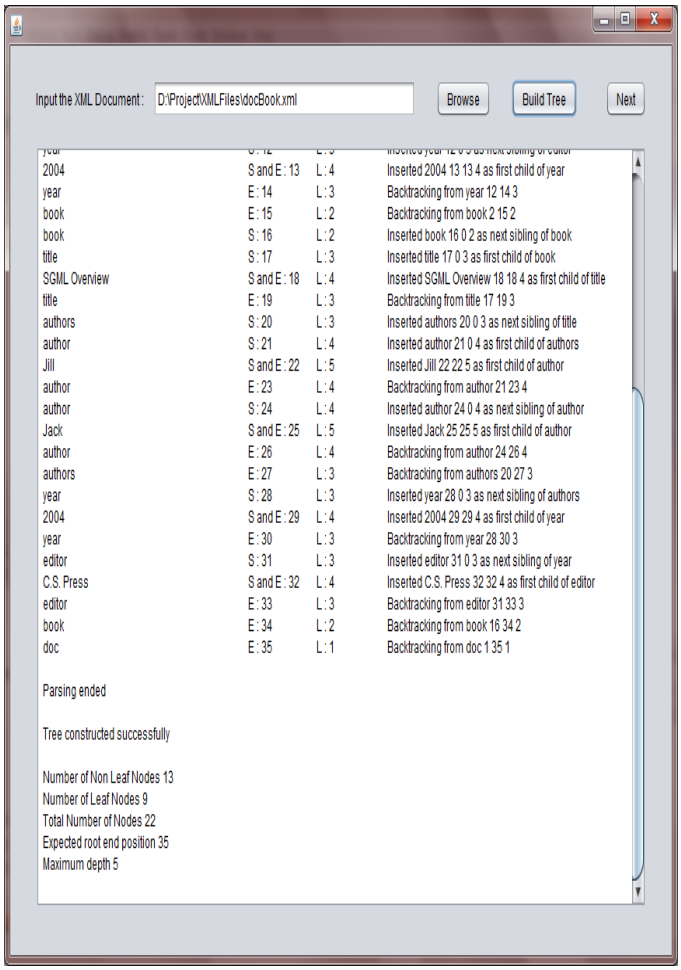

Fig. 10. Document tree for docBook.xml

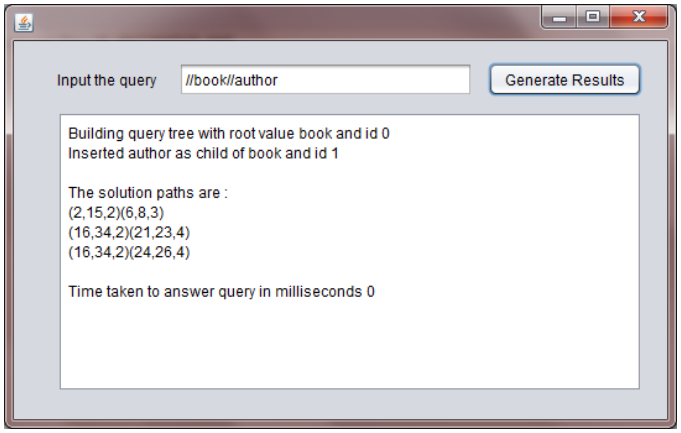

Fig. 11. Twig Results of //book//author

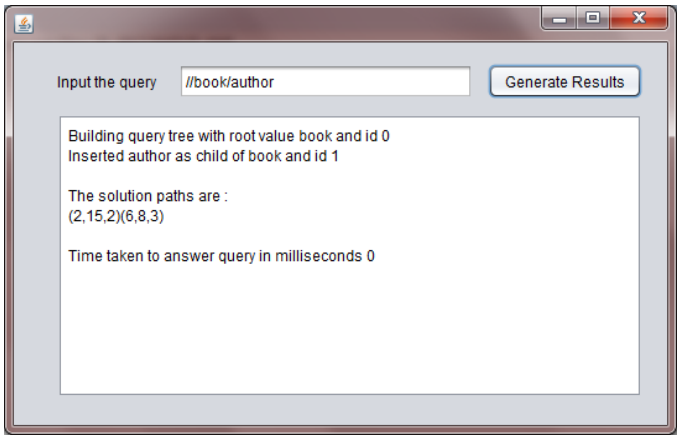

Fig. 12. Twig Results of //book/author

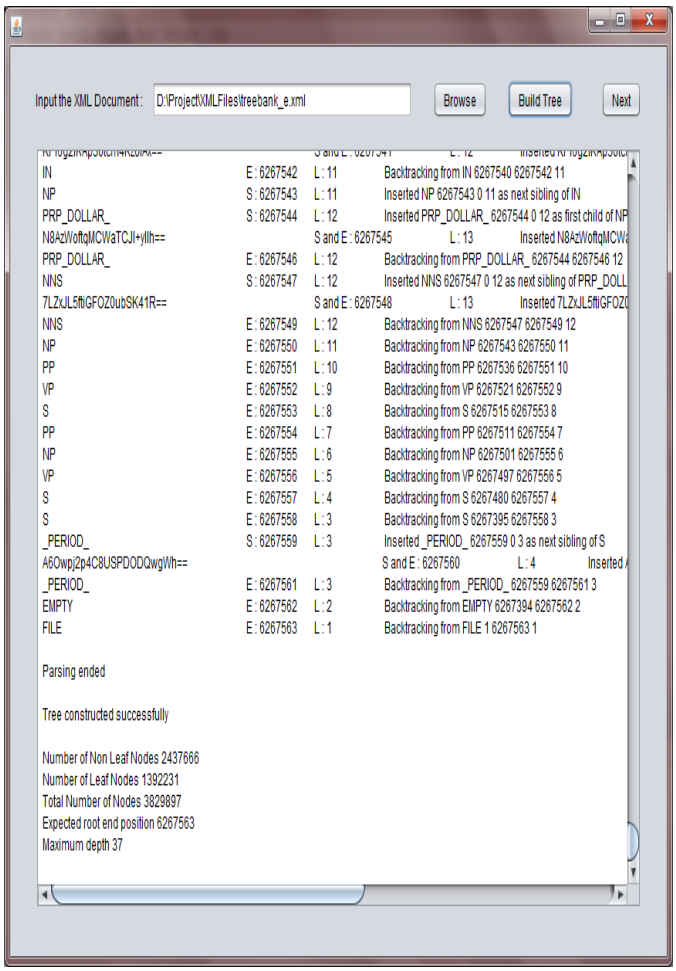

Fig. 13. Document tree for treebank_e.xml

ISBN: 978-1-61804-228-6

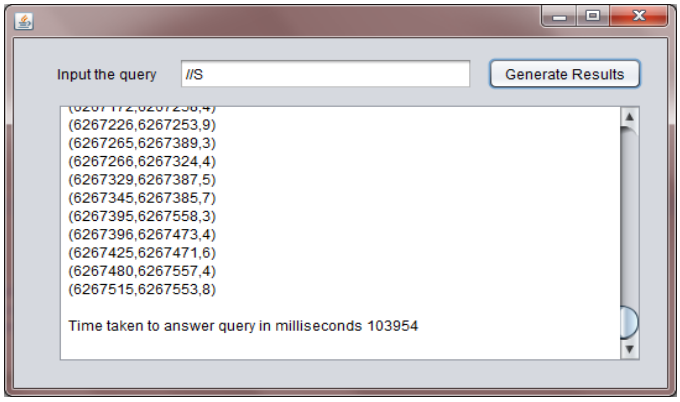

Fig. 14. Twig Results of //S

VIII. CONCLUSION

Holistic twig joins are critical operations for XML queries. In this paper, a novel approach for holistic computing of twig patterns using an algorithm called TwigMerge, which gracefully extends the I/O and CPU optimality to twigs with AD as well as PC edges, was presented. Analytical study was performed with regard to the validity and performance of the approach and its accompanying algorithms, and concluded with optimal I/O and optimal CPU on twigs with arbitrary AD and/or PC edges. This work supports only plain twigs which have only query nodes. As future work, the approach can be extended to boolean twigs or Btwigs i.e. twigs which support any arbitrary combination of AND/OR/NOT boolean predicates as well.

REFERENCES

[1] D. Che, T.W. Ling, W.C. Hou, "Holistic Boolean-Twig Pattern Matching for Efficient XML Query Processing", *IEEE Transactions on Knowledge and Data Engineering*, vol. 24, no. 11, pp. 2008-2024, Nov. 2012.

[2] N. Bruno, N. Koudas, and D. Srivastava, "Holistic Twig Joins: Optimal XML Pattern Matching", Proc. ACM SIGMOD International Conference on Management of Data (SIGMOD' 02), pp. 310-321, June 2002.

[3] H. Jiang, H. Lu, W. Wang, "Efficient Processing of Twig Queries with OR-Predicates", Proc. ACM SIGMOD Int'l Conf. Management of Data (SIGMOD' 04), pp. 59-70, 2004.

[4] J. Lu, T. Chen, and T.W. Ling, "Efficient Processing of XML Twig Patterns with Parent Child Edges: A Look-ahead Approach", Proc. 13th ACM Int'l Conf. Information and Knowledge Management (CIKM' 04), pp. 533-542, Nov. 2004.

[5] T. Yu, T.W. Ling, and J. Lu, "twigstacklist¬: A Holistic Twig Join Algorithm for Twig Query with Not-Predicates on XML Data", Proc. 11th Int'l Conf. Database Systems for Advanced Applications (DASFAA' 06), pp. 249-263, 2006.

[6] Univ. of Washington XML Repository, http: //www.cs.washington.edu / research/xmldata sets/, 2012.

Divya Rajagopal completed her Bachelor's degree in Computer Science and Engineering from Amrita School of Engineering, Amrita Vishwa Vidyapeetham University, Coimbatore, Tamilnadu, India. She completed a 4-month internship with Infosys Ltd. and worked for a year as Systems Engineer in the Education and Research (E&R) department of Infosys Ltd., Mysore, India. She is currently pursuing her Master's degree in Computer Science and Engineering from Government College of Technology, Coimbatore, Tamilnadu, India.

Dr. Miraclin Joyce Pamila J.C. is an Assistant Professor (Senior Grade) in the Department of Computer Science and Engineering, Government College of Technology, Coimbatore, Tamilnadu, India. She received her Master and Doctoral degree in Computer Science and Engineering from Anna University, Chennai, India. Her fields of interest include Mobile Computing, Data Management Systems, Network Security and Recovery system design for mobile networks. She is a life member of ISTE. She teaches and guides courses at both B.E. and M.E. levels in Computer Science and Information Technology. She has published 30 technical papers in national and international conferences and journals.

Code Optimization and Performance Analysis of Oceanographic Software Package NEMO for GPGPU Systems

Plamenka Borovska, Desislava Ivanova

***Abstract*—** The paper presents our experience in code optimization and performance analysis of software package NEMO on hybrid parallel computer systems with accelerators. NEMO Ocean is a software package for oceanology, simulating ocean gyres and sea-ice models. Code optimization and performance analysis are performed for the case study of NEMO ORCA2_LIM configuration. All experiments are conducted on a heterogeneous IBM Blade Center comprising Blade Servers and NVidia Tesla M2075 accelerators. The parallel software for oceanology NEMO has been optimized for GPGPU systems. For this purpose an optimization has been implemented and verified. The experimental results show that the optimized NEMO code provides considerably better performance than the original code.

***Keywords*—** High-Performance Computing, Graphical Processing Accelerators, Parallel Code Optimization, NEMO Ocean software, Parallel Performance Analysis

I. Introduction

Parallel systems with general purpose graphical processing units (GPGPU) or also known like hybrid parallel systems are designed by standard central processing units (CPU) and graphical processing units (GPU). The reason for develop such a system is that the current CPUs can't provide higher computing capabilities on the same level of energy consumption. There is also a need of chip to provide thousands of parallel operations per cycle or to provide lots of operations per core [1, 3, 5].

We are in the era of parallel systems with new architectures designs. Huge amount of software for the conventional HPC systems is started to be rewritten for graphical processors. The hybrid systems provide greater computing power over less consumed energy and make plausible to calculate with greater precision and speed. This is thanks to the better consistency of the graphical chip for computing and the optimized energy consumption. Thus we can tell that the future for the HPC systems, for the moment, is pointed to the hybrid systems with accelerators [1, 2].

Apart of the high computing capabilities these systems provide small energy consumption, but there are some challenges: it is needed a special programming language and compilers. This makes the traditional programming languages like C and FORTRAN useless for porting on graphical devices. There are compilers which provide such a function. The compilers are not free and sometimes they don't provide the expected optimization. From one side the optimization of the code is depending on how good the parallel code is written – how often there is communication between the CPUs and what amount of data is exchanged. From the other side the optimization depend from the time for allocating, initializing, freeing and copying the data to and from the GPU.

There is a problem with the free compilers for FORTRAN, because the compilers support optimization just for C and C++ programming languages. This makes us to rewrite the most time consumption functions for implementation on GPU devices. This work required to use wrappers and interfaces for calling these functions in FORTRAN and back.

II. Comparison Analysis of Hybrid Computer Systems with GPUs

The need of highly performance calculations grow in many different fields of science, medicine, engineering and finances. NVidia continues with their innovations so they can keep up and develop incredibly powerful GPU architectures. The existing NVidia GPUs with Fermi architecture already predefined and accelerate the capabilities of the modern high-performance computer systems in fields like processing data from seismic activity, biochemical simulations, modeling the weather and climate, dynamic of the fluids and analyzing of huge amounts of data [3, 4, 5].

Table 1 Comparing GPU and CPU capabilities

	Nvidia Fermi	AMD Magny-Cours
Cores	448	12
Operations/cycle	1	4
Double Precision	515 GFlops	101 GFlops
Bandwidth	144 GB/s	27,5 GB/s

This work was supported by the scientific project DCVP02/1, Ministry of Education and Science, Bulgaria.

P. Borovska is a Head of Computer Systems Department, Technical University of Sofia, 1000 Sofia, Bulgaria, Kl. Ohridski 8, bl. 1, office 1201 phone: +359 2965 25 24; e-mail: pborovska@tu-sofia.bg.

D. Ivanova is an Assist. Prof. at the Computer Systems Department, Technical University of Sofia, 1000 Sofia, Bulgaria, 1000 Sofia, Bulgaria, Kl. Ohridski 8, bl. 1, office 1205 phone: +359 2965 22 24; e-mail: d_ivanova@tu-sofia.bg.

The performance of the GPU is five times greater than the CPU, Table 1. The performance of the software application depends from the computer system, i.e. how good it is implemented for a given architecture.

The Kepler GPU architecture give us performance of 1 TFlop in double precision, which is with 80% better and with 60% to 65% greater performance compared with Fermi architecture. The energy consumption is better and gives up to three times better performance per watt compared with Fermi. This is due to the better utilizing of the chip and integrating some innovations like [2, 3, 5]:

- Dynamic parallelism dives the capability of the GPU to generate work for itself, synchronize results and control the workflow with hardware pipelines without the interruption of the CPU. This gives flexibility for adapting to the amount of data and size of the parallel task during application runtime.

- Hyper-Q gives the opportunity on one GPU to be started several blocks of threads simultaneously. The Hyper-Q increases the connections with host code and the GPU device and due to the number of CUDA streams, number of MPI (Message Passing Interface) tasks or even multiple threads from a single task can port to the CUDA device is increased.

- Grid management unit imports the dynamical parallelism. The grid management unit controls the grids (blocks of threads), which will be computed on the GPU device. This unit can interrupt the creation of new grids, queue them or cancel them, until they are ready to be executed. This way of parallelism has flexibility.

III. NEMO Ocean Software Package and Code Optimization

NEMO Ocean is a software package for oceanology, simulating ocean gyres and ice masses, weather broadcast and others. NEMO is open source software and it is available in some main configurations [6, 9]:

- Ocean dynamics – NEMO-OPA;
- Sea-ice model and thermodynamics – NEMO-LIM;
- Biogeochemistry – NEMO-TOP;

NEMO Ocean consists from 1613 file with an average length of 300 lines, which are around 400 thousands lines of code. The software is written in FORTRAN 90/95 which makes it difficult for optimization on GPU devices, because not every device support it, and give us too little freedom and flexibility like modern programming languages [7, 8].

These limit us to use one of the possibilities:

- ✓ Rewrite the code, so it can be executed on GPU devices – as the amount of code is too huge as mentioned earlier and it will cost a lot of time for one person to do it, this option is not suitable;
- ✓ Use compilers, which support porting FORTRAN to GPU devices – these compilers are not cheap; the license is about $3000 - $4000 per year. Also they don't always give the expected optimization, so this opportunity is not suitable too;
- ✓ Use interfaces and wrappers for calling functions written to execute on GPU devices and functions in FORTRAN – this option is modification on the first option with the difference, that it will be needed to rewrite only the time-consuming functions and write some interfaces for connecting them with the FORTRAN code. The disadvantage of this method is the transition from FORTRAN to C/C++ or CUDA C and linking the object files in executable file.

This paper discusses the last option – using interfaces and wrappers. The experimental framework consists of NEMO Ocean configuration ORCA2_LIM, which provides 200 MB, input raw data in 32 files and hardware platform heterogeneous IBM Blade Center located at Computer Systems Department, Technical University of Sofia.

Additional software and libraries required:

- CUDA tool chain version 5.0;
- HDF5 library version 1.8.9;
- NetCDF library version 4.1.3;
- Zlib library version 1.2.7;
- Szip library version 2.1 (optional);
- MPI compilers and libraries;
- PDToolkit version 3.18.1;
- Papi library version 5.1.0;
- And TAU profiling tool.

Code optimization requires pre-processing work connecting to determine the most time consuming functions for the current test environment. This is done by using Tuning and Analysis Utilities (TAU) profiling tool, Fig. 1.

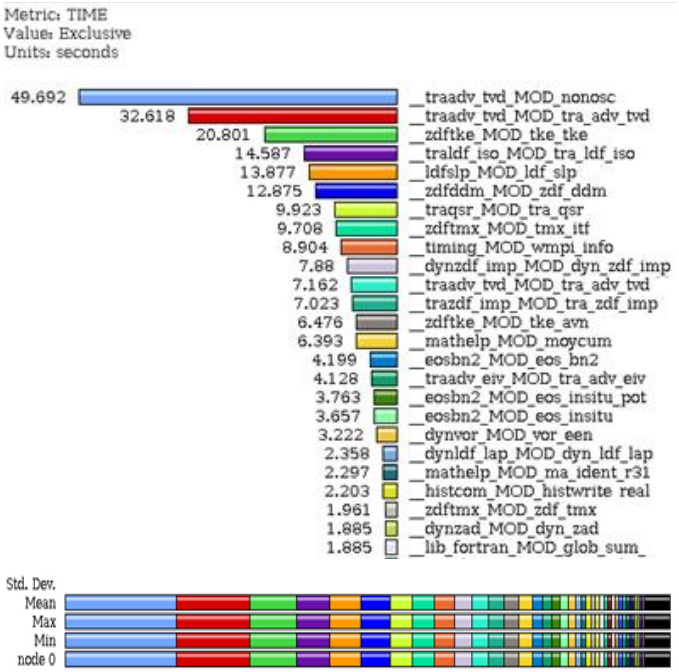

Fig. 1 GUI of TAU profiling tool

TAU software is used in high-performance computer systems for dynamic code analysis of parallel applications during runtime. It gives the opportunity to see which functions of the program are the most time consuming and need optimization.

TAU software is a portable profiling and tracing toolkit for performance analysis of parallel programs written in FORTRAN, C, C++, UPC, Java and Python. TAU profiling

tool gives the opportunity to analyze code which is executed on CUDA (NVidia GPUs) [10].

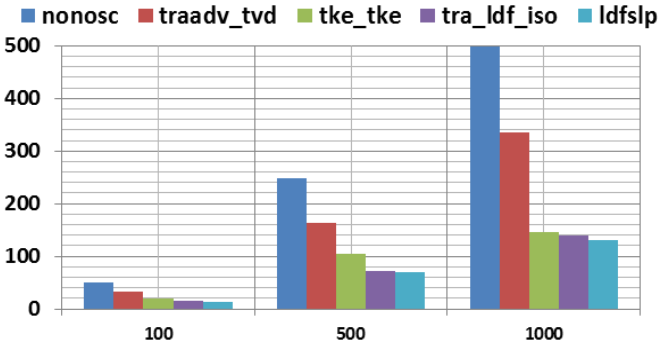

Fig. 2 Average execution time of the time consuming functions with different load.

The results of executed simulations for different load (number of iteration steps) are presented on Fig. 2. These results give better perspective of that which functions need optimization. As it is seen, the most time consuming functions are *nonosc* and *traadv_tvd*, which can be found in the module *file traadv_tvd.F90*. The curve of the execution time of the simulations in the chart also follows the changes in the average execution time of these functions, Fig. 3.

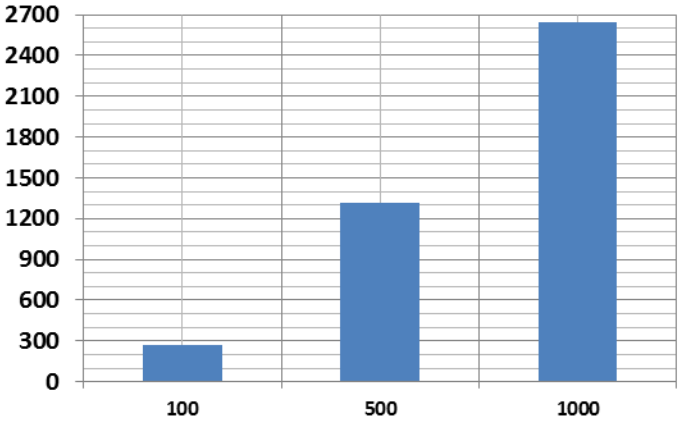

Fig. 3 Total simulation execution time for various workloads

The simulation results of the most time consumption functions show some requirement which must be taken into consideration for writing interfaces for FORTRAN and C/C++ or CUDA C and vice versa:

- The transition variables must be pointers, no matter their type;
- Defining wrappers and interfaces for calling functions in C/C++ functions from FORTRAN and opposite;
- During the transition of arrays (one-, two-, three- or N-dimensional) or dynamically allocated memory, it must be transited a variable for each of their dimension;
- N-dimensional arrays in Fortran are passed as one-dimensional in C/C++ or CUDA C;
- The starting index of arrays in FORTRAN is 1, but in C/C++ or CUDA C – 0.

Thus NEMO Ocean is composed from FORTRAN module files, for declaration the interfaces, which will be used for calling C/C++ or CUDA C functions. The following example module file can be used:

```
Module nemo_cuda
Use par_kind
Use iso_c_binding

Implicit None

Public <interface_to_function>, <interface_to_function2>

Interface <interface_to_function>
   Module Procedure <function_name>
End Interface <interface_to_function>

Interface <interface_to_function2>
   Module Procedure <function_name2>
End Interface <interface_to_function2>

Contains
   Subroutine <function_name> (<parameters>) bind(c)
   ! Declarating parameters
   End Subroutine <function_name>

   Subroutine <function_name2> (<parameters2>) bind(c)
   ! Declarating parameters
   End Subroutine <function_name2>
End Module nemo_cuda
```

The first and last row declare the beginning (Module <name_of_module>) and the ending (End Module <name_of_module>) of the module file, the declaration of functions (subroutines) and interfaces. After these are included additional module files (Use <name_of_module_file>): park_kind – containing information about the size of the type REAL in FORTRAN, single or double precision; iso_c_binding – contains procedures and directive for binding FORTRAN ran with C (includes the bind(c) directive). With the phrase Implicit None, we show that the variables which will be used in the current file must be decelerated. If this phrase is not included, all variables will be considered as new and will be initialized with default types and values.

Using the word Public it is tell which functions and interfaces will be available in other module files and could be used. These are the interfaces for connecting with C functions. Next are defined the interfaces separately and showing which function to be call when an interface is called for execution. There could be more than one function to be call from one interface, but the functions (subroutines) have to be different from each-other by at least one variable.

The last thing is the declaration of the prototypes of the C/C++/CUDA C functions. This is done after the word Contains which shows the functions and subroutines contained in the module file.

ISBN: 978-1-61804-228-6

After defining module for the interfaces, there is need to define wrappers for calling FORTRAN functions from C/C++ or CUDA C code. The following module file is responsible for defining wrappers:

```
Module nemo_f_wrappers
Use<module_files_with_needed_functions>
Use par_kind
Use iso_c_binding

Contains
   Subroutine <wrapper_function1> (<parameters3>)
bind(c)
   ! Declarating parameters
   ! Additional Fortran code (if needed)
   Call<function_from_module_file1>(<parameters4>)
   End Subroutine <wrapper_function1>
End Module nemo_f_wrappers
```

There no new things compared with the previous module file except that it is needed to include the module files (Use<module_files>) which contains the functions called from the wrapper functions (subroutines) (Call <function_from_module_file>).

The next step is code optimization for the accelerators. First of all in a C/C++ header file must be defined a preprocessor directive like this:

```
#ifdef DOUBLE_PRECISION
#define real double
#else
#define real float
#endif
```

In this way when compiling the code for double precision calculations will be needed to make changes in the FORTRAN module file *par_kind* (for changing the size of FORTRAN REAL type) and use the option *–DDOUBLE_PRECISION* for compiling the code for the graphical device. In the same header file, there is need to define prototypes of the FORTRAN wrappers, which is defined earlier:

```
extern "C" void <wrapper_function1> (<parameters3>);
```

After defining all prototypes for all the wrappers and/or macros for save memory allocation or functions call, it is time to peak in writing the code for the graphical device. In this section is described how to write a function allocating and freeing memory on the GPU and computing function on it.

```
__global__ void gpu_kernel1(<size_params>,
<gpu_params>){
   Int tid= blockIdx.y*size_param2*size_param3 +
blockIdx.x*size_param3 + threadIdx.x;

gpu_param3[tid] = gpu_param2[tid] +
   +gpu_param1[tid];
// Other calculations
}

extern "C" void <function_name> (<cpu_parameters>){
// Declaration of local variables
// Declaration of GPU variables (gpu_param)

// Allocating and uploading data to GPU
cudaMalloc(&gpu_param1, size1);
   cudaMemcpy( gpu_param1,
         cpu_param1, size1,
         cudaMemcpyHostToDevice);
// Uploading the rest of the variables

// Calling function for
// computing on the GPU
dim3 blockGrid(size_param1, size_param2);
dim3 threadsperBlock(size_param3, 1);
gpu_kernel1 <<blockGrid, threadsperBlock>>
(<size_params>, <gpu_parameters>);

// After execution download calculated data
cudaMemcpy( cpu_param1,
      gpu_param1, size1,
      cudaMemcpyDeviceToHost);
// Freeing variables allocated on the GPU
cudaFree(gpu_param1);
}
```

First it is needed to define all functions, which will be executed on the graphical unit *(gpu_kernel1, gpu_kernel2, … , gpu_kernelN)*, and to use the attribute __global__, which gives the opportunity to call these function from the host (CPU) and execute them on the device (GPU).

Second using similar declarations (as same as defining the wrapper function prototypes in the header file), we will define the functions, which will use the interfaces defined in FORTRAN module files. Moreover, declarations of the local host variables and the variables for the GPU are required. Finally we need to execute the code on the GPU.

The amount of code (in rows) which is optimized on CUDA C and the number of rows of FORTRAN NEMO code is shown in Fig.4.

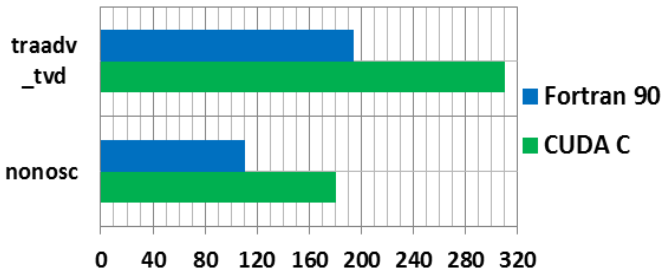

Fig. 4 Comparison of the amount of the original code and optimized functions for GPU execution

The simulation results and performance analysis of the NEMO code will be presented in the next section.

ISBN: 978-1-61804-228-6

IV. Simulation Results and Performance Analysis

The simulation experiments are conducted for NEMO ORCA2_LIM configuration. The input package of data for this configuration is 200MB and the output data is around 600 MB after structuring and post processing. The NEMO ORCA2_LIM configuration needs about 10 minutes to complete on HPC system with 32 cores or four to five hours on single core (for 5745 simulation steps).

Once again TAU profiling tool is used in addition to obtain good results and perform analysis. First we have tested an experimental unimproved MPI version coming with the original NEMO code and then make some tests with the optimized code for graphical units.

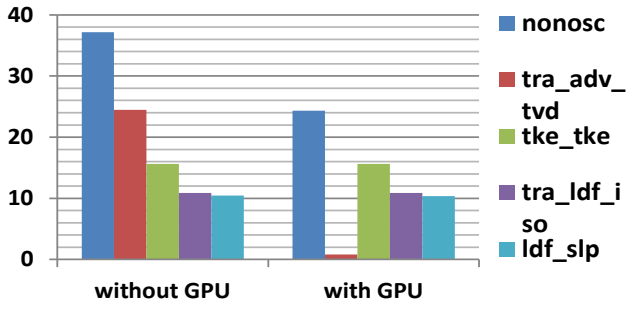

Fig. 5 Comparison between the basic test (without GPU acceleration) and the optimized test (with GPU acceleration)

The simulation results have been conducted on the IBM Blade and the performance results have been obtained. The average execution time of the function *nonosc* is reduced by at least 30% compared with the execution time without the GPU acceleration, as for the function *tra_adv_tvd*, the execution time is reduced 20 times, Fig. 5.

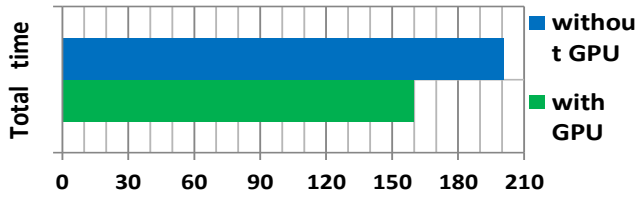

Fig. 6 Comparison of the total execution time with and without GPU

Although we have optimized only two functions of NEMO code, we get performance during program execution. The execution time is with 30% less compared with the execution time of the original NEMO code written in FORTRAN. This also leads to reducing total execution time by 30%, Fig. 6.

The development and investigations are implemented on computer system with only one graphical unit. We expect greater acceleration on high-performance computer systems, with more cores and graphical processors for the case of bigger configurations with bigger package of input data.

For now the biggest NEMO Ocean configuration is ORCA12, the input data amount is about 20GB and the output amount is around 150GB raw data, the needed time for completing this simulation is about 30 astronomical hours.

If the whole NEMO software package is optimized to use graphical devices, we expect greater reduction in execution time. Our future work is to verify it.

V. Conclusion

The parallel software for oceanology NEMO has been optimized for GPGPU systems. The optimized NEMO code is ported, compiled and executed on IBM Blade Center. It is best suited to work in combination of MPI tasks and threads.

Parallel performance evaluation of NEMO code has been investigated experimentally. Parallel performance parameter such execution time has been measured. The performance estimation and analyses show that the performance of the optimized NEMO code is better than an original MPI code written in FORTRAN. The total execution time is decreased by approximately 30%.

The investigations are part of tasks included in the PRACE project and the Supercomputing Applications – SuperCA++ project. The main objective is to optimize the NEMO code for Exascale Computer Systems with thousands and millions of cores. The optimized code is universal and can be apply for other similar research projects and experiments in the field of oceanology and will allow researchers to conduct their experiments on even more powerful supercomputers. They will be able to perform simulations with very large amounts of data.

Acknowledgment

The results reported in this paper are part of a research project DCVP02/1, supported by the National Science Fund, Bulgarian Ministry of Education and Science.

References

[1] Che-Lun Hung ; Hsiao-Hsi Wang ; Jieh-Shan Yeh ;Yu-Chen Hu ; Chun-Yuan Lin ; Yaw-Ling Lin, Preference Utility algorithm using GPGPU architecture, Computer and Information Science (ICIS), 2013 IEEE/ACIS 12th International Conference on Digital Object, pp. 155 – 160

[2] Zhi Tang ; Youjip Won , Multithread Content Based File Chunking System in CPU-GPGPU Heterogeneous Architecture, Communications and Processing (CCP), 2011 First International Conference on , 10.1109/CCP.2011.20, pp. 58 – 64

[3] NVidia Website: http://www.nvidia.com/

[4] Alan Gray - GPU System Architecture http://www.training.prace-ri.eu/uploads/tx_pracetmo/GPU_Architecture.pdf

[5] Mark Volett – Nvidia Kepler GK110 defines next generation GPU computing - http://blog.trentonsystems.com/nvidia-kepler-gk110-defines-next-gen-gpu-computing

[6] NEMO Home Page – NEMO Website: http://www.nemo-ocean.eu/About-NEMO

[7] FORTRAN 90/95 - Programming Manual (University College London): http://books.openlibra.com/pdf/Fortran-90-95-manual.pdf

[8] FORTRAN Standard Documents http://gcc.gnu.org/wiki/GFortranStandards

[9] NEMO book v3.4: http://www.nemo-ocean.eu/Media/Files/NEMO_book_3_42

[10] TAU/Tuning and Analysis Utilities: http://www.cs.uoregon.edu/Research/paracomp/papers/tau_sc99flyer.pdf

Prof. PhD Plamenka Borovska is a Head of Computer Systems Department at the Technical University of Sofia. She is an expert in High-Performance Computing, Parallel Computer Architecture, Parallel Algorithms, System Area Networks, GRID and Cloud Computing, Metaheuristics, Bioinformatics and e-Health. She is a leader of High-Performance and GRID Computing Group and manages national and European research and scientific projects.

Desislava Ivanova is an Assist. Professor at the Computer Systems Department, Technical University of Sofia. She is responsible for teaching of High-Performance Computing, Parallel Computer Architecture, Cloud and GRID Computing courses. Desislava Ivanova participates in different research and scientific projects in the areas of High-Performance and Cloud Computing.

ISBN: 978-1-61804-228-6

FPGA Implementation of Modular Exponentiation Using Single Modular Multiplier

M. Issad, B. Boudraa, M. Anane, S. Seddiki

***Abstract*—** This paper presents the FPGA implementation of Modular Exponentiation (ME), based on Software/Hardware (SW/HW) approach. Indeed, in Rivest, Shamir and Adleman (RSA) cryptosystem, ME which is computed by series of Modular Multiplications (MM's), is the main function to encrypt and decrypt data. In order to achieve the best trade-off between area, speed and flexibility, we propose in this work an embedded system, where ME algorithm is managed in SW, using the processor MicroBlaze of Xilinx. The MM is implemented as a HW core around the processor. Because, the MM is usually considered as a critical arithmetic operation, the Montgomery modular multiplication, requiring simple shifts and additions is used to realize the HW architecture of our MM core. The results show that the application to RSA 1024-bits, the execution time of the ME is about 109.5 ms. While, in terms of hardware resources, the device requires 1645 slices.

***Keywords*—** Modular Exponentiation, Montgomery Modular Multiplication, Microblaze, RSA**.**

I. Introduction

Modular Exponentiation (ME) is a common function used in several public key cryptosystem, such as, Rivest, Shamir and Adleman (RSA) protocol [1] and Diffie-Hellman key exchange scheme [2].

Most algorithms developed in literature for computing the ME, have shown that this function is based on the iterative computation of the modular multiplication. In order to optimize the performance execution of the basic arithmetic operation, namely, the modular multiplication, an efficient algorithm was developed by Montgomery [3]. This algorithm transforms the modulus reduction to a series of additions and right shifts. Therefore, the implementation of RSA requires two parts. The first part is dedicated to the calculation of the Montgomery modular multiplications (MMM's). The second one is used to control the execution of the ME.

In this paper, our main aim is the Software/Hardware (SW/HW) implementation of the ME for RSA. The proposed embedded system is based on the soft processor core MicroBlaze [4].

This work was supported by the Ministère de l'Enseignement Supérieures et de la Recherche Scientifique, Algeria.

M. Issad is with the Centre de Développement des Technologies Avancées, Cité 20 Aout 1956, Baba Hassen BP 17, Algeries, Algeria (email: missad@cdta.dz).

B.Boudraa is with the Université des Sciences et de la Technologie Houari Boumediene, Bab ezzouar, Algeria (email: b.boudraa@yahoo.fr).

M.Anane is with the Ecole Supérieur d'informatique, Oued Smar, Algeria (email: m_anane@esi.dz).

S. Seddik is with the Centre de Développement des Technologies Avancées, Cité 20 Aout 1956, Baba Hassen BP 17, Algeries, Algeria (email: S.Seddiki@cdta.dz).

Indeed, although the timing complexity optimization is still a major problem of cryptographic systems designers, the enhancement in terms of hardware resources and flexibility remains a binding constraint. Therefore, in order to achieve the best trade-off between area, speed and flexibility, we propose to implement in HW single Montgomery modular multiplier. The overall control of the ME algorithm is completely executed in SW by the processor Microblaze.

However, in such implementations, the MMM requires first an optimisation, in order to adapt its execution to the processor data path. In this work, we propose also a high radix implementation of the MMM, based on its sequential version [5].

The rest of this paper is organized as follows: In section II, the RSA algorithm is described. In section III, the MMM and the proposed method for its hardware implementation are presented. In section IV, we present the modular exponentiation algorithm. In Section V, the FPGA methodology of the proposed embedded system is reported. Section VI, discusses the experimental results and some comparisons with some recent works. The conclusion is given in section VII.

II. RSA Algorithm

Generally, the implementation of RSA requires the design of three abstraction levels [1].

The first level corresponds to cryptographic schemes where the public key (E, N) and the private key (D, N) are first generated. To calculate N, E and D, two large random prime numbers p and q are generated and two equations are used:

$$N = p \times q \tag{1}$$

$$D \times E \equiv 1 \bmod [(p-1)\times(q-1)] \tag{2}$$

E is chosen in the range $1 < E < (p - 1) \times (q - 1)$ such that,

$$gcd[E,(p-1)\times(q-1)] = 1 \tag{3}$$

The key (E, N) is made public. p, q and D are kept secret. Therefore, breaking the RSA security is believed to be as hard, because crackers will never know the values of p and q. Even though, E and N are known, it is still hard to find D.

The second level consists of the ME computation. Indeed, to encrypt a plaintext message M and decrypt the encrypted message P, we apply the expressions (4) and (5), respectively.

ISBN: 978-1-61804-228-6

$$P = M^E \bmod N \quad (4)$$

$$M = P^D \bmod N \quad (5)$$

E and D are respectively the public and the private exponents. N is the modulus.

The third level is often considered as the calculation of the modular multiplication over Galois field GF(N) [6]. This operation can be executed by using multiplication and division. However, in literature many methods are proposed to compute the modular multiplication in order to avoid the division, as this latter is a complex operation. Among these methods, MMM is often used.

III. Montgomery Modular Multiplication

The MMM using radix r ($r=2^k$) of two operands X and Y is defined by the following expression [3]:

$$S = X \times Y \times R^{-1} \bmod N \quad (6)$$

N is an odd integer coded on n digits. R is the Montgomery constant, chosen such that $R = 2^{k \times n}$, with pgcd (2^k, N) = 1. In the RSA, this condition is satisfied, because N is an odd number.

Since the MMM result is obtained with additional factor, namely R^{-1}, the MMM requires the conversion of X and Y to Montgomery representation and then performs the expression (6). The result is converted back to recover it in the classical domain [3].

Many works have been conducted on the hardware implementation of the MMM [7], [8] in order to improve its execution time. However, the resulting architectures require more resources and are not applicable for the design that we target. In [9], we have proposed an approach using radix-2, in order to reduce the occupied resources. The results showed low temporal performances, because the MMM radix-2 algorithm requires high number of iterations.

Indeed, the effective approach to implement the MMM around the embedded processor is to use its sequential version (Digit-serial) [5]. In this version, inputs and output of the algorithm are first decomposed into n digits of k bits, 2^k being the chosen radix. Then arithmetic operations are performed digit-by-digit in a serial mode. In addition, to adapt the execution of the MMM to the processor, the intuitive choice of the parameter k corresponds to the data path size of the processor. In this work, as we use Microblaze which is a 32 bits soft core, the value of k is of 32.

In the original MMM algorithm, a final subtraction is used at the end. This subtraction is necessary because the operands X and Y must satisfy the condition $0 \leq X, Y < N$. However, the reduction of S mod N if $S \geq N$ can be omitted using a modified version of the MMM algorithm. In this case, inputs and output can be higher than N ($0 \leq X, Y, S < 2 \times N$) with $R = 2^{(n+1) \times 32}$. Then, the operands X and Y become coded on (n+1) instead of n digits. Our work is based on this variant, called MMM algorithm without final subtraction [10].

Indeed, the MMM algorithm is based on the iterative calculation of the intermediate results $S_{(i+1)}$ which are given by the expression (7) [5].

$$S_{(i+1)} = (S_{(i)} + (X[i] \times Y) + (q_{(i)} \times N)) / 2^{32} \quad (7)$$

In radix $r=2^{32}$, the operands X, Y, the modulus N and the intermediate results $S_{(i+1)}$ are represented by:

$$X = \sum_{i=0}^{n} X[i] \times 2^{i \times 32}, \; Y = \sum_{j=0}^{n} Y[j] \times 2^{j \times 32},$$

$$N = \sum_{j=0}^{n} N[j] \times 2^{j \times 32} \quad S_{(i+1)} = \sum_{j=0}^{n} S[j]_{(i+1)} \times 2^{j \times 32},$$

with N[n]=0.

As the operands are coded on succession of digits, to calculate $S_{(i+1)}$, an outer and an inner loops are used. They are defined respectively by the indices (i) and (j). (i) denotes the $(i)^{th}$ digit of the operand X. (j) defines the digit-position of Y, N and $S_{(i)}$. Thus, at each iteration (i) where only one digit of the operand X is selected, we begin by the computation of $q_{(i)}$ using the expressions:

$$q_{(i)} = (H[0]_{(i)} \times N') \bmod 2^{32} \quad (8)$$

where, $H[0]_{(i)} = S[0]_{(i)} + (X[i] \times Y[0])$ and $N' = -N[0]^{-1} \bmod 2^{32}$

Then, the arithmetic operations are performed using digit-serial mode with a precision of 32 bits. To obtain $S_{(i+1)}$, we have used two intermediate variables $H_{(i)}$ and $W_{(i)}$. The values of their $(j)^{th}$ digits, i.e., $H[j]_{(i)}$ and $W[j]_{(i)}$ depend on both multiplications $X[i] \times Y[j]$ and $q_{(i)} \times N[j]$, respectively. If we consider that,

$$X[i] \times Y[j] = Pr1[j]_{(i)} + (C1[j]_{(i)} \times 2^{32}) \quad (9)$$

and

$$q_{(i)} \times N[j] = Pr2[j]_{(i)} + (C2[j]_{(i)} \times 2^{32}), \quad (10)$$

therefore $H[j]_{(i)}$ and $W[j]_{(i)}$ are written as:

$$(cy_2^j \times 2^{32}, cy_1^j \times 2^{32}, H[j]_{(i)}) = Pr1[j]_{(i)} + C1[j-1]_{(i)} + S[j]_{(i)} + cy_1^{j-1} + cy_2^{j-1} \quad (11)$$

$$(cy_4^j \times 2^{32}, cy_3^j \times 2^{32}, W[j]_{(i)}) = Pr2[j]_{(i)} + C2[j-1]_{(i)} + H[j]_{(i)} + cy_3^{j-1} + cy_4^{j-1} \quad (12)$$

with j varying from 0 to n.

$C1[j-1]_{(i)}$ and $C2[j-1]_{(i)}$ are the most significant digits of both multiplications, respectively. cy_1^{j-1}, cy_2^{j-1} and cy_3^{j-1}, cy_4^{j-1} are the carriers calculated at the iteration (j-1). These carriers, as $C1[j-1]_{(i)}$ and $C2[j-1]_{(i)}$, are initialized at the beginning of the $(i)^{th}$ loop. Using these notations, the computation of the expressions (11) and (12) may be carried out sequentially, where we calculate first the $(j)^{th}$ digit of $H_{(i)}$ followed by the $(j)^{th}$ digit of $W_{(i)}$. Then, according to the expression (7), the $(j)^{th}$ digits of the intermediate results $S_{(i+1)}$ are obtained considering only the (n+1) most significant digits of $W_{(i)}$.

In order to implement the MMM in embedded cryptosystem, the arithmetic operations presented above are performed in an Arithmetic Unit (AU). In the following, we present its hardware implementation.

Hardware Implementation of the Arithmetic Operations

The architecture of the AU is shown in Fig. 1. This latter is based on the DSP48E cores [11] to implement the multiplication of the expressions (8), (9) and (10).

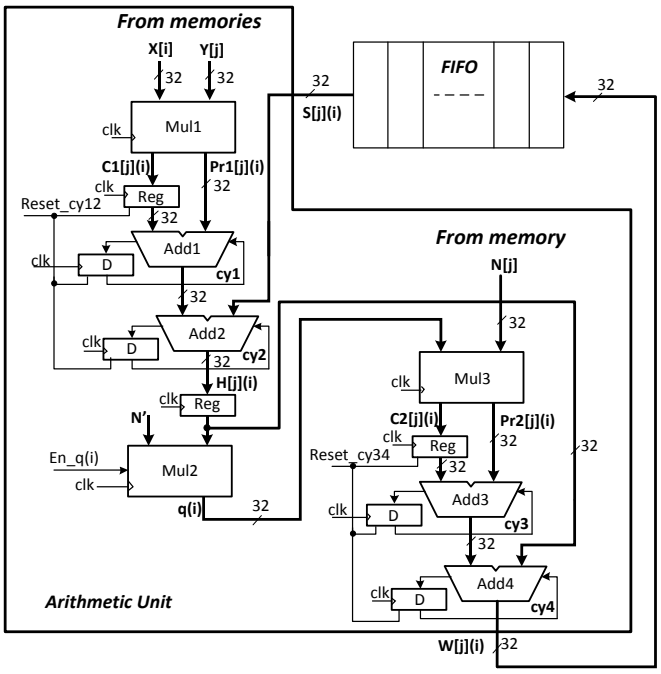

Fig.1 Architecture of the Arithmetic Unit

It consists of three multipliers, four carry propagate adders, registers and D flip-flops. The implementation of the expression (7) supposes that the operands X, Y and N are stored in memories. The intermediate results $S_{(i)}$ are stored in FIFO. Indeed, at each iteration (i), where the $(i)^{th}$ digit of the operand X is selected, the value of $q_{(i)}$ can be considered as constant. $q_{(i)}$ is calculated by the Mul2 according to the expression (8). In addition to the input data, the AU receives three control signals which are En_q(i), Reset_cy12, and Reset_cy34. The first allows to maintain $q_{(i)}$ constant. The second and the third are used respectively to initialize the carries ($C1[j-1]_{(i)}$, cy_1^{j-1}, cy_2^{j-1}) and ($C2[j-1]_{(i)}$, cy_3^{j-1} , cy_4^{j-1}) at the beginning of the iteration (i). Carries are delayed by one clock cycle and added with the next computed digits. Therefore, the computation of the $(j)^{th}$ digit of $W_{(i)}$ is split into six clock cycles as flow:

1. Address generation to get Y[j].
2. Reading Y[j] from memory and computing the product X[i]×Y[j] by the Multiplier Mul1.
3. Computation of $H[j]_{(i)}$ by the adders add1 and add2.
4. Address generation to get N[j].
5. Reading N[j] from memory and computing the product $q_{(i)}$×N[j] by the Multiplier Mul3.
6. Computation of $W[j]_{(i)}$ using the adders add3 and add4.

Thus, to compute the expressions (11) and (12), where (j) varying from 0 to n, the iteration (i) requires (n+1) cycles. Taking into account the number of cycles corresponding to $W[j]_{(i)}$ computation and the size of the operand X, the clock cycle count CCC to get the MMM result is given by the expression (13).

$$CCC = (n+7)\times(n+2) \tag{13}$$

IV. Modular Exponentiation Algorithm

For large exponents, the modular exponentiation is a complex function. Since, many algorithms have been developed to optimize its performances. In our work, the binary R-L (Right to Left) method is utilized [12]. This latter is based on the binary representation of the exponent scanned bit-by-bit from Right to Left. At each iteration of the algorithm, squaring and multiplication are performed. The multiplication is executed only if each bit of the exponent is equal to 1. The binary R-L algorithm is given below.

Binary R-L Algorithm

Inputs: $D = \sum_{i=0}^{e-1} d(i) \times 2^i$

$P = \sum_{j=0}^{n} X[j] \times 2^{j\times 32}$, $N = \sum_{j=0}^{n} N[j] \times 2^{j\times 32}$, $N[n] = X[n] = 0$

Pre- computed: $N'=-N[0]^{-1} \bmod 2^{32}$, with pgcd $(N, 2^{32})=1$

$R^2 \bmod N$, with $R=2^{(n+1)\times 32}$

Intermediate variables: $CC_i = \sum_{j=0}^{n} CC_i[j] \times 2^{j\times 32}$,

$Sq_i = \sum_{j=0}^{n} Sq_i[j] \times 2^{j\times 32}$

Output : $M = \sum_{j=0}^{n-1} M[j] \times 2^{j\times 32} = P^D \bmod N$

Begin

1. Sq_{-1}= Montgomery($X, R^2 \bmod N, N, N'$)
2. CC_{-1}= Montgomery($1, R^2 \bmod N, N N'$)
3. ***for*** i ***from*** 0 ***to*** $e-1$ ***do***
4. Sq_i= Montgomery($Sq_{i-1}, Sq_{i-1}, N, N'$)
5. ***If*** $d(i) = 1$ ***then*** CC_i=Montgomery($CC_{i-1}, Sq_{i-1}, , N, N'$)
6. ***else*** $CC_i = CC_{i-1}$
7. ***end for***
8. M=Montgomery($CC_{e-1}, 1, N, N'$)

Return M

In this algorithm, input/output data and intermediate results are represented in radix $r=2^{32}$, except the exponent D, coded in radix 2. The *Montgomery(.)* function corresponds to the computation of the MMM. At each iteration, it receives: two operands, the modulus and the constant N' to provide two intermediate results denoted by CC_i and Sq_i. These results correspond to the modular multiplication and squaring, computed in the Montgomery domain, respectively.

V. Architecture of the Embedded System

The hardware architecture of the proposed embedded system for computing the modular exponentiation is shown in Fig. 2.

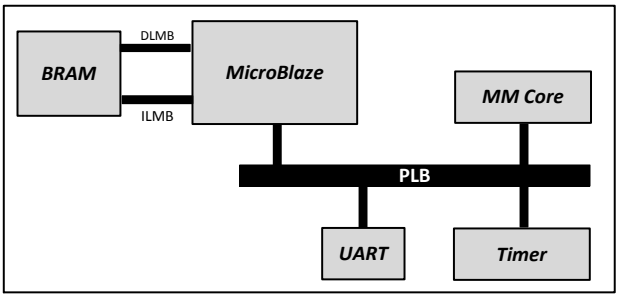

Fig.2 Hardware architecture of the embedded system

This architecture was built on Xilinx Virtex-5 XC5VLX50T Genesys development board [13] and designed using XPS 13.2 (Xilinx Platform Studio) environment.

The proposed embedded system contains the following components: Microblaze processor, memory BRAM, Local Memory Bus (LMB), Processor Local Bus (PLB), Universal Asynchronous Receiver Transmitter (UART), Timer and our accelerator MM core. This latter communicates with the processor via the memory-mapped-registrer [14].

Microblaze accesses either instruction through ILMB or data through DLMB. These two buses are 32 bits. All the peripherals communicate with the processor through the PLB bus which is of 32 bits. The BRAM is configured to 16 KB memory space. The UART is integrated in the system to allow the communication between the processor and the RS232 port of the board. The Timer is used to gather informations about how many clock cycles are required for executing a single MMM and a modular exponentiation.

The device drivers of each peripheral are used to develop the main program description which is executed by Microblaze. Indeed, for computing single ME given by $M=P^D \text{mod} N$, Microblaze receives, as inputs from UART, the exponent D, the message P, their sizes, the modulus, the constant N' and the value of R^2 mod N. Before performing this function, the processor begins by restoring all the inputs data according to their representation in radix 2^{32}, then both MMMs required for executing an iteration of the ME algorithm, are calculated sequentially by the MM core. This latter, receives the operands from the memory BRAM through the processor, at each iteration of the modular exponentiation algorithm. The MMM result will be then transferred to the BRAM to be used as operand in next computations. When the ME is achieved, the processor starts by splitting the result M into 8-bits digits and sends it outside FPGA via the UART; starting from least significant digit to most significant digit.

The important component of our embedded system is the designed MM core. In the following, let us consider its implementation.

MM core Implementation

The integration of the MM core in the embedded system requires not only the design of its hardware architecture and an interface circuitry to communicate with the PLB bus, but also the accompanied device drivers running on the processor. The programs of these drivers are implemented using the C code and designed on two layers. The first is the high level driver. It consists of the *ExpBinary(.)* function which allows to perform the modular exponentiation algorithm. The second is the low level driver. It consists of three functions *Getbitindex(.), Write_Modulus_N'(.)* and *Montgomery(.). Getbitindex(.)* is executed by the processor. Its role is to perform the right shift of the exponent D and provide the $(i)^{th}$ bit at the beginning of each iteration (i) of the ME algorithm. *Write_Modulus_N'(.)* allows for transmitting to MM core the modulus and the constant N'. *Montgomery(.)* is used by Microbaze to ensure the monitoring of the MMM computation. Except of the first function, the others depend of the hardware interface circuitry and allow the communication between the processor and the MM core. Indeed, the process of making the hardware interface can be time consuming task. Thus, our work is based on using the IPIF (Intellectual Property Interface) of Xilinx [15]. The block diagram of our accelerator MM core based on a single Montgomery modular multiplier is show in Fig. 3. It consists of the interface IPIF and of the MonMul multiplier which can be used as black box. This latter is responsible of the MMMs execution. It mainly consists of: Memory data, our AU, Control Unit and Memory FIFO. The IPIF uses a standard back-end interface called IPIC (IP Interconnect) which helps to connect our core to the IPIF services.

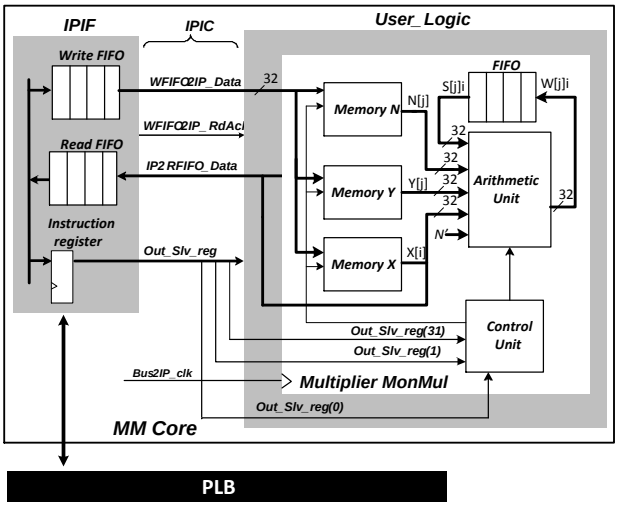

Fig. 3 Block diagram of the MM core

To allow the communication between Microblaze and the multiplier MonMul, the internal components configured in the interface IPIF are: Write FIFO, Read FIFO, and instruction register. The write FIFO is used to transfer the operands, the modulus and the constant N' to MonMul. The read FIFO ensures the reading of the result. The processor controls the multiplier MonMul using instructions. These latter are defined in the device drivers as opcodes and are transmitted through the instruction register. Table I lists the instructions and their opcodes.

TABLE I
INSTRUCTION FORMAT

Opcode	Instruction	Description
0000…..0001	Reset_MonMul	Initialization of the multiplier MonMul after each MMM execution
1000…..0001	Run_Write_N_N'	Loading the modulus N and the constant N'
0000…..0000	Run_Write_X_Y	Transferring two operands to MonMul
0000…..0010	Run_MMM	MMM execution

The signals of the IPIC are defined as follows:

- *Bus2IP_clk :* Clock signal.
- *WFIFO2IP_data:* Output data bus of the write FIFO.
- *WFIFO2IP_RdAck:* Using an active high pulse, this signal indicates, that a data on the WFIFO2IP_Data bus is valid for reading at the next rising edge of the clock signal. This pulse is a signal used inside the multiplier MonMul, to control the loading of the input data into local memories.
- *IP2RFIFO_data:* Input data bus of the read FIFO.
- *Out_Slv_reg(31)* and Out_Slv_reg(0): These signals are the most significant and the least significant bits of the instruction register, respectively. The first is used to enable the loading of the modulus and the N', independently of both operands. The second allows the initialization of the multiplier MonMul and enabling the loading of two operands X and Y after performing each MMM.

- *Out_Slv_reg(1):* This signal is the second bit of the instruction register. It allows to active the execution of the MMM arithmetic operations.

In order to perform the modular exponentiation, the MonMul multiplier receives at each iteration two operands namely, X and Y. According to the modular exponentiation algorithm, X and Y can be the message P, the constant R^2 mod N, or the intermediate results CC_i and Sq_i. Thus, for performing one modular exponentiation, Microblaze starts by sending first using the instruction *"Run_Write_N_N'"*, to start the loading of the modulus and the constant N'. Then the execution process becomes identical for all MMMs. The basic operations for computing one MMM are as follows:

Before starting the MMM computation, Microblaze transmits first the instruction *"Run_Write_X_Y"* to enable the transfer of two operands X and Y which will be stored in local memories. Once both operands are entirely received, Microblaze sends the instruction "*Run_MMM"* to start the execution of the MMM. The transfer of the result from the multiplier MonMul to Microblaze is based on the status of the read FIFO link. During the transfer of data from processor to MM core and when performing the MMM, this link is high. In other words, the data bus IP2RFIFO_data transmits 0xFFFFFFFF value to Microblaze. When the multiplier MonMul completes the execution of one MMM, it initializes the read FIFO by 0x00000000. After that, it sends the (n+1) digits of the result. At the end, Microblaze reinitializes the multiplier MonMul, using the instruction "*Reset_MonMul*".

VI. Implementation Results

The embedded system presented in this paper has been designed by using Xilinx ISE design suite 13.2. To verify the correctness of the MM core integration, functional simulation was made using ModelSim SE 6.4 10.0C. The architecture description of the multiplier MonMul was coded using VHDL language. The memory blocks and DSP48E cores were generated with the Core Generator tool of ISE.

The timing report showed that a maximum frequency $f_{max}=1/t_{clk}$ of 100.26 Mhz can be achieved where t_{clk} is the clock period. This latter is computed from the AU critical path, having the maximal delay. This delay corresponds to the computation time of the products X[i]×Y[j] and $q_{(i)}$×N[j] which require one 32-bits multiplier.

Table II shows the execution time results, where the proposed embedded system is clocked by 100 Mhz.

TABLE II
Temporal performances

Bit width	f Mhz	T_{MMM} (ms)	T_{ModExp} (ms)
short exponent	100	7171 10^{-5}	2.6
Long exponent	100	7171 10^{-5}	109.5

The encryption is applied for RSA 1024 bits with short and long exponent. The short exponent is set to D=65537= $(10000000000000001)_2$. The long exponent is an integer with 1024 bit-width. This sample has 515-bits non-zero which is close and higher than the average case where the bit string non-zero is about 512-bits.

In this table, T_{MMM} and T_{ModExp} are the execution times of a single MMM and of the modular exponentiation, respectively. These times are computed by the multiplication of the necessary clock cycles given by the Timer with the clock period.

In this analysis, we are interested by the delay T_{ModExp} which depends on several factors, namely: loading the modulus and the constants N' into the MM core (T_1); executing a single MMM which includes the data transfer (operands and result) between the processor and the MM core (T_2); shifting the exponent and testing its $(i)^{th}$ bit (T_3). Finally, the T_{ModExp} depends also of number of bits equal to zero in the exponent.

According to modular exponentiation algorithm, when using short exponent D=65537, the complexity in terms of number of MMMs and shifts is of (3×MMMs)+(17×(Shift and test))+(19×MMMs). 3×MMMs are the MMMs required to convert the execution of the modular exponentiation algorithm in the Montgomery domain and to represent the result in the classical domain. The results show that the first three factors (T_1, T_2, and T_3) required in terms of number of clock cycles are 814, 7171 and 53, respectively. We note that the number of clock cycles required for computing a single MMM is high. Indeed, according to expression (13) of section III, for RSA 1024 bits where the length of the data is 33 digits (n=32 bits), the execution of single MMM by our AU requires only 1248 clock cycles instead of 7171. This difference is mainly due to the data exchanged (operands and result) between the processor and the MM core. Precisely, the transfer of a single digit between the two parts requires approximately 61 clock cycles. Thus, we can consider that the communication between the processor and our customized MM core can be seen as a bottleneck.

Table III shows the occupied resources by our embedded system on the target FPGA circuit. These results are listed in terms of number of slices, of select RAM blocks (36 kb and18 kb) and of DSP48E cores. In order to evaluate the costs of the MM core, we have implemented the basic embedded system without our MM core. The result shows that the difference is about 607 slices and 6 select RAM blocks. In addition, the proposed Arithmetic Unit (AU) uses 11 DSP48E cores.

TABLE III
Occupied resoures

	Slices	Select RAM	DSP48E
Our embedded system	1645	10	14
Basic embedded system	1038	4	3
MM core	607	6	11

Table IV compares our work with some previous implementations of the modular exponentiation. Note that, in the present work, our main goal is not the optimization of the execution time, but to achieve the best trade-off between area, speed and flexibility.

In [16], a hardware implementation of the modular exponentiation is presented. This work is based on the modified Booth encoder and on the carry save representation to accelerate the MMM execution. In [17], the authors present a SoC based on the Nios processor of Altera which includes a variety of Intellectuals Property (RSA, ECC,…). In this work, the modular exponentiation is implemented as single core. In [18], a hardware implementation of the Modular exponentiation is presented. This work promotes the optimisation of the hardware resources, instead of the execution time. In order to optimize the memory blocks

number, the author uses single block RAM of 36kbits where all the input data are stored.

TABLE IV
PERFORMANCES COMPARISON

	Design	Area	T_{ModExp} Z=65537 (ms)	T_{ModExp} 1024 bits (ms)	Devices
Our	SW/HW	1645 slices 14 DSPs 10 RAMs	2,6	109,6	Virtex-5
Ghoreishi [16]	HW	26640 slices	0.189	19.405	Virtex-2
Hani [17]	SW/HW	12881(Logic Elements)	-	31,93	ep1s40f780c5
Song [18]	HW	180 slices 1 DSP 1 RAM	-	36.37	Virtex-5

VII. CONCLUSION

In this paper, we have presented the FPGA implementation of modular exponentiation, using SW/HW approach. In the first step, we have optimized the HW implementation of the MMM. Then, we have adapted the execution of this operation to the soft processor core Microblaze. This methodology allows the implementation of the ME algorithm with the best trade-off between the area, speed and flexibility. The execution time of our embedded system depends on several factors. We have shown that the communication between the processor and our MM core can be considered as a bottleneck. Indeed, the data transfer clock cycles (operands and result) may take up to 82,59 % of the total clock cycles required to compute a single MMM. However, through the performances comparison, we note that our approach can easily take part in an environment where the reduction of the area is a binding constraint.

REFERENCES

[1] R.L. Rivest, A. Shamir, and L. Adleman,"A method for obtaining digital signatures and public-key cryptosystems", *Communication ACM*, vol 21, No.2, pp.120-126, 1978.

[2] W. Diffie and M.E. Hellman, "New directions in cryptography", *IEEE Transactions on Information Theory*, vol.IT22, No.6, pp.644–654, 1976.

[3] P.Montgomery, "Modular multiplication without trial division", *Mathematics of Computation*, vol. 44, pp.519-521, 1985.

[4] "MicroBlaze Processor Reference Guide", UG081 (v13.2), Xilinx, 2011.

[5] C.K.Koc, T.Acar, S.Burton and J.Kaliski , "Analyzing and comparing Montgomery multiplication algorithms", *IEEE Micro*, vol.16, No.33, pp.26-33,1996.

[6] J.P Deschamps, G.J.A Bioul, G.D. Sutter, "*Synthesis of Arithmetic Circuits FPGA, ASIC, and Embedded Systems*", (A John Wiley & Sons, 2006).

[7] N.Nedjah and L.M.Mourelle, "A Review of Modular Multiplication Methods and Respective Hardware Implementation" *Informatica*, vol.30, pp.111-129, 2006.

[8] C. McIvor, M. McLoone, J. McCanny, A. Daly, and W. Marnane, "Fast Montgomery Modular Multiplication and RSA Cryptographic Processor Architectures", *In Proceedings of 37th Annual Asilomar Conference on Signals, Systems and Computers*, pp.379–384, 2003.

[9] M.Issad, M.Anane and N.Anane, "An optimised architecture for radix-2 Montgomery modular multiplication on FPGA", *International Journal of High Perform System Architecture*, vol.3, No.4, pp.175-185, 2011.

[10] C.D. Walter, "Precise Bounds for Montgomery Modular Multiplication and some Potentially Insecure RSA Moduli", Lecture Notes in Computer Science,Topics in Cryptology - CT-RSA, pp.30–39, 2002.

[11] Virtex-5 FPGA XtremeDSP Design Considerations User Guide UG193 (v3.5) January 26, 2012.

[12] Ç.K. Koç, "RSA Hardware Implementation", RSA Laboratories, RSA Data Security, Version 1.0, 1995.

[13] Genesys Board Refference Manuall, Revision: Feb, 2012.

[14] P.R.Schaumont, "*A Practical Introduction to Hardware/Software Codesign*", Springer, 2010.

[15] PLB IPIF (v2.02a), DS448, 2005.

[16] S. S. Ghoreishi, M.A. Pourmina, H. Bozorgi, M. Dousti, "High Speed RSA Implementation Based on Modified Booth's Technique and Montgomery's Multiplication for FPGA Platform", In *Proc*. CENICS '09, pp.86-93, 2009.

[17] M. K.Hani, H. Y. Wen, A. Paniandi, "Design And Implementation Of A Private And Public Key Crypto Processor For Next Generation IT Security Applications", *Malaysian Journal of Computer Science*, vol. 19, No 1, pp.29 – 45, 2006.

[18] B. Song, K. Kawakami, K. Nakano and Y. Ito, "An RSA Encryption Hardware Algorithm using a single DSP Block and single Block RAM on the FPGA", In *Proc. First International Conference on Networking and Computing*, pp.140-147, 2010.

Stability Analysis of Impedance type Haptic Interface

Neelu Nagpal[1] and Jyoti Ohri[2]

Abstract— One of the most important elements to facilitate the user for creation of immersive reality with in virtual environment is Haptic interface. In this paper the analysis of the haptic interaction 1-DOF discrete-time impedance haptic system when interacting with static wall with delay is carried out. The classical control analysis has been utilized for determining the stability of one degree of freedom of haptic interface colliding with virtual wall and obtained the stability region without delay and with delay. The proposed Jury stability test provides the information regarding stable values of virtual coupling elements and also establishes a linear condition between stiffness, damping and system delay for haptic systems, which was not possible with the Routh-Hurwitz.

***Keywords*—** Jury Stability Test, Haptic Interface, Impedance type, Stability Region, Virtual Coupling.

I. Introduction

HAPTIC system is a computer-controlled system that allows us to physically interact with the virtual or remote environment through the sense of touch. The design of such system enables to produce/receive kinesthetic stimuli for/from human movements and the user is being able to touch, feel, and manipulate objects in an environment, in addition to seeing (and/or hearing) them, gives a sense of compelling immersion in the environment that is otherwise not possible.
The advanced interaction systems offers attractive applications in surgical and rehabilitation robotics, power assist-devices, training simulation systems, etc. The most critical issue in these systems is how to ensure stable and safe interaction with a high fidelity of reproduction of a virtual environment.
Haptic system involves bidirectional interaction with the user and forces are displayed to the user by a "haptic loop". The haptic loop is a closed loop control system that determines the nature of interaction of the haptic device with the user based on the position and velocity of the end effector. Such a control system describes an impedance type haptic device, reducing the mass and friction effects while increasing structural rigidity and force feedback capability. However, these goals introduce conflicting requirements on actuators, structures and closed-loop implementation and there exists difficulty in realizing the ideal transparency.

Neelu Nagpal is a research scholar, NIT , Kurukshetra and Assistant Professor, with the Electrical & Electronics Engineering Department, MAIT, Delhi, India (e-mail: nagpalneelu1971@gmail.com).

Dr. Jyoti Ohri is a Professor with the Electrical Engineering Department, NIT, Kurukshetra,India (e-mail: ohrijyoti@gmail.com).

Numerous attempts have been made in the recent years to maintain stable haptic interaction. Minsky et al. [1] investigated the stability of haptic interaction and derive a condition for stability of haptic device based on the considerations of sampling rate of the controller. They expressed the stability of the discrete force law as the upper limit on the maximum stiffness that can be achieved by virtual wall. Colgate et al. [2] presented a theoretical analysis of the passivity of the stiff wall and in [3], provided a condition the haptic device must satisfy to exhibit passive behavior. Adams and Hannaford [5] represented the haptic interface as a linear two-port with terminals for a human operator and a virtual environment. They proposed the unconditionally stable condition that the two-port network should be passive and a design procedure using virtual coupling to guarantee the stability. Although this approach has the advantage that the design problem can be decoupled from the design of virtual environment, the solution is not the best in the viewpoint of transparency. In paper [3], comparison of haptic devices in response to the shape and size of their regions stability is proposed. These regions are designated in their studies as the "Z-Width" of the device as it covers the whole of impedances that can be implemented therewith. Gil.et al. [6] computed the exact stability boundary for virtual damping and stiffness for one degree of freedom of haptic interface for static environment using Routh-Hurwitz criterion.

Our work propose Jury stability test that can be directly applied to the discrete characteristics equation without solving for roots and is applicable to the polynomial with real and complex coefficient.

The paper is organized as follows: Section 2 presents brief description of haptic system. Section 3 summarizes the mathematical model of haptic system. In Section 4, classical control methods are applied to analysis of the stability and discussed the main results. Section 5 compares the stability regions of two commercial available devices and important conclusions are stated in Section 6.

II. SYSTEM DESCRIPTION

There are two main types for a haptic system: impedance type and admittance type. The impedance display type will sense the position from the manipulator and a computer simulation will calculate the force output\ to the manipulator. Most haptic interfaces use impedance displays.

But the admittance type haptic system outputs motion from force input, and the energy in the system always dissipates. This indicates that the impedance type haptic system has less passivity than the admittance type haptic system.

The block diagram of the basic components of haptic system is shown in Fig 1.Between haptic device and virtual environment, virtual coupling block composed of virtual stiffness (*K*) and virtual damping (*B*) acts as an artificial link. This viscoelastic impedance model is used to compute the force of environment. The design of virtual coupling elements plays an important role for the stability of haptic system as well as for the safety of the device.

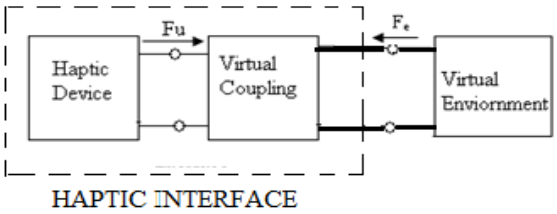

Figure 1: Block Diagram of a basic Haptic System.

When introducing a time delay by a discrete-time implementation of a virtual environment, an impedance type haptic system can generate energy which can induce the instability. Colgate et al. showed an example of squeezing and releasing a virtual spring that result in generation of energy [2].

III. MODEL DESCRIPTION

The model of an Impedance type haptic system which is composed of a robot manipulator and static virtual environment connected by an artificial link known as virtual coupling network (usually a spring and damper) is considered. The function of virtual coupling is to restore the virtual force that must be restored to the human operator as a function of the positions and velocities of both the user and the virtual object.

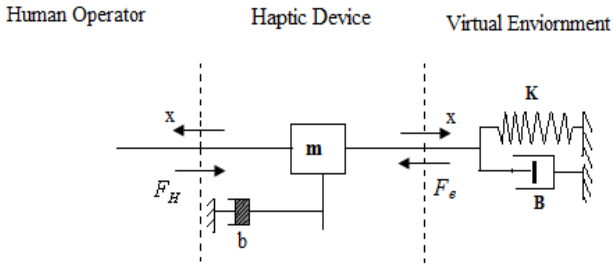

Fig 2: Ideal Force model of Ideal Haptic system

Consider single degree of freedom of an ideal haptic system depicted by Fig 2. The simplified model of an impedance type haptic device consists of a physical inertia, *m* and has viscous damping,*b*. The Virtual properties of the environment are stiffness, *K* and damping,*B* defining the desired dynamics of the interaction and used to calculate the contact force. In real case, the environment usually is more complicated.

The model of the haptic system is composed of continuous part (haptic device) and discrete part (virtual coupling controller). The stability analysis can be performed after transforming all blocks of control loop into the same domain i.e. in discrete time domain before performing any stability test for determine the stability boundary. Fig. 3 shows the model of haptic device colliding with virtual wall with discrete delay.

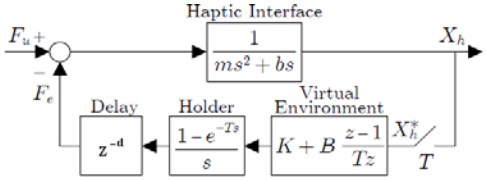

Figure 3: Simplified Linear model of a Haptic System

Assuming coulomb friction and user contributing to only positive effect in stability, the effect of delay is considered alone and the resulting characteristics equation obtained is written as (1):

$$1+z^{-d}\,Z\,[ZOH\ G(s)]\ C(s) = 0 \qquad (1)$$

$$Z[ZOH.G] = \left[\frac{1-e^{-Ts}}{s}.\frac{1}{ms^2+bs}\right]$$

The characteristics equation obtained in discrete form is

$$1+z^{-d}\left[\left\{\frac{\left(e^{-bT/m}-1+\frac{bT}{m}\right)z+1-\left(1+\frac{bT}{m}\right)e^{-bT/m}}{(z-1)(z-e^{-bT/m})\frac{b^2T}{m}}\right\}\right][K+B\frac{z-1}{Tz}] \qquad (2)$$

Without any change in the contact force law, the dimensional normalized parameters can be used for the stability analysis. The parameters used in the (2) are normalized as in Table 1:

Table 1: Dimensionless Parameters

Symbol	PARAMETER	Dimensionless Variable
x	position	
m	mass	
T	sampling interval	
b	physical damping	$\delta = \frac{bT}{m}$
B	virtual Damping	$\beta = BT/m$
K	virtual stiffness	$\alpha = KT^2/m$
t_d	Delay	$d = t_d/T$

Both real and dimensionless parameters can theoretically take any value ($m > 0$, $b > 0$, and $T > 0$ and $t_d \geq 0$).

Equation (2) in terms of normalized parameters can take the form as:

$$\delta^2(z-\varepsilon)(z-1)^{d+1} - (1-\varepsilon-\delta)(\alpha+\beta)z^2 + [(1-\varepsilon-\delta\varepsilon)(\alpha+\beta) + (1-\varepsilon-\delta)\beta]z - (1-\delta\varepsilon)\beta = 0 \quad (3)$$

By substituting normalized variables, the characteristic equation (3) becomes independent of the physical system parameters *m*, *b* and *T*. The benefit of normalizing the parameters is that for different haptic devices having different values of mass and damping, the overall shape of the stability boundary of system in the *α-β* plane remains same .

The same region of α and β is obtained for stability and the amount of computation required is much less than that required with real parameters in Routh- Hurwitz stability criterion.

Stability boundaries for a system can be found using traditional stability tests such as Routh-Hurwitz [6] with conformal mapping or Jury stability test and described in section 4.

IV. STABILITY ANALYSIS

Implementation of Routh-Hurwitz and Jury stability test is done after identification of characteristics equation of the block diagram of the system assuming static environment.

A. *Stability Analysis using Routh-Hurwitz Criterion*

Routh-Hurwitz criterion is applicable to time domain, the bilinear transformation is implemented that maps the unit circle of *z*- plane with the left *w*- plane. The criterion is implemented to modified characteristics equation (3) to draw the region of *α* and *β* after assuming the value of mass*(m)* as 0.5 Kg , physical damping coefficient *(b)* as 0.1 Ns/m and sample time(*T*) is given the value 1 ms.

The characteristics equation (3) obtained in discrete form without delay i.e. d=0 is written as:

$$P(z) = a_0z^3 + a_1z^2 + a_2z + a_3 = 0 \; where \; a_3 > 0; \quad (4a)$$

In the stability analysis using bilinear transformation coupled with the Routh stability criterion, substitute $z = \frac{1+w}{1-w}$ in (4) and get the equation as:

$$a_3\left(\frac{1+w}{1-w}\right)^3 z^3 + a_2\left(\frac{1+w}{1-w}\right)^2 z^2 + a_1\left(\frac{1+w}{1-w}\right)z + a_0 = 0 \quad (5)$$

Then, clearing the fractions by multiplying both sides of this last equation by$(1-w^2)$, the modified equation is

$$Q(w) = b_3w^3 + b_2w^2 + b_1w + w_0 = 0; \; b_3 > 0 \quad (6a)$$

Implementation of Routh stability criterion results in the following inequality equation

$$b_1b_2 - b_0b_3 > 0 \quad (7a)$$

The characteristics equation (3) obtained in discrete form with delay i.e. d=1 is written as:

$$a_0z^4 + a_1z^3 + a_2z^2 + a_3z + a_4 = 0; where \; a_4 > 0 \quad (4b)$$

After bilinear transformation in the same manner the characteristics equation (4b) obtained in discrete form with delay i.e. d=1 is written as:

$$Q(w) = b_4w^4 + b_3w^3 + b_2w^2 + b_1w + w_0 = 0 \quad (6b)$$

Again after implementation of the Routh stability Criterions, the inequality of equation results in expression given in 7(b):

$$b_1b_2b_3 - b_1^2b_4 - b_3^2b_0 > 0 \quad (7b)$$

Substituting numerical values of parameters of different haptic systems, the inequality of equation (7a) and (7b) defines the region of stability (drawn in figs.4 & 5) means the locus of values of α and β which ensure stability of the device

B. *Stability Analysis using Jury Stability Criterion*

Jury stability criterion for discrete-time system is applied to the characteristics equation (3) written as a function of z.

Case (1). *Without delay i.e. d=0* :The system representing the discrete characteristics equation (4a) is stable if the following conditions are all satisfied.

Condition 1:$|a_3| < |a_0|$

Condition 2: $P(z)\big|_{z=1} > 0$

Condition 3: $P(z)\big|_{z=1} < 0$ as $n = 3$ is odd

Condition4:$|b_2| > |b_0|$

where $b_2 = \begin{vmatrix} a_3 & a_0 \\ a_0 & a_3 \end{vmatrix}$ and $b_0 = \begin{vmatrix} a_3 & a_2 \\ a_0 & a_1 \end{vmatrix}$

Also $|c_1| > |c_0|$

where $c_1 = \begin{vmatrix} b_2 & b_0 \\ b_0 & b_2 \end{vmatrix}$ and $c_0 = \begin{vmatrix} a_3 & a_2 \\ a_0 & a_1 \end{vmatrix}$

The Jury stability criterion is implemented to discrete characteristics equation to draw the region of *α* and *β*. In order to confirm the results with Routh Criterion, the same values of *m*, *b* and *T* are considered .

The following inferences are drawn from the Jury stability criterion applicable to 1 dof haptic system interacting with static virtual wall without delay:

(i) From first condition of Jury test i.e$|a_3| < |a_0|$, It is found that the value of *β* should be less than 2.0003. This maximum value of *β* put maximum limit on the value of virtual damping *B* as 1000.

(ii) Second condition of Jury stability test implies that the value of α should be greater than zero or Virtual stiffness should have finite positive value for the system stability.

(iii) Third condition of Jury test can be used to receive the analytical stability condition of the system and derive the linear relationship between the system parameters.

(iv) Fourth condition enables to draw the stability boundary of the haptic system as shown in Fig 4.

Case(2) With delay i.e. for d= 1, the system representing the discrete characteristics equation (4b) is stable if all the following conditions are satisfied

.Condition 1: $|a_4| < |a_0|$

Condition 2: $P(z)\big|_{z=1} > 0$

Condition3: $P(z)\big|_{z=1} > 0$ as $n = 4$ is even

Condition4: $|b_3| > |b_0|$

where $b_3 = \begin{vmatrix} a_4 & a_0 \\ a_0 & a_4 \end{vmatrix}$ and $b_0 = \begin{vmatrix} a_4 & a_3 \\ a_0 & a_1 \end{vmatrix}$

and $|c_2| > |c_0|$

where $c_2 = \begin{vmatrix} b_3 & b_0 \\ b_0 & b_3 \end{vmatrix}$ and $c_0 = \begin{vmatrix} b_3 & b_2 \\ b_0 & b_1 \end{vmatrix}$

The following inferences are drawn from the Jury stability criterion applicable to 1 dof haptic system interacting with static virtual wall with delay:

First condition of Jury test i.e. $|a_4| < |a_0|$, put a limit on the maximum value of β i.e. on virtual damping.

Second condition of Jury stability test implies that the value of α should be greater than zero or Virtual stiffness should have finite positive value for the system stability.

Third condition of Jury test can be used to receive the analytical stability condition of the system and derive the linear relationship between the system parameters.

Fourth condition enables to draw the stability boundary of the haptic system as shown in Figure 4.

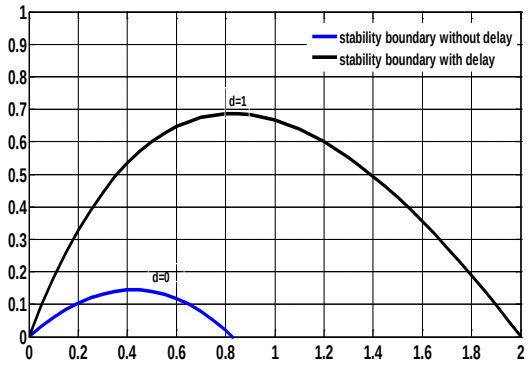

Fig 4: Stability Boundary in terms of normalized parameters with and without delay.

V. CASE STUDY

This section shows the simulation results of the stability regions of two different types of haptic devices i.e. Freedom 6 and Phantom 1.0. The Physical Parameters of both devices are shown in Table 2. The algorithm developed for Routh stability criterion and Jury stability test, the stability region obtained is same for both tests are shown for both types of devices in Fig 5 and Fig 6.

Table 2: Physical Parameters of Devices

Device	*m* *[Kg]*	*b* *[Ns/m]*	*T* *[ms]*
Phantom 1.0	0.072	0.005	1
Freedom 6	0.25	0.01	1

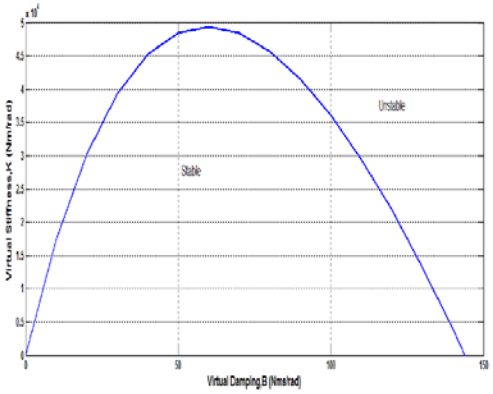

Fig 5: Stability Boundary for Phantom 1.0 Haptic Device

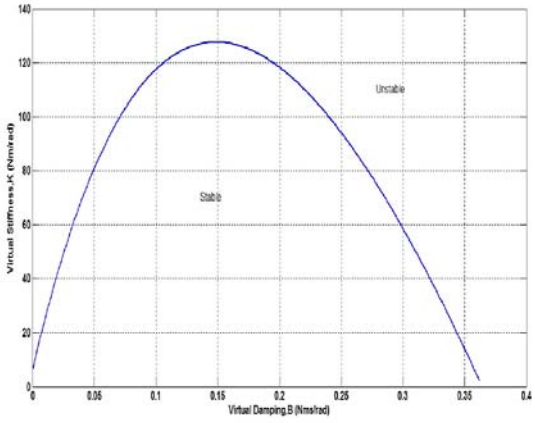

Fig 6: Stability Boundary for Freedom 6 Haptic Device

The shape of stability region curve is the same for both types of devices although the stability region of Phantom 1.0 is much larger than Freedom 6.

ISBN: 978-1-61804-228-6

VI. Conclusion

The stability of single degree of haptic interface system is studied using Jury Stability criterion and stability region is obtained. The results are compared with Routh-Hurwitz criterion. The proposed Jury stability test provides the information regarding stable values of virtual coupling elements and also establishes a linear condition between stiffness, damping and system delay for haptic systems, which was not possible with the Routh-Hurwitz.

The stability analyses are utilized for the selection of parameters of virtual coupling elements and results are presented in the form of the stability region of haptic interface which is of great importance for evaluating the performance of the device. The results are validated through simulations and are consistent with the performance of a variety of commercial haptic device. The studies are useful for the system designer in planning and selection of haptic devices.

References

[1] Minksy, M. Ouh-young, O. Steele, F. P. Brooks Jr., and M. Behensky. Feeling and seeing: Issues in force display. IEEE Computer Graphics and Applications, Vol. 24, no. 2, 1990.

[2] J. E. Colgate, P. E. Grafing, M. C. Stanley, and G. Schenkel. Implementation of stiff virtual walls in force reflecting interfaces. In Proceedings of IEEE Annual Virtual Reality International Symposium, 1993, pp. 202–208.

[3] J. E. Colgate and J. M. Brown. Factors affecting the z-width of a haptic display. In Proceedings of IEEE International Conference on Robotics and Automation, 1994, pp. 3205–3210.

[4] J. E. Colgate and G. G. Schenkel. Passivity of a class of sampled-data systems: Application to haptic interfaces. JournalRobot System, 1994, vol. 14, no. 1,pp. 37–47, 1997.

[5] Richard J. Adams and Blake Hannaford. Control Law Design for Haptic Interfaces to Virtual Reality. IEEE Transaction on Control System Technology, Vol. 10, No 1, January, 2002.

[6] Jorge Juan Gil, Alejo Avello, Angel Rubio, and Julian Florez. Stability Analysis of a 1 DOF Haptic Interface Using the Routh–Hurwitz Criterion. IEEE Transactions on Control Systems Technology, Vol. 12, No. 4, July, 2004.

[7] Jorge Juan Gil Sanchez.Emilio, T. Hulin, C. Preusche, and G. Hirzinger. Stability Boundary for Haptic Rendering: Influence of damping and Delay. Journal of Computing and Information Science in Engineering, March 2009, Vol. 9 / 1-1.

[8] K. Ogata. Discrete-time control systems,Chapter 4: Design of Discrete-Time Control Systems by Conventional Methods,Prentice-Hall, Inc. Upper Saddle River, Second Edition,NJ, SA, 1995J.

[9] Blake Hannaford, Prof. Allison Okamura. Handbook of Robotics,Chapter 30: Haptics, Springer Handbook of Robotics**,** 2008, ISBN 354023957X.

First A. Author Neelu Nagpal did her B.E.(Eelectrical Engg.) and M. Tech. in Control System from DTU Delhi and is presently Phd scholar at NIT Kurukshetra , India.

Dr Jyoti Ohri is currenly professor in Eectrical Engg Deptt

Investigation of Antenna based of New Frequency Selective Surface (FSS) for WLAN Applications

Moufida Bouslama [1], Moubarek Traii[1], Ali Gharsallah[1], and Tayeb A. Denidni[2], Senior Member, IEEE

[1] Laboratory of Electronic, Faculty of sciences of Tunis
Elmanar2092 Tunis, Tunisia
[2] University of Quebec, INRS-EMT, Place Bonaventure, 800 Gauchtière the West, Office 6900, Montreal (Quebec) H5A1K6

Abstract—In this paper, a FSS unit with filtering property is designed. This new frequency selective surfaces (NFSS) printed on a very small dielectric layer. A patch antenna is the excitation source; Software CST Microwave Studio is used to study this antenna. The input impedance, gain and radiation pattern of the E-field and H were presented. We perceive that the NFSS offer better directivity and better gain antenna for WLAN applications. The gain can be improved to approximately 17.4 dBi.

Keywords—Frequency Selective Surface (FSS), antenna resonant cavity, WLAN applications.

I. INTRODUCTION

With the appalling growth of wireless markets, antennas with periodic elements have attracted the attention of many researchers. These antennas are low cost and light weight. However, improved directivity, gain and suppression of surface waves are the properties that can offer this type of antenna. These periodic structures are electromagnetic band gap [1]-[2]-[3], meta-materials [4]-[5], or frequency selective surface [6]-[7] and even dielectrics. These FSS structures are like high reflective superstrats offering a better principal lobe with increased levels of radiation. Furthermore these NFSS not suffer mutual coupling which can degrade the performance of the antenna [8]. For years, the FSS are the subject of various studies [9]-[10] and one of the properties very used by FSS is frequency filtering. After transit of the electromagnetic wave through the FSS, some frequency are transmitted while others are reflected. Reaction of an FSS face is determined by the geometry designs periodic , by their properties of dispersion and by the step of lattice [7]-[11]. In this design, a new FSS form is proposed. These patterns are presented in a discontinuous circular shape combined with the FSS hybrid form is placed above the basic patch antenna which is excited with SMA cable. The idea of this contribution is to minimize the number of FSS structures used in creating a directional antenna with high gain and low side lobe.

II. ANTENNA AND FSS CONFIGURATION

A. New FSS unit cell

A new FSS form acting as a filter is designed the first at the beginning. The new FSS element is a discontinuous circle combined with the hybrid FSS printed on a substrate. The structure and parameters of the FSS unit are shown in the Fig.1.(a) and 1.(b). The resonance frequency is influenced by the unit cell dimensions of knowing that by decreasing the size of the FSS, the resonance frequency shifts to the high frequency range. Furthermore, the permittivity of the substrate affects the resonance frequency and bandwidth. Length of the unit cell FSS is 36 mm and the distance between the units is 8mm.

The substrate is TMM6 of Rogers with the dielectric constant is ε_r=6, and the height of the substrate is h=0381 mm. The software CST Microwave is used for the analysis of these items with a plane wave for excitation.

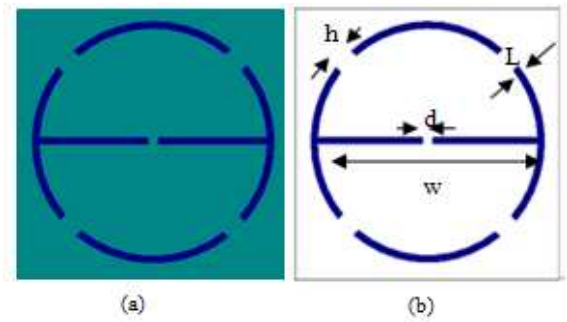

Fig.1 (a) Structure of unit cell FSS, (b)parameters of unit cell.

Table I. Final dimensions of proposed FSS cell (MILLIMITERS)

Parameters	L	h	d	w
Values	1	3	1	30

ISBN: 978-1-61804-228-6

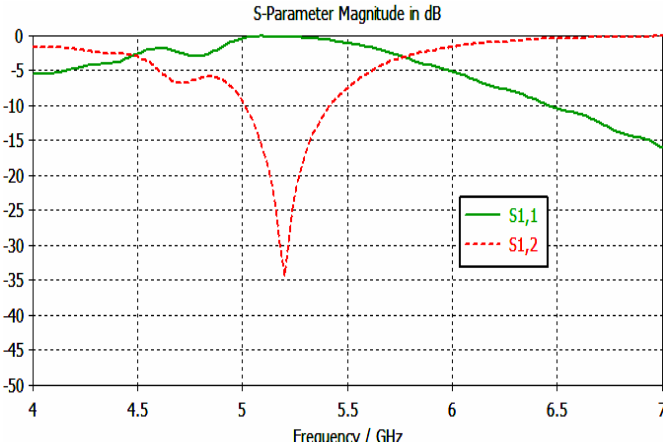

Fig.2 Simulated transmission and reflection responses of proposed FSS.

Fig.2 presents the transmission and reflection coefficient of the FSS unit cell. The FSS provides a non-conducting state at the frequency 5.2 GHz allowing the properties have a filter. For this result, a combined resonant circular ring with a discontinuous line. According to this new unit cell

we observed a stop band of the electromagnetic wave to the frequency range of 5 to 5.4 GHz.

B. Proposed Antenna with NFSS

The principle mentioned above will be applied to develop a prototype of new ground FSS operating at 5.2 GHz. Fig 3 shows the geometry of the proposed antenna. This antenna is composed of layer frequency selective surface which is placed at above the antenna.

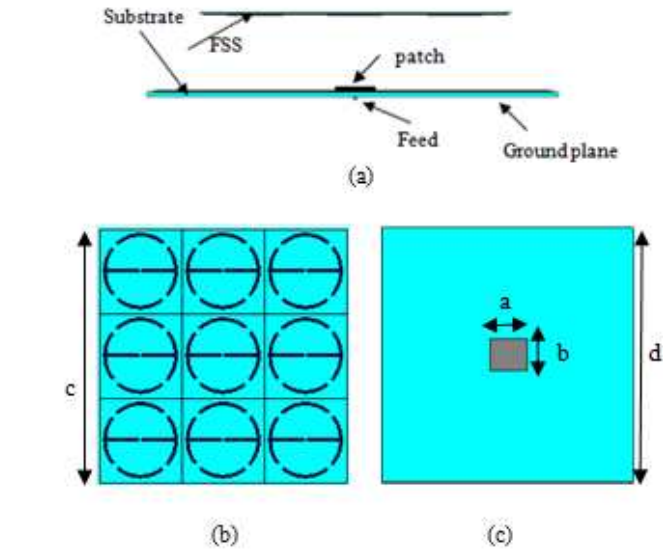

Fig.3 (a) Structure of the proposed antenna (b) Proposed hybrid FSS screen (c) Antenna patch.

Fig 3.a shows the proposed antenna excited by an SMA cable is adapted to50 Ω. The distance between the antenna and NFSS is $\lambda/2$. Fig3.b shows the configuration distributed of the new NFSS sheet. The NFSS surface is designed not only to imitate a locking / transparent surface to frequencies around 5.2 GHz, but also for controlling radiation and performance of the proposed antenna. The substrate of the antenna is RT / duroid 5870 with a permittivity equal to 2.33 and height H.

Table II. Final dimensions of proposed antenna (MILLIMITERS)

Parameters	A	b	c	d	H
Values	20.995	17.403	108	140	1.575

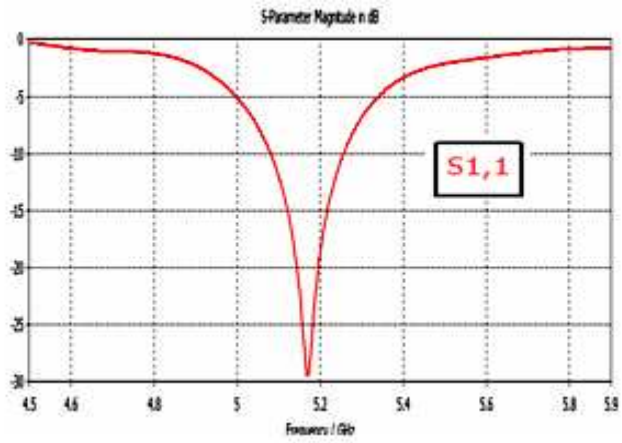

Fig.4 Antenna patch matching, simulation results.

The simulation result of the return Loss of the antenna shown in Fig.4. The final dimensions of the NFSS are used in the simulations are shown in the first part. The return loss shows that all the proposed antenna has good adaptation around 5.2 GHz. In addition, the antenna offers an adaptation in the frequency band 5.08 to 5.25 GHz.

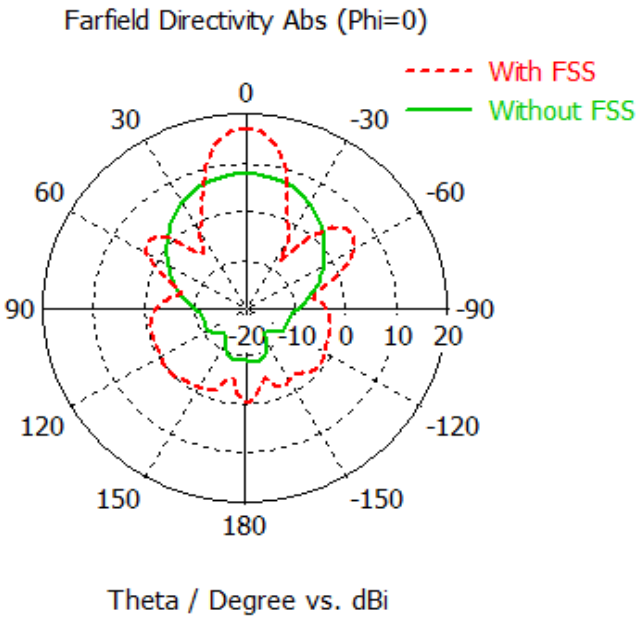

Fig.5 Gain of the antenna with and without FSS for the E-plane.

ISBN: 978-1-61804-228-6

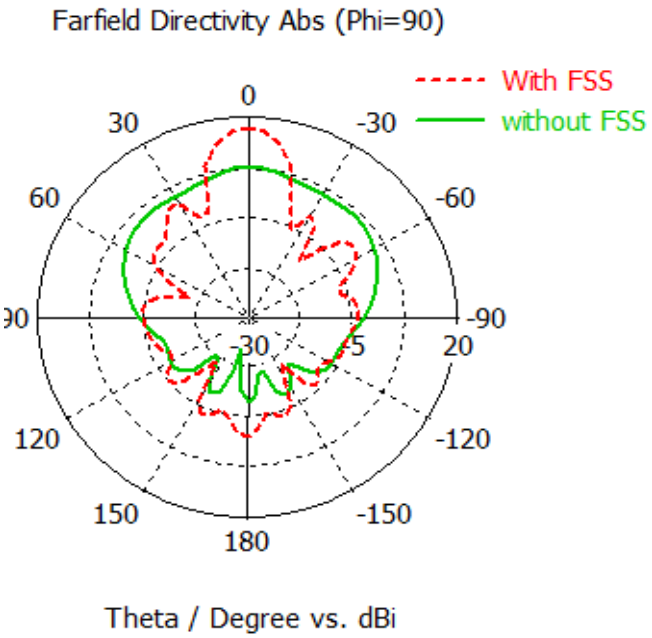

Fig.6 Gain of the antenna with and without FSS for the H-plane.

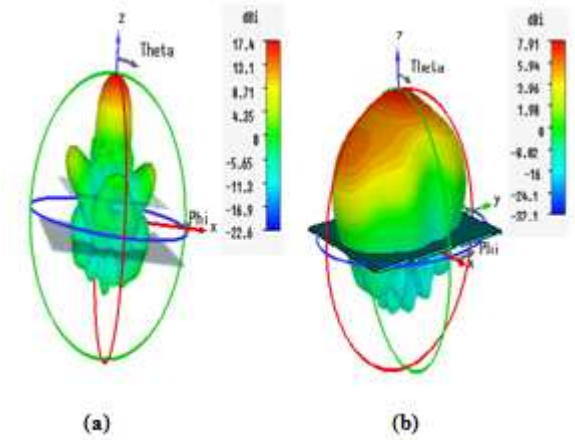

Fig.7 Gain of the antenna in 5.2 GHz : with FSS (a)and without FSS(b) .

To study the influence brought by the proposed antenna, the system is simulated. Simulation results show that the bandwidth at -3 dB experiencing a remarkable change, the principal lobe increases and will have a appearance directive. The depth of the resonance increases almost 10 dB . The transmission efficiency of the proposed antenna is better about 60%. The results are shown in Fig 5 and Fig 6.

The gain of the antenna is simulated around 5.2 GHz. We note that the gain has increased in a remarkable way since the gain of the antenna with FSS reached 17.4dBi while it was only 7.94 dBi antenna without FSS. Therefore, it is noted that the proposed antenna provides high gain over a wide frequency band.

III. CONCLUSION

In this paper, a FSS unit is designed and it is analyzed by the software CST microwave studio. The simulation results show that the filtering function may be exercised by the NFSS. In addition, an antenna resonant cavity based on the structure of the NFSS was presented. The proposed antenna has a simulated gain 17.4 dBi at 5.2 GHz. Thanks to these characteristics, the new antenna based FSS may be used for WLAN applications.

ACKNOWLEDGEMENT

Authors acknowledges the support of the University of Quebec, INRS-EMT.

REFERENCES

[1] Kanso, R. Chantalat, M. Thevenot, E. Arnaud and T. Monediere "Offset Parabolic Reflector Antenna Fed by EBG Dual Band Focal Feed for Space Application",IEEE Antennas and Wireless Propagation Letters, Vol 9, accepted August14,2010.

[2] L. Leger, T. Monédière, B. Jecko. *Enhancement of gain and radiation bandwidth for a planar 1-D EBG antenna*, IEEE Antennas and Wireless Propagation Letters, Vol. 15, N°9, September 2005.

[3] D. Nashaat, H. A. Elsadek, E.t Abdallah, H. Elhenawy and M. F. Iskander, "Enhancement of Microstrip Monopole Antenna Bandwidth by Using EBG Structures published in IEEE Antennas and Wireless Propag., Letters, vol. 8, pp.959-963, 2009.

[4] Chen, Xi ; Hui Feng Ma ; Ying Zou, Xia ; Jiang, Wei Xiang ;Cui, Tie Jun " Three-dimensional broadband and high-directivity lensantenna made of metamaterials" Journal of Applied Physics, vol 110, 044904 - 044904-8 ,2011

[5] Dhouibi, A. ; Burokur, S.N. ; de Lustrac, A. ; Priou, A. " Low-Profile Substrate-Integrated Lens Antenna UsingMetamaterials" Antennas and Wireless Propagation Letters, IEEE 43-46, 2013

[6] Bayatpur,F. ; Sarabandi,K. "Miniaturized FSS and Patch Antenna Array Coupling for Angle-Independent, High-Order Spatial Filtering" Microwave and Wireless Components Letters, IEEE, Vol 20,79-81,20107

[7] Munk, «Frequency Selective Surfaces : Theory and Design.» *J. Wiley Interscience, US*, 2000.

[8] Yang, F. and Y. Rahmat-Samii, \Microstrip antennas integrated with Electromagnetic Band-Gap (EBG) structures: A low mutual coupling design for array applications," *IEEE Trans.Ant. Propag.*, Vol. 51, No. 10, Oct. 2003.

[9] R. Orta, R. Tascone, R. Zich, "Scattering from finite extent Frequency selective surface illuminated by arbitrary sources", Electronics Letters, Vol.21, No3, 1985

[10] Chich-Hsing Tsao ; Mittra, R. "Spectral-domain analysis of frequency selective surfaces comprised of periodic arrays of cross dipoles and Jerusalem crosses "Antennas and Propagation, IEEE Transactions , vol 32,478-486,1984

[11] LI Xiao-qiu, GAO Jing-song "Effects of Y loop element FSS structure parameter on frequency response" Optics and Precision Engineering.Vol.6 pp.1070-1075, 2006.

Square Root Generator for Galois Field in Multiple-Valued Logic – Larger Systems

Nabil A. Abu-Khader and Nesreen F. Al-Nashashibi

Abstract— This paper is based on our previous paper entitled "Square Root Generator for Galois Field in Multiple-Valued Logic"[1] where we have discussed several patents in the area of Multiple-Valued Logic in Galois Fields. In [1], we have presented two pipelined square root circuits for Galois field in Multiple-Valued Logic (MVL) for smaller systems as well as various patents. We also discussed basic Galois Field properties. We have used composite Galois fields in a MVL approach to generate the required square root value in the field. The fact that less literals are used in our approach speeds up the calculation operation. The MVL approach of calculating the square root in a composite Galois field is novel. In this review, we present the application of this approach in larger Galois Field systems. It is highly recommended for readers to review [1,2] before proceeding with this paper since it contains rich reference material.

Keywords— MVL, Galois Field, Larger Systems.

I. Introduction

GALOIS FIELD $GF(p^k)$ is a polynomial field, and $GF((p^n)^m)$ is a composite field, where $k = nm$ and p is a prime number. p is the base and it was chosen to be = 2 since the base of the binary system consists of 0 and 1. k will give a series of 0s and 1s from the coefficients of a polynomial. This polynomial is generated using an irreducible polynomial. If we split $k = nm$, then we will have $GF((2^n)^m)$. In the quaternary system, we have four different states, that is why n should equal to 2. Then we have $GF((2^2)^m)$ as the Galois quaternary field. To have an equivalent system for $GF(2^4)$, m should equal to 2, and to have the equivalent system for $GF(2^6)$, m should equal to 3 and so on.

This work was prepared by the following authors:
Dr. N. A. Abu-Khader, Regional Training Manager – Middle East for Compressor Controls Corporation, Abu-Dhabi, UAE. (Phone: 971-2- 446 9671; fax: 971-2-446 96712; e-mail: nabil_abukhader@hotmail.com).
N. F. Al-Nashashibi, Electrical and Computer Engineer, Dubai, UAE (e-mail: nesreen_nashashibi@yahoo.com).

Based on our approach in [1] and in [3,4], we have used a 4-level system to encode the elements of Galois field. On the other hand, the extension of our idea to an 8-level system design will be an interesting idea. In this case, Galois field will be of the form $GF((2^4)^m)$ for any m. The main challenge in these kinds of circuits is to design an 8-level Galois field adder and multiplier circuits which remains as future look.

In this paper, we will illustrate how to deal with larger Galois field systems. In the previous paper [1], we dealt with smaller Galois Field $GF((2^2)^2)$. Here, we will expand our quaternary basis to the case where $m = 3$, i.e., $GF((2^2)^3)$. Several equations are being used to illustrate the expansion principle. Binary Galois field $GF(2^6)$ table is illustrated below. The primitive element $\alpha = 010000$, and the primitive irreducible polynomial = $x^6 + x + 1$.

α	**Polynomial**	**4-tuple**
α^{∞}	0	000000
α^0	1	100000
α^1	x	010000
α^2	x^2	001000
α^3	x^3	000100
α^4	x^4	000010
α^5	x^5	000001
α^6	$1+x$	110000
α^7	$x+x^2$	011000
α^8	x^2+x^3	001100
α^9	x^3+x^4	000110
α^{10}	x^4+x^5	000011
α^{11}	$1+x+x^5$	110001
α^{12}	$1+x^2$	101000
α^{13}	$x+x^3$	010100
α^{14}	x^2+x^4	001010
α^{15}	x^3+x^5	000101
α^{16}	$1+x+x^4$	110010

ISBN: 978-1-61804-228-6

α^{17}	$x+x^2+x^5$	011001
α^{18}	$1+x+x^2+x^3$	111100
α^{19}	$x+x^2+x^3+x^4$	011110
α^{20}	$x^2+x^3+x^4+x^5$	001111
α^{21}	$1+x+x^3+x^4+x^5$	110111
α^{22}	$1+x^2+x^4+x^5$	101011
α^{23}	$1+x^3+x^5$	100101
α^{24}	$1+x^4$	100010
α^{25}	$x+x^5$	010001
α^{26}	$1+x+x^2$	111000
α^{27}	$x+x^2+x^3$	011100
α^{28}	$x^2+x^3+x^4$	001110
α^{29}	$x^3+x^4+x^5$	000111
α^{30}	$1+x+x^4+x^5$	110011
α^{31}	$1+x^2+x^5$	101001
α^{32}	$1+x^3$	100100
α^{33}	$x+x^4$	010010
α^{34}	x^2+x^5	001001
α^{35}	$1+x+x^3$	110100
α^{36}	$x+x^2+x^4$	011010
α^{37}	$x^2+x^3+x^5$	001101
α^{38}	$1+x+x^3+x^4$	110110
α^{39}	$x+x^2+x^4+x^5$	011011
α^{40}	$1+x+x^2+x^3+x^5$	111101
α^{41}	$1+x^2+x^3+x^4$	101110
α^{42}	$x+x^3+x^4+x^5$	010111
α^{43}	$1+x+x^2+x^4+x^5$	111011
α^{44}	$1+x^2+x^3+x^5$	101101
α^{45}	$1+x^3+x^4$	100110
α^{46}	$x+x^4+x^5$	010011
α^{47}	$1+x+x^2+x^5$	111001
α^{48}	$1+x^2+x^3$	101100
α^{49}	$x+x^3+x^4$	010110
α^{50}	$x^2+x^4+x^5$	001011
α^{51}	$1+x+x^3+x^5$	110101
α^{52}	$1+x^2+x^4$	101010
α^{53}	$x+x^3+x^5$	010101
α^{54}	$1+x+x^2+x^4$	111010
α^{55}	$x+x^2+x^3+x^5$	011101
α^{56}	$1+x+x^2+x^3+x^4$	111110
α^{57}	$x+x^2+x^3+x^4+x^5$	011111
α^{58}	$1+x+x^2+x^3+x^4+x^5$	111111
α^{59}	$1+x^2+x^3+x^4+x^5$	101111
α^{60}	$1+x^3+x^4+x^5$	100111
α^{61}	$1+x^4+x^5$	100011
α^{62}	$1+x^5$	100001

Table 1: Binary Galois field $GF(2^6)$

The conversion parameter $\beta = \alpha^s$ can be found as [5]:

$$s = \frac{2^{nm}-1}{2^n-1} = \frac{2^6-1}{2^2-1} = 21 \quad \Rightarrow \beta = \alpha^{21} \qquad \text{....(1)}$$

The conversion matrix T can be found by finding the representation of an element in $GF((2^2)^3)$ in terms of $GF(2^6)$. From [1], we have:

$$A = \sum_{i=0}^{m-1} a_i'\alpha^i = \sum_{i=0}^{2} a_i'\alpha^i = a_0' + a_1'\alpha + a_2'\alpha^2 \qquad \text{....(2)}$$

Using our approach in [1] and Equation (2), then *A* can be represented as:

$$A = a_{00} + a_{01}\beta + (a_{10} + a_{11}\beta)\alpha + (a_{20} + a_{21}\beta)\alpha^2 \qquad \text{...(3)}$$

Substituting $\beta = \alpha^{21}$, then by reducing the resulting terms using the irreducible polynomial $x^6 + x + 1$, we will have:

$$A = (a_{00} + a_{01} + a_{11} + a_{21}) + (a_{01} + a_{10})\alpha + (a_{11} + a_{20})\alpha^2 + (a_{01} + a_{21})\alpha^3 + (a_{01} + a_{11})\alpha^4 + (a_{01} + a_{11} + a_{21})\alpha^5 \qquad \text{...(4)}$$

$$\Rightarrow a_0 = a_{00} + a_{01} + a_{11} + a_{21}$$

$$\Rightarrow a_1 = a_{01} + a_{10}$$

$$\Rightarrow a_2 = a_{11} + a_{20}$$

$$\Rightarrow a_3 = a_{01} + a_{21}$$

$$\Rightarrow a_4 = a_{01} + a_{11}$$

$$\Rightarrow a_5 = a_{01} + a_{11} + a_{21}$$

This will form the following matrix equation:

$$\begin{bmatrix} a_0 \\ a_1 \\ a_2 \\ a_3 \\ a_4 \\ a_5 \end{bmatrix} = \begin{bmatrix} 1 & 1 & 0 & 1 & 0 & 1 \\ 0 & 1 & 1 & 0 & 0 & 0 \\ 0 & 0 & 0 & 1 & 1 & 0 \\ 0 & 1 & 0 & 0 & 0 & 1 \\ 0 & 1 & 0 & 1 & 0 & 0 \\ 0 & 1 & 0 & 1 & 0 & 1 \end{bmatrix} \cdot \begin{bmatrix} a_{00} \\ a_{01} \\ a_{10} \\ a_{11} \\ a_{20} \\ a_{21} \end{bmatrix} \quad \ldots(5)$$

Then, our conversion matrix T will be:

$$T = \begin{bmatrix} 1 & 1 & 0 & 1 & 0 & 1 \\ 0 & 1 & 1 & 0 & 0 & 0 \\ 0 & 0 & 0 & 1 & 1 & 0 \\ 0 & 1 & 0 & 0 & 0 & 1 \\ 0 & 1 & 0 & 1 & 0 & 0 \\ 0 & 1 & 0 & 1 & 0 & 1 \end{bmatrix} \quad \ldots(6)$$

The Matrix T gives the representation of an element in the binary Galois field $GF(2^6)$ given its representation in the composite Galois field $GF((2^2)^3)$. The inverse transformation, i.e., the conversion from $GF(2^6)$ to $GF((2^2)^3)$, requires the computation of T^{-1},

$$T^{-1} = \begin{bmatrix} 1 & 0 & 0 & 0 & 0 & 1 \\ 0 & 0 & 0 & 1 & 1 & 1 \\ 0 & 1 & 0 & 1 & 1 & 1 \\ 0 & 0 & 0 & 1 & 0 & 1 \\ 0 & 0 & 1 & 1 & 0 & 1 \\ 0 & 0 & 0 & 0 & 1 & 1 \end{bmatrix} \quad \ldots(7)$$

The irreducible polynomial for $GF((2^2)^3)$ can be found as:

$$F(x) = (x+\alpha)(x+\alpha^4)(x+\alpha^{16})$$

$$= x^3 + (\alpha + \alpha^4 + \alpha^{16})x^2 + (\alpha^5 + \alpha^{17} + \alpha^{20})x + \alpha^{21}$$

$$= x^3 + x^2 + \alpha^{42}x + \alpha^{21}$$

$$= x^3 + x^2 + \beta^2 x + \beta \quad \ldots(8)$$

Using the MVL representation Table from [1], the irreducible polynomial becomes:

$$F(x) = x^3 + x^2 + 3x + 2 \quad \ldots(9)$$

II. THE RELATION BETWEEN THE FIELDS $GF(2^6)$ AND $GF((2^2)^3)$

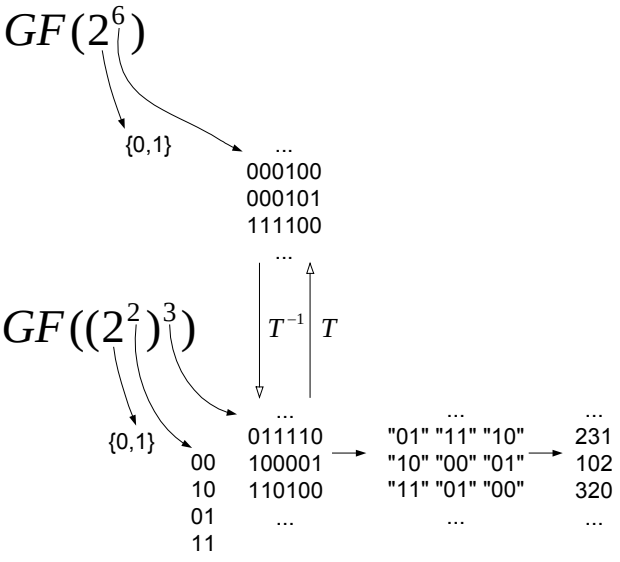

III. MULTIPLICATION EXAMPLE ON THE LARGER FIELDS

Suppose we want to find the multiplication of two elements in both fields $GF(2^6)$ and $GF((2^2)^3)$.

Let $A=\alpha^3$, $B=\alpha^{15}$, and

$F(x)=x^3+x^2+3x+2$.

To find AB in $GF(2^6)$:

$$AB=\alpha^3\alpha^{15}=\alpha^{(18)\bmod(2^6-1)}=\alpha^{18\bmod 63}=\alpha^{18}$$

From the Table 1, we find that $\alpha^{18}=111100$.

Now, to find AB in $GF((2^2)^3)$:

Using T^{-1}, we find the representation of A and B in $GF((2^2)^3)$:

$$A=<011110>\equiv 2+3\alpha+\alpha^2\equiv<231>,$$

$$B=<100001>\equiv 1+2\alpha^2\equiv<102>.$$

Then, we can multiply the resulting polynomials to find the product AB as:

$$AB=(2+3\alpha+\alpha^2)(1+2\alpha^2)$$
$$=2+3\alpha+\alpha^2+3\alpha^2+\alpha^3+2\alpha^4 \quad \ldots(10)$$

Using the given irreducible polynomial $F(x)=x^3+x^2+3x+2$, we reduce the powers of Equation (10) by substituting:

$$\alpha^3=\alpha^2+3\alpha+2$$

$$\alpha^4=2\alpha^2+\alpha+2$$

Then we have:

$$AB=2+3\alpha+\alpha^2+3\alpha^2+\alpha^2+$$
$$3\alpha+2+2(2\alpha^2+\alpha+2) \quad \ldots(11)$$

Using our approach in [1], Equation (11) becomes:

$$AB=3+2\alpha \quad \ldots(12)$$

This forms the pair <320> which is equivalent to $<110100>$ as per our assumption in [1].

Using the matrix T:

$$\begin{bmatrix}a_0\\a_1\\a_2\\a_3\\a_4\\a_5\end{bmatrix}=\begin{bmatrix}1&1&0&1&0&1\\0&1&1&0&0&0\\0&0&0&1&1&0\\0&1&0&0&0&1\\0&1&0&1&0&0\\0&1&0&1&0&1\end{bmatrix}\cdot\begin{bmatrix}1\\1\\0\\1\\0\\0\end{bmatrix}=\begin{bmatrix}1\\1\\1\\1\\0\\0\end{bmatrix}\equiv 111100$$

So the answer is the same in both systems.

IV. SQUARE ROOT ALGORITHM

The $\sqrt{A}$ operation can be found from the below property [1]:

$$A^{2^k-1}=1 \rightarrow A^{2^k}=A$$

$$A^{(2^k)/2}=\sqrt{A} \rightarrow A^{2^k2^{-1}}=\sqrt{A}$$

$$\Rightarrow \sqrt{A}=A^{2^{(k-1)}}$$

Here in this larger system $k = 6$, then the above equation might be written as:

$$\sqrt{A}=A^{2^5}=A^{32\ \bmod(2^6-1)} \quad \ldots(13)$$

V. SQUARE ROOT CALCULATION EXAMPLE

Let $A=\alpha^3$, and $F(x)=x^3+x^2+3x+2$.

To find $\sqrt{A}$ in $GF(2^6)$:

$$\sqrt{\alpha^3}=(\alpha^3)^{32\ \bmod(2^6-1)}=\alpha^{33}$$

From the Table 1, we find that $\alpha^{33}=010010$.

ISBN: 978-1-61804-228-6

Now, to find $\sqrt{A}$ in $GF((2^2)^3)$ we need to

calculate $\sqrt{A} = A^{2^5} = A^{10} = A^2A^2A^2A^2A^2$

$A =< 011110 > \equiv 2 + 3\alpha + \alpha^2 \equiv < 231 >$ from the above example, then calculate $A^2 = AA$ then $\sqrt{A} = A^2A^2A^2A^2A^2$:

$$\sqrt{A} = A^2A^2A^2A^2A^2 = 2 + 2\alpha^2 \equiv < 202 >$$

This forms the pair <202> which is equivalent to

$< 010001 >$ as per our assumption in [1].

Using the matrix T:

$$\begin{bmatrix} a_0 \\ a_1 \\ a_2 \\ a_3 \\ a_4 \\ a_5 \end{bmatrix} = \begin{bmatrix} 1 & 1 & 0 & 1 & 0 & 1 \\ 0 & 1 & 1 & 0 & 0 & 0 \\ 0 & 0 & 0 & 1 & 1 & 0 \\ 0 & 1 & 0 & 0 & 0 & 1 \\ 0 & 1 & 0 & 1 & 0 & 0 \\ 0 & 1 & 0 & 1 & 0 & 1 \end{bmatrix} \cdot \begin{bmatrix} 0 \\ 1 \\ 0 \\ 0 \\ 0 \\ 1 \end{bmatrix} = \begin{bmatrix} 0 \\ 1 \\ 0 \\ 0 \\ 1 \\ 0 \end{bmatrix} \equiv 010010$$

So the answer is the same in both systems.

VI. CONCLUSIONS AND FUTURE DEVELOPMENTS

We have presented a unique encoding technique to interpret the binary signals into MVL signals in an equivalent content using the quaternary system. In this review, we have shown that our unique encoding technique is expandable for larger systems to any Galois field order. This method can be applied in applications in [6,7]. In this paper, we have added a new and innovative way to do calculations in larger Galois Fields for MVL. We believe that the interpretation technique for MVL signals using composite Galois fields made our approach successful. This work complements our Galois Field calculations in MVL so a full 8-level Galois Field CPU can be designed. The main challenge in these kinds of circuits is to design an 8-level Galois field adder and multiplier circuits which remains as future look.

ACKNOWLEDGMENT

The authors declare no acknowledgements to this particular paper.

REFERENCES

[1] N. Abu-Khader, et al., "Square Root Generator for Galois Field in Multiple-Valued Logic", Recent Patents on Electrical Engineering, Vol. 4, No. 3, Sep. 2011, Pages 209-213.
[2] N. Abu-Khader, and P. Siy, "Systolic Galois Field Exponentiation in a Multiple-Valued Logic Technique", Integration, the VLSI Journal, Vol. 39, Issue 3, Jun 2006, Pages 229-251.
[3] C. P. Chen, Y. C. Hung, L.L. Lin, "Cryptography System and Elliptic Curve Operation Method" US20070198824 A1 (2007).
[4] Y. Stein, J. A. Kablotsky, "Compound Galois field engine and Galois field divider and square root engine and method" US7895253B2 (2011).
[5] B. Sunar, E. Savas, CK. Koc, „Constructing composite field representations for efficient conversion", IEEE Trans Comput 2003; 52 (11): 1391-1398.
[6] B. Schneier, "Applied cryptography", John Wiley & Sons, Inc. 1996.
[7] MR. Schroeder, "Number theory in science and communication", Springer-Verlag, 2nd Edition, 1986.

Formant Frequency Tuning in Professional Byzantine Chanters

Georgios Chrysochoidis and Georgios Kouroupetroglou

Abstract**—** In this study we present the digital signal processing of formant frequency tuning in the context of the Byzantine chant voices. The DAMASKINOS prototype acoustic corpus of Byzantine Ecclesiastic professional voices was adopted for the selection of the recordings for the analysis. We have investigated recordings from 2 different professional chanters in ascending and descending musical scales of the diatonic genre, for the five vowels /a/, /e/, /i/, /o/ and /u/. The method of analysis included a semi-automatic segmentation of the audio material, extraction of the pitch and formant frequencies in PRAAT and final post-processing in MATLAB. For pitch analysis we implement a robust analysis algorithm that performs acoustic periodicity detection on the basis of an accurate autocorrelation method. Formant values were calculated with the Burg algorithm. Results show clear evidence that chanters tend to use personal formant tuning strategies throughout their vocal range.

Keywords**—** singing analysis, chanting processing, formant tuning, pitch.

I. Introduction

IN 1960, Gunnar Fant presented the theory of a source-filter production model for vowels, in his work "Acoustic Theory of Speech Production" [1]. According to this model, the voice source produces a harmonic series, consisting of the fundamental frequency $f0$ and a large number of harmonic frequencies, the partials [1].

Specifically, when applied to vowel production, the speech signal could be thought as the result of the source signal, produced by the glottis, and the resonator or vocal tract filter. A linear mathematical model supports this theory, which allows for relatively simple handling of calculations. The vocal tract filter can be further considered as a linear time-invariant filter for very short periods of time, making the system even more mathematically tractable. The source-filter theory of vowel production is summarized in the following equation:

$$P(f) = U(f)\, T(F)\, R(f)$$

where P(f) id the radiated sound pressure spectrum of speech, U(f) refers to the volume velocity and is used because of vocal folds act like a source of air pulses. T represents the transfer function and R denotes the radiation characteristics. For the current work we consider the terms U(F) and R(f) to be constant a different vowels are produced. Therefore, different vowels can be described as variations in the transfer function T(f) and the radiated spectrum P(f).

The resonance frequencies of the vocal tract are called formants, designated as F1, F2, F3, etc. in ascending order, and they can be displayed as spectral peaks in the frequency response of the vocal tract filter [1]. The vocal tract has four or five important formants that are used to amplify and dampen certain frequencies. The length and shape of the vocal tract determine the formant frequencies, resulting in the production of the different vowel sounds of the radiated speech signal. The lowest two formants F1 and F2 largely determine the vowel [1], while the remaining higher order formants are related to the quality of tone [2].

Adjusting the vocal tract in order to align formants with harmonics, thereby amplifying certain portions of the vocal spectrum, is known as formant tuning [3]. This intuitive act, that is highly dependent upon the vertical laryngeal positions, has been used from trained singers in the past, in cases where the singing voice should be heard across large spaces along with other sound sources, like for example music orchestras [3].

In the past, research concentrated on the relation between the quality of the voice and the formants. Later works [4], [5], revealed the existence of the singer's formant, which can be explained acoustically as a clustering of formants, F3 and F4, or F4 and F5, and even in some cases F3, F4, and F5. The singer's formant enables a singer to be heard over an orchestra, since there is little competition from the orchestra near the frequency range of the singer's formant [4]. This is a way for the singer to save some vocal effort, in other words it results in "vocal economy" [3].

Formant tuning is considered as another vocal strategy used by trained singers when trying to produce the ideal voice and economizing on vocal effort. Several works have been

This work has been co-financed by the European Union (European Social Fund – ESF) and Greek national funds through the Operational Program "Education and Lifelong Learning" of the National Strategic Reference Framework (NSRF) - Research Funding Program: "THALES - Investing in knowledge society through the European Social Fund", under the project: "ERASITECHNIS: Processing, Analysis, Synthesis and Context-Based Retrieval for Multimedia Music-Related Data Bases of Traditional Music and Dancing Recordings", MIS 375435.

G. Chrysochoidis is with the Division of Signal Processing and Communication, Department of Informatics and Telecommunications, National and Kapodistrian University of Athens, GR 15784 Athens, Greece (e-mail: geoxry@di.uoa.gr).

G. Kouroupetroglou is with the Division of Signal Processing and Communication, Department of Informatics and Telecommunications, National and Kapodistrian University of Athens, GR 15784 Athens, Greece (e-mail: koupe@di.uoa.gr).

published concerning formant tuning strategies applied by classically trained Western operatic voices [6], [2], [8], [9], as well as contemporary [10] and traditional [11] ones. Recent works [8], [9] give a description of the formant tuning literature with details about the different methods and their limitations [9]. Three trends seem to be the dominant ones: a) F1 and F2 are tuned to a partial, b) F1 and F2 are not related anyhow to harmonics of the $f0$ and c) F1 and F2 are tuned just above their nearest partial in a way so that they don't coincide.

While literature on formant tuning continues to grow for other types of vocal music genres, Byzantine Ecclesiastic chant voice hasn't been studied extensively in the same context. Following our work on the existence of formant tuning in Byzantine chant [7] our current investigation tries to answer whether formant tuning strategies exist in Byzantine chant, which is examining if chanters use intentionally formant tuning to produce the desired acoustical result.

II. Byzantine chant music

Byzantine Chant Music (BCM) is a religious type of monophonic vocal performance practiced mainly in churches. Its main purpose is to serve the religious needs of the Orthodox Christian worship, providing a musical accompaniment for the ecclesiastical poetry [12], [13]. BCM follows aesthetical rules formed over the course of centuries, traditionally transferred from master performers to apprentices. It is a microtonal music since it contains intervals smaller than the conventional contemporary Western theory semitone.

The temperament used in modern Byzantine chant is based on a 72 equal divisions of the octave, called moria (plural form of morio) [13]. Compared to the 12-tone equal temperament followed by the Western theory, a Western semitone would equal to 6 moria in this 72-tone equal temperament system. Byzantine music uses the term echos to refer to a specialized type of musical mode [12], [13], denoting not only the musical scale being applied in a melody with a definite "tonic" or main note called vasi (Greek word for "base"), but also specific musical phrasing [13].

There are three musical genera in Byzantine chant: the diatonic, the chromatic and the enharmonic [12], [13]. The fundamental intervallic differences between the three genera, apart from musical aesthetics, serve different musical meanings, when considered in a specific lyric context. This leads to another classification of the three genera and its subdivisions, based on the ethos of the music genre, as Chrysanthos of Madytos, one of the main three reformers of the modern Byzantine music theory, named it [12], [14].

The musical scale used by the chanters in this work belongs to the diatonic genre shown in Figure 1.

III. Materials

The measurements used in our analysis were acquired using the PRAAT software. PRAAT is a valuable software tool in the field of phonetics and voice analysis in general [18]. It is a flexible tool, which provides functionality that could handle most of the tasks needed in this work. It handles all the widely used audio file formats by importing the audio files as objects on which various operations can be applied. Apart from sound files, PRAAT can create and make use of tagging files in the form of layers called tiers. Tiers consist of boundaries and intervals between them. Labels can be added at these intervals making it easy to tag sound recordings. Several tiers can form a TextGrid object. To summarize the main PRAAT features we used in our analysis: a. it handles large audio files, b. it extracts measurements of the vocal parameters using its built-in functions, c. it uses tagging layers for audio file annotation, and d. it uses a scripting language for automating processing. Indeed, PRAAT can manipulate, edit and analyze long stereo audio files. Annotation of the files is done with tagging layers, using boundaries to mark time exact points in the recording, and the intervals in-between them to insert the metadata. One of the most powerful features of PRAAT is inevitably its scripting language. This language includes variables, loops, jumps, formulas, procedures, arrays, etc. which provide the flexibility to implement complex algorithms in combination with the ready-to-use analysis commands found in PRAAT.

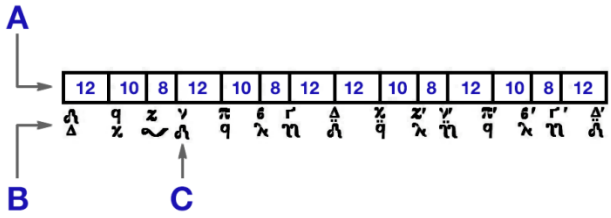

Figure 1. Diatonic genre scale used in Byzantine chant. A: Scale intervals measured in moria (72-tone equal temperament). B: Symbols used for the scale degrees. C: Scale's tonic.

The functions that were mostly used in our measurements are the ones for pitch and formant analysis. For pitch analysis PRAAT uses an algorithm that performs an acoustic periodicity detection on the basis of an accurate autocorrelation method [19].

Formant values are calculated with the algorithm by Burg [20], [21]. PRAAT is a commonly used speech analysis tool and its accuracy has been thoroughly tested in several related papers [22], [23], [24]. Furthermore, PRAAT measurements are used in many investigations as the baseline for accuracy comparisons [25], [26], [27], [28].

We started processing the audio files by using a series of PRAAT scripts that analyzed intensity and pitch, in order to annotate the audio file, by marking the basic musical units, which correspond to the scale's degrees [17]. Our final purpose was to extract separate audio files for each scale's degree. This was a three-step process: 1. voiced – unvoiced parts of the audio file were labeled using a tag layer, 2. for each voiced part boundaries were placed at pitch transitions between the scale's degrees, and 3. intervals in-between boundaries were labeled according the audio segment's average pitch. Before moving forward to the next step we were able to fine-adjust the placement of the boundaries. The transition zones between notes have been excluded. Each audio segment between boundaries was extracted to a separate audio file with average time duration of 1 sec.

ISBN: 978-1-61804-228-6

Next, we analyzed each of the extracted files, using PRAAT's readily available functions, in order to acquire the actual measurements we needed. Three vocal parameters were measured every 10 msec: pitch value for f0, frequency values for the formants F1 and F2. Other measurements, like sound intensity level, formant bandwidths, formant levels and partials levels were also extracted, although not used in the current work. All data were stored in tab-delimited text files.

Final processing was done in Matlab. First the data files were imported, the mean values were calculated for pitch and formant frequencies and the corresponding graphs were plotted.

Our aim was to be able to compare both ascending and descending scales for each vowel in order to be able to determine if formant tuning was used intentionally by the chanters.

IV. Results

Displaying and analyzing the actual measurements for each chanter was the next step in our investigation. This involves plotting the frequency tracks of the two lowest formants F1 and F2, along with the partials h2-h8, where $hn = n \cdot f0$ and f0 is the fundamental frequency of the vowel. Figure 2 and 3 present these measurements for each chanter respectively. Both axes represent frequency values in semitones, measured from D2 (73 Hz).

In order to be able to easily compare ascending and descending scales, the descending part was plotted using vertical mirroring as to overlay over the ascending part.

The pitch range that draws our attention is the one referred to as the passaggio, which is D4-G4 for tenors and B3-E4 for baritones [6], [9], [29]. It has been found that formant tuning is mostly observed in and above this range [9]. This can be easily seen in our results. Most chanters tend to tune their F1 and F2 to partials at this pitch range, although there were cases of formant tuning at lower scale degrees.

Considering an accuracy margin of about 20 Hz for the tuning of the formant frequencies [32], [9], as well as the maximum distance criterion of 50 Hz between the formant and its nearest harmonic, used in similar works [9], a 2 semitone approximate distance between the formant F1 and the partial h2, in the frequency range of E4, could still be counted as tuning [9]. This could easily explain the distance between the F1 and h2, found in the results for chanter 1, since it can be considered inside the formant tuning tolerance limits.

The distance in semitones between each formant F1, F2 and their closest partial for all vowels, is displayed in Fig. 2. The data presented in the graphs are for the ascending and descending diatonic scales, for both chanters.

Results for chanter 1 (Fig. 2) show a clear tendency of the F1 and F2 formants to follow the slope of the h2 and h4 respectively, inside the passaggio area, although sometimes h3 and h4 are also used for the tuning of f1 and f2. Formant tuning is evident in four of the total five vowels.

Formants F1 and F2 of chanter 2 (Fig. 3) show signs of formant tuning especially at the passaggio range and above. The second chanter represents a typical example of the formant tuning phenomenon since f1 is in most cases aligned with the h2 harmonic in all 5 vowels.

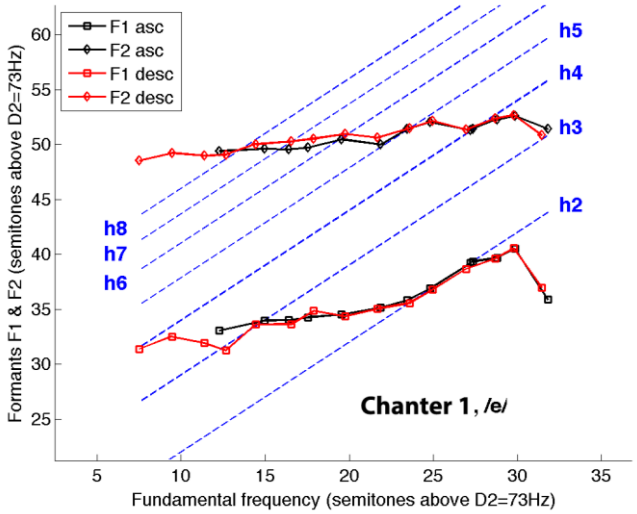

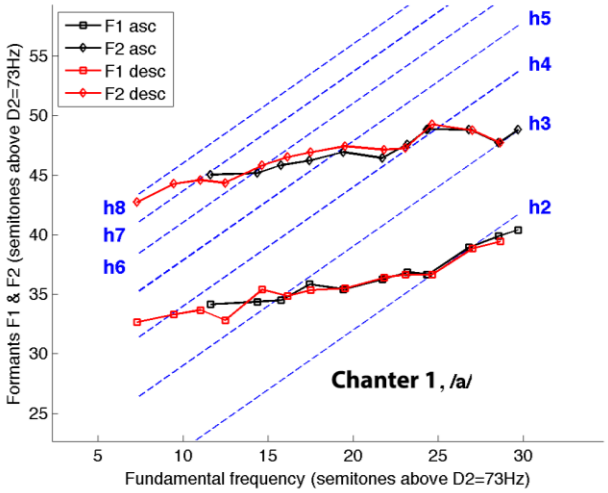

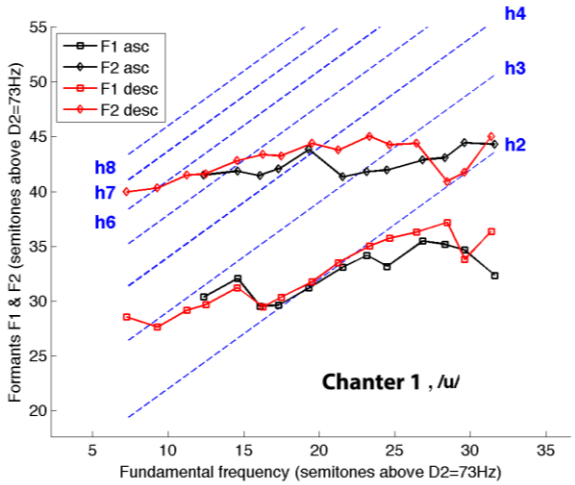

ISBN: 978-1-61804-228-6

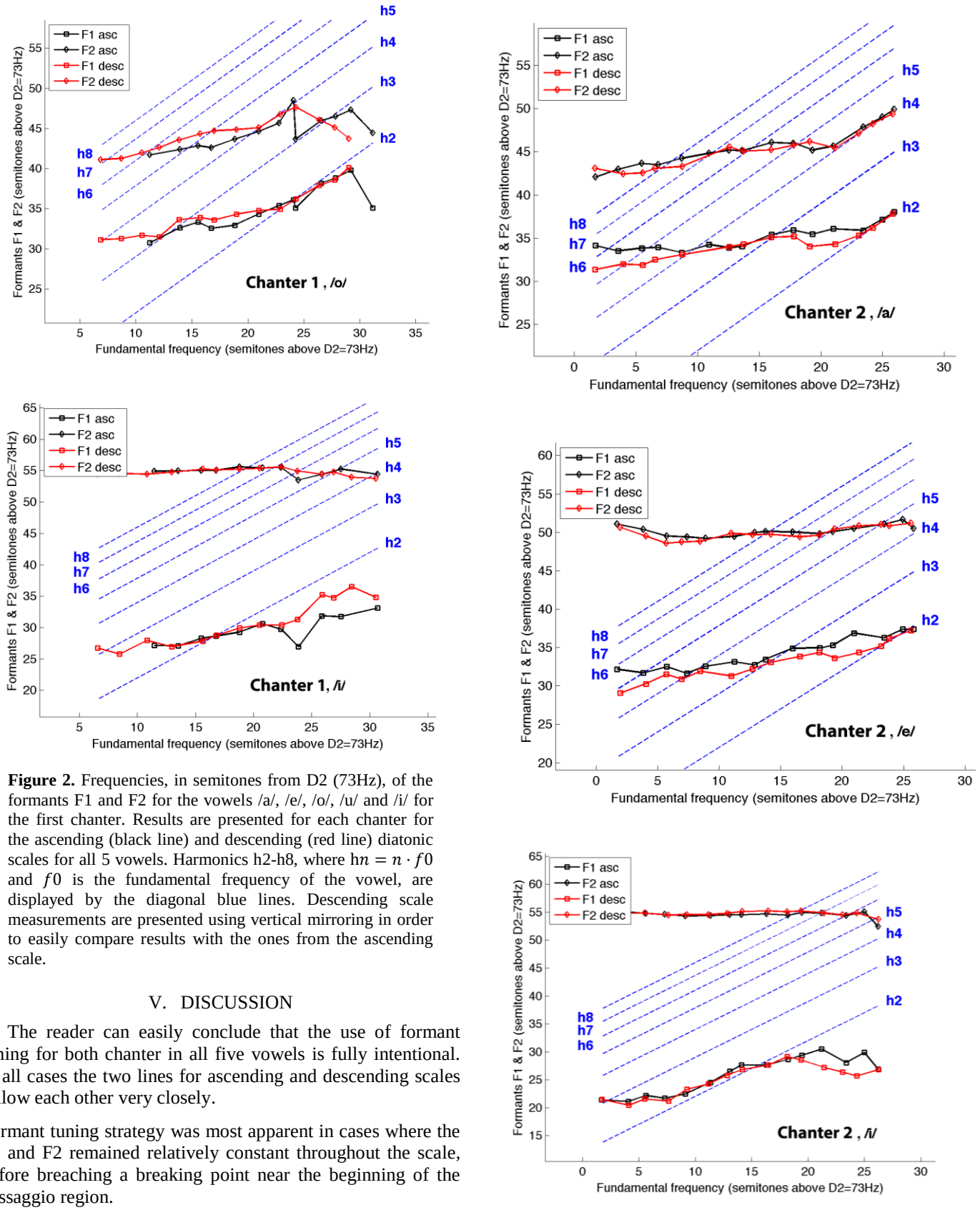

Figure 2. Frequencies, in semitones from D2 (73Hz), of the formants F1 and F2 for the vowels /a/, /e/, /o/, /u/ and /i/ for the first chanter. Results are presented for each chanter for the ascending (black line) and descending (red line) diatonic scales for all 5 vowels. Harmonics h2-h8, where h$n = n \cdot f0$ and $f0$ is the fundamental frequency of the vowel, are displayed by the diagonal blue lines. Descending scale measurements are presented using vertical mirroring in order to easily compare results with the ones from the ascending scale.

V. DISCUSSION

The reader can easily conclude that the use of formant tuning for both chanter in all five vowels is fully intentional. In all cases the two lines for ascending and descending scales follow each other very closely.

Formant tuning strategy was most apparent in cases where the F1 and F2 remained relatively constant throughout the scale, before breaching a breaking point near the beginning of the passaggio region.

ISBN: 978-1-61804-228-6

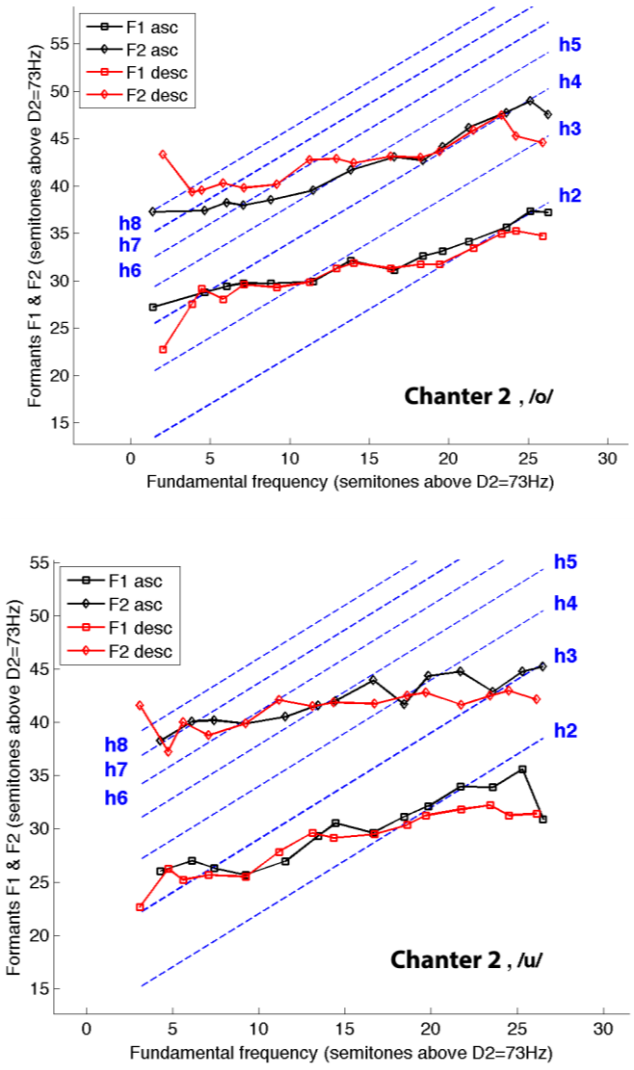

Figure 3. Frequencies, in semitones from D2 (73Hz), of the formants F1 and F2 for the vowels /a/, /e/, /o/, /u/ and /i/ for the second chanter. Results are presented for each chanter for the ascending (black line) and descending (red line) diatonic scales for all 5 vowels. Harmonics h2-h8, where h$n = n \cdot f0$ and $f0$ is the fundamental frequency of the vowel, are displayed by the diagonal blue lines. Descending scale measurements are presented using vertical mirroring in order to easily compare results with the ones from the ascending scale.

Regarding the question as to whether there is a common tuning strategy followed by most chanters, the answer is not obvious. Although in many cases we observed similarities between the chanters for F1 and F2, we tend to believe that each chanter follows his own personal strategy to achieve the aesthetic result he desires.

In order to be able to give a safe answer whether Byzantine chanters use common strategies in formant tuning a larger sample of the corpus must be analyzed. This analysis will be part of our future work.

Going through the examples of formant tuning found in our results, formant F1 coincided, in most cases, with the partial h2 and h3, while formant F2 was tuned either to h3 or h4, in all cases.

VI. FUTURE WORK

Future work will mainly cover extracting and displaying more data from the DAMASKINOS corpus. For a start, this would include retrieving data from all the chanters of the corpus. Analyzing data from other vowels as well, would give us a clear picture as to whether chanters show a preference in formant tuning for specific vowels.

Another important and interesting part of a future investigation would be the comparison of formant tuning strategies followed by BCM performers who have also been trained as professional opera singers and vice versa. The design of the DAMASKINOS corpus has included singers that meet the above conditions.

Finally, searching for a possible relation between formant tuning and different genera in BCM could also lead to important facts, both about the modern practice of Byzantine chant performance and also about the intentionality factor stated before.

REFERENCES

[1] G. Fant, *Acoustic Theory of Speech Production*. Walter de Gruyter, 1970.
[2] G. Carlsson and J. Sundberg, "Formant frequency tuning in singing," *J. of Voice*, vol. 6, no. 3, pp. 256–260, 1992.
[3] J.A. Stark, *Bel canto: a history of vocal pedagogy*. University of Toronto Press, 2003.
[4] J. Sundberg, "The acoustics of the singing voice," *Sci. Am.*, vol. 236, no. 3, pp. 82–91, 1977.
[5] J. Sundberg, *The Science of the Singing Voice*. Northern Illinois Univ, 1987.
[6] D.G. Miller and H.K. Schutte, "Formant tuning in a professional baritone," *J. of Voice*, vol. 4, no. 3, pp. 231–237, 1990.
[7] G. Chrysochoidis, G. Kouroupetroglou, D. Delviniotis, S. Theodoridis: "Formant Tuning in Byzantine Chant" Proceedings of the Int. Conference Sound and Music Computer, pp. 217-223, Stockholm, Sweden, July 30-August 3, 2013.
[8] J. Sundberg, F.M.B. Lã, and B.P. Gill, "Professional male singers' formant tuning strategies for the vowel /a/," *Logoped Phoniatr Vocol*, vol. 36, no. 4, pp. 156–167, 2011.
[9] J. Sundberg, F.M.B. Lã, and B.P. Gill, "Formant Tuning Strategies in Professional Male Opera Singers," *J. of Voice*, Dec. 2012.
[10] M.E. Bestebreurtje and H.K. Schutte, "Resonance strategies for the belting style: Results of a single female subject study," *J. of Voice*, vol. 14, no. 2, pp. 194–204, 2000.
[11] N. Henrich, M. Kiek, J. Smith, and J. Wolfe, "Resonance strategies used in Bulgarian women's singing style: A pilot study," *Logopedics Phonatrics Vocology*, vol. 32, no. 4, pp. 171–177, 2007.
[12] D.G. Panagiotopoulos, *Theoria kai Praxis tis Byzantinis Ecclesiastikis Mousikis*, 6th ed. Athens: Sotir, 1997.

ISBN: 978-1-61804-228-6

[13] D. Delviniotis, G. Kouroupetroglou, and S. Theodoridis, "Acoustic analysis of musical intervals in modern Byzantine Chant scales," *J. of the Acoustical Society of America*, vol. 124, no. 4, pp. EL262–EL269, 2008.

[14] M. Chrysanthos and P.G. Pelopides, *Theoretikon mega tes mousikes*. En Tergeste : ek tes typographias Michael Vais (Michele Weis), 1832.

[15] D. Delviniotis and G. Kouroupetroglou, "DAMASKINOS: The Prototype Corpus of Greek Orthodox Ecclesiastical Chant Voices", in *Proc. Int. Conf. Crossroads | Greece as an Intercultural Pole of Musical Thought and Creativity*, Thessaloniki, Greece, pp.1-14, 2011.

[16] G. Kouroupetroglou, D. Delviniotis, and G. Chrysochoidis, "DAMASKINOS: The Model Tagged Acoustic Corpus of Byzantine Ecclesiastic Chant Voices," *in Proc. ACOUSTICS Conf.*, Heraclion, Greece, 2006, pp. 68–76.

[17] G. Chrysochoidis, D. Delviniotis, and G. Kouroupetroglou, "A semi-automated tagging methodology for Orthodox Ecclesiastic Chant Acoustic corpora," in *Proceedings of the Int. Conf. Sound and Music Computing*, Lefkada, Greece, 2007, pp. 126–133.

[18] P. Boersma, "Praat, a system for doing phonetics by computer," *Glot International*, vol. 5, no. 9/10, pp. 341–345, 2002.

[19] P. Boersma, "Accurate short-term analysis of the fundamental frequency and the harmonics-to-noise ratio of a sampled sound," in *IFA Proceedings 17*, 1993, pp. 97–110.

[20] N. Andersen, "On the calculation of filter coefficients for maximum entropy spectral analysis," *Geophysics*, vol. 39, no. 1, pp. 69–72, Feb. 1974.

[21] D. G. Childers, *Modern spectrum analysis*. IEEE Press : sole worldwide distributor (exclusive of IEEE), Wiley, pp. 252-255, 1978.

[22] P. Boersma and G. Kovacic, "Spectral characteristics of three styles of Croatian folk singing," *The Journal of the Acoustical Society of America*, vol. 119, no. 3, p. 1805, 2006.

[23] P. Escudero, P. Boersma, A. S. Rauber, and R. A. H. Bion, "A cross-dialect acoustic description of vowels: Brazilian and European Portuguese," *The Journal of the Acoustical Society of America*, vol. 126, no. 3, p. 1379, 2009.

[24] T. Wempe and P. Boersma, "The interactive design of an F0-related spectral analyser," in *Proc. 15th ICPhS*, 2003, pp. 343–346.

[25] I. Jemaa, O. Rekhis, K. Ouni, and Y. Laprie, "An evaluation of formant tracking methods on an Arabic database," in *10th Annual Conference of the International Speech Communication Association-INTERSPEECH 2009*, 2009.

[26] H. Boril and P. Pollák, "Direct time domain fundamental frequency estimation of speech in noisy conditions," in *Proceedings of EUSIPCO 2004 (European Signal Processing Conference)*, 2004, vol. 1, pp. 1003–1006.

[27] D. G. Silva, L. C. Oliveira, and M. Andrea, "Jitter Estimation Algorithms for Detection of Pathological Voices," *EURASIP Journal on Advances in Signal Processing*, vol. 2009, no. 1, p. 567875, 2009.

[28] K. Bunton and B.H. Story, "A test of formant frequency analyses with simulated child-like vowels", Presented at the 161st Acoustical Society Meeting, 129(4), pt. 2 of 2, 2011.

[29] D. Delviniotis, "*Byzantine chant analysis by using signal processing techniques*," PhD Theses, National and Kapodistrian University of Athens, Department of Informatics and Telecommunications, 2002.

[30] L. Dmitriev and A. Kiselev, "Relationship between the Formant Structure of Different Types of Singing Voices and the Dimensions of Supraglottic Cavities," *Folia Phoniatrica et Logopaedica*, vol. 31, no. 4, pp. 238–241, 1979.

[31] T.F. Cleveland, "Acoustic properties of voice timbre types and their influence on voice classification," *J. of the Acoustical Society of America*, vol. 61, p. 1622, 1977.

[32] N. Henrich, J. Smith, and J. Wolfe, "Vocal tract resonances in singing: Strategies used by sopranos, altos, tenors, and baritones," *J. of the Acoustical Society of America*, vol. 129, p. 1024, 2011.

Design of 0.05-5 GHz LNA for Cognitive Radios Receiver

W. Farrag[1], A. Ragheb[2], N. Rashid[3]
[1]Electrical dep., Al-Azhar University, Cairo, Egypt, eng_alex22@yahoo.com.
[2]Electronics dep., National Telecommunication Institute (NTI), Cairo, Egypt, ahmed.ragheb@nti.sci.eg.
[3]Electrical dep., Al Jouf University, Al Jouf, Saudi Arabia, nasrrashid@ju.edu.sa.

***Abstract*—This paper presents a design of Low Noise Amplifier (LNA) for Cognitive Radios (CRs) receiver and it operates from 50 MHz to 5 GHz. The proposed design is consisted of two stages, the first one is a combination of cascode with common gate stage to improve the gain, power consumption, and the input matching. The second stage is a common source (CS) for canceling the noise and distortion of CG of the first stage. This design achieves a noise figure 4.1-4.8 dB, input reflection coefficient less than -11 dB, output reflection coefficient below -10dB, the power gain from 10.2 dB to 12.5 dB and the consummation power 7.14 mW supplied from 1 V. The proposed LNA is designed using 0.18 μm CMOS technology.**

***Index Terms*—LNA, Cognitive Radios, noise cancellation, current reuse, common gate.**

I. Introduction

Recently it has become a common use of application of wireless standards such as GSM, DECT, Bluetooth, GPS, and WLAN on the same device. To keep pace with this evolution found CRs receivers. CRs receivers are unlike the conventional wireless transceivers, which operate in a specific bands, CRs utilize any unoccupied channel in a wide range of frequencies from several megahertz up-to several gigahertz [1]. This idea based on sensing and detecting an available channels before the communication initialized [1], [2].

As known, LNA is the first building block in the RF receivers, so it has a significant impact in the over all performance of the receiver. Therefore, achieving a good performance parameters like high gain, low power consumption, low noise figure, and good input and output matching over the band of interest, is one of the biggest challenge of the receiver design. Also, when the operation bandwidth of LNA increase, the difficulty of achieving the desired performance parameters will increase. The design of CRs LNA is very difficult, where it needs to operate at low frequency and high frequency as well.

Newly found many designs that are interested in wideband low noise amplifier such as [3], [4], [5] where they are wideband techniques, high gain, low noise, and good input and output matching, but they operate at high frequency only. Also the design in [6] it does not work at low frequency and high power consumption. The proposed design combines between low and high frequency with relatively low power consumption, good matching, and acceptable gain, NF.

This paper is organized as follows, section II describes the circuit design of the proposed CRs LNA. Section III discusses the simulation results of the proposed LNA. Finally, the conclusion is presented in section IV.

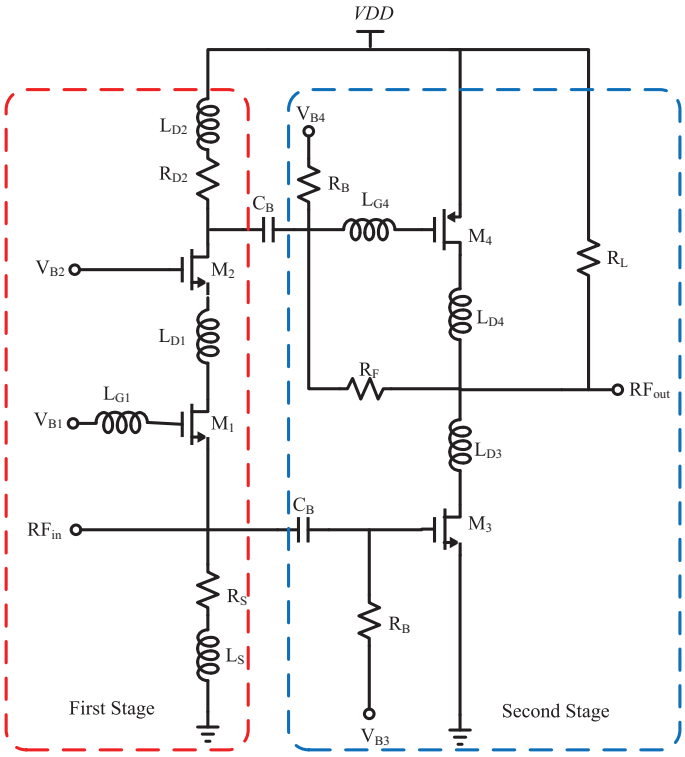

Figure 1: Schematic of the proposed CRs LNA

II. Circuit Design of LNA

The proposed LNA was designed by a standard $0.18\mu m$ CMOS process. Fig. (1) shows the schematic of the proposed CRs LNA. It consists of two stages, each stage has a different tasks.

The first stage includes two main parts, the first part is the input matching network to provide the input return loss of the LNA at low and high frequencies, and it contains the CG transistor M_1, L_{G1}, L_S, and R_S. Where the input impedance of CG transistor M_1 calculated as following

$$Z_{in} = \frac{1}{g_{m1} + J\omega C_{gs1}} \quad (1)$$

where g_{m1} is the transconductance of $M_1$and C_{gs1} is the gate-to-source parasitic capacitance of M_1. At low frequency

ISBN: 978-1-61804-228-6

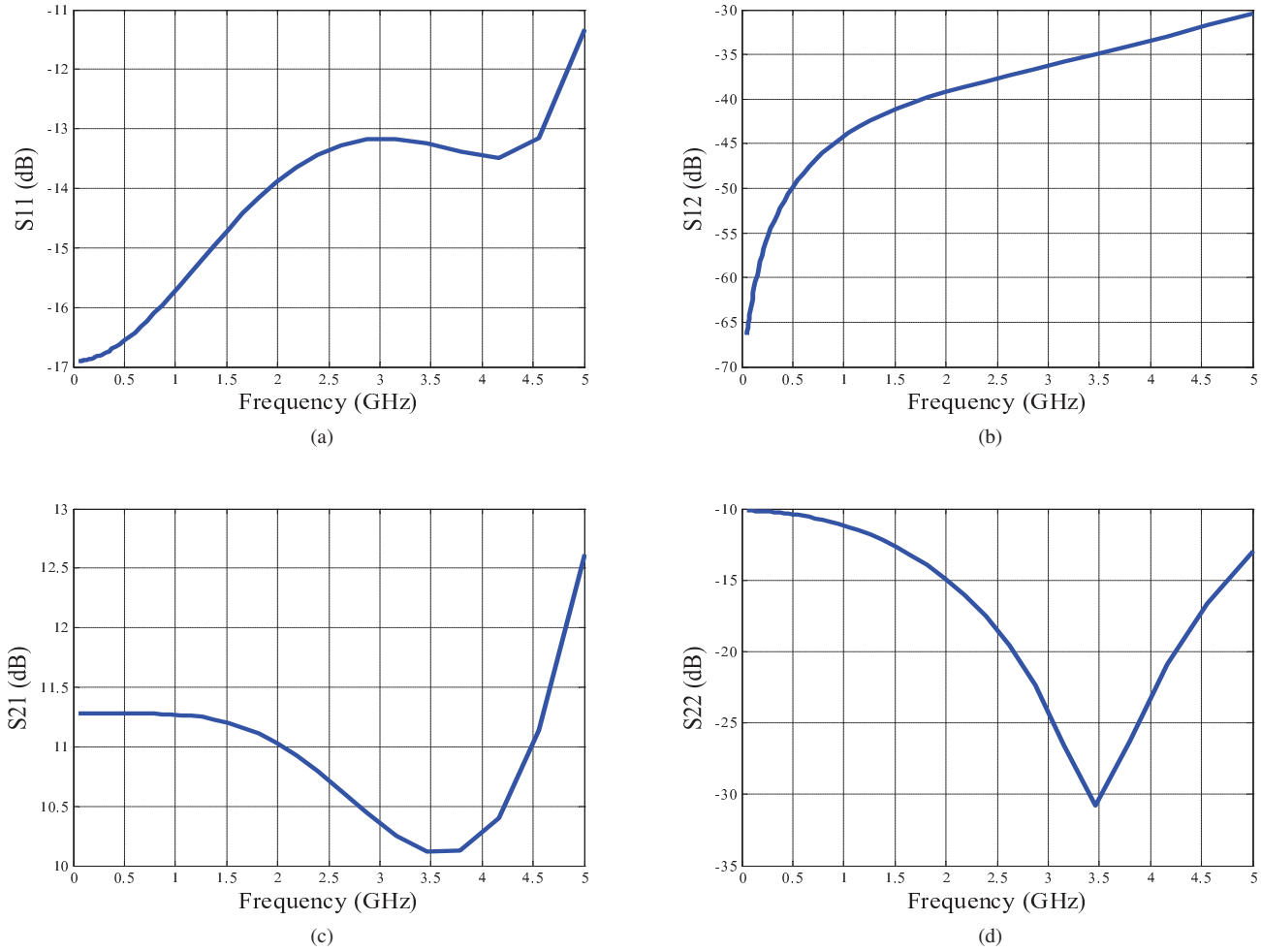

Figure 2: S-Parameter results of the proposed CRs LNA: (a) Input reflection coefficient S_{11}, (b) Reverse isolation S_{12}, (c) Power gain S_{21}, (d) Output reflection coefficient S_{22}

$Z_{in} \approxeq \frac{1}{g_{m1}}$, but at high frequency the negative impact of C_{gs1} will appear so the gate and source inductors L_{G1} and L_S, respectively, are used to resonate with C_{gs1}, and in order to extend the bandwidths in low frequency the R_S is used [1]. The second part is the cascode topology that used to provide the gain and isolation between input and output. This part consists of M_2 and the peaking inductor L_{D2} is used as the load of the first stage which it's impedance increase with the increasing of the operating frequency and because it's less at low frequencies R_{D1} is added to increase the gain at low frequency.

The second stage consists of two techniques, the first one is the noise cancellation technique which depends on CS transistor M_3which applied to cancel the noise of M_1[1]. The second technique is the current reuse where the PMOS transistor M_4 is used to reuse the current of M_2[3], [4].

The gate inductor L_{G4} and drain inductor L_{D3} and L_{D4} are added for inductive shunt peaking and series peaking,receptively. R_F is the negative feedback for preventing the variation of output voltage. Finally the resistor R_L is used to decrease variation of the output impedance and achieve good output reflection coefficient.

Table I: Parameters values for the proposed CRs LNA

parameter	value	parameter	value
$(W/L)_1$ (μm)	120/0.18	L_{G4}	481 pH
$(W/L)_2$ (μm)	100/0.18	L_{D3}	1.75 nH
$(W/L)_3$ (μm)	100/0.18	L_{D4}	2.54 nH
$(W/L)_4$ (μm)	250/0.18	R_S	2.5 KΩ
L_S	12.9 nH	R_F	700 Ω
L_{D2}	6.7 nH	R_L	10 KΩ
L_{G1}	1.68 nH	R_{D1}	180 Ω
L_{D1}	3.26 nH	R_{B1}	2KΩ
C_B	102.5 nF	R_{B2}	5KΩ

The proposed CRs LNA is designed by 0.18 μm CMOS process and the component parameters values are listed in table I.

III. Simulated Results

Design of the proposed wideband CRs LNA was carried out using Spectre simulator from Cadence Design Suite. The

ISBN: 978-1-61804-228-6

Table II: The performance of the proposed LNA and comparison with existing architecture

	Technology (CMOS)	BW (GHz)	V_{dd} (V)	S_{11}(dB)	S_{21}(dB)	NF (dB)	P_c (mW)
[6]	130 nm	1.2	1.8	-	16.4	2.1-3.4	14.4
[7]	65 nm	0.1-4	1.2	<-10	18	2 @ 2GHz	12
[8]	130 nm	0.2-3.8	1	-	13	2.8-3.4	5.7
[9]	180 nm	1.05-3.05	1.8	<-10	10.9	2.57@1.2 GHz	12.6
[10]	180 nm	1.2	2.2	<-9	14	3	15.8
[11]	130 nm	1.9-2.4	1.2	<-13	14-10	3.2-3.7	17
[12]	130 nm	1.8-2.4	1.2	<-12	26-28	3.2-3.4	9.6
[13]	65 nm	10	1	<-12	10.5	2.7-3.3	13.7
	65 nm	5.2	1	<-7.5	10.7	2.9-5.4	7
This work	180 nm	.05-5	1	<-11	10.9	4.1-4.8	7.14

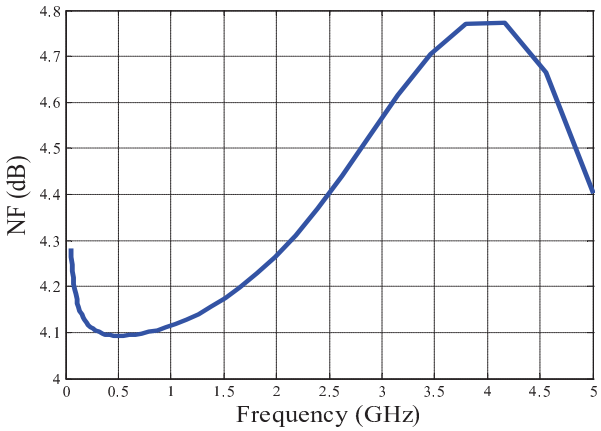

Figure 3: Noise figure of the proposed CRs LNA

circuit has been designed by using standard 180nm CMOS technology and it consumes 7.14 mW from 1 V supply.

Fig. (2a) illustrates the input return loss S_{11} is less than -11 dB over all the bandwidth and the reason behind this, the proposed CG topology with input matching network at the first stage and by controlling the parameters of L_{G1}, L_S, and R_S which resonate and prevent the impact of C_{gs1} and $C_{gs3}$of $M_1$and M_3, respectively.

Fig. (2b) shows the revers isolation S_{12}between output and input over the .05- 5 GH_Z band of interest where it is less than -30 dB. The good isolation because of the usage of CG, cascode, and current reuse topologies.

Fig. (2c) shows the simulated power gain S_{21} versus frequency characteristics of the proposed CRs LNA. High and flat S_{21} of 10.1-12.5 dB was achieved over the .05- 5 GH_Z band of interest.

Fig. (2d) presents the output return loss S_{22} where it less than -10 dB. The most important factors that affect the output matching are M_3, M_4, L_{G4}, R_L, and R_F.

The simulated noise figure NF is shown in fig. (3), NF of the proposed CRs LNA achieves 4.1-4.8 dB. The relatively high noise figure is due to the number of transistor that are used and operating this circuit in low frequency.

The performance of the proposed CRs LNA and a comparison with existing architectures are summarized in Table II.

IV. Conclusions

This paper proposes a wideband LNA for a cognitive radios receivers over the .05- 5 GHz band of interest. The proposed architecture based on the CG topology to provide the input matching, cascode with current reuse techniques to improve the gain, power consumption, and isolation, and noise cancellation technique to provide the noise figure of this design. The proposed LNA operates by 1 V supply and consumes 7.14 mA for the band of interest. Finally, it has been designed by 0.18 μm CMOS process.

References

[1] Ansari, A.; Yavari, M., "A very wideband low noise amplifier for cognitive radios," Electronics, Circuits and Systems (ICECS), 2011 18th IEEE International Conference on , vol., no., pp.623,626, 11-14 Dec. 2011.

[2] Razavi, B., "Cognitive Radio Design Challenges and Techniques," Solid-State Circuits, IEEE Journal of , vol.45, no.8, pp.1542,1553, Aug. 2010.

[3] Ragheb, A. N.; Fahmy, G.A.; Ashour, I.; Ammar, A., "A 3.1–10.6 GHz low power high gain UWB LNA using current reuse technique," Intelligent and Advanced Systems (ICIAS), 2012 4th International Conference on , vol.2, no., pp.741,744, 12-14 June 2012.

[4] Ahmed Ragheb, Ghazal Fahmy, Iman Ashour, and Abdel Hady Ammar, "A Novel Reconfigurable MB-OFDM UWB LNA Using Programmable Current Reuse," International Journal of Microwave Science and Technology, vol. 2013, Article ID 924161, 5 pages, 2013.

[5] Heng Zhang, Xiaohua Fan, Sinencio, and E.S, "A Low-Power, Linearized, Ultra-Wideband LNA Design Technique," IEEE J. Solid- State Circuits, vol. 44, no. 2, pp. 320-330, Feb. 2009.

[6] Y.-H. Yu, Y.-S. Yang, and Y.-J. E. Chen, "A compact wideband CMOS low noise amplifier with gain flatness enhancement," IEEE J. Solid- State Circuits, vol. 45, no. 3, pp. 502–509, Mar. 2010.

[7] X. Wang, W. Aichholzer, and J. Sturm, "A 0.1–4 GHz resistive feedback LNA with feedforward noise and distortion cancelation," in Proc. Eur. Solid-State Circuits Conf. (ESSCIRC), Sep. 2010, pp. 406–409.

[8] H. Wang, L. Zhang, and Z. Yu, "A wideband inductorless LNA with local feedback and noise cancelling for low-power low-voltage applications," IEEE Trans. Circuits Syst. I, Reg. Papers, vol. 57, no. 8, pp. 1993–2005, Aug. 2010.

[9] J. Kim, S. Hoyos, and J. Silva-Martinez, "Wideband common-gate CMOS LNA employing dual negative feedback with simultaneous noise, gain, and bandwidth optimization," IEEE Trans. Micorw. Theory. Tech., vol. 58, no. 9, pp. 2340–2351, Sep. 2010.

[10] D. Im, I. Nam, H.-T. Kim, and K. Lee, "A wideband CMOS low noise amplifier employing noise and IM2 distortion cancellation for a digital TV tuner," IEEE J. Solid-State Circuits, vol. 44, no. 3, pp. 686–698, Mar. 2010.

[11] M. El-Nozahi, E. Sanchez-Sinencio, and K. Entesari, "A CMOS low-noise amplifier with reconfigurable input matching network," IEEE Transactions onMicrowaveTheory and Techniques, vol. 57, no. 5, pp. 1054–1062, 2009.

ISBN: 978-1-61804-228-6

[12] A. Slimane, M. T. Belaroussi, F. Haddad, S. Bourdel, and H. Barthelemy, "A reconfigurable inductor-less CMOS low noise amplifier for multi-standard applications," in Proceedings of the IEEE 10th International Conference on New Circuits and Systems Conference (NEWCAS '12), pp. 57–60, 2012.

[13] Ke-Hou Chen ; Shen-Iuan Liu ," Inductorless Wideband CMOS Low-Noise AmplifiersUsing Noise-Canceling Technique", IEEE Circuits and Systems Society,vol.59,pp.305 – 314,Feb. 2012.

An Improved Genetic Algorithm for PID Parameter Tuning

Jyoti Ohri , Naveen Kumar, Minakshi Chinda

Abstract— Genetic algorithms are computer based search techniques patterned after the genetic mechanism of biological organisms Their capability to find high performance areas in large domains makes them ideal choice for function optimization problems. However it is seen that GA does not always guarantee an optimum solution. This paper presents an improved genetic algorithm, which combines the concept of immunity, variable probabilities and multi objective optimization. PID parameter optimization is an important problem in control field. This improved genetic algorithm is used in PID parameter optimization. The algorithms are simulated with MATLAB programming. The simulation result shows that the PID controller with improved genetic algorithm shows better performance in comparison with canonical GA**s.**

.

***Keywords*—** Genetic Algorithms, Immune Genetic Algorithms, Improved Genetic Algorithms, Parameter Optimization, PID Parameter Tuning, Variable Probability.

I. INTRODUCTION

Genetic Algorithms or in short GAs are stochastic algorithm based on principles of natural selection and genetics [1, 2]. Genetic Algorithms (GAs) are a stochastic global search method that mimics the process of natural evolution. These robust genetic algorithms have been successfully applied to problems in a variety of fields of study, and their popularity continues to increase due to their effectiveness, their applicability and their ease of use [2, 3, 6]. Their capability to find high performance areas in large domains makes them ideal choice for function optimization problems [1-3]. Advances and research in GA techniques has opened a new field for various control techniques. PID control is one such control technique.

PID control has been in use in a large no. of industrial applications. But tuning PID parameter is still an important task because the system parameters in almost all the industrial processes are constantly changing [5, 7]. Thus GA because of its random search proves to be an efficient tuning method. GA's have outperformed standard tuning practices, e.g. Ziegler Nichols, in designing PID controllers for industrial processes. However it is seen that GA does not always guarantee an optimum solution [9,10] One can't rely on the final solution of GA. Keeping this fact in mind in this paper, an improved version of canonical genetic algorithm is introduced in order to avoid the uncertainty in the final solution. Concept of immunity with elitism [10], variable probability functions [12] and multi objective functions [3] are integrated to make GA work faster and better [14,15, 16]. Concept of immunity helps in convergence to optimum solution. Due to variable probabilities as GA moves towards a better solution, number of crossovers and number of mutations are decremented to reduce the simulation time. A multiobjective fitness function which simultaneously maximizes different objectives is included to give better solution than other performance indices. Performance analysis is carried out using MATLAB and simulation results indicate that the improved GA overcomes many of the difficulties associated with canonical GA and conventional tuning methods. It is also shown that the improved GA produces optimum or near optimum results for systems that are normally considered difficult to tune.

II. GENETIC ALGORTIHMS

A. Genetic Algorithms

Genetic Algorithms are search and optimization techniques inspired the process of natural selection [1]. GAs controls not just one possible solution to a problem but a collection of potential solutions. These solutions are known as population. The potential solution in the population is called individuals or individual. These individuals are the encoded representations of all the parameters of the solution. Each individual is evaluated for their fitness. Individuals are then given a fitness rating based on relative fitness.

To give better solutions, the GA uses genetic operators or evolution operators such as crossover and mutation for the creation of new individuals from the existing ones in the population. This is achieved by either merging the existing ones in the population or by modifying an existing individual.
The selection mechanism for parent individuals takes the fitness of the parent into account. This will ensure that the better solution will have a higher chance to select and donate their beneficial characteristic to their offspring.

A genetic algorithm is typically initialized with a random population consisting of between 20-100 individuals. This population or also known as mating pool is usually represented

.
Jyoti ohri is Professor ,Electrical Engg Deptt.with the National Institute of Technology, Kurukshetra,India136119; e-mail: ohrijyoti@ rediffmail.com.
Naveen Kumar is M.Tech. Student with the National Institute of Technology, Kurukshetra,India136119; naveenvermaindia@gmail.com
Meenakshi Chinda was M.Tech. Student with the National Institute of Technology,Kurukshetra,India136119;e-mail: minakshi_chinda@rediffmail.com.

by a real-valued number or a binary string called a individual. How well an individual performs with respect to its fitness is measured and assessed by the objective function or fitness function. The objective function assigns each individual a corresponding number called its fitness. The fitness of each individual is assessed and a survival of the fittest strategy is applied. There are three main stages of a genetic algorithm; these are known as *reproduction, crossover* and *mutation*.
During the reproduction phase the fitness value of each individual is evaluated. This value is used in the selection process to provide bias towards fitter individuals. Just like in natural evolution, a fit individual has a higher probability of being selected for reproduction.

Once the selection process is completed, the crossover algorithm is initiated. The crossover operation swaps certain parts of the two selected strings in a way to capture the good parts of old individuals and create better new ones. The crossover probability indicates how often crossover is performed.

Mutation is the occasional random alteration of a value of a string position. It is used for adding some new information in the individual. It is considered a background operator in the genetic algorithm .The probability of mutation is normally low because a high mutation rate would destroy fit strings and degenerate the genetic algorithm into a random search.

The steps involved in creating and implementing a genetic algorithm:
1. Generate an initial, random population of individuals for a fixed size.
2. Evaluate their fitness.
3. Check whether the termination criterion is satisfied or not
4. Reproduce using a probabilistic method (e.g., roulette wheel).
5. Implement crossover operation on the reproduced individuals (Choosing probabilistically both the crossover site and the mates)
6. Execute mutation operation with low probability.
7. Repeat step 2 until a predefined convergence criterion is met.
The convergence criterion of a genetic algorithm, is a user-specified condition for example the maximum number of generations or when the string fitness value exceeds a certain threshold.

B. Problem with Genetic Algorithm

Genetic algorithm has a number of potential solutions in almost all fields of engineering. But still most of its applications are still in papers and under research. The reason being that GA does not always converge to an optimum solution [3, 9], because GA is a random technique. The genetic operators like crossover and mutation works randomly. This random search which was an advantage in covering the complete search space comes out to be a disadvantage for convergence. So some proper control on genetic processes is needed for convergence purposes

III. IMPROVED GENETIC ALGORITHMS

GA with the mutation probability P_m, crossover probability P_c, and proportional selection will never converge to the global optimum regardless of initialization, crossover operator, and objective function. In order to solve this problem, the advantages of immune genetic algorithm (to converge to optimum or near optimum), variable probabilities (to make genetic faster) and multiobjective function (to solve various objectives) are combined to make some refinements in GA.

A. Immune Genetic Algorithms

The biological immune system is a highly parallel and distributed adaptive system that has powerful information processing capability. Through extracting some properties from the immune system, the researchers have developed many artificial immune systems and immune algorithms to solve complex engineering problems. The idea of immunity is mainly realized through two steps i.e. a vaccination and an immune selection, of which the former is used for raising fitness and the latter is for preventing the deterioration. Now they are explained as follows.

Vaccination

Given an individual, a vaccination means modifying the genes on some bits in accordance with priori knowledge so as to gain higher fitness with greater probability. This operation must satisfy the following two conditions.
Vaccination on individuals is done by comparing it with the optimal one or the best one. Each gene of the individual is compared with the optimal one and if it is different with antibody than vaccination is provided to improve that individual.

The Immune Selection

This operation is accomplished by the following two steps. The first one is the immune test, i.e. testing the antibodies. If the fitness is smaller than that of the parent, which means serious degeneration must have happened in the process of crossover or mutation, then instead of the this antibody, previous antibody will participate in the next competition; the second one is the annealing selection, i.e., to inject number of antibodies in the population.
Assume that $v = \{v_1, v_2 \ldots v_n\}$ is the antibody and $w = \{w_1, w_2 \ldots w_n\}$ is any individual in a given y population. Their root mean square (rms) difference is represented by d (v, w) and their fitness values are represented by f_v and f_w respectively. Assume that ε is a small positive constant. If

$$J(v,w) = \{d(v,w) + \alpha \, I \, f_v - f_w \, I \} \leq \varepsilon \qquad (1)$$

is satisfied, it means that the individual has passed the immune test clearly and that can participate in next generation .$\alpha > 0$ is a tunable parameter that controls the relative importance of the fitness difference $|f_v - f_w|$ versus the *rms* difference d (v, w) in J(v, w).
d (v, w) reflects the similarity of the two antibodies in their structures and $|f_v - f_w|$ reflects the similarity of the two

antibodies in their performance or qualities. The *rms* difference between the antibodies v and w is defined as:

$$d(v,w)=\sqrt{\left\{\sum_{i=1}^{n}(v_i-w_i)^2\right\}/n} \qquad (2)$$

where *n* is the number of bits or genes in the individual
Substituting *rms* difference into (1), we obtain:

$$J(v,w)=\left\{\sqrt{\sum_{i=1}^{n}(v_i-w_i)^2\}/n}+\alpha\left|(f_v-f_w)\right|\right\}\le\in \qquad (3)$$

Secondly, by adjusting the parameter α, IGA can balance the diversity of antibody population and its convergence speed in the evolutionary process so as to rapidly produce the globally optimal solution. If similarity in structure is more important, a larger α can be selected (α >1). On the contrary, if one hopes the similarity in quality (fitness) is more important, a smaller α can be selected (α <1).

A. Variable Probabilities

Crossover rate P_c and mutation rate P_m decide the performance of GA. In the conventional mechanism, the crossover rate and mutation rate are held constants. Higher crossover rate can increase the generation of new individuals in the searching process, it perhaps also raise the probability to destroy superior individuals in the crossover process, so it can prevent leading to local optimal solution. And in order to prevent converging to local optimal solution, we can't use too small mutation rate, but higher mutation rate may make GA like a completely random search. So we use the adaptive probabilities of crossover and mutation mechanism, it can adaptively change the crossover rate and mutation rate according to the current situation of evolution. This work presents a method in which crossover probability will diminish with generation increase, gives a computing method about crossover probability.

$$P_c=P_{c_1}(1-\frac{m}{M}) \qquad (4)$$

where, m is evolution generation, M is the total generation, generally P_{c1} is 0.6- 0.8.
Mutation probability can keep the algorithms from local convergence, while fixed probability may destroy perfect individuals easily. We adopt mutation probability method.

$$P_m=P_{m_1}(1-\frac{m}{M}) \qquad (5)$$

where, m is evolution generation, M is the total generation, generally P_{m1} is 0.1.

The advantage of this method is that initially as we are starting from a random point, we need to cover a large search space but as number of generation is increasing and we are moving towards a better solution we can decrease probabilities and hence number of crossovers and mutations to make genetic search faster and better.

B. Multiobjective Fitness Function

The most crucial step in applying GA is to choose the objective functions that are used to evaluate fitness of each chromosome. Some works use performance indices as the objective functions.Many authors' uses Mean of the Squared Error (MSE), Integral of Time multiplied by Absolute Error (ITAE), Integral of Absolute Magnitude of the Error (IAE), and Integral of the Squared Error (ISE) as performance index [8,9].

As we need to minimize the error. So fitness function is taken as inverse of error .i.e. performance index, because the smaller the value of performance indices of the corresponding chromosomes the fitter the chromosomes will be, and vice versa, we define the fitness of the chromosomes as:

$$fitness\ value=\frac{1}{Performance\ index}$$

For many real world decisions making problems there is a need for simultaneous optimization of multiple objectives. If there are more than two objectives to be optimized, it might be possible to find a solution which is best with respect to the all objectives.

Classical methods for multi objective optimization include a method of objective weighting, where multi objective functions f_i are combined into overall objective function *F*

$$F(x)=\sum_{i=1}^{k}w_i f_i(x) \qquad (6)$$

where the weights $w_i\in[0,1]$ and $\sum_{i=1}^{k}w_i=1$.

Different weight vectors provide different solutions.
For the genetic implementation of a PID controller settling time, rise time and peak over shoot can also be a performance criterion [19]. So we can a make an objective function which takes into account these three objectives.

$$M.O=w_1*m_p+w_2*t_s+w_3*t_R \qquad (7)$$

where m_p is the maximum overshoot t_s is the settling time, t_r is the rising time, w_1, w_2 and w_3 are the corresponding weight which depends on the problem and requirement.
Consider a step input R (t) and the output response Y(t).The following objectives are stated for design.
Minimizing the maximum overshoot of the output

$$F_1=M_P=\max Y(t) \qquad (8)$$

Minimizing the settling time of the output

$$F_2=t_s \qquad (9)$$

Such that

$$0.98R\le Y(t)\le 1.02R,\ \forall t\ge t_s$$

Minimizing the rise time of the output

$$F_3=t_r=t_1-t_2 \qquad (10)$$

Such that $Y(t_1)=0.1R$ & $Y(t_2)=0.9\ R$
Fitness function will be

$$fitness\ \ function=\frac{1}{MO} \qquad (11)$$

Some other multi objective function can be made by combining peak overshoot, settling time, rise time with error criterion e.g.

$$F = w_1 * m_p + w_2 * MSE \quad (12)$$

Following is the algorithm of improved GA

Step 1: Initialize genetic algorithm by defining population size, probabilities etc

Step 2: Randomly generate initial population.

Step 3: Initialize iteration counter.

Step 4: For each individual:

(a) Convert bit string to find variables value.

(b) Calculate fitness of each individual

(c) Determine the individual which has the largest fitness in the population and save it as antibody

Step 5: Calculate average fitness and hence relative and cumulative fitness.

Step 6: Do the roulette wheel selection

Step 7: Perform crossover operations on the population based on variable crossover probability function (11).

Step 8: Perform mutation operations on the population based on variable mutation probability function (12).

Step 9: For each individual repeat step 5 and Determine the individual which has the largest fitness in the population and save it as present antibody if this antibody fitness is larger than previous antibody replace the antibody.

Step 10: Replace population with this new population

Step 11: If number of iteration is less than maximum iteration number return to Step 5; otherwise, give the optimal values of variable

IV. DESIGNING OF PID USING IMPROVED GENETIC ALGORITHM

Tuning of PID parameters is difficult because of variable system parameters. Random search of GA makes it a good tool for PID parameter tuning. A PID Controller is designed using Improved GA in this chapter.

A. Objective Function of the Improved Genetic Algorithm

Most challenging part of creating a genetic algorithm is writing the objective function. . An objective function was created to find a PID controller that gives the smallest overshoot, fastest rise time or quickest settling time. Each individual in the population is passed into the objective function one at a time. The individual is then evaluated and assigned a number to represent its fitness, the bigger its number the better its fitness. The genetic algorithm uses the individual's fitness value to create a new population consisting of the fittest members. The P, I and D gains are used to create a PID controller according to the equation below.

$$C_{PID} = \frac{K_D s^2 + K_p s + K_I}{s} \quad (13)$$

PID controller is placed in a unity feedback loop with the system transfer function. The controlled system is then given a step input and the error is assessed using performance criterion.

B. Parameter Coding and Decoding

Coding is mapping a parameter to be optimized into one individual from code space to parameter space by some rules. Because binary system coding is easy for genetic algorithms operation [2,3], we code parameter K_p, K_i, K_d into 5 digits binary system code and put them into one individual. Mapping from binary coding to real numbers is as shown,

$$x = \min + \frac{(\max - \min)}{2^n - 1} \times binary\,value \quad (14)$$

where, max and min are upper and lower limits of K_p, K_i or K_d respectively, binary value is a binary system value.

K_p	K_d	K_i

Fig 1. Coding of PID parameters as a bit string

Here, we randomly assign a value for each individual in a specifies variable range and convert it into the parameters of the fitness function value i.e K_p, K_i and K_d when evaluating the fitness population members.

C. Initial Population and Selection Operation

Initial population is randomly generated. They are converted to bit strings and fitness is assigned. Their relative fitness and cumulative fitness is assigned. During the selection stage, the strings are selected to copy themselves according to their cumulative probability according to their fitness value. Based on nature's survival-of the-fittest mechanism, the individuals with higher fitness values have higher probabilities to produce offspring by copying themselves [1, 2, 3]. Here we use a proportion method, which computes the fitness values and the cumulative probability of each individual by fitness function.

D. Crossover and Mutation

Crossover and mutation operators are used to keep algorithm search space diverse and to improve the individual based on crossover and mutation probability. This work uses (4) as crossover probability method in which crossover probability will diminish with generation increase.

Mutation probability given by (5) can keep the algorithms from local convergence, while fixed probability may destroy perfect individuals easily.

E. Immune Operator

To introduce the concept of immunity in the algorithm, immune operator is introduced in to the algorithm Immune operator consists of these following steps:

Antibody selection and replacement

The best individual of first generation is made antibody for the further generation. In next generation best individual is compared with antibody if fitness of that individual is more than the antibody it is made the antibody for the next generation. In each generation this process keeps on going.

Antibody similarity:

Function used for antibody comparison is as following

$$J(v,w)=\{\sqrt{\sum_{i=1}^{n}(v_i-w_i)^2\}/n}+\alpha\left|(f_v-f_w)\right|\}\leq\in$$

As said in earlier section parameter α has advantage of keeping similarity in structure and quality. High value of α decrease the population diversity while lower value increases convergence speed.

Antibody injection:

Antibody injection in the population is done after comparing all individuals with the antibody. If value of J is less than ε, the individual is replaced by antibody. Number of replacements can be made fixed or variable. In this dissertation number of injections are fixed to one third of population size i.e. maximum concentration of antibody in population is given as

$$C_i=\frac{popsize}{3} \quad (15)$$

where C_i is the antibody concentration and pop size is the size of the population

F. Elitism

In the process of the crossover and mutation-taking place, there is high chance that the optimum solution could be lost. To avoid this, the elitist models are often used. In this model, the best individual from a population is saved before any of these operations take place. When a new population is formed and evaluated, the elite member is inserted so that best member remains in the process.

G. Functions with Time Delay

Time delays are components that introduce time-lag in systems response. . As delay always reduces stability of minimum phase systems (systems which don't have poles and zeros in the right half of s-plane), it is important to analyses the stability of systems with time delay. Time delays make the system tough to deal. The time delay in the function has to be replaced by some approximations.

As first order lag plus delay (FOLPD) is used in most of the industries, it is given as

$$G(s)=\frac{e^{-sT_d}}{1+sT} \quad (16)$$

where T_d is the time delay.

Some approximations need to be done for effect of delay. In this paper delay will be approximated with a first order function

$$e^{-sT_d}=\frac{1-0.5sT_d}{1+0.5sT_d} \quad (17)$$

So system is now modified as follows

$$G(s)=\frac{1-0.5sT_d}{(1+sT)(1+0.5sT_d)} \quad (18)$$

System can now be easily evaluated.

H. Complete algorithm

Step 1: Define the population size m, the maximum iteration number M, number of variables, number of bits, crossover probability, mutation probability etc;

Step 2: Based on the property and application condition of the given controlled object, determine the ranges and numerical precisions of K_p, K_i, and K_d, respectively.

Step 3: Randomly generate m individual to constitute the initial population

Step 4: Set the iteration counter t=1.

Step 5: For each individual k (k=1-m):

(a) Determine the PID gains K_p, K_i, and K_d

(b) Send these gains into the PID controller and perform a simulation experiment on the controlled system using the unit step signal as the system input, and then calculate fitness

(c) Determine the individual which has the largest fitness in the population and save it as antibody

Step 6: Calculate average fitness and hence relative and cumulative fitness.

Step 7: Do the roulette wheel selection

Step 8: Perform crossover operations on the population based on variable crossover Probability function (11).

Step 9: Perform mutation operations on the population based on variable mutation Probability function (12).

Step 10: For each individual k repeat step 5 and Determine the individual which has the largest fitness in the population and save it as present antibody if this antibody fitness is larger than previous antibody replace the antibody.

Step 11: Replace population with this new population

Step 12: t←t+1. If t≤ M, return to Step 5; otherwise, output the optimal PID gains K_p, K_i, and K_d

Step 13: Plot step response of plant with optimum value of K_p, K_i, and K_d.

V. SIMULATION AND RESULTS

Improved genetic algorithm is tested for two systems for analysis for their response. A third order system is firstly taken. Then a first order system with lag plus delay (FOLPD) is taken. Tool used is MATLAB .

The block diagram of the controlled system is shown in Fig.2

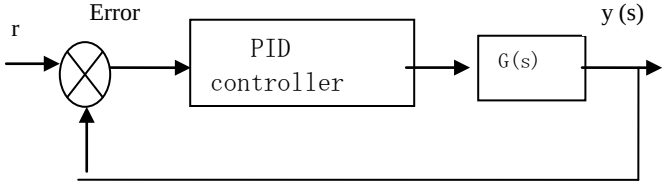

Fig 2. Block diagram of the controlled system.

Parameters taken for analysis . of GA are listed in Table 1

Table 1. List of system parameters

Parameter	Value
Population size	30
Maximum no. of generation	50
Mutation probability (P_{m1})	0.1
Crossover probability (P_{c1})	0.66
Number of bits per variable	5
Upper limit of gains	25
Lower limits of gain	25
$\in$	10
α	1
w_1	0.6
w_2	0.3
w_3	0.1

SIMULATION FOR SYSTEM 1

The following third order system is taken for analysis

$$G(s) = \frac{1}{[s(s+1)(s+5)]} \qquad (19)$$

Figure 3 shows the step response of system1 (19) with Ziegler Nicholas method. Fig 4 shows the response with classical GA using MSE criterion. Fig 5. shows the step response with improved GA as proposed in this paper. Table 2 shows the results for these simulations. It is seen from Fig 5 that GA is finally converging to the optimum solution. Fig 6 shows the graph of K_P,K_I, & $K_{D,}$. Fig 7 shows the plot of average fitness for the system.

Table 2 Comparison of Improved GA with canonical GA and ZN method.

Method	Mp	%Mp	Ts	Tr	Kp	Kd	Ki
ZN	1.62	62%	10	.577	6.322	17.99	12.8
Canonical GA (MSE)	1.11	0	1.85	.442	1.85	2.5	0.1
Improved GA(MO)	0	0	None	1.46	6.451	7.258	0.1

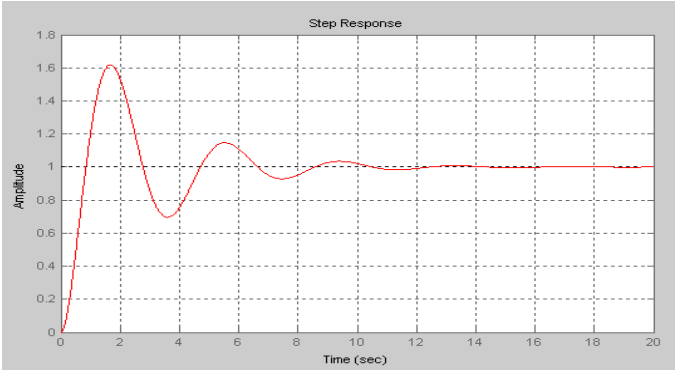

Fig. 3 Step response with Ziegler Nicholas method for system1

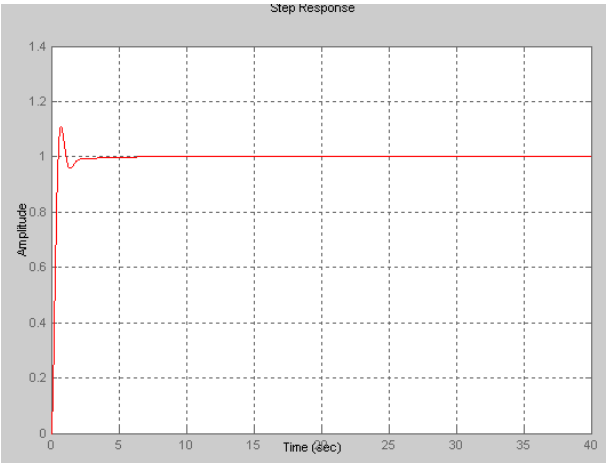

Fig 4. Step response with classical GA using MSE criterion

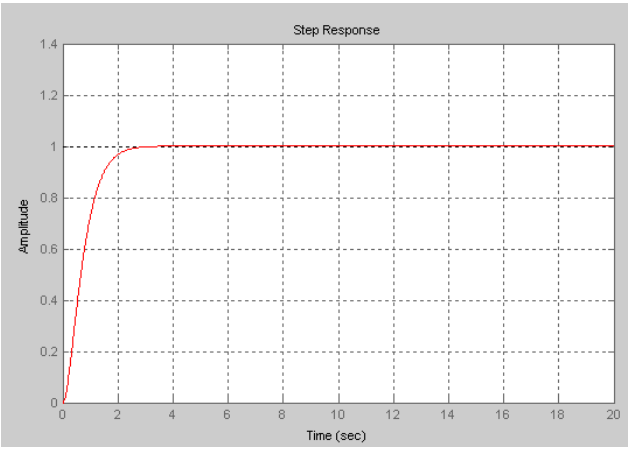

Fig 5. Step response with improved GA with multiobjective function

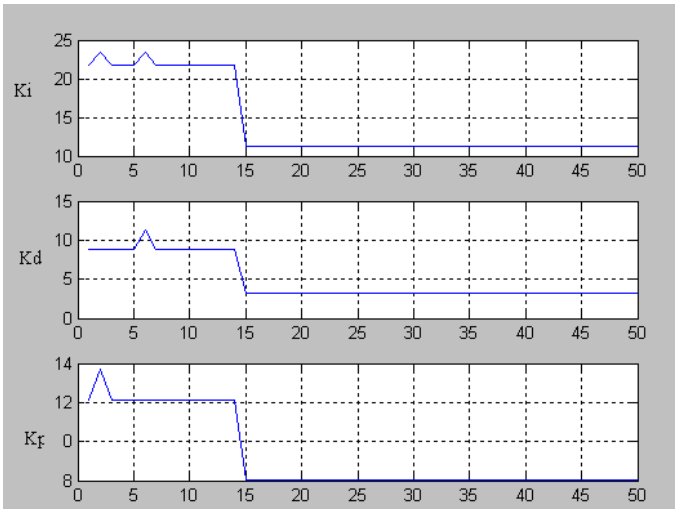

Fig 6. Plot of variables (K_p, K_i and K_d) for improved GA

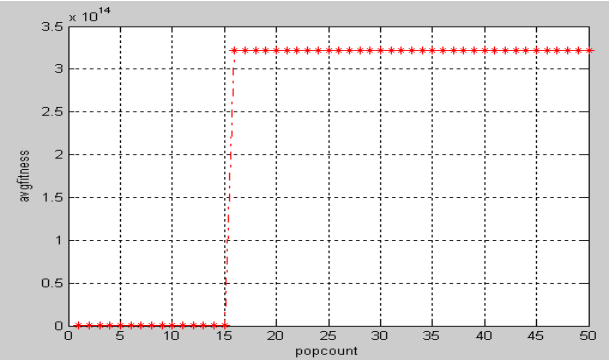

Fig 7 average fitness for improved GA

Calculation of computation time

Improved GA because of its variable probabilities takes comparatively lesser simulation time. Table 3 shows the comparison data of the computation efficiency of canonical GA and improved GA. Table 3 shows that improved GA reduces the computation time by 40%. The reason for reduction in computation time is due to reduction in number of crossovers and number of mutation in improved GA with increase in iteration counts.

Table 3. Comparison of computation time

Algorithms	**Average CPU time per iteration (sec)**
Canonical GA	2.5
Improved GA	1.5

Results

- Improved GA is finally converging to optimum or near optimum solutions.
- With improved GA peak overshoot as compared to classical GA is reduced to zero.
- Settling time is also reduced to zero.
- Rise time can be reduced by adjusting the weight criterion.

SIMULATION FOR SYSTEM 2

A first order system with time delay is selected as System 2

$$G(s)=\frac{e^{-0.1s}}{1+0.5s} \qquad (20)$$

By approximating delay with first order approximation i.e

$$e^{-sT_d}=\frac{1-0.5sT_d}{1+0.5sT_d}$$

System becomes,

$$G(s)=\frac{1-0.05s}{(1+.5s)(1+0.05s)} \qquad (21)$$

The parameters of the PID Controller for System 2 i.e. FOLPD system are tuned with (1) Zeigler Nicholas tuning method, (2) with classical GA and then (3)with improved GA. Figure 8 shows the responses for the above three cases. The comparison of results of the above three cases is shown in Table 4.

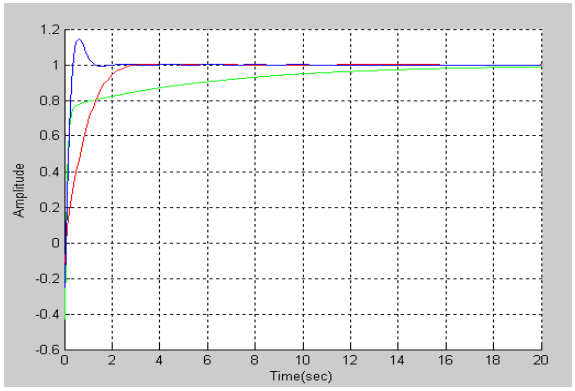

Fig 8.Step Responses of controlled system 2

Green line shows the case 1 performance (ZN Method)
Blue line shows the case 2 performance (classical GA.)
Red line shows the case 3 performance (Improved GA.)

Table 4. Comparison of Improved GA with classical GA and ZN Method for system 2

Method	**Mp**	**Mp%**	**Ts**	**Tr**	**Kp**	**Kd**	**Ki**
ZN	0	0	13.8	3.37	8	0.3	1.2
Improved GA (MSE)	1.15	15%	1.09	0.267	4.83	0.2	17.74
Improved GA (MO)	0	0%	2.39	1.6	1.0483	0.1	2.5

Results

As shown in Fig 8 and Table 4

- ZN method gives seriously under damped response.
- Improved GA with MSE even if the peak overshoot increases, it reduces the settling time and rise time by about 92 %

ISBN: 978-1-61804-228-6

- Improved GA with MO does not give any overshoot and it also reduces the settling time by 82% and rise time by 52 %

VI. Conclusion

This paper presents an improved genetic algorithm for PID control and its inherent advantages. The responses as shown in previous section show that the designed PID with improved GA has much better response than using the canonical GA method and other techniques. The classical method is good for giving us as the starting point of what are the PID values.
The improved GA designed PID is much better in terms of the overshoot and settling time and with the concept of immunity it does converge to an optimum or near optimum solution. The concept of variable probabilities also decreases the processing time. This improved GA is tested for a third order system and a time delay system. It is seen that it gives optimum or near optimum values for both system

Consequently, the improved genetic algorithms are better than simple genetic algorithms and they are feasible and effective optimization algorithms.

.

References

[1] Holland, J.J. *Adaptation in Natural and Artificial Systems*, University of Michigan Press. I975

[2] Goldberg, David E., *Genetic Algorithms in Search, Optimization and Machine Learning*. Addison-Wesley Pub. Co. 1989.

[3] Michalewicz Z. , *Genetic algorithms + Data structure = Evolution Programs.*, Springer Publications., 1999

[4] Ogata K, *Modern Control Engineering*, 4th edition, Pearson publications,2002

[5] Visioli Antonio, *Practical PID Control*, *SPRINGER* Publication, 2006.

[6] Qing Wang, Pieter Spronck, Rudolf Tracht, "An overview of genetic algorithms applied to control engineering problems**",** Proceedings of the Second International Conference on Machine Learning and Cybernetics, Wan, 2-5 November 2003.

[7] Kiam Heong Ang, Gregory Chong , and Yun Li, "PID Control System Analysis, Design, and Technology" *IEEE Transactions On Control Systems Technology*, Vol. 13, No. 4, July 2005.

[8] Kwok D.P., Wang P. "Fine tuning of classical PID Controller" Emerging Technologies and Factory Automation, *IEEE*, 1992.

[9] O' Mohanty, T., Downing,C.J. and Klaudiuz, F., 'Genetic Algorithms for PID Parameter Optimisation: Minimising Error Criteria' [online], URL: http://www.pwr.wroc.pl/~i-8zas/kf_glas00.pdf

[10] Licheng Jiao ,"A novel genetic algorithm based on immunity", *IEEE* Trans. on systems, man, and cybernetics—part a: systems and humans, vol. 30, no. 5, september 2000.

[11] Guanzheng Tan, Bin Jiang, Liming Yang. "A Novel Immune Genetic Algorithm-Based PID Controller Design and Its Application to CIP-I Intelligent Leg" Third International Conference on Natural Computation (ICNC 2007).*IEEE*

[12] Xiangzhong Meng, Baoye Song. "Fast Genetic Algorithms Used for PID Parameter Optimization" , Proceedings of the *IEEE* International Conference on Automation and Logistics, 2007, China

[13] Andri Mirzal, Shinichiro Yoshii, Masashi Furukawa, "PID Parameters Optimization by Using Genetic Algorithm*", ISTE Journal Of Science And Technology Policy*, 2006

[14] Guili Yuan, Yan-guang Xue, and Jizhen Liu , "Adaptive Immune Genetic Algorithm and Its Application in PID Parameter Optimization for Main Steam Temperature Control System" Proc. of Third International Workshop on Advanced Computational Intelligence August 25-27, 2010 - Suzhou, Jiangsu, China

[15] Amira. Sayed A. Aziz *et.al*. "Artificial Immune System InspiredIntrusion Detection System Using Genetic Algorithm" Informatica 36 (2012)347–357.

[16] M. Rabiej, "Application of Immune and genetic algorithms to the identification of a polymer based on its X-ray diffraction curve", *Journal of Applied Cryst*.(2013), 46, 1136-1145.

Jyot Ohri is Professor in Electrical Engg Deptt., NIT Kurukshetra. Having interest in robot control , robust control and Soft computing techniques.

Naveen Kumar is M.Tech. Student in Electrical Engg. Deptt. with the National Institute of Technology, Kurukshetra,India136119; naveenvermaindia@gmail.com.

Meenakshi chinda was student of M.tech in Electrical Engg , NIT Kurukshetra and now working in a software company in India.

An Efficient Load Balancing Algorithm for virtualized Cloud Data Centers

Ali Naser Abdulhussein Abdulhussein, Jugal Harshvadan Joshi, Atwine Mugume Twinamatsiko, Arash Habibi Lashkari, Mohammad Sadeghi

***Abstract*—**Cloud computing has become a new computing paradigm as it can provide scalable IT infrastructure, QoS-assured services and customizable computing environment. Although there are many research activities or business solutions for Cloud computing, most of them are focused on single-provider Cloud. As a key service delivery platform in the field of service computing. Cloud Computing provides environments to enable resource sharing in terms of scalable infrastructures, middleware and application development platforms, and value-added business applications .This study examined the latest technology in the field Cloud Computing. The main study focused on load balancing for virtual machines inside single cloud data center. There different algorithms for balancing, one of them called Throttled load balancing which treats the virtual machines based on two values that can send to the intended virtual machine or send it to the remote ones .A proposed modification has been proposed to solve some of the key features in this algorithm like Process migration, Fault tolerant and Overload Rejection. The idea is to send even when all the virtual machines heavily loaded by determining the most respectable hardware specifications of the virtual machines.

***Keywords*—** Cloud Computing, cloud Virtualization, load balancing, Cloud Data Center

I. Introduction

Cloud computing refers to both the applications delivered as services over the Internet and the hardware and systems software in the data centers that provide those services. With a connection over the internet, a consumer is able to access various resources, be it premium or free in order to perform certain functionality and all these constitute a cloud; The services themselves have long been referred to as Software as a Service (SaaS). Some vendors use terms such as IaaS (Infrastructure as a Service) and PaaS (Platform as a Service) to describe their products. This is to say with cloud computing, a cloud is formed over the amalgamation of various services be it physical or virtual over a network to perform certain services (Parhizkar B. et.al, 2013).

By deploying IT infrastructure and services over the network, an organization can purchase these resources on an as needed basis and avoid the capital costs of software and hardware. With cloud computing, IT capacity can be adjusted quickly and easily to ac-commodate changes in demand. While remotely hosted, managed services have long been a part of the IT landscape, a heightened interest in cloud computing is being fueled by ubiquitous networks, maturing standards, the rise of hardware and software virtualiza-tion, and the push to make IT costs variable and transparent .

Great interest in cloud computing has been manifested from both academia and private research centers and numerous projects from industry and academia have been proposed. In commercial contexts among the others, we highlight: amazon elastic compute cloud, IBM's blue cloud, etc .There are several scientific activities driving toward open cloud-computing middleware and infrastructures such as reservoir and eucalyptus, etc (Parhizkar B. et.al, 2013).

Clouds aim to power the next generation data centers as the enabling platform for dynamic and flexible application provisioning. This is facilitated by exposing data center's capabilities as a network of virtual services (e.g. Hardware, database, user-interface, and application logic) so that users are able to access and deploy applications from anywhere in the Internet driven by the demand and QoS (Quality of Service) requirements. Similarly, IT companies with innovative ideas for new application services are no longer required to make large capital outlays in the hardware and software infrastructures. By using clouds as the application hosting platform, IT companies are freed from the trivial task of setting up basic hardware and software infrastructures. Thus they can focus more on innovation and creation of business values for their application services.

II. Related works

According to Abhay Bhadani and Sanjay Chaudhary (Bhadani A. et.al, 2010), they propose a Central Load Balancing Policy for Virtual Machines (CLBVM) to balance the load evenly in a distributed virtual machine/cloud

This manuscript is part of the final projects of three students who worked in cloud computing together in Postgraduate Centre of Study (PGC), Limkokwing University of Creative Technology, Cyberjaya, Malaysia.

Mr. Jugal Harshvadan Joshi, Ali Naser Abdulhussein Abdulhussein, and Atwine Mugume Twinamatsiko were students in the cloud computing research group (jugal90@gmail.com, ali.naser2010@yahoo.com, twinmugume@gmail.com).

Dr. Arash Habibi Lashkari was supervisor of this group and advisor of research projects in Postgraduate Centre of Study (PGC), Limkokwing University of Creative Technology (a_habibi_l@hotmail.com).

Mr. Mohammad Sadeghi is head of Postgraduate Centre of Study (PGC), Limkokwing University of Creative Technology (m.sadeghi@limkokwing.edu.my).

computing environment. This effort tries to compare the performance of web servers based on their CLBVM policy and independent virtual machine(VM) running on a single physical server using Xen Virtualizaion. The paper discusses the value and feasibility of using this kind of policy for overall performance improvement.

The proposed CLBVM policy is at an inception stage and requires work for I/O as well as memory availability on the target server. The CLBVM policy has the potential to improve the performance of the overall N Servers though it does not consider fault tolerant systems. They tried to make the system completely distributed such that, if the performance of the VM gets affected by another VM, it can move itself to lightly loaded server on the go (Bhadani A. et.al, 2010).

Glauco Estácio Gonçalves et. al (Gonçalves, G. E. et.al ,2013), proposed algorithms for allocation of computing and network resources in a Distributed cloud (D-Cloud) with the objectives of balancing the load in the virtualized infrastructure and of considering constraints, such as processing power, memory, storage, and network delay. The evaluation of the algorithm shows that it is indeed adequate for link allocation across different physical networks. It considers that links are unconstrained in terms of capacity. They argue that this situation is well-suited to a pay-as-you-go business plan, very common in Cloud Computing and it allows a better usage of the resources than the common idea of link capacity reservation. The proposed algorithms were tested through simulations, focusing on the improvements brought by the minimax path strategy. The experiments showed that the minimax path strategy can offer better load balancing, in terms of maximum link stress than heuristics from the literature as the rate of requests increases (Gonçalves, G. E. et.al, 2013).

Zehua Zhang and Xuejie Zhang (Zhang Z. et.al , 2010), proposed a load balancing mechanism based on ant colony and complex network theory in open cloud computing federation in this paper, it improves many aspects of the related Ant Colony algorithms which proposed to realize load balancing in distributed system, Furthermore, this mechanism take the characteristic of Complex Network into consideration. Finally, the performance of this mechanism is qualitatively analyzed, and a prototype is developed to enable the quantitative analysis, simulation results manifest the analysis.

This mechanism improves many aspects of the related Ant Colony algorithms which proposed to realize load balancing in distributed system, and the characteristic (small-world and scale-free) of Complex Network have been taken into consideration (Zhang Z. et.al , 2010).

Srinivas Sethi et. al (Sethi S. et.al , 2012) , they introduced the novel load balancing algorithm using fuzzy logic in cloud computing, in which load balancing is a core and challenging issue in Cloud Computing. The processor speed and assigned load of Virtual Machine (VM) are used to balance the load in cloud computing through fuzzy logic. It is based on Round Robin (RR) load balancing technique to obtain measurable improvements in resource utilization and availability of cloud-computing environment.

The network structure or topology also required to take into consideration, when creating the logical rules for the load balancer. Two parameters named as the processor speed and assigned load of Virtual Machine (VM) of the system are jointly used to evaluate the balanced load on data centers of cloud computing environment through fuzzy logic (Sethi S. et.al, 2012).

Pengfei Sun et. al, They presented a new security load balancing architecture-Load Balancing based on Multilateral Security (LBMS) which can migrate tenants' VMs automatically to the ideal security physical machine when reach peak-load by index and negotiation. They have implemented their prototype based on CloudSim, a Cloud computing simulation. Their architecture makes an effort to avoid potential attacks when VMs migrate to physical machine due to load balancing (Sun P. et.al, 2011).

Shu-Ching Wang et.al (Wang S. et.al, 2010), they introduced a two-phase scheduling algorithm under a three-level cloud computing network is advanced. The proposed scheduling algorithm combines OLB (Opportunistic Load Balancing) and LBMM (Load Balance Min-Min) scheduling algorithms that can utilize more better executing efficiency and maintain the load balancing of system.

The goal of this study is to reach load balancing by OLB scheduling algorithm, which makes every node in working state. Besides, in their research, the LBMM scheduling algorithm is also utilized to make the minimum execution time on the node of each task and the minimum whole completion time is obtained. However, the load balancing of three-level cloud computing network is utilized, all calculating result could be integrated first by the second level node before sending back to the management. Thus, the goal of loading balance and better resources manipulation could be achieved (Wang S. et.al, 2010).

He-Sheng WU et.al (Wu H. et.al, 2013), discussed the new characteristics the load balancing should have in cloud computing. In cloud computing, load balancing manages virtual machine in the cloud instead of actual one. Therefore, load balancing system should be provided with the function of elastic management of back-end resource, i.e. to dynamically add or delete back-end server (existing in the form of virtual machine in the cloud) based on actual network load condition.

Since the virtual machine for load balancing management in cloud computing can be dynamically applied and released, an algorithm of prediction-based elastic load balancing resource management (TeraScaler ELB) is presented to overcome the drawbacks.

Experiments have shown that the required number of virtual machines change in compliance with the change of network load, thus TeraScaler ELB is able to dynamically adjust the processing capacity of back-end server cluster with the applied load. Besides it could make full use of the 'use on demand' feature of cloud computing, TeraScaler ELB leads to a better application of prediction based load balancing in cloud

computing. It concludes that compared with the traditional elastic resource management algorithm, TeraScaler ELB is more reasonable for providing scalability and high availability (Wu H. et.al, 2013).

Jiann-Liang Chen, et. al (Chen J. et.al , 2012), this paper presents a study to improve cloud computing systems performance based on Eucalyptus cloud platform. An optimal load balancing mechanism called EuQoS system for scheduling VMs is proposed. Extending EuQoS to accommodate real-time services, Hadoop platform is integrated into the EuQoS system. Log processing services are utilized to investigate the performance of system throughput. Experimental results indicate that the proposed EuQoS system can improve system throughput by 6.94% compared with the basic Eucalyptus platform with Hadoop mechanisms.

According to Xiaona Ren et. al (Ren X. et. al , 2011), Considering the unique features of long-connectivity applications, an algorithm is proposed, Exponential Smoothing forecast-Based on Weighted Least-Connection ESBWLC. ESBWLC optimizes the number of connections and static weights to actual load and service capability, and adds single exponential smoothing forecasting mechanism. Finally, experiments show that ESBWLC can improve the load of real servers effectively.

Analysis of Previous Load Balancing Algorithms

The throttled algorithm has been chosen to be modified based on the simulation conducted as it has better results compared with the other algorithms especially if it is working with response time algorithm and based on recommendations of the experts that we have found in the articles (Shiraz M. et. al , 2012). Throttled algorithm is also known as the threshold algorithm as it has two values (tUpper and tUnder) which specify the load on the virtual machines. If the load is greater than the value of tUpper then, it will send the process to the remote processor, otherwise if the load if less than the value of tUnder then it will process it locally and if the virtual machine is overloaded then it will update the other virtual machines of its state. The algorithm has a low inter-process communication as most of the load is processed locally which leads in performance as there is not much sending and receiving of jobs (Sanei Z. et. al, 2012).

There many metrics that govern the load balancing in a virtualized data centers, the threshold algorithm guarantees most of them except some which are as follows (Sharma S. et.al, 2008):

Overload Rejection: If Load Balancing is not promising additional overload rejection measures are needed. When the overload situation ends then first the overload rejection measures are stopped. After a short guard period Load Balancing is also closed down.

Fault Tolerant: This parameter gives that algorithm is able to bear twisted faults or not. It enables an algorithm to continue operating properly in the event of some failure. If the performance of algorithm decreases, the decrease is relational to the seriousness of the failure, even a small failure can cause total failure in load balancing.

Process Migration: Process migration parameter provides when does a system decide to migrate a process? It decides whether to create it locally or create it on a remote processing element. The algorithm is capable to decide that it should make changes of load distribution during execution of process or not.

III. Proposed New Algorithm

As a result we can conclude that when the virtual machines is heavily loaded and also the other virtual machines overloaded then it will not send any incoming jobs to the remote processor as it is overloaded and it will process it locally. our idea is when a virtual machines is overloaded, the algorithm can still send to the most respectable virtual machine in terms of physical hardware specifications, this will lighten the burden of one virtual machine to the other as it will make the strongest virtual machines handle the load while the others processing until the others will finish the jobs and back to the original state. This will help solving some the metrics that should be found in the load balancing algorithms like overload rejection (Abhijit A. et.al, 2012). This modification will make a queue of new incoming jobs for the strongest virtual machines respectively as the load on one overloaded processor can be much higher than on other overloaded processors, causing significant disturbance in load balancing, and increasing the execution time of an application.

Table 1: Analysis of Throttled algorithm (Abhijit A. et.al, 2012)

Parameters	Threshold Algorithm
Nature	Static
Overload Rejection	Yes
Reliability	Less
Adaptability	Less
Stability	Large
Predictability	More
Forecasting Agency	More
Cooperative	Yes
Fault Tolerant	Yes
Resource Utilization	Less
Process Migration	Yes
Preemptiveness	Non-preemptive
Response Time	Less
Waiting Time	More
Turnaround Time	Less
Execution System	Decentralized
Throughput	Low
Processor Thrashing	No

IV. Simulation and Results

In this section, this paper will try to show some the simulations conducted to choose the throttled algorithm as the algorithm to modify. First simulation was conducted to test

throttled algorithm with the closest data center as the service broker whereby it chooses the closest data center to the user request. The second simulation was conducted for the throttled algorithm but in regard to the best response time of the data centers the request was made to. In the third round the simulation was tested for throttled in regard to reconfiguring dynamically of the data center located around the world whereby the requests can be directed flexibly according to the best data center that can serve the request.

THROTTLED WITH CLOSEST DATA CENTER:

The first round was tested using the Throttled algorithm for the load balancing strategy with the Closet Data Center as the Data Center broker policy. The simulations were conducted for 100 virtual machine and a total of 1000 requests per user per hour, with an average of 10000 users in a peak hours and 100 in off-peak hours with 6 user bases located in different locations around the world and 6 Data Centers also located in different locations around the world as shown in figure 1.

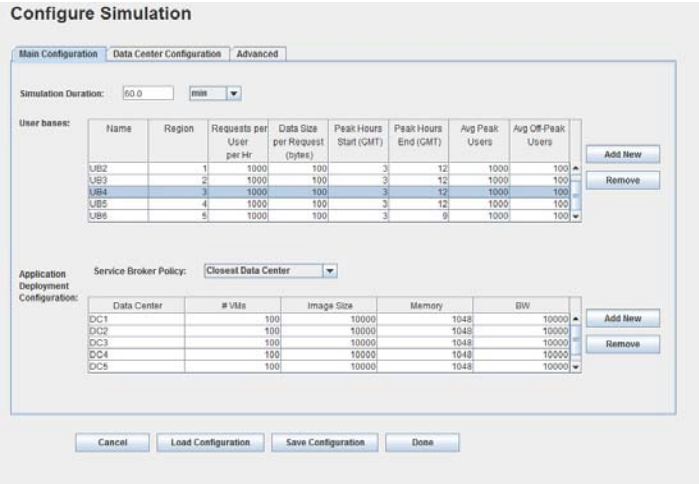

Figure 1: User base specification and service broker policy for the data center

In figure (2, 3), explanation on how to do the configuration for the simulation that is going to be tested on, Whereby the selection of the user requests that can be made per hour and whether it's a peak hour or normal hours to simulate a real world events as well as the starting and ending times for these requests. The data center broker that will govern the behavior of the data center have been identified as well ,for example in this simulation ,the closest data center which means the closest one for the requests to be entertained around the world. Hardware specifications of the data centers like the memory , CPU speed , the number of cores inside each CPU ,the operating system, the number of virtual machines inside each data centers and the cost that for each virtual machine to use the memory and CPU cores have been defined as well .

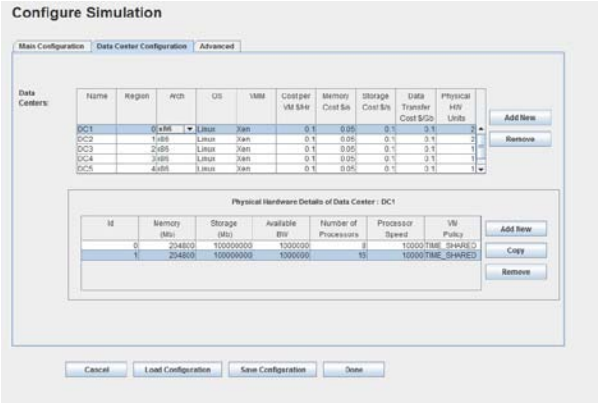

Figure 2: Data Center specifications

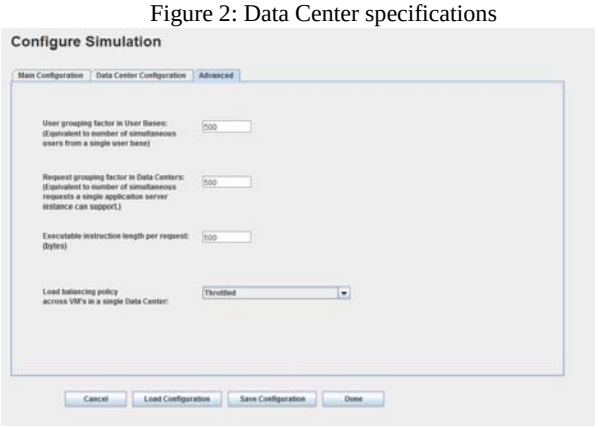

Figure 3: User requests and the load balancing algorithm

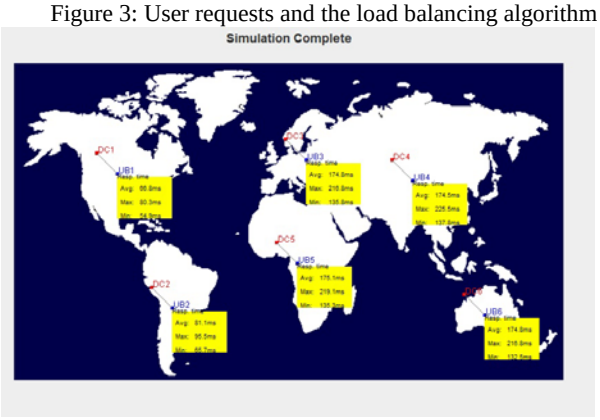

Figure 4: Data center locations and user bases requests

In figure 4, it shows the geographical location of each data center with their average, minimum and maximum execution time that can be taken in consideration when simulating with respect to each user request and whether this request is made from single user or multiple.

The results for the simulation conducted based on the specification provided in the above figures that shows the overall response time for the data centers and the cost for the virtual machines to serve the requests if the broker is set to closest data center.

Results:

	Avg (ms)	Min (ms)	Max (ms)
Overall response	141.35	54.87	225.52
Data Center processing time	91.72	12.65	167.76

Cost:

Total Virtual Machine Cost ($)	Transfer Cost ($)	Grand Total ($)
60.00	5.76	65.76

THROTTLED WITH OPTIMIZE RESPONSE TIME:

The second round was tested using the Throttled algorithm for the load balancing strategy with the Closet Data Center as the Data Center broker policy. I have conducted a simulation for 100 virtual machine and a total of 1000 requests per user per hour, with an average of 10000 users in a peak hours and 100 in off-peak hours with 6 user bases located in different locations around the world and 6 Data Centers also located in different locations around the world as shown in figure 5.

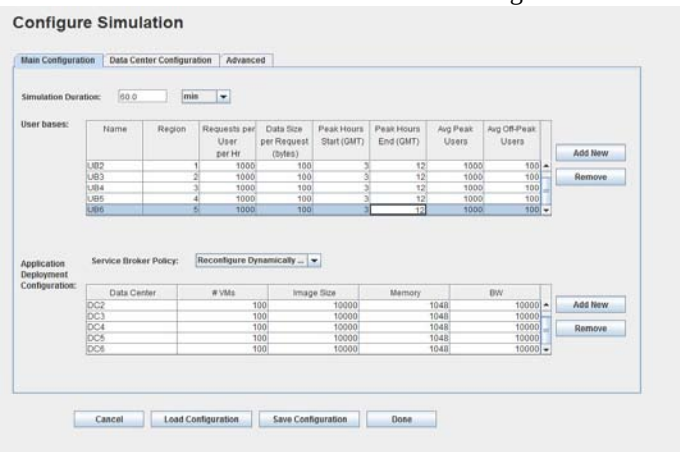

Figure 5: User base specification and service broker policy for the data center

In figure (6, 7), explanation on how to do the configuration for the simulation that is going to be tested on, Whereby the selection of the user requests that can be made per hour and whether it's a peak hour or normal hours to simulate a real world events as well as the starting and ending times for these requests. The data center broker that will govern the behavior of the data center have been identified as well ,for example in this simulation ,optimize response time which means the best data center that responded to the request to be process around the world based on the hardware specifications of the data centers like the memory , CPU speed , the number of cores inside each CPU ,the operating system, the number of virtual machines inside each data centers and the cost that for each virtual machine to use the memory and CPU cores have been defined as well .

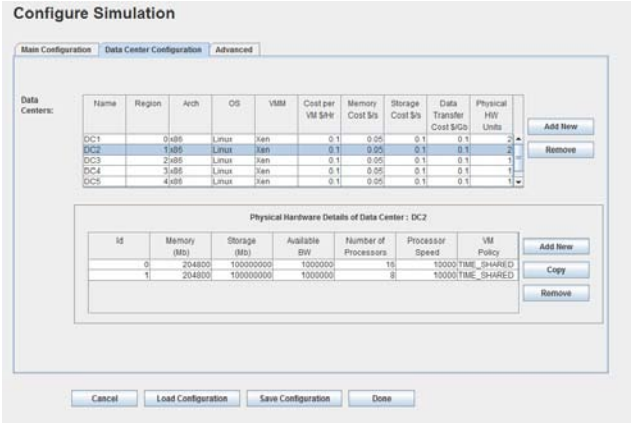

Figure 6: Data Center specifications

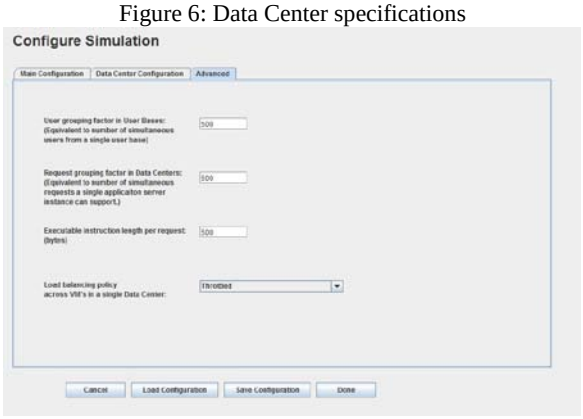

Figure 7: User requests and the load balancing algorithm

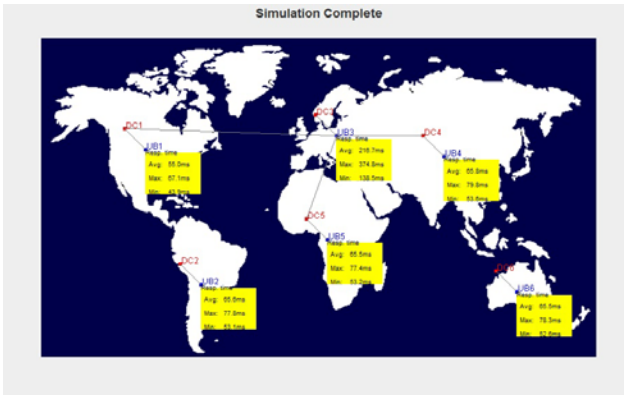

Figure 8: Data center locations and user bases requests

In figure 8, it shows the geographical location of each data center with their average, minimum and maximum execution time that can be taken in consideration when simulating with respect to each user request and whether this request is made from single user or multiple.

The results for the simulation conducted based on the specification provided for the data centers and the virtual machines shows a better results if the broker set to optimize response time in terms of data center execution time and cost of the virtual machines.

Results:

	Avg (ms)	Min (ms)	Max (ms)
Overall response time	89.14	43.86	374.83

ISBN: 978-1-61804-228-6

Data Center processing time	26.43	3.31	162.01

Cost:

Total Virtual Machine Cost ($)	Total Data Transfer Cost ($)	Grand Total ($)
50.50	5.76	56.26

THROTTLED WITH RECONFIGURE DYNAMICALLY:

The third round was tested using the Throttled algorithm for the load balancing strategy with the Closet Data Center as the Data Center broker policy. I have conducted a simulation for 100 virtual machine and a total of 1000 requests per user per hour, with an average of 10000 users in a peak hours and 100 in off-peak hours with 6 user bases located in different locations around the world and 6 Data Centers also located in different locations around the world as shown in figure 9.

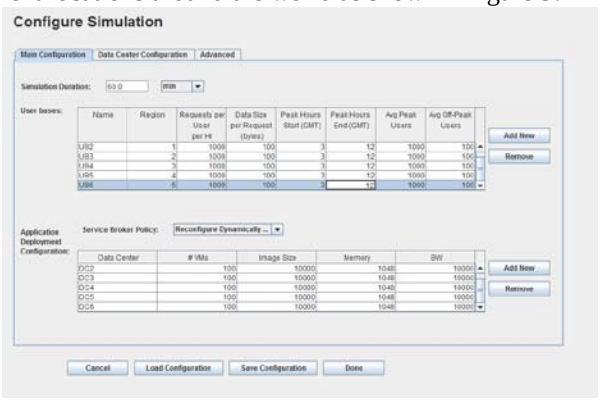

Figure 9: User base specification and service broker policy for the data center

In figure (10, 11), explanation on how to do the configuration for the simulation that is going to be tested on, Whereby the selection of the user requests that can be made per hour and whether it's a peak hour or normal hours to simulate a real world events as well as the starting and ending times for these requests. The data center broker that will govern the behavior of the data center have been identified as well ,for example in this simulation ,reconfiguration dynamically which means the data centers can serve the requests respectively but if there are other data centers available which are better than the current one, it will switch automatically to the best one accordingly. Hardware specifications of the data centers like the memory , CPU speed , the number of cores inside each CPU ,the operating system, the number of virtual machines inside each data centers and the cost that for each virtual machine to use the memory and CPU cores have been well-defined as well .

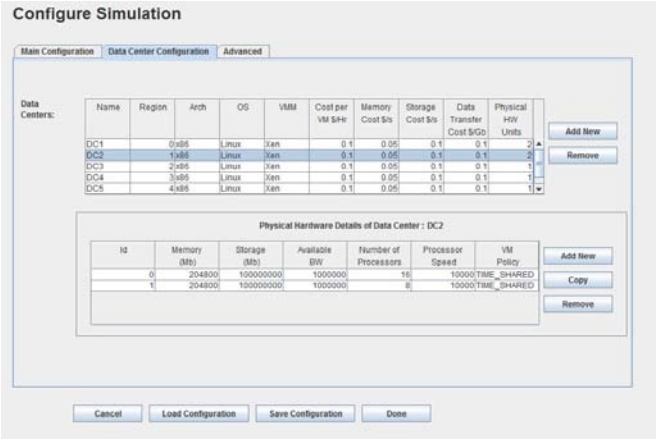

Figure 10: Data Center specifications

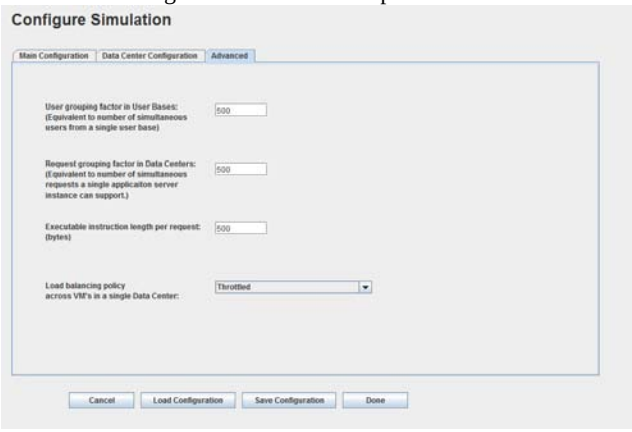

Figure 11: User requests and the load balancing algorithm

Figure 12: Data center locations and user bases requests

In figure 12, it shows the earthly location of each data center with their average, minimum and maximum execution time that can be taken in consideration when simulating with respect to each user request and whether this request is made from single user or multiple.

The results for the simulation conducted based on the specification provided for the data centers and the virtual machines shows a higher results if the broker set to reconfigure dynamically in terms of data center execution time and cost of the virtual machines than the optimize response time.

ISBN: 978-1-61804-228-6

Results:

	Avg (ms)	Min (ms)	Max (ms)
Overall response time	139.98	44.29	227.18
Data Center processing time	90.35	3.90	169.44

Cost

Total Virtual Machine Cost ($)	Total Data Transfer Cost ($)	Grand Total ($)
53.47	5.76	59.50

V. Conclusion

Cloud computing is a new edge technology that is versatile, fast and developing at a fast rate. In this report, different models of implementation of cloud computing has been studied. It is obvious that the cloud concept is a way to-go method of technology implementation these days. The trend of development is high, though much has been accomplished there is still a lot to do in this field of cloud computing for the future generation. One of the biggest buzz terms in technology today is cloud computing. Companies all over the world are utilizing the cloud for their businesses, allowing users to access their technology anytime, anywhere. Essentially, organizations who are using the cloud, or cloud computing, have their files, software, information and resources available anywhere in a virtual network. A modification for throttled algorithm has been identified to increase the efficiency of its response time and data center processing execution time and cost. Implementation of this modification in the CloudSim and Cloud Analyst will conducted as a future work. Cloud analyst has been chosen to simulate the current throttled algorithm in respect with different service broker. The results show that throttled algorithm is the chosen algorithm to modify as it has better results in terms of overall response time and data center processing.

VI. Acknowledgement

The special thank goes to our helpful supervisor Dr. Arash Habibi Lashkari from Postgraduate school for his unrivaled supervision and guidance in our dissertation and final project.

References

[1] Bhadani, A., & Chaudhary, S., Performance evaluation of web servers using central load balancing policy over virtual machines on cloud. Proceedings of the Third Annual ACM Bangalore Conference on - COMPUTE '10, 1–4. doi:10.1145/1754288.1754304, (2010).

[2] Gonçalves, G. E., Endo, P. T., Palhares, A. A., Santos, M. A., Kelner, J., & Sadok, D. (2013). On the load balancing of virtual networks in distributed clouds. Proceedings of the 28th Annual ACM Symposium on Applied Computing - SAC '13, 625. doi:10.1145/2480362.2480481, (2013).

[3] Larosa, Y. T. Optimal QoS load balancing mechanism for virtual machines scheduling in eucalyptus cloud computing platform. 2012 2nd Baltic Congress on Future Internet Communications, 214–221. doi:10.1109/BCFIC.2012.6217949, (2012).

[4] Muhammad Shiraz, Abdullah Gani, Rashid Hafeez Khokhar, Ejaz Ahmed, An Extendable Simulation Framework for Modeling Application Processing Potentials of Smart Mobile Devices for Mobile Cloud Computing, Proceedings of Frontiers of Information Technology 2012, Pakistan, 19-21 December 2012

[5] Parhizkar, B., Naser, A., Abdulhussein, A., & Joshi, J. H. (2013). A Common Factors Analysis on cloud computing models, 10(2), IJCSI International Journal of Computer Science Issues, Vol. 10, Issue 2, No 1, ISSN (Print): 1694-0814 | ISSN (Online): 1694-0784 523–529. March (2013).

[6] Ren, X., Lin, R., & Zou, H. A dynamic load balancing strategy for cloud computing platform based on exponential smoothing forecast. 2011 IEEE International Conference on Cloud Computing and Intelligence Systems, 220–224. doi:10.1109/CCIS.2011.6045063, (2011).

[7] Rajguru, A. A., & Apte, S. S. A Comparative Performance Analysis of Load Balancing Algorithms in Distributed System using Qualitative Parameters, International journal of recent Technology and Engineering (IJRTE) , ISSN:2277-3878, Volume-1 , Issue -3. Ausgust (2012).

[8] Sethi, S., Sahu, A., & Kumar, S. (2012). Efficient load Balancing in Cloud Computing using Fuzzy Logic, 2(7), 65–71, IOSR Journal of Engineering (IOSRJEN) ISSN 2250-3021 Volume 2, Issue 7(July 2012), PP 65-71 ,July 2012.

[9] Sun, P., & Chen, Y. POSTER: LBMS: Load Balancing based on Multilateral Security in Cloud, Proceedings of the 18th ACM conference on computer and communications security pages 861-864, (2011).

[10] Sharma, S., Singh, S., & Sharma, M. Performance Analysis of Load Balancing Algorithms, World Academy of Science, Engineering and Technology 269–272. (2008).

[11] Wang S. Yan k Liao W Wang S. Towards a Load Balancing in a Three-level Cloud Computing Network, Computer Science and Information Technology (ICCSIT), 3rd IEEE International Conference on (Volume:1). (2010).

[12] Wu, H. Wang C. XIE J., TeraScaler ELB-an Algorithm of Prediction-based Elastic Load Balancing Resource Management in Cloud Computing, 27th International Conference on Advanced Information Networking and Applications Workshops (2013).

[13] Zohreh Sanaei, Saeid Abolfazli, Abdullah Gani, Rashid Hafeez Khokhar, Tripod of Requirements in Horizontal Heterogeneous Mobile Cloud Computing. 1st International Conference on Computing, Information Systems and Communications (CISCO'12), May 14-16, Singapore, (2012).

[14] Zhang Z. and Zhang X., A Load Balancing Mechanism Based on Ant Colony and Complex Network Theory in Open Cloud Computing Federation, 2nd international conference on industrial mechatronics and automation. (2010).

[15] R. J. Vidmar. (1992, August). On the use of atmospheric plasmas as electromagnetic reflectors. *IEEE Trans. Plasma Sci.* [Online]. *21(3).* pp. 876—880. Available: http://www.halcyon.com/pub/journals/21ps03-vidmar

Reducing the number of sub-trees for frequent itemsets mining

Supatra Sahaphong and Gumpon Sritanratana

***Abstract*—**This paper aimed to develop a new algorithm to mine all frequent itemsets from a transaction database. A new mining algorithm called vertical index list (VIL) tree which performs database only once and without generating any candidate itemsets. The decision maker can change of the minimum support threshold without rescanning of the database. The VIL-tree algorithm uses sorted VIL, so a mount of the frequent itemsets are generated at first. The next trees are resized down which reduced trees construction and its traversal, and the number of recursive of mining steps. When the node construction and sub-trees are reduced, resulting in a reduction in run time and memory consumption. The experiments in which run time and memory consumption of the proposed algorithm are tested in comparison with frequent pattern (FP) growth algorithm. The experiments of both algorithms are evaluated by applying to the bench mark synthetics datasets. The experimental results demonstrate that VIL-tree provides better performance than FP-growth in terms of run time and space consumption.

***Keywords*—**Association rule mining, data mining, frequent itemsets mining, knowledge discovering.

I. Introduction

Frequent itemsets mining is an essential step in association rule mining. The association rule mining is to decompose into two major subtasks. First, the generation of all the frequent itemsets which satisfy the minimal support threshold. Second, the extraction of all high confidence rules from frequent itemsets found in previous step. Our work focuses on the first subtask. The first classic algorithm is Apriori which is proposed in [1]. The Apriori principle is "If an itemsets is frequent, then all of its subsets must also be frequent" [2]. The Apriori algorithm uses a level-wise and breadth-first search approach for generating association rule. It uses the support-based pruning to control the exponential growth of candidate itemsets. The algorithms based on generated and tested candidate itemsets have two major problems which are shown as follows. The database must be scanned multiple times to generate candidate sets which increase the I/O load and is time-consuming. Moreover, the generation of huge candidate sets and calculation of their support will consume a lot of CPU time. The drawbacks which presented as above were overcome by using the next generation of algorithm, called the FP-growth algorithm [3]. The advantages of mining of frequent itemsets by using the FP-growth algorithm are shown as follows. The database is scanned only two times, so time consuming is decreased. The generating of candidate sets is not required, so the I/O load is reduced. The FP-growth algorithm performs depth-first search approach in the search space. It encodes the data set using a compact data structure called FP-tree and extracts frequent pattern directly from this prefix tree [4]. The following researches have improved this idea. In reference [5], the H-mine algorithm was introduced by using array-based and trie-based data structure. The Patricia Mine algorithm was proposed in [6] that compressed Patricia trie to store the data sets. The FPgrowt* algorithm reduced the FP-tree traversal time by using array technique [7]. In reference [8], the SFI-Mine algorithm which constructs pattern-base by using a new method which is different from pattern-base in FP-growth and mines frequent itemsets with a new combination method without recursive construction of conditional FP-tree. However, most of the FP-tree algorithm base has the following drawbacks. First, mining of frequent itemset from the FP-tree, it generates huge of conditional FP-tree and takes a lot of time and space. Second, when the changing of minimum support, this algorithm may restart and scan database twice. Many researchers have proposed ways to scan database once. The Eclat algorithm was proposed by using the join step from the Apriori property to generate frequent pattern [9]. In Reference [10], the new data structure, called LIB-graph is proposed to contain data when database is scanned and discovery of frequent patterns by using recursive conditional FP-tree. The Sorted-List structure which created from the Vertical Index List was proposed to contained data from scanning database once and mining of frequent itemsets by using depth-first search [11]. Moreover, in case that the decision maker wants to change the minimum support threshold, an algorithm is performed without rescanning of database [12].

This paper proposed a new algorithm to mine all frequent itemsets. The feature of the proposed algorithm presented as follows. The database is scanned only one time to mine frequent itemsets and a new algorithm mines frequent itemsets without generation of candidate sets. The decision maker can

This work was supported in part by Ramkhamhaeng University, Ramkhamhaeng Raod, Bangkapi District, Bangkok 10240, Thailand.

Supatra Sahaphong is with the Department of Computer Science, Faculty of Science, Ramkhamhaeng University, Ramkhamhaeng Raod, Bangkapi District, Bangkok 10240, Thailand (corresponding e-mail: supatra@ru.ac.th, supatra@hotmail.com).

Gumpon Sritaratana is with the Department of Mathematics, Faculty of Science, Buriram Rajabhat University, Muang, 31000, Thailand (e-mail: sgumpon@gmail.com).

change of the minimum support threshold all time without rescanning of the database. The proposed algorithm reduced the number of sub-trees and loops in mining steps. Therefore, the proposed method can reduce both run time and space consumption, the experiments in which the run time and memory consumption are tested for the VIL-tree and FP-growth algorithm. The results of this method are still obtaining complete and correct frequent itemset. This paper is organized as follows. The prior knowledge is presented in section II, follows by the approach which is presented in section III, the results and discussions is shown in section V and the finally, the conclusion is addressed in section VI.

II. Prior Knowledge

This section introduces basic concepts for mining of frequent itemsets. The following definition is proposed by Han et al in [4, 12].

Let $I = \{x_1, x_2, ..., x_m\}$ be a set of items and $DB = \{T_1, T_2, ..., T_n\}$ be a transaction database, where $T_1, T_2, ..., T_n$ are transactions that contain items in *I*. The support, or *supp* (occurrence frequency), of a pattern *A*, where *A* is a set of items, is the number of transactions containing *A* in DB. A pattern *A* is frequent if *A*'s support is no less than a predefined minimum support threshold, *minsup*. Given a DB and a minimum support threshold *minsup*, the problem of finding a complete set of frequent itemsets is called the frequent-itemsets mining problem.

A data structure called a vertical index list (VIL) which introduced in [2, 9, 11] is summarized as follows. Let $T_i = \{x_1, x_2, ..., x_m\}$ be a transaction in DB, where $i = 1,2,...,m$ and x_j is an item for $j = 1,2,...,n.$ A vertical index list (or VIL) is the structure constructed from a scan of each T_i in DB only once. Each row in VIL contains an item in *I*, support of item in I, and transactions in DB which contain such an item. The set of transaction will be written in order according to the ascending of its identification number. The set of items will be written in order according to the descending of its support. The algorithm in Fig. 1 shows how to construct the VIL.

The construction VIL is presented in Fig.1.

```
Algorithm1: The instruction of VIL
Input: DB, minsup
Output: sorted VIL
Begin
   Scan DB once.
   Create all items to VIL
   Define all support of items in VIL is zero
   For each transaction in DB do
      For each item in transaction do
         Insert transaction of item to TID-set which
           corresponding with item
         Count support of item
      End //For
   End //For
         Sort support of items of VIL   //descending sort
End //Begin
```

Fig. 1 The instruction of VIL

III. The Approach

This section introduces a new algorithm called VIL-tree. The feature of the proposed algorithm presented as follows. The transaction database is scanned only one time to mine frequent itemsets. The VIL-tree algorithm mines frequent itemsets without generation of candidate sets, reduces the number of sub-trees and loops in mining steps. Therefore, the proposed method can reduce both of run time and space consumption.

The transaction database is scanned once to construct a VIL. Then an itemset-tree structure is a general tree structure constructed from the VIL, called a vertical index list-tree of itemsets, denoted by VIL-tree (itemsets). It is a finite set of one or more nodes. It consists of the root of tree, a set of item subtrees as the children of the root, and a set of header tables. Each node in tree comprises five fields. There are two fields of value which are item-name and support and there are three fields of pointer which are same-item, parent and child. Each member of the *header table* consists of two fields, item-name and head of node link. Each node of tree is of the form (frequent itemset : support).

The algorithm in Fig. 2 shows how to construct VIL-tree and the algorithm in Fig. 3 shows how to mine all frequent itemsets.

ISBN: 978-1-61804-228-6

```
Algorithm2: VIL-tree(Frequent item) construction
Input: VIL
Output: VIL-tree (Frequent item)
Begin
  Create header table
  Read item in VIL    //supp(item) is not less than minsup
  Create root R and initial supp(R) to 1
  Link R to header table
  For each transaction of root R do
    While next frequent item <> (last frequent item)+1 do
      Read next frequent item (N) that has same transaction
          with R
      Call InsertTree (N,R)
    End//While
  End//For
End //Begin
Procedure InsertTree (N,R)
Begin
  If VIL-tree(R) has a node C such that
     C.item-name = N.item- name then Increment supp(N) by 1
  Else
    Create new node N and initial supp(N) to 1
    Link N to N's parent; Link N to N's header table
    Link N to same-item
  End //If
End //Begin
```

Fig. 2 The construction of VIL-tree

```
Algorithm3: Mining frequent itemsets from VIL
Input: VIL, VIL-tree (frequent itemset), minsup
Output: WFS  //WFS is the set of all frequent itemsets
Begin
    For each frequent item in VIL do
      Find a set of frequent itemset length 1 (or FI-1) from VIL
        //FI-1 is a set of all frequent items which
        // supp(frequent item) not less than minsup
      Save FI-1 to FS-1 // FS-1 is the set of frequent itemsets
            length 1
    End //For
    For all FI-1 do
      Create VIL-tree from FI-1 and then create a set of
          sub-header-1 (or SH-1)
      Generate candidate root of sub-tree(FI-1) from FI-1 and
          SH-1
      For all candidate root do
        While (candidate root is not in FS-m and level of tree
              is not equal 2) do   //where m=2,3,…,n
            Create sub-tree(FI-m) and then create a set of
                sub-header-m (or SH-m)
            Generate candidate root of sub-tree(FI-m) from
                FI-m and SH-m
          End //While
          Combine root node.child node and save it to FS-m
      End //For
    End //For
    Union all FS-m and save to WFS
End //Begin
```

Fig. 3 VIL-tree algorithm

IV. Results and Discussion

This section presents the experiments in which the run time and memory consumption are tested for the VIL-tree and FP-growth algorithm with two synthetic datasets and varying minimum support thresholds. The experiments were performed on a Microsoft Windows 7 Home Premium, processor is (Intel (R) Core (TM) i5-2467M, and 4 GB of RAM. All algorithms were coded using C language. The two synthetic datasets generated by the IBM Almaden Quest research group [13-14] were used for presented the experimental results. The datasets serve as the FIMI repository, which is a result of the workshops on frequent itemset mining implementations [15-16]. The two original databases of synthetic datasets are T10I4D100K and T40I10D100K.

In Fig. 4 and Fig. 5, when the minimum support is high, the number of frequent itemsets is low. The minimum support is low, many frequent itemsets are obtained. VIL-tree is always faster than FP-growth method because frequent item in VIL is performed in order of high support. The node construction and sub-trees are reduced, resulting in a reduction in run time and memory consumption. The Fig. 6 and Fig. 7 show that the memory consumption of VIL-tree is less than FP-growth in every minimal support threshold. This is because the node construction and the size of trees are reduced, so memory consumption is decreased.

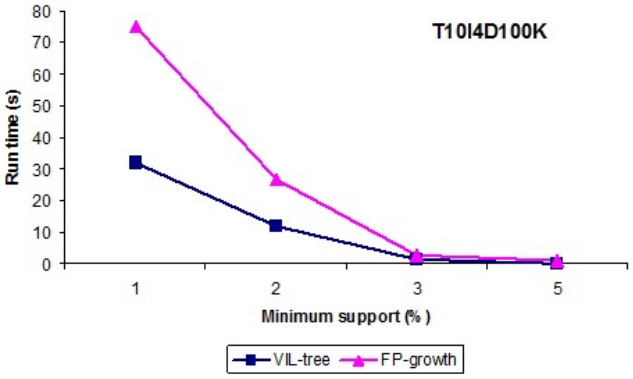

Fig. 4 Run time of mining on T10I4D100K

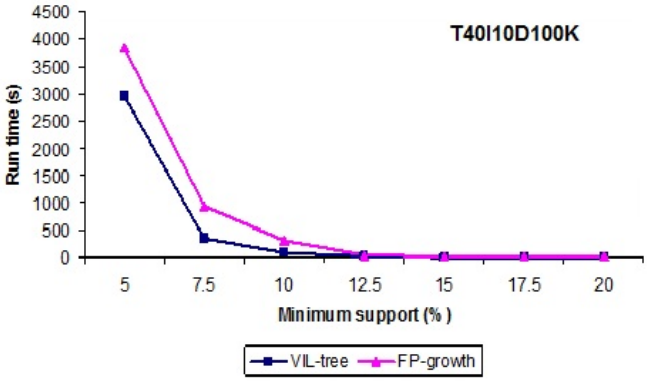

Fig. 5 Run time of mining on T40I10D100K

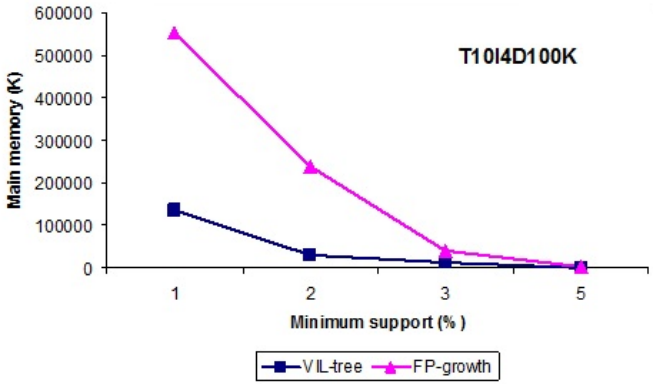

Fig. 6 Memory consumption of mining on T10I4D100K

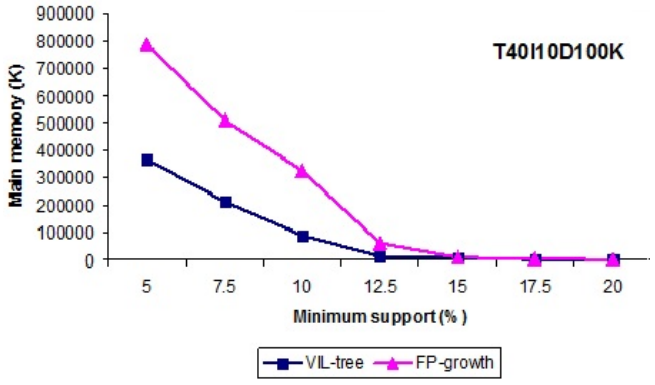

Fig. 7 Memory consumption of mining on T40I10D100K

V. Conclusion

This paper aimed to develop a new algorithm to mine all frequent itemsets from a transaction database. A new mining algorithm called vertical index list (VIL) tree which performs database only once and without generating any candidate itemsets. The decision maker can change the minimum support threshold without rescanning of the database at anytime. The research provided the experiments in which run time and memory consumption are tested in comparison with frequent pattern (FP) growth algorithm. The experiments of both algorithms are evaluated by applying to the bench mark synthetic datasets. The experimental results demonstrate that VIL-tree provides better performance than FP-growth in terms of run time and space consumption. We summarized the feature of this research as follows. The VIL-tree algorithm scans database only once, moreover, the VIL-tree algorithm uses sorted VI so that the amount of frequent itemsets are generated at first. The next VIL-tree is resized down and sub-trees are reduced which reduced the number of loops of mining steps. Therefor, run time and space consumption are reduced. The experiments of both algorithms are evaluated by applying to the bench mark synthetics datasets. The experimental results demonstrate that VIL-tree provides better performance than FP-growth in terms of run time and space consumption.

Acknowledgment

We deep appreciation and gratitude to Associate Professor Dr. Veera Boonjing of the Department of Mathematics and Computer Science, Faculty of Science, King Mongkut's Institute of Technology Ladkrabang, Thailand for his guidance and suggestions. We would like to express our appreciation and gratitude to Associate Professor Dr. Tawesak Tanwandee of Mahidol University, Thailand for his help in proof reading of this paper.

References

[1] R. Agrawal and R. Srikant: Fast Algorithm for Mining Association Rules, *Proceedings of the 20th International Conference on Very Large Data Bases*, Chile, September 1994, 487-499.

[2] P-N. Tan, M. Steinbach, & V. Kumar, *Introduction to Data Mining* (Pearson Education Inc., 2006).

[3] J. Han, J. Pei, & Y. Yin: Mining Frequent Pattern without Candidate Generation, *Proceedings of the 2000 ACM SIGMOD international conference on Management of Data*, Texas, May 2000, 1-12.

[4] J. Han, J. Pei, Y. Yin, & R. Mao: Mining Frequent Pattern without Candidate Generation: a Frequent Pattern Tree, *Springer, vol.* 8, 2004, no 1, 53-87.

[5] J. Pei, J. Han, H. Lu, S. Nishio, S. Tang, & D. Yang: Hmine: Hyper-Structure Mining of Frequent Patterns in Large Databases, *Proceedings of the 2001 IEEE International Conference on Data Mining*, USA, November 2001, 441-448.

[6] A. Pietracaprina, & D.Zandolin: Mining Frequent Itemsets Using Patricia Tries, *Proceedings of the 3rd IEEE International Conference on Data Mining*, Florida, USA, November 2003.

[7] G. Grahne, & J. Zhu: Efficiently Using Prefix-Trees in Mining Frequent Itemsets," *Proceedings of the 3rd IEEE International Conference on Data Mining*, Florida, USA, November 2003.

[8] S. Sahaphong, & V. Boonjing: The Combination Approach to Frequent Itemsets Mining, *Proceedings of the 2008 International Conference on Convergence and hybrid Information Technology*, Korea, November 2008, 565-570.

[9] M.J. Zaki, Scalable Algorithms for Association Mining, *IEEE Transaction on Knowledge and Data Engineering, vol.* 12, no. 3, 2000, 372-390.

[10] D. J. Chai, L. Jin, B. Hwang, & K. H. Ryu: Frequent Pattern Mining Using Bipartite Graph, *Proceedings of the 18th International Conference on Database and Expert Systems Applications*, Germany, August 2007, 182-186.

[11] S. Sahaphong, Frequent Itemsets Mining Using Vertical Index List, *Proceedings of the 2nd IEEE International Conference on Computer Science and Information Technology*, China, August 209, 480-484.

[12] J. Han, & M. Kamber, *Data Mining: Concepts and Techniques*, Elsevier, Maryland Heights MO, 2006.

[13] Frequent Itemset Mining Dataset Repository, "T10I4D100K". Available: http://fimi.cs.helsinki.fi/data/
[14] Frequent Itemset Mining Dataset Repository, "T40I10D100K".Available:http://fimi.cs.helsinki.fi/data/
[15] Workshop on Frequent Itemset Mining Implementations. Available: http://fimi.ua.ac.be/fimi03/
[16] Workshop on Frequent Itemset Mining Implementations. Available: http://fimi.ua.ac.be/fimi04/

Supatra Sahaphong received her B.S. (Computer Science) from Ramkhamhaeng University (RU), Thailand, in 1990, a M.S. (Information Technology) from King Mongkut's Institute of Technology Ladkrabang (KMITL), Thailand, in 1998, and a Ph.D. (Computer Science) from KMITL in 2011. From 1991 to 1999, she worked at Institute of Computer, RU and has joined Department of Computer Science, Faculty of Science, RU in 1999, where she is currently an Assistant Professor. She has been invited to be a program committee member and organizing committee of many international conferences as well as reviewer of many journals. She had received the best paper award from the Second International Workshop on Frontiers of Information Technology, Applications and Tools. Her research interests include data mining, knowledge discovering, and image segmentation.

Gumpon Sritanratana is an Assistant Professor at the Department of Mathematics, Faculty of Science, Buriram Rajabhat University, Thailand. He received Ph.D. in Mathematics from Chiang Mai University, Thailand. He worked at Department of Mathematics, Mahidol Univerisity, Thailand. He has been invited to be a program committee member and organizing committee of many international conferences and reviewer of many journals. His research activities involve partial differential operators such as the laplacian, ultra-hyperbolic and domain operators etc. His interest is in certain partial differential equations involving temper distribution solution. Another area of interest involves distribution theory and matrix calculus, especially some matrix convolutions of functions and distributions.

Performance of Frame Synchronization Symbols for an OFDM System in Dispersive Channels

Ali A. Eyadeh

***Abstract*—** In this paper, the problem of frame synchronization in orthogonal frequency division multiplexing (OFDM) system is considered. For an OFDM system, frame synchronization is achieved by forcing the receiver to start its FFT at the right time. One way in which this may be achieved is to precede the OFDM data with a special synchronization symbol. Two synchronization symbols are proposed to achieve frame synchronization for an OFDM, the wobbulation symbol and a training symbol based on IEEE 802.11a. These symbols are evaluated in a two-ray multipath channel, and performances are compared in terms of the probability of correct synchronization.

***Keywords*—**Communication channels, OFDM, Frame synchronization, Synchronization symbols

I. Introduction

DATA transmission systems depend to a great extent for their efficiency upon correct synchronization. Correct synchronization occurs by organizing the data into reliable synchronized frames [1], [2]. Each frame includes a synchronization symbol followed by data symbols. At the receiver the synchronization symbol indicates the starting position of the frame. In a noisy communication link, the received data are not always correct, so there is no certainty of being able to recognize the synchronization symbol when it is sent or to detect it by chance when it is not sent, so two factors are essential for designing a synchronization system:

1. The synchronization symbol must be sufficiently unlikely to occur by chance in random data symbols.
2. The receiver must be designed to permit a suitable margin of errors.

In OFDM systems the frame synchronization task is to align the FFT window at the correct received sample. If this is not achieved, then the samples from the adjacent OFDM symbol can be included in the FFT block, resulting in ISI. Several techniques have been proposed for OFDM synchronization [3]-[10].

In this paper two synchronization symbols are proposed to achieve frame synchronization for an OFDM-based indoor wireless data transmission system, the wobbulation symbol and a training symbol based on IEEE 802.11a.

A. A. Eyadeh is with the Electrical Engineering Department, Al-Jouf University, Sakaka, Saudi Arabia, on leave from Yarmouk University, Irbid, Jordan (e-mail: aeyadeh@yu.edu.jo).

II. OFDM System

OFDM is a special case of multi-carrier modulation system [10], based on the discrete Fourier transform in which a high bit rate stream is separated into a large number of low data rate sub-channels each of which modulates a single carrier. Sub-carriers are spaced by the reciprocal of the sub-channel data rate and are thus orthogonal. The block diagram for an OFDM system is shown in Fig. 1.

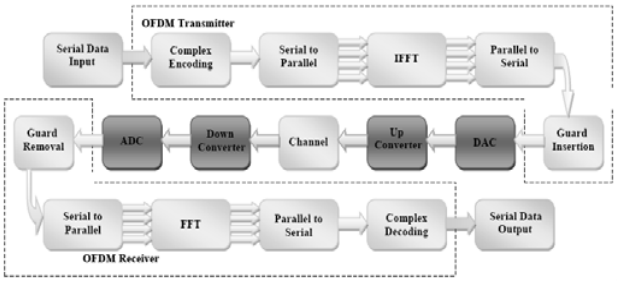

Fig. 1 block diagram of an OFDM system

The incoming serial data with a high data rate *R* is first encoded in a complex modulation format. The choice of modulation format may also influence the equalization requirements. Differential decoding requires no Phase equalization.

The encoded data stream is converted from serial to parallel to provide N complex data sub-channels with a data rate R/N for each sub-channel. The sequence of N parallel complex data sub-channels is transferred from frequency domain into time domain by the inverse fast Fourier transform (IFFT) process, to generate an OFDM signal. The OFDM signal is then converted back to serial data for transmission.

The orthogonality between different sub-carriers can be disturbed by intersymbol interference (ISI) caused by multipath propagation in the radio channel, so in order to combat this effect a guard interval is introduced. The discrete symbols are converted to analogue and low-pass filtered for radio frequency (RF) upconversion.

The OFDM receiver is essentially the inverse of the OFDM

transmitter as shown in Fig. 1. The incoming signal is mixed down to base-band, filtered and converted to digital words. The FFT at the receiver extracts the phase and amplitude of each sub-carrier from the block of the received samples. To demodulate the received signal successfully the receiver must start its FFT at the beginning of one of the OFDM data blocks, so frame synchronization is essential for an OFDM system.

III. Frame Synchronization in OFDM System

There are two types of synchronization that an OFDM receiver must achieve. The first one is the synchronization of the carriers for the receiver and the transmitter. This is important for the orthogonality between subcarriers, which is essential to avoid ICI.

The second synchronization task is to align the FFT window at the correct received sample. If this is not achieved then, the samples from the adjacent OFDM symbol can be included in the FFT block, resulting in ISI.

Here we have concentrated on the second synchronization task "FFT window alignment" in which we have introduced a complex OFDM synchronization marker.

In Fig. 2, a generalized OFDM receiver structure with synchronization block is given. Typically, the frame synchronizer operates on the data in the time domain and its output is used as an alignment point in serial to parallel conversion.

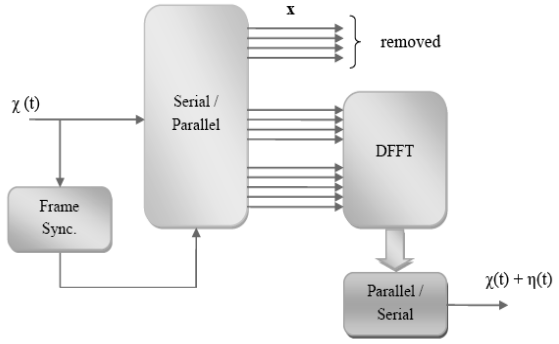

Fig. 2 generalized OFDM receiver structure with synchronization

IV. Synchronization Symbols

The two proposed synchronization symbols are:

A. Wobbulation Symbol

The wobbulation symbol is described by (1), (*i* is the time-sample):

$$x_i = e^{j\pi i^2 / N} \tag{1}$$

(except in the range $0 \le i < \Delta\mu_{\max}$ and $N - \Delta\mu_{\max} < i < N - 1$, in which x_i is zero)

$\Delta\mu_{\max}$ is the maximum uncertainty of the null symbol search (in samples) from the correct position. *N* is the number of active carriers.

B. Training Symbol based on IEEE 802.11a

The frame format of OFDM-based IEEE 802.11a contains three parts, the short training sequence (STS), long training sequence (LTS) and OFDM data symbol sequence. A short training sequence consists of ten repeated short symbols (ST1 to ST10), and the long training sequence consists of a double-protection interval (GI2) and two repeated long symbols (LT1 and LT2). Each of the short symbols are composed of 16 samples, and each of the long symbols are composed of 64 samples. STS and LTS sequences form a preamble or a synchronization symbol used to indicate the start position of each OFDM frame, as shown in Fig. 3 below:

ST1	ST2	ST3	……	ST10	GI2	LT1	LT2

Fig. 3 IEEE 802.11a standard preamble

V. OFDM Signal Burst and Model

An OFDM signal comprises a large number of digitally modulated carriers, which are orthogonal to each other within a certain length of the signal period. An OFDM symbol period (*T*OFDM=*TU* + *TG*) consists of an effective OFDM symbol period (*TU=64TS*) and a guard interval (*TG*=8*TS*), which is used to mitigate the effect of intersymbol interference (ISI).

In this paper, the performance of frame synchronizations using wobbulation symbol and a training symbol based on IEEE 802.11a. is investigated considering an OFDM N-subcarrier baseband transmitted under the influence of dispersive channel: two ray multipath channel.

A block diagram of an OFDM simulation model is shown in Fig. 4 and the transmitted OFDM data block is shown in Fig. 5.

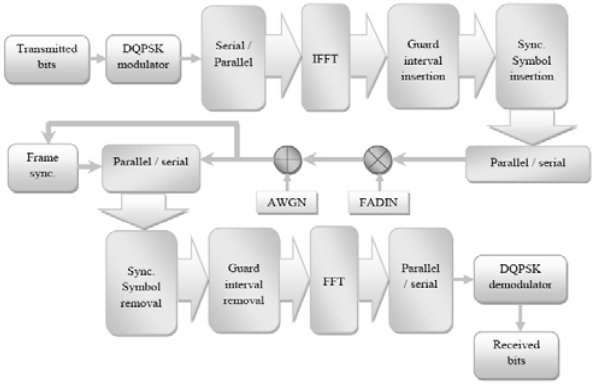

Fig. 4 simplified OFDM system model with synchronization

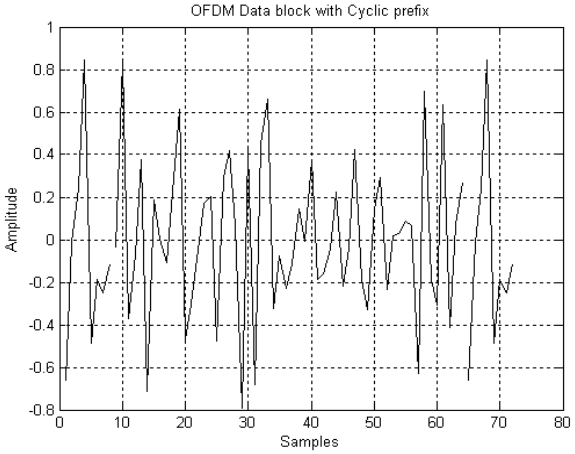

Fig. 5 transmitted OFDM data block with cyclic prefix

A. Simulation Parameters

Simulation was conducted using DQPSK for the modulation scheme; each burst consists of one reference symbol and six consecutive data symbols.

Each of the OFDM symbol uses 48 useful sub-carriers and 64 samples in the time domain (64TS), plus eight additional time sampling durations (8TS) as a guard interval. Thus one OFDM symbol duration (TOFDM=72TS=2.88μS). Simulation Parameters are shown in Table I.

TABLE I
SIMULATION PARAMETERS

Modulation/detection	DQPSK/differential detection	
Channel spacing	1/T	25MHz
FFT size	N	64
Subcarrier spacing	1/NT	391 KHz
Number of used subcarriers	N_u	48
Total number of virtual subcarriers	V_c	16
guard	T_g	$8T_S$
Doppler frequency	f_d	50Hz

B. Frame Synchronization Circuit

The frame synchronization circuit structure is shown in Fig. 6. The purpose of this circuit is to provide the receiver with the proper frame indices (i.e., the frame starting and ending samples) this circuit has an important roll in aligning the FFT window at the receiver.

As can be seen, this circuit consists of a shift register, correlator circuit, and a comparator. The shift register provides for a sliding correlation window of the reference symbol length (i.e. wobbulation symbol or IEEE sequence). The correlator performs the cross-correlation operation between the reference symbol and the incoming data stream. The resulting correlation-coefficients are fed to the comparator which compares its value to a pre specified threshold and decides weather a new frame is presents or not. In other words, it can be said that synchronization circuit's function is to hunt for the SYNC symbol in the received bit stream.

The output of the synchronization circuit for an ideal channel is shown in Fig. 7.

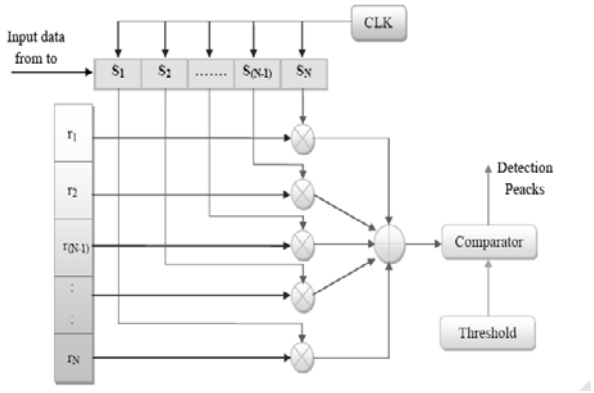

Fig. 6 synchronization circuit structure

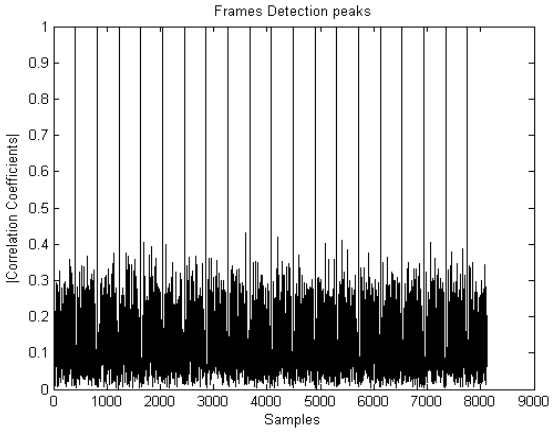

Fig. 7 output of the frame synchronization circuit, for ideal channel

VI. SIMULATION RESULTS

In this paper the performance of frame synchronization for an OFDM system using wobbulation symbol and IEEE sequence is investigated under the influence of dispersive (two-ray multipath) channels.

Random data were transmitted over the same channel for both synchronization symbols, and the probability of correct synchronization (*Pcs*) was calculated. Fig. 8 shows the probability of correct synchronization *Psc* for different values of SNR for the two synchronization symbols under the influence of dispersive channels.

ISBN: 978-1-61804-228-6

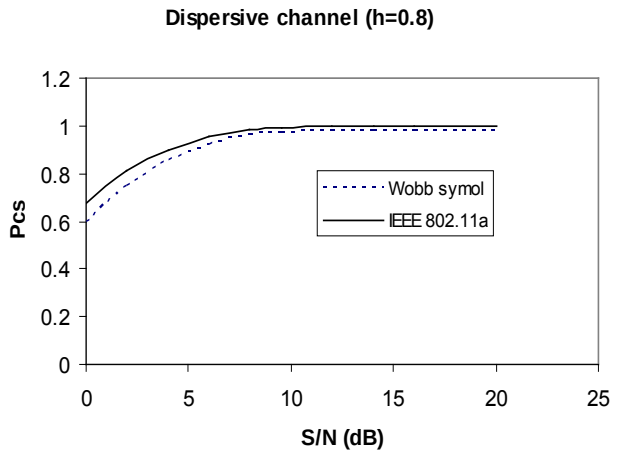

Fig. 8 probability of correct synchronization (*Psc*) for the two synchronization symbols under the influence of dispersive channels

VII. Conclusion

Frame synchronization for an OFDM-based indoor wireless data communication system has been presented. Two different synchronization symbols, the wobbulation symbol and the IEEE sequence, were used. The performance of the system has been analyzed under the influence of dispersive channels. The probability of correct synchronization for both symbols was found and the simulation results presented here provide some indication of the improvements available by using the IEEE 802.11a sequence as a synchronization symbol for frame synchronization.

References

[1] P. Driessen, "Improved Frame Synchronization Performance for CCITT Algorithms Using Bit Erasures", *IEEE Trans. Comm.*, vol. 4, no. 6, pp. 2016-2019, 1995.

[2] K. Luong, A. Mokraoui, P. Duhamel, and N. Trung., "Time Synchronization Algorithm in IEEE 802.11A Communication System," *20th European Signal Processing Conference*, Bucharest, Romania, 2012, pp. 1628-1632.

[3] R. A. Scholtz, "Frame Synchronization Techniques", *IEEE Trans. Comm*., vol. 28, pp. 1204-1212, 1980.

[4] T. Fusco and M. Tanda, "A Data-Aided Symbol Timing and Frequency Offset Estimation Algorithm for OFDM Systems", *Wireless Personal Communications: An International Journal*, vol. 35, no. 1-2, pp. 201-212, 2005.

[5] M. Bank, M. Bank, M. Haridim, and B. Hill, "OFDM Simulation Methods Based on Stuffing," *proceedings of 12th WSEAS International Conference on COMMUNICATIONS*, Heraklion, Greece, July 2008, pp. 220-224.

[6] C. Kishore and V. Reddy, "A Frame and Frequency Offset Estimation Algorithm for OFDM System and its Analysis," *EURASIP Journal on Wireless Communications and Networking*, vol. 6, pp. 46-61, 2006.

[7] T. Haiyun, K. Lau, and R. Brodersen, "Synchronization Schemes for Packet OFDM System," *Proceeding of IEEE International Conference on Communications*, USA (ICC 03), vol. 5, 2003, pp. 3346-3350.

[8] R. Thakur, and K. Khare, "Synchronization Techniques in OFDM Systems," *International Journal of Computer Networks and Wireless Communications*, vol. 2, no. 6, pp. 693-696, 2012.

[9] A. Eyadeh, "Frame Synchronization Symbols for an OFDM System," *International Journal of Communications*, vol. 1, no. 2, pp. 126-134, 2008.

[10] A. Akan, E. Onen, and L. Chaparro, "A New Time-Frequency Based Channel Estimation Approach for Wireless OFDM Systems," *WSEAS Transactions on Communications*, Issue 8, Vol. 5, pp. 1033-1038, 2006.

Ali A. Eyadeh was born in Irbid province, Jordan, on July 13, 1962. He received the bachelor degree in the department of electrical engineering, Jassy University, Romania in 1986, and M.Sc. and Ph.D. degrees in communication engineering from University of Wales, Swansea, UK in 1995 and 1997 respectively.

He is an associate professor in the department of electrical engineering, Al-Jouf University, Saudi Arabia, on leave from Yarmouk University, Hijjawi faculty for engineering technology, Jordan. He taught in several universities in Jordan, United Arab Emirates (UAE), Syria and Saudi Arabia. His research interests include synchronization in digital communication systems, digital signal processing and data compression.

Analysing and Devising a Model for Trustworthy Software

Bekim Fetaji [1]
South East European University,
Contemporary Sciences and Technologies, Computer Science
Ilindenska bb, 1200 Tetovo, Republic of Macedonia
b.fetaji@seeu.edu.mk

Nasih Reci [2], Majlinda Fetaji [3]
South East European University,
Contemporary Sciences and Technologies, Computer Science
Ilindenska bb, 1200 Tetovo, Republic of Macedonia
nr07178@seeu.edu.mk , m.fetaji@seeu.edu.mk

Abstract— The research study is focused on the exploration and analyses of development methodologies of trustworthy software and proposes a model and a framework for approaching such development, while applied it on a particular practical application PRIME DB were has been implemented and tested the proposed model as well as evaluated with the users. Analyses of the current methodologies and best practices involved in the development of software that can be used to increase reliability in software has been realized. Also developed a software solution to test the model and apply the framework as well as tested and evaluated it with the users using questionnaire. In conclusions insights are provided and recommendations are stated based on the study results realized.

Keywords—trustable software, reliable software, model for trustable software, software engineering reliability

I. INTRODUCTION

Today many software systems govern our life, so the software engineers must accept the responsibility to develop systems that will be preserving and protecting our work and the integrity of the system. Software is becoming the most important component of a system. According to [1] during the last 50 years, two other components, computer networks and hardware separately, have reached a much higher level of reliability and performance. The cost of poor quality of software is becoming increasingly critical, particularly emphasizing the fact that the cost of software development and life expectancy has surpassed that of hardware. Improve quality of this software reduces costs dramatically, because 80 to 90% of this amount goes then in regulation, adaptation, extension and maintenance of software [3]. Nearly 40% of the cost of software development nowadays goes for tests, to fix errors and defects. The frequency of failures in software compared to hardware failures today goes up to 100:1 [3].

The proposed model from this research study for developing trustable software is based on project management tools, techniques and methodologies that are characterized by key elements: infrastructure that provides the necessary leadership and communication, training and rewards within organization that will provide strong support for software development as reliable process. Also a system for the collection of reliable data that accurately identify user requirements during different phases of software development; methods to optimize the design of software and addressing different user requirements, such as reliability, cost, and duration; establishing protocols for coding and testing various arrangements for adequate time, this strategy provides cost and time efficient process. Because in this way the information about possible failures would be available at any time; standardization of best practices [2], [5] and establishment of quality planning tools [11] as QFD (Quality Function deployment) and FMEA (Failure Modes and Effects Analysis); using innovative tools for software development as Design objects Oriented (OOD), Extreme Programming (XP) and means known as CASE tools.

In order to develop a trustworthy system, the conclusion is based on the evaluation realized [1] that the development process must be reuse oriented and integrate formal languages and rigorous methods in all phases of system development life – cycle process [4], [6], [8]. The second aim of this research was to give such a software engineering process model that consists of several parallel tracks of activities, and the central concern in all this activities was to ensure trustworthiness.

As contribution the study as outcome developed software application based on the previously devised model and a framework with a set of tools supporting the spectrum of formal development activity from modeling to deployment, focusing in:

1. Design, and improve trustworthy software systems.
2. Focus on customer-centered issues as first class structural elements of trustworthiness attributes such as reliability, dependability, safety, security, availability and upgradeability.
3. Validate, test, evaluate, integrate, maintain and upgrade software to ensure proper function and reliability.
4. Integrate additional techniques such as systems thinking, process management, standardization and adequate documentation.
5. Use tools and techniques for developing trustworthy software and to describe the challenge of Trustworthy Software Systems.

II. Research Focus

The main goals of this research study are:

1. Analyze reliable and trustable software systems.

2. Focus on issues that relate to the users' requirements and to establish them as structural elements of the first class, such as: reliability, security, stability, availability, protection, and updating software reliability.

3. Validate, test, evaluate, integrate, and maintain software to ensure the proper functioning of the software.

4. Develop a model to integrate, to engineer systems thinking, management processes, standardization and adequate documentation.

5. Utilize and use advanced tools and techniques to increase reliability during software development and describe the challenges for achieving these goals.

III. Hypotheses

The main hypotheses addressed in this research study are as follows:

1. What are the methodologies and best practices involved in the development of software and that can be used to increase reliability in software?

2. In order for the Software to be credible or reliable is a reliable hardware needed?

3. Which technologies can improve productivity and quality of software, based on components or Object Oriented Programming?

4. After five decades of software development, do we need a new paradigm and genuine involvement of management in the development of increasingly complex applications?

IV. Analysis of the Causes of Loss of Credibility in the Software

Reliability in software presents social problem and is taking the recent global importance [9]. Following are some of the main causes:

Lack of commitment of managers: the most common reasons that have to do with the quality problems are lack of commitment, involvement and support of the managers. This also applies to software to hardware.

Inappropriate interactions with users: This happens when not properly understand the users' requirements. This means that the voice of the customer must be heard and their demands should be understood and interpreted adequately. However, software development usually involves very little user involvement have been written after the program specifications. This lack of interaction with users and their requirements change, which occurs rarely be detected and corrected during software development [11]. This is one of the main causes of problems that have to do with the quality of software.

Increasing complexity, software systems are facing problems more and more complex and often no equivalent solution to understand the nature of the problem and the level of difficulty. Complex software systems used for automatic flight control, search engines, e-commerce and global money transfer, have no equivalent manual comparison. Moreover, such applications may not have the previous experiment with to be based on them.

Lack of not agreeing criteria: In the complex software systems, system developer often ends in establishing criteria that may or may not meet the requirements of users.

The limited scope of automation: development and use of software is human and interactive. CASE tools and automation as object oriented design, have helped, but the extent of automation in software is limited compared with hardware.

Internet Connection: Integration of software systems to the Internet, exposes systems to risks and viruses. These risks may be large. They range from identity theft to the massive financial fraud and national security threats.

V. Proposed Model for Developing Reliable Software

As noted above, the software unreliability is always the result of errors during design or human error. According to [4] philosophy and the systems proposed in this paper provide a different methodology, which means that the systems developers must first identify the optimal requirements and definitions so that applications be as powerful and reliable. These elements are taken from the model proposed below.

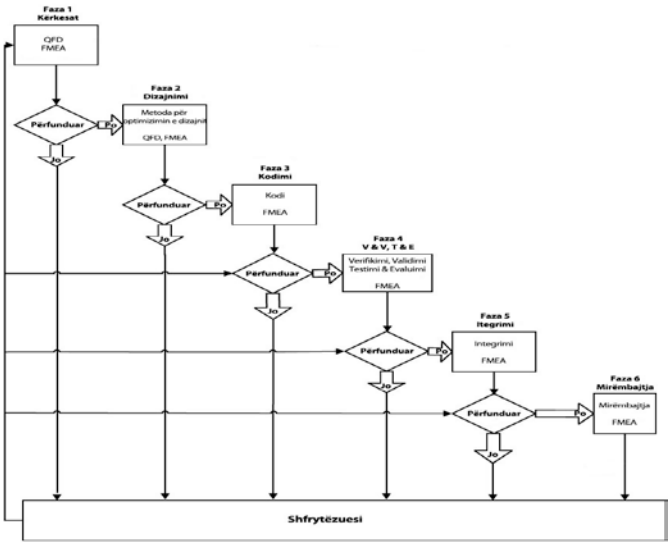

Fig. 1. Proposed model of trusted software development

This model includes seven components of the process of developing reliable software. This model is based on strong management and proven tools, techniques and methodologies that are characterized by the following key elements:

Infrastructure that provides the necessary leadership and communication, training and rewards within the organization that will provide strong support for the process of developing reliable software.

System for the collection of reliable data that accurately identify the users' requirements during various phases of software development.

Method for optimizing the design of software and addressing the different requirements of users, such as reliability, cost, and duration.

Creating practices for coding and testing for different arrangements for adequate time. This strategy provides process cost and time efficient, because in this way information about possible failures would be available at any time.

Standardization of best practices and planning the placement of qualitative as QFD and FMEA Failure Modes and Effects Analysis.

The use of innovative tools for software development as Object Oriented Design, Extreme Programming and appropriate tools known as CASE tools [7].

If the reference model for the development of powerful software and process design of reliable software we can say that the model describes the process, while the process is illustrated by the model.During the last decades several models have been developed for applications development. Many of them like the waterfall model, Spiral Model, and the V-model, have originated in the aerospace industry and do not always reflect the reality of the software development process [11], [12].

This model is an iterative process that offers interactions with users always considering voice, the users' requirements during the application development process. Among others, is powerful and flexible and can be adapted to any process for software development. It should be noted that the software companies where technology is an important activity, the software development process is very important for you only left to software engineers. It is the responsibility of the executive team to provide the necessary leadership, proper management infrastructure, and creating an environment suitable for the development of reliable software.

VI. Software For Media Presence (PrimeDB)

PrimeDB developed as software to monitor all national television, print, radio, web and networks (portals) in Kosovo during the social 24/7/365. Media Presence service that is derived from the monitoring process PrimeDB media company. Media monitoring is a process that involves reading, watching and listening to the editorial content of ongoing media resources, with the aim of identifying and analyzing the content of interest.

Search is the same as in Google, you can find any media content that you care for only a few seconds.

With a few more clicks, you can have accurate statistics of media presence to your business, your competitors ads, in TV interviews, news or what others say about you and not only.

Furthermore, PrimeDB experts are ready to help you in generating tools, complex statistical reports for your reports more complicated and detailed.

Presence of media content generated by the spectrum of media to monitor. The margin of error in media monitoring of PrimeDB intended to be less than 2% in total.

In the event of any claim by a third party for infringement of copyright, or other similar rights to the materials provided by the presence of the media, the media source material assumes any liability and potential inconsistency.

Fig. 2. PrimeDB Media Presence

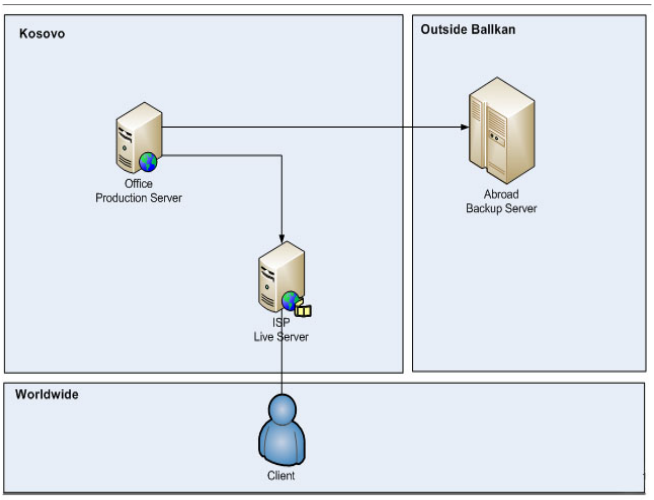

Fig. 3. The business plan online operation

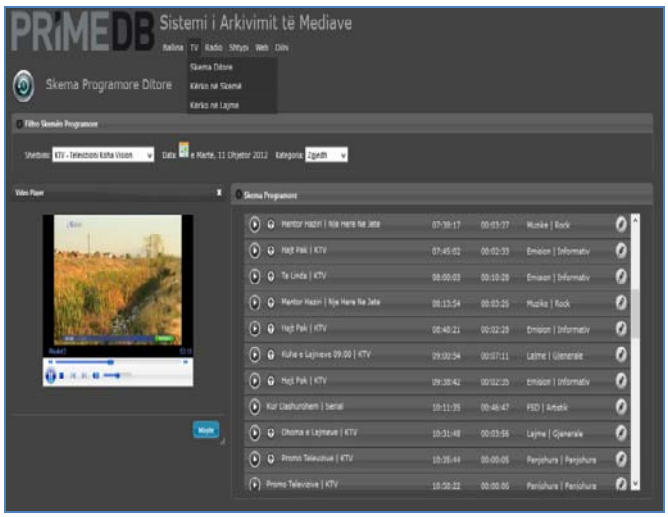

Fig. 4. The media archiving system – video

VII. Data Analyses

Periodic analysis is part of Media Presence service, which enables to generate statistics about the media presence of a certain period, based on filtering the form below:

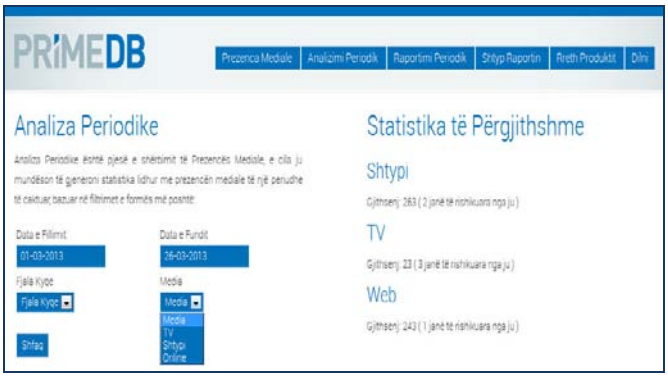

Fig. 5. The media archiving system – video

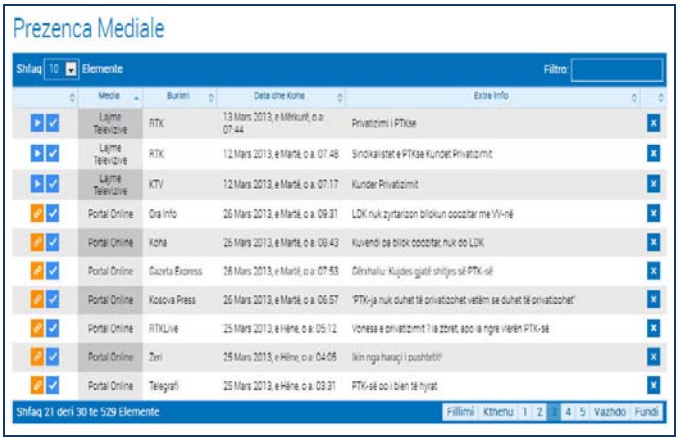

Fig. 6. The presence of the media shown the table

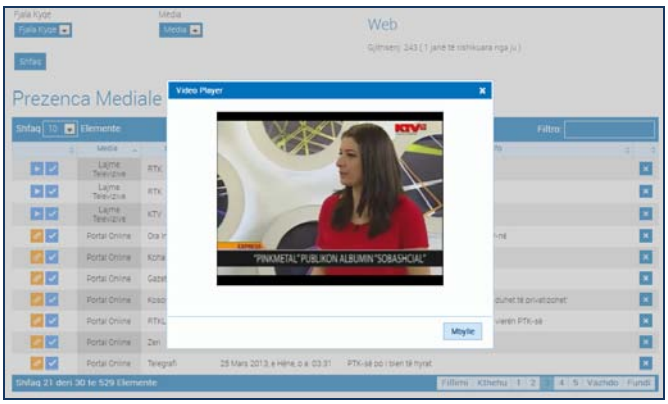

Fig. 7. The visual elements of video

In the right part of the screen could notice of general statistics, a total of 263 elements Press (2 are revised by the user), TV total of 23 elements (3 are reviewed by the user), the Web has had 243 (1 are reviewed by the user).

As shown in order search results table, in this case we have made a search from 01-03-2013 until 26-03-2013 in all media. Statistics show total number of results found and how they are reviewed by the current employee.

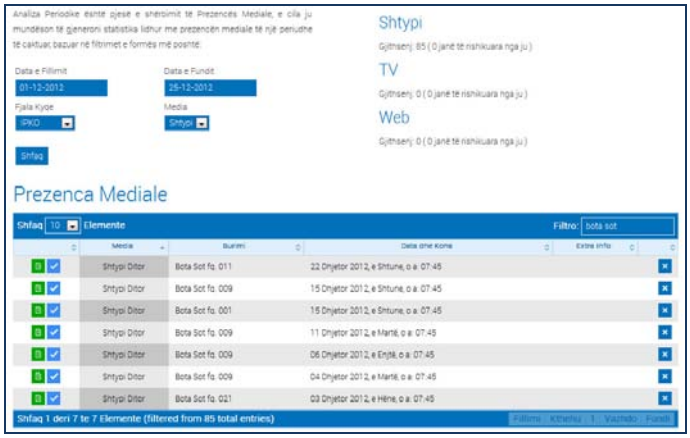

Fig. 8. Searching by keyword and filter only as "the world today"

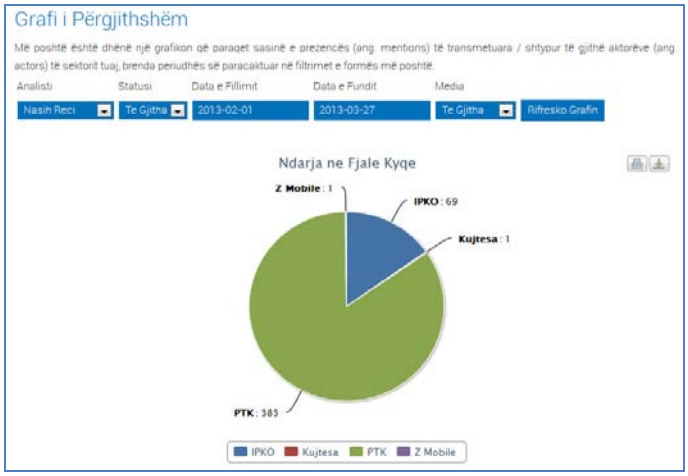

Fig. 9. Periodic Reporting

Fig. 10. Graph of PR reports on a daily basis

ISBN: 978-1-61804-228-6

VIII. User Feedback Analyses

There were 70 software engineers that have participated in the study filling the questionnaire that had 10 questions and addressed the main identified issues regarding trustable software.

Does trustworthy software requires trustworthy hardware in order to fulfill its attributes?

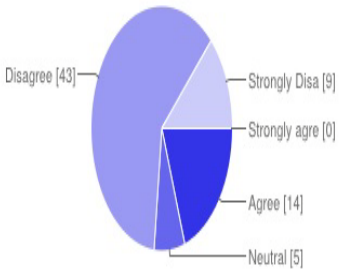

Strongly agree	0	0%
Agree	14	20%
Neutral	5	7%
Disagree	43	61%
Strongly Disagree	9	13%

Do we need a new paradigm to develop increasingly complex software systems?

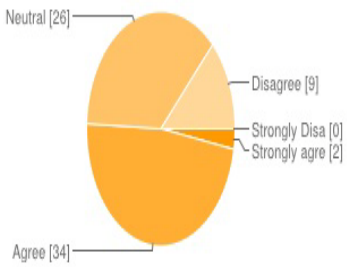

Strongly agree	2	3%
Agree	34	48%
Neutral	26	37%
Disagree	9	13%
Strongly Disagree	0	0%

In order to develop a trustworthy system, do you think the development process should be reused oriented and integrate formal languages and rigorous methods in all phases of system development life – cycle process?

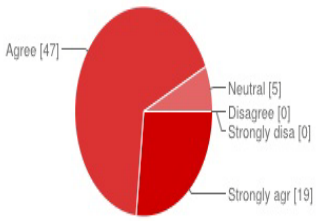

Strongly agree	19	27%
Agree	47	66%
Neutral	5	7%
Disagree	0	0%
Strongly disagree	0	0%

Please select the most important structure elements of trustworthiness:

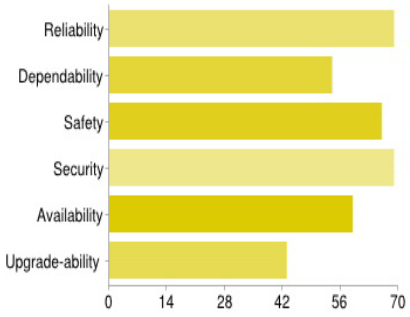

Reliability	69	19%
Dependability	54	15%
Safety	66	18%
Security	69	19%
Availability	59	16%
Upgrade-ability	43	12%

Do you think that the organizational infrastructure is a key element in developing trustworthy software?

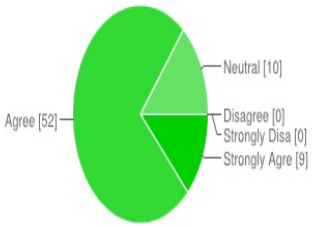

Strongly Agree	9	13%
Agree	52	73%
Neutral	10	14%
Disagree	0	0%
Strongly Disagree	0	0%

Which basic tools should be used in developing trustworthy software?

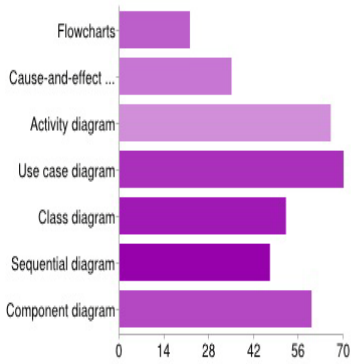

Flowcharts	22	6%
Cause-and-effect diagrams	35	10%
Activity diagram	66	19%
Use case diagram	70	20%
Class diagram	52	15%
Sequential diagram	47	13%
Component diagram	60	17%

Please select which additional techniques should be integrated in order to improve software trustworthiness:

Systems thinking	62	19%
Process management	69	21%
Standardization	66	20%
Adequate documentation	63	19%
Failure Modes and Effects Analysis	66	20%

Does the opportunity to extract user requirements in every phase of software development process is a must component in developing trustworthy software?

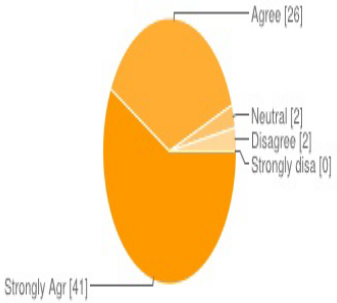

Strongly Agree	41	58%
Agree	26	37%
Neutral	2	3%
Disagree	2	3%
Strongly disagree	0	0%

ISBN: 978-1-61804-228-6

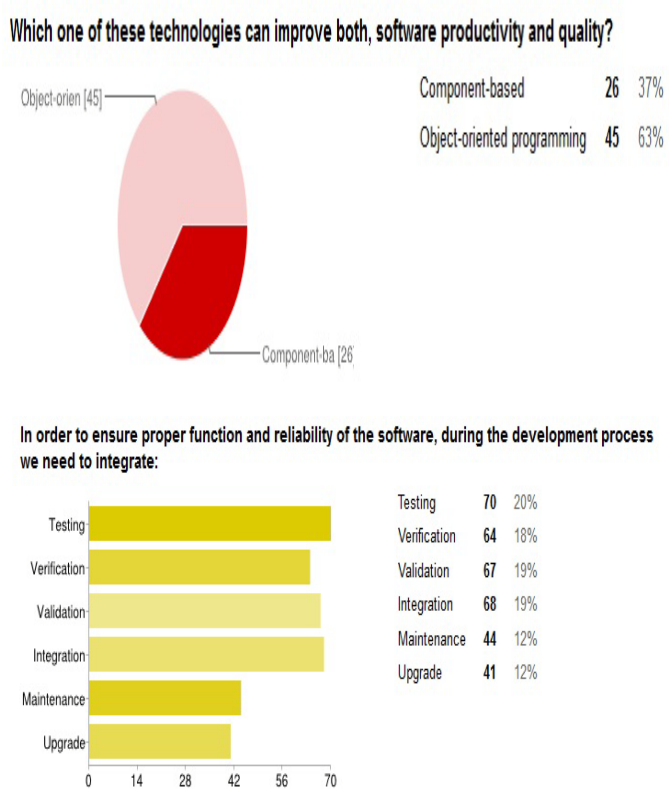

Fig. 11. User Feedback analyses

IX. Conclusions

As contribution the study as outcome developed software application based on the previously devised model and a framework with a set of tools supporting the spectrum of formal development activity from modeling to deployment, focusing in:

1. Design, and improve trustworthy software systems.

2. Focus on customer-centered issues as first class structural elements of trustworthiness attributes such as reliability, dependability, safety, security, availability and upgradeability.

3. Validate, test, evaluate, integrate, maintain and upgrade software to ensure proper function and reliability.

4. Integrate additional techniques such as systems thinking, process management, standardization and adequate documentation.

5. Use tools and techniques for developing trustworthy software and to describe the challenge of Trustworthy Software Systems.

The result of this study is to model the development of reliable software along with a set of tools that support the spectrum of formal software development, from design to implementation, focusing on:

1. Conceptual design and improvement of the model and the framework for development of software to increase reliability in them.

2. Focus on the issues related to customers as structural elements for achieving first class of credibility as security, stability, availability, protection, maintenance and updating of software.

3. Validation, testing, evaluation, integration, maintenance and updating to ensure the proper functioning of the software.

4. Integration of additional techniques such as systems thinking as engineers, management processes, standardization and adequate documentation.

5. Development and use of the model, framework, techniques and tools for software development and reliable description of the challenges in the future to increase the reliability of software systems.

Seven components of the software development process credible proposed model are:

1. The possibility to extract the requirements of users in different stages.

2. Adequate documentation.

3. Optimization of application (design) from the bottom up.

4. Oriented development artifacts.

5. Feedback and interaction between phases.

6. Analysis of risks in different stages

7. Early return on investment.

The quality of software can be described as the level at which a system, component or process fulfills the requirements or expectations of users. This includes various requirements of users, such as reliability, security, data assurance, the availability of other, but most importantly safety remains. In addition to these, the concept of Software reliable, I also added the ability for users to achieve reliability and to meet the needs of their declared and not declared even unexpected ones. Software developer should know to hear the voice and demands of the customers, to interpret them properly and can develop reliable software in accordance with their requirements.

Quality as attribute has a number of features, and therefore should be clearly understood customer prospects during the duration of the application. This not only helps in detecting the needs of users, but also to avoid excessive costs, delays and unnecessary complications. However, to address all issues pertaining to software quality, especially when it comes to large applications, strategies should be drawn up with little detail. Software development process should be sustainable to ensure interoperability can with users, identifying their requirements expressed and unexpressed during the term of the software. Be enabled feedback (feedback) and repetition between two or more stages during software development. To create an instrument for optimizing the design for reliability (or other attributes), cost, and duration. To ensure return on

ISBN: 978-1-61804-228-6

investment, proper documentation, analysis of risks in different phases of software development to be directed at objects.

The proposed model is based on strong management and proven tools, techniques and methodologies that are considered key elements: infrastructure that provides the necessary leadership and communication, training and rewards within the organization that will provide strong support for the software development process reliable; system for collecting reliable data to accurately identify the users' requirements during various phases of software development, optimization methods for the design of software and addressing the different requirements of users, such as reliability, cost, and duration; coding practices for creating and testing for different arrangements for adequate time, this strategy provides process cost effective and time, because in this way information about possible failures would be available at any time, standardization of best practices and planning the placement of qualitative as QFD and FMEA, use of innovative tools for software development as design oriented objects, extreme programming and the proper tools known as CASE tools.

It should be noted that the software companies where technology is an important activity, the software development process is very important for you only left to software engineers. It is the responsibility of the executive team to provide the necessary leadership, proper management infrastructure, and creating an environment suitable for the development of reliable software.

To be a reliable software, you have to work and function properly in different conditions of use and operation. My claim is that the software is also powerful reliable software, because it is specified performs as expected and desire are also under unfavorable circumstances. When we specify certain functions to applications, it is necessary to identify power quality or reliability as explicit in quantitative or qualitative terms. These qualities are essential. If the application performs the desired function successfully without error, then it is reliable application (always performs what is expected to perform).So, this application is also powerful.

In the final analysis, technology development of reliable software is concerned with the construction and improvement of competitive skills. This is done only if the company takes leadership seriously and passionately such a thing. If this technology is taught, acquired and implemented effectively, creates competitive advantage terrible, not only for large companies specialized for software development, but also for small companies. The essence of this technology lies in its implementation across the company.

The next step in the process of developing reliable software systems is further expansion of this process even in other projects. Any new project should benefit and learn from previous projects and it must be ongoing. Learning that comes from the review, and continuous evaluation of such projects is crucial. During these processes may also develop new techniques and technologies or new models, but only effective processes will gain consistency. The real lesson not start learning these techniques and technologies, but started practicing their initiative.

Based on the feedback and evaluations we can conclude that this study has indications to have positive effect on the improvement of the design concept of reliable software, as well as serve as a good reference for the further studies on the development of software powerful and reliable.

REFERENCES

[1] Aileen Patricia Cater-Steel B.Bus. (2004). An evaluation of software development practice and assessment - based process improvement in small software development firms. Submitted in fulfilment of the degree of Doctor of Philosophy in Griffith University , 56.

[2] Alagar, V., & Mohammad, M. (2007). Specification and verification of trustworthy component-based real-time reactive systems. SAVCBS .

[3] Avritzer, A., & Weyuker, E. J. (1998). Investigating Metrics for Architectural Assessment. Fifth International Software Metrics Symposium (p. 210). Bethesda, Md: Proc. IEEE.

[4] Booch, G. (1994). Object-Oriented Analysis and Design with Applications (Vol. 2nd Ed.). Menlo Park, CA: Addison-Wesley.

[5] Curtis, B. (1980). Measurement and experimentation in software engineering. Proceedings of the IEEE, vol. 68, no. 9, (pp. 1144-1157).

[6] Dobbins, J. H., Schulmeyer, G. G., & McManus, J. I. (1999). Handbook of Software Quality Assurance. Prentice Hall PTR, p. 196.

[7] F. Coenen, & T. Bench-Capon. (1993). Maintenance of Knowledge-Based Systems: Theory, Techniques and Tools. . Cornwall, UK: Hartnolls Ltd, Bodmin.

[8] Gary S. Wasserman. (2003). Reliability Verification, Testing, and Analysis in Engineering Design. New York: Marcel Dekker, p. 41

[9] Lientz, & Swanson. (2011, April 14). Developing and Maintaining Secure and Reliable Software in the Real World. Retrieved January 2013, from Building Real Software: http://swreflections.blogspot.com/2011/04/lientz-and-swanson-on-software.html

[10] Littlewood, B., & Strigini, L. (2000). Software Reliability and Dependability. A Roadmap, the 22nd International Conference on Software Engineering (p. 2). Proc. ICSE.

[11] Tool, T. (2007). Tool for Modeling and Implementation of Embedded Systems. Retrieved from http://www.timestool.com

[12] Van Vliet, H. (2000). Software Engineering:Principles and Practices, 2nd Edition. . West Sussex, England: John Wiley & Sons.

Analysis of ECDH Key Agreement protocol through linear temporal logic

Ashwini Kumar
Computer Science Department
IERT
26 Chatham lines, Prayag Allahabad (UP) INDIA
simplyashwini@gmail.com

Abstract—the Elliptic curve cryptography (ECC) an emerging favorite because it requires less computational control, memory, and communication bandwidth when compared to other existing cryptography systems. In this paper we present Elliptic curve cryptography Diffie–Hellman key agreement protocol, it provide the base for various key-agreement protocol, it provides the basis for a diversity of legitimate protocols, and is used to opportunity for web browsers application using secure application. Communication protocols are an important class of concurrent algorithms that pose a difficult challenge for existing verification technologies. To achieving this goal lies in by means of formal methods, which based on mathematical languages, technique, and method for specifying and verifying such systems. Use of formal analysis doesn't priori assurance of precision. However, they can greatly increase our understanding of a system by revealing inconsistencies, ambiguities, and incompleteness's that might otherwise go undetected. Model checking is a very popular technique used for ensuring the correctness of hardware and software systems.

Keywords—ECDH; key agreement; security ;LTL; model cheking ;publlic key cryptography

I. INTRODUCTION

Computer program correctness has, for decades, concerned industry and been studied in academia. The formal methods follow a line of investigation in particular, how formal logic can be practically implies in the analysis of computer programs and their designs. Most effort has been spent on the development of semantic frameworks for formalizing logics and developing systems that can formally prove that a software artifact satisfies a formula in some logic. Model checking and theorem proving are examples of such attempts to mechanize proofs of correctness [1]. The primary aim of protocol analysis is to establish confidence in the cryptographic security of a protocol. A key establishment protocol is operational if, in the absence of active adversaries and communications errors, honest participants who comply with its specification always complete the protocol having computed a common key and knowledge of the identities of the parties with whom the key is shared [2].

A. Objectives and properties

ECDH Cryptographic protocols involving message interactions require specific designation of both the messages to be exchanged and the proceedings to be taken by each party. The subsequent types of protocols may be notable, based on aim as indicated:

1. Authentication protocol – to provide to one party some degree of assurance regarding the identity of another with which it is purportedly communicating;

2. Key establishment protocol – to establish a shared secret;

3. Authenticated key establishment protocol – to establish a shared secret with a party whose identity has been corroborated [3].

B. Analysis methods

Common approaches for analyzing ECDH cryptographic protocol include the following:

1. Ad hoc and practical analysis. This approach consists of any variety of convincing arguments that any successful protocol attack requires a resource level greater than the resources of the perceived adversary. Protocols which survive such analysis are said to have intended to increase the probability of solving some safekeeping problem, with security here characteristically in the computational sense and adversary implicit to have set assets. Points of view often take for granted to secure building blocks. Protocols are typically designed to counter standard attacks, and shown to follow accepted principles. Practical arguments (paralleling complexity-theoretic arguments) involving constructions which assemble basic building blocks may justify security claims. While perhaps the most commonly used and practical approach, it is in some ways the least satisfying. This approach may uncover protocol flaws thereby establishing that a protocol is bad. However, claims of security may remain questionable, as subtle flaws in cryptographic protocols typically escape ad hoc analysis; unforeseen attacks remain a threat.

2. Reducibility from hard problems. This technique consists of proving that any successful protocol attack leads directly to the ability to solve a well-studied reference problem, it considered computationally infeasible given current knowledge and an adversary with bounded resources. Such analysis yields so-called provably secure protocols, although the security is conditional on the reference problem being difficult.

A challenge in this approach is to establish that all possible attacks have been taken into account, and can in fact be

equated to solving the identified reference problems. This approach is considered by some to be as good a practical analysis technique as exists. Such provably secure protocols belong to the larger class of techniques which are computationally secure.

3. complexity-theoretic analysis. An appropriate model of computation is defined, and adversaries are modeled as having polynomial computational power (they may mount attacks involving time and space polynomial in the size of appropriate security parameters). A security proof relative to the model is then constructed. The continuation of fundamental cryptographic primitives with precise properties is typically assumed. An objective is to design cryptographic protocols which require the fewest cryptographic primitives, or the weakest assumptions. As the analysis is asymptotic, care is required to determine when proofs have practical importance. Polynomial attacks which are viable beneath such a model may nevertheless in practice be computationally infeasible. Asymptotic scrutiny may be of limited weight to tangible problems in practice, which have finite size. Notwithstanding these issues, complexity-theoretic analysis is priceless for formulating fundamental principles and confirming intuition.

4. information-theoretic analysis. This approach uses mathematical proofs involving entropy relationships to prove protocols are unconditionally secure. While unconditional security is ultimately desirable; this approach is not applicable to most practical schemes for several reasons. These include: many schemes, such as those based on public-key techniques, can at best be computationally secure; and information-theoretic schemes typically either involve keys of impractically large size, or can only be used once. This approach cannot be combined with computational complexity arguments because it allows unlimited computation.

5. Formal methods. So-called formal analysis and verification methods include logics of authentication (cryptographic protocol logics), term re-writing systems, expert systems, and various other methods which combine algebraic and state-transition techniques. The most popular protocol logic is the Burrows-Abadi-Needham (BAN) logic [4]. Logic-based methods attempt to reason that a protocol is correct by evolving a set of beliefs held by each party, to eventually derive a belief that the protocol goals have been obtained. This category of analysis is somewhat disjoint from the first four. Formal methods have proven to be of utility in finding flaws and redundancies in protocols, and some are automatable to varying degrees. On the other hand, the “proofs” provided are proofs contained by the specified formal environment, and cannot be interpreted as absolute proofs of security. One-sidedness remains: the absence of discovered flaws does not imply the absence of flaws. Some of these techniques are also unwieldy, or applicable only to a subset of protocols or classes of attack. Many require (manually) converting a concrete protocol into a formal specification, a critical process which itself may be subject to subtle flaws [12].

A flaw in a cryptographic protocol may become a real security thread [1]. Even a seemingly small protocol may produce a great number of possible behaviors. One of the methods to formally consider protocols correctness is model checking by representing the protocol as Buchi automata M, specifying every checked property as an LTL temporal formula and checking satisfiability of the formula in the model

M |= _ [5, 6, 7].

II. Model Checking and Linear Temporal Logic

Key establishment and authentification cryptographic protocols can be modeled as automata so that their properties, described as temporal formulas, can be checked. The main problem is to keep such a model effectively verifiable. The satisfiability of the formulas in the model should increase confidence in the security of the protocols. Thus it is crucial to explicitly list requirements such a model must comply with. The environment in which the protocol is studied is considered an important matter [8, 9,10]. All the desirable properties of the protocol are written down as LTL logic formulas. The formulas contain references to variables from the protocol model.

Then one can try to proof that the program meets its specification. The approach is known as formal methods. It is most recognize efforts to guarantee the correctness of system design and behaviors. Especially, framework checking now called model checking [5] provides method for verifying concurrent system. In model checking, the model M is transition system and the properties are formula in temporal logic to verify that a system satisfies a property [11]. The system is finite state create environment efficient verification Model checking, despite reasoning about infinite behavior [1, 5]. If during the verification response is acceptable, then the system meets its specification otherwise fail to agree with its specification. Temporal Logic provides key inspiration for model checking [11]. It can be use to describe the ordering of the events in time without introducing time explicitly. Temporal properties are basically used to describe safety or correctness.

LTL logic temporal language gives opportunity to offer key inspiration for the model checking [12]. Due to use of Cyclic group property used in ECDH the ordering of the events in time without introducing time precisely and clearly communicated [13]. Temporal properties are basically used to describe safety or correctness and vitality properties. Inspired by [12,13], In the proposed approach we build a transitions system for ECDH Key Encryption Protocol[3,13], which describe the allowed evolutions of the protocol then we use Linear Temporal Logic to verify the correctness or safety properties of ECDH Protocol[5,12, 13].

Model checking is widely acceptable technique used for verification of any system. Model checking begin with the model modeled by the user and try to find out whether the attributes account by the user are reasonable on the given model. The model checking can be completely done by first building the Kripke structure [14] which represents the transition system, then expressing the properties by a temporal formula and using model checking to check whether the Kripke structure is a model of this formula. There are various temporal logics used in model checkers, like LTL, CTL, CTL* etc [15]. In this paper we focus on Linear Temporal which specifies temporal properties on linear computation path [15].

ISBN: 978-1-61804-228-6

III. THE SYNTACTIC AND SEMANTICS OF LTL

Linear Temporal Logic allows us to refer to the future [14]. It models time as a chronological sequence of states, extending infinitely to future. LTL is built up from a set of atomic formula p, q, r… the usual logic connectives ¬ (negation), v (disjunction), ^ (conjunction), (implication) and the following temporal operators:

a) Y means next state

b) W means all future states (Globally)

c) E means some future state (Eventually)

d) R means until

e) T means release

The first three operators are unary, so that Y f is a well formed formula whenever p is a well-formed formula. The last two operators are binary, so that p U q is a well-formed formula whenever p and q are well-formed formulas. Some often used temporal logic symbols are:

□p = Wp

◊p =Ep

○p = Yp

A. *Type of Temporal Properties*

x. Safety (bad things never happens)

W ¬ (ack1 ^ ack2) "mutual exclusion"

W (req→(reqUack)) "req must hold until ack"

y. Liveness (something good happens)

W (req→ Eack) "if req, eventually ack"

z. Fairness

WE req→WE ack "if infinitely frequently req, infinitely over and over again ack"

B. *Transition System*

Let AP be a non-empty set of singlet operation propositions:

A Transition System is a structure M = (ST, →, L) Where

ST	Finite set of states
→	Binary relation on S, such that every t ЄST has some st ' Є ST with st → st'
L: ST→2^{AP}	Labeling function, which labels each state with the singlet operation propositions which hold in that state.

The interpretation of the labeling function is that each state s has a set of atomic propositions L (st) which are true that particular state. Example of Transition System .see figure no 1

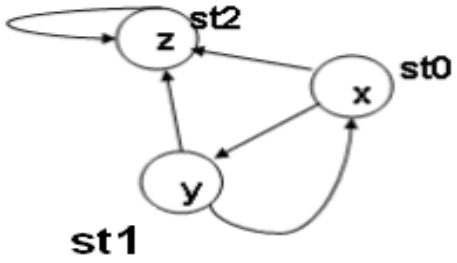

Fig no 1: Transition system

ST = {st0, st1, st2}

Transitions = st0→ st1, st1 → st0, st1 → st2, st0 → st2, st2 → st2

L (st0) = {x}

L (st1) = {y}

L (st2) = {z}

C. *Paths*

A path in a Model M = (ST,→, L) is an infinite sequence of states st0, st1, st2… in ST such that for each i >= 0, sti→ si+1.

We use Π to denote the suffix of the path. Here Π =st0, st1, st2...starting from some initial state. A path is any maximal sequence of state through which a computation may go. We right paths as st1→st2→st3→ we can unwind the transi tion system to obtain an infinite reckoning tree (see figure no. 2) to represent all the possible executions of the system, whose behavior is described by the Transition System M starting from the initial state.

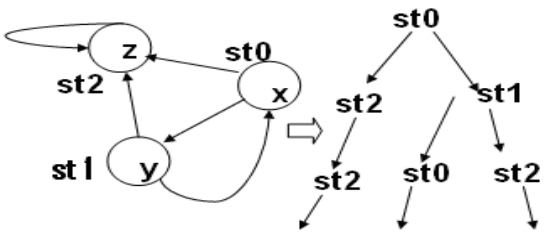

Fig no. 2: unwinding the transition state to obtain an infinite computation tree

D. *Semantics of LTL*

Suppose M = (ST, st0, R, L) is Kripke Structure, st0→…… be a path in M and f be an LTL formula. Then Π f (f is valid along Π) is defined as follows.

Π |= ⊤

Π |≠ ⊥

Π |= p iff pЄst0)

Π |=¬p iff not Π |= p

Π |= pvq iff Π |= p and M, Π |= q

Π |= p^q iff Π |= p or M, Π |= q

Π |= p→q iff Π |= q whenever M, Π |= p

$\Pi \models Ep$ iff there is some $i \geq 1$ such that $\Pi^i \models p$

$\Pi \models Yp$ iff $\Pi^1 \models p$

$\Pi \models Ep$ iff all $i \geq 0$: $\Pi^i \models p$

$\Pi \models pUq$ iff every $i \geq 0$: $\Pi^i \models q$ and all $j < i$: $\Pi^j \models p$

$\Pi \models pRq$ iff all $i \geq 0$: $\Pi^i \models q$ or every $i \geq 0$: $\Pi^i \models p$ and all i:

$\Pi^j \models q$

An LTL of knowledge formula f does not hold in a Kripke structure which represents the transition system, denoted $M \not\models f$, iff there is a path Π in M, Such that $\Pi\ 0 = S0$ and $\models \neg f$ and it is also possible that both $M \not\models f$ and $M \not\models \neg f$ hold.

E. Checking LTL Specs in SPIN

Checking LTL Specs in SPIN [2, 5] define as the predicates/propositions using #define in sys.prom file (using lowercase letters to begin predicate names)

e.g., #define bigx x > 1000

Formalize requirement as an LTL formula

e.g. “eventually x is greater than 1000” becomes <>(bigx)

Put the negation of the desired LTL property in file req.ltl

e.g., (!<>(bigx))

Execute SPIN to generate a verifier based on the property

spin –a –F req.ltl sys.prom

Compile

gcc –o pan.exe pan.c

Run with command-line option (-a) specifying that a liveness property is being checked

pan.exe –a

Display error trail

spin –t sys.prom

IV. DIFFIE-HELLMAN KEY EXCHANGE USING ELLIPTIC CURVE (DHECC)

A. Elliptic Curve Cryptography

Elliptic curve cryptography (ECC) [3] is relatively new technology compared to other public key cryptography such as RSA. Elliptic key operates on minor key magnitude. A 160-bit key in ECC is considered to be as secured as a 1024 bit key in RSA. ECC operates on the points in the elliptic curve $y^2=x^3+ax+b$, where $4a^3+27b^2 \neq 0$. The above equation of elliptic curve is in real coordinate. To make elliptic curve operation efficient and accurate the elliptic curve can be defined in finite fields. Elliptic curve in two finite fields, prime field and binary field, are defined by standard. In prime field operation the elliptic curve equation is modified as y2mod $p=x^3+ax+b$ mod p, where $4a^3+27b^2$ mod $p \neq 0$. The ECC standards are specified in SEC, Standards for Efficient Cryptography [3, 16].

B. Domain parameters

There are certain public constants that are shared between parties involved in protected and trusted ECC communication. This includes curve factor a, b. An originator point G in the chosen curve, the modulus p, order of the curve n and the cofactor h [3, 17]. There are several standard domain parameters defined by SEC, Standards for Efficient Cryptography [17].

C. Point multiplication

Point multiplication is the central operation in ECC. In point multiplication a point P on the elliptic curve is multiplied with a scalar k using elliptic curve equation to obtain another point Q on the same elliptic curve. i.e. k*P=Q

Point multiplication is achieved by two basic elliptic curve operations · Point addition, adding two points J and K using elliptic curve equation to obtain another point L i.e., L = J + K. · Point doubling, adding a point J to itself using elliptic curve equation to obtain another point L i.e. L = 2J. Here is a simple example of point multiplication. Let P be a point on an elliptic curve. Let k be a scalar that is multiplied with the point P to obtain another point Q on the curve. i.e. to find Q = k*P. If k = 23 then k*P = 23*P = 2(2(2(2P) + P) + P) + P. In the ECC explanations given below upper case letter indicates a point in the elliptic curve and the lower case letter indicates a scalar.

D. One Way function in ECC

The security of ECC depends on the difficulty of Elliptic Curve Discrete Logarithm Problem. Let P and Q be two points on an elliptic curve such that k*P = Q, where k is a scalar. Q can be easily obtained from P and k but given P and Q, it is practically infeasible to find k, if k is sufficiently large. k is the discrete logarithm of Q to the base P[3].

Elliptic Curve Cryptography (ECC) is promising as a pretty public-key cryptosystem for mobile/wireless world. Compare to long-established cryptosystems like RSA, ECC offers comparable defense mechanism with smaller key sizes, which results in faster calculation; lower energy consumption, as well as memory and bandwidth savings. An elliptic curve E which is over the finite field Fp is given through an equation. An equation determine by

$Y^2 = X^3 + aX + b,$

$a, b \in Fp$, and $-(4a^3 + 27b^2) \neq 0$

Please note that as stated in the beginning of the section, the “=” should be replaced by “≡” in the above definition. Another comment is that when we speak about partial derivatives we indicate the “formal partial derivate” and this formal partial derivate can be defined over an arbitrary field.

Suppose two communication parties, Alice and Bob, want to agree upon a key which will be later used for encrypted communication in conjunction with a private key cryptosystem. They first fix a finite field Fq, an elliptic curve E defined over

it and a base point B∈ E (the base point will be with high order). To generate a key, first Alice chooses a random n_{Alice}∈ Fq (this random is of high order) which she keeps secret. Next she calculates n_{Alice}*G ∈ E which is public and sends it to Bob. Bob does the same steps, i.e. he chooses a random integer n_{Bob} (this random integer will be secret) and calculates n_{Bob}*G which is sent to Alice. Their secret common key is then P = n_{Alice} n_{Bob}*G ∈ E. Definition An elliptic curve E over the field F is a smooth curve in the so it is called"long transform"

$$Y^2 + a_1XY + a_3Y = X^3 + a_2X^2 + a^4X + a_6,\ a_i \in F$$

We let $E_p(F)$ denote the set of points (x, y) ∈ F2 these points satisfy this equation, they are also along with a "point at infinity" which is denoted by O. Remember that smooth curve means that is the curve in which there is no point in E (F) where both partial derivatives vanish. The definition given above is valid for any field. In cryptography we are only paying attention in finite fields. Taking into consideration only finite fields we get a "feasible" equation. Two finite fields are of particular interest. The finite field Fp with p ∈ E elements, because of its structure, and the finite field Fqm with q = pr Elements, since setting p = 2 the arithmetic in this field will be well suited for implementations in hardware. For generating a shared secret between Alice and Bob using ECDH, both have to agree up on Elliptic Curve domain parameters. An overview of ECDH is given below.

E. Key Agreement Algorithm

E1.User Alice and User Bob want to agree on a shared key. Alice and Bob compute their public and private keys

E2. Alice Private Key = n_{Alice}

Alice Public Key = p_{Alic} = n_{Alice}*G

E3. Bob Private Key = n_{Bob}

Bob Public Key = p_{Bob} = n_{Bob}*G

User Alice and User Bob send each other their public keys.

Both Users take the product of their private key and the other user's public key.

E4. Alice → $Seckey_{Alice}$ = n_{Alice}* p_{Bob}= n_{Alice}* n_{Bob}*G_p

E5. Bob → $Seckey_{Bob}$ = n_{Bob}* p_{Alice}= n_{Bob}* n_{Alice}*G_p

E6. Shared Seckey= $Calc\_Seckey_{Alice}$= $Calc\_Seckey_{Bob}$

F. ECDH - Mathematical Explanation

To confirm the approved shared undisclosed $Seckey_{Alice}$ and $Seckey_{Bob}$ at both User Alice and Bob are the same From E2, E4 and E5.

$Seckey_{Bob}$ = n_{Bob}*$p_{Alice=}$ n_{Bob}*(n_{Alice}*G_p)= n_{Alice}^n_{Bob}^ FiG_p = n_{Alice}^ p_{Bob}= $Seckey_{Alice}$

Hence Seckey= $Seckey_{Alice}$= $Seckey_{Bob}$

Since it is virtually impracticable to find the private key n_{user} from the others public key p_{user}, it's not possible to obtain the shared secret for a third party.

V. Analysis of ECDH Protocol using Linear Temporal Logic

A. State variables

1. Key_BobAlice , to generation of an asymmetric key needed between Bob Alice .
2. Req_abq , to request for global public element a,b,q
3. Req_G , to request point $G(x_1,y_1)$in $E_p(a,b)$
4. Choose_a , to select ECC 'a' parameter
5. Choose_b , to select ECC 'b' parameter
6. Choose _q , to pick a large interger q which is either a prime numbers p or an interger of th form 2^m .
7. Find_E_q , to find elliptic group of points $E_p(a,b)$ with parameter a, b
8. Find _n , to find the order of n of a point on elliptic curve is the smallest positive integer n such that nG=O.Eq(a,b) and G are partner of the cryptosystem known to all participant.
9. Find_G_p , to choose a base point $G(x_1,y_1)$ in Eq(a,b) whose order is a very large value n .

B. Key generation

1) User Bob key generation

10. Sel_n_{Bob} , to select private key n_{Bob} such that n_{Bob}<n by User Bob .
11. Calc_ p_{Bob} , to select public key $p_{Bob(}n_{Bob}$*G) by User Bob .

2) User Alice key generation

12. Sel_n_{Alice} , to select private key n_{Alice} such that n_{Alice}<n by User Alice .
13. Calc_ p_{Alice} , to select public key $p_{Alice(}n_{Alice}$*G) by User Alice .

C. Exchange of public keys and Secret key calculation

14. Send_p_{bob} , to send public key p_{Bob} by User Bob to User Alice .
15. Send_p_{alice} , to send public key p_{Alice} by User Alice to User Bob .
16. Recv_p_{Bob} , to receive value of p_{Bob} by User Bob from User Alice .
17. Recv_p_{Alice} , to receive value of p_{Alice} by User Alice from User Bob
18. Calc_$Seckey_{Bob}$, to calculate secret key $Seckey_{Bob}$ (n_{Bob}* p_{Bob})by User Bob .
19. Calc_$Seckey_{Alice}$, to calculate secret key $Seckey_{Alice}$ (n_{Alice}* p_{Alice})by User Alice .
20. Calc_Seckey= $Calc\_Seckey_{Alice}$* $Calc\_Seckey_{Bob}$

D. Assumptions

21. GPE_Gen1 , which result in selection of global public element of ECC parameter a,b,q .
22. GPE_Gen2 , which result in selection of global public element $G_p(x,y)$ on ECC of order large value of n.
23. G_{Bob}_keyGen , which result in selection of n_{Bob} then calculation of public key P_{Bob} and finally sending of value P_{Bob} to User Alice.
24. G_{Alice}_keyGen , which result in selection of n_{Alice} then calculation of public key P_{Alice} and finally sending of value P_{Alice} to User Bob .
25. Gen_seckey_{Bob} , which result is calculation of secret key by User Bob.
26. Gen_seckey_{Alice} , which result is calculation of secret key by User Alice .

E. Symbolic Representation

27. GPE_Gen1 = userAlice≠ none ^ userBob ≠ none ^ Key_BobAlice ^ choose_a ^ choose_b^ choose_q.
28. G_{Bob}_keyGen= $Find\_G_p$^ Sel_n_{Bob}^ Calc_ p_{Bob}
29. G_{Alice}_keyGen= $Find\_G_p$^ Sel_n_{Alice}^ Calc_ p_{Alice}
30. Gen_seckey_{Bob} = Sel_n_{Bob}^ Calc_ $p_{Alice=}$ Sel_n_{Bob}^(Sel_n_{Alice}^ $Find\_G_p$)= Sel_n_{Alice}^ Sel_n_{Bob}^ $Find\_G_p$ = Sel_n_{Alice}^ Calc_ p_{Bob}= Gen_seckey_{Alice}

F. Requirement

Now we define the requirement of protocol using linear temporal Logic.

31. P1: Whenever generation of a symmetric key is needed between User Bob and Alice , the two parties need to choose two numbers a, b, and q.
    G1(Key_BobAlice→choose_a^choose_b^choose_q))
    G2 (G_p→ $Find\_E_q$^ Find _n)
32. P2 : if both user choose private key such that (n_{Bob}, n_{Alice}) <n & n_{Bob}= n_{Alice} i.e. not smooth then intruder could not get secret key .
    G3((G_p^Calc_p_{Bob}= intruder) → ¬sel_n_{Bob})
    G4((G_p^Calc_p_{Alice}= intruder) → ¬sel_n_{Alice})
33. P3 : As with the exchange system, a n encryption / Decryption system require a point G and an Elliptic group E_q(a,) as parameter. Each user Bob & Alice select a private key n_{Bob} & n_{Alice} respectively and generate own public key $p_{Bob(}n_{Bob}$*G) & $p_{Bob(}n_{Bob}$*G) respectively.

G. Message exchange

1. If User Bob want to send a message m to User Alice, Bob chose a random positive integer K_{Bob} and produce a encrypted ciphers text c_{Bob} consisting of the pair of points $c_{Bob}=\{K_{Bob}G, m_{Bob} + K_{Bob}p_{Alice}\}$.
   Note: Note that User Bob used User Alice's Public Key p_{Alice} .
2. To decrypt the cipher $c_{Bob}=\{K_{Bob}G, m_{Bob} + K_{Bob}p_{Alice}\}$, User Alice multiply the first pair of point by Alice's secret Key and subtract the result from the second point
   $= m_{Bob} + K_{Bob}p_{Alice} - n_{Alice}(K_{Bob}G)$
   $= m_{Bob} + K_{Bob}(n_{Alice}G) - n_{Alice}(K_{Bob}G)$ ∴ $(p_{Alice} = n_{Alice}G)$
   $= m_{Bob}$
3. Even if intruder known the private key value of User Bob Alice. For the attacker to recover the message, attacker would have to compute K given G and Kg , which assumed hard . This is called discrete logarithm problem for elliptic curves.

H. Encryption Decryption

4. Sel_m_{Bob} , to select m_{Bob} an integer as message by User Bob.
5. Sel_m_{Alice} , to select m_{Alice} an integer as message by User Alice.
6. Sel_ K_{Bob} , to select random integer element such that $K_{Bob} < Gen\_seckey_{Bob}$ by User Bob.
7. Sel_ K_{Alice} , to select random integer element such that $K_{Alice} < Gen\_seckey_{Alice}$ by User Alice .
8. $Calc\_c_{Bob}$, to calculate cipher c_{Bob} ($K_{Bob}G$, $m_{Bob} + K_{Bob}p_{Alice}$) by User Bob using User Alice's Public Key (p_{Alice}).
9. $Calc\_c_{Alice}$, to calculate cipher c_{Alice} ($K_{Alice}G$, $m_{Alice} + K_{Alice}p_{Bob}$) by User Alice using User Bob's Public Key (p_{Bob}).
10. $Send\_c_{Bob}$, send value of c_{Bob} by User Bob to User Alice.
11. $Send\_c_{Alice}$, send value of c_{Alice} by User Alice to User Bob.
12. Recv_ c_{Bob}, to receive value c_{Bob} by User Alice from User Bob .
13. $Recv\_c_{Alice}$, to receive value c_{Alice} by User Bob from User Alice .
14. $Clac\_d_{Alice}$ to decrypt the cipher recive from User Bob and retrieve message $[(m_{Bob} + K_{Bob}p_{Alice} - n_{Alice}(K_{Bob}G)) \equiv m_{Bob} + K_{Bob}(n_{Alice}G) - n_{Alice}(K_{Bob}G) \equiv m_{Bob}]$ by User Alice using own private key (n_{Alice}) and public element participant.

ISBN: 978-1-61804-228-6

15. Clac_d_{Bob} to decrypt the cipher receive from User Alice and retrieve message [$(m_{Alice} + K_{Alice}p_{Bob} - n_{Bob}(K_{Alice}G))\equiv m_{Alice} + K_{Alice}(n_{Bob}G) - n_{Bob}\ (K_{Alice}G) \equiv m_{Alice}$] by User Bob using own private key (n_{Bob}) and public element participant.

I. Assumptions

16. Gen_c_{Bob} , which result of calculation of c_{Bob} made by User Bob.
17. Gen_c_{Alice} , which result of calculation of c_{Alice} made by User Alice.
18. Gen_d_{Alice} , result of decrypted message d_{Alice} made by User Bob .
19. Gen_d_{Bob} , result of decrypted message d_{Bob} made by User Alice .

Symbolic representations

20. Gen_c_{Bob}= Sel_m_{Bob}^ Sel_ K_{Bob}^ Sel_n_{Bob}^ Calc_ p_{Alice} ^ Send_c_{Bob}
21. Gen_c_{Alice}= Sel_m_{Alice}^ Sel_ K_{Alice}^ Sel_n_{Alice}^ Calc_ p_{Bob}^ Send_c_{Alice}
22. Gen_d_{Alice} = Recv_c_{Bob}^ n_{Alice} ^Sel_K_{Alice}.
23. Gen_d_{Bob} = Recv_c_{Alice}^ n_{Bob} ^Sel_K_{Bob}.

VI. FEATURES OF ECDH

1. You get one-way certification for at no cost. I.e., if User Bob has User Alice's public ECDH key, and uses it to communicate to someone; User Bob knows that someone is User Alice, restricted of doing any additional checks. Now, User Alice has no idea who she's talking to; on the other hand, for some scenarios, User Alice really doesn't care.
2. You don't need a reply from User Alice to get her ECDH public value; you already know it. This may permit you to use one fewer protocol round. If User Bob needs to do is share a symmetric key so he can fire User Alice a message, he doesn't require any replies from User Alice at all; he can create his public key, and the message ciphered and validated with a key derivative from the shared secret.
3. The big drawback of ECDH is the highly computation-intensive nature of its underlying cryptographic operations, causing long execution times and high energy consumption.

VII. CONCLUSION

The Diffie–Hellman scheme is one of the exchanging key cryptosystem, no massages are involved in this scheme, in this report, and we try to benefit from this scheme by use the key (which exchange it) as a secret key. We are using Diffie–Hellman scheme in Elliptic curve cryptography for encryption and Decryption. We have presented a formal approach to analyze the ECDH Key agreement protocol in LTL (Linear Temporal Logic). More ever we build a transitions system, which describe the allowed evolutions of the protocol starting from some initial state, the system move from one state to another state by performing some actions. Finally with the help of LTL formulas we try to find out whether these formulas are satisfied on transition system. Future work will include the progress in analysis of other complex protocol using LTL and hope to discover new complex logic and errors.

REFERENCES

[1] Schneider S., Ryan P., Modelling and analisis of security protocols, Addison–Wesley (2001).

[2] Sapiecha P., Krawczyk U., Validation of cryptographic protocols using model checker spin, CECC (2010).

[3] A. M. Fiskiran and R. B. Lee. "Workload characterization of elliptic curve cryptography and other network security algorithms for constrained environments". IEEE International Workshop on WWC-5, 2009

[4] M. Burrows, M. Abadi, and R. Needham. A Logic for Authentication. In *Proceedings of the Royal Society of London*,volume 426, pages 233–271, 1989.

[5] Merz S., Model Checking: A Tutorial Overview, Technical report M¨unchen University(2000)

[6] Mukund M., Linear-time temporal logic and B¨uchi automata, SPIC Mathematical Institute,Madras, India (1997)

[7] Tauriainen H., Automated testing of B¨uchi automata translators for linear temporal logic,Helsinki University of Technology (2000

[8] Compagna L., Armando A., Carbone R., LTL model checking for security protocols 23 (2009).

[9] Gordon A. D., Progress on provable implementations of security protocols, TechnicalReport, Microsoft Research (2009).

[10] Stamer H., Verification of cryptographic protocols, Technical Report, University of Kassel (2005).

[11] Sapiecha P., Krawczyk U., Validation of cryptographic protocols using model checkerspin, CECC (2010).

[12] Long Shigong and Wang Lijun, "Analysis of Cryptographic Protocol using LTL of knowledge," International conference on Networking and Digital Society, pp. 463-466, 2010.

[13] Yufang Huang, "Algorihtm for elliptic curve diffie-Hellman key exchange based on DNA title self assembly In Proceedings of 46th IEEE Theories and Applications,pp.31-36, 2008.

[14] Michael Huth and Mark Ryan, Logic in Computer Science, Cambridge University Press, pp 172-243, 2004

[15] A Pnueli, "The temporal logic of programs", In proceedings of the 18th IEEE Symposium Foundations of Computer Science (FOCS 1977), pp. 46 – 57, 1977.

[16] N. Koblitz,"Elliptic curve cryptosystems," Mathematics of Compution, vol. 48, no.177, pp.203-209, Jan 1987.

[17] Certicom, Standards for Efficient Cryptography, SEC 1: Elliptic Curve Cryptography,Version 1.0, September 2000

Segmentation of Brain MRI Image Based on Clustering Algorithm

Siti Noraini Sulaiman, Noreliani Awang Non, Iza Sazanita Isa, Norhazimi Hamzah

***Abstract*—** Medical images are widely used by the physicians to find abnormalities in human bodies. The physicians used the findings to plan further treatment for the patient. However the images sometimes are corrupted with a noise which normally exist or occurs during storage, or while transfer the image and sometimes while handling the devices. Therefore the need to enhance the image is crucial in order to improve the image quality. Segmentation technique for Magnetic Resonance Imaging (MRI) of the brain is one of the method used by radiographer to detect any abnormality happened specifically for brain. The method is used to identify important regions in brain such as white matter (WM), grey matter (GM) and cerebrospinal fluid spaces (CSF). In this project, the image segmentation via clustering method is used to cluster or segment the images into three different regions which represent the white matter (WM), grey matter (GM) and cerebrospinal fluid spaces (CSF) respectively. These regions are significant for physician or radiographer to analyse and diagnose the disease. The clustering method known as Adaptive Fuzzy K-means (AFKM) is proposed to be used in this project as a tool to classify the three regions. The results are then compared with fuzzy C-means clustering. The segmented image is analysed both qualitative and quantitative. The results demonstrate that the proposed method is suitable to be used as segmentation tools for MRI brain images using image segmentation.

***Keywords*—** Image Processing, Image Segmentation, Brain MRI image, Clustering.

I. Introduction

MEDICAL image normally used by the physicians to detect abnormalities in body system. It is also used for the treatment planning. Various medical images techniques used to sense the irregularities in human bodies such as Magnetic Resonance Imaging (MRI), Computerized tomography (CT), and Ultrasound (US) imaging. In such a case, the radiographer used a tool to make the decision of medical images analysis easier. It also helps radiographer make accurate decision about the corresponding image. The radiologist use medical image to identify the tumours, tissues, and its anatomical structures [1].But there are many problems faced when performing MRI procedure. The problems are the image generally have non-linear characteristics and sometimes are corrupted with noise These problems make the radiologist faced difficulties in identifying of tumors, tissues and its location as well as difficulties to study the anatomical abnormal growth of glands. Finally, these may lead to inconveniences in making decision [1].

Many segmentation methods have been introduced in the literature [2]. In digital image processing, segmentation refers to the process of splitting observe image data to a serial of non-overlapping important homogeneous region [3]. Clustering algorithm is one of the process in segmentation. In the analysis of medical images for computer-aided diagnosis and therapy, a preliminary processing task often required is segmentation [3, 4]. Besides that, by using computer aided, image processing can be applying image reconstruction. It is very important to medical field because radiologist can identify the abnormality happen at the brain. Since radiologist can determine abnormality in the patient brain, they can give the best treatment for the patient.

There various image segmentation techniques based on clustering. For examples of clustering algorithm are K-means (KM) clustering, Moving K-means (MKM) clustering and Fuzzy C-means (FCM) clustering. Clustering is the process of separating data into group of similarity [5]. It also known as procedure of organizing objects into groups whose members are similar in certain way, whose goal is to identify structures or clusters existing in a group of unlabelled data[6]. Clustering algorithm are normally being used in computer, engineering and mathematics field [7]. In the past few decades, the uses of clustering algorithm have been broadening to medical fields. Thus is due to the development and advancement of medical imaging fields. Examples of medical images are image of brain, bone, and also chest. Clustering algorithm is suitable in biomedical because it will make the analysis easier.

Segmentation via clustering can also be used to detect the three regions at the brain image. Magnetic Resonance Image (MRI) of brain is one of medical imaging tools used to detect abnormality in brain. From the MRI brain images, the radiologist normally interested to look for three significant regions. The three regions are white matter (WM), grey matter (GM) and cerebrospinal fluid spaces (CSF) [3, 6]. Figure 1 shown three regions of normal MRI brain image. The precise

S. N. Sulaiman is a Senior Lecturer at Faculty of Electrical Engineering, Universiti Teknologi MARA (UiTM), 13500 Permatang Pauh Penang, Malaysia. (Phone: +604 3822619; fax: +604 3822810; e-mail: sitinoraini@ppinang.uitm.edu.my).

N. Awang-Non, was undergraduate student at Faculty of Electrical Engineering, Universiti Teknologi MARA (UiTM), 13500 Permatang Pauh Penang, Malaysia. (e-mail: noreliani@yahoo.com).

I. S. Isa. is a Lecturer at Faculty of Electrical Engineering, Universiti Teknologi MARA (UiTM), 13500 Permatang Pauh Penang, Malaysia (e-mail: izasazanita@ppinang.uitm.edu.my).

N. Hamzah is a Lecturer at Faculty of Electrical Engineering, Universiti Teknologi MARA (UiTM), 13500 Permatang Pauh Penang, Malaysia (e-mail: norhazimi880@ppinang.uitm.edu.my).

measurement of these three regions is important for quantitative pathological analyses and so becomes a goal of lots of method for segmenting MRI brain image data.

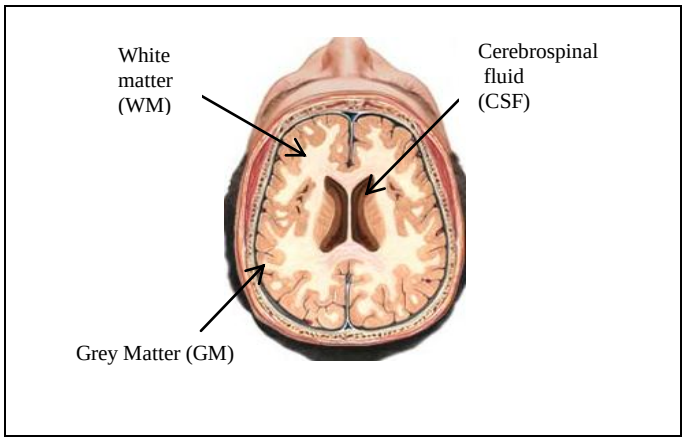

Figure 1: The normal brain MRI image

In this paper segmentation via clustering method named Adaptive Fuzzy K-means (AFKM) clustering is used to segment the MRI brain image into three different regions. The AFKM method is proposed to prove that it can classify and segment the MRI brain image better than conventional method. AFKM clustering algorithm is combination of KM, MKM and FCM clustering. The features of AFKM are to provide a better and more adaptive clustering process.

The remaining of the paper is organized as section II presents about AFKM clustering algorithm is proposed. Section III describe data analysis of MRI brain image. Section IV presents a result analysis comparison of performance of FCM and AFKM clustering algorithm. Besides that, the comparison detail of qualitative and quantitative also presented. Lastly, Section V concludes of this paper.

II. METHODOLOGY

In medical field, Medical Resonance Image (MRI) is one of the methods used to detect abnormalities in human body. The clustering algorithm for image segmentation was introduced to the MRI images in order to segment the image.

In this paper, a new method of clustering algorithm based segmentation known as technique is recommended [6]. The segmentation technique used to be implemented medical image like MRI. It use to exquisite soft tissue contrast between normal tissue and pathologic tissue. The proposed method for this paper is then comparing with conventional method known as Fuzzy C-means (FCM). In this section algorithm FCM and AFKM are briefly discussed in II(A) and II(B).

A. Fuzzy C-means (FCM) clustering Algorithm

Bezdek is the person who introduced Fuzzy C-means (FCM) algorithm. The FCM is one of the most commonly used clustering algorithm [6, 7]. FCM clustering is constructed based on the same idea of definition cluster centers by iteratively regulating their locations and minimizing an objective function as K-Means (KM) algorithm [6]. The advantage of FCM is, it allows more flexibility when dealing with multiple cluster by introducing multiple fuzzy membership grades [6].

B. Adaptive Fuzzy K-Means (AFKM) clustering Algorithm

In this paper, AFKM method is recommended to be used to process MRI images. It is the latest type of clustering algorithm proposed by [7]. The AFKM is combination of fundamental theories of conventional K-means and MKM clustering algorithm (i.e., assigning each data to its closet centre or cluster) and the conventional Fuzzy C-means (FCM) clustering algorithm (i.e., allows the data to belong to two or more clusters or centres). The objective function of AFKM is calculated using the equation:

$$J = \sum_{k=1}^{n_c}\sum_{t=1}^{N}\left(M_{kt}^{m}\right)\left\|v_t - c_k\right\|^2 \tag{1}$$

where M_{kt}^{m} the fuzzy membership function and m is the fuzziness exponent. The degree of being in a certain cluster is related to the inverse of the distance to the cluster. The new position for each centroid is calculated using the equation:

$$C_k = \frac{\sum_{t=1}^{N}\left(M_{kt}^{m}\right)'v_t}{\sum_{t=1}^{N}\left(M_{kt}^{m}\right)'} \tag{2}$$

where,

$$\left(M_{kt}^{m}\right)' = M_{kt}^{m} + \Delta M_{kt}^{m} \tag{3}$$

where $\left(M_{kt}^{m}\right)'$ is the new membership and is defined as:

$$\Delta M_{kt}^{m} = \alpha\left(c_k\right)\left(e_k\right) \tag{4}$$

and e_k is error of belongingness. Then, the value of e_k is calculated by

$$e_k = B_k - \hat{B}_k \tag{5}$$

The AFKM algorithm improved the clustering with the introduction of belongingness concept where it measures the degree relationship between centre and its members. The degree of belongingness is calculated using;

$$B_k = \frac{c_k}{M_{kt}^{m}} \tag{6}$$

The objective is to minimize the objective function from equation (1). The process is repeated iteratively until the center is no longer moved all data have been considered.

ISBN: 978-1-61804-228-6

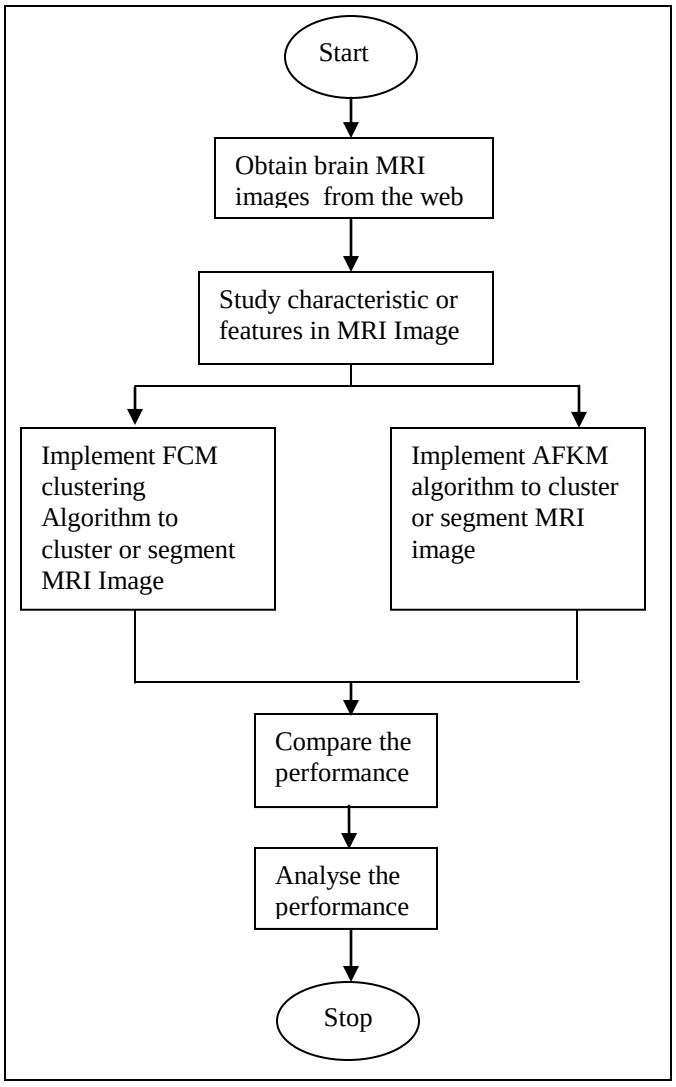

Figure 2: Flow chart of the segmentation clustering algorithm

Images of brain MRI are obtained from internet database. The images are processed with AFKM and FCM clustering algorithm and comparison is made between the two clustering algorithms. The flow chart for the whole process is depicted in Figure 2.

III. Data Acquisition and Analysis

The method Adaptive Fuzzy K-means (AFKM) clustering algorithm is introduced to segment a MRI brain image but usually the MRI brain image used computer-aided to detect any irregularities happened. In this paper, six of MRI brain images obtained from internet databases are chosen to be tested the AFKM algorithm, as shown in Figures 3(a) until 3(f) respectively.

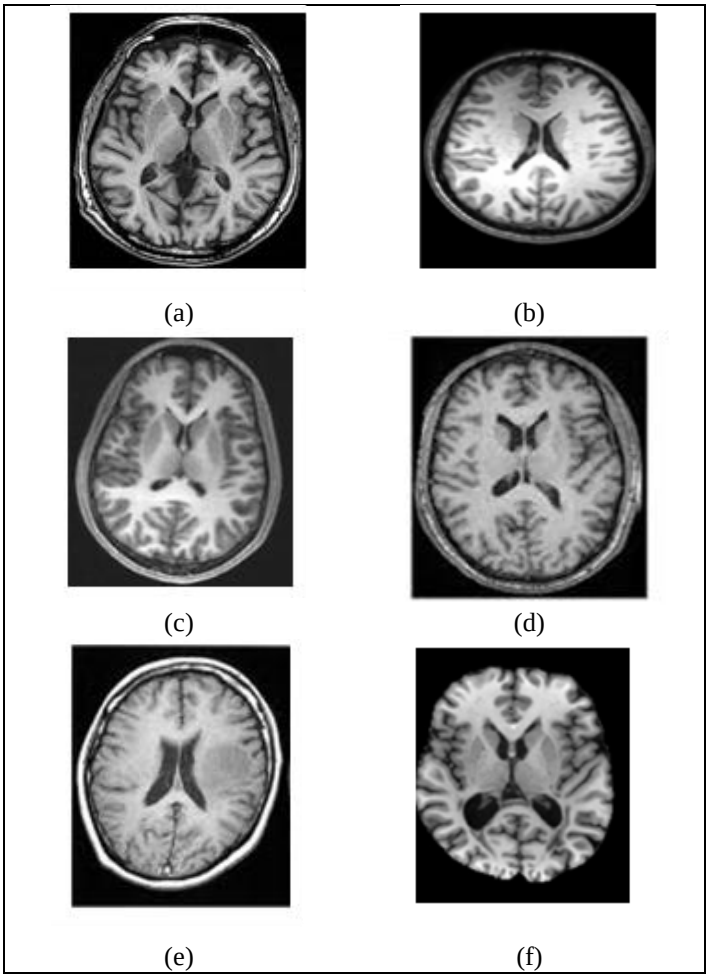

Figure. 3. The original image of MRI brain images: (a) image 1, (b) image 2, (c) image 3,(d) image 4,(e) image 5,(f) image 6.

To implement the performance analysis, qualitative and quantitative are considered. There are three evaluation functions used in quantitative analysis obtain from Liu and Yang [8]:

$$F(I)=\sqrt{R}\sum_{i=1}^{R}\frac{e_i^{\,2}}{\sqrt{A_i}} \tag{7}$$

Equation *F'(I)* and *Q(I)* are proposed by Borsotti [9] where the *Q(I)* is the improved version of *F(I)*. The equations are givens follow:

$$F'(I)=\frac{1}{1000(NxM)}\sqrt{\sum_{A=1}^{Max}[R(A)]^{1+1/A}}\sum_{i=1}^{R}\frac{e_i^{\,2}}{\sqrt{A_i}} \tag{8}$$

$$Q(I)=\frac{1}{1000(NxM)}\sqrt{R\sum_{i=1}^{R}\left[\frac{e_i^{\,2}}{1+\log A_i}+\left(\frac{R(A_i)}{A_i}\right)^2\right]} \tag{9}$$

For evaluation of the cluster quality, the most fundamental benchmark is the mean squared error (MSE). It could be described as follows:

$$MSE = \frac{1}{N}\sum_{j=1}^{M}\sum_{i\in s_j}\left\|x_i - c_j\right\|^2 \quad (10)$$

IV. Result and Discussion

From these images, the performance analysis of qualitative and quantitative are implemented. The qualitative analysis depends on the human visual. Human visual can interpret the images based on capability and segmentation algorithm of conventional method like FCM and the new method proposed which is AFKM. It can detect the region of interest like GM, WM and CSF. For quantitative analysis, it refers to the performance of segmentation of the image. It produces by proposed algorithm. The conventional algorithm will compared with a new proposed algorithm. The result of quantitative analysis taken based on three evaluation functions. The three functions of quantitative analysis are F(I), F'(I) and Q(I). The image size can calculate from N x M. For evaluation of the cluster, the mean squared error (MSE) is the one most fundamental benchmark. Besides that, these functions related more to the visual judgement. For the better result of segmentation, AFKM values of F(I), F'(I) and Q(I) are smaller than FCM values. Both of result of qualitative and quantitative will be presented in section IV (A) and IV (B).

A. Qualitative Analysis

For the result in qualitative analysis, six images are used. Qualitative analysis is to examine usually whether the resultant image is good or not.The performance is examine visually in qualitative analysis. The segmentation performances are compared with conventional methods of FCM and new method proposed of AFKM. Clustering algorithm used in this paper is to segment the MRI brain image into here regions i.e the GM, WM and CSF,therefore the clustering algorithm is chosen to have three clusters.The result is then compared with FCM algorithm. From the result shown in Figures 4 to 5, it can be observed that quality of image is not perfect compared to the AFKM method. The weakness of FCM method is it over segment the image which lead to image become too bright. But using AFKM,it can segment the image clearly and the region of interest is more sharp.

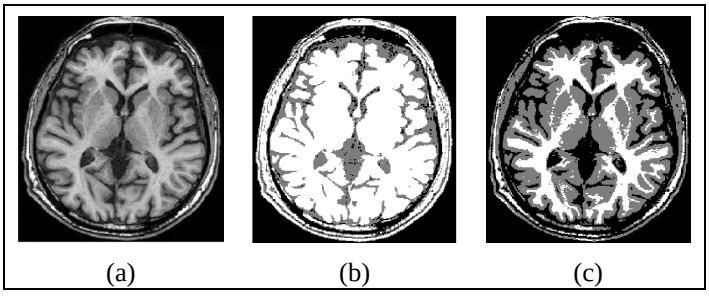

Figure 4: The image 1 of segmentation image with three clusters: (a) Original image. (b) FCM. (c) AFKM

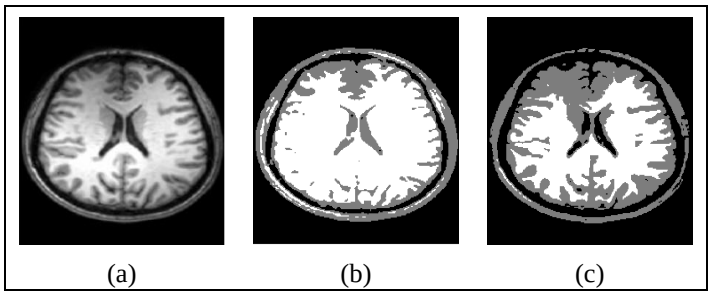

Figure 5: The image 2 of segmentation image with three clusters: (a)Original image. (b) FCM. (c) AFKM

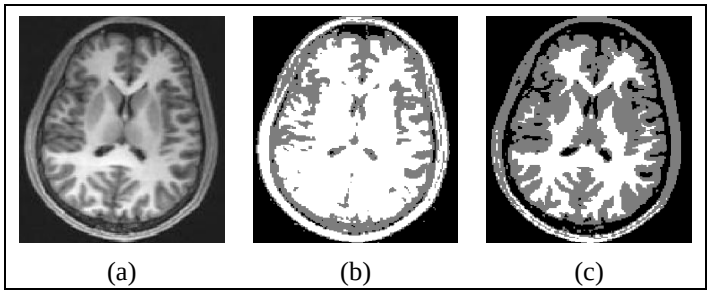

Figure 6: The image 3 of segmentation image with three clusters: (a) Original image. (b) FCM. (c) AFKM

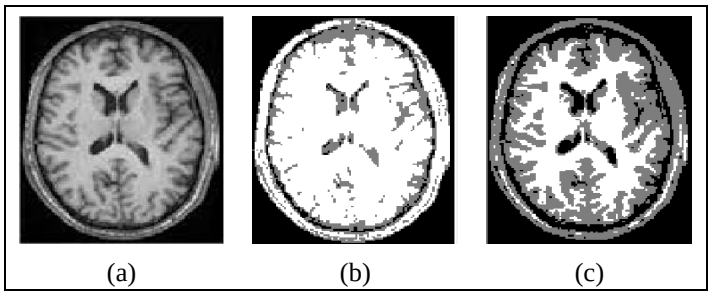

Figure 7: The image 4 of segmentation image with three clusters: (a) Original image. (b) FCM. (c) AFKM

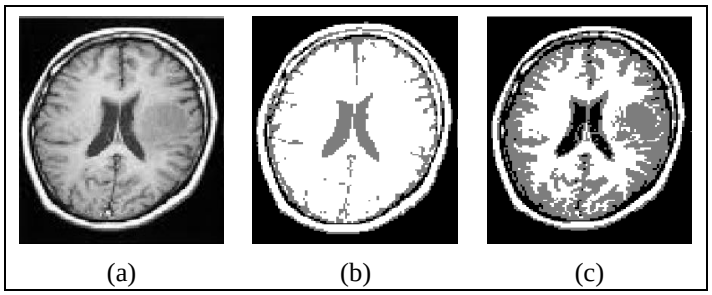

Figure 8: The image 5 of segmentation image with three clusters: (a) Original image. (b) FCM. (c) AFKM

After implementing AFKM algorithm, the image looks clearly in the visual compared to the conventional method of FCM. The resultant images are shown in Figures. 6 and 7. By FCM, the MRI brain image is brighter compared to AFKM. It happens because the FCM have over segment of the image. It

can give effect on segmentation and three regions cannot be detected clearly. The images of AFKM become sharper and clearer.

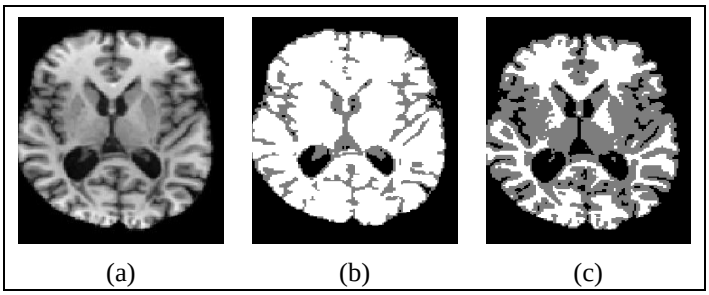

(a) (b) (c)

Figure 9: The image 6 of segmentation image with three clusters: (a) Original image. (b) FCM. (c) AFKM

By using FCM, the image is unclear. It is because the image becomes bright and not meet a criteria of segmentation. But when AFKM method applied, the images are sharp and the segment of WM, GM and CSF are correctly. The resultant images are shown in Figures. 8 and 9, respectively.

From the resultant images are shown in Figures. 4 to 9, a new method proposed of AFKM can give better performance of segmentation technique compared the conventional method of FCM.

B. Quantitative Analysis

The analysis of quantitative is evaluated based on the three benchmark functions. It is also mentioned in section III. The analysis also evaluates by fundamental benchmark is mean squared error (MSE).The quantitative analysis is to support the qualitative finding in section III(A). The result of quantitative analysis show in Tables 1to 4. These tables summarize the segmentation of the quantitative estimation. All the result gets from a comparison of FCM and AFKM clustering method. From the comparison, new method of AFKM produces the better result compared to conventional method of FCM. The new method proposed of AFKM produce the smaller values of all MSE, F(I), F'(I) and Q(I) analysis. So; it can be conclude that the AFKM method is successful segmentation. It is because AFKM can detect the three regions at MRI brain. In addition, the proposed AFKM manages to segment the image successfully with less noisy pixel. Generally, these interpretations specify that the AFKM might be a better methodology in terms of image segmentation application.

TABLE 1. *MSE* Evaluation of quantitative

No of images	MSE for three cluster	
	FCM	AFKM
1	815.76	**519.64**
2	1019.61	**533.69**
3	890.91	**398.58**
4	931.96	**498.74**
5	935.64	**560.1**
6	739.44	**443.61**

TABLE 2. *F(I)* Evaluation of quantitatives

No of images	F(I) for three cluster	
	FCM	AFKM
1	5837.95	**4088.74**
2	3242.73	**1259.42**
3	1806.05	**551.67**
4	1382.49	**530.84**
5	1117.05	**601.11**
6	857.27	**434.69**

TABLE 3. *F'(I)* Evaluation of quantitatives

No of images	F'(I) for three cluster	
	FCM	AFKM
1	618.92	**434.72**
2	363.21	**137.36**
3	195.47	**60.24**
4	149.14	**56.52**
5	119.18	**63.23**
6	95.06	**48.14**

TABLE 4. *Q(I)* Evaluation of quantitaves

No of images	Q(I) for three cluster	
	FCM	AFKM
1	19087.99	**14629.71**
2	10656.03	**4205.06**
3	3225.98	**835.36**
4	1858.97	**665.41**
5	1353.32	**620.26**
6	1459.95	**618.94**

Note: for the rest of the Tables, bolded numbers show the best result obtained for each analysis.

V. CONCLUSION

A. Figures and Tables

In this paper, the new method of AFKM clustering algorithm is present. The AFKM clustering is combination with MKM, KM and FCM. The result can prove that using AFKM can get sharper and clearer of segmentation in MRI brain image. This process is a good method for segmentation. The technique was used to segment the three regions in MRI brain image using clustering algorithm. The results get from the qualitative and quantitative of MRI brain image. In the future, AFKM method can apply in engineering field, agriculture field and also nutrition field.

REFERENCES

[1] M. V. Kumar, and. Sumitra. M. G, "An improved clustering Based Segmentation Algorithm For Brain MRI," vol. 2, p. 126, 2013.

[2] W. Zhi Min, S. Qing, and S. Yeng Chai, "MRI brain image segmentation by adaptive spatial deterministic annealing clustering," in Biomedical Imaging: Nano to Macro, 2006. 3rd IEEE International Symposium on, 2006, pp. 299-302.

[3] T.-s. L. L. L. and. T. W. Xiao-li Jin, "Multi-Spectral MRI Brain Image Segmentation Based On Kernel Clustering Analysis," vol. 34, 2012.

[4] S. Saha and S. Bandyopadhyay, "MRI brain image segmentation by fuzzy symmetry based genetic clustering technique," in Evolutionary Computation, 2007. CEC 2007. IEEE Congress on, 2007, pp. 4417-4424.

[5] J. Sheng-Yi and L. Xia, "A Hybrid Clustering Algorithm," in Fuzzy Systems and Knowledge Discovery, 2009. FSKD '09. Sixth International Conference on, 2009, pp. 366-370.

[6] Limin Luo. and. Jun Ohya. Rong Xu, Segmentation of MRI Image, 2012.
[7] S. N. Sulaiman and N. A. M. Isa, "Adaptive fuzzy-K-means clustering algorithm for image segmentation," Consumer Electronics, IEEE Transactions on, vol. 56, pp. 2661-2668, 2010.
[8] Y. H. Yang. J.Liu, "Multiresolution color image segmentation," IEEE Transaction on Pattern Analysis and Machine Intelligence, vol. 16, pp. 689-700, 1994.
[9] P. Campadelli. M.Borsotti, R.Schettini, "Quantitative evaluation of color image segmentation result," Pattern Recognition Letters, vol. 19, pp. 741-747, 1998

BIOGRAPHIES

Siti Noraini Sulaiman obtained her B.Eng (Hons) in Electrical and Electronics Engineering from Universiti Sains Malaysia in 2000, MSc and PhD in Biomedical Engineering (focusing on Medical Imaging) from the same university in 2003 and 2012 respectively. Siti Noraini currently holds the position of senior lecturer at Faculty of Electrical Engineering, Universiti Teknologi MARA, Penang, Malaysia. She specializes in the area of image processing, intelligent systems, neural networks for medical applications, and algorithms.

Nureliani Awang Non is a diploma holder in Electrical Engineering (Electronic) from Universiti Teknologi MARA (UiTM) Pulau Pinang in 2010. She is currently persuing her Bachelor in Electrical (Hons.) Engineering at the same university and expected to graduate in the middle of January 2014.

Iza Sazanita Isa started joining Universiti Teknologi MARA, Pulau Pinang in year 2006. She received her first honour degree from UiTM Shah Alam in 2004 and MSc from Universiti Sains Malaysia in 2009. She is currently a lecturer at Universiti Teknologi MARA, Pulau Pinang. Her current research is biomedical engineering, advanced control system and related area in signal and image processing

Norhazimi Hamzah received the B. Eng in electrical and electronics from Universiti Teknologi Petronas (UTP) in 2002. After 3 years working experience in the industry as an engineer, she continued her master study at Universiti Teknologi Malaysia (UTM). She obtained Master in Engineering (Electrical Engineering) in 2007. She joined Universiti Teknologi MARA (UiTM) as a lecturer in 2008. Her research interest include sliding mode control, nonlinear control, artificial intelligence, automotive control, process control and biomedical.

Investigating factors that influence e-school management in high schools in Macedonia

Majlinda Fetaji [1]
South East European University,
Contemporary Sciences and Technologies, Computer Science
Ilindenska bb, 1200 Tetovo, Republic of Macedonia
b.fetaji@seeu.edu.mk

Bekim Fetaji [2]
South East European University,
Contemporary Sciences and Technologies, Computer Science
Ilindenska bb, 1200 Tetovo, Republic of Macedonia
m.fetaji@seeu.edu.mk

Abstract— The focus of this research study is on investigating concepts, analyses and development of e-school management system. High schools in Macedonia still utilize the manual classical paper-based administration and school management. Therefore, e-School Management System (e-SMS) is developed to facilitate teaching and administration staffs to manage school activities in high schools and parents to have in-time information about the performance of their child. As a result, users found that they are willing to use e-SMS which also showed to have improved the quality of the management process in schools and improved information and communication among teachers, parents, students and the general public and. Empirical research is conducted to evaluate the satisfaction of e-SM and the attitude towards using this system in the future. Furthermore, the factors that influence the usage and the positive and satisfactory level of attitude towards electronic school management will be identified. Findings are presented and recommendations are provided.

Keywords— e-SM, e-SMS, e-school management, e-school management system, web services, Regression Model of Statistical Significance of Results

I. INTRODUCTION

In Macedonia, the classical method of management and administration of learning and school activities is practiced in all secondary schools. The fact is that this classical approach of management is not appropriate and contains various deficiencies such as keeping records on paper, face-to-face miscommunication, misuse of a position, not-in-timely information and communication, inadequate communication and information among school staff itself, students and parents and other deficiencies. Therefore, e-School Management System (e-SMS) is developed to facilitate teaching and administration staff to manage school activities in high schools and parents to have in-time information about the performance of their student/child. This school management e-Model will offer tasks such as registering students, teachers, forming classes, keeping track of teachers' and students' status and profiles; generating reports, official transcript, etc.

II. HYPOTHESIS

Formulated are the following hypotheses which this paper should give answers to:

H0: The electronic school management will improve the quality of school management processes and information and communication between the school staff, students, parents and the general public.

H1: The experience in using e-applications previously and the confidence on e- applications influence and increase the satisfactory level of attitude towards e-school management.

III. RESEARCH METHODOLOGY

The study is conducted through qualitative testing method using a questionnaire consisted of 20 questions about the profilization, academic background, computer skills; usage and attitude towards different features of electronic school management activities and have they used and do they believe e-applications. Participants were students, teaching and administrative staff and parents of 3 high schools-in Kumanovo, RM. 15 teachers, 41 parents and 5 administrators filled-in an online questionnaire that contained multiple-choice questions. For some of the questions students had to denote their own attitude. The questionnaire was alienated into four sections: "General information", "Computer skills", "Attitude towards different features of electronic school management", „Attitude towards reliability and quality of management in e-school management" and „have they used and believe e-applications".

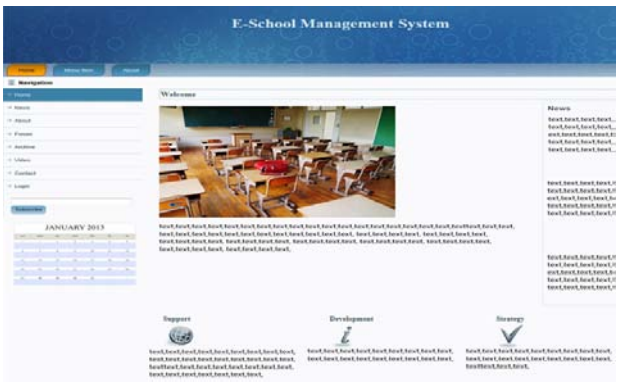

Fig 1. A screen shot of welcome screen

ISBN: 978-1-61804-228-6

The results are presented in tables of percentages, graphics and diagrams. Screen shots of the welcome screen is shown in the given figure 1.

IV. Results and Findings

Precondition for successful utilizing an e- management application is having a computer and internet access at home/neighbor cafeteria. It is evident that the percentage of owned computers in high schools in deployed countries in the world increases every day. In our target high schools, the results shown in the figure 3 and 4, we found that the lack of computer and/or internet access is not an obstacle. We can see that 95% of users have a computer at home, while 87% have an internet access.

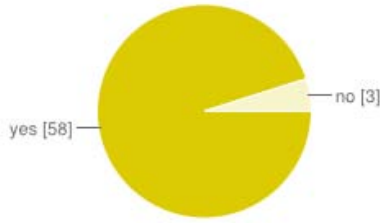

Fig 2. Percentage of owned computers (100%)

Fig 3. Percentage of having internet access (89%)

The results about the question Q12: Is the school management administered this way improved compared to the classical manual method; and Q14: Does the approach of using e-SMS offer better quality management, which are shown in the figure 4 and figure 5.

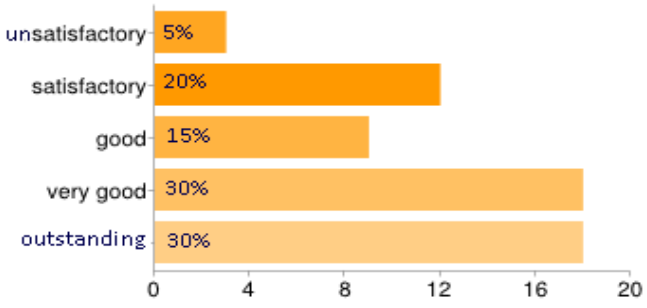

Fig 4. The e-SMS management improvement compared to the classical manual method**.**

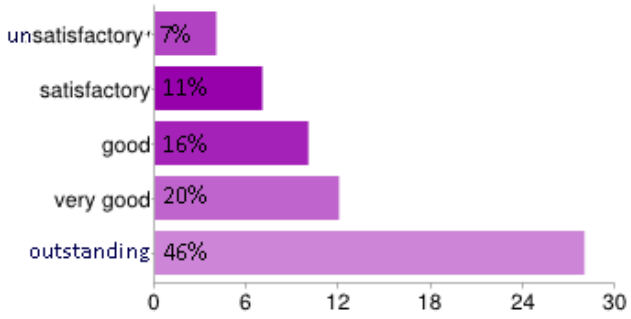

Fig 5. The e-SMS management offers better quality management

60% of users claim there is improvement in the school management using e-SMS, 15% claim it is good while 25% do not see any improvement in e-SMS management vs. manual management. 66% of users claim that e-SMS offers better quality management, 10% say the e-management is good while 18% are not satisfied with the quality of the e-management. These results indicate that the electronic school management is outstanding in aspect of improvement and better quality of management compared to the classical manual management which is expected, but still there are a percentage of users that are not satisfied.

These results verified our hypothesis H0 is true.

Furthermore, we are interested in the usage and positive attitude of users towards electronic school management. This is investigated by the survey question Q15: Are you satisfied the way school management is organized vs. classical way?; and Q16: Do you like using this school management application, shown in the figure 6 and figure 7. The answers of the question Q17: If you do not like the electronic school management, what is the reason?, tell us some of main reasons why users do not like e-school management, which are shown in figure 8.

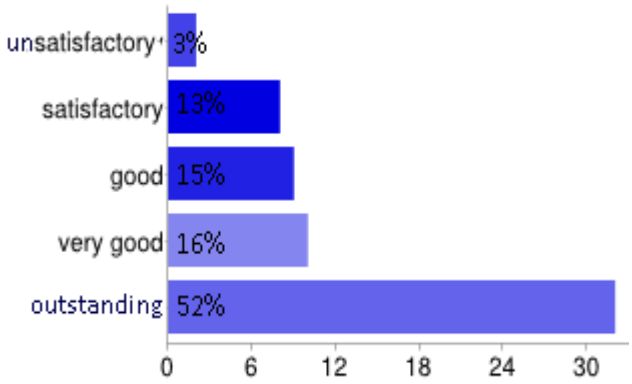

Figure 6. Satisfaction of the way e-school management is organized vs. classical manual method

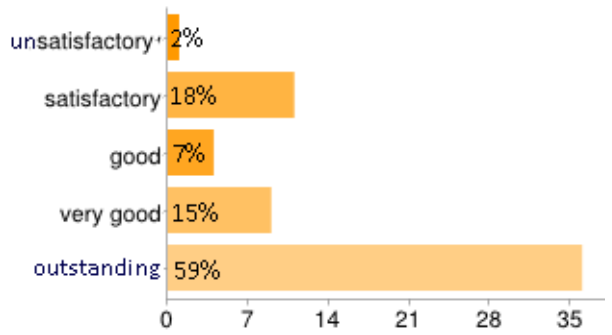

Figure 7. Satisfaction of performing e- school management (e-SM)

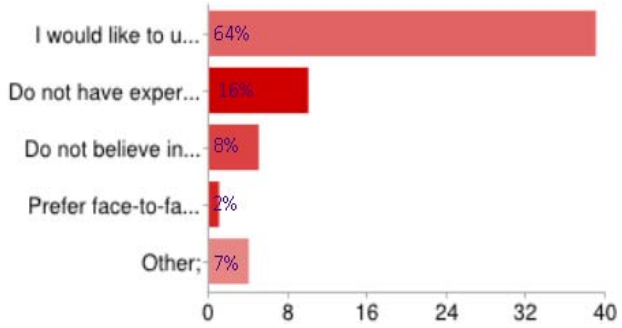

Figure 8. Reasons users do not like to use e- school management system

From the results we see that users' satisfaction how the school management is organized vs. classical manual way is in high percentage 68% outstanding and very good, while 16% are not satisfied with the electronic management, 15% think it is good. About 74% of users are outstanding and very good satisfied using the e-SMS for school management, 20% are not satisfied, while 7% say it is good. From the question if the users would not like to perform e-school management, 64% answered they would like to use the e-SM, while 45% of those who would not like to use stated the reason that they do not have experience in using e-applications, 23% stated that they do not believe in the security of e-applications, just 5.5% prefer face-to-face communication, and 19.5% stated other reason. The highest percentage of users who do not like electronic school management stated their experience in using e-applications as a reason. The next higher percentage is of those that do not believe e-applications. Also, the percentage of users that would not like to use e-management is very high 45%. That is a good reason to look for what influences the still high percentage of unwillingness to use e-management, even though the percentage of users with very good and outstanding attitude is very high 64%. Therefore, we want to investigate the influence of previous experience in using e-applications and the users' confidence in e-applications in the increase of the satisfactory level of attitude towards electronic school management. Also, we want to investigate how does the role of the user in the education process influence the satisfactory level of attitude towards electronic school management. The main independent variables of our investigation are the previous experience in using e-applications and confidence towards e-applications, where the initial questions to which the students had to answer was "The level of previous use of e-applications", "The level of confidence towards e-applications" and "Are they satisfied the way school management is organized using e-management". They were given five options to answer: Unsatisfactory (1); Satisfactory (2); Good (3); Very Good(4) and Outstanding(5). The results about dependency of satisfactory level of attitude towards electronic school management on the previous experience in using e-applications and confidence in e-applications and the role of the user in the education process are shown in the following table 2, table 3 and table 1 and fig 10, fig 11 and fig 12.

Table 1. Satisfactory level of attitude towards electronic school management on the role of the user

Level of satisfaction of e-school management	Role in the education process		
	Teacher	Parent	Administration Officer
Unsatisfactory	2%	2%	
Satisfactory		13%	
Good	2%	3%	2%
Very good	10%	3%	3%
Outstanding	11%	46%	2%

Table 2. Dependency of satisfactory level of attitude towards electronic school management on the previous use of e-applications

Level of satisfaction of e-school management	Level of previously used e-applications				
	Never	Sometimes	Intermediate	Frequently	Always
Unsatisfactory	3%				
Satisfactory	3%	8%	7%		
Good	2%	2%	2%	2%	
Very good	5%	3%	2%	5%	2%
Outstanding	3%	2%	3%	40%	11%

Table 3. Dependency of satisfactory level of attitude towards electronic school management on the level of confidence on e-applications

Level of satisfaction of e-school management	Level of confidence towards e-applications				
	Unsatisfactory	Satisfactory	Good	Very Good	Outstanding
Unsatisfactor	3%				

y					
Satisfactory	5%	8%			
Good	2%	2%	2%	2%	
Very good	7%	3%		2%	5%
Outstanding	3%	2%	2%	36%	16%

According to the results shown in tables 2 and 3, we can see that 50% / 33% of users which **have never/ sometimes** used e-applications have an outstanding and very good level of satisfaction on attitude towards electronic school management, while 38% / 54% are not satisfied with the e-management, 13% / 13% think it is good. The satisfactory level of attitude towards **electronic school management** resulted to be outstanding and very good with the highest percentage of 96%/100% of users which level of previously used e-applications is outstanding and very good, while 4% / 0% think it is good and there are no unsatisfied users. We have similar results from the influence of the confidence towards e-applications in satisfaction towards e-management. 50% / 33% of users which **have unsatisfactory/satisfactory level** of confidence towards e-applications have an outstanding and very good level of satisfaction on attitude towards electronic school management, while 40% / 54% are not satisfied with the e-management, 10% / 13% think it is good. 96% / 100% of users which **have outstanding/very good level** of confidence towards e-applications have an outstanding and very good level of satisfaction on attitude towards electronic school management, while 4% / 0% think it is good and there are no unsatisfied users. We can conclude that previous use of e-applications and level of confidence on e-applications directly influence the level of satisfaction on attitude towards electronic school management. Even the users that have not previously used e-apps and have no confidence in e-apps have a positive attitude towards electronic school management. Those that have an experience in using e-apps and confidence in e-apps have a strongly positive and a high level of satisfaction on attitude towards electronic school management. From the results presented in table 1 and fig 13, only 8% of teachers are not satisfied and do not have positive attitude towards electronic management, while 84% have outstanding and very good satisfactory level on attitude towards e-management. 73% of parents have outstanding and very good satisfactory level on attitude towards e-management while just 23% are unsatisfied with e-management. Administration officers have declared themselves as highly satisfied with the e-management.

Moreover, after investigating their correlation, it was found that there is a strong correlation among satisfactory level of attitude towards e-school management with the 2 indicators, shown in the following fig 9, which is strong enough (closer to 1 – stronger) to say that by increasing the level of use of e-apps and level of confidence towards e-apps, the satisfactory level of attitude towards electronic school management increases. Hereby, the hypothesis H1 is proved.

	likeuseesm
likeuseesm	1.0000
usedpreviо~y	0.6482
believecon~e	0.6594

Figure 9. Correlation of the level of satisfaction towards e-SM with the used previously e-apps and confidence on e – apps

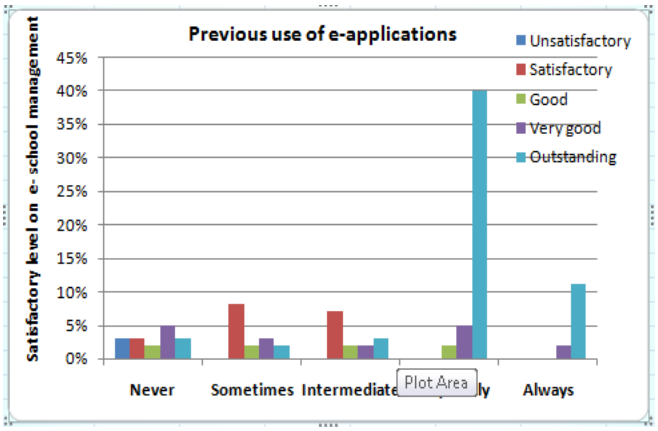

Figure 10. Satisfaction level towards e-SM vs. previous use of e-applications

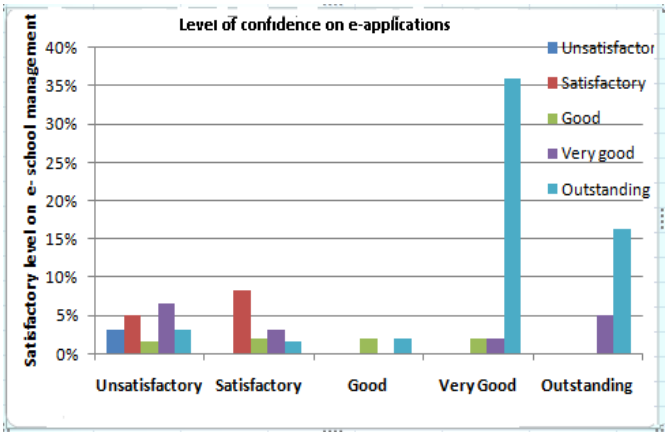

Figure 11. Satisfaction level towards e-SM vs. confidence on e-applications

ISBN: 978-1-61804-228-6

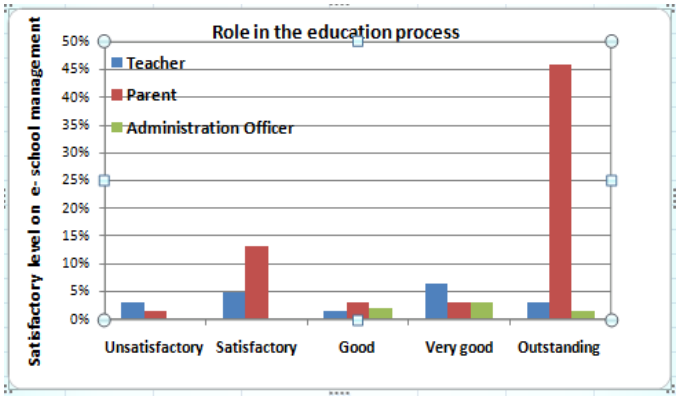

Figure 12. Satisfaction level towards e-SM vs. role in the education process

Moreover, we want to prove the significance of the obtained results using regression model of statistical significance.

V. The Regression Model of Statistical Significance of Results

Regression analysis is a statistical tool to investigate the relationships between variables and to develop a model that is useful for predicting the value of the dependent variable for given values of the independent variable. We want to prove the statistical significance of the proof of hypothesis. Actually we want to determine the fundamental effect of the independent variable(s) upon dependent variable—"satisfactory level of attitude towards electronic school management". To explore these issues we gathered data on the variables of interest and use regression to estimate the quantitative effect of the fundamental variables upon the variable that they influence. We also evaluate the "statistical significance" of the estimated relationships, that is, the degree of self-reliance that the true relationship is close to the estimated relationship.

First we define the research hypothesis that is H="higher levels of previous experience in using e-applications and higher levels of confidence on e- applications influence and increase the satisfactory level of attitude towards e-school management", H0="There is no relationship between levels of previous experience in using e-applications and higher levels of confidence on e- applications and the satisfactory level of attitude towards e-school management".

To investigate this hypothesis, we have gathered set of measured values on levels of previous use of e-applications and levels of confidence on e-applications. Let x symbolize levels of previous use of e-applications and let y symbolize satisfactory level of electronic school management. We suppose that factors other from x which are being unobserved (noise) influence it. Accordingly, we suppose that: i) users from the group which level of previous use of e-apps is "never and sometimes" might show higher satisfactory level on attitude towards e-SM (we had such results, see figures 10-figure 12.) and ii) satisfactory level on attitude towards e-SM increases above this baseline (called intercept parameter b0 [10]). Our hypothesis may be written as a regression equation as follows: y= b0+ b1* x+ e, where b1 is slope parameter, b0 is intercept parameter and e is disturbance in the relationship between y and X.

VI. Conclusions

Now we have to test how good this regression equation predicts values of y, for given values of Xi , i=1,.., 5. We use stata_9. The results of regression are shown in the following Tables 4-5. Results are presented in the following regression equations:

Y=2.2 + 0.59 * X,

Coefficients (slope) b1=0.59 is positive which means that for each increase level in use of e-applications, the satisfactory level of attitude towards e-SM increases respectively by b1=0.59. The constants b0 is the initial position: the satisfactory level of attitude towards e-SM would be about b0=2.2, (meaning would be mostly good and– among level 2 and 3) for users that have never used e-applications.

Table 5. Regression of satisfactory level of attitude towards e-SM vs. level of previous use of e-apps

Source	SS	df	MS	Number of obs =	60
				F(1, 58) =	42.03
Model	37.1140143	1	37.1140143	Prob > F =	0.0000
Residual	51.2193191	58	.883091708	R-squared =	0.4202
				Adj R-squared =	0.4102
Total	88.3333333	59	1.49717514	Root MSE =	.93973

likeuseesms	Coef.	Std. Err.	t	P>|t|	[95% Conf.	Interval]
usedpreviously	.5938242	.0915992	6.48	0.000	.4104684	.77718
_cons	2.236738	.3214685	6.96	0.000	1.593249	2.880227

Table 6. Regression of satisfactory level of attitude towards e-SM vs. level of confidence on e-apps

Source	SS	df	MS	Number of obs =	60
				F(1, 58) =	44.62
Model	38.4087462	1	38.4087462	Prob > F =	0.0000
Residual	49.9245872	58	.860768744	R-squared =	0.4348
				Adj R-squared =	0.4251
Total	88.3333333	59	1.49717514	Root MSE =	.92778

likeuseesms	Coef.	Std. Err.	t	P>|t|	[95% Conf.	Interval]
believeconfidence	.5473931	.0819459	6.68	0.000	.3833604	.7114257
_cons	2.369393	.2945118	8.05	0.000	1.779863	2.958922

The probability of the F statistic, the test for statistical significance of the regression equation (an F-value > 4.0 is usually statistically significant), for which we got the values of F=42, means that the regression equations help us to understand the relationship between level of previous use of e-apps X and y. The probability of the F statistic for the overall regression relationship, the p value describes the statistical

ISBN: 978-1-61804-228-6

significance of the test: it is significant at 99% level, because the p value is 0.000. The values of r-squared, r2=0.42, which is the measure of relationship and indicates that with the known value of X (the level of previous use of e-apps), we can explain 42% of the variance in y (the satisfactory level towards e-SM). We reject the null hypothesis that there is no relationship. The standard error is very small, approximately Std. Err.=0.09. A t-test that indicates statistical significance of the coefficient b1 (a t-value > 2.0 is usually statistically significant) which is large in our case t=6.48, and we can conclude that there is a statistically significant relationship. This means that the independent variable or X, (level of previous use of e-apps) should be kept in the regression equation, since it has a statistically significant relationship with the dependent variable or y (satisfactory level of attitude towards e-SM).

We got similar results when investigating the second independent variable "level of confidence on e-apps". The regression equation is formulated as: Y=2.3 + 0.54 * X,

Coefficients (slope) b1=0.53 is positive which means that for each increase level in confidence in e-applications, the satisfactory level of attitude towards e-SM increases respectively by b1=0.54. The constants b0=2.3 meaning the satisfactory level of attitude towards e-SM would be about b0=2.3, (meaning would be mostly good and– among level 2 and 3) for users that have no confidence on e-applications. The F value F=42, means that the regression equations help us to understand the relationship between level of confidence on e-apps X and y. The p value describes the statistical significance of the test: it is significant at 99% level, because the p value is 0.000. The values of r-squared, r2=0.43, indicates that with the known value of X (the level of confidence on e-apps), we can explain 43% of the variance in y (the satisfactory level towards e-SM). We reject the null hypothesis that there is no relationship. We support the research hypothesis that there is a statistically significant relationship between the level of confidence on e-apps and the satisfactory level of attitude towards e-SM. A t-test is t=6.48, we can conclude that there is a statistically significant relationship. This means that the level confidence on e-apps has a statistically significant relationship with the dependent variable (satisfactory level of attitude towards e-SM). We have verified the statistical significance of data and conclusions. Level of previous use of e-apps and level of confidence on e-apps are highly significant. We recommend giving effort to increase the user experience on e-applications and also increase the confidence towards e- applications by organizing trainings and by presenting users (teachers, parents and administration officers) the real advantages of e-management.

REFERENCES

[1] 1] Douglas C. Montgomery, Elizabeth A. Peck (2006) "Introduction to Linear Regression Analysis", John Wiley & Sons Inc, Wiley-Interscience, ISBN: 0471754951, New York.

[2] [2] Chong, G., & Jun, Ch., (2005) "Performance of some variable selection methods when multicollinearity is present", Chemometrics and Intelligent Laboratory Systems, Elsevier B.V, Volume 78, Issues 1-2, 28 July 2005, Pages 103-112 (doi:10.1016/j.chemolab.2004.12.011)

[3] Curtis, B. (1980). Measurement and experimentation in software engineering. Proceedings of the IEEE, vol. 68, no. 9, (pp. 1144-1157).

[4] Van Vliet, H. (2000). Software Engineering:Principles and Practices, 2nd Edition. . West Sussex, England: John Wiley & Sons.

FSS Shielding and Antenna Discrimination Effect on Interference Mitigation Techniques

Lway F. Abdulrazak

***Abstract*—** This paper extracts the rules of shielding from basic measurements to mitigate the interference of IMT-Advanced on Fixed Satellite Service. The IMT-Advanced system is represented by a 20 MHz bandwidth WiMAX IEEE802.16e base station. Co-existence analysis is done for Co-Channel Interference (CCI) and Adjacent Channel Interference (ACI) with guard bands equal to 0 MHz, 5 MHz and 12 MHz, respectively. The guard bands are used with shielding attenuation of 0 and 20 dB for each scenario. The proposed Interference-to-Noise ratio (I/N) is used as a pre-requisite for a desensitization-proof receiver. A case study of using signal generator, VSAT unit and different shielding materials are considered. The testing is performed in the Anechoic Chamber as well as outdoor, and deployment is designed to fulfill FSS signal receiving criteria. A set of key path loss parameters are calculated, followed by the computations of positive horizon angles imposed by losses over various terrains for different deployment areas. The Antenna discrimination has been discussed alongside the shielding absorption coefficients of the suggested materials. Then the antenna discrimination proposal is demonstrated with a high degree of capability to reduce the harmful power interference from IMT-Advanced base station towards the FSS receiver.

***Keywords*—** IMT-Advanced, interference, mitigation, satellite, shielding.

I. Introduction

A Tractable approach of dealing with interference issues imposed by the co-existence scenarios of FSS receiver and IMT-Advanced system is presented in this paper. Hereby, shielding is used to attenuate the Electromagnetic Incompatibility (EMI) between sources (IMT-Advanced) and susceptible equipment (FSS receiver). The mechanism of shielding is described as follows: when terrestrial waves hit the shield, a part of its energy will be reflected because of the shield surface; another part of the energy will be absorbed and transformed to other shapes of energy (thermal and electrical energy). Part of the electrical energy will be discharged through the ground and the rest will pass through the shielding. So, basically the site shielding is about physical obstruction built to reduce the interference from the interferer to the victim receiver [1].

This work was supported in part by the Malaysian Communication and Multimedia Commission (MCMC). The author would like to express his acknowledgment to Cihan University – Sulaimanyia for covering the publication expenses.

L. F. Abdulrazak is a lecturer at the Computer Science Department, Cihan University, Sulaimanyia City, Iraq. Phone: 00964-7700616304; e-mail: audayt@yahoo.com.

Most of the studies recommended that shielding can reduce the harmful interference [2-8]. The best isolation happened when the enclosure is fabricated as one homogeneous piece. The shielding material choice is wide, but each material differs in its ability to attenuate the electromagnetic waves. Shielding can be natural by locating the FSS dish in around the back of building or hill. It can be done artificially by adding one or two walls on the path between victim and interferer [1]. Two walls will be much better because it will duplicate the amount of attenuation. The dish elevation angle should be considered during shielding deployments to prevent signal blocking by the shielding shape [9]. By putting the dish as low as possible, and with high shielding all around except in the direction of the beam to satellite, will help to avoid the interference. The signal reception will be better, because the more the dish is hidden the greater the reduction in interference level [10].

A sharing studies based on simulation have been conducted in Japan for the frequency 3400-4200MHz. The results of sharing studies based on the interference model using the existing ITU-R Recommendations as well as those of new sharing studies taking into account the shielding effect by the artificial objects observed in a real environment is also included.

A new practical shielding mitigation technique is needed to achieve the minimum separation distance. This technique can further increase the possibility of sharing between these systems using guard band insertion between the two services. Deterministic analysis, adjacent channel interference ratio (ACIR), field strength, and path loss propagation are all covered in this research for the co-channel interference (CCI) and adjacent channel Interference (ACI) scenarios. The shielding strategy developed base on test bed measurements to evaluate the attenuation of the proposed materials. Matlab™ has been used as a simulation tool, whereas the IMT-Advanced parameters have been characterized by WiMAX IEEE802.16e. The impact of different FSS channel bandwidths, guard band separations, shielding effects, antenna heights and different deployment areas on co-existence feasibility are considered.

II. Propagation Model and Systems Parameters

The shielding technique (R) can attenuate the interference power, where R may take a value between 0 dB to 40 dB depending on the materials and shielding arrangement, as clarified below [11]:

$$20\log(d) = -I + EIRP_{Interferer} - 92.5 - 20\log(F) - A_h + G_{vs}(\alpha) - R \quad (1)$$

Where A_h is the factor related to the territories as described earlier in this chapter, d is separation distance, R is the shielding loss, *EIRP*: is the effective isotropic radiated power transmitted from the interferer, F is the frequency and G_{vs} is related to the typical receiving FSS antenna gain [12], [13].

Intuitively by introducing clutters, smaller separation distance is achieved and vice versa. Path loss prediction in the case of Line Of Sight (LOS) is obtained by including the losses produced by the line-of-sight situation together with the losses produced by clutter models as shown in Equation (2) [14]:

$$L(d) = 92.44 + 20\log_{10} f_{GHz} + 20\log_{10} d_{Km} + 10.25e^{-d_k}\left[1 - \tanh\left[6\left(\frac{h}{h_a} - 0.625\right)\right]\right] - 0.33 \quad (2)$$

Where d is the distance between the interferer and the victim receiver in kilometers, f is the carrier frequency in Gega Hertz and d_k is the distance in km from nominal clutter point to the antenna (d_k =0.02 km, 0.02 km, 0.025 km and 0.1 km for the four deployment environments dense urban, urban, sub-urban and rural , respectively), h is the antenna height (m) above local ground level and ha is the nominal clutter height above local ground level (h_a= 25 m, 20 m, 9 m and 5 m for the four deployment environments).

The receiving gain of FSS station is called off axis antenna $G_{vs}(\alpha)$. The off axis angle value depends on the earth station location and the main receiving beam, where a typical receiving antenna gain can be calculated as Equation (3) [15]:

$$G_{vs}(\alpha) = \begin{cases} G_{\max} - 2.5\times10^{-3}(\frac{D}{\lambda}\phi)^2 & 0 < \alpha < \phi_m \\ 52 - 10\log_{10}(\frac{D}{\lambda}) - 25\log_{10}(\alpha) & 3.6^o < \alpha < 48^o \\ -10dBi & 48^o < \alpha < 180^o \end{cases} \quad (3)$$

Where G_{max} is the maximum antenna gain (38dBi), D=1.8m (satellite diameter) and λ is the wave length in meter and ϕ_m is given by:

$$\phi_m = \frac{20\lambda}{D}\sqrt{G_{\max} - 2 - 15\log_{10}(\frac{D}{\lambda})} \quad (4)$$

In the simulation a value of -10 dB was considered to represent the local case study (the FSS elevation angle at the experiment location was 74^o).

In addition to the deterministic approach, other critical parameters, such as the receiver blocking and Adjacent Channel Interference Ratio (ACIR) are considered in this work. These resulted from the introduction of the Spectrum Emission Mask (SEM) of the interferer and the blocking filter capability of the victim. It is worth mentioning that receiver blocking and ACIR calculations are based on transmitter SEM and victim filter response powers [16]. The receiver blocking is considered in order to find the power degradation in decibel. This can be calculated as follows:

$$\text{Receiver Blocking} = \begin{cases} ACS\ \text{Reduction} & if\ BW_{interferer} < BW_{victim} \\ 0\,dB & if\ BW_{interferer} \geq BW_{victim} \end{cases} \quad (5)$$

Such a SEM is the 20 MHz channel bandwidth type-G WiMAX spectrum emission mask in [17]. In order to calculate the adjacent channel interference, the ACIR should be considered by reducing the interference powers of the interferer ACLR and the victim ACS which are located on different central frequencies [18]. The ACIR is given by:

$$ACIR = 10\log_{10}\left[\left(10^{ACLR_{IMT}/10}\right)^{-1} + \left(10^{ACS_{FSS}/10}\right)^{-1}\right]^{-1} \quad (6)$$

With the carrier frequency at 4 GHz, the overall propagation model may be rewritten as follows:

$$20\log_{10}(d) = -I + EIRP_{WiMAX} + G_{vs}(\alpha) - 104.58 + ACIR + corr\_band - (10.25e^{-d_k}\left[1 - \tanh\left[6\left(\frac{h}{h_a} - 0.625\right)\right]\right] - 0.33) \quad (7)$$

Corr_band is the correction factor of the band ratio, which is equal to 0 dB when BWWiMAX < BWFSS. Otherwise, Corr_band = -10log (BWWiMAX/BWFSS), when BWWiMAX > BWFSS. Therefore, when the bandwidth of FSS is 230 kHz, the correction band is given by the following expression:

$$Corr\_band = -10l\log_{10}(\frac{20\times10^6{}_{WiMAX}}{230\times10^3{}_{FSS}}) = -19.4dB \quad (8)$$

The value of correction band is used in the simulation processes.

III. Tools, Specifications and Field Measurements

The VSAT unit used for running the field test, which receives the internet signal at 4040 MHz. A harmful interference was applied on the FSS receiver using synthesized signal generator to generate interfered signal within the range 3700-4200 MHz. The FSS unit is installed to receive an internet Bandwidth (Burstable to 256Kbps downlink and 9.6 kbps uplink) through MEASAT III Geostationary Satellite

Orbit.

The synthesized signal generator was used to generate an interference signal to assess the interference of 1MHz bandwidth. This is done to verify the effect of adjacent interference level as well as the in-band interference. The MEASAT 3 satellite orbit position is 91.5^0 E, while the dish is located at latitude of 1.558^0 N and longitude 103.6^0 E Longitude. The distance of the earth station to the satellite is 35955 km. The signal delay is 239 ms for MEASAT-3. For the receiver unit, antenna diameter is 1.8m, centre frequency (F_c) is 4040 MHz, elevation angle is 74^0, azimuth is 263.7^0, height is 1.8m, Bandwidth is 230kHz and Theoretical Interference level (I) equal to -165 dBw/230 KHz. For the Broadband wireless access, centre frequency is 4040MHz, peak output power is 20dBm, channel bandwidth 1MHz, antenna gain 10dBi and antenna height is 2.2m.

The measurements procedure with the shielding technique is started with antenna measurements, where a Horn antenna is used in the shielding experiment to represent the BWA sector. The measured return loss of the horn antenna gave a good response for the frequency band 3700-4200 MHz.

An empirical experiment has been conducted using the anechoic chamber to measure the free line of sight signal level. Concurrently, a Broadband Wireless Access (BWA) signal generator is used as a WiMAX transmitter. Having set such a typical ambience, various types of metals are located in between the transmitter and the receiver. This is aimed at measuring the signal penetration through different materials in order to obtain the power loss through several barriers. The results of attenuation obtained with different shielding materials are reported in Table I.

Table I: Measurements of signal losses for 4040 MHz Radio paths obstructed by common materials

Material type	Loss (dB)
Aluminium shield (0.1cm thickness)	22.1
Aluminium mesh wire shielding (0.2cm wire spacing)	20.9
Copper shielding (0.1cm thickness)	24.5
Copper mesh wire shielding (0.2cm wire spacing)	23.3
Zinc shield (0.1cm thickness)	20

The losses obtained are in the range of 20 to 22.1 dB for the materials used as shown in Table I. For cost-effective deployment, a zinc metal of 0.1cm thickness is used for shielding the FSS as shown in Fig. 2.

Fig.1. FSS shielding using Zinc sheet material

The study has practically proved that best shielding condition occurs when the FSS receiver antenna is entirely shielded except for the top side. Furthermore, the shield should be separated at least 1 m from the basement of antenna and 0.5 m higher than the antenna's body. It must also be grounded. If a shield is deployed in the direction of the satellite, the angle of elevation from the bottom of the antenna reflector to the top of the shield should be about 5 degrees less than the satellite elevation.

A BWA synthesized signal generator is used to generate an interfering signal, which ranges from 3400 to 4200 MHz. This frequency range covers both cases of CCI and ACI as shown in Fig.1. A 20 dBm signal with a bandwidth of 1 MHz was generated and broadcasted in the direction of FSS receiver. The frequency of the interferer was varied from 3800 MHz to 4100 MHz, which resulted in 0 kb/s downlink signal in the FSS receiver. However, when the transmitter power of interferer is reduced by 1 dBm significant decrease in interference was observed. In order to have a minimum separation distance required for the co-existence in CCI scenario, the deterministic calculation is given by:

$$20\log(d)=EIRP(\text{-}65\text{dBw})\text{-}I(\text{-}165\text{dBW}/0.23\text{MHz}) +G_r(\text{-}10)\text{-}92.44\text{-}20\log f(4.02\text{GHz});\ d=0.187\ \text{Km} \quad (9)$$

Where d is the separation distance in km, $EIRP$ is the effective isotropic radiation power of the interferer, I is the interference level, G_r is the received gain, f is the receiving frequency of FSS. A 0.187 km is a large separation distance for a small transmitted power like 20 dBm. Therefore, the experiment has shown that co-existence scenarios based on co-channel sharing is almost practically impossible. The analyzed interfered signal collected in Table II was used to ensure the wave propagation attenuation after and before the FSS frequency carrier.

Table II: Effect of BWA signal on the FSS carrier with and

ISBN: 978-1-61804-228-6

without shielding

Parameter		20 dBm Signal generator			
		Without shielding		With 0.1cm Zinc	
		before carrier	after carrier	before carrier	after carrier
ACS (dB)	5 MHz Offset	15	50	35	70
	10 MHz Offset	31	60	61	105
	15 MHz Offset	55	70	0	0

As clearly shown in Table II, the higher the transmission frequency, the higher is the propagation losses; and reducing the transmitted power corresponds to a reduced ability to penetrate the walls. Therefore, the effects of interference, with or without shielding, at different frequency offsets is summarized in Fig.2. The threshold value is defined at -125 dBm.

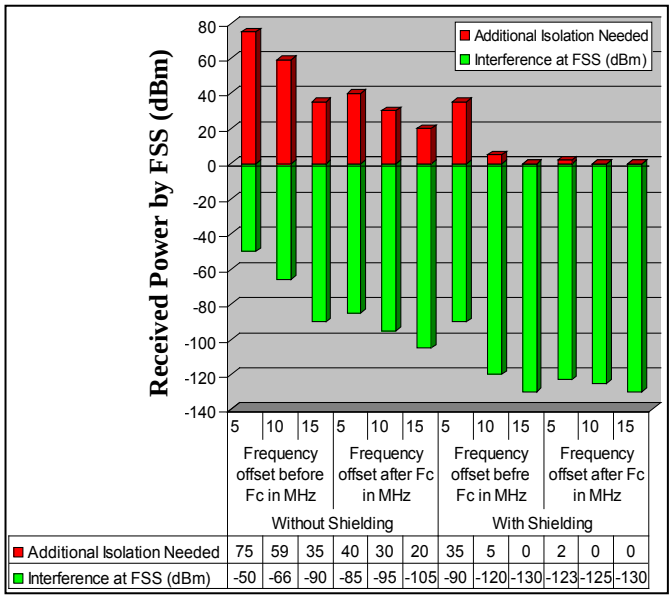

Fig.2: The additional isolation needed for the FSS protection.

Fig.2 clearly shows that signal ability to interfere is bigger when it has less value than FSS frequency carrier and vice versa. In addition, signal attenuation is higher when shielding technique is used compared to the signal attenuation before the shielding. It is also shown in the figure that co-existence is achieved with 20 dB shielding attenuation and 15 MHz frequency offset. It can be concluded that it is possible to reduce down the harmful interference to 10% by increasing the shielding attenuation to 20 dB and the separation distance can be reduced down to 1% for 40 dB shielding attenuation.

IV. The Co-existence analysis of FSS with WiMAX using Shielding

The intersystem interference model in the CCI and ACI depends essentially on the wave propagation model; it consists of free space propagation and clutter loss effects. According to the shielding experiment at CCI scenario, the zero-guard band and guard bands separation channel are simulated to represent the interference scenarios. A minimum separation in two dimensions (frequency and distance) for different deployment areas with and without using the shielding technique has been covered.

Firstly, when the interfering signal shares the same band with the victim FSS receiver and thus separation distance is desired. Secondly, when the interfering signal is contiguous to the victim band and finally when a guard band is in between the bands in question. The worst case of sharing between WiMAX and FSS receiver is simulated when both the interfering and victim antennas are opposite-tower-mounted and facing each other. An FSS antenna of variable heights (1.8 m and 5m) has been used to emphasize that positioning the FSS receiver onto the ground can effectively reduce the separation.

In Fig.3, the 20 dB shielding mitigation technique is used to reduce the separation distance between the two services, which corresponds to the reduction of 10 % of the original distance.

Fig.3: The separation distance between WiMAX and FSS

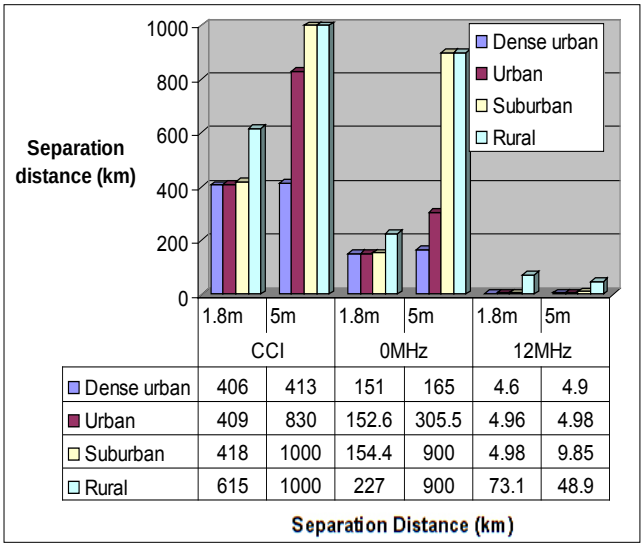

when FSS bandwidth is 0.23 MHz for four deployment areas for CCI, zero guard band and 12 MHz Guard band with 20 dB shielding attenuation.

The reduced separation obtained in Fig.3 (with the insertion of 12 MHz guard band and 20 dB Shielding) is not sufficient for practical deployment of the future communications systems. Obviously, a minimum separation distance is calculated for 36 MHz FSS bandwidth when shielding attenuations are 0 and 20 dB, respectively. Figure 4 shows the results for 36 MHz FSS (1.8 m) bandwidth when $\Delta f = 0$ (CCI),

ISBN: 978-1-61804-228-6

28 (zero guard band), 33 (12 MHz guard band) and 40 MHz for the four deployment areas.

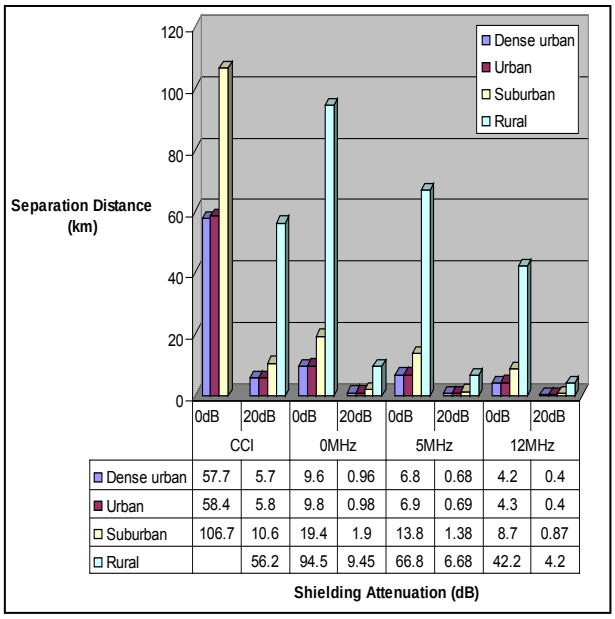

	CCI		0MHz		5MHz		12MHz	
	0dB	20dB	0dB	20dB	0dB	20dB	0dB	20dB
Dense urban	57.7	5.7	9.6	0.96	6.8	0.68	4.2	0.4
Urban	58.4	5.8	9.8	0.98	6.9	0.69	4.3	0.4
Suburban	106.7	10.6	19.4	1.9	13.8	1.38	8.7	0.87
Rural		56.2	94.5	9.45	66.8	6.68	42.2	4.2

Fig.4: The separation distance between WiMAX and FSS when FSS bandwidth is 36 MHz in the four deployment areas for CCI, zero guard band and 12 MHz Guard band and 40 MHz with 0 and 20 dB shielding attenuation.

From Fig.4, it is noticed that separation distance reduced to 0.4 km when 12 MHz is used as guard band (with a 20 dB as a shielding attenuation in dense urban area deployment). However co-existence in the CCI scenario is still difficult due to large separation distance required. Since base station-to-base station is the main scenario of interference, complete analyses on the antenna discrimination effect should be done by using the smart antenna, being a suggested technology for next generation of mobile communication.

V. ANTENNA DISCRIMINATION IMPACTS

An Antenna Discrimination Loss (ADL) is the difference in azimuth between the interferer antenna direction and the victim receiving direction. Thus, pointing the beams of antenna victim and interferer are not aligned on each other, and it could lead to degradation in the interferer gain toward the victim. In order to highlight this issue, the separation distance results obtained in Fig.5 for a dense urban area deployment is incorporated in the ADL simulation. Figure 5 shows the varying values of minimum separation distance using ADL in the range of 0 to 15 dB of the CCI, with 0 and 12MHz guard band separation. Definitely, the ADL technique proposes another mitigation technique which supports the smart antenna technology. However, a scenario of intersystem interference is also considered in order to compare the effect of three sectored terrestrial base station and electrically shifted beam base station on the FSS earth station.

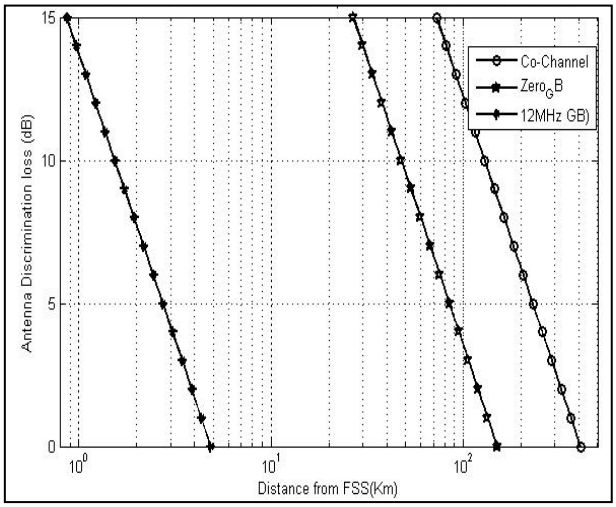

Fig.**5:** Antenna discrimination loss and minimum separation distance when FSS bandwidth is 0.23 MHz in dense urban area with 20 dB shielding Attenuation.

In the cases of co-channel co-existence, zero guard band and adjacent channel, a 15 dB antenna discrimination loss can decrease the physical separation from 406 km, 165 km and 49 km to 72 km, 26.8 km and 0.86 km, respectively, for 20 MHz WiMAX channel bandwidth and 1.8m FSS height with 20dB shielding protection in dense urban area.

VI. CONCLUSION

The proposed shielding technique proves resilient in the presence of interference (with or without the guard band). The technique may thus be considered as a viable alternative to many other commercial-of-the-shelf (COTS) mitigation solutions. On the shielding mitigation technique, it was found that different materials have different levels of signal attenuation. The proposed shielding material (0.1mm thickness Zinc sheet) was a balanced choice, providing a high attenuation (about 20 dB) at a lower cost, compared to other metals. It was also found that it is possible to reduce the harmful interference up to 10 % by increasing the shielding attenuation up to 20 dB. Consequently the separation distance can be minimized to 1% for 40 dB shielding attenuation. This method can be applied to other satellite systems, because different channel bandwidths were simulated for the victim FSS receiver. The simulation results have shown that both the interference and separation distance decrease with an increasing channel bandwidth.

Co-channel interference scenario in the rural area is the most difficult compared to other scenarios. However, it requires a long coordination distance in the range of 6150 km and 86 km without shielding effect for a 0.23 MHz and 36 MHz FSS channel bandwidths, respectively, given an FSS antenna height of 1.8m. By adding 40 dB shielding attenuation, the coordination distance will correspondingly be reduced to 61 km and 0.86 km. These are the highest reduction

that could be achieved without guard separation. These findings emphasize that the shielding technique can significantly improve the FSS immunity against the interference as well as the signal reception via FSS. However, adjacent channel interference scenario with frequency offsets from the carrier of 12 MHz in dense urban area shows the best co-existence scenario with 40 dB shielding attenuation. For instance, it needs 0.49 km and 0.04 km geographical separation for 0.23 MHz and 36 MHz FSS channel bandwidths, respectively, when FSS antenna height is 1.8 m. This indicates that the dense urban area is the best area for co-existence and intersystem interference coordination.

From the deployment standpoint, different areas are considered and it is shown that the dense urban type of environment is the most convenient type for successful co-existence scenarios, whereas the rural one is the worst for frequency sharing and coordination in the same band. From the shielding perspective, it is worth mentioning that this technique is applicable to any antenna size at various heights. For the ADL, it is concluded that other mitigation techniques should be researched to enhance the co-existence between the two services by reducing the separation distance.

REFERENCES

[1] WiMAX Forum (white paper). *Compatibility of Services using WIMAX Technology with Satellite Services in the 2.3 - 2.7 GHz and 3.3 - 3.8 GHz Bands*. 2007.

[2] ITU-R WP 8F/975-E. *Analysis of interference from IMT to FSS in the 3400-4200 MHz and 4500-4800 MHz*. Aug. 2006.

[3] Recommendation ITU-R S.1432. *Apportionment of the Allowable Error Performance Degradations to Fixed-Satellite Service (FSS) Hypothetical Reference Digital Paths Arising From Time Invariant Interference for Systems Operating Below 15 GHz*. October, 2008.

[4] APT Report. *The Co-Existence of Broadband Wireless Access Networks in The 3400-3800 MHz Band and Fixed Satellite Service Networks in The 3400-4200 MHz Band.* Draft No. APT/AWF/REP-5. Edition: March 2008.

[5] NTIA Report TR-99-361, Technical Characteristics of Radiolocation Systems Operating in the 3.1 – 3.7 GHz Band and Procedures for Assessing EMC with Fixed Earth Stations Receivers. December, 1999.

[6] Radiocommunication Study Groups. *Experimental Evaluation on Robustness Against Potential Interference to TVRO Terminal From IMT-Advanced Transmitter in The 3 400-4 200 MHz Band.* Document 8F/1233-E. Japan. May 2007.

[7] IST-2006-027756 WINNER. *WINNER II Spectrum Sharing Studies*. D5.10.3 v1.0. 2007.

[8] Radiocommunication Study group. *Sharing Studies between FSS and IMT-Advanced Systems In The 3400-4200 And 4 500-4 800 MHz Bands*. R03-WP8F-C-1015. 2008.

[9] RSAC Paper. *Assessment of Potential Interference between Broadband Wireless Access Systems in the 3.4 – 3.6 GHz Band and Fixed Satellite Services in the 3.4 – 4.2 GHz Band*. Hong Kong. February 2006.

[10] Radiocommunication Study group. *Update of Sharing Studies between IMT-Advanced and Fixed Satellite Service in the 3 400-4 200 and 4 500-4 800 MHz Bands.* Document 8F/927-E. August 2006.

[11] Seidenberg, P. Althoff, M.P. Schulz, E. Herbster, G. Kottkamp, M. Statistical of Minimum Coupling Loss in UMTS/IMT-2000 Reference Scenarios. *Vehicular Technology Conference VTC'99, IEEE VTS 50th*. Vol:2, Publication Year: 1999, pp: 963 - 967.

[12] ITU-R SF.1486. *Sharing methodology between Fixed Wireless Access Systems in the Fixed Service and Very Small Aperture Terminals in the Fixed-Satellite Service in the 3 400-3 700 MHz Band. ITU-R R WP4-9S, Geneva, Switzerland*. November, 2000.

[13] ITU-R Recommendation SF.1006. *Determination of the interference potential between earth stations of the fixed-satellite service and stations in the fixed service*. Apr. 1993.

[14] Han-Shin Jo, Hyun-Goo Yoon, JaeWoo Lim and Jong-Gwan Yook. An Advanced MCL Method for Assessing Interference Potential of OFDM-Based Systems beyond 3G with Dynamic Power Allocation. *Proceedings of the 9th European Conference on Wireless Technology*. UK. September 2006. pp. 39-42.

[15] ITU-R WP8F Contribution. *Proposed MIMO Channel Model Parameters for Evaluation of Air Interface Proposals for IMT-Advanced.* Document 8F/1149-E, Question ITU-R 229/8, ITU-R WP8F Meeting in Cameroon, January 2007. http://www.itu.int/md/meetingdoc.asp?lang=en&parent=R03-WP8F-C&PageLB=225.

[16] X. Li and L. J. Cimini Jr. Effects of clipping and filtering on the performance of OFDM. *IEEE Commun. Letters*. May 1998. vol. 2, pp. 131-133.

[17] Recommendation ITU-R P.452-12. *Prediction Procedure for the Evaluation of Microwave Interference between Stations on the Surface of the Earth at Frequencies above about 0.7 GHz*. Geneva, Switzerland. May, 2007.

[18] Document AWF-3/17 .*Assessment of potential interference between Broadband Wireless Access (BWA) in 3.4-3.6 GHz band and Fixed Satellite Service (FSS) in 3.4-4.2 GHz band*. Office of the Telecommunications Authority (OFTA) Hong Kong. September 2006. http://www.esoa.net/v2/ docs/public_cband/ ESOA_CBand_APTReport.pdf.

Dr. Lway F. Abdulrazak (M'07) was born in Baghdad, 1982. He was a Research Fellow with the Wireless Communication Center, Faculty of Electrical Engineering, Universiti Teknologi Malayisa (UTM), Malaysia, (September 2007-October 2011). He obtained his PhD and M.Eng. from Universiti Teknologi Malaysia (UTM), Malaysia, in Electrical, Electronics and Telecommunications Engineering in 2011 and 2007, respectively. He received the B.Eng. degree in Electronics and Communications Engineering from Omer Al Mokhtar University, Libya, in 2005. His research interests include LTE-Advanced system, WiMAX Technology, Antenna Design and Simulation, coexistence and spectrum sharing analysis, OFDM System, and propagation channel prediction, HAPS systems and deployments.

Currently, he is a lecturer and course Tutor at the Computer Science Department, Cihan University-Sulaimanyia, Iraq. He is teaching Computation Theory, MATLAB Programming, Microprocessor, Statistics and Numerical analysis. He has more than 25 publications in the field of Wireless Communications.

Dr. Abdulrazak, is a member of Iraqi Association of Professional Engineerings since 2012, and he got many awards of appreciation from the Cihan University and other local associations.

Considering the Design of Cloud Computing Structures on Computer Systems: New Designs in Global Economic Development

J. S. Boyce,

Abstract-Cloud computing is using massive computing resources, deployed among virtual datacenters, dynamically allocated to specific users and tasks and accessed as a service via an user interface (UI), such as a web browser. This presentation will examine the technical cloud computing structures, consider the technical and ethical issues in designing effective sites, and consider the impact of cloud computing on reshaping computer education programs to include enterprise systems.

Keywords— Cloud computing; enterprise systems; global management

I. INTRODUCTION

What is Cloud Computing?

Cloud computing is using massive computing resources, deployed among virtual datacenters, dynamically allocated to specific users and tasks and accessed as a service via an user interface (UI), such as a web browser.

Tim Jones in his description of Open Stack comments, "Cloud computing architectures tend to focus on a common set of resources that are virtualized and exposed to a user on an on-demand basis. These resources include compute resources of varying capability, persistent storage resources, and configurable networking resources to tie them together in addition to conditionally exposing these resources to the Internet."

The physical cloud resources may reside in a number of locations, the details of which are not typically known to the service's users. Cloud resources are offered as a service on an as needed basis. The cloud itself typically consists of large numbers of commodity-grade servers, harnessed to deliver highly scalable and reliable on-demand services for established enterprise software vendors; the cloud introduces a range of significant issues. Cost reduction is promised via the cloud means massive reinvestment in profitable products to make them cloud-ready, and deep uncertainty about whether such products can be priced at a point that will continue to ensure the lush margins to which the industry has grown accustomed. These investments make the investments made legacy systems obsolete such that they must be altered or replaced to take advantage of dynamic allocation of resources. How will organizations define and analyze the costs to transfer to a cloud base data system. Criteria to analyze the intended benefits include metrics to combining the Advantages of Cloud and Enterprise Security, weigh the differences between Private/Public/Hybrid Clouds, levels of Security provided to the users; end-to-end factors such as storage, network, meta-data, and determinations of internet versus intranet storage.

Several ways are used to customize for verticals: these include

- By application or SOA – financial, media, healthcare
- By customer – strategic/tactical
- By case – e.g. SLA customized to ROI

All cloud providers promise turnkey and automated management, but hidden costs include the transition and training costs for the organizations data gatherers and data transfer protocols. Changes in procedures become less flexible as they cannot be incurred internally. Below is a table of some basic cloud technologies with their strengths and weaknesses [1].

ISBN: 978-1-61804-228-6

Technology	Key Feature	What's Missing
Grid Computing	Job scheduling across many machines	Difficult to administer; Lacks broad applicability of cloud computing
Virtualization	Virtual machines decouple OS from hardware	Fail to fundamentally solve scale and reliability
IaaS Infrastructure-as-a-Service	Computational infrastructure available for rent	Lacks security , vertical solutions,
SaaS Software-as-a-Service	Application availability through the cloud	SaaS is an application on the cloud, not a cloud by itself
Utility Computing	Packaged computing, application, and storage sold as a service	Describes a business model, not a technology or architecture

Cloud Models

II. Structures

Basically this approach to business opens up new technology partners and organization want to be current and trendy. The emergence of an entire new set of companies and service providers try to capitalize on the term "Cloud" to further their business interests. They provide provide technology and services where cloud-based business applications can be deployed and tailored to a business' or partner's needs - by market or industry. Each cloud service provider claims its cloud platform is unique in its formation and history; they combine terms such as in Global Management, Enterprise Security, and Virtualization. The partnership is touted as a mutually beneficial, to ensure the success of relationship. Graphic models are used to allow businesses to grasp the concepts. Corporations such as Aleric International were quick to produce consulting and mentoring options for their clients.

IBM joined the cloud IAAS world in 2010 with their representation called OpenStack [2]:

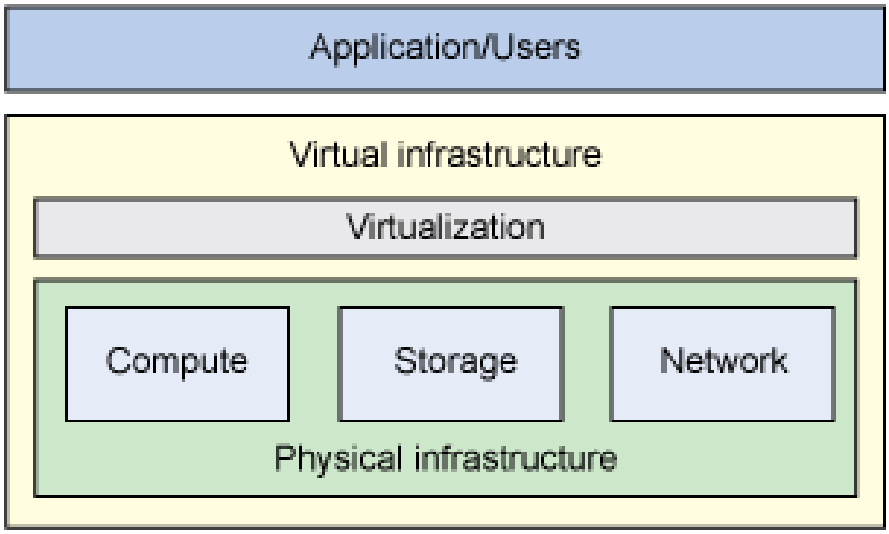

Open Stack Design

ISBN: 978-1-61804-228-6

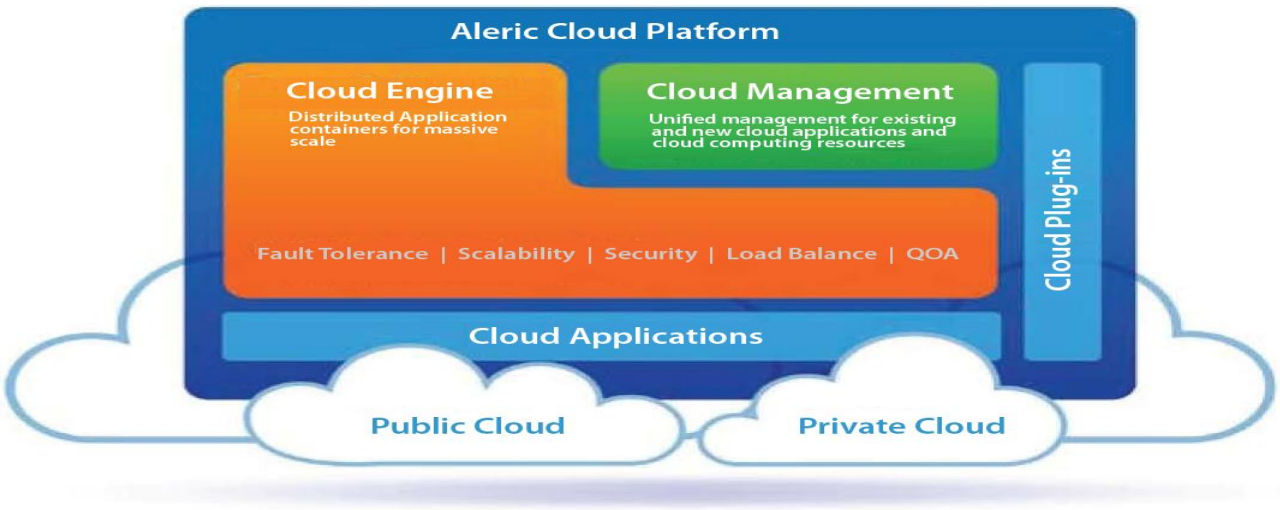

Aleric Cloud Model

The shift to cloud changes the hardware and platform requirements as the organization reevaluates its enterprise structure [3]. Some say the tangible becomes intangible, and money is fungible. As personnel are reduced, so is the visibility of the process. Management roles become more virtual, and data security becomes the key element.

III. Impact on Computer Science Education

Why should Computer Education care?

Fundamentally it changes the way we do implement computer systems, acquire clients, distribute goods and services, and assess productivity. Educational programs will need to add Enterprise computing structures to their curriculums. It also changes the job market while altering current management models.

Changing the Curriculum

Information Systems will need to make drastic modifications in their curriculum as the closed models of IT in organizations have been redefined. A course in Cloud Computing should become part of the Information Systems Curricula. Below are some sample outcomes for a basic course in Cloud Computing which requires a basic understanding of business processes.

More advanced technical courses in IT management will evolve as organizations assess Return on Investment and Cost/Benefit Analyses over time. Training costs for personnel to transition to these new processes will also create an entirely new market for education and training.

What about Software Skills?

Cloud computing requires an understanding of enterprise systems as well as considerable knowledge in Web design and Architecture. The platform of most cloud systems in Unix/Linux. In Jones discussion of Open Stack,

> Cloud computing architectures tend to focus on a common set of resources that are virtualized and exposed to a user on an on-demand basis. These resources include compute resources of varying capability, persistent storage resources, and configurable networking resources to tie them together in addition to conditionally exposing these resources to the Internet. [2]

IV. Curriculum Recommendations

The curriculum for an Information systems program that focuses on Cloud development would include the following*:

Web Architecture Design and Application Development

- Service-Oriented Architecture (SOA) implementation
- Object-Oriented Analysis and Design
- Java Platform, Enterprise Edition (Java EE) Application Development
- Web 2.0 Application Development

ISBN: 978-1-61804-228-6

Mainframe Development

- Systems Analysis and Design
- COBOL/CICS/DB2 Development
- Database Design

Web Application Integration

- Web-enabling back-end applications
- Integrating legacy systems
- Accessing back-end database resources

*It is interesting to see the reemergence of COBOL and DB2 in IBM's definition of required skills for their Open Stack development team. [4]

Upon completion of this course a student will be able to
Define open source cloud computing structures and procedures for enterprise implementation.
Explain the economics of cloud computing at the enterprise level.
Examine the concepts of web application and consider the viability of various web applications.
Integrate the concepts of virtualization with the install/practice of virtualization systems.
Compare and contrast the merits of best practices in cloud services.
Model distributed storage and security structures and discuss issues in cloud computing, including risks and disaster recovery tools.
Explore the next generation of cloud computing architectures/models/tools.

Cybersecurity is an Ethical as well as Technical Issue!

Cloud computer changes the privacy of data, as it changes the autonomy of the company. As a differentiating solution, the utility of computing becomes an enterprise level concern. Key to success is the carrier reliability and geo- and application targeted networks. Business models need to be reinvented to be more community-drive and clouds built for the benefit of all participation.

How Do We Accomplish Virtualization?

As IT technology becomes the Global Cloud, it will be necessary to evolve into a next generation of computing with patent-pending security structures, and open cloud applications platforms. The focus of the business model has been core competence and forming partnerships with leaders. New modes of community, defined on a global scale, will require corporate changes in the definition of participants, management, and customers. New

ISBN: 978-1-61804-228-6

networks will also rely more heavily on mobile interfaces that are more flexible, reliable, and secure. For computer education programs at colleges and universities, it will require new methods of teaching system designers, and database managers, where portability, expandability and risk management will become central components of the curriculum. Texts will have to be redesigned and research projects created to create metrics for productivity and IT success.

Thus cloud computing opens and new era of computing education that shifts the emphasis from the local to the global.

References

[1] Hunter, R. (22 Dec 2011), "Why Cloud?" Gartner Report.

[2] Jones, T. (2012) developer Works, Cloud Computing, http://www.ibm.com/developerworks/cloud/library/cl-openstack-cloud/ pp. 1+.

[3]Aleric International, (2013), http://www.aleric.biz/.

[4] Schaffhauser, D. (3 June 2011) "IBM Tackles Education Analytics with SaaS Suite". Campus Technology.

Dynamic Voltage Restorer behaviour

F. Ghezal[1]; S. Hadjeri[1]; M.Benghanem[2]; S. Zidi[1]

1) *Intelligent Control and Electrical Power Systems Laboratory ICEPS*
Electrical Engineering Departement
Djillali Liabes university, Sidi Bel Abbes, Algeria
2) Mohamed boudiaf university USTO, Oran , Algeria

,

Nour73_fac@yahoo.fr , shadjeri2@yahoo.fr

Abstract— Power quality is one of major concerns is the present era. The power quality disturbances are voltage sag, swell, notch, spike and transients… etc. Custom power devices are the good solution to resolve these problems. One of those devices is named Dynamic voltage restorer (DVR), which is used in distribution system network. This paper presents the comparison of DVR the simulation using simpowersystems/Mtalab blocs and the simulation using RT_LAB simulator in real time domain.

Index Terms— DVR, real time, voltage sags, voltage swell, RT_LAB simulator

I. INTRODUCTION

To overcome the power quality related problems occurring in the transmission system, FACTS (Flexible AC Transmission System) devices play a major role. These are also referred to as Utility based solutions. Similarly Custom Power devices, which normally targeted to sensitive equipped customers, are used to overcome power quality problems in the distribution network [1].

Power quality problems in industrial applications concern a wide range of disturbances, such as voltage sags and swells, flicker, interruptions, harmonic distortion [2, 3].
IEEE 519-1992, IEEE 1159-1995 describes it as in Table 1.

Disturbance	Voltage	duration
Voltage sags	0.1-0.9 pu	0.5-30 cycles
Voltage swell	1.1-1.8 pu	0.5-30 cycles

Table 1: IEEE definitions for the voltage sags and swells

Power quality in the distribution system can be improved by using a custom power device DVR for voltage disturbances such as voltage sags, swells, harmonics, and unbalanced voltage. The function of the DVR is a protection device to protect the precision manufacturing process and sophisticate sensitive electronic equipments from the voltage fluctuation and power outages [4].

II. DYNAMIC VOLTAGE RESTORER

The Dynamic Voltage Restorer (DVR) (Gosh and Ledwich, 2002; Vilathgamuwa et al., 2002) has been proposed to protect sensitive loads from such voltage sags. The DVR is connected in series with the sensitive load or distribution feeder and is capable of injecting real and reactive power demanded by the load during voltage sag compensation. The output of the DVR inverter is usually provided with an output LC filter to attenuate the harmonic contents appearing in injected voltage. The filter parameters are designed according to certain design aspects such as depth of the sag to be mitigated and the load voltage [4, 6].
The general DVR configuration consists of an injection/Booster transformer, a Harmonic filter, a Voltage source converter (VSC), DC charging circuit and a Control and Protection system as shown in Figure (1) [5] [6].

II.1 principles operations of DVR

The DVR has two modes of operation which are: standby mode and boost mode. In standby mode (Vinj=0), the voltage injection transformer's low voltage winding is shorted through the converter. No switching of semiconductors occurs in this mode of operation, because the individual inverter legs are triggered such as to establish a short-circuit path for the transformer connection. The DVR will be most of the time in this mode. In boost mode (Vinj>0), the DVR is injecting a compensation

voltage through the voltage injection transformer due to a detection of a supply voltage disturbance [6, 7].

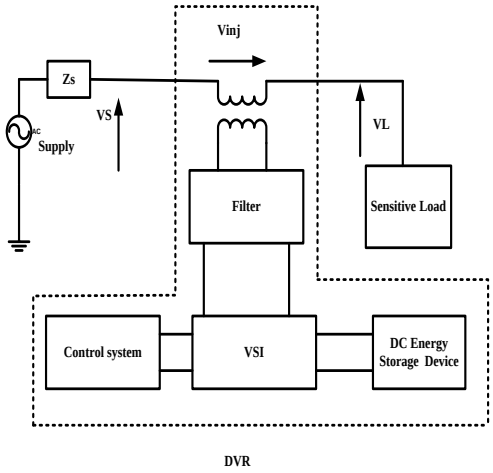

Figure 1: Dynamic Voltage Restorer (DVR) schematic diagram

II.2 Compensation technique in DVR

The most popular voltage injection strategies are [4], [5], [9]:

(a) Pre-sag compensation method
(b) In-phase compensation method
(c) In-phase advanced compensation method
(d) Voltage tolerance method with minimum energy injection

II.3 Control system

The basic functions of a controller in a DVR are the detection of voltage sag/swell events in the system, which determines the reference voltage that should be injected by DVR and the VSI control which is in this work consists of PWM with PI controller. The controller input is an error signal obtained from the reference voltage and the value of the injected voltage (Figure 2). Such error is processed by a PI controller then the output is provided to the PWM signal generator that controls the DVR inverter to generate the required injected voltage. The commutation pattern is generated by means of the sinusoidal pulse width modulation technique (SPWM); voltages are controlled through the modulation [6], [7], [8].

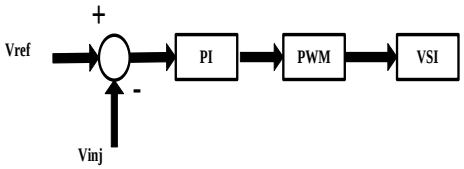

Figure 2: DVR Control scheme

III. SIMULATIONS AND RESULTS

This paper presents simulation results under SimPowerSystems – MATLAB/Simulink and DVR based real time simulation. The scheme of the system under study is shown in figure 3 and figure 4.

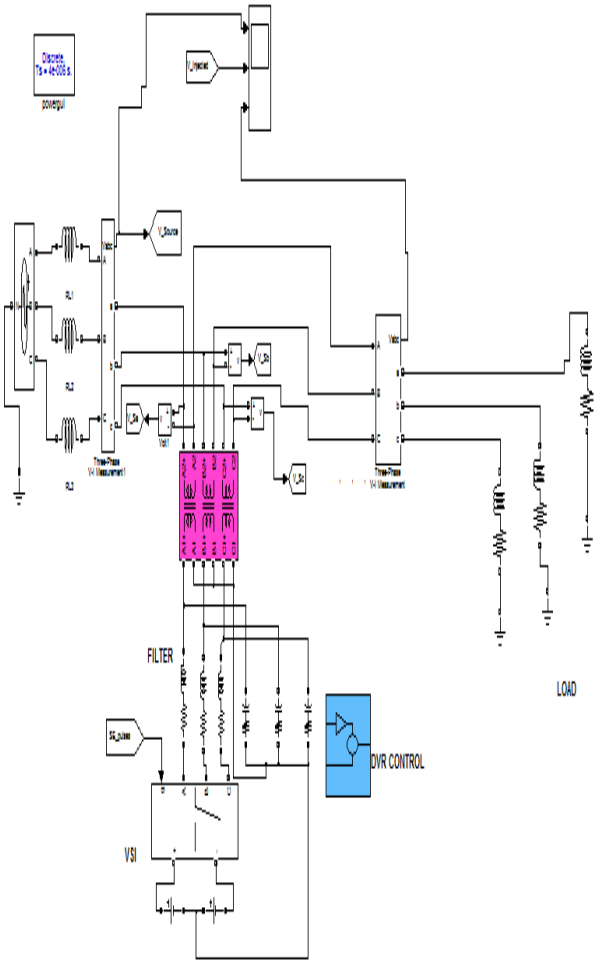

Figure 3: SIMULINK Model of the simulated system

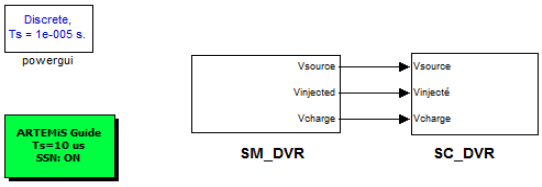

Figure 4 :RT_LAB/ SIMULINK Model of the simulated system

Using real time simulation under RT_Lab/Simulink the model is divided on two subsystems figure 4: SM_DVR: Master subsystem, and SC_DVR: Console subsystem. The two subsystems are shown in figure 5, 6.

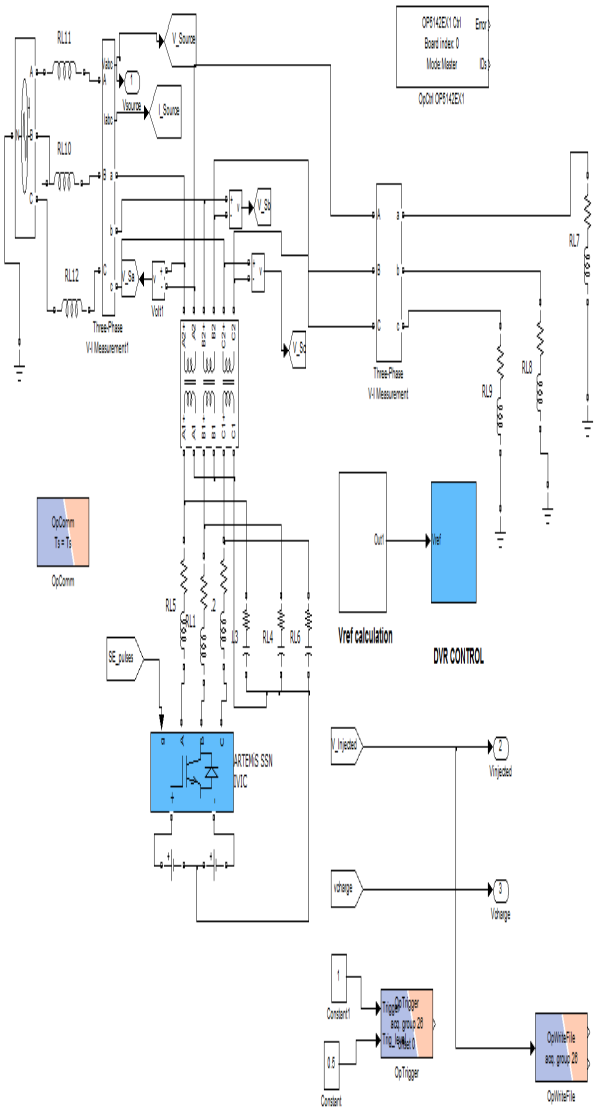

Figure 5: RT_LAB/ SIMULINK Model of the Subsystem SM_DVR

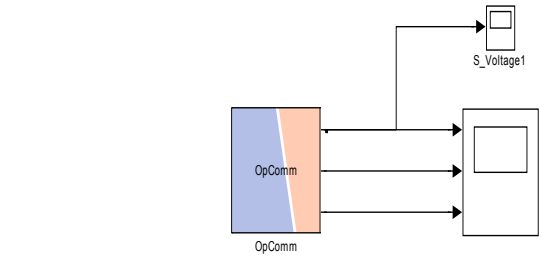

Figure 6: RT_LAB/ SIMULINK Model of the Subsystem SC_DVR

Figure 7 shows the real-time model of the proposed scheme as implemented in RT-Lab environment.

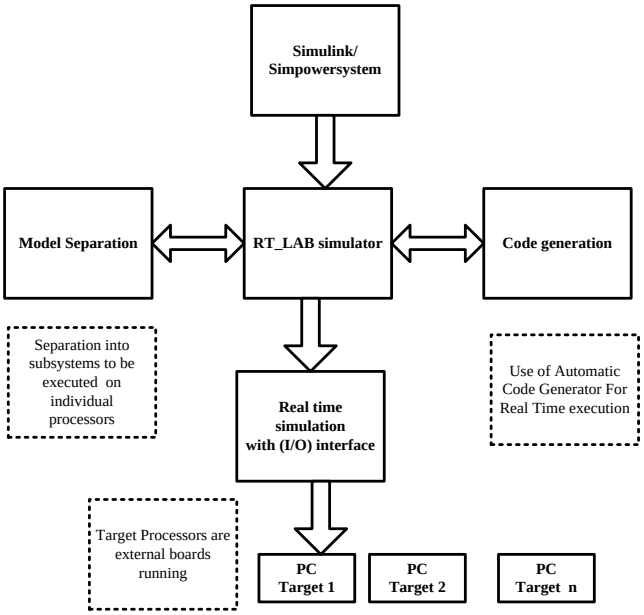

Figure 7: Real-time simulation using RT-Lab simulator.

The real-time platform RT-LAB™ provides also special libraries which allow the improvement of the system performance using Simulink/SimPowerSystems blocks for real-time simulation. ARTEMIS (Advanced Real- Time ElectroMechanical Simulator) is a tool integrated into the blockset SimPowerSystems of Simulink. It provides improved algorithms allowing simulation in realtime. RT-EVENTS Blockset is an add-on that works with MATLAB/Simulink to improve the efficiency and accuracy of continuous-time and discrete-time systems simulations whose dynamics are affected by discrete events [10].
The system parameters are shown in table 2

ISBN: 978-1-61804-228-6

Supply voltage	220
Line impedance	19.26e-7 H
Series transformer turn ratio	1
DC bus voltage	850 V
Filter inductance	1 mH
Filter capacitance	80µ F
Load resistance	10/3
Load inductance	60 mH
Line frequency	50Hz

Table 2 : system parameters

Three-phase 25 % voltage swell are simulated for two cases. The first one is trough Matlab/ simulink and the second is the real time simulation using RT_LAB simulator. For simplification the results of only one phase are shown. Voltage swell is initiated at 0.1 s and it is kept until 0.3 s, with total duration of 0.2 s. Figure 8 shows the DVR performance through MATLAB simulation, the DVR inject the voltage in order to correct the load voltage. As can be seen from the results the load voltage is kept at the nominal load value.

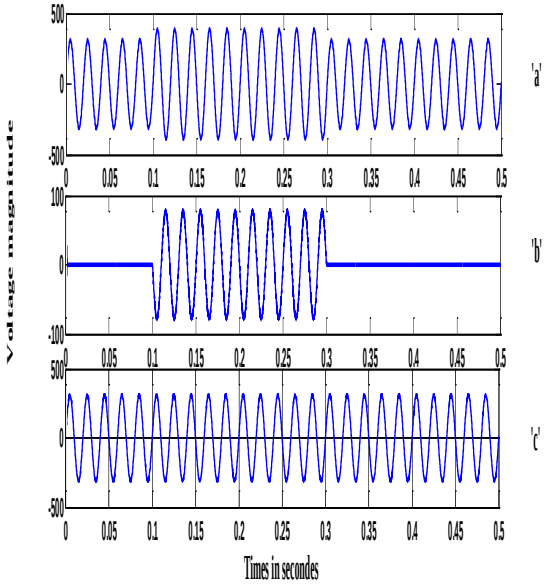

Figure 8: DVR performances with 25% voltage swell ‘a’ Voltage source
‘b’ Injected voltage
‘c’ Load voltage

.

Figure 9 shows the real time simulation of the DVR we can see the DVR performance with fixed step time of 10 µs, the DVR inject the voltage in order to correct the load voltage. As can be seen from the real time simulation results the load voltage is kept at the nominal load value. And this real time simulation justify that the proposed system can be used for the experimental part.

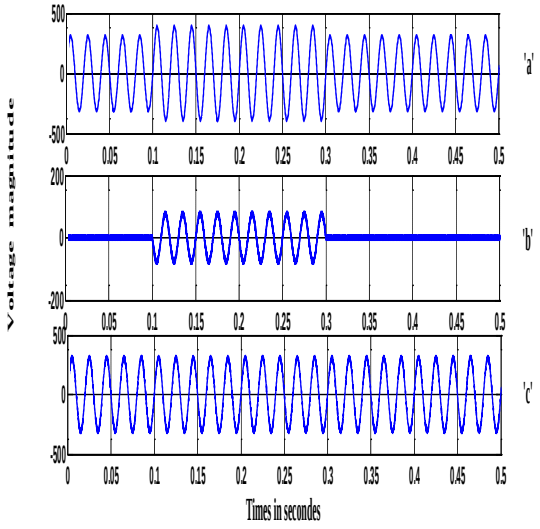

Figure 9: Real time DVR performances with 25% voltage swell ‘a’ Voltage source
‘b’ Injected voltage
‘c’ Load voltage

Three-phase 20 % voltage sags are simulated for two cases. The first one is trough Matlab/ simulink and the second is the real time simulation using RT_LAB simulator. For simplification the results of only one phase are shown. Voltage sags is initiated at 0.1 s and it is kept until 0.2 s, with total duration of 0.1 s. Figure 10 shows the DVR performance through MATLAB simulation, the DVR inject the voltage in order to correct the load voltage. As can be seen from the results the load voltage is kept at the nominal load value.

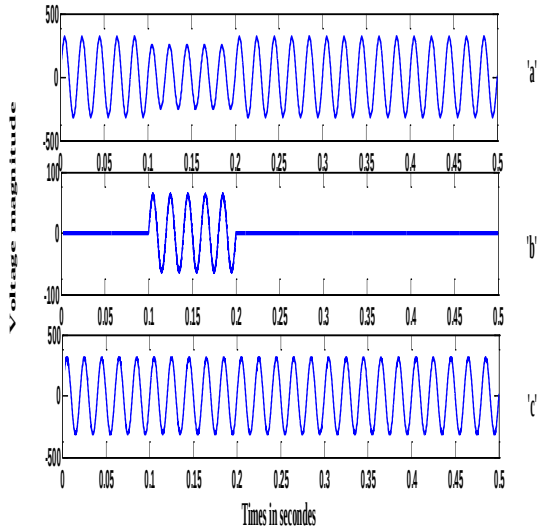

Figure 10: DVR performances with 20% voltage sags ‘a’ Voltage source
‘b’ Injected voltage
‘c’ Load voltage

ISBN: 978-1-61804-228-6

Figure11 shows the real time simulation of the DVR we can see the DVR performance with fixed step time of 10 µs, the DVR inject the voltage in order to correct the load voltage. As can be seen from the real time simulation results the load voltage is kept at the nominal load value concerning sags voltage. And this real time simulation justify that the proposed system can be used for the experimental part.

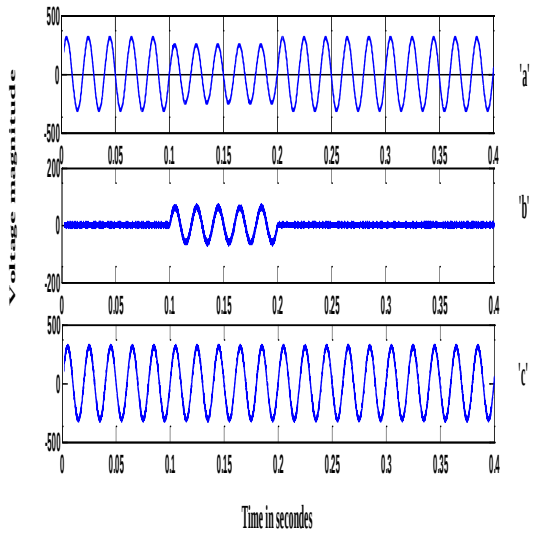

Figure: 11 Real time DVR performances with 20% voltage sags 'a' Voltage source 'b' Injected voltage 'c' Load voltage

IV. CONCLUSIONS

This paper has presented result from DVR simulation, and DVR real time simulation at the distribution line. The DVR is designed to protect the sensitive load. The PWM has been presented. The main advantage of this DVR is its simple control. The real time RT_LAB platform has been presented. The simulation results showed clearly the performance of the DVR to compensate voltage sags/ swell without any difficulties and injected the appropriate voltage to correct rapidly any anomaly in the supply voltage to keep the load voltage at the nominal value. The DVR real time simulation using RT_LAB platform has shown the ability of the proposed system to compensate voltage sags/swell at the distribution line rapidly and efficiently. This real time simulation success can be changed to the experimental prototype in the future work.

.

V. REFERENCES

[1] M. V. Kasuni Perera "CONTROL OF A DYNAMIC VOLTAGE RESTORER TO COMPENSATE SINGLE PHASE VOLTAGE SAGS" Master of Science Thesis, Stockholm, Sweden 2007.

[2] Rosli Omar,Nasrudin Abd rahim, Marizan Sulaiman MODELING AND SIMULATION FOR VOLTAGE SAGS/SWELLS MITIGATION USING DYNAMIC VOLTAGE RESTORER (DVR) ", Journal of Theoretical and Applied Information Technology page(s) 464-470; 2009.

[3] Nagendrababu Vasa, Sreekanth g, Narender reddy Narra, Dr. Srujana A "SERIES COMPENSATION TECHNIQUE FOR VOLTAGE SAG MITIGATION" IOSR Journal of Engineering (IOSRJEN), Volume 2, Issue 8 (August 2012), PP 14-24

[4] Anita Pakharia, Manoj Gupta «DYNAMIC VOLTAGE RESTORER FOR COMPENSATION OF VOLTAGE SAG AND SWELL: A LITERATURE REVIEW » International Journal of Advances in Engineering & Technology, July 2012, Vol. 4, Issue 1, pp. 347-355

[5] M. A. Taghikhani "PHASE ADVANCED DYNAMIC VOLTAGE RESTORER CONTROL SYSTEM DESIGN" International Journal of Control Science and Engineering 2012, 2(4):pp 60-68

[6] Rosli Omar,Nasrudin Abd rahim, Marizan Sulaiman, « NEW CONTROL TECHNIQUE APPLIED IN DYNAMIC VOLTAGE RESTORER FOR VOLTAGE SAG MITIGATION » American J. of Engineering and Applied Sciences 3 (1): 42-48, 2010

.

[7] B. Ferdi, C. Benachaiba, S. Dib, R. Dehini, « ADAPTIVE PI CONTROL OF DYNAMIC VOLTAGE RESTORER USING FUZZY LOGIC», Journal of Electrical Engineering: Theory and Application (Vol.1-2010/Iss.3) pp. 165-173.

[8] Rosli Omar,Nasrudin Abd rahim,« MITIGATION OF VOLTAGE SAGS/SWELLS USING DYNAMIC VOLTAGE RESTORER (DVR) » ARPN Journal of Engineering and Applied Sciences, Vol. 4, N0 4, June 2009, pp 50-56

.

[9] Tarek El-Shennawy, Mahmoud El-Gammal, Amr Abou-Ghazala, Abdel Monem MoussaMitigation of Voltage Sags in a Refinery with Induction Motors Using Dynamic Voltage Restorer (DVR)" European Journal of Scientific Research, Vol.36 No.1 (2009), pp.118-131.

[10] Steeve Beaulieu, Mohand Ouhrouche, Christian Dufour, Pierre-François Allaire "REAL-TIME MODELLING AND SIMULATION OF AN ACTIVE POWER FILTER" lASTED International Conference on Power and Energy Systems PES 2007, Clearwater, Florida, U.S.A.

Single Carrier Multi-Tone Modulation Scheme

Roman M. Vitenberg
Guarneri Communications Ltd , Israel
roman@guarneri-communications.com

Abstract—
In this paper, we propose a modulation scheme, which can improve the performance of a variety of wired and wireless communication systems.
We call this scheme "Single Carrier Multi-Tone" (SCMT) because it is a name well describes the physical principles on which it is made. This scheme was developed based on a study known SC-FDMA, OFDM and SC-FDE technologies. The aim of this research was to improve the performance of existing communication systems for terrestrial television broadcasting. The proposed modulation scheme combines the advantages of known technologies and devoid of their shortcomings. The several key characteristics of the SCMT are illustrated by the results of MATLAB simulation.

Keywords — **SC FDMA, OFDM, TV Broadcasting, SC FDE, ATSC, PAR, QAM, VSB, multipath, single carrier, Multi-tone.**

I. INTRODUCTION

Orthogonal Frequency Division Multiplexing (OFDM) is the most popular transmission technology in digital terrestrial broadcasting (DTTB), adopted by many DTTB standards.

The big advantage of OFDMA is its robustness in the presence of multipath signal propagation [2]. The immunity to multipath arises from the fact that the OFDMA system transmits information to the *M* orthogonal frequency carriers, each of which operates at 1/*M* times the bit rate of the information signal. On the other hand, the OFDMA waveform exhibits noticeable envelope fluctuations resulting in a high peak-to-average power ratio (PAPR). Signals with a high PAPR require highly linear power amplifiers to avoid excessive intermodulation distortion. To achieve this linearity, the amplifiers have to operate with a large back off from their peak power. The result is low power efficiency (measured by-the ratio of transmitting power to the power dissipated), which poses significant difficulties on portable wireless terminals.

Another problem with the OFDMA scheme in wireless transmissions derives from the inevitable offset in frequency references among the transmitted and receiver terminals. Frequency offset destroys the orthogonality of the transmissions, thus introducing subcarriers interference.

To overcome these drawbacks, 3GPP is studying a modified form of OFDMA for uplink transmissions in the "long-term evolution (LTE)" of cellular systems [12] – [15]. A modified version of OFDMA, called Single Carrier FDMA (SC-FDMA), has been described in several standard documents [13, 14] and researches [1, 12]. As in OFDMA, the transmitter in the SC-FDMA uses number orthogonal frequencies (subcarriers) to transmit information symbols. Compared to OFDMA, the mechanism significantly reduces variations in the envelope of the transmitted signal. Therefore, SC-FDMA signals have inherent lower PAPR then OFDMA signals [1].

Nevertheless, in cellular systems with severe multipath, SC-FDMA signals are sent to the base station with substantial inter-symbol interference. The base station uses an adaptive equalization in the frequency domain to cancel the interference. This arrangement makes sense in a cellular system because it reduces the distortions of the linear amplification in the portable terminal, at the cost of complexity of signal processing (frequency domain equalization) on the base station.

A similar occurs in the design terrestrial TV broadcasting systems. The great importance in such systems has the efficiency of RF transmitters.

Currently for terrestrial TV broadcasting systems is being used a single carrier 8VSB system in the United States (ATSC A/53) and OFDM system in Europe (DVB-T, DVB-T2) and Asia (ISDB-T, DTMB-T).

The OFDM DVB standard provides a large number of configurations, and useful features but requires a transmitter peak power at 6dB more than the peak power of the ATSC transmitter A/53. As a result, the benefits of DVB, obtained through the use of the LDPC code, high constellation QAM256 and decrease the number of pilots, reduced.

The indisputable advantage of DVB is the high performance of communications in a multipath channel. Therefore, the DVB terrestrial TV broadcasting system provides better connectivity with mobile objects than A/53.

The logical solution would be to use a new SC FDMA modulation for future terrestrial TV Broadcasting systems, but it is possible only after a significant improvement in the SC FDMA technology. This paper is structured as follows: in the next section describes the SC FDMA modulation scheme and discusses its shortcomings, further in the third section will be described offered by us SCMT modulation scheme. The fourth section presents the results of MATLAB simulations. In conclusion, we describe the main results of this paper.

II. SC FDMA Modulation Scheme

SC-FDMA transmitter converts the binary input signal into a sequence of modulated subcarriers. To do this, it performs the signal processing illustrated in Figure 1. Signal processing is performed during the repetitive time intervals called blocks. A block is the time used for the formation one SC FDMA symbol. During this interval, a system generates all subcarriers once. Several SC FDMA symbols combined in a transmission frame for continuous transmission.

The input binary sequence comes to the QAM Modulator, which converts binary entering into a multi-level sequence of complex numbers. The QAM modulator uses one of several possible modulation formats, including binary phase shift keying (BPSK), quaternary PSK (QPSK), 16 level quadrature amplitude modulation (16-QAM) and 64-QAM. The system adapts the modulation format and thus the bit rate according to the current channel condition of the terminal.

The transmitter sends groups of the complex numbers x (t) by packets, each of which contains N symbols. In the first stage of the SC-FDMA modulation scheme is performed N-points discrete Fourier transform (DFT), to get a frequency domain representation of the input symbols X (f). Then, it maps each of N DFT outputs to one of inputs of M-point IDFT core (M > N). Others inputs of IDTF core are connected to zero. The IDFT core generates M orthogonal subcarriers, which may be transmitted over the channel. As in OFDMA, a typical value of M is 256 subcarriers and N = M / Q is an integer divisor of M (a typical value of Q is 16). Q is bandwidth expansion factor of the sequence of characters.

As in OFDMA, the M-point inverse DFT (IDFT) converts the amplitudes of the subcarriers into the time domain signal (SC FDMA symbol) Y (t). These symbols are transmitted sequentially.

The transmitter performs two other signal processing operations prior to transmission. It inserts a set of symbols referred to as a *cyclic prefix* (CP) in order to provide a guard time to prevent inter-block interference (IBI) due to multipath propagation. .

If the length of the CP is longer than the maximum delay spread of the channel, or roughly, the length of the channel impulse response, then, there is no IBI. In general, CP is a copy of the last part of the block which is added at the beginning of each block for several reasons. . First, CP acts as a guard time between successive blocks. . Second, since CP is a copy of the last part of the block, it converts a discrete time linear convolution into a discrete time circular convolution.

Thus transmitted data propagating through the channel can be modeled as a circular convolution between the channel impulse response and the transmitted data block, which in the frequency domain is a point wise multiplication of the DFT frequency samples. Then, to remove the channel distortion, the DFT of the received signal can simply be divided by the DFT of the channel impulse response. A point-wise or a more sophisticated frequency domain equalization technique can be implemented to remove multi-path distortions.

The transmitter also performs a linear filtering operation referred to as pulse shaping in order to reduce out-of-band signal energy.

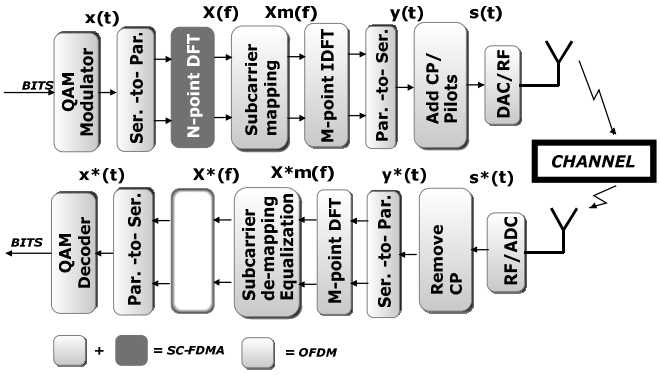

Figure 1: SC FDMA functional diagram.

OFDM has much in common with SC-FDMA. The only difference between SC FDMA and OFDM is the presence of the N-point DFT in the SC-FDMA transmitter and the N-point IDFT in the SC-FDMA receiver. For this reason, SC-FDMA is sometimes referred to as DFT-spread OFDMA. Several approaches to mapping transmission symbols X (f) to SC-FDMA subcarriers are currently under consideration. They are divided into two categories; distributed and localized. For terrestrial TV broadcasting, only localized transmission can be used.

In the localized subcarrier mapping mode, N consecutive subcarriers of IDFT are occupied by the DFT outputs of the input data resulting in a continuous spectrum that occupies a fraction of the total available bandwidth.

As it is well known, the main drawback of OFDM is the high level of peak-to-average power ratio (PARP). While PARP for the signal of a single carrier modulation is about 5~7dB, the PARP for OFDM signal is significantly higher (up to 12 dB).

PARP in SC-FDMA system is significantly lower than in the OFDM because the transmitted signals have different statistical characteristics.

Suppose that we exclude cyclic prefixes from the transmitted signal and connect the outputs of DFT appropriate to firsts N-inputs IDFT. In this case, the transmitted signal is equal to Q-times up sampled sequence of input QAM symbols. Evident that the transmitted signal will have the same statistical characteristics, including PARP, as the QAM input signal. As cyclic prefixes are represented segments of the transmitted signal y (t) that their statistical characteristics the same as the signal y (t). Therefore, PAPR of the transmitted signal s (t) is the same as PAPR of the sequence of QAM symbols x (t) passed through the output filter.

In the case of SC-FDMA modulation, the function of output filter is performed by FFT core. This filter has a rectangular shape and the bandwidth is exactly equal to $W = N*\Delta F$, where ΔF is a frequency shift between subcarriers.

ISBN: 978-1-61804-228-6

This form of the spectrum is not optimal from the point of view of obtaining the minimal PAPR, but cannot be changed in the SC-FDMA scheme.

As a result the PAPR SC-FDMA output signal (in localized subcarrier mapping mode) is significant higher than in case of using optimal output filter [5].

Unlike OFDM SC-FDMA requires an additional N-point DFT core in transmitter and N-point IDFT core in the receiver.

Below we offer an improved system that overcomes the drawbacks of the SC-FDMA.

III. Single Carrier Multi-Tone Modulation

A functional diagram of the proposed communication system is shown in Figure 2. This modulation scheme which we called the SCMT is different from the well-known scheme SC-FDMA presence up-sample unit in the transmitter and down-sample unit in the receiver. Unlike SC FDMA Transmitter, which comprises N-point DFT core and M-point IDFT core, the SCMT Transmitter comprises M-point FFT and M-point IFFT cores. Respectively, the SC FDMA Receiver comprised M-point DFT core and N-point IDFT core, unlike the SCMT Receiver, which comprises M-point FFT core and M-point IFFT core.

. Since FFT and IFT transactions can be executed with the same FFT/IFFT core at different time intervals, the complexity of SCMT equipment is the same as for OFDM. Additional in SCMT transmitter included a programmable digital filter that allows us to change the shape of the spectrum of the transmitted signal with the purpose to obtain the minimum PAPR.

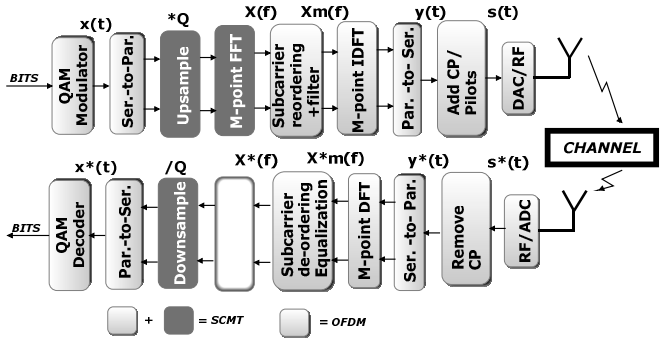

Figure 2: SCMT functional diagram.

In the proposed scheme as well as in SC-FDMA symbols generated by QAM modulator are combined into groups of N characters. These groups are converted into groups of M symbols by up-sampling. Up-sampling coefficient Q = M/N is typically 2 or 4 depends from characteristics of RF filters in transmitter equipment. M-group characters on FFT output represent a mapping of up-sampled input signal into the frequency domain. In the frequency domain the up-sampled signal occupies bandwidth equal Q*W and comprises Q copies of the input spectrum. Each FFT output is multiplied on coefficient that corresponds to a frequency characteristic of the optimal output filter. Filtered subcarriers are divided in two groups first of them occupied the lower part of spectrum, second occupied higher part of the spectrum. The reordering process performs relocation of these groups around selected carrier frequency. Wherein first group of subcarriers is placed above carrier frequency and the second group of subcarriers is placed below the carrier. Figure 3 shows the signal spectra at various stages of processing.

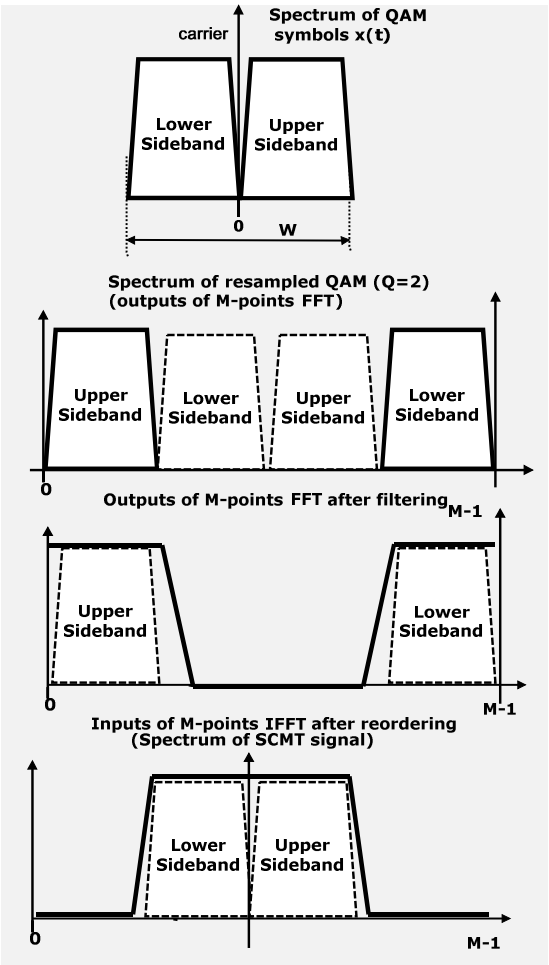

Figure 3: SCMT spectrum diagram.

The SCMT receiver performs an inverse allocation of subcarriers so the subcarriers above carrier frequency are shifted to the lower part of the spectrum and subcarriers below carrier frequency are placed at the end of the spectrum. After equalizing and re-ordering received subcarrier are processed by M-point IFFT. From the output of IFFT the groups of M-character comes to down-sampling unit. The

down-sampling unit transforms these groups in N-character packets of QAM symbols.

The proposed modulation scheme allows extensive opportunity to control the shape of the spectrum of the transmitted signal.

In particular, it is possible to create a single sideband communication system, the signal spectrum of which will correspond to the signal 8VSB. Such system can be fully backward compatible with a valid TV broadcast ATSC system. At the same time, thanks to using multi-tone technology this system can provide reliable communications with mobile devices. SCMT as OFDM are using precision equalization in the frequency domain, so both systems can use QAM modulation of high-level: 1024QAM and 4096QAM. In the case of VSB modulation, the SMNT system can operate with 16VSB, 32VSB and 64VSB signals. Therefore, the use of a single sideband SCMT modulating in future ATSC 3.0 standard TV Broadcast systems will significantly increase the speed of transmission of information.

Figure 4 shows a functional schematic of the SCMT system with single sideband transmission.

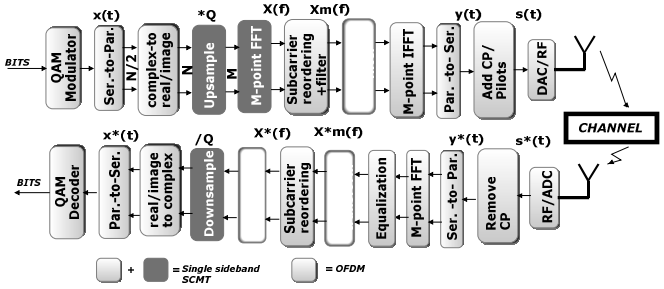

Figure 4: Single sideband SCMT functional diagram.

A single sideband SCMT transmitter comprises a sideband filter, which produces an output signal with the spectrum, which corresponds to the desired shape. In the case of an ATSC compatible broadcasting system, the sideband filter forms a spectrum of the output signal similar to a spectrum of 8VSB signal. Since the single side signal has a bandwidth W/2, then such a system transmits information with bitrate equal ½ of the bitrate double side system. Therefore, the QAM symbols are packed in N/2-character group, each of them subsequently converted into a group of N-real numbers (PAM symbols).

The single sideband receiver includes Hilbert Transform unit, which restores the suppressed sideband. This unit is placed after an equalizer and before IFFT unit. As a result, on the output of IFFT are generated M real numbers. After down-sampling N real numbers are converted into N/2 complex QAM symbols, which subsequently come to the input of QAM decoder. Figure 5 shows the signal spectrum in different processing stages.

As is clear from the functional diagram Figure 4 considered the system can operate in two modes, one with a single sideband modulation, for example VSB, and signal bandwidth W/2 and other with dual sideband QAM modulation and signal bandwidth W.

This fact may be interesting for developers of a new ATSC 3.0 standard because allows to create a TV broadcast system that will be in one mode full compatible with existing A/53 and A/153 standards and 6-MHz television channel and in other mode will be used wide 12-MHz channel. Because of using multi-tone signals and high level of QAM constellations,

This system will provide aggregate bit rate up to 72 Mbps for 6-MHz channel and up to 144 Mbps for the 12-MHz channel.

The information bit rates will be corresponding up to 60 Mbps for 6-MHz channel and up to 120 Mbps for the 12-MHz channel.

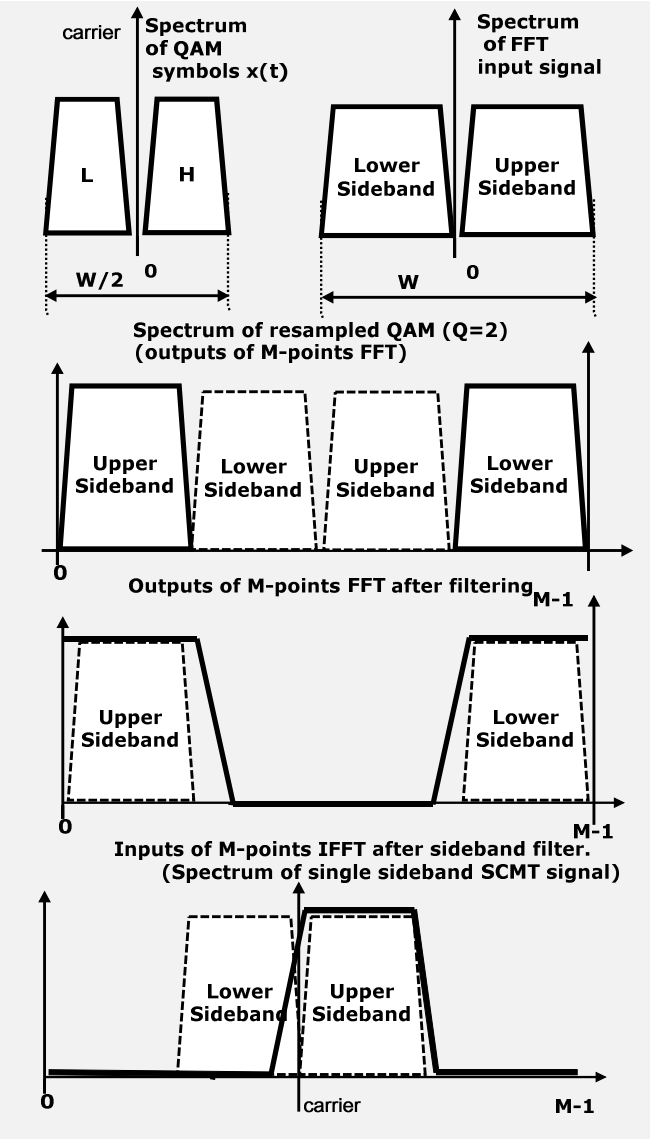

Figure 5: Single sideband SCMT spectrum diagram.

An important advantage of the proposed SCMT modulation is the possibility of inclusion in the output signal additional impulses, such as the segment sync and frame sync, which are necessary for compatibility with existing ATSC equipment. With the addition of sync pulses, the orthogonality between subcarriers is not broken, as is the case in systems with OFDM. Indeed, in OFDM system the sync pulses may be added only to the output of IFFT by summation subcarriers and said pulses. The spectrum of the sync pulses is uniformly distributed over the entire bandwidth (W) of the transmitted signal that leads to a distortion in amplitude and phase of each subcarrier. In SCMT system the sync pulses can be inserted directly in the input data stream as a specific sequence of bits.

Because this sequence is successively exposed first FFT operation and then the IFFT operation of the same dimension, waveform of signal on FAT input coincides with the envelope of signal on IFFT output. Hence, instead of OFDM, carriers' orthogonality will not fail.

The sync pulses can be easily extracted in the receiver. This process is carried out by correlation of the received signal with the pattern of modulated sync pulse. Figure 6 illustrates the process of segment sync pulse insertion in the ATSC compatible system.

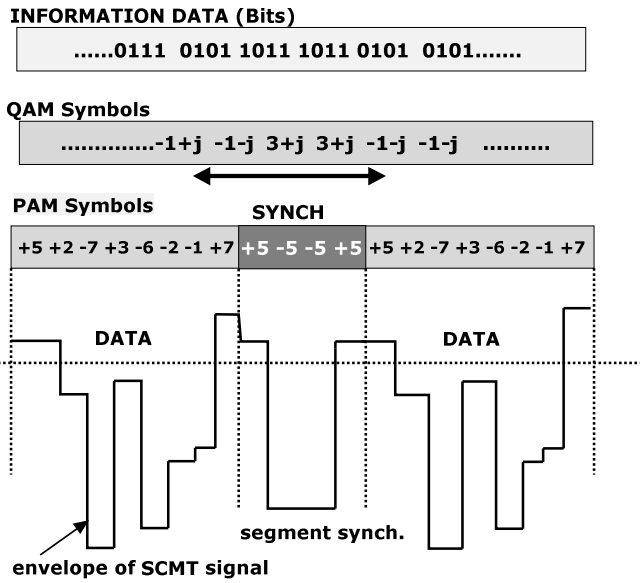

Figure 6: Insertion of segment synchronization pulse.

The described terrestrial TB broadcasting system uses a single-sideband transmission by 2048 carriers in 6 MHz bandwidth. The spectrum of the transmitted signal is similar to the spectrum of the existing system using 8VSB modulation.

The designed scheme uses the same structure of the transmitted signal as the current system. Partially the frame and segment sync signals are identical. Data frames of transmitting signal can include as data fields, which use existing technology in accordance with A/53 and A/153 standards, so a data field with SCMT technology.

Figure 7 shows the data field of the transmitted signal of our proposed broadcasting system that will be fully compatible with the existing A/53 and A/153 standards. The data field has the standard length 24.2 ms and comprises a standard field synchronization block FS and exactly 52 data symbols each of them includes one IFFT symbol, cyclic prefix, windowing interval and 6 segment sync impulses. The Data's symbol has a length equal 464us. The cyclic prefix length is about 17% of data symbol.

The system utilizes the same clock frequency as existing A/53 systems and can simultaneously transmit standard A/53, A/153 and SCMT data fields.

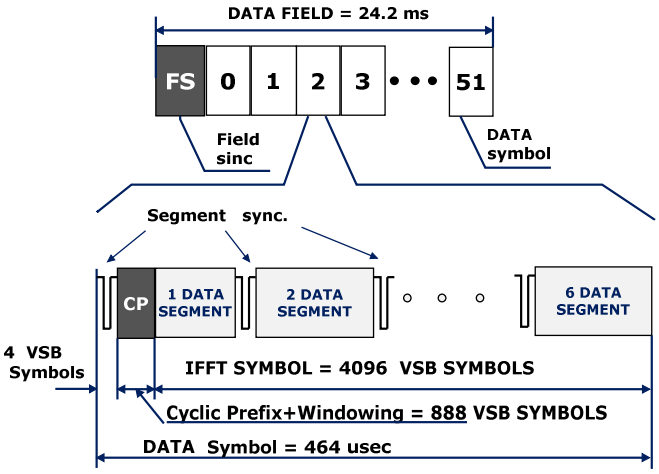

Figure 7: Data field of TV broadcast SCMT system

Instead of standard frames, which use only 8VSB modulation, SCMT frames may carry signals of 16VSB, 32VSB or 64VSB modulation. Thus, the SCMT data frames can significantly increase throughput of the TV broadcast system.

IV. MATLAB Simulations of the SCMT System

Below we report results of MATLAB simulations SCMT TV Broadcast system with next parameters:

1. Frequency Bandwidth : 6 MHz
2. IFFT/FFT size : 8K
3. Number of carriers : 2K
4. Type of system : single sideband
5. Modulation : 8VSB, 16VSB, 32VSB, 64VSB

Figure 8 shows the spectrum of designing system in the case of the filter with a rectangular shape and bandwidth W = 2K* ΔF.

Figure 9 shows PAPR of output signal in this case.

Figure 10 shows spectrum of system with raised-cosine filter and roll-off factor 0.25.

ISBN: 978-1-61804-228-6

Figure 11 shows PAPR for output signal a system with raised-cosine filter.

Figure 12 illustrates a low level of the peaks in the output signal of SCMT system

Figure 13 shows a constellation diagram in single sideband SCMT system on the output of QAM decoder for 16VSB mode of operation

Figure 13 shows a constellation diagram in single sideband SCMT system on the output of QAM decoder for 64VSB mode of operation

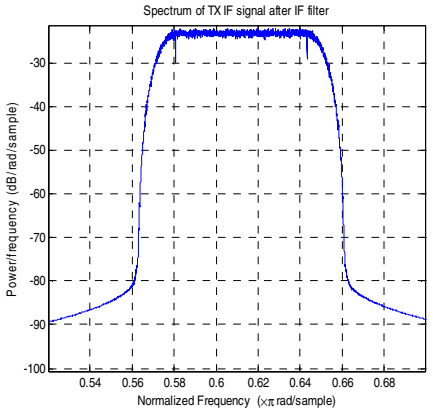

Figure 10: Spectrum of output signal (Raised-cosine filter)

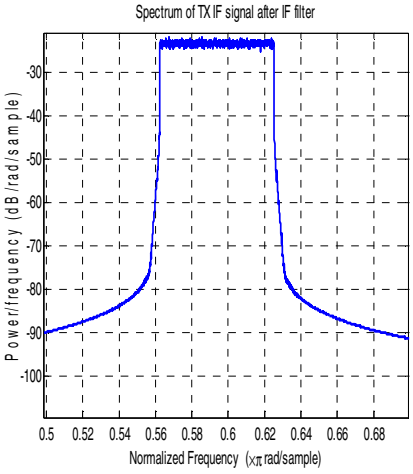

Figure 8: Spectrum of output signal (filter with a Rectangular shape)

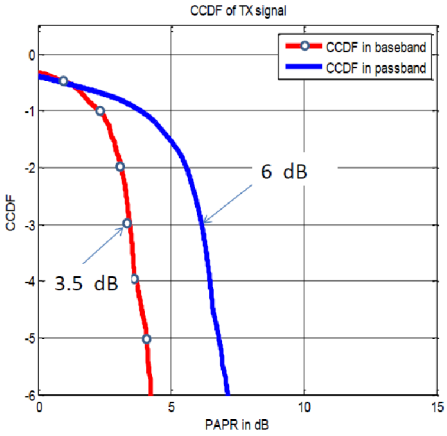

Figure 11: PAPR of output signal (Raised-cosine filter)

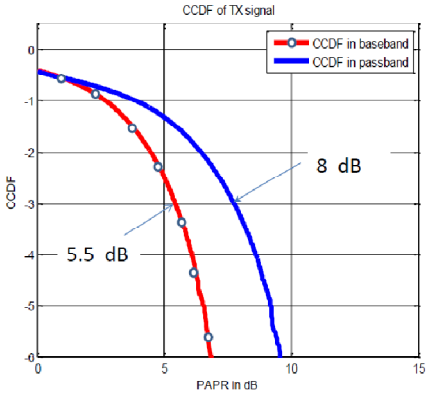

Figure 9: PAPR of output signal (filter with a Rectangular shape)

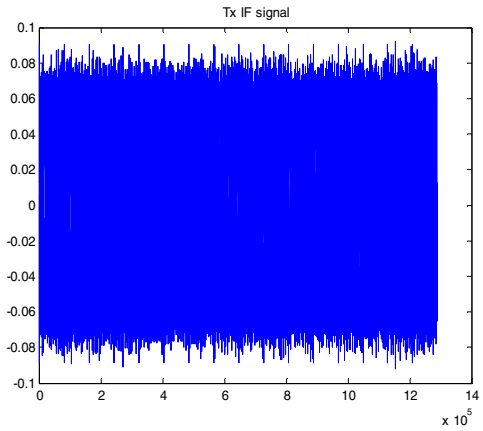

Figure 12: SCMT output signal (PARP ~ 6 dB)

ISBN: 978-1-61804-228-6

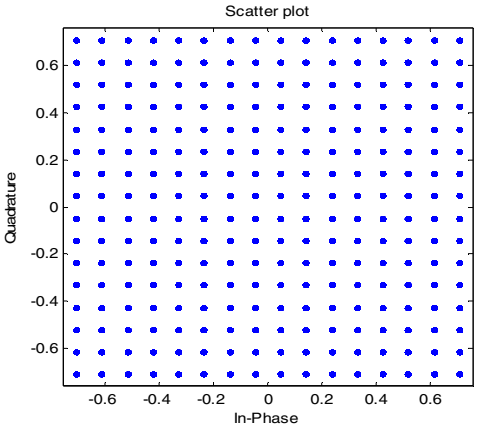

Figure 13: Constellation of received signals. (16VSB mode)

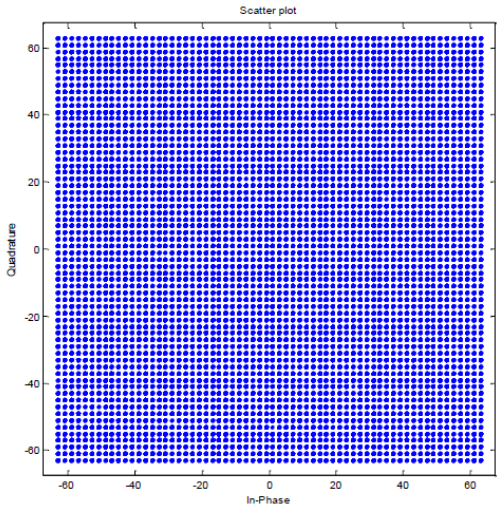

Figure 14: Constellation of received signals. (64VSB mode)

V. CONCLUSIONS

We have presented the results of a study of a Single Carrier Multi-Tone modulation scheme, which can be successfully used in TV broadcast terrestrial systems and other communication devices that require reliable communication in the presence of reflected signals. Instead of OFDM, proposed system demonstrates low peak-to-average power ratio of the output signal and, therefore, can use low power transmitters. The proposed system provides better performance than known SC-FDMA system and can be used for single sideband transmission. The MATLAB simulations show that SCMT modulation can be a real candidate for a new physical layer for future terrestrial TV broadcasting system and can be used in developing of ATSC 3.0 standard.

REFERENCES

[1] H. G. Myung, J. Lim, and D. J. Goodman, "Single carrier FDMA for uplink wireless transmission," *IEEE Veh. Technol. Mag.*, vol. 1, no. 3, pp. 30–38, 2006.
[2] N. Benvenuto, R. Dinis, D. Falconer, and S. Tomasin, "Single carrier modulation with nonlinear frequency domain equalization: an idea whose time has come–again," *Proc. IEEE*, vol. 98, no. 1, pp. 69–96, 2010.
[3] D. Wulich and L. Goldfeld, "Bound of the distribution of instantaneous power in single carrier modulation," *IEEE Trans. Wireless Commun.*, vol. 4, pp. 1773–1778, July 2005.
[4] S. Daumont, B. Rihawi, and Y. Lout, "Root-raised cosine filter influences
on PAPR distribution of single carrier signals," in *Proc. 2008 Int. Symp. Commun., Contr. and Signal Process.*, pp. 841–845.
[5] Hideki Ochiai, "On Instantaneous Power Distributions of Single-Carrier FDMA Signals" IEEE WIRELESS COMMUNICATIONS LETTERS, VOL. 1, NO. 2, APRIL 2012
[6] M. Tanahashi and H. Ochiai, "On the distribution of instantaneous power in single-carrier signals," *IEEE Trans. Wireless Commun.*, vol. 9, pp. 1207–1215, Mar. 2010.
[7] H. Ochiai, "Exact and approximate distributions of instantaneous power for pulse-shaped single-carrier signals," *IEEE Trans. Wireless Commun.*, vol. 10, pp. 682–692, Feb. 2011.
[8] T. Frank, A. Klein, and T. Haustein, "A survey on the envelope fluctuations of DFT precoded OFDMA signals," in *Proc. IEEE ICC 2008*, pp. 3495–3500.
[9] D. Falconer, "Linear precoding of OFDMA signals to minimize their instantaneous power variance," *IEEE Trans. Commun.*, vol. 59, no. 4, pp. 1154–1162, 2011.
[10] D. Falconer, S.L. Ariyavisitakul, A. Benyamin-Seeyar, and B. Eidson, "Frequency Domain Equalization for Single-Carrier Broadband Wireless Systems," *IEEE Commun. Mag.*, vol. 40, no. 4, pp. 58–66, Apr. 2002.
[11]. H. Sari, G. Karam, and I. Jeanclaude, "Transmission Techniques for Digital Terrestrial TV Broadcasting," *IEEE Commun. Mag.*, vol. 33, no. 2, pp. 100–109, Feb.1995.
[12]. J. Lim, H.G. Myung, and D.J. Goodman, "Proportional Fair Scheduling of Uplink Single-Carrier FDMA Systems," to be presented at *The 17th Annual IEEE International Symposium on Personal, Indoor and Mobile Radio Communications (PIMRC'06)*, Helsinki, Finland, Sep. 2006.
[13] *3rd Generation Partnership Project (3GPP); Technical specification group radio access network; Physical layer aspects for evolved UTRA (Release 7)*
[14] 3rd Generation Partnership Project; Technical Specification Group Radio Access Network, *Physical Layer Aspects for Evolved Universal Terrestrial Radio Access (UTRA)*, 3GPP TR 25.814 V7.1.0, Sep. 2009.
[15] *Evolved Universal Terrestrial Radio Access (E-UTRA); User Equipment (UE) radio transmission and reception (Release 8)*, 3GPP TS 36.101 v8.7.0, Sep. 2009.

AREA EFFICIENT MULTIBAND FREQUENCY DIVIDER

C.Jagadeeshwaran, C.Sundarrasu

[1]*Department of ECE, Sasurie College of Engineering, India*

E-mail: jagadeeshwaranpc@gmail.com

[2]*Department of ECE, Sasurie College of Engineering, India*

E-mail: Sundar24940@gmail.com

Abstract:

In this paper the prescaler circuit which is used by frequency synthesizers of Bluetooth, zigbee and WLAN is proposed with multi modulus 32/33/47/48 prescaler, New E-TSPC 2/3 prescaler, P-counter and S-counter. This proposed prescaler can divide the frequency in three bands 0f 2.4-2.484GHz, 5.15-5.35GHz and 5.725-5.825GHz with a resolution selectable from 1-25MHz.The Area and power consumed by the multimodulus prescaler circuit is minimized.

Keywords:

DFF, frequency synthesizer, E-TSPC, wireless LAN (WLAN), true single phase clock (TSPC)

1. INTRODUCTION

Wireless LAN (WLAN) in the multigigahertz bands, such as HiperLAN II and IEEE 802.11a/b/g, are the leading standards for high-rate data transmissions, and standards like IEEE 802.15.4 are recognized for low-rate data transmissions. The demand for lower cost, lower power, and multiband RF circuits increased in conjunction with need of higher level of integration. The frequency synthesizer, usually implemented by a phase-locked loop (PLL) is one of the power-hungry blocks in the RF front-end, and the first-stage frequency divider consumes a large portion of power in a frequency synthesizer. The integrated synthesizers for WLAN applications at 5GHz reported in [3] consume up to 25mW in CMOS realizations.

The frequency synthesizer reported in [4] uses an E-TSPC prescaler as the first-stage divider, but the divider consumes around 6.25mW. A low-power clock multiband divider for Bluetooth, Zigbee, and IEEE 802.15.4 and 802.11 a/b/g WLAN frequency synthesizers based on pulse-swallow topology is reported in [1], and it is implemented using a 0.18µm CMOS technology. The multiband divider consists of a wide band multimodulus 32/33/47/48 prescaler and swallow (S) counter and p-counter. In this proposed system the E-TSPC 2/3 prescaler in [1] is replaced by the New E-TSPC 2/3 prescaler[2], which consumes low power and area when compared to the existing design.

2. BLOCK DIAGRAM

In the existing system, a dynamic logic multiband flexible integer-N divider based on pulse-swallow topology is proposed, which uses a low-power wide band 2/3 prescaler and a wide band multimodulus 32/33/47/48 prescaler as shown in Fig.1. The divider also used an improved low-power loadable bit-cell for the Swallow S-counter and P- Counter. Fig.2 shows the proposed multi modulus 23/33/47/48 prescaler block with New E-TSPC 2/3 Prescaler [2]

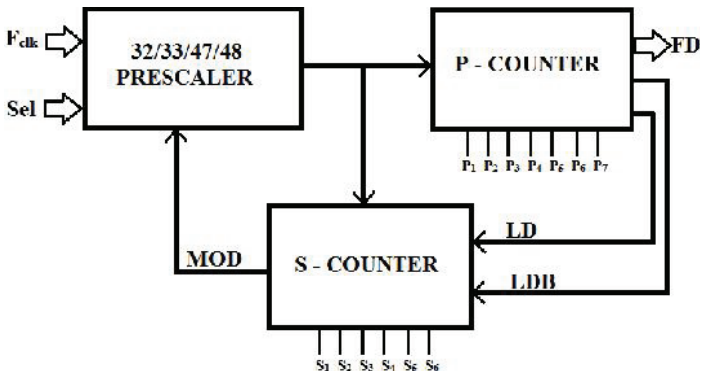

Fig.1. Multiband Divider Block

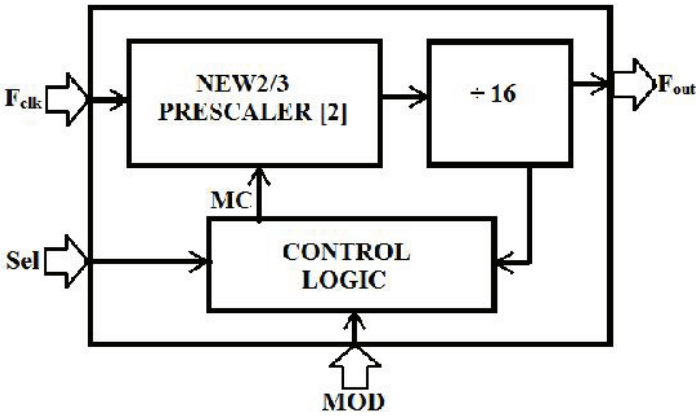

Fig.2. Proposed Multi-Modulus 32/33/47/48 Prescaler

3. NEW E-TSPC 2/3 PRESCALER

This New low power E-TSPC 2/3 prescaler is introduced from [2] which is shown in Fig.3, and this is the further improved version of the Existing prescaler. It consist of two flipflops and the and gate as like previous design. The OR gate used for the divide control is replaced with a PMOS transistor, it act likes a switch. Note that there is a negation bubble at one of the AND gate's input. The output *Q* of FF1 is thus complemented before being fed to FF2. When the switch is open, the input from FF1 is disconnected and FF2 alone divides the clock frequency by 2. When the switch is close, FF1 and FF2 are linked to form a counter with three distinct states. Besides the speed advantage, E-TSPC FFs are particularly useful for low voltage operations because of the minimum height in transistor stacking.

ISBN: 978-1-61804-228-6

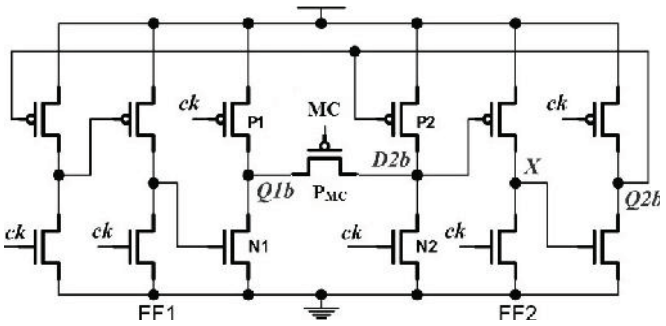

Fig.3. New E-TSPC 2/3 Prescaler

Other than the two E-TSPC FFs, only one pMOS Transistor (P_{MC}) is needed. The pMOS transistor controlled by the divide control signal serves as the switch. The AND gate plus its input inverter are achieved by way of wired-AND logic using no extra transistors at all. The proposed design scheme is far more sophisticated than the measure of simply adding one pass transistor may suggest. First of all, unlike any previous designs, the E-TSPC FF design remains intact without any logic embedding. Both speed and power behaviors are not affected, which indicates a performance edge over the logic embedded FF design. Secondly, the inverter to complement the one of the two E-TSPC FF outputs for divide-by-3 operations is removed in the proposed design. The circuit simplification, again, suggests the improvements in both speed and power performances.

4. 32/33/47/48 PRESCALER

The proposed wide band multimodulus prescaler is shown in Fig.4, which can divide the input frequency by 32, 33, 47, and 48. It is similar to the 32/33 prescaler. But it consists of additional inverter and a multiplexer as like existing design. This prescaler performs additional divisions (divide- by-47 and divide-by-48) without any extra flip-flop, thus saving a considerable amount of power and also reducing the complexity of multiband divider which will be discussed below. The multimodulus prescaler consists of New E-TSPC 2/3 prescaler [2], four divide-by-2 circuits ((AD)=16) and combinational logic circuits for getting multiple division ratios. Beside the usual MOD signal for controlling N/(N+1)) divisions, the additional control signal Sel is used to switch the prescaler between 32/33 and 47/48 modes.

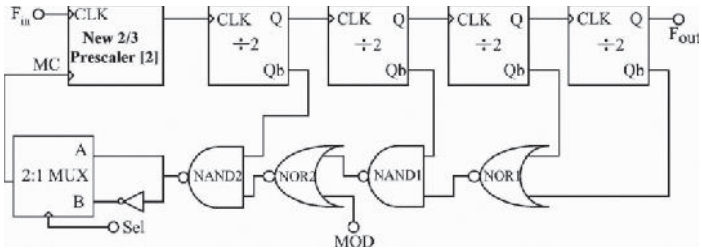

Fig.4. Multimodulus 32/33/47/48 Prescaler Using New E-Tspc 2/3 Prescaler

4.1. CASE 1: Sel= '0'

When Sel = '0' , the output from the NAND2 gate is directly transferred to the input of 2/3 prescaler and the multimodulus prescaler operates as the normal 32/33 prescaler, where the division ratio is controlled by the logic signal MOD. If MC='1', the 2/3 prescaler operates in the divide-by-2 mode and when MC='0', the 2/3 prescaler operates in the divide-by-3 mode. If MOD = '1', the NAND2 gate output switches to logic "1" (MC = '1') and the wide band prescaler operates in the divide- by-2 mode for entire operation. The division ratio N of the multimodulus prescaler is

$$N= (AD*N_1) + (0* (N_1 + 1)) = 32. \quad (1)$$

Where N_1 = '2' and AD = '16' is fixed for the entire design. If MOD = '0' , for 30 input clock cycles 'MC' remains at logic "1", where wideband prescaler operates in divide-by-2 mode and, for three input clock cycles, 'MC' remains at logic "0" where the wideband prescaler operates in the divide-by-3 mode. The division ratio N+1 of the multimodulus prescaler is

$$N+1 = ((AD - 1) * N_1) + (1 * (N_1 +1)) = 33. \quad (2)$$

4.2 CASE 2: Sel = '1'

When Sel = '1', the inverted output of the NAND2 gate is directly send to the input of 2/3 prescaler and the multimodulus prescaler operates as a 47/48 prescaler, and the division ratio is controlled by the signal 'MOD'. If MC='1', the 2/3 prescaler operates in divide-by-3 mode and when MC='0', the 2/3 prescaler operates in divide-by-2 mode'. If MOD='1', the division ratio N +1 performed by the multimodulus prescaler is same as (1) except that the wide band prescaler operates in the divide-by-3 mode for the entire operation given by

$$N +1 = (AD * (N_1 + 1)) + (0 * N_1) = 48 \quad (3)$$

If MOD = '1', the division ratio N performed by the multimodulus prescaler is

$$N = ((AD - 1) * (N_{1+1})) + (1 * N_1) = 47 \quad (4)$$

5. MULTIBAND FLEXIBLE DIVIDER

The single-phase clock multiband flexible divider which is shown in Fig.1, consists of the Proposed multimodulus 32/33/47/48 prescaler, a 7-bit programmable P-counter and a 6-bit swallow S-counter. The multimodulus 32/33/47/48 precaler is briefly discussed in Section IV. The control signal Sel decides whether the divider is operating in lower frequency band or higher band. The operation of P-counter and S-counter are same as the existing system[1]

6. SIMULATIONS

The proposed multimodulus prescaler has the maximum operating frequency of 7.2 GHz (simulation)[1]. The simulation results of this proposed multimodulus prescaler in different mode of operation (32/33/47/48) is shown in the Fig.7. These simulation waveforms are carried out by using Modelsim 6.4c(Verification tool)

(a)

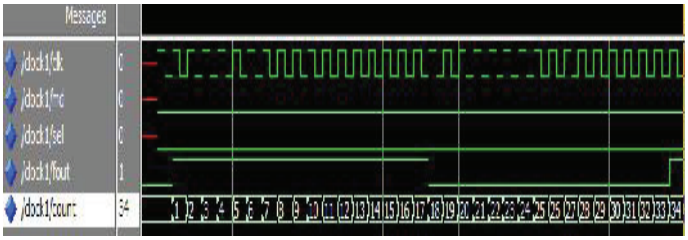

(b)

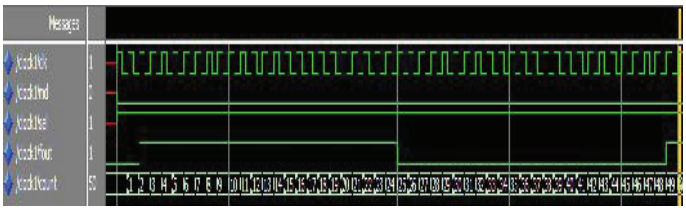

(c)

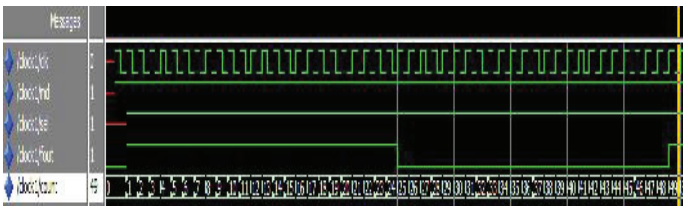

(d)

Fig.7. Simulation Result of Multimodolus Prescaler during (a)divide by 32 mode, (b) divide by 33 mode, (C) divide by 47 mode, (d) divide by 48 mode.

The simulation waveform of the entire divider block including P & S counter and "FD" for some clock cycles is shown in the Fig. 8.

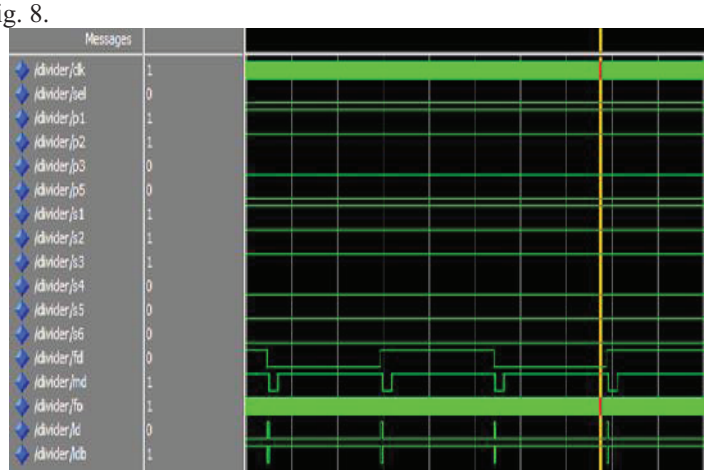

Fig.8. Simulation Waveform of Multiband Divider

The proposed design is implemented using Xilinx ISE 10.1i (Synthesis Tool). The area utilization (Equivalent gate count) of the proposed multiband divider using New E-TSPC 2/3 prescaler is less, when compared to the existing design [1], without any change in the operation sequence. The area utilization of proposed and existing system is shown in the Fig.9. The result comparison are shown in the Table 1

Device Utilization Summary			
Logic Utilization	**Used**	**Available**	**Utilization**
Total Number Slice Registers	29	9,144	1%
Number used as Flip Flops	19		
Number used as Latches	10		
Number of 4 input LUTs	51	9,144	1%
Logic Distribution			
Number of occupied Slices	51	3,072	1%
Number of Slices containing only related logic	45	45	100%
Number of Slices containing unrelated logic	0	45	0%
Total Number 4 input LUTs	62	9,144	1%
Number used as logic	51		
Number used as Shift registers	1		
Number of bonded IOBs	12	178	6%
Number of GCLKs	1	4	25%
Number of GCLKIOBs	1	4	25%
Total equivalent gate count for design	636		
Additional JTAG gate count for IOBs	624		

(a)

Device Utilization Summary			
Logic Utilization	**Used**	**Available**	**Utilization**
Total Number Slice Registers	29	9,144	1%
Number used as Flip Flops	19		
Number used as Latches	10		
Number of 4 input LUTs	51	9,144	1%
Logic Distribution			
Number of occupied Slices	45	3,072	1%
Number of Slices containing only related logic	45	45	100%
Number of Slices containing unrelated logic	0	45	0%
Total Number of 4 input LUTs	51	9,144	1%
Number of bonded IOBs	12	178	6%
Number of GCLKs	1	4	25%
Number of GCLKIOBs	1	4	25%
Total equivalent gate count for design	508		
Additional JTAG gate count for IOBs	624		

(b)

Fig.9. (a) Area Utilization of Existing Design, (b) Area Utilization of Proposed Design.

Table 1 Result Comparison.

Logic Utilization	In This Paper	Existing Design [1]
Total No. of Slice Registers	29	29
No. of Occupied Slice	45	51
Total No. of 4 Input LUTs	51	62
Total Equivalent Gate Count	508	636

ISBN: 978-1-61804-228-6

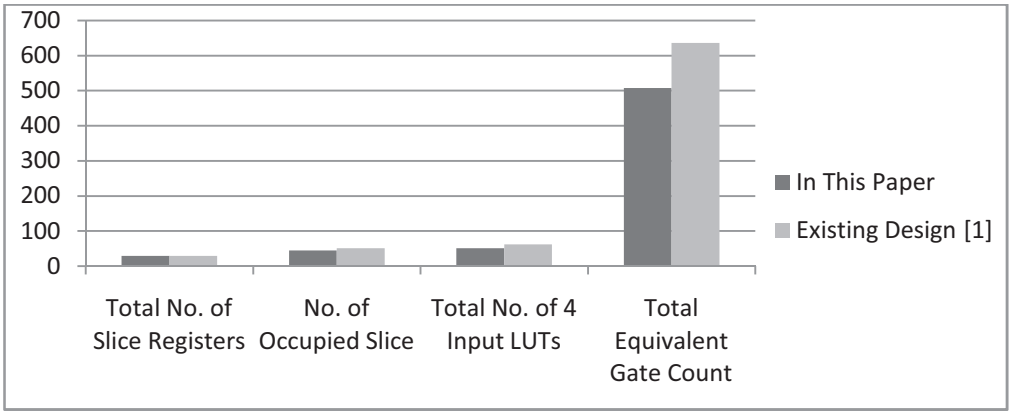

7. CONCLUSION

In this paper, New E-TSPC 2/3 prescaler is used in wide band multimodulus 32/33/47/48 prescaler. A dynamic logic multiband flexible integer-N divider is designed which uses E-TSPC 2/3 prescaler [2]. The P-counter and S-counter values are programmable and it is programmed to the divider between the range of 1 to 6.2 GHz with finest resolution of 1 MHz and variable channel spacing. since interest lies in the 2.4- and 5–5.825-GHz bands of operation, the P- and S-counters are programmed accordingly. The proposed multiband flexible divider also uses an improved loadable bit-cell for P & S counters. The overall equivalent gate count of the design is reduced to 508 from 636.

REFERENCES

[1] Vamshi Krishna Manthena, Manh Anh Do, Chirn Chye Boon, and Kiat Seng Yeo, "*A Low-Power Single- Phase Clock Multiband Flexible Divide,r*" IEEE Transactions On Very Large Scale Integration (VlSI) Systems, Vol. 20, No. 2, February 2012

[2] Yin-Tsung Hwang and Jin-Fa Lin "*Low Voltage and Low Power Divide-By-2/3 Counter Design Using Pass Transistor Logic Circuit Technique*" IEEE Transactions On Very Large Scale Integration (VLSI) Systems, Vol. 20, No. 9, September 2012

[3] H.R.Rategh et al., "*A CMOS frequency synthesizer with an injectedlocked frequency divider for 5-GHz wirless LAN receiver,*" IEEE J. Solid-State Circuits, vol. 35, no. 5, pp. 780–787, May 2000.

[4] S. Pellerano et al., "*A 13.5-mW 5 GHz frequency synthesizer with dynamic-logic frequency divider*," IEEE J. Solid-State Circuits, vol. 39, no. 2, pp. 378–383, Feb. 2004.

[5] X. P. Yu et al., "Design *of a low power wideband high resolution programmable frequency divider*," IEEE Trans. Very Large Scale Integr. (VLSI) Syst., vol. 13, no. 9, pp. 1098–1103, Sep. 2005.

Analysis of Voice Over Wi-Fi in a Wireless Lan with IEEE 802.11b Standard

Zubeir Izaruku Dafalla and Mayyada Harmoshi
Salalah College of Applied Sciences,
Department of Information Technology,
Sultanate of Oman.
E-mail: zubeir.sal@cas.edu.om

Abstract

Voice over Wi-Fi (VoWi-Fi) emerged after Voice over IP (VoIP) proved to be a useful technology to replace usual coaxial cable phone system. The breakthrough in VoWi-Fi may affect the cell phone business in the near future due to its lower cost, mobility and portability. In this paper, performance analysis of voice quality over the Wi-Fi network based on the IEEE 802.11b standard was done through simulation and the results analyzed in detail.

1. Introduction

The idea of VoWi-Fi actually comes from mobile applications where mobile terminals that were predominantly meant for voice only services can support other data related applications such as SMS (short message services) few years ago. The idea of VoWi-Fi was derived from the fact that the existing wireless local area networks, which were initially design to support data communications, can eventually support voice communication. However, there are issues pertaining to the voice quality that a wireless network can support due to its limited resources. This resulted in many manufacturers like Cisco, SpectraLink, Meru Networks and AirFlow Networks coming out with their own designs and implementations to support voice over wireless network. Even IEEE 802.11 Task Group E came out with the standard 802.11e which is dedicated for multimedia applications like voice and video over the wireless networks. In this paper, we attempted to see how voice can be delivered over WLAN. Services provided by MAC as well as Real Time Transport Protocol (RTP) and Real Time Transport Control Protocol (RCTP) will be discussed. The rest of the paper is organized as follows: Section 2 covers medium access control methods used in Wi-Fi, Section 3 coverers voice encoding and compression techniques used in wired and wireless networks, section 4 covers simulation methodology and results discussion and finally section 5 concludes the paper.

2. Medium Access control Methods for Transmitting Voice over Wi-Fi

The proliferation of internet protocol (IP) into wireless domain like GPRS, 3G and Wireless LAN has further increase the challenge of delivering real time services like voice and video over these bearers. Data is transmitted over IEEE 802.11 medium by using either the Distributed Coordination Function (DCF) or Point Coordination Function (PCF).

2.1 Distributed Coordination Function (DCF)

DCF is used as the core mode of operation for distributed infrastructure (star) network. It uses a contention based access method. A mobile node that is ready to transmit a frame will sense the medium. If the medium is busy, it will wait for an additional predetermined period of time of DIFS length. During that contention period, the mobile node will calculate the random back-off time by multiplying the time slot picked up in the window by a random number. The mobile number ticks down the random back-off time, checking to see if the medium is busy. The mobile

ISBN: 978-1-61804-228-6

node with the shortest time gain access to the medium first and transmits its frame. The collisions can now occur only when two or more mobile nodes select the same time slot to transmit. These mobile nodes will have to re-enter the contention procedure to select the same time slot to retransmit the collided frames [2].

2.2 Point Coordination Function (PCF)

PCF is specified in IEEE 802.11 as an optional protocol framing method. PCF was designed to accommodate those services requiring both voice and data transaction. PCF works in round robin fashion [2].

Version	P	CRC Count	Marker	Payload Type	Sequence	#
Timestamp						
Synchronization Source (SSRC) Identifier						
Contributing Source (CCRC) Identifier						
Payload						

Figure 1. The real-time transport protocol (RTP) used to deliver real-time data such as voice and video over the network whether it is wireless or wired networks [2]

3. Voice Encoding and Compression Techniques

The real key to sending voice over any packet data network (wireless or wired) is encoding and compression. Encoding digitizes analog signal like voice. Compression offers several advantages, one of which is the reduction of raw bandwidth required to support the information transfer [2]. VoWi-Fi like VoIP makes use of Digital Signal Processors (DSP) which is the engine for voice coders to compress as well as convert analog voice signal into data packet (RTP packet) so that they can be transported over an IP-based network [2]. The term DSP refers to the combined effort of DSPs and codec (compression and decompression) to perform the conversion of analog and digital signals into IP communication flows. There are a few voice encoding and compression technique like PCM (G.711), ADPCM (G.726) and many others.

3.1 Pulse Code Modulation

Pulse Code Modulation or PCM is a digital scheme for transmitting analog signal. The signals in PCM are binary, where there are two possible states: logic 1 (high) and logic 0 (low). This is always true no matter how complex the waveform happens to be. PCM is possible to digitize all form of analog data, including motion video, voice, music, telemetry and virtual reality (VR). To obtain PCM from analog waveform at the transmitting end of a communication system, the analog amplitude is sampled at regular intervals. The sampling rate is several times the maximum frequency of the analog waveform in cycles per second or Hertz. The instantaneous amplitude of the analog waveform at each sampling is round off to the nearest level. This process is known as quantization. The number of levels is always a power of 2 such as 4, 8, 16, 32, and 64.

3.3 Real Time Transport Protocol

Real-time Transport Protocol (RTP) is an application layer protocol. It is an IP-based protocol providing support for the transport of real-time data such as video and voice. It used lover level protocol such as User Data Protocol (UDP) and Transport Control Protocol (TCP) for the transport across the network [2]. See figure 1 for details.

In most situations UDP is used instead of TCP especially for transmitting multimedia applications like voice and video across a wireless network. UDP has less overhead since it does not provide several functions such as sequencing the datagrams. It sends, packet receipt verification, missing packet retransmission and other flow control services. Regardless of the underlying network protocol used, RTP provides data transport for real-time data like voice. It provides several functions to ensure data is synchronized for all users and will be recombined correctly at the receiving end by using the information contained in the RTP packet [2].

However, an RTP packet is still just a packet and there are several problems packets have that are magnified when dealing with real-time information. First, packets may or may not be received when they are, they may not be in the same order as when they were sent. This makes reconstructing the packet stream in the proper order and requesting missing packets very important [2]. This resulted in the design of another protocol known as Real-time Transport Control Protocol which works along side with RTP to provide feedback for flow control to manage several aspects of the delivery of real-time content [2].

ISBN: 978-1-61804-228-6

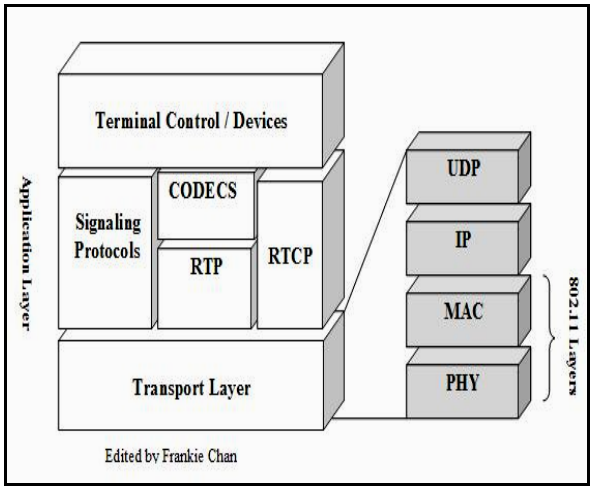

Fig. 2. The Voice over Wi-Fi (VoWi-Fi) protocol [2].

3.4 Problems Faced by Voice over Wi-Fi

Voice over Wi-Fi has its shortcomings. The 802.11 WLAN standard was originally design for data services and not for voice. Therefore it faces problems such as scalability, quality of services (QoS), delay impairments etc.

3.4.1 Scalability Problem

The IEEE 802.11 standard uses a mechanism known as Carrier Sense Multiple Access with Collision Avoidance (CSMA/CA) which was based on Ethernet wired network which uses Carrier Sense Multiple Access with Collision Detection (CSMA/CD) mechanism. Since the CSMA/CA is also based on a binary exponential back-off algorithm that only grant user access whenever there is no other user transmitting in the network. Stations essentially do their best to listen for transmissions and avoid collisions. The problem is the scheme is largely ineffective applied in situations where multiple clients are active such as applying in VoWi-Fi network. Like the Ethernet hub, which will cause performance to degrade considerably in populated and crowded networks, the wireless LAN is subject to prohibitive scalability issues. When a large number of nodes are active, typically six to ten, running either voice applications (voice calls) or data transmission, the network slows down as the nodes or stations constantly collide, back-off and wait [1].

3.4.2 Quality of Services (QoS) Problem

Furthermore, the 802.11 standard lacks the mechanism to be able to recognize voice and apply QoS at layer 2 in order to avoid packet delay and loss. Voice packets are treated identical to any other data packet. Wired networks today have the ability to control QoS at the Internet Protocol, IP layer (layer 3) because Ethernet switching capacity (layer 2) is high enough to ensure packets will be transmitted with minimal loss and with minimal retransmission. By contrast, WLAN today lack the ability to control contention with the efficiency of wired Ethernet switches. Therefore QoS suffers “over-the-air” (at layer 2) before any IP (layer 3) QoS mechanisms have a chance to make any effect [1].

3.4.3 Delay Impairments

Like any network, Voice over Wi-Fi also cannot escape from delay problems. Basically there are a few major delays that will affect the voice quality over the Wi-Fi network. They are propagation delay, packetization delay, medium access control delay, jitter buffer delay and transport delay.

4. Simulation Results and Discussion OPNET Modeler was used to simulate the voice performance over the IEEE 802.11b Wi-Fi network which has a maximum data rate of 11 Mbps. An office environment Wi-Fi network with 2 mobile subnets (2 AP domains) which can cover up to an area of 300m x 300m was designed. We started from 2 mobile nodes per AP domain, increased it to 4 and 6 mobile nodes per AP domain to observe the voice performance. The statistics that we obtained are voice packet end-to-end delay and packet delay variation as follow.

4.1 Voice Packet End-to-End Delay

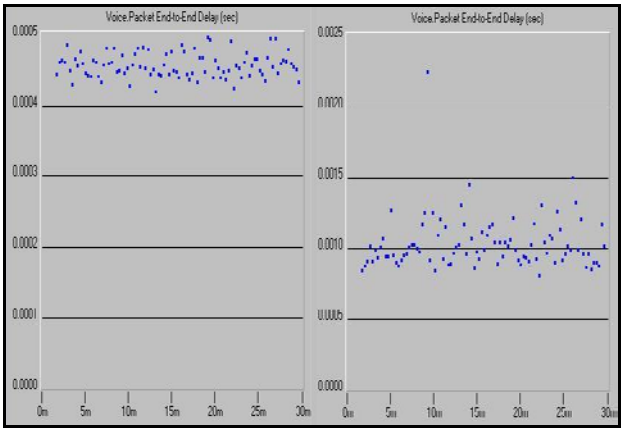

Fig. 3. Comparing voice packet end-to-end delay between 2 Mobile Nodes per AP Domain (left figure) and 4 Mobile Nodes per AP Domain (right figure).

Voice packet end-to-end delay is the time a voice packet takes to travel from the sender process (calling mobile node) to the receiver process (called mobile node). It is actually the sum of the processing, queuing, transmission and propagation delay. It can clearly be observed from figures 3 and 4 that when more active mobile nodes running voice applications (voice calls) simultaneously are added into a Wi-Fi network, the voice packet end-to-end delay increases significantly. From 0.0004s-0.0005s range for 2 mobile nodes per AP domain, it increases to 0.0005s-0.0025s range for 4 mobile nodes per AP domain. It later increases to a range of 0s-3s for 6 mobile nodes per AP domain.

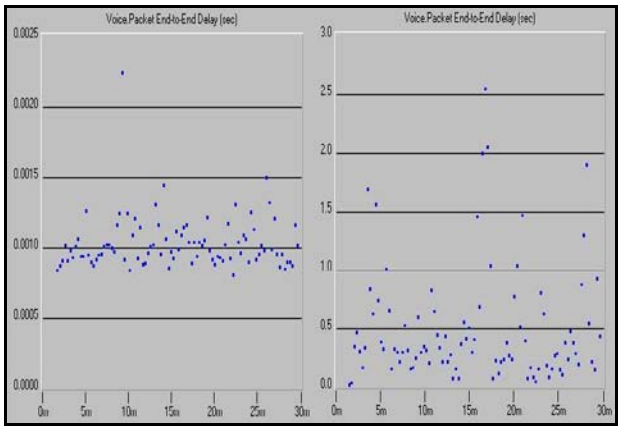

Figure 4. Comparing voice packet end-to-end delay between 4 Mobile Nodes per Access Point (left figure) and 6 Mobile Nodes per Access Point (right figure).

According to International Telecommunication Union (ITU) standard, the packet end-to-end delay has to be less than 0.4s in order to protect and preserve the voice quality over the wireless network. Therefore, the design of Wi-Fi network to have 2 and 4 mobile nodes per AP domain is therefore ideal to implement VoWi-Fi applications. However, for more mobile nodes per AP domain, the contention to use the scarce network resources certainly increases. This will eventually cause the network or voice packet end-to-end delay to rise which will result in poor voice quality over the Wi-Fi network.

5. Conclusions

Simulation results and statistics have shown that VoWi-Fi applications are applicable to Wi-Fi network with less mobile networks (less than 6). When active mobile nodes are running voice applications such as voice calls and audio streaming over the Wi-Fi network, the contention for network resources will increase and this eventually causes increase in voice packet end-to-end delay in Wi-Fi network. This results in poor voice quality over the Wi-Fi networks. In order to support voice applications over the Wi-Fi network, it is recommended that Wi-Fi network with higher data rates such as IEEE 802.11g which supports up to 54 Mbps has to be used. Our next research work will address this issue. It expected that 802.11g will provide better performance for voice applications over the Wi-Fi network in terms of voice quality as well as support more concurrent voice calls over the Wi-Fi networks. IEEE 802.11g standard can support up to approximately 4 to 5 times the amount of voice calls as compared to IEEE 802.11b which was investigated in this study.

6. References

[1] The enterprise is read for voice over WLAN. Is voice over WLAN ready for enterprise? Meru Networks, November 2003.
[2] M. Shiva Kumar, Voice over WLAN, April 2002.

Bibliography

[1] Jan Linden, Jan Blom, Voice over 802.11 Case Study Wireless VoIP: The Next Step in Communications Evolution, 2003.
[2] A. Ganz, A. Phonphoem, N. Llopis, I. Kim, K.Wongtavarawat, Converged Voice,
Video and Data Wired-Wireless LANs Testbed, *IEEE Military Coomunications*
Conference Proceedings: 1297-1301 vol.2, 1999.
[3] Dr Harry Bims, Enabling Voice over WLANs, Airflow Networks, September 2003.
[4] Charles N. Thurwachter, *Wireless Networking*, Prentice Hall, 2002.
[5] B. Walke, *Mobile Radio Networks: Networking, Protocols and Traffic Performance*, Wiley, 2001.
[6] J. H. James, Bing Chen, Laurier Garrison, Implementing VoIP: A Voice Transmission Performance Progress Report, *IEEE Communication Magazine:*
36-41, July 2004.
[7] Al Patrick, Voice Services over 802.11 WLAN.

Authors Index

ISBN: 978-1-61804-228-6